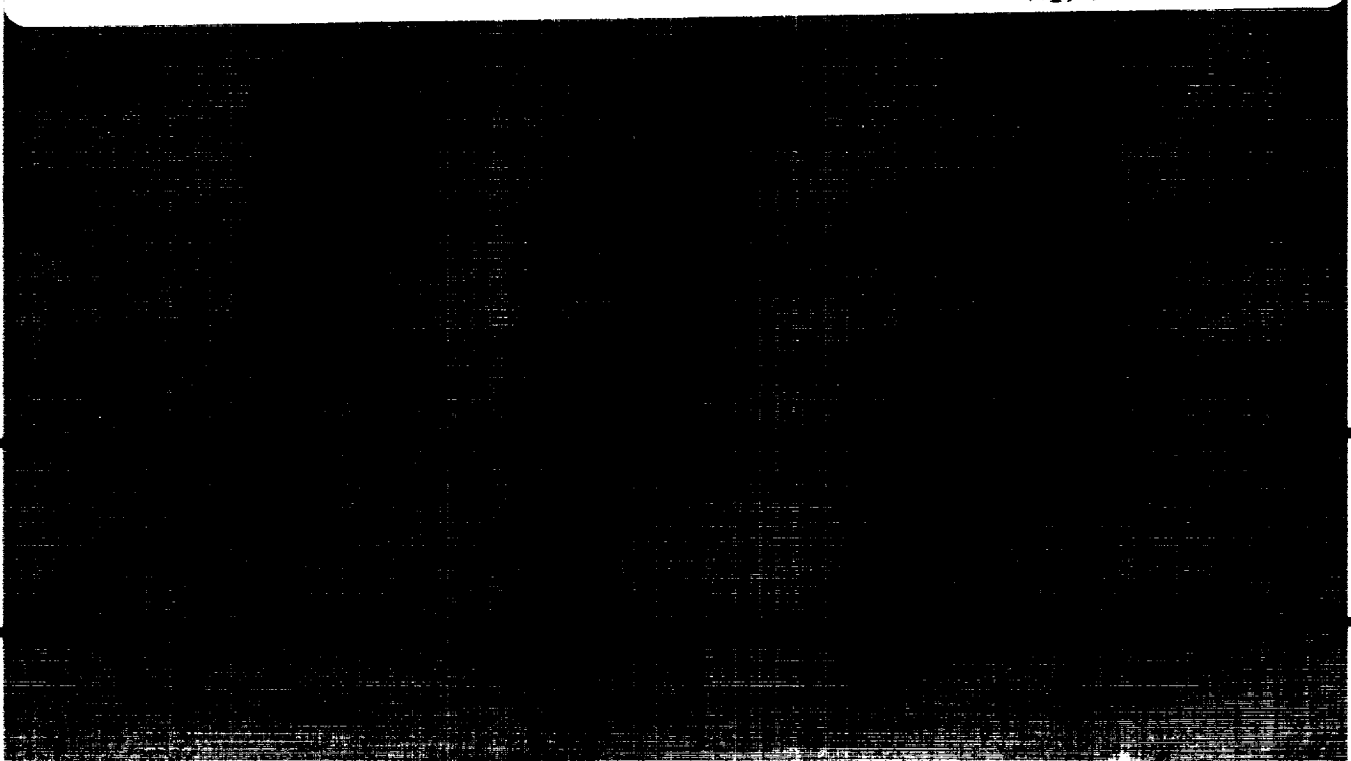


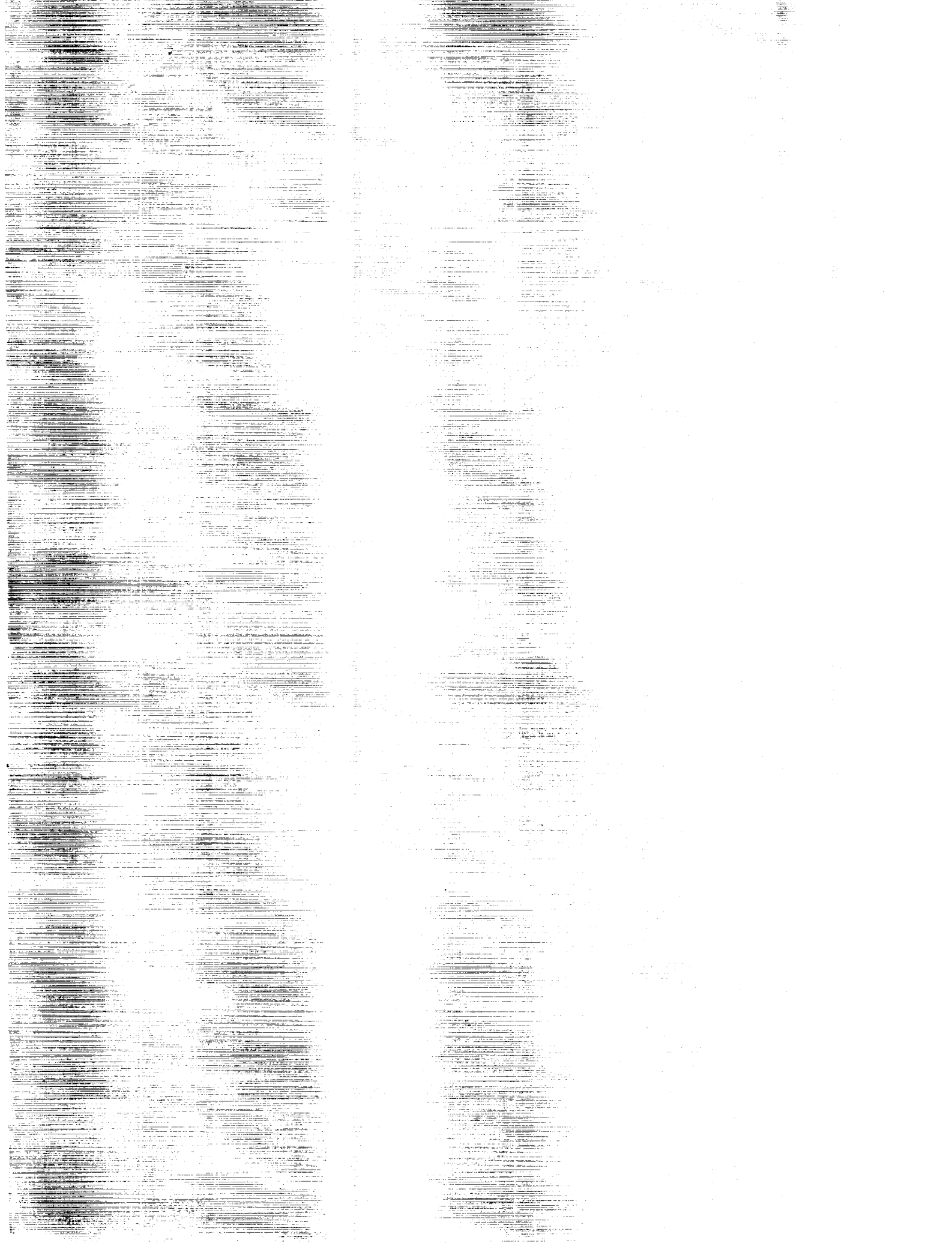
Aeropropulsion '87

(NASA-CP-3049) AEROPROPULSION 1987 (NASA)
498 p CSCL 21E

N92-22510
--THRU--
N92-22543
Unclass

H1/07 0000037





NASA Conference Publication 3049

Aeropropulsion '87

Proceedings of a conference held at
NASA Lewis Research Center
Cleveland, Ohio
November 17-19, 1987



National Aeronautics and
Space Administration
Office of Management
Scientific and Technical
Information Division

1990

FOREWORD

The Aeropropulsion '87 conference was held on November 17 to 19, 1987, at the NASA Lewis Research Center in Cleveland, Ohio. In attendance were approximately 500 high-level representatives of aeropropulsion, airframe, and related industries, numerous smaller companies, several government agencies, and the academic world. The purpose of the conference was to present to industry an unclassified, but otherwise comprehensive, summary of the aeropropulsion research accomplished by the Lewis Research Center during the early and middle 1980's, with emphasis on the 1985 to 1987 work.

This publication records the Proceedings of Aeropropulsion '87. Its organization parallels that of the conference itself. Introductory presentations by senior management of both Lewis Research Center and NASA Headquarters reviewed some past accomplishments and discussed the philosophy, major thrusts, and trends foreseen in the ongoing NASA aeropropulsion program. The technical presentations were grouped into six plenary sessions, dealing with, respectively, (1) materials research, (2) structures research, (3) internal fluid mechanics research, (4) instrumentation and controls research, (5) subsonic propulsion technology, and (6) high-speed propulsion technology. The leadoff presentation for each session consisted of an overview or perspective on the topic by the appropriate session chairperson.

Authorship credit is listed with each paper in these Proceedings. All authors are from Lewis Research Center unless noted otherwise. In addition, the overall conference was planned, organized, and managed by members of the Lewis Research Center aeropropulsion staff, and was conducted with the assistance of Sverdrup Technology, Inc.

Edward A. Willis, Jr.
NASA Lewis Research Center

CONTENTS

	Page
THE 1987 AEROPROPULSION CONFERENCE: CHANGE AND CHALLENGE	
Robert Rosen, NASA Headquarters	1
IMPACT AND PROMISE OF NASA AEROPROPULSION TECHNOLOGY	
Neal T. Saunders and David. N. Bowditch	13
SESSION 1 - AEROPROPULSION MATERIALS RESEARCH	
LEWIS MATERIALS RESEARCH AND TECHNOLOGY: AN OVERVIEW	
Salvatore J. Grisaffe	37
HIGH-TEMPERATURE POLYMER MATRIX COMPOSITES	
Michael A. Meador	45
CREEP AND FATIGUE RESEARCH EFFORTS ON ADVANCED MATERIALS	
John Gayda	55
DEVELOPMENT OF A NEW GENERATION OF HIGH-TEMPERATURE COMPOSITE MATERIALS	
P.K. Brindley	65
SELF-LUBRICATING COATINGS FOR HIGH-TEMPERATURE APPLICATIONS	
Harold E. Sliney	79
CERAMICS FOR ENGINES	
James D. Kiser, Stanley R. Levine, and James A. DiCarlo	91
SESSION 2 - AEROPROPULSION STRUCTURES RESEARCH	
AEROPROPULSION STRUCTURES	
Lester D. Nichols	105
DETERMINING STRUCTURAL PERFORMANCE	
Edited by Michael A. Ernst	113
LIFE PREDICTION TECHNOLOGIES FOR AERONAUTICAL PROPULSION SYSTEMS	
Michael A. McGaw	129
INTEGRATED ANALYSIS AND APPLICATIONS	
Dale A. Hopkins	141
SESSION 3 - INTERNAL FLUID MECHANICS RESEARCH	
INTRODUCTION TO THE INTERNAL FLUID MECHANICS RESEARCH SESSION	
Brent A. Miller and Louis A. Povinelli	155
INLETS, DUCTS, AND NOZZLES	
John M. Abbott, Bernhard H. Anderson, and Edward J. Rice	157

TURBOMACHINERY

Robert J. Simoneau, Anthony J. Strazisar, Peter M. Sockol, Lonnie Reid, and John J. Adamczyk	175
---	-----

CHEMICAL REACTING FLOWS

Edward J. Mularz, U.S. Army Aviation Research and Technology Activity - AVSCOM, and Peter M. Sockol	197
--	-----

CONCLUDING REMARKS TO THE INTERNAL FLUID MECHANICS RESEARCH SESSION

Brent A. Miller and Louis A. Povinelli	209
--	-----

SESSION 4 - INSTRUMENTATION AND CONTROLS RESEARCH

INSTRUMENTATION AND CONTROLS RESEARCH SUMMARY	211
--	------------

I - INTRODUCTION

Norman C. Wenger	213
----------------------------	-----

II - RESEARCH SENSORS

David R. Englund	217
----------------------------	-----

III - OPTICAL MEASUREMENT SYSTEMS

Daniel J. Lesco	225
---------------------------	-----

IV - HIGH-TEMPERATURE ELECTRONICS

Lawrence G. Matus and Gary T. Seng	233
--	-----

V - FIBER OPTICS FOR CONTROLS

Gary T. Seng	243
------------------------	-----

VI - DIRECTIONS IN PROPULSION CONTROL

Carl F. Lorenzo	251
---------------------------	-----

VII - INSTRUMENTATION AND CONTROLS RESEARCH REFERENCES

261

SESSION 5 - SUBSONIC PROPULSION TECHNOLOGY

OVERVIEW OF THE SUBSONIC PROPULSION TECHNOLOGY SESSION

G. Keith Sievers	271
----------------------------	-----

SMALL ENGINE TECHNOLOGY PROGRAMS

Richard W. Niedzwiecki	279
----------------------------------	-----

ROTORCRAFT TRANSMISSIONS

John J. Coy	303
-----------------------	-----

THE NASA AIRCRAFT ICING RESEARCH PROGRAM

Robert J. Shaw and John J. Reinmann	315
---	-----

AIRCRAFT ENGINE HOT SECTION TECHNOLOGY - AN OVERVIEW OF THE HOST PROJECT

Daniel E. Sokolowski and Marvin H. Hirschberg	343
---	-----

OVERVIEW OF NASA PTA PROPFAN FLIGHT TEST PROGRAM	
Edwin J. Graber	363
ADVANCED PROPELLER RESEARCH	
John F. Groeneweg and Lawrence J. Bober	383
SESSION 6 - HIGH-SPEED PROPULSION TECHNOLOGY	
NASA THRUSTS IN HIGH-SPEED AEROPROPULSION RESEARCH AND DEVELOPMENT - AN OVERVIEW	
Joseph A. Ziemianski	407
SUPERSONIC STOVL PROPULSION TECHNOLOGY PROGRAM - AN OVERVIEW	
Bernard J. Blaha and Peter G. Batterton	413
PROPULSION CHALLENGES AND OPPORTUNITIES FOR HIGH-SPEED TRANSPORT AIRCRAFT	
William C. Strack	437
SUPERSONIC THROUGHFLOW FANS FOR HIGH-SPEED AIRCRAFT	
Calvin L. Ball and Royce D. Moore	453
HIGH-SPEED INLET RESEARCH PROGRAM AND SUPPORTING ANALYSIS	
Robert E. Coltrin	469
HYPERSONIC PROPULSION RESEARCH	
G. Burton Northam, Langley Research Center	487

THE 1987 AEROPROPULSION CONFERENCE:

CHANGE AND CHALLENGE

Dr. Robert Rosen, Deputy Associate Administrator
Aeronautics and Space Technology at NASA Headquarters

Dr. Colladay asked me to express his apologies for not being here. In our view this is a very important conference. Unfortunately, we are less than a week away from Gramm-Rudman, and Ray is involved this morning in some discussions on its potential impact on the agency.

The first line of Charles Dickens' *A Tale of Two Cities* is "it was the best of times, it was the worst of times." It seems appropriate to me for the last year or so to apply that to aeronautics. On the one hand, we have incredible opportunities in front of us. We have the potential to develop not just evolutionary aircraft, but new aircraft, the kind this world has never seen before. NASP will soon be a reality. A high speed transport is something we are very seriously thinking about. X-wing is at the beginning of flight testing. The tilt rotor will very shortly be a military inventory aircraft. We're also looking into other kinds of aircraft, the ASTOVL and supermaneuverability concepts, all of which provide an incredible opportunity, the kind of opportunity that probably has not been here since World War I.

But there is also a change going on in the world. The preeminence that the United States had in aeronautics may not exist in the future. Where we were once unchallenged in our technical endeavors, in our market share, in absolute terms we may no longer be. While we have an opportunity that we have never had before, we also have a challenge that we have never had before. So today I want to talk about some of the changes we see in aeropropulsion and to consider how those changes are affecting what we will do in the future.

Let us look at the challenges. There are challenges for the agency, for industry and academia, and for the rest of government. We need to determine how we can meet the challenges that we have before us. I think all of us are here because we all like a challenge; we like to look at, and prepare for, the future.

Let me talk about some of the changes we face, most of which you have heard before, but let us consider them in total. The first has to do with market change. For a long time the airline market was fixed. We knew what we were going to fly, what kind of range we needed, what kind of speeds were involved. But now we have a dramatically growing interest in long-haul aircraft. The market for transoceanic flights is predicted to be something like 300,000 passengers per day by the year 2000, and we believe it is going to double 25 years after that. That's an incredible new market and the figure of 300,000 passengers per day probably does not take into account the benefits that we will acquire from high speed aircraft. We see commercial aviation going to a high speed arena to take advantage of this very large new market. We see other changes having to do with revolutionary concepts in envelope expansion, range and maneuverability, like ASTOVL and NASP. On the other hand, we have also predicted that aviation fuel prices were going to go up, but in fact they have been fairly steady. So this predicted change did not come about and thus is affecting the way we think about future operation and development costs.

But those are not all the changes. The biggest change, one that is on everyone's mind, has to do with competitiveness. Where the U.S. once had a 90% market share in commercial aircraft, where we had a very sound general aviation industry, where our rotorcraft industry was very strong, we now have significant challenges from overseas. I am not going to go into that any further, as we're all too aware of it. The competitive change has also led to closer ties with the Europeans than ever before. This has obviously been in response to others impacting what used to be a U.S. dominated market. Over the long haul, the Japanese and Europeans are very consciously looking at those technologies which will strengthen their position in the market. Our belief right now is that while they haven't specifically targeted a high speed transport, they are certainly pursuing those technologies which will allow them to gain greater capability and thus offer greater competition.

Then there are technological changes which have come about in the last few years: computational methods are stronger now than ever before. Supercomputers are more available and are being used to a greater extent. Some of the revolutionary concepts I mentioned earlier really drive propulsion/air frame integration as well as control system integration, and many of these concepts have to be explored through the use of computers.

The final change I want to mention has to do with R&D support. The national debt is creating pressures which are very, very severe; in fact, Dr. Colladay is not here today because of the national budgetary pressure we are facing. At this point we do not know what is going to be the impact on the NASA budget with all the problems involved with reducing the national debt. But one thing we are sure about is that there isn't going to be any easy money. It is not a simple task for us to go to OMB and say, for instance, that somebody at Lewis has a good idea in

aeropropulsion, and since it is a good idea we need additional funding. That just will not work. The competition for government funds is very severe these days. And when you have successfully achieved one hurdle, the next one is just as big. You're not sure what your budget will be until the last hurdle is cleared. The resulting effect is that our programs have to be extremely strong and they have to have broad support. It's not just because we're the National Aeronautics and Space Administration and we do good work that we get funded. We will get funding for programs that are well-supported by industry and academia, and that have good technical merit behind them. If the support and merit are not there, our budget requests will not be accommodated.

With the opportunities that we have and with the changes that are occurring, we must take the world as it is today and seek ways to do the job we are doing now and do it better. That is a challenge for each one of us and that is the challenge we will now consider.

I think the right way to approach today's challenges is to pick up on the opportunities and decide that we must do things a bit differently than we have done them before. We must decide that we need greater teamwork between industry, government, and academia. Teamwork will allow us to overcome some of the shortcomings of the past. The reason we have to do this is simple: we can not achieve the kind of leadership that we've known in the aeronautics industry and in aeropropulsion without doing things differently than in the past. For the past 50 to 70 years we worked with the aeronautics industry in a predictable, constant way and we achieved a wonderful market share. We achieved incredible technical leadership. But things have changed. As a result of the changes mentioned earlier, instead of a 90% market share in commercial aircraft, we now have a 70% market share. That's proven to us something very clear: 90% is not our birthright. American airlines are not going to buy only from American aircraft manufacturers. European

airlines and airlines in the rest of the world will go where the price and the technology are best. The U.S. has come down from that 90% equilibrium position. In my view, the U.S. situation was in equilibrium for a long time, but now that equilibrium has been disturbed. Now the U.S. is at 70%, which may not be an equilibrium position.

What I would like to see is that we work together to achieve the strongest position that we can for aeronautics. There are many factors that enter into the 90% to 70% decline, and into what is going on right now in industry. You know the factors; they include government subsidies, insurance settlements, and several other things which are not technological factors. We have to address those things somehow, but I will not address them here today. I'm not going to tell you about government subsidies or insurance settlements. But what I am going to talk to you about is technology. I feel that in the overall scheme of things, technology is really the key.

In spite of government subsidies and whatever else is going on in the economics of aeronautics, one thing is certain: if U.S. aircraft don't have the best technology, they will not be bought, and we will not succeed. We cannot overcome foreign government subsidies with inferior technology. Thus, I want to talk about ways we can work cooperatively to improve the technology that is on our aircraft. In particular, I want to talk about the challenges that exist for NASA, for industry, for DOD, and for academia with respect to improving technology in today's environment.

Let me start out with NASA-Lewis first. Lewis works in a number of technology fields. They have a solid foundation in turbomachinery, materials and structures, and guidance and control systems. They have a growing expertise in internal fluid mechanics and validation of its applications. They are fostering and developing innovative concepts in aeropropulsion. The advanced turboprop, which is something we are all very proud of, is an example of developing an

innovative concept to the point where it is utilized by industry. This is another strength of NASA-Lewis: the ability to transfer technology to industry and other government agencies. They have an outstanding spectrum of experimental facilities; you have an opportunity to tour those facilities during this conference. I urge you to use that tour to look at the facilities that are here, to think about how these facilities can help you, how these facilities can be made available for your needs, and how can you apply them. NASA Headquarters is interested in making these facilities available to you; I know NASA Lewis is interested in doing this as well.

But there is a challenge to the Lewis Research Center to help improve on what you are doing and at the very same time to develop closer ties with industry. Let me offer some specific challenges to Lewis to move closer towards the goal of superior aer propulsion technology. First, do not compete with industry. The Lewis Research Center has certain capabilities which are outstanding, but the Center is not in the business of *developing* engines. Don't try to develop engines. Try to develop the long-term fundamental research which you can do best of all and leave the engine development to the people who can do that best, the aer propulsion industry. Work on the long-term research, but while you are working on the long-term research, think about the partnership that I challenged you with earlier. Think about how you can make your long-term research consistent with what is going on in industry. Look for ways to accomplish intermediate goals within that long-term research and transfer it to industry as it comes along. Make sure that you transfer your research accomplishments so that industry has immediate access to newly developed technology. Get closer to the people who are doing the research in industry and find out what their needs are so in fact your research becomes relevant; so that your near-term objectives in your long-term effort become relevant to industry's needs.

Another way in which NASA Lewis can draw closer to industry is to work aggressively to seek joint programs and cooperative adventures with industry. The Center is doing a considerable amount of research. There is a lot of similar work going on in industry. Find ways of pulling those programs together so you can work as partners, so you can benefit from what is going on in industry, and industry can benefit from what is going on at the Center. In the end, you will be collectively stronger. My promise is that I personally will do what I can to break down the natural and bureaucratic barriers that seem always to occur, so that these cooperative programs can occur as easily as possible.

With respect to the academic community, I challenge NASA Lewis to increase its involvement with that community as well. Take advantage of the academic community as a source of ideas, both fundamental and technical ideas and innovative concepts. Use that talent, get that talent into the Center and spread those ideas throughout the Center. Provide access to universities as a way of working hand-in-hand with the facilities through your computers so that a partnership is built. I think ICOMP, the Institute for Computational Mechanics in Propulsion, is a good example. It was started at Lewis a couple years ago and it's already having some very good results. I urge you to continue that program and to develop similar ones to establish coordination and cooperation with the academic community.

Last, I urge NASA Lewis to plan its programs in such a way as to take advantage of what your real strengths are: your researchers and the stability you offer those researchers to do sound, fundamental work. I believe the program at Lewis can be extremely strong technically because of what you can offer to the people who work here. This country does not need a mediocre aeropropulsion program in the National Aeronautics and Space Administration. What this country needs is an absolutely in-depth, first class research program; and I think that the resources that

are here at this Center can be brought to bear on that research program. I urge you to follow through as strongly as possible in planning high quality technical research, the kind of research that industry is anxious to utilize. If you do that, the partnership between NASA and industry will become very strong. There will not be competition, but rather, support, cooperation, and eagerness on the part of industry for your research programs.

Now that I have talked specifically about challenges to NASA Lewis, let me tell you what I believe are the challenges for industry. There is, of course, an economic challenge which I will not talk about here. Rather, I will talk about the challenge of technology development. The industry-sponsored R&D work that goes on is a critical and special ingredient in our equation for national technical strength in aeronautics. By and large the work that comes out of industry on its own has been excellent. But I believe there is something which industry can do better; industry should take advantage of the strength at the NASA Centers, in particular, the Lewis Research Center. There's a tremendous capability here in people, resources, and facilities. I think that industry ought to view the NASA Centers not merely as a funding source, but also as one element in their overall corporate research activity. The Center is here and much of its reason for being is to support industry. So the challenge I offer to industry is to form a better working relationship with NASA and strive to become an equal partner. Do not utilize NASA merely as a fund source; utilize it as an equal partner in research.

Let me suggest some ways that industry might do that. When I talked about challenges for the Center, I mentioned closer cooperation with industry and the idea of working towards joint programs: that challenge applies equally to industry. Industry can also work with the Centers for joint programs. Seek ways in which to do research and ways in which to work cooperatively with the NASA Centers. There are some excellent examples of successful joint programs. I see no

reason why those programs cannot be expanded and continued to promote closer cooperation between industry and NASA.

Effective technology transfer is also of interest. You heard that earlier from Lawrence Ross. What industry must do to succeed at this is to identify and work towards the particular areas where you think cooperation could exist and then approach NASA. Let NASA know that you have a program you want to work on cooperatively. Try to be creative when doing some of these things. Let NASA personnel spend some time in industry. Often what happens in a cooperative program that uses a Center facility, a wind tunnel or other type of facility, is that industry sends someone to the Center to work there for a while. Isn't there also some benefit to having NASA researchers work in industry for a while? Isn't there something industry can gain from that? I see real benefits in this to both NASA and industry.

Let me digress for just a second and tell you something about our budget process. When we determine what we're going to request from the Administration in any given year, we go through a number of hoops and discussions. We look at what our opportunities are, what is needed, what we can convince the Administration of, and then what we can convince Congress of. We get advice from within NASA that we discuss at Headquarters; we get advice from the field centers; and we get advice from industry. We have advisory committees that we rely upon very heavily in determining what direction our agency ought to take. I urge industry to take the position of an equal partner, to get involved with our advisory committees. The advisory committee structure that we have is fairly broad, and I suspect that everyone in this room is close to someone on an advisory committee for the Office of Aeronautics and Space Technology. Because of the ties you have to advisory committee members, everybody in this room has the ability to impact NASA's programs. Do it! It happened last year when we were going through the interaction process of

putting the budget together. We were undecided about a few elements; we got our advisory committee in, had an all-day session discussing what should be the approach, and which direction we ought to take, and the feedback we got was clear. The feedback was certain as to what direction industry wanted us to go and that's the direction we took. Take advantage of a very effective advisory committee structure. I was in industry some time ago and I didn't know that the advisory committee structure existed, to tell you the truth. NASA uses the advisory committee in formulating our budget, in deciding the directions we want to go, in looking at our programs' strengths, and in defending our programs. So it's an opportunity for all of industry, and I advise and urge you to take that opportunity.

There is another way we can interact. It has to do with industry programs and the support you have for NASA programs and aeropropulsion. We at Headquarters have recently been taking a very aggressive position towards the growth we think is essential in aeronautics. We think we've had some success over the last couple years, and we're excited about obtaining more success in the future. But industry involvement in the whole process is extremely critical. You have options: you can participate and help us collectively, or, you can choose not to help us.

Let me give you an example of an external source that is very effective. One of the things NASA does and ought to do is planetary science. The space part of our business is the most well-known; the public views planetary science as essentially what the agency does. Planetary science produces lots of good science and lots of good PR; we have all seen the wonderful photographs that have come back from outer space. I happen to be in favor of planetary science; I think it's one of those things the agency ought to do, and I don't want anyone to misinterpret these remarks. The external planetary science community has decided it can be most effective by having a strong lobby with NASA and in Congress and they have succeeded. The budget for planetary science in

the agency is about equivalent to the budget for aeronautics in the agency. I don't think the budget for planetary science is too large, but I think when you make a comparison between planetary science and aeronautics, the aeronautics budget ought to be a lot larger. For that to happen, we're going to need some help from industry; the kind of help that the science people in the agency are getting from the planetary science community. That's an opportunity to make your needs known. In order to make your needs known, you need to break down some of the rivalry that exists between competing companies. Consider the good for all, and that good for all includes the good work NASA is doing. Industry should not give us credit for anything we don't do, but you should give NASA credit and tell others about the things we do for you.

I want to talk now about the universities. I said a minute ago that industry should not consider NASA merely as a funding source. Universities have a different problem. They need money but they don't get money from anywhere except places like NASA. So we have to be viewed as a funding source by the universities. The challenge to academia is to be more flexible and willing to move into and support some of the new work that is going on. High speed technology, supermaneuverability, and ASTOVL are all going to require new kinds of research in new areas. So the challenge I offer to academia is to take the steps to go in the new direction that aeronautics is going in. Discontinue the work that is not quite as productive as it used to be, and take this opportunity to think about moving into a new area, an area where we can make large strides and where you in fact can support an important goal or direction of the country.

With respect to the other government agencies: there is a challenge for them as well. A coordinated, cooperative, government research program is essential to sustain the kind of resources that we have had in the recent past. When we discuss our budget request with the Office of Management and Budget, the number one question to us is what is the Air Force doing

in this area? We must always justify the work that we do compared with what is going on in the Air Force or the DOD in general. OMB realizes that in the kind of budget situation we are in now, we can't afford to duplicate work. In fact, we must do work that is complimentary. The challenge here is to shed some of the territorial prerogative that we have all had in the past, and look towards working cooperatively so that the DOD program, or the FAA program, and the NASA program will fit together to strengthen each agency's programs.

I also suggest that the DOD and other government agencies as well look for partnerships with industry. Find ways to work cooperatively to strengthen our overall programs. The Lewis Research Center has a vision for the future in aeropropulsion that you will hear more about. I know that vision has been discussed widely within the Center; it has also been discussed at NASA Headquarters. It is something that we all believe in. While you attend this conference, think about this vision, and discuss with NASA personnel what you like about it, perhaps ways in which it can be improved. What NASA really wants is to have a very strong, high quality program. That is what the U.S. needs, that is what industry needs, that is our reason for being. Our goal in conferences like this one is to do everything we can to make sure that the program we have in aeropropulsion is at the leading edge, that the technology is well-transferred, and that the cooperation between the government and the rest of the aeropropulsion community is as good as it possibly can be. I urge you to use this conference as a first step towards developing this cooperation. While you are here for the next few days, think about meeting these challenges for a stronger aeropropulsion community.

IMPACT AND PROMISE OF NASA AEROPROPULSION TECHNOLOGY

Neal T. Saunders
and
David N. Bowditch

SUMMARY

The aeropropulsion industry in the United States has established an enviable record of leading the world in aeropropulsion for commercial and military aircraft. NASA's aeropropulsion propulsion program (primarily conducted through the Lewis Research Center) has significantly contributed to that success through research and technology advances and technology demonstrations. Some past NASA contributions to engines in current aircraft are reviewed, and technologies emerging from current research programs for the aircraft of the 1990's are described. Finally, current program thrusts toward improving propulsion systems in the 2000's for subsonic commercial aircraft and higher speed aircraft such as the High-Speed Civil Transport and the National Aerospace Plane (NASP) are discussed.

INTRODUCTION

In 1987 the aeronautics community commemorated the 50th anniversary of the first successful operation of a turbojet engine. This remarkable feat by Sir Frank Whittle represents the birth of the turbine engine industry, which has greatly refined and improved Whittle's invention into the splendid engines that are flying today. During the past 50 years, the U.S. aeropropulsion industry has developed an enviable record in leading the world in the continual development of new aircraft engines with improved performance, durability, environmental compatibility, and safety. NASA, as did its predecessor NACA, takes pride in assisting the development of this record as a long-time partner with U.S. industry in the creation and development of advanced technologies which have spurred each new generation of engines.

This paper highlights some of the recent contributions of NASA's aeropropulsion research and technology efforts (fig. 1). Several technology advances that emerged from NASA research efforts in the 1970's and early 1980's were instrumental in the development of high-bypass turbofan engines that are powering today's fleet of commercial transports (such as the Boeing 767 shown at the lower left). And some of our more recent efforts have been key to the development of advanced turboprop engines which will lead to the introduction of a new generation of transports (center) in the mid-1990's. Also, we will describe some of the current research efforts that are aimed at advanced propulsion systems that might power transports in the 21st century. This includes advanced engines for both subsonic transports and high-speed transports such as the High-Speed Civil Transport (HSCT) and the National Aerospace Plane (NASP) (upper right).

Fifty years after the Whittle engine first ran, it is interesting to review the improvement in efficiency of commercial turbofan engines, shown in figure 2. The thermal efficiency of the Whittle engine was relatively low because of its low pressure ratio and low maximum temperature. As improved materials and aerodynamics became available, these parameters increased dramatically, improving the core thermal efficiency for first-generation turbine engines. Second- and third-generation turbine engines benefited from further increases in thermal efficiency and also obtained major improvements in propulsive efficiency by increasing the bypass ratio of the turbofan engine. Advanced turboprop engines will obtain further dramatic increases in propulsive efficiency by increasing the bypass ratio to its ultimate practical value.

NASA AEROPROPULSION CONTRIBUTIONS

Base Research and Technology Program

Base research and technology contributions of NASA's aeropropulsion program have been many and varied, and some of the more significant technologies are listed in figure 3. One of the most significant technology advances involved improved aerodynamic designs for fans and compressors. In the 1970's NASA, through both in-house and contract efforts, built and tested more than 100 single- and multiple-stage compressors and fans to develop and verify advanced design concepts such as high tip speeds, low source noise, controlled-diffusion blading, and low-aspect-ratio blading. These technologies were combined in the design of the compressors and fans of the Energy Efficient Engine Program, which provided unprecedented performance improvements. These components provide the basis for the fans and compressors on the newest commercial turbofan engines. The other major NASA contributions listed in figure 3 (composite materials and structures, thermal barrier coatings, reduced noise and emissions, and advanced controls) are described in later figures.

NASA Lewis Research Center has been a leader in the development of composite materials and the structural analysis necessary to provide significant reductions in engine weight and fuel usage (fig. 4). A PMR-15 polymer developed at Lewis is currently the nonmetallic composite matrix with the highest use temperature (550 to 600 °F). Composites using graphite fibers in a PMR-15 matrix have been used to produce a lightweight fan duct for the F404 engine, as illustrated on the left side of this figure. Current research is aimed at extending the use temperature to 800 °F. For higher temperatures Lewis is investigating metal and ceramic-matrix composite materials.

To efficiently use the anisotropic composite materials, new analytical methods and computer codes had to be developed. Composites micromechanics and laminate theories have been developed through Lewis programs and incorporated into the Integrated Composites Analyser (ICAN) code (right side of figure) to predict the material properties necessary to design components such as fan or propeller blades. These contributions have provided significant weight reduction and permitted improved aerodynamics through thinner blades without the dampers necessary on the older metal blades.

Ceramic thermal barrier coatings are being used in many of today's engines to extend the lives of metal parts used in combustors and turbines. The use of thermal barrier coatings by applying a ceramic coating onto a metal burner or

turbine part to protect the metal and reduce its temperature was recognized in the 1960's. However, early applications were frustrated by the coating spalling off after short periods of use. NASA led research on those coatings which identified the failure mode as oxidation of the underlying metal and developed bond coatings and application procedures that have successfully prevented the coating failure. Increased reliability has resulted in the increased use of coatings in engines during the past two decades (fig. 5). Initial use was limited to a band-aiding approach to extend the life of combustor liners (left). During the 1980's improved thermal barrier coatings have been applied to selected areas, such as turbine vane platforms (center), to extend life and reduce cooling air requirements. As the technology of these coatings reaches full maturity, thermal barrier coatings will be extended to more critical areas, such as the aerodynamic surfaces of turbine blades (right).

NASA has played a dual role in noise reduction of commercial turbine-powered aircraft by contributing to the technology and by providing unbiased expert consulting to the FAA in its rule-making role. This role, combined with industry programs, has resulted in dramatic reduction in noise generated by the modern turbofan aircraft (fig. 6), making them the good neighbors they are today. NASA Lewis did extensive research in the sources of noise, acoustic treatment to suppress the emitted noise, and necessary procedures to measure noise in ground test facilities so that flight noise could be estimated. This understanding was used by NASA and the industry to design new components, engines, and installations that reduced airport noise to an acceptable level.

The trend in turbine engines toward more controlled variables to get improved performance and efficiency, as shown in figure 7, has made it necessary to switch from the old reliable hydromechanical control to a modern, flexible digital control. The many technical barriers to this transition have been a subject of research at Lewis since a J-85 engine was first operated under digital control in 1970. To develop a formalized procedure to design controls for so many simultaneous variables, multivariable control theory for turbine engines was developed by Lewis and demonstrated in the F100 Multivariable Control Program. Since the most unreliable components of the control are the engine sensors, Lewis developed algorithms to allow the failure of sensors to be detected and accommodated while continuing to safely control the engine. Digital control is currently being used on the F100 in a supervisory trimming mode with a hydromechanical control and is being demonstrated in flight in a full authority mode in the digital electronic engine control (DEEC) for the F100 engine. This type of control system will be on most of the new high-performance engines of the 1990's and 2000's.

Advanced Turboprop Program

The effect of bypass ratio on civil transport engines in terms of fuel usage is shown in figure 8. The specific fuel consumption (SFC) of turbine engines has declined as the bypass ratio has been increased. When turbine engines were first introduced in commercial service, they were a great success as long as the fuel price was very low. To improve fuel efficiency, the bypass ratio was first increased to about 2 for the low-bypass engine and finally to about 7 for the high-bypass engines with resulting large decreases in SFC. When the fuel crisis hit in the mid-1970's, it became apparent that further

decreases in SFC were very desirable. Therefore, the further reduction in SFC available with the ultimate in high bypass, the propeller, was recognized as a goal worth investigating.

As a result of earlier turboprop experience, it was initially difficult to get the reintroduction of propellers for propulsion of commercial aircraft taken seriously. To compete with turbofan aircraft, similar speed and cabin comfort were required. Therefore, as shown in figure 9, the initial research at Lewis in the late 1970's was aimed at demonstrating desirable performance and noise at higher cruise speeds than had previously been obtained with propellers. The success of this research indicated the feasibility of achieving major reductions in fuel usage with advanced propellers. However, studies and analyses indicated that the full turboprop system had to be demonstrated in flight tests. So research in mechanical systems, such as gearing and pitch-change mechanisms, and propulsion integration were initiated in the early 1980's. While single-rotation propeller systems are simpler and have application to many types of aircraft, it was recognized that the swirl loss of about 8 percent could be avoided with counterrotation. The additional benefit of propulsion integration on aircraft with tail-mounted engines further increased interest in counterrotation so that research was started in the mid-1980's. These programs have culminated in flight demonstrations of the technology by Lockheed on a Gulfstream II, by Boeing on a 727, and by McDonnell Douglas on an MD90. NASA has been actively involved as a partner in all of these flight tests.

The Advanced Turboprop Program has included NASA in-house research in both experimental and analytical aerodynamic, acoustic, and structural technologies. These programs have contributed to the understanding of flutter, acoustics, and aerodynamics of swept transonic propeller blading. Some recent results, shown in figure 10, represent Euler solutions of the flow over the blades. At low forward speeds the leading-edge vortex system displayed in the left picture explains the good aerodynamic performance not predicted by the simpler two-dimensional aerodynamics. Unsteady Euler solutions predict the time-varying propeller aerodynamic forces obtained at angle-of-attack (shown in the center picture), and the unsteady forces on the blades in a counterrotation propeller system (shown in the right picture).

As a result of ongoing successful flight programs demonstrating the advanced turboprop technology, applications will be following in the near future. As the price of fuel inevitably increases, the increased efficiency of turboprop systems will be even more attractive, and transport aircraft such as the proposed Boeing 7J7 and McDonnell Douglas MD93 should become production aircraft. Advanced cargo aircraft, such as shown in figure 11, are being considered to provide improved range and efficiency and to replace military aircraft such as the C141 and the C130.

Hot Section Technology (HOST) Project

In the early 1980's, the life of commercial engine hot sections was considerably shorter than desired. NASA's HOST Project was conducted to focus technologies for aerothermodynamic and structural analysis of combustors and turbines toward more accurate predictions of hardware life (fig. 12). Therefore, for the first time, the aerothermodynamics to predict the thermal environment, heat transfer, and resulting thermal loads on components were combined

with materials behavior to predict the structural response and resulting life. Before the HOST Project, life prediction was a primarily empirical art; if a new component differed significantly from previous experience, life prediction was inaccurate and ultimately dependent on life testing and redesign if problems arose. HOST has combined the analytical approach with the development of advanced instrumentation used in benchmark quality experiments to better characterize the actual hot-section environment and to verify computer codes. As a result, more accurate analytical predictions of hot-section life are now possible.

The HOST instrumentation program focused on two types of instrumentation: instrumentation for characterizing the environment in the hot-section region and instrumentation for measuring the effect of that environment on the hot-section components. Examples of each type are shown in figure 13. The thermocouple probe is capable of measuring dynamic gas temperature fluctuations with a frequency response out to 1000 Hz. Tests of this probe at the combustor exit of an F-100 engine showed rapid dynamic gas-temperature excursions from as low as the compressor-exit temperature to near stoichiometric temperatures. The lower left picture is a view of a fuel nozzle in an engine operating at full power, obtained by using the new fiber optic combustor viewing system. Not only can it get such views in an operating engine for the first time, but by using laser light as an illumination source and filtering out the combustion-generated light, it can look through the flame and view the opposite wall during operation. Heat flux measurement on an operating turbine vane is another new capability developed in the HOST Project. These and other new instruments are giving new understanding of the environment in the hot sections of operating turbine engines.

Predictions of the HOST codes for a turbine blade in an operating engine are illustrated in figure 14. The variation of load with time associated with engine operation during a typical flight is shown in the upper left of the figure. The aerothermodynamic codes are used to predict the mechanical and thermal loading on the blade shown in the upper right. Heat-transfer codes are used to predict the temperature distribution in the blade, as shown in the lower left, at each instant of time. Mechanical and thermal loading distributions are used in structural analysis codes to determine the stress and strain distributions in the turbine blade. By evaluating the time-varying stress and strain using a life model, failure can be predicted; in this case, at about the center of the blade leading edge. Understanding the failure mechanisms in this manner allows a designer to correct life-limiting parts before the engine runs for the first time.

TURBINE BLADE MATERIALS TRENDS

From the beginning of the turbine engine in the 1930's, the materials have limited its efficiency and maximum thrust. In the 1950's and 1960's turbine blade materials were first wrought and later conventionally cast. During that period, use temperatures increased at a moderate pace (fig. 15). Beginning in the 1970's, new materials processing methods accelerated the pace at which use temperature increased. During this period, Lewis developed oxide-dispersion-strengthened (ODS) superalloys in-house and through contracts, and subsequently spun off the technology to industry to provide commercial alloys. The 1950's Lewis experience with tungsten-fiber-reinforced superalloys has been recently used to manufacture the first silicon-carbide-fiber/titanium-aluminide-matrix

composite material and to characterize it. These materials, combined with Lewis-developed thermal barrier coatings, will provide surface use temperatures up to 2300 °F in the 1990's. The Advanced High Temperature Engine Materials Program, beginning this year, will develop materials like the silicon-carbide-fiber/reaction-bonded-silicon-nitride material identified in the Lewis in-house program for use in the 21st century at temperatures of 2500 °F and higher. These new materials, through new higher values of use temperature, provide the opportunity of reaching new heights in turbine engine efficiency and thrust at speeds from subsonic to high supersonic if the accompanying aerodynamic and structural technologies can also be developed to allow maximum use of the material capabilities.

FUTURE COMMERCIAL SUBSONIC ENGINES

Returning to figure 2, which shows the historical increases in efficiency obtained in commercial engines, the future gains obtainable with the full potential of advanced technology have been added to identify the ultimate goal for subsonic engines (fig. 16). The left portion of the goal corresponds to advanced turbofans and the right portion to the turboprop with its higher propulsion efficiency. Reaching that goal requires new levels of performance from all the engine components by integrating the advanced technology in materials, aerodynamics, and structures.

The effect of overall pressure ratio on core thermal efficiency is shown in figure 17 for several levels of maximum cycle temperature and whether the hot-section components are cooled. For current component capabilities of 2300 °F with cooling, there is only a minor benefit with increasing pressure ratio. However, if the components could be operated uncooled at 2300 °F (with improved materials), significant increases in efficiency could be obtained if the pressure ratio of the core was increased to 60 or more. In addition, if advanced components with improved aerodynamic efficiency were available, further increases in thermal efficiency could be obtained at 2300 °F if the pressure ratio was further increased to 100. Increasing advanced component operating temperature to 3000 °F uncooled (with ceramic and carbon/carbon components) requires even higher pressure ratios to obtain maximum efficiency. It is important to note that increased temperature must be combined with more efficient components and unprecedented levels of cycle pressure ratio in order to realize major increases in core efficiency.

The core pressure ratios necessary to realize the full potential of new materials will require new aerodynamic technology for both the high compressor and turbine. As shown in figure 18, at pressure ratios of 100 or more, new materials will be needed in the latter stages of the compressor where the temperatures reach 1600 °F and higher. These last stages will also have very low corrected weight flow and the minute passage heights characteristic of small engines. Since small engines (with centrifugal/radial flow components) have had relatively low performance when compared with commercial turbofan engines, NASA has been directing significant effort at understanding the loss mechanisms associated with these components and developing technology to minimize these losses. Thus, our small-engine technology efforts might well play a key role in the future development of improved large engines.

As part of our research efforts for small engines, we are currently assembling a large-scale, low-speed centrifugal compressor to investigate the internal three-dimensional flows so that they can be understood and controlled with

resulting efficiency improvements. The rotor, shown in figure 19, is 5 ft in diameter and large enough to install instrument rakes in the passages and to instrument the vanes and walls with static pressures. The casing is also constructed with access for laser anemometry to document the interior flow fields. Analytical codes are being developed in parallel with the experimental efforts. The left figure illustrates the initial results of a quasi-three-dimensional thin-layer analysis which represents the expected flow on the meanline of the passage. Results of this research should eventually lead to improved performance of centrifugal compressors for use in small engines or the latter stages of large commercial engines.

Another element in our small engine technology efforts involves ceramic, uncooled, radial-flow turbomachinery. For several years Lewis has managed the Automotive Gas Turbine Program for the Department of Energy. The major emphasis of this program is to advance the technology of ceramics to a point where these brittle materials can be considered as serious candidates for use in high-performance turbomachinery. The goal of this program is to produce and demonstrate ceramic components capable of operation in a small-engine environment at temperatures of 2500 °F. Significant progress has been made. Fabrication technology has progressed from the manufacture of simple test bars and laboratory specimens to engine quality, complex parts, as shown in figure 20. Static parts, like those in the figure, have been rig tested at the target temperature of 2500 °F for extended periods. All the ceramic parts, including the turbine rotor, have been demonstrated in an engine at 2200 °F for 85 hours at 70 percent of design speed. A turbine rotor has been tested in an engine at 1950 °F and 100 percent of design speed for several hours. Future work is aimed at component reliability through improved materials, design, and manufacturing techniques to increase the overall reliability of ceramic engine components.

In addition, Lewis has NASA-sponsored research efforts aimed at extending the use temperature of ceramics to 3000 °F with life similar to current engines. Thus, emphasis is on high-temperature use of ceramics and on their structural and environmental durability and reliability. The program is interdisciplinary in nature with major emphasis on materials and processing and significant efforts in design methodology and life prediction.

LONG-RANGE, HIGH-SPEED FLIGHT

While NASA Lewis will continue to work on subsonic propulsion technology, the major part of its aeropropulsion program is shifting toward propulsion systems for long-range supersonic and hypersonic aircraft (fig. 21). The bottom picture represents configurations being studied for second-generation commercial supersonic transports that will probably be limited to turbine engine propulsion and hydrocarbon (JP-type) fuels. The Mach 5 military aircraft in the center of the figure is a configuration that Lewis has been investigating jointly with Langley Research Center and represents aircraft that cruise at speeds beyond those possible with turbine engines and hydrocarbon fuels. Lewis is also heavily involved in technology maturation efforts for propulsion systems being considered for the National Aerospace Plane Program represented by the aircraft in the upper left of the figure. The NASA aeropropulsion program will study propulsion systems for these aircraft to provide technology for improved efficiency, specific thrust, and environmental compatibility.

Most of the propulsion concepts under study at NASA for high-speed flight are shown in figure 22. Many of them have turbine engine hardware in the prime propulsion stream, but some nonturbomachinery systems are being studied for special applications, such as acceleration missions (for example, the air liquefaction cycle and scramjet cycle). High-speed cruise missions usually use turbine engines for acceleration and cruise, unless the cruise temperature is excessive for the engine. In these very high speed cases, either ramjet or scramjet propulsion is used in a dual cycle. For supersonic cruise of a commercial transport, NASA, in a joint program with industry, is studying many turbine engine cycles, including the turbofan with a supersonic-throughflow fan which appears to be a promising new concept.

High-Speed Civil Transport

Returning to the efficiency figure (fig. 2), a supersonic cruise aircraft goal has been added (fig. 23). Because of the large ram-pressure-ratio in supersonic flight, the Concorde propulsion system achieves a relatively high overall efficiency in spite of its 1960's technology. However, at the termination of the NASA Supersonic Cruise Program in the early 1980's, variable-cycle engines for supersonic cruise were estimated to offer a significant increase in efficiency over the Concorde engine's value of 40 percent. The goal of the current NASA program is to increase that efficiency to at least 60 percent through the use of advanced materials, structures, aerodynamics, and cycles like the one using a supersonic-throughflow fan.

Supersonic Throughflow Fan Technology

The advantages of the supersonic fan relative to a baseline afterburning turbofan are illustrated in figure 24. The simpler inlet and fan are lighter weight and more efficient by avoiding the complexity of slowing the external flow to subsonic speeds before introducing it to the fan. These advantages provide about a 10-percent decrease in specific fuel consumption and about a 25-percent reduction in propulsion weight, which leads to a 22-percent increase in aircraft range. Since the feasibility of maintaining supersonic flow through a turbomachinery stage has never been demonstrated, Lewis has initiated an exploratory program to investigate the feasibility of the supersonic fan component.

A cross section of the supersonic fan experimental hardware currently being constructed at Lewis is shown in figure 25, together with several computer solutions used in its design and analysis. The supersonic fan rotor and stator are located in the center of the installation downstream of an annular sliding block nozzle, which generates the supersonic flow into the rotor. A similar sliding nozzle is located downstream of the stator to slow the flow before it enters the exhaust duct. The quasi-three-dimensional thin-layer Navier-Stokes solution shown on the left was used to optimize the pressure distribution on the blading in the presence of the blade boundary layer. The analytical results shown at the bottom of the figure illustrate the unsteady interaction between the rotor and stator flow fields. The analytical results are processed to look like a schlieren photograph of the flow.

Very High Speed Propulsion

As we direct attention to higher speed regimes, hybrid propulsion systems beyond turbomachinery cycles must be considered. Figure 26 presents the specific impulse of the basic airbreathing propulsion cycles and compares them with the best rockets. The cycles with turbomachinery provide the highest specific impulse at speeds up to about Mach 5 where it becomes too hot for the turbomachinery to produce enough pressure ratio to overcome the inefficiency of its components. The subsonic ramjet then provides the highest specific impulse until about Mach 10 where molecular dissociation reduces its impulse below that of the scramjet. Airbreathing cycles always have a higher impulse than rockets but are much more difficult to operate at the higher Mach numbers. Work at Lewis and other NASA centers is aimed at extending the use of airbreathing cycles to Mach numbers higher than the Mach 3+ flown by the YF12.

A joint study of a military Mach 5 cruise aircraft by Lewis and Langley Research Centers and industry partners identified an over/under turboramjet cycle to provide desirable acceleration and cruise performance. The Mach 5 inlet illustrated in figure 27 represents the ramjet configuration with the turbine engine compartmented off for high-speed cruise. The experimental inlet hardware was recently delivered to Lewis for test in the 10- by 10-Foot Supersonic Wind Tunnel. Results of a fully viscous three-dimensional analysis displayed in the figure indicate that the sidewall boundary layer will collect on the cowl side of the inlet sidewall and cause separation, which would probably cause inlet unstart. Analytical results such as these were used to design a bleed system for the experimental hardware that will be tested in the near future.

While supersonic combustion ramjets (scramjets) were envisioned over 20 years ago, no one has yet proven their practical use. Langley has led NASA's scramjet propulsion research and recently demonstrated positive thrust on a scramjet configuration similar to the one shown in figure 28. Similar work is now planned by the NASP contractors, as the successful operation of the scramjet cycle is necessary to achieve a single-stage-to-orbit vehicle. The environment of a scramjet module is extremely hot and can be created in test facilities on the ground for only a few minutes at Mach numbers up to 10. Therefore, scramjet operation at higher Mach numbers will be critically dependent on computational fluid dynamics for analyzing and designing future scramjet configurations.

CONCLUDING REMARKS

The U.S. aeropropulsion industry has been very successful in competing in the world market for powering modern aircraft. NASA takes great pride in its contributions to that success, some of which have been reviewed in this paper. As the world competition grows, it will become harder to maintain our current leadership. NASA's current aeropropulsion program will continue to support that leadership by emphasizing technology that will provide future opportunities for major advances in propulsion efficiency and durability. While we have reviewed the highlights of that program, we could not cover it in sufficient detail nor describe enough of its programs to gain a full appreciation of its breadth and scope. Also, we have primarily concentrated on propulsion technology for commercial aircraft applications; however, much of NASA's propulsion technology advances are also applicable to military aircraft systems. The

papers that follow will provide a broader description of the NASA aeropropulsion program, which should help lead the industry into continuing to produce the best propulsion systems for commercial and military aircraft into the 21st century.

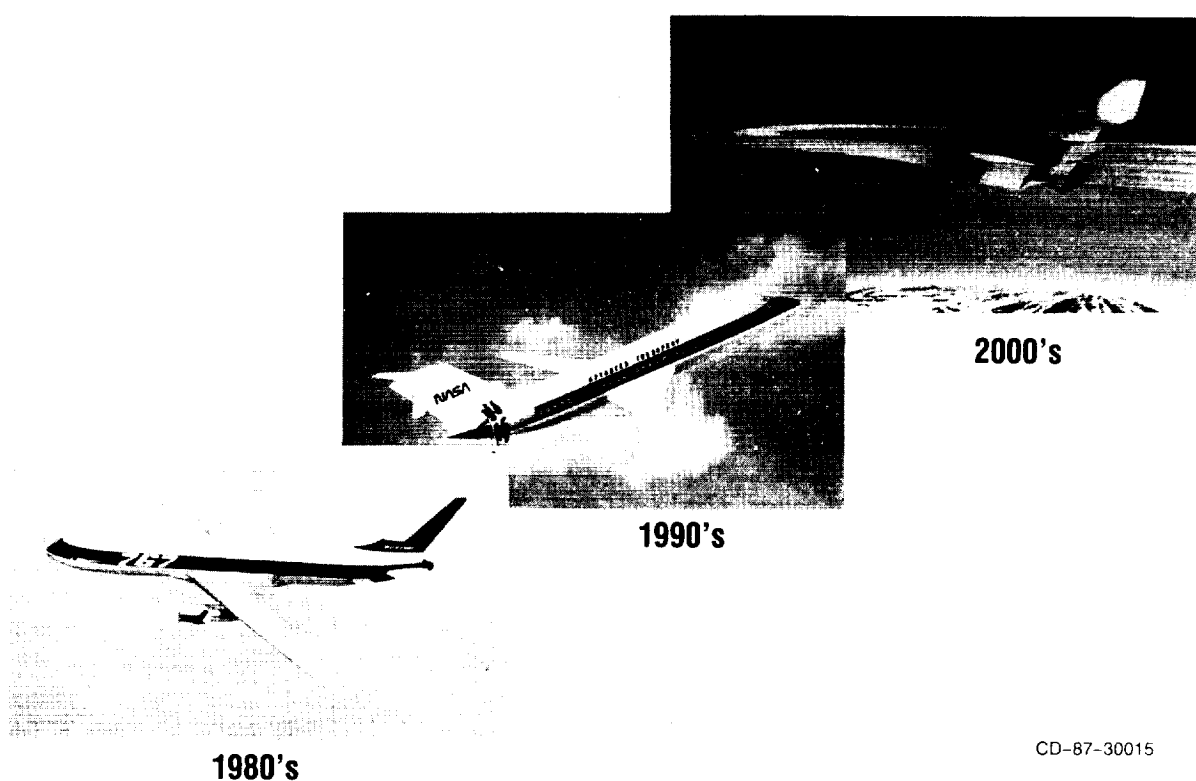


Figure 1. - Current and future aircraft benefiting from NASA's Aeropropulsion Technology Program.

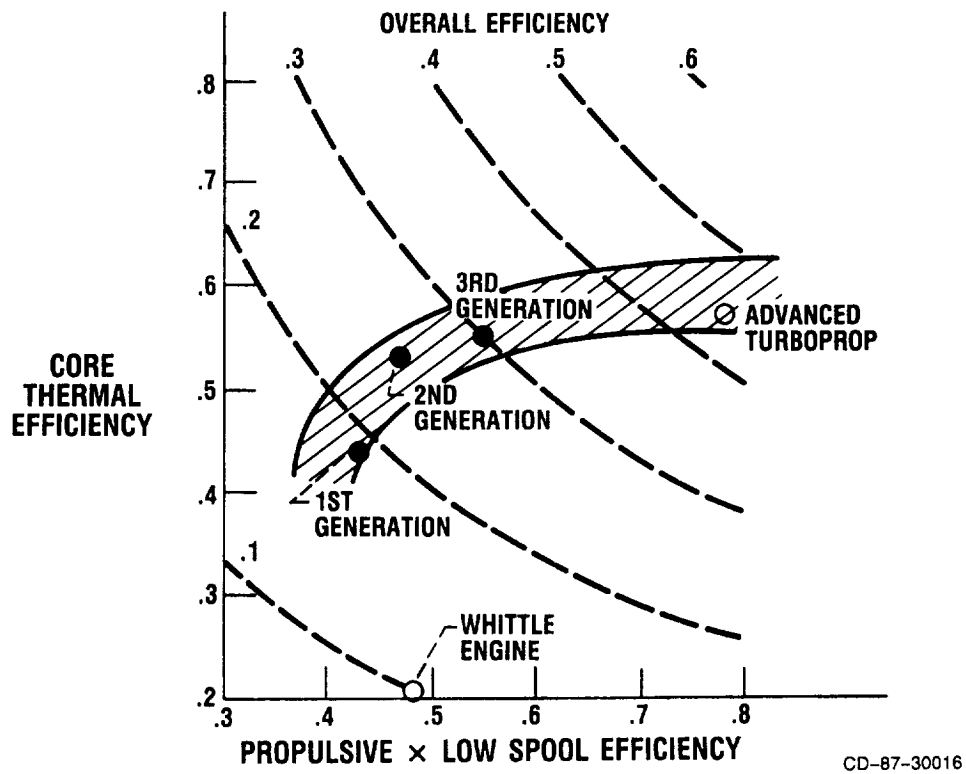
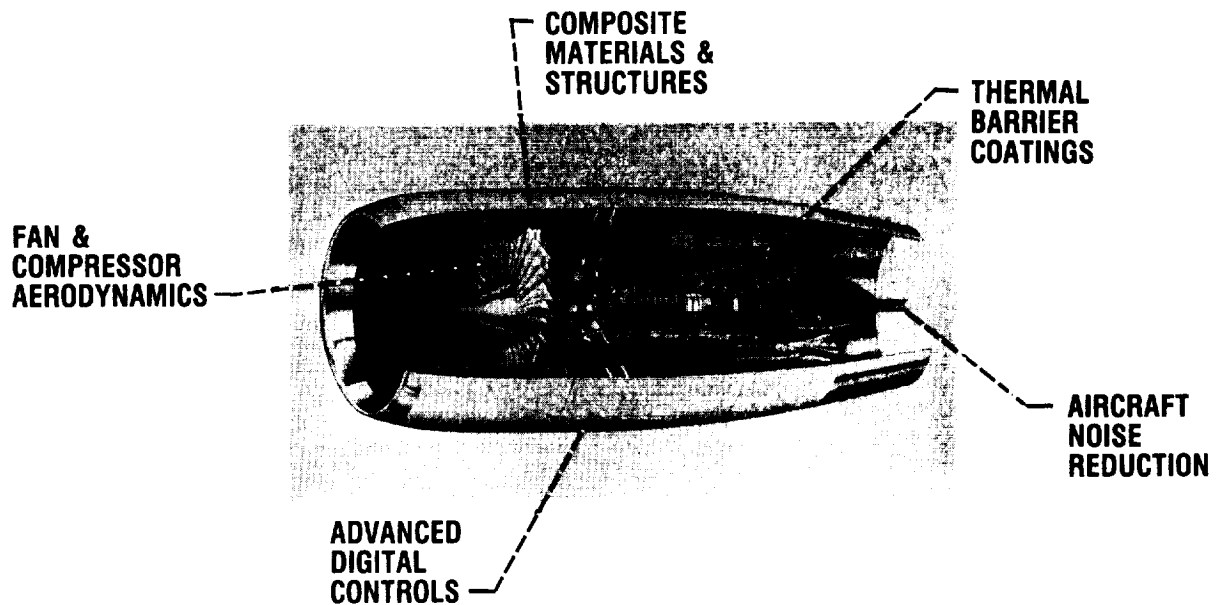
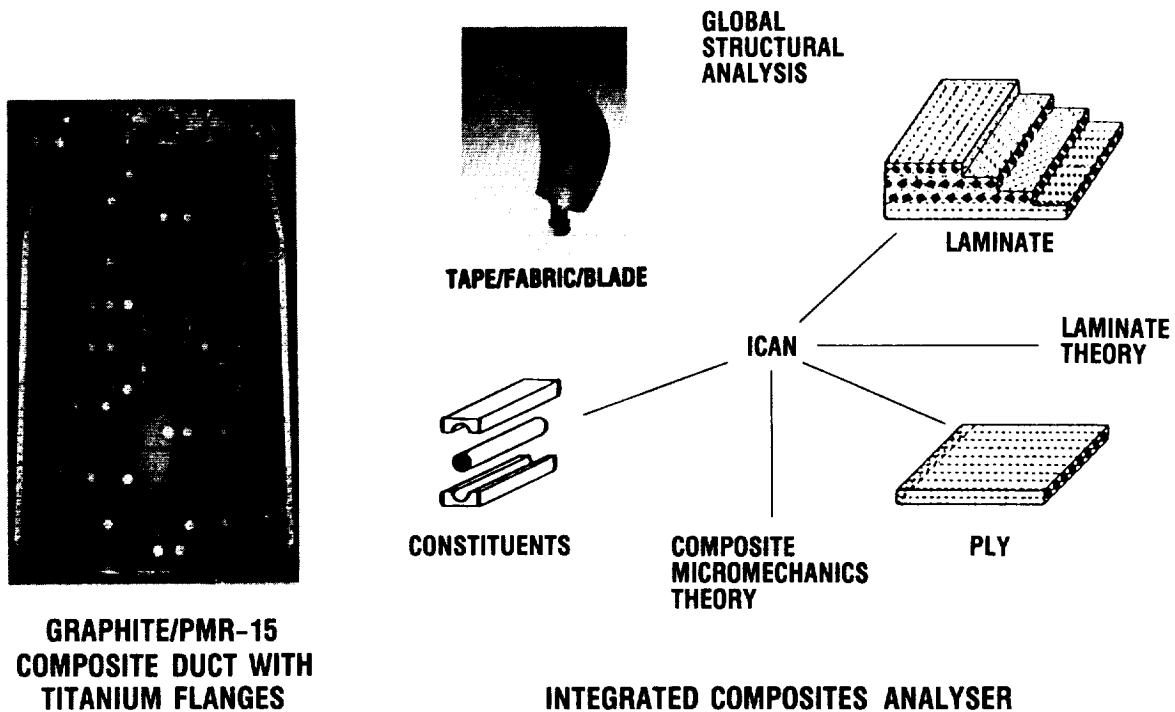


Figure 2. - Efficiency trends for commercial subsonic turbine engines.



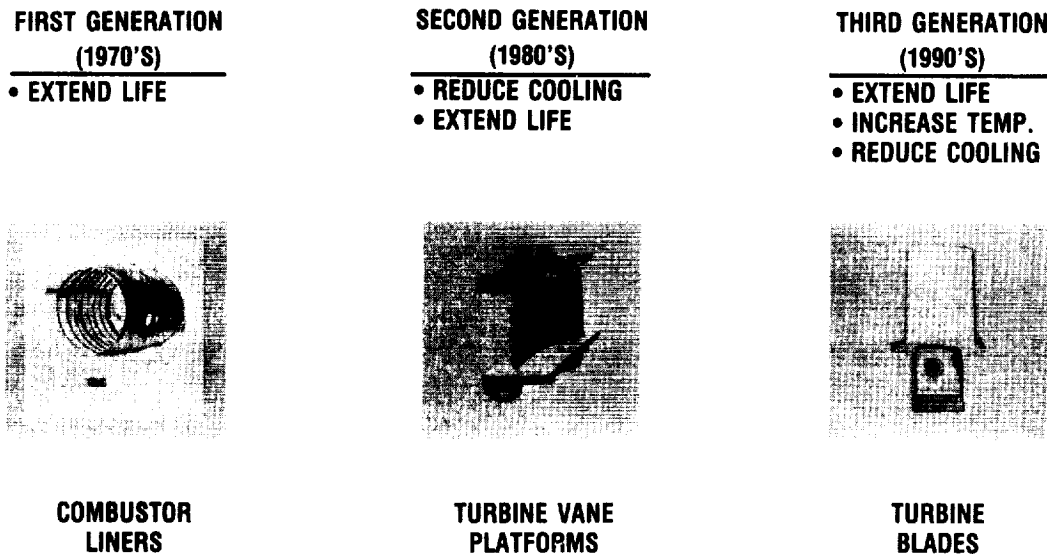
CD-87-30017

Figure 3. - Contributions to modern turbofan engines from the NASA Lewis aeropropulsion program.



CD-87-30018

Figure 4. - Contributions of the Lewis aeropropulsion program to advanced composite materials and structures technology in modern turbine engines.



CD-87-30024

Figure 5. - Applications for Lewis thermal barrier coating technology.

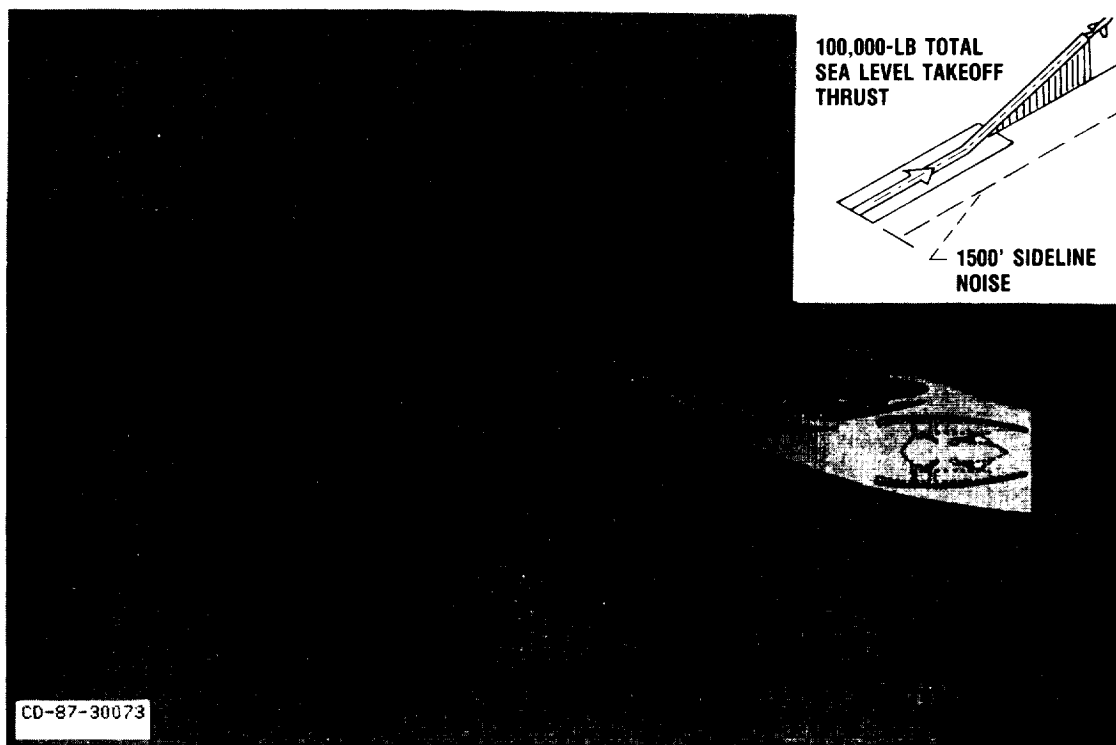


Figure 6. - Historic aircraft noise reduction due mainly to advanced aeropropulsion technology.

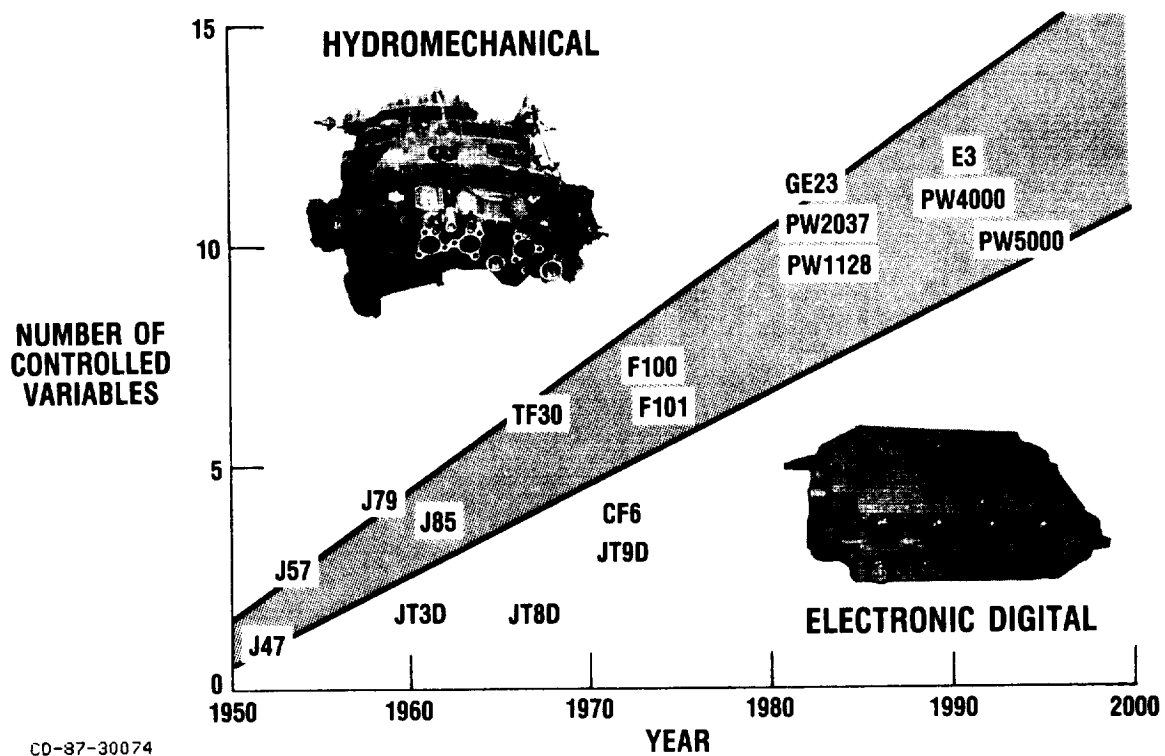


Figure 7. - Advanced electronic digital controls provide unprecedented flexibility and capacity for increasing the number of controlled turbine engine variables.

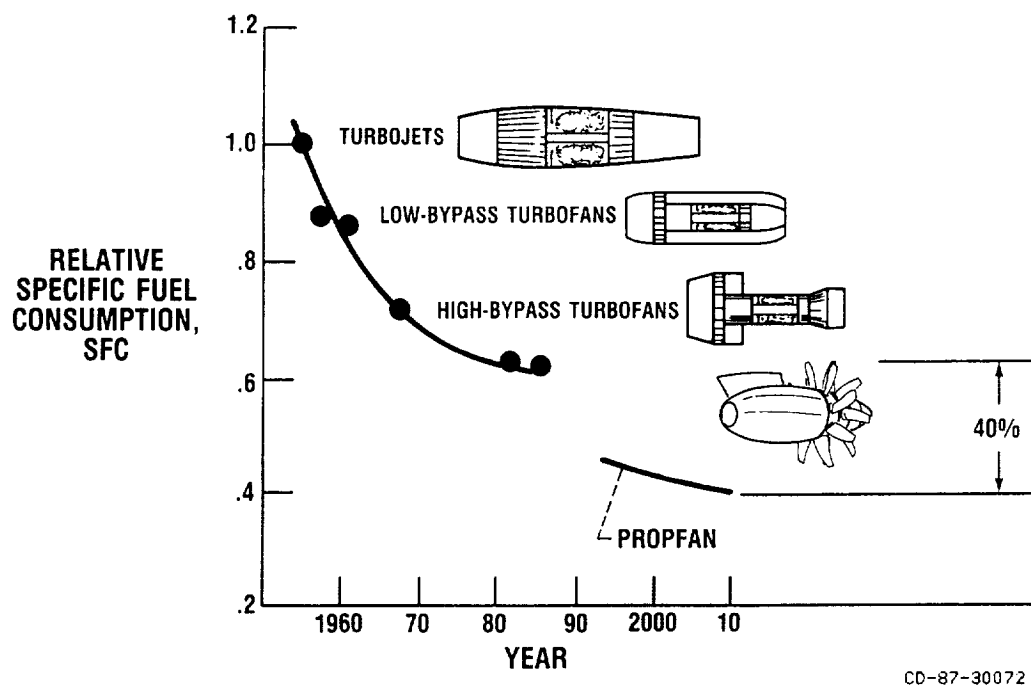


Figure 8. - High-bypass engines have better subsonic performance.

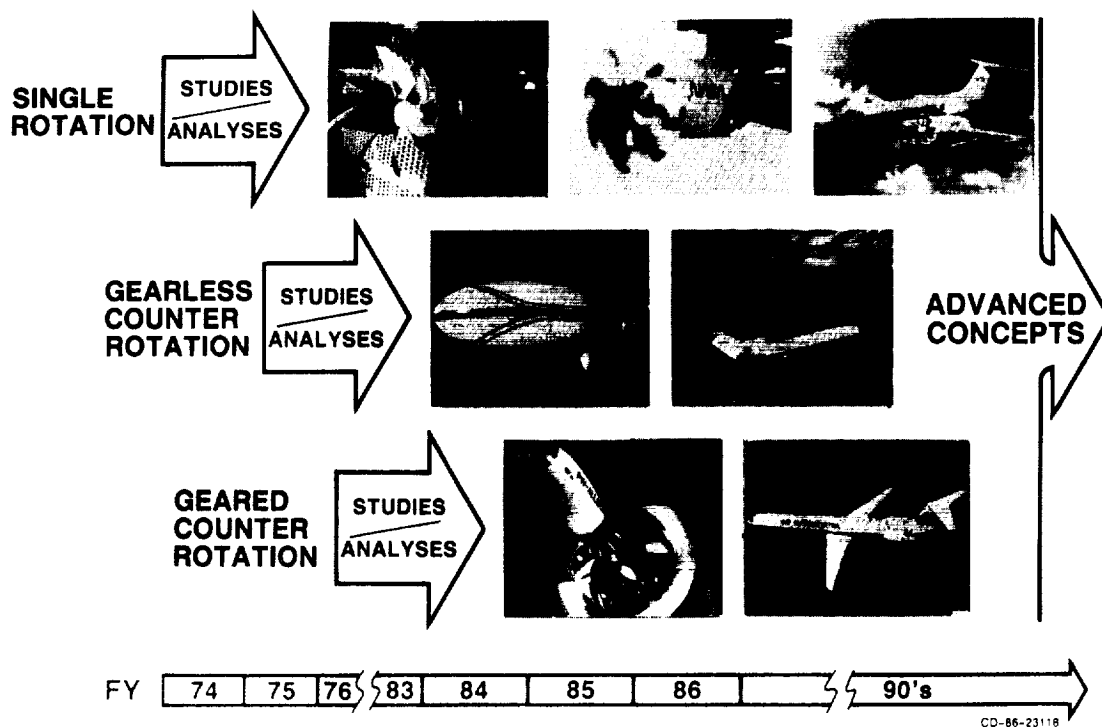
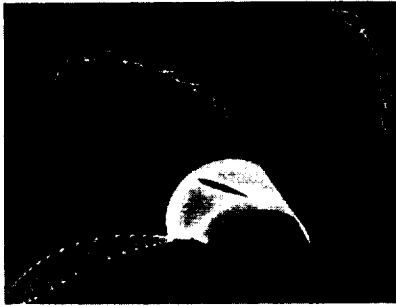
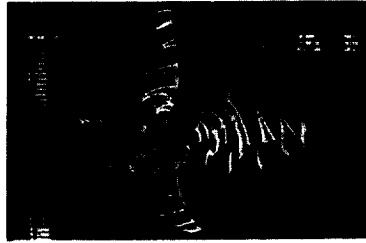


Figure 9. - Advanced Turboprop Program.



**LEADING EDGE VORTEX
AERODYNAMICS
AT LOW SPEED**



**UNSTEADY AERODYNAMICS
AT ANGLE OF ATTACK**



**UNSTEADY COUNTERROTATING
BLADE ROW INTERACTIONS**

CD-87-30041

Figure 10. - Advanced computational fluid dynamics analysis for propeller flow fields.

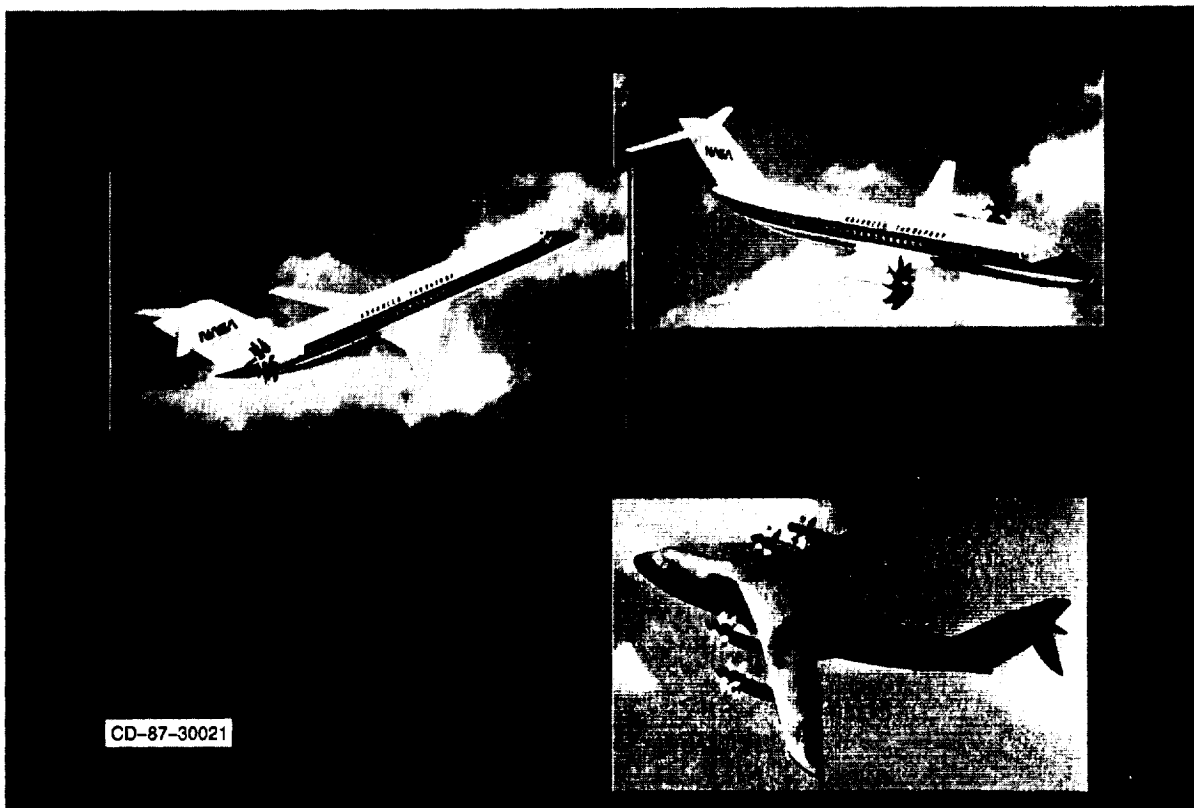
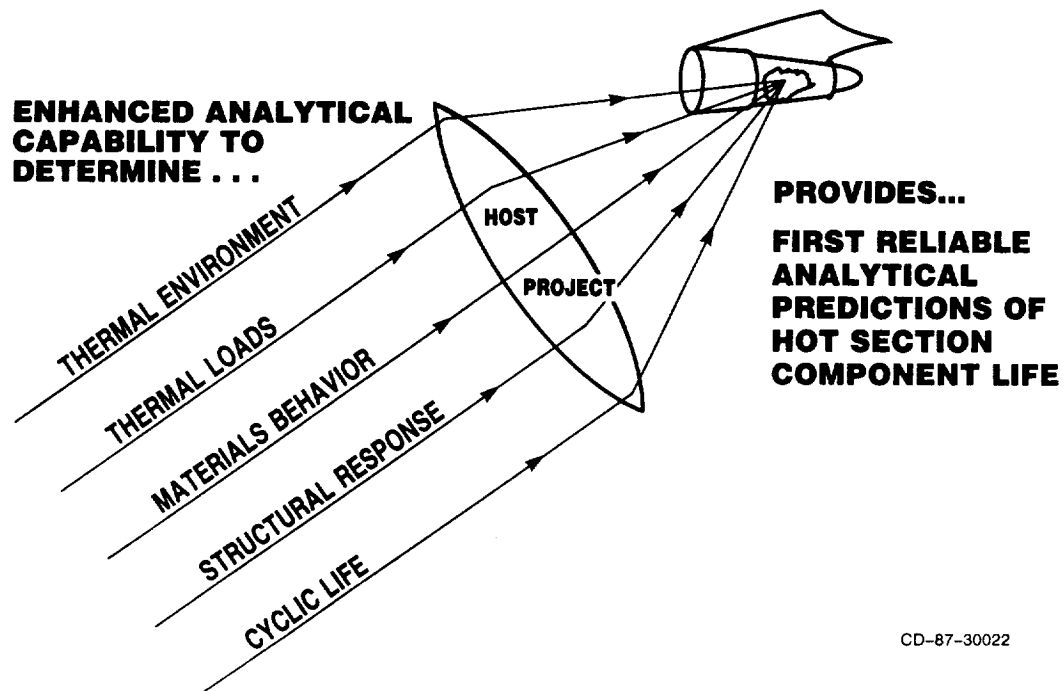
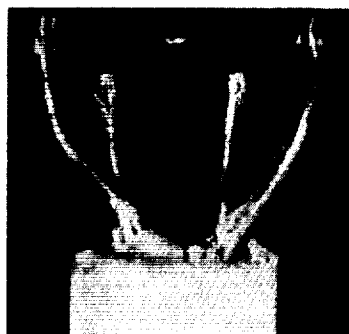


Figure 11. - Potential future advanced turboprop applications.

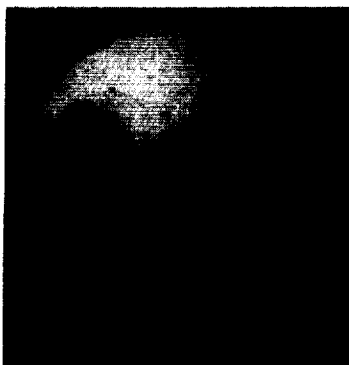
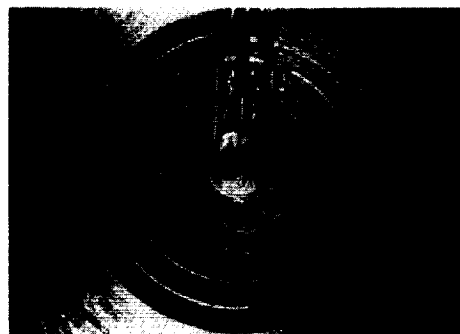


CD-87-30022

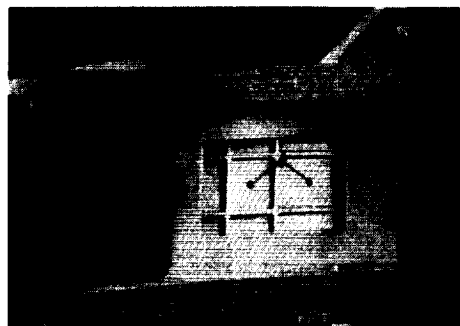
Figure 12. - NASA's Hot Section Technology (HOST) Project.



1000-Hz
THERMOCOUPLE
PROBE



COMBUSTOR
VIEWING
SYSTEM



HEAT FLUX GAGE INSTALLATION IN VANE

CD-87-30025

Figure 13. - HOST project instrumentation technology.

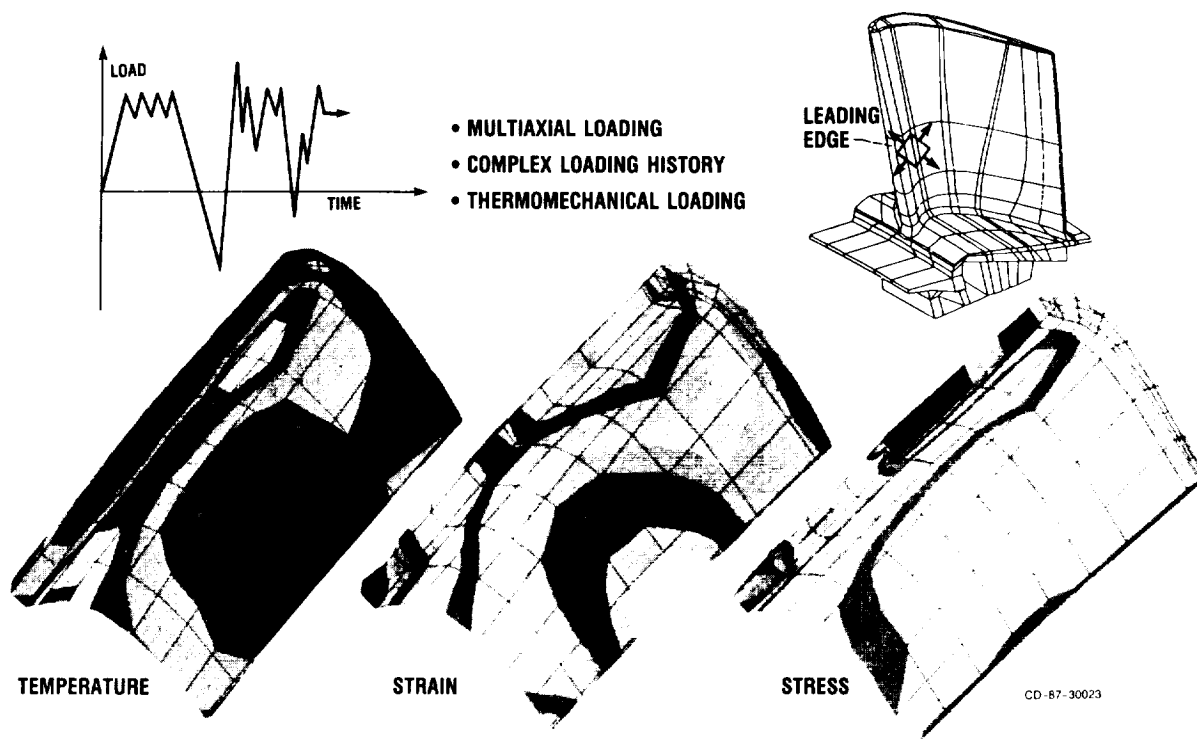


Figure 14. - HOST prediction of operating conditions and life.

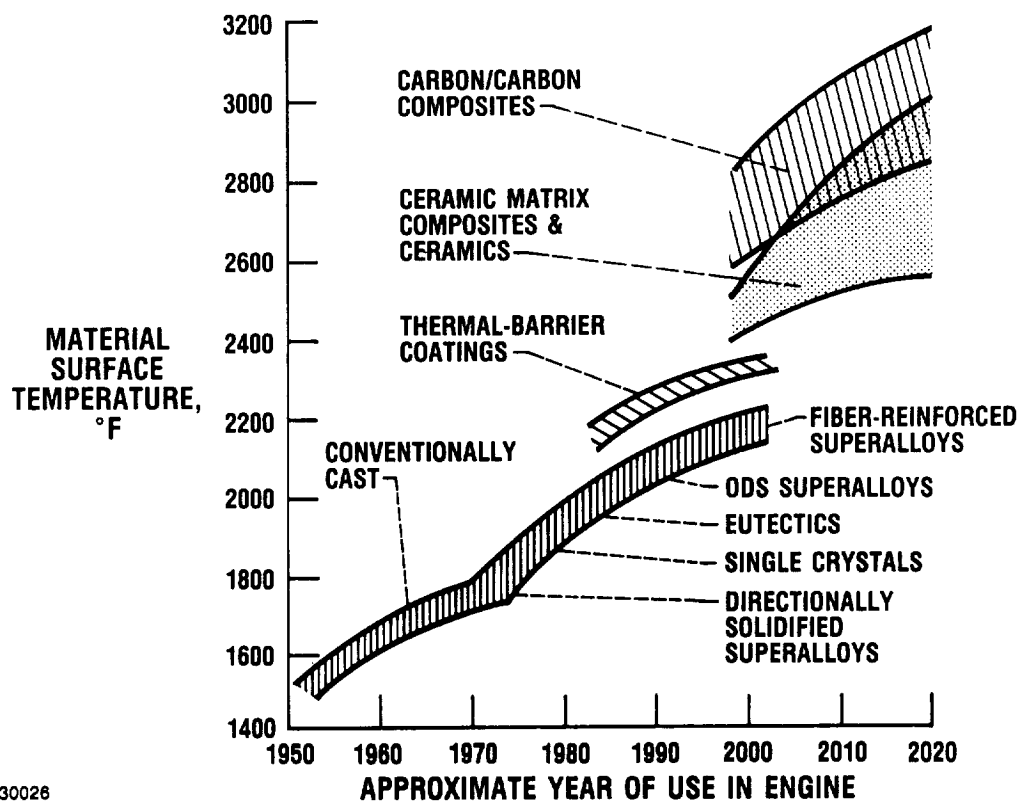


Figure 15. - Historic and projected turbine blade materials trends.

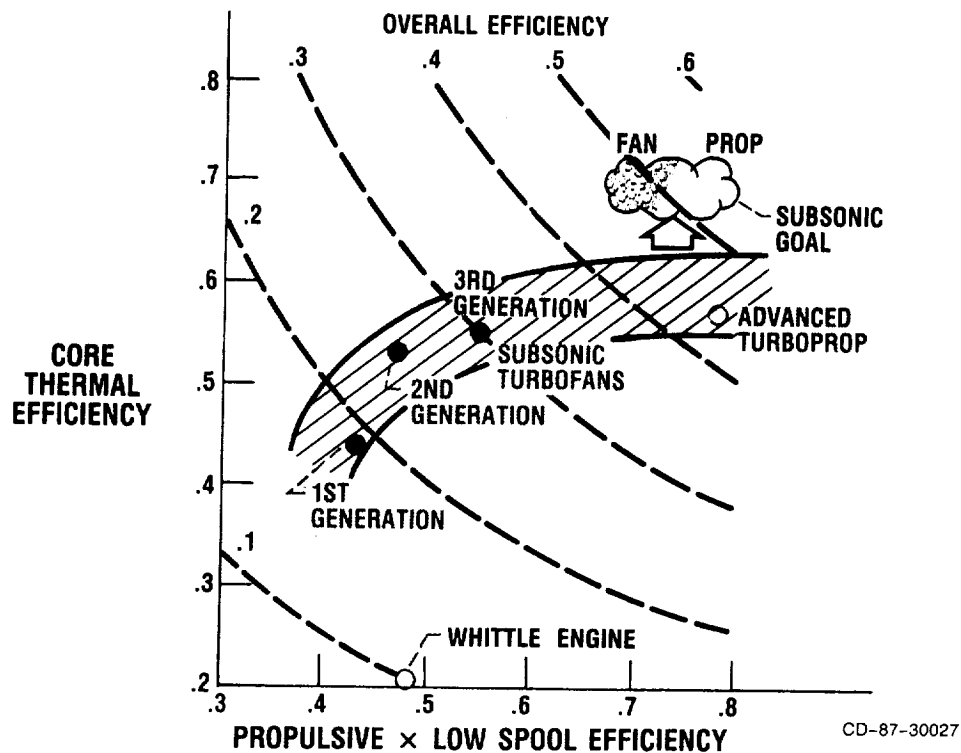


Figure 16. - Goal for future commerical turbine engine efficiency.

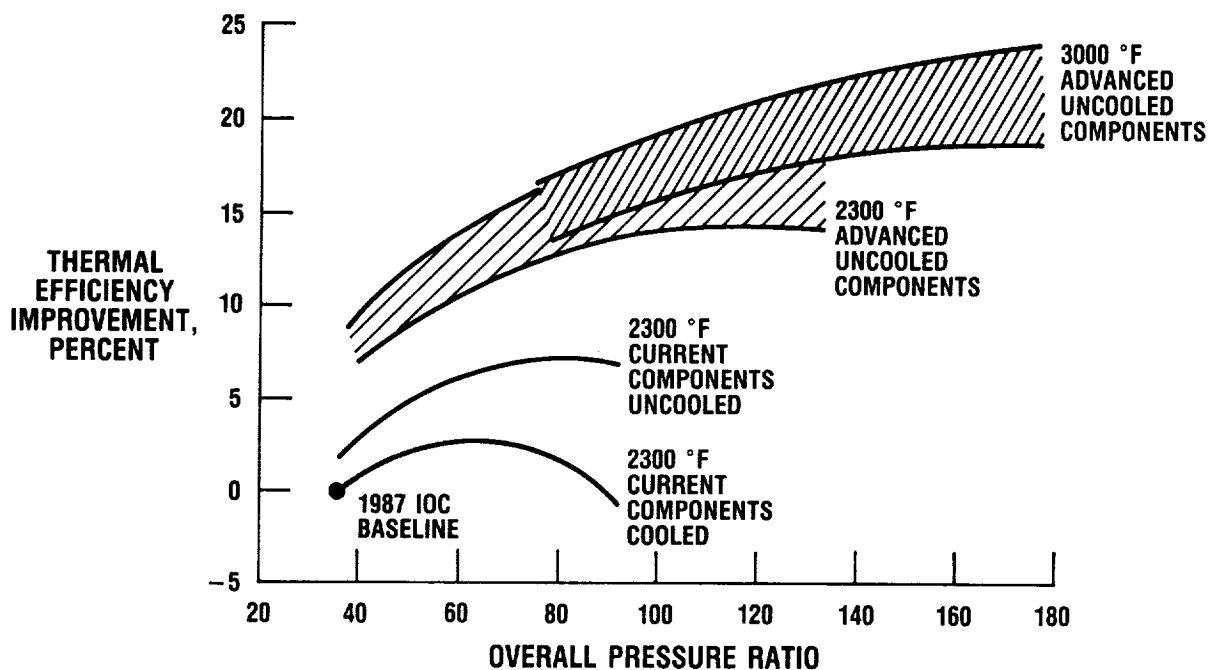
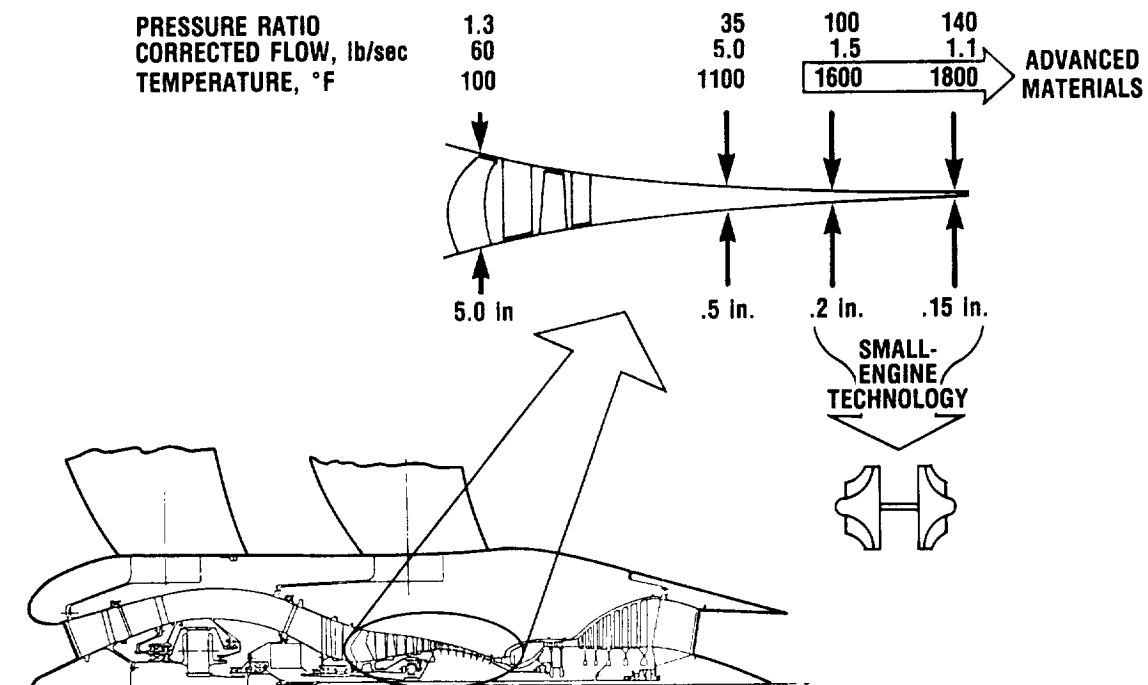


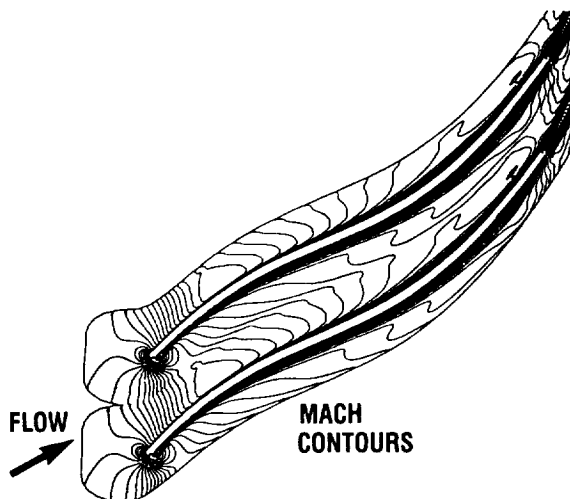
Figure 17. - Core technology effect on turbine engine thermal efficiency.



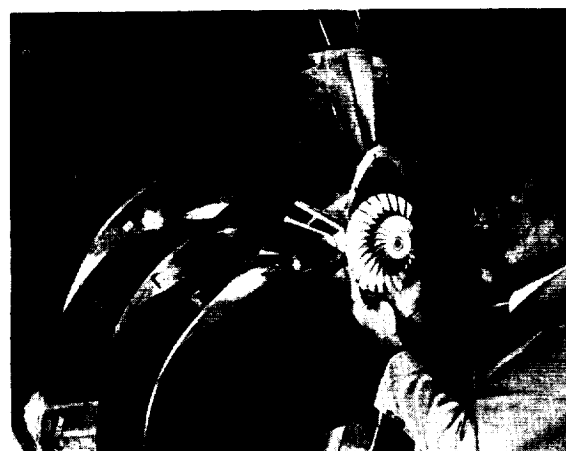
CD-87-30029

Figure 18. - Impact of very high core pressure ratio on required compressor technology.

ORIGINAL PAGE
BLACK AND WHITE PHOTOGRAPH



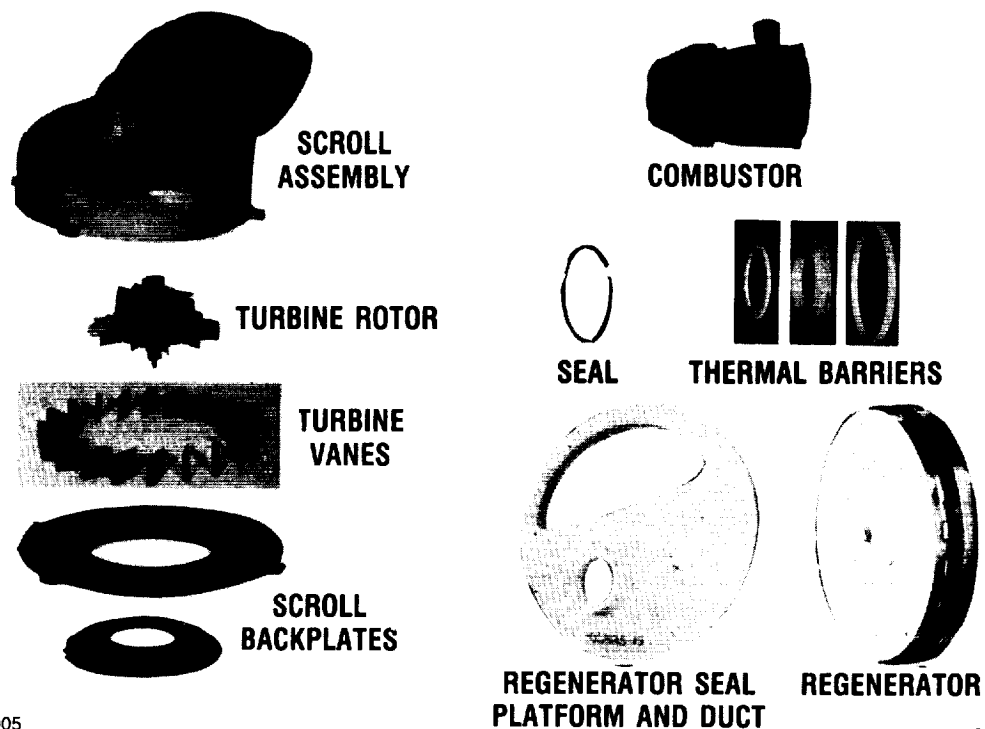
QUASI-3D THIN-LAYER ANALYSIS



INSTRUMENTED ROTOR

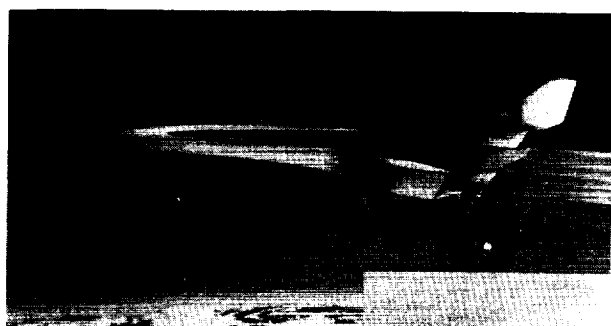
CD-87-30030

Figure 19. - Large, low-speed centrifugal compressor.



CD-87-29905

Figure 20. - Advanced ceramic engine components, Lewis/DOE Automotive Gas Turbine Program.



ORIGINAL PAGE
BLACK AND WHITE PHOTOGRAPH



CD-87-30039

Figure 21. - Aircraft requiring advanced propulsion for long-range supersonic flight.

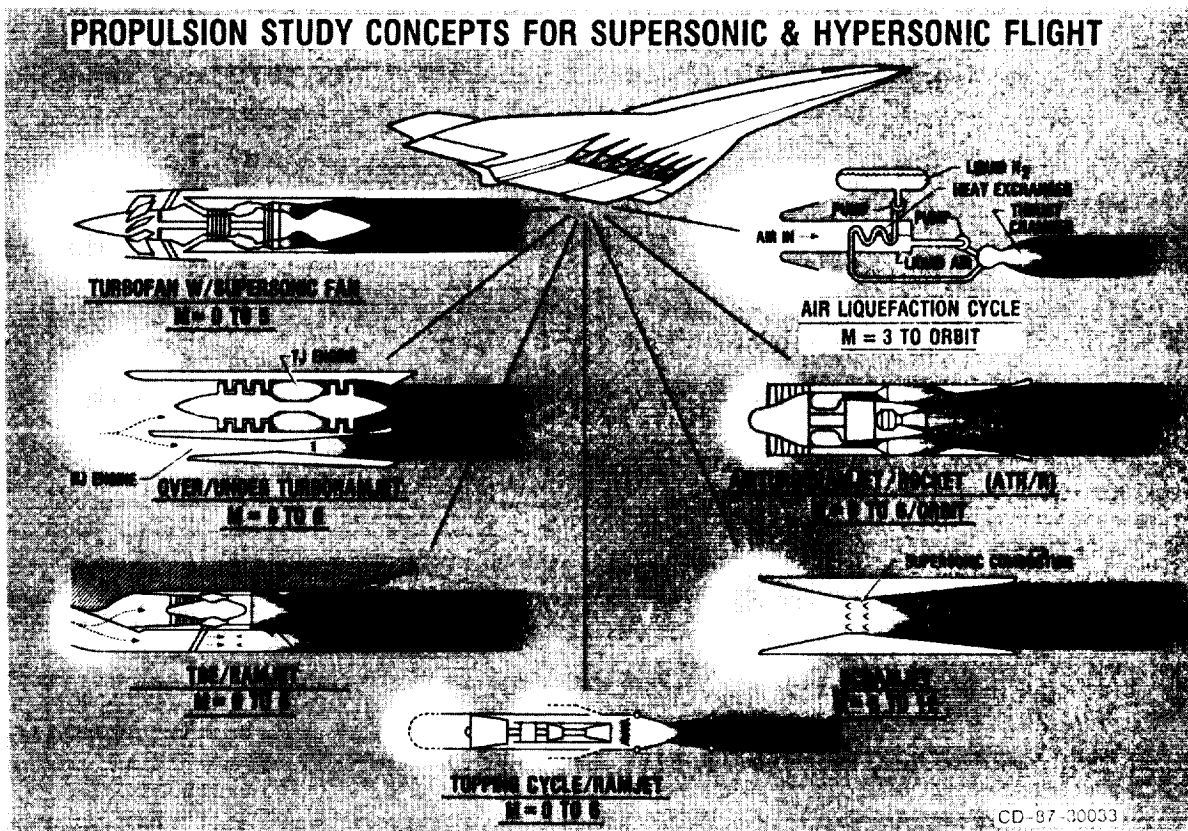


Figure 22. - Advanced propulsion study concepts for supersonic and hypersonic flight.

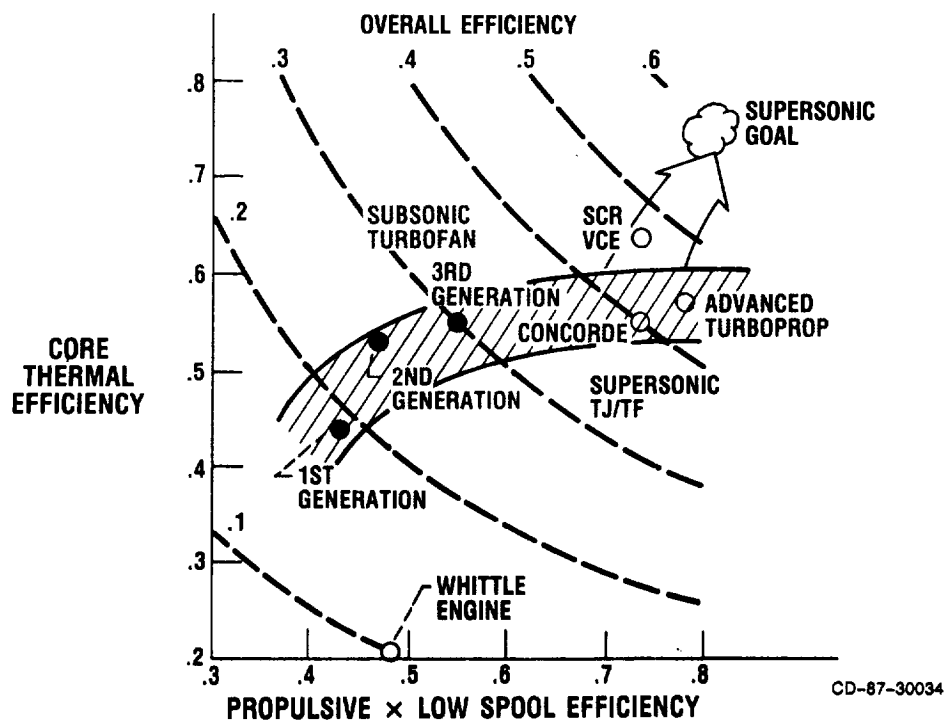


Figure 23. - Turbine engine efficiency goal for high-speed supersonic cruise.

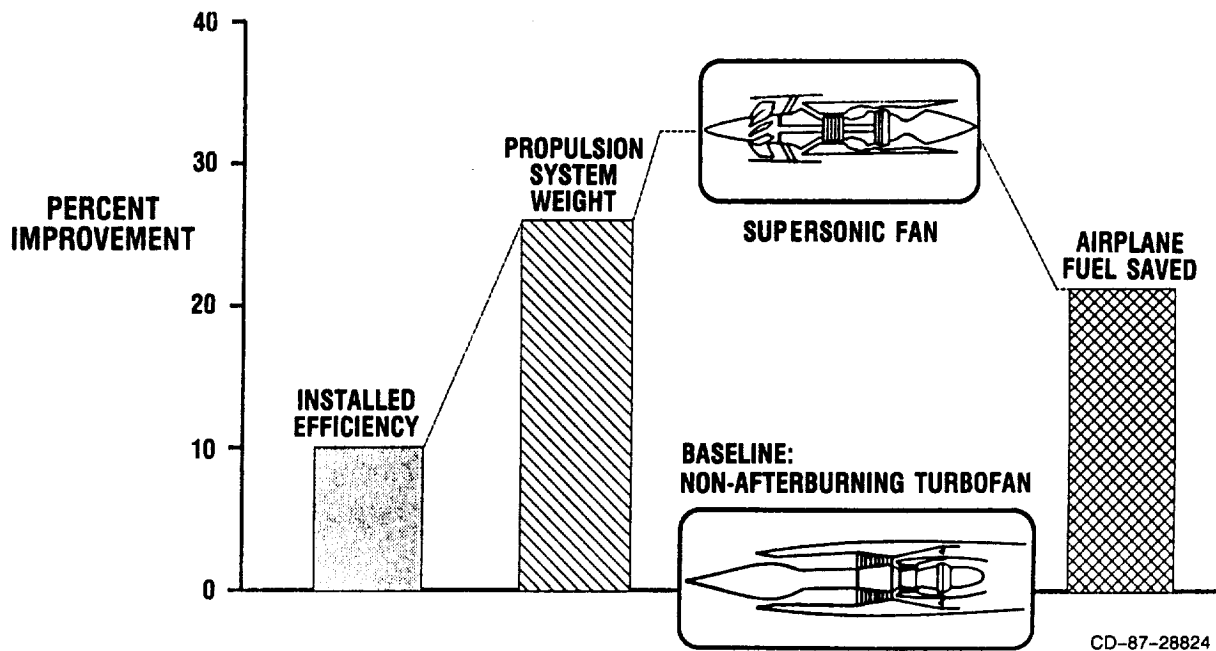


Figure 24. - Supersonic throughflow turbofan benefit for a 300-passenger, Mach 3 commercial transport with 5500-nmi range.

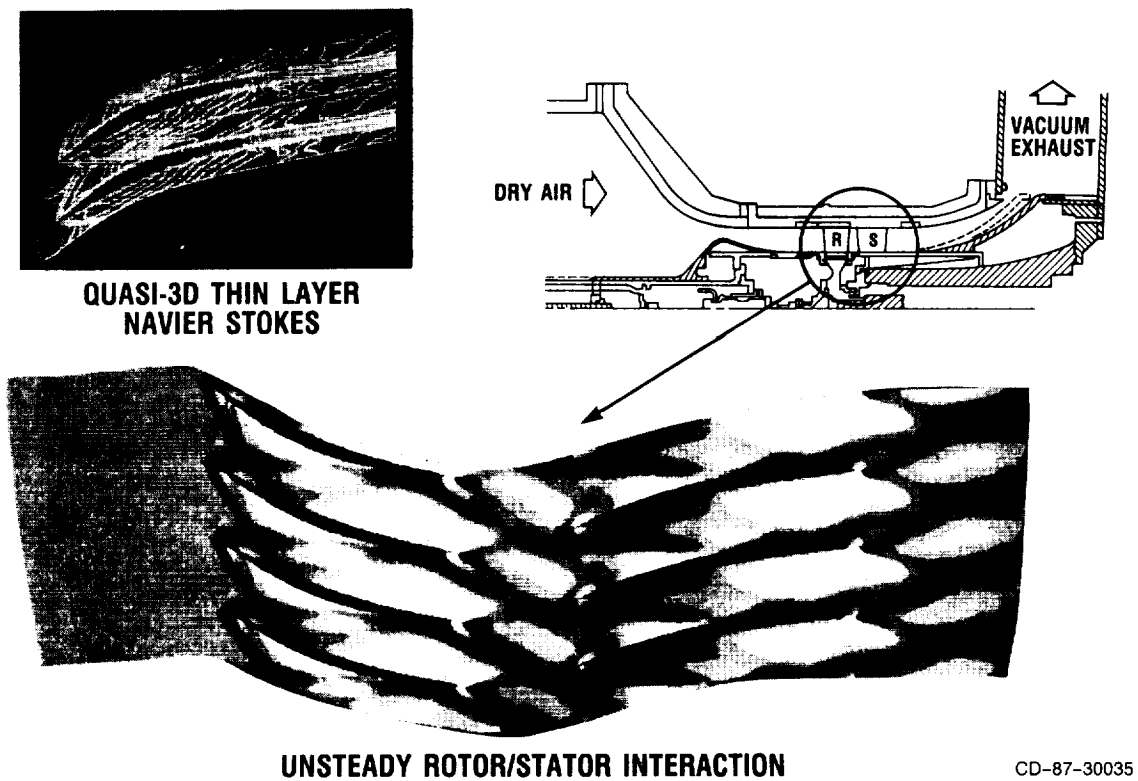
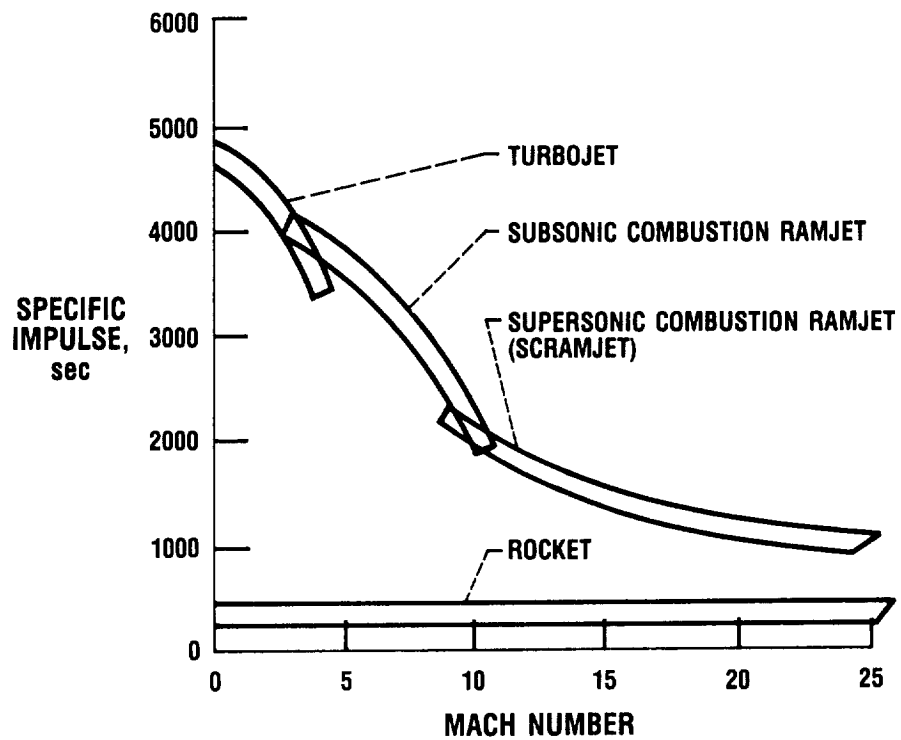
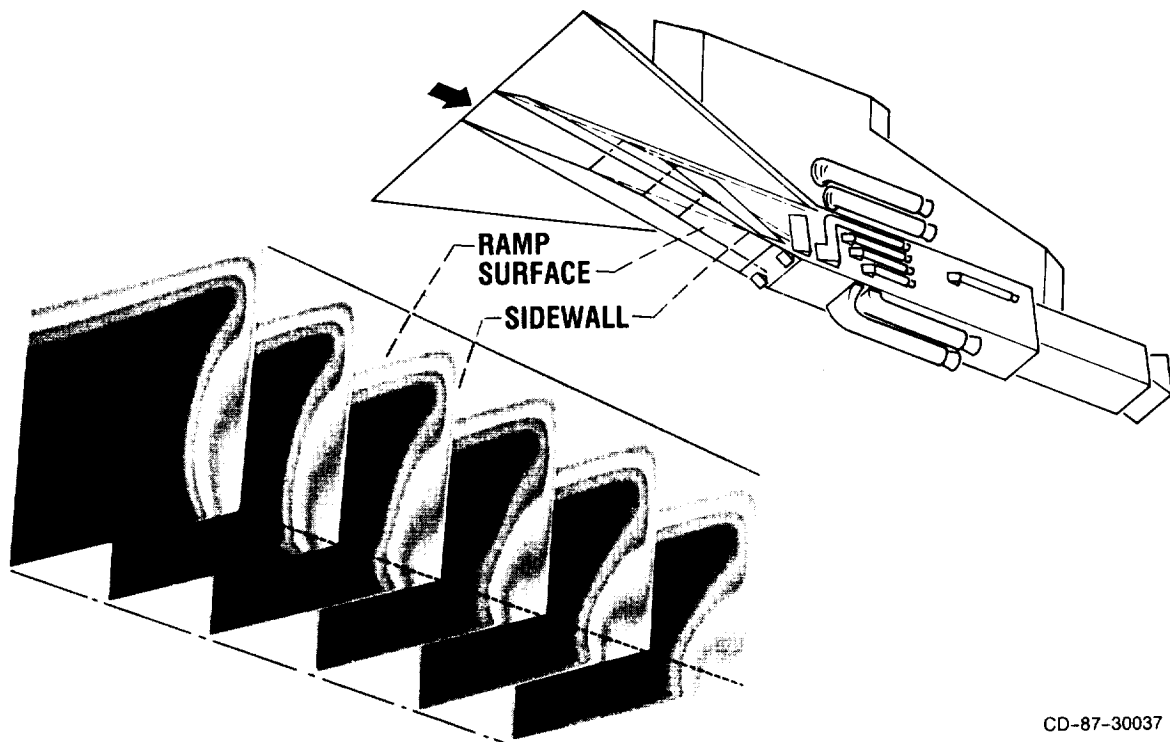


Figure 25. - Hardware and analysis for supersonic fan feasibility demonstration.



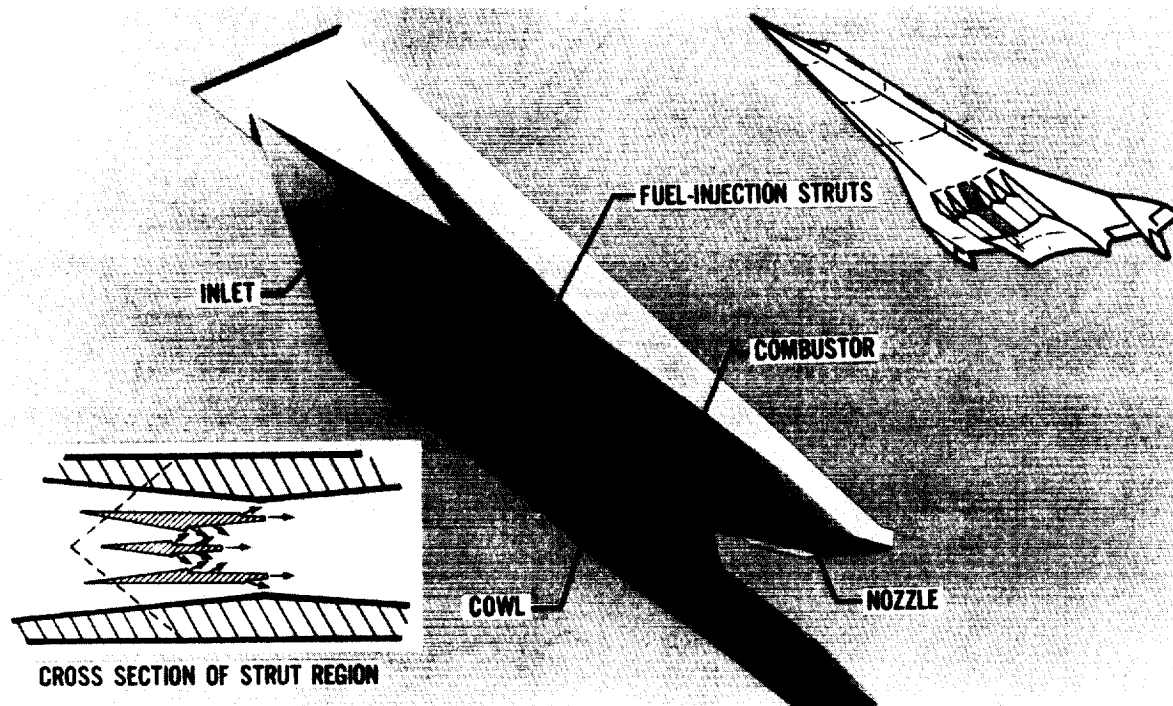
CD-87-30036

Figure 26. - Performance comparison of high-speed airbreathing and rocket propulsion.



CD-87-30037

Figure 27. - Test model and analysis for investigation of Mach 5 inlet concept.



CD-87-30038

Figure 28. - Langley Research Center concept for airframe integrated supersonic combustion ramjet (scramjet).

SESSION 1 - AEROPROPULSION MATERIALS RESEARCH

LEWIS MATERIALS RESEARCH AND TECHNOLOGY: AN OVERVIEW

Salvatore J. Grisaffe

SUMMARY

The Materials Division at the Lewis Research Center has a long record of contributions to both materials and process technology as well as to the understanding of key high-temperature phenomena. This paper overviews the division staff, facilities, past history, recent progress, and future interests.

INTRODUCTION

The Materials Division at the Lewis Research Center is NASA's focal point for high-temperature materials research aimed at aerospace propulsion and power systems needs (fig. 1). Lewis is NASA's largest materials research group. Currently the staff consists of about 99 civil servants (over 45 percent have earned Ph.D.'s) and 73 National Research Council (NRC) postdoctoral fellows, university consortia members, support service contractors, and industrial guest investigators. Their backgrounds cover all the materials disciplines. Thirty percent of our staff are recent graduates, and this reflects an ongoing commitment to fresh ideas and new talent. Our facilities give us the capability to make, consolidate, and fabricate new materials and to test and analyze them. With the Center's powerful computational capabilities, we can also model, compute, and predict material behavior.

Our job is to create new materials and new understanding in support of NASA's needs and specific materials goals. We then work to transfer the resulting knowledge, technology, and processes to the broad user community.

For those industrial organizations and universities interested in collaboration on research of potential mutual interest, a description of our key facilities can be obtained on request. To help us respond, your request should outline your specific interests.

HISTORICAL MATERIALS DIVISION CONTRIBUTIONS

In the past Lewis has made many contributions to the technology of high-temperature, high-performance materials (fig. 2). In our laboratories, as well as in conjunction with industry, Lewis has fostered the advance of such concepts as

(1) Metal matrix composites. Continuous fiber reinforced metal composites were born at Lewis, and the rule of mixtures was applied to property estimation. More recently, our arc spray monotape fabrication

process (U.S. patent No. 4,518,625; license available) has opened this arena to commercial applications.

(2) Refractory metals and compounds. New W and Mo+Re alloys were discovered at Lewis and then were strengthened by Hf and C additions. We conducted much of the early work on HfC and TaC.

(3) Ceramics. Lewis conducted the first engine tests on brittle cermets, developed early blade root designs for brittle materials, identified the potential of ceramic ball bearings, and generated early data on the oxidation and thermal shock resistance of Si_3N_4 and SiC ceramics indicating their potential for gas turbine service. More recently, a SiC fiber reinforced silicon nitride (U.S. patent No. 4,689,188; license available) was developed which has the best high-temperature strength of any current ceramic composite material.

(4) Coatings. Lewis research resulted in the early identification of NiCrAl and FeCrAl as surface protection systems for superalloys. Our research also produced the first thermal barrier coatings (TBC's) to work in actual gas turbine engine environments and to be tested on blades in engines.

(5) Polymer Composites. PMR-15 was discovered at Lewis, and we supported it through commercial introduction to flight engines.

Today, propulsion system performance limits are pacing aircraft advances. Achievement of viable high thrust-to-weight aircraft; Mach 2 to 6 transport aircraft; very high efficiency/pressure ratio subsonic transport aircraft; vertical, short takeoff and landing aircraft (VSTOL); the National Aerospace Plane (NASP); and other aircraft depends on advances in engine materials. Similarly, in the whole arena of space propulsion and space power, the availability of high-performance materials is controlling advances. Many of the same needs exist for both types of systems. Indeed, as we move toward hypersonic, cryogenic-fueled aircraft and multiple reuse rockets, the temperature, performance, and life demands show significant overlap (fig. 3). One major remaining area of difference is in the environments such materials experience during service.

BASIC RESEARCH

In response to the preceding requirements, the Materials Division is directing its efforts toward advanced high-temperature composites capable of meeting NASA and industry needs for the year 2000 and beyond. Our work involves basic research, focused research, and new concept exploration. The basic studies (about 20 percent of our effort) are aimed at understanding key barrier phenomena. Some of these areas are shown in figure 4. Note that as part of our efforts to mathematically characterize and predict material responses, we have a growing modeling activity supporting our experiments.

Solidification and casting, friction and wear, and chemical synthesis and deposition are major areas of basic interest. This research is thus heavily focused on the basics of processing effects on materials' microstructures and on the understanding of the resultant properties and their degradation during service.

FOCUSED RESEARCH AND TECHNOLOGY

About 65 percent of our effort involves focused research - looking at long range NASA system needs and attacking those issues that either enable or strongly enhance system performance. Such research covers a very broad range of NASA and industry interests (fig. 5). In the area of hypersonic engine structures (and advanced rocket nozzles) we are looking for high-strength/high-conductivity systems such as W fiber/copper composites for cooled applications as well as for high-temperature ceramic composites for hard-to-cool components. Long-life materials for high-speed turbopump blades, bearings, etc. are being sought. Ceramic materials, intermetallic composites, and polymer conductors are all being pursued to provide lightweight, high-performance alternatives to current technology. In the high-temperature superconductor arena we are supporting efforts aimed at NASA-specific applications. To enhance satellite performance and the space station's effectiveness, we are working on improved space lubricants as well as supporting microgravity science and its applications, including the commercial use of space. Here we do focused research on basic microgravity processing issues. In our Microgravity Materials Science Laboratory we work with industry and university investigators to help clarify their ideas and to lay the groundwork for potential space experiments or processing hardware.

SYSTEMS DEVELOPMENT

About 15 percent of our effort supports systems where NASA has a major role in development (fig. 6). For example, our work on the SP-100 (a space nuclear power generation concept) includes materials for lightweight radiators, research that is clarifying the basis for Ge-Si/GaP thermoelectric performance improvements, and high-strength refractory composites for lithium-cooled heat pipes. Our support for the space station includes identifying salts for thermal storage and corrosion-resistant materials for their containment. Our work on advanced chemical propulsion engines is focused on new concepts to extend turbopump and nozzle cycle resistance. In the auto gas turbine program that NASA manages for the Department of Energy (DOE), we have done much to raise the reliability and reproducibility of monolithic ceramics and to characterize factors that currently limit their use. In the NASP program we have a small role but are contributing to intermetallic and ceramic materials development efforts.

NASA recognized the growing relationship between materials availability and system performance limits. So this year a new effort was started. It is called the Advanced High-Temperature Engine Materials Technology Project (fig. 7). This base R&T augmentation will concentrate on accelerating the exploratory and the focused types of our research and will be aimed primarily at eliminating key barriers to consideration of high-temperature composites for engines. With this effort we will be moving to tie together both the materials development and the structural analysis efforts from the start in an attempt to reduce the 12 to 15 year time that new materials normally take to reach system use. We are also trying to create new linkages between ourselves, industry, and the universities. This coordination will benefit U.S. aeropropulsion by concentrating a diversity of views and backgrounds on moving such revolutionary materials forward. Specifically, we expect future advances in ceramics, intermetallics, refractory metals, and polymer composites as well as in the following areas:

- (1) Fibers (improved fiber properties and temperature limits, fiber coating to control interface bonding and reactions as well as new interface characterization methods)
- (2) Composite fabrication (optimizing current processes, but looking for better ways so as to create options to make complex shapes economically in a reliable manner)
- (3) Testing and analysis (new methods and facilities to generate high-temperature property data and to verify the new analytical codes and models to guide layup and fabrication)
- (4) Life and failure analysis (better ways to relate multiphase microstructures to properties and, eventually, properties to component performance)
- (5) Ideas (new ideas to help create a "next generation" basic industry capable of a strong role in world trade)

CONCLUDING REMARKS

We certainly plan to take full advantage of the expected new interactions with industry and the universities to deal with these kinds of problems. We also look at the expanded interactions between materials and structures research as a way to lower the time it takes to validate a new materials idea or analysis method.

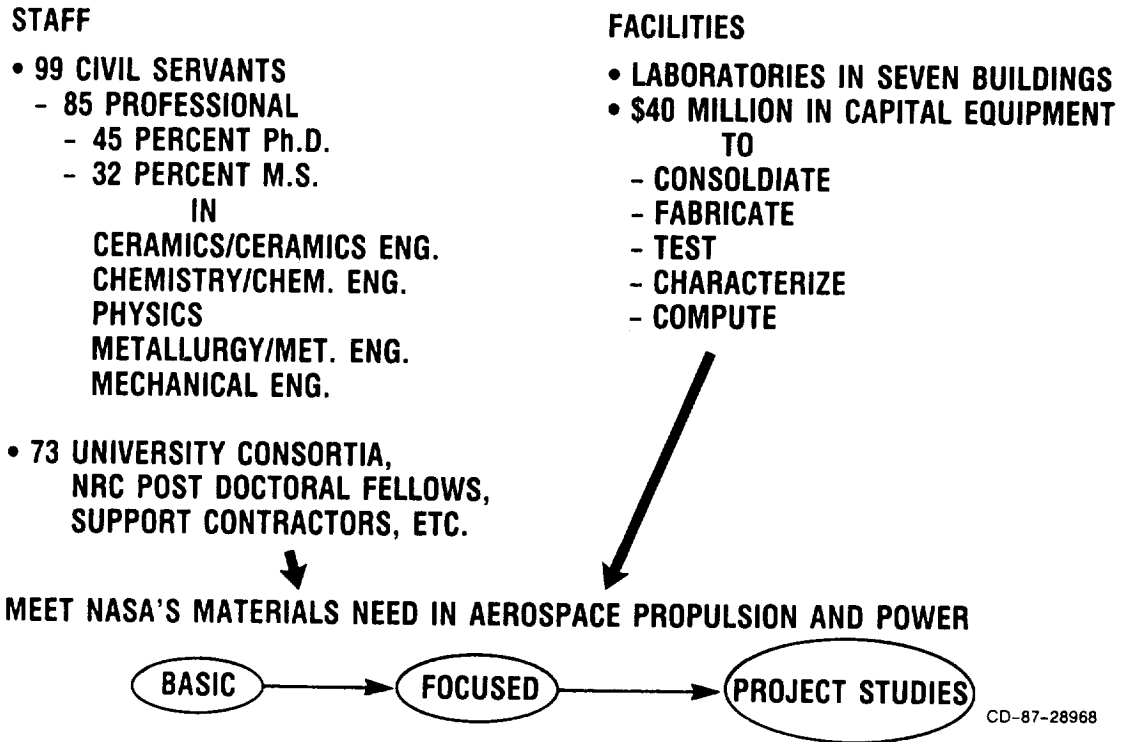


Figure 1. - Lewis Materials Division.

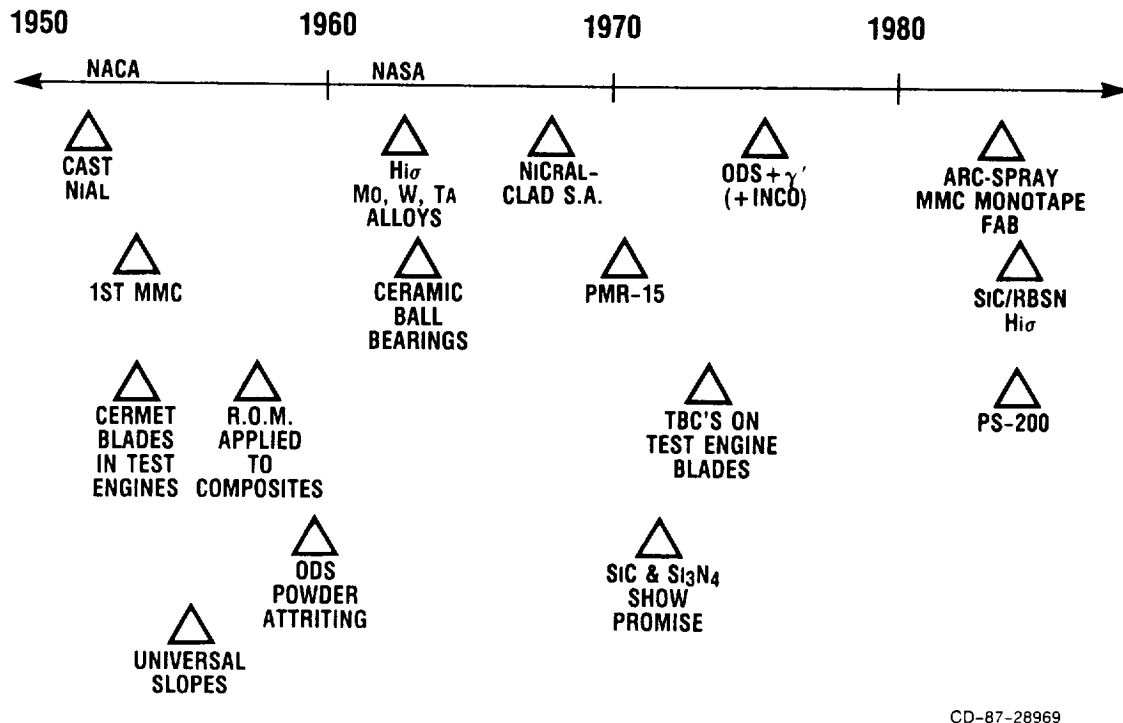
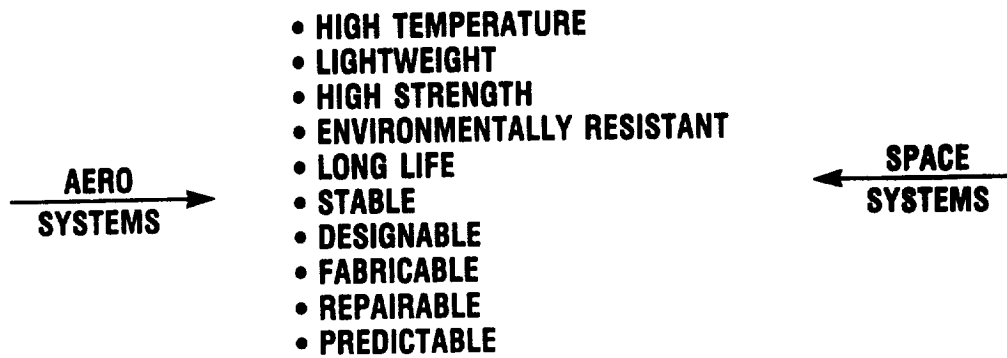
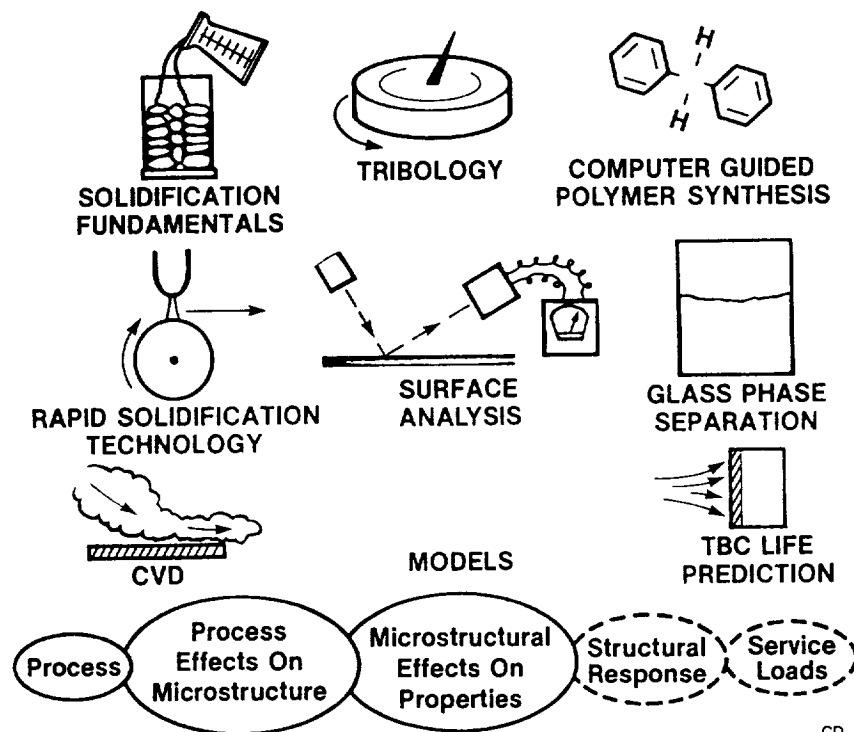


Figure 2. - Some Materials Division contributions.



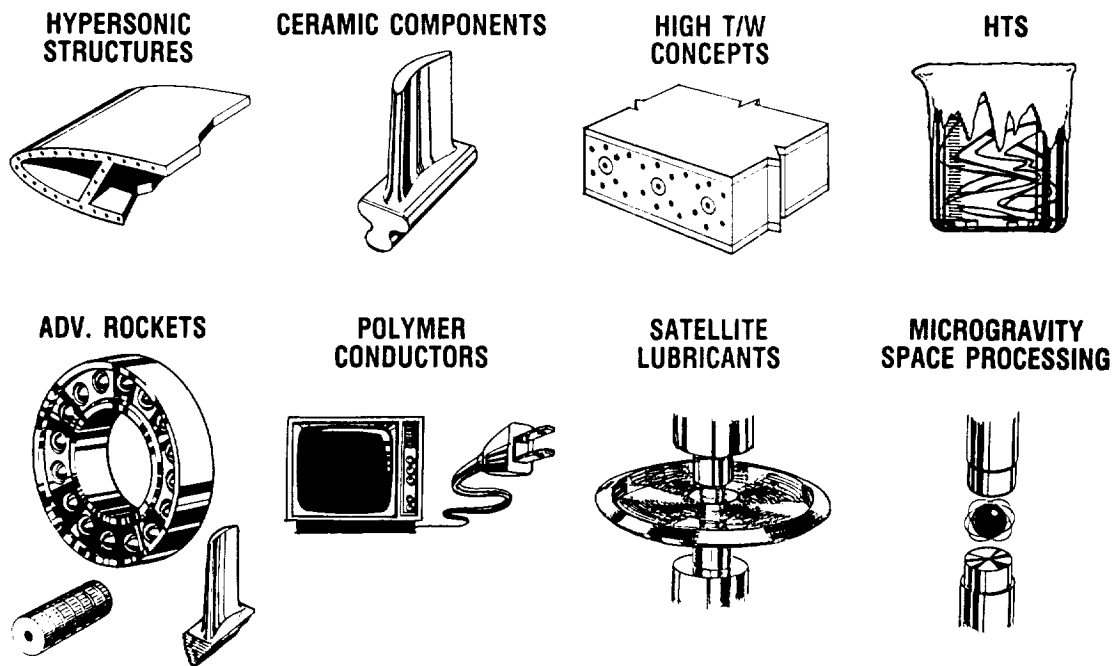
CD-87-28970

Figure 3. - Common material needs.



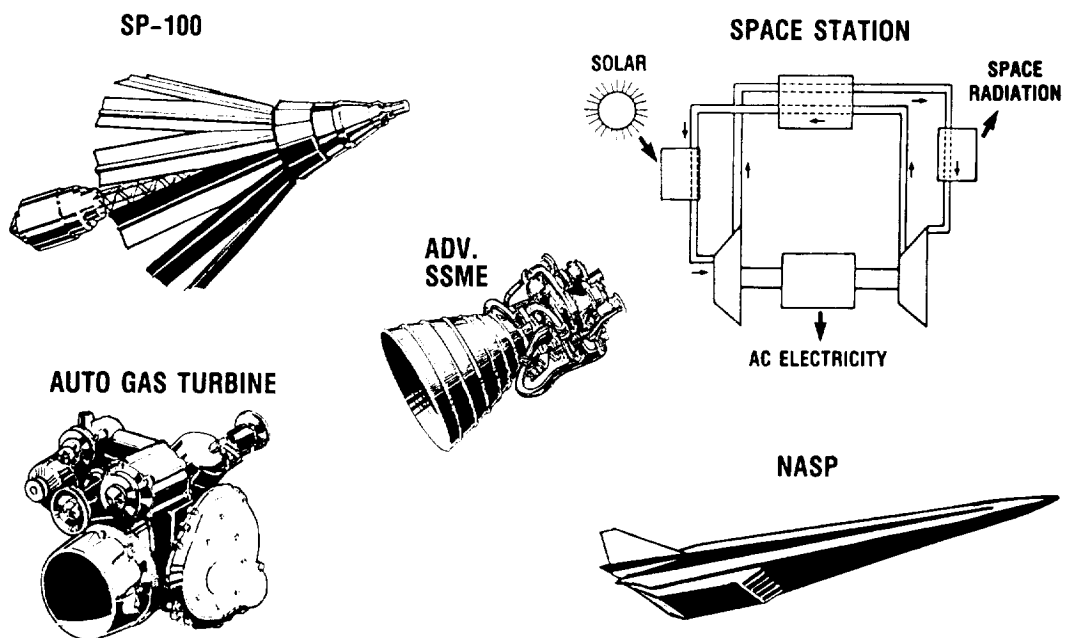
CD-87-28971

Figure 4. - Basic research.



CD-87-28972

Figure 5. - Focused research and technology.



CD-87-28973

Figure 6. - Systems support.

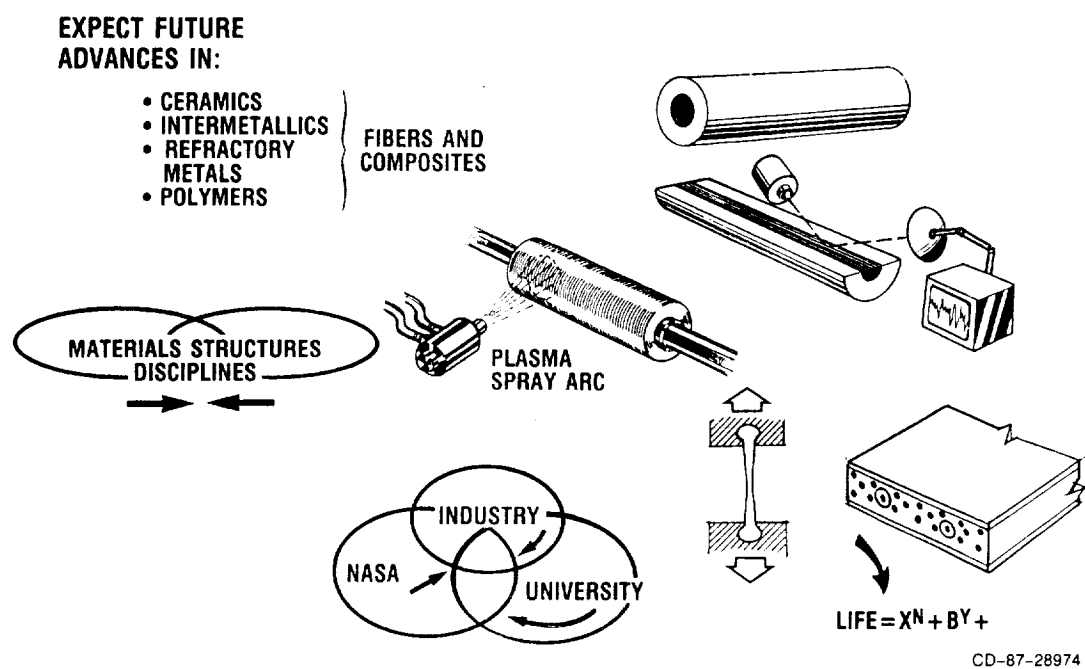


Figure 7. - The Advanced High-Temperature Engine Materials Technology Project 1988 to 1993.

HIGH-TEMPERATURE POLYMER MATRIX COMPOSITES

Michael A. Meador

An increasing emphasis on high-performance aircraft and high thrust-to-weight systems has driven the need to develop and use new, lightweight, high-specific-strength materials in aeropropulsion. These newer materials (in particular, composites) must not only offer a weight savings over more conventional materials, but should also be amenable to fabrication into complex shapes and designs, be resistant to the threats of their use environment (thermal and thermal oxidative degradation, corrosion, etc.), have good mechanical properties, and be cost effective.

Current state-of-the-art polymer matrix composites will withstand extended use at temperatures as high as 600 to 650 °F in oxidizing environments. While this may limit their application as aeropropulsion materials, polymer matrix composites can be shaped or molded easily during processing, are corrosion resistant, and can be chemically modified to provide a variety of specific properties, for example, increased toughness, and increased electrical or thermal conductivity (fig. 1). Where appropriate, the use of polymer matrix composites in aeropropulsion and other material applications can offer savings not only in weight, but in production costs as well.

The first polymer matrix composites to find use in aircraft engines were fiberglass/epoxy systems (fig. 2). The earliest uses of polymer matrix composites were in noncritical applications, and were also severely limited by the upper use temperatures of epoxies (250 to 300 °F). Since that time, further research has led to polymer matrix composites with higher and higher use temperatures (e.g., 600 °F for graphite/polyimides). In addition, time has seen the acceptance of these materials move from noncritical to critical structural applications. Current research in the Polymers Branch at the NASA Lewis Research Center is directed at advanced polymers and polymer matrix composites for extended use at 700 °F and beyond.

A major concern in the processing of polymer matrix composites is the production of voids. These voids can arise from a number of sources: the evolution of volatile byproducts during processing, contaminants, degradation, or poor resin flow. Regardless of their origin, voids are not only potential sources for mechanical failure but can also lead to enhanced thermal oxidative degradation in the composite. Therefore, one of the major goals of polymer matrix composite processing is the minimization of void content. One approach to this (fig. 3) involves a two-step cure procedure. Generally, the first step (condensation reaction) of this procedure involves the formation of a low-molecular-weight prepolymer. This first step also produces some quantity of volatile byproducts which escape during this step. The prepolymer formed in this step is endcapped with a group which undergoes a cross-linking reaction at a higher temperature (addition reaction) to form a more thermally

stable polymer network. Unlike the first step, the cross-linking addition reaction proceeds with no formation of byproducts. The result is a highly processable, void-free composite.

In the early 1970's researchers at the NASA Lewis Research Center developed an addition-curing polyimide resin system known as PMR (polymerization of monomer reactants) polyimides (ref. 1). These polyimides (in particular, PMR-15) afford exceptional thermal oxidative stability coupled with good processability by way of a number of conventional techniques. The useful lifetimes of PMR-15 in air (60 psia) are 10 000 hr at 550 °F and 1500 hr at 600 °F (fig. 4).

PMR-15 represents the state of the art in 550 °F matrix resins and has found a wide range of use in both aeropropulsion and nonpropulsion applications. A study prepared by General Electric (ref. 2) under contract to the Navy concluded that the inclusion of graphite/PMR-15 composites in a number of military aircraft engines, such as the F-404, F-110, and F-101, could result in considerable savings in weight and manufacturing costs (fig. 5). As a result of this study and a joint Navy-NASA Lewis funded program, General Electric is currently producing a graphite/PMR-15 duct for their F-404 engine (fig. 6). Originally made out of titanium, this duct was manufactured by forming and machining titanium plates followed by chem-milling to reduce the final weight. The graphite/PMR-15 replacement duct, on the other hand, is autoclave molded in two pieces. In initial tests, the graphite/PMR-15 replacement duct successfully completed over 1000 engine test cycles for a total engine exposure time of 700 hr. Replacement of the original titanium duct by the graphite/PMR-15 duct has resulted in a total weight savings of 7 pounds per engine, as well as in a substantial reduction both in production costs and in the use of titanium.

Offering the combination of good processability and thermal/oxidative stability, PMR-15 is a recognized leader in high-temperature polymer matrix resins. It is one of the most widely used resins for 550 °F applications and is available from a number of suppliers (fig. 7).

Since the development of PMR polyimides, the Polymers Branch at NASA Lewis has responded to industry needs for improvements in these resins, for understanding the mechanisms for their thermal/oxidative degradation (ref. 3), and for developing quality control procedures (ref. 4). (See fig. 8.) For example, modification of the original PMR-15 formulation has produced a toughened polyimide, designated PMR-T (ref. 5), with an increase in failure shear strain and failure impact energy (fig. 9).

One concern that has arisen with graphite/PMR-15 and other polymer matrix composites is that they experience some microcracking during thermal cycling, which can affect mechanical properties. The NASA Lewis Polymers Branch has approached this problem from two angles - one a chemical solution, the other an engineering solution. The use of PMR-T in place of PMR-15 resulted in a 50-percent reduction in the composite transply crack density after 1000 thermal cycles (0 to 450 °F). Use of a random fiber mat finish on a graphite/PMR-15 composite virtually eliminated microcracking during the same thermal cycling test (fig. 10).

A major thrust of the Polymers Branch at Lewis has been in developing PMR polyimides with improved thermal oxidative stability over PMR-15. One such

improvement is PMR-II (ref. 6), a 1977 I-R 100 Award winner. Increased thermal oxidative stability was achieved in this system by substituting more thermally stable monomers into the original PMR-15 formulation. The result is a lower weight loss and better retention of mechanical properties at 600 °F in air than PMR-15 (fig. 11). A higher molecular weight formulation of PMR-II, PMR-II-700, shows promise as a 700 °F resin candidate (ref. 7). This resin experiences only a slight loss of mechanical properties after 200 hr in air (60 psia) at 700 °F and has a weight loss roughly a third of that of PMR-15 under these conditions (fig. 12).

Mechanistic studies have revealed that the end cap is responsible for much of the thermal oxidative instability of PMR polyimides at high temperatures (above 600 °F). The polyimide PMR-II-700 represents one approach to counteracting the deleterious effects of these end caps. By increasing the formulated molecular weight of the polymer, such as is done in PMR-II-700, the overall weight percent of endcap is reduced. The result is improved thermal oxidative stability with some sacrifice in processability (higher molecular weight polymers do not flow as well as their lower molecular weight analogs).

However, it is clear that to achieve higher and higher use temperatures in polymer matrix composites, alternatives to PMR polyimides must be developed. These alternatives may be anything from simply changing to a more thermal, oxidatively stable end cap to developing entirely new polymer systems. A recent effort in the Polymers Branch has been focused on finding new addition-curing polymers which offer improved thermal oxidative stability over PMR polyimides, while at the same time affording good processability. The polyimide MARVIMIDE (ref. 8) is one product of this effort (fig. 13). This linear ladder polyimide combines thermoplastic processing behavior with high softening temperatures (glass transition temperatures (T_g 's) as high as 790 °F) and good thermal oxidative stability. Figure 14 shows a comparison of the short-term weight loss (obtained by thermal gravimetric analysis (TGA)) of samples of MARVIMIDE and PMR-15. The MARVIMIDE has a (131 °F, 55 °C) higher onset of decomposition than the PMR-15. More recently prepared formulations of MARVIMIDE exhibit onsets of decomposition approaching 1150 °F (620 °C). Graphite/MARVIMIDE composites are currently being prepared, and their long-term thermal oxidative behavior is under investigation.

Polymers research at the NASA Lewis Research Center has produced high-temperature, easily processable resin systems, such as PMR-15. In addition, the Polymers Branch has investigated ways to improve the mechanical properties of polymers and the microcracking resistance of polymer matrix composites in response to industry need for new and improved aeropropulsion materials. Current and future research in the Polymers Branch is aimed at advancing the upper use temperature of polymer matrix composites to 700 °F and beyond by developing new resins, by examining the use of fiber reinforcements other than graphite, and by developing coatings for polymer matrix composites to increase their oxidation resistance.

REFERENCES

1. Serafini, T.T.; Delvigs, P.; and Lightsey, G.R.: Thermally Stable Polyimides From Solutions of Monomeric Reactants. J. Appl. Polym. Sci., vol. 16, No. 4, Apr. 1972, pp. 905-915.

2. Stotler, C.L.: Development Program for a Graphite/PMR-15 Polyimide Duct for the F404 Engine. The 1980's - Payoff Decade for Advanced Materials, SAMPE, 1980, pp. 176-187.
3. Alston, W.B.: Structure-to-Property Relationships in Addition Cured Polymers. I. Thermooxidative Stability of Norbornenyl-Cured Polyimide Resins. Polym. Prepr., vol. 27, no. 2, Sept. 1986, pp. 410-411.
4. Roberts, G.E.; and Lauver, R.W.: Quantitative Analysis of PMR-15 Polyimide Resin by HPLC. J. Appl. Polym. Sci., vol. 33, no. 8, June 1987, pp. 2893-2913.
5. Vannucci, R.D.; and Bowles, K.J.: Graphite/PMR Polyimide Composites With Improved Toughness. 17th National SAMPE Technical Conference, SAMPE, 1985, pp. 352-363. (NASA TM-87081).
6. Serafini, T.T.; Vannucci, R.D.; and Alston, W.B.: Second Generation PMR Polyimides. NASA TM X-71894, 1976.
7. Vannucci, R.D.: PMR Polyimide Compositions for Improved Performance at 371 °C. Advanced Materials Technology '87, R. Carson et al., eds., SAMPE, 1987, pp. 602-612. (NASA TM-88942).
8. Meador, M.A.B.: Addition Polymers From 1,4,5,8-Tetrahydro-1,4,5,8-diepoxyanthracene and Bis-dienes: Processable Resins for High Temperature Applications. Polym. Prepr., vol. 28, no.2, Aug. 1987, pp. 375-376. (NASA TM-89838).

- CAN BE SHAPED OR FORMED EASILY
- LIGHTWEIGHT
- CORROSION RESISTANT
- CAN BE TAILORED TO SPECIFIC NEEDS

CD-87-29452

Figure 1. - Properties of polymer matrix composites.

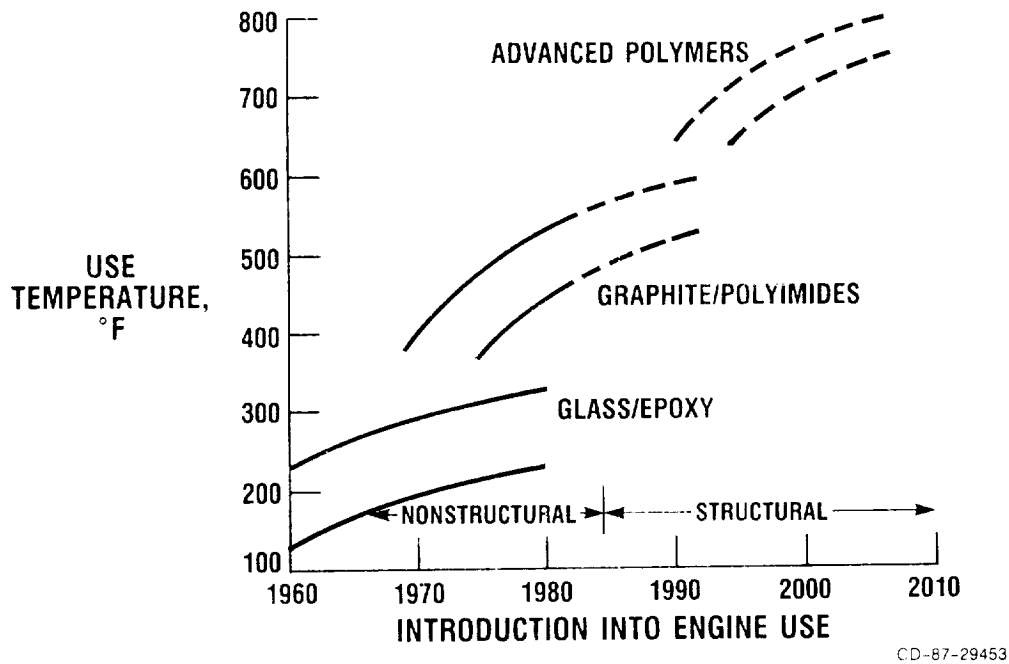


Figure 2. - Trends for polymer composites in engines.

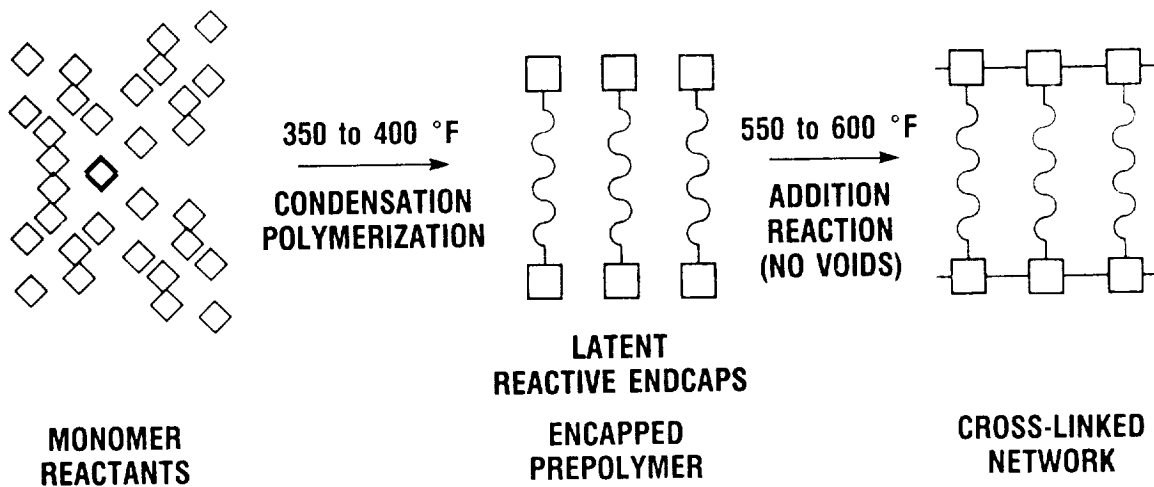


Figure 3. - Reaction scheme for addition polyimides.

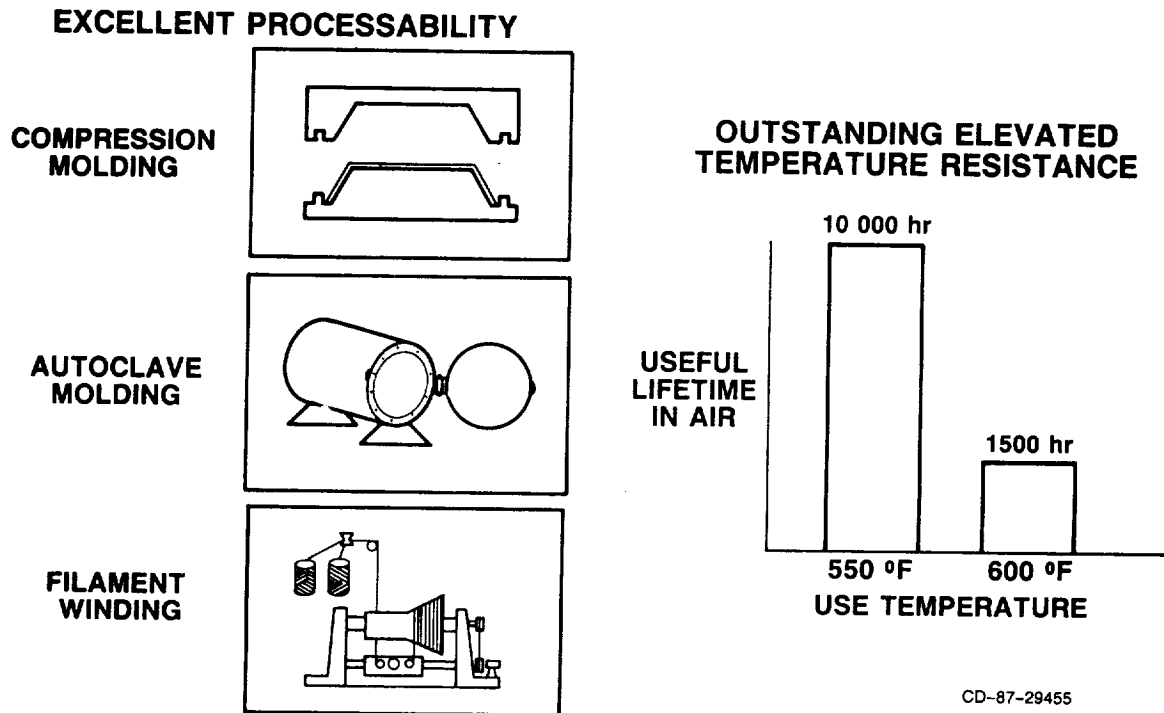


Figure 4. - Lewis-developed PMR-15 polyimide technology.

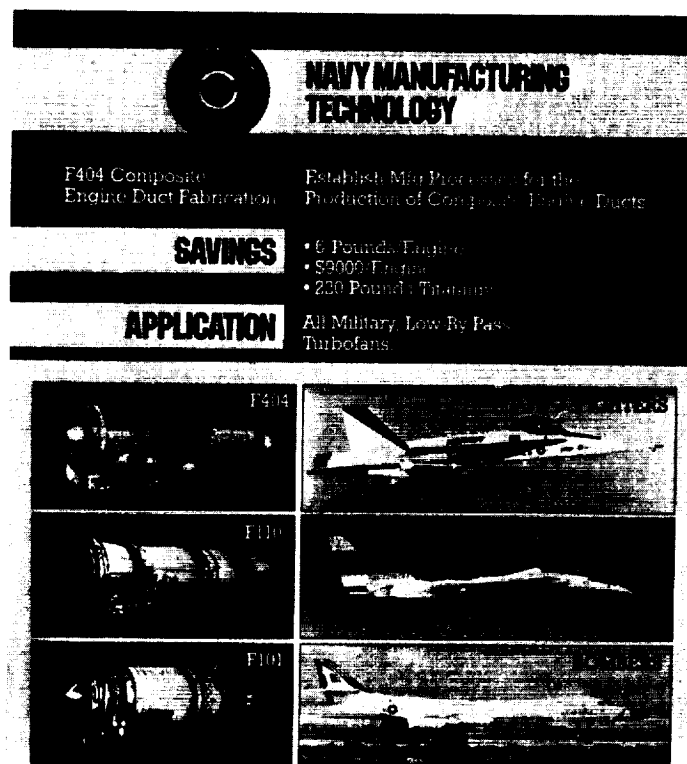


Figure 5. - Navy manufacturing technology.

**WEIGHT
SAVINGS**

7 POUNDS/ENGINE

PRODUCTION QUALITY DUCT



CD-87-24957

Figure 6. - Graphite/PMR-15 titanium replacement F-404 duct (Navy/NASA Lewis/GE joint development).

- PMR RESINS DEVELOPED IN RESPONSE TO NEED FOR A *PROCESSABLE*, HIGH TEMPERATURE MATERIAL
- EIGHT *COMMERCIAL* LICENSES FOR PMR RESINS. MAJOR SUPPLIERS: AMERICAN CYANAMID, CIBA-GEIGY, FERRO, FIBERITE, HEXCEL, U.S. POLYMERIC, HYSOL/GRAFIL, TRIBON.
- ONE OF THE MOST *WIDELY USED* MATRIX RESINS FOR 550 °F APPLICATIONS.

CD-87-29458

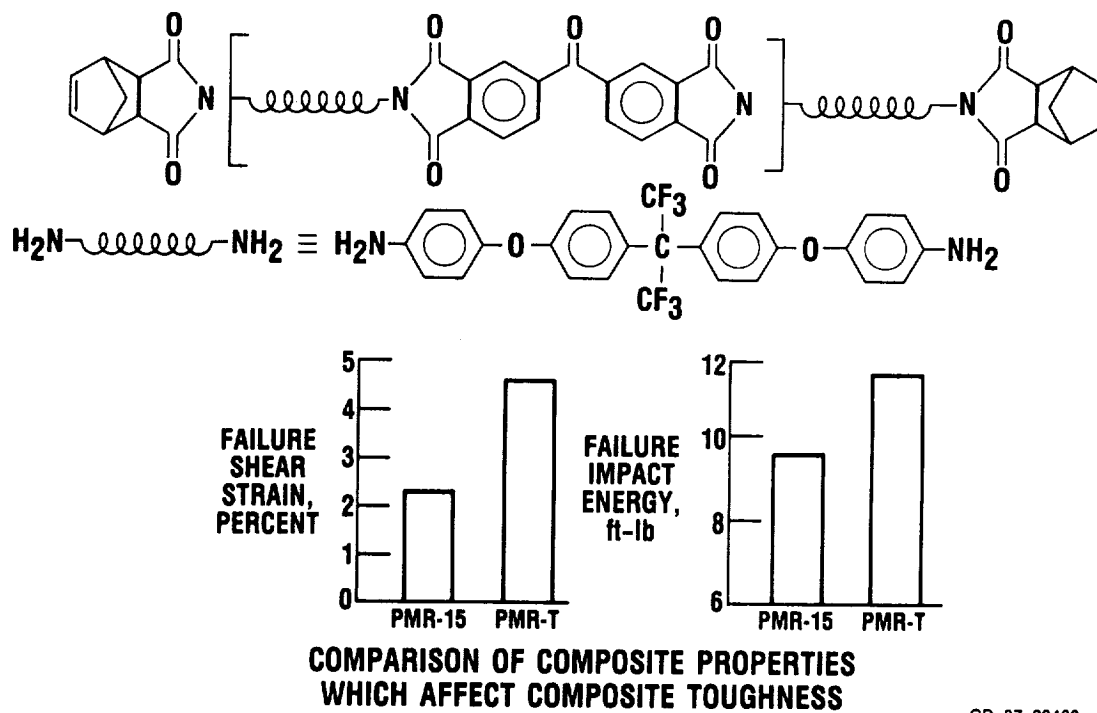
Figure 7. - PMR-15: recognized leader in high-temperature polymer matrix resins.

- IMPROVED TACK/EASIER HANDLING PMR
- LOWER CURE TEMPERATURE MATERIALS
- MECHANISTIC STUDIES
- UNDERSTANDING OF STRUCTURE/PROPERTY RELATIONSHIPS
- DEGRADATION STUDIES
- IMPROVED TOUGHNESS
- IMPROVED THERMAL STABILITY
- QUALITY CONTROL PROCEDURES

THIS WORK HAS LED TO OVER SEVENTY SCIENTIFIC PUBLICATIONS, TWELVE PATENTS AND SEVEN PATENTS PENDING.

CD-87-29459

Figure 8. - Lewis Polymers Branch response to industry needs for improvements and further understanding of polyimides.

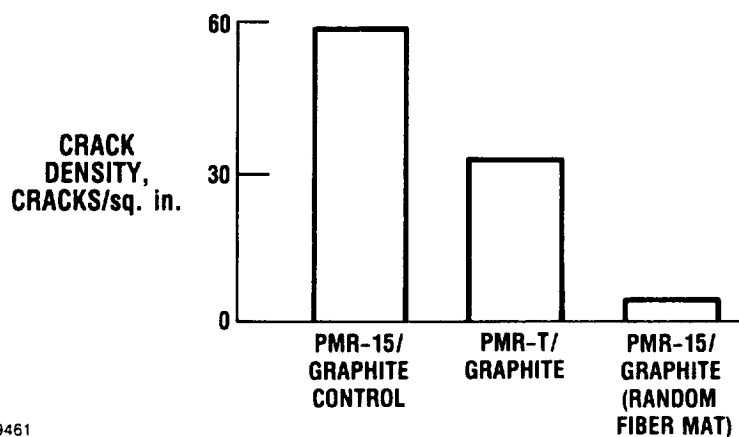


CD-87-29460

Figure 9. - PMR polyimides with improved toughness.

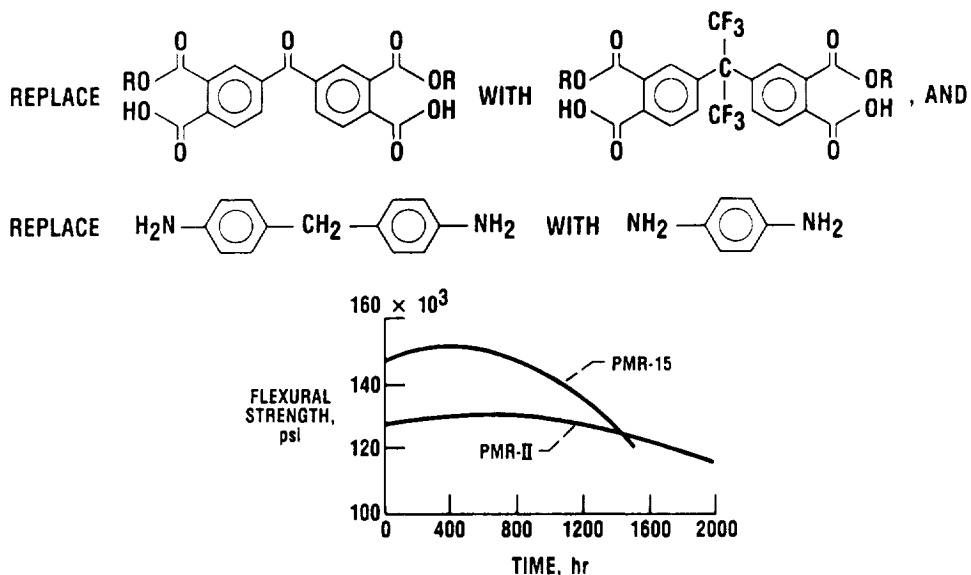
APPROACHES TO ELIMINATE IN-SERVICE MICROCRACKING:

- 1) TOUGHER POLYMER MATRIX RESIN
- 2) REPLACING SOME UNIDIRECTIONAL PLIES WITH RANDOM FIBER MAT



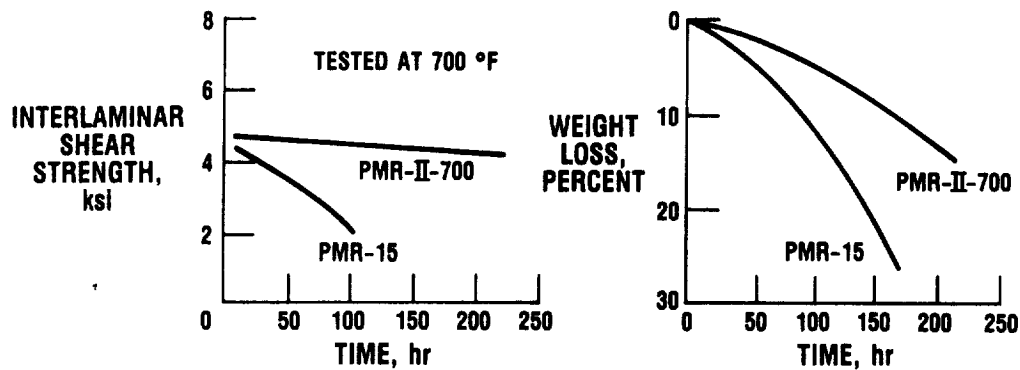
CD-87-29461

Figure 10. - Eliminating microcracking during in-service thermocycling.



CD-87-29462

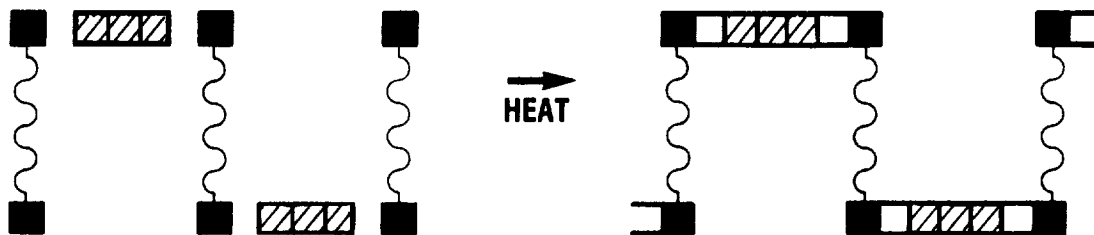
Figure 11. - PMR-II: better retention of properties through use of more stable monomers.



**PROPERTIES OF GRAPHITE FIBER/PMR RESIN COMPOSITES
AFTER EXPOSURE TO AIR AT 700 °F AND 60 PSIA**

CD-87-29463

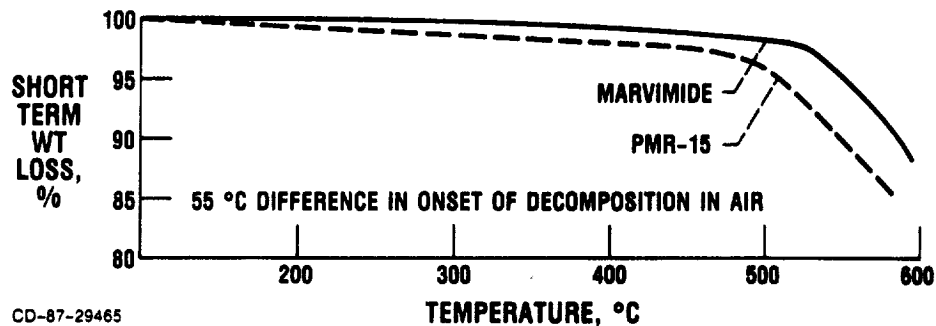
Figure 12. - PMR-II-700: entry into 700 °F applications.



- PROCESSABLE (THERMOPLASTIC ?)
- HIGH SOFTENING TEMPERATURES
- STABLE LADDER STRUCTURES

CD-87-29464

Figure 13. - MARVIMIDES: linear addition copolymers with partial ladder structure.



CD-87-29465

Figure 14. - Comparison of short-term weight loss of samples of MARVIMIDE and PMR-15.

CREEP AND FATIGUE RESEARCH EFFORTS ON ADVANCED MATERIALS

John Gayda

SUMMARY

Two of the more important materials problems encountered in turbine blades of aircraft engines are creep and fatigue. To withstand these high-temperature phenomena modern engines utilize single-crystal, nickel-base superalloys as the material of choice in critical applications. This paper will present recent research activities at Lewis on single-crystal blading material related to creep and fatigue. The goal of these research efforts is to improve the understanding of microstructure-property relationships and thereby guide material development.

Although single crystals exhibit creep properties which are superior to conventionally cast, polycrystalline blading material, recent work at Lewis and other aerospace laboratories has shown that greater improvements can be attained by developing single-crystal alloys with a "rafted" microstructure. In this microstructure, the small, cuboidal γ' precipitates that strengthen these alloys are converted into nearly continuous layers or "rafts" of γ' . The factors, both internal and external, which affect raft formation have been studied from an experimental and analytical standpoint. These include the effect of stress, temperature, lattice misfit, and elastic constants of the precipitate and matrix.

In addition to creep damage, thermomechanical fatigue (TMF) of single-crystal blading material has received much attention in recent years because it is often found to be life limiting. TMF damage results from simultaneous fluctuations of temperature and mechanical loads. Recent work at Lewis on coated single crystals has identified an environmentally driven damage mechanism for the deleterious out-of-phase TMF cycle. Experimental evidence for this mechanism is presented, together with a qualitative model describing the damage mechanism.

INTRODUCTION

The harsh operating environment encountered in the turbine section of an aircraft engine gives rise to numerous materials problems. Two of the more important problems are associated with creep and fatigue damage of turbine blades. Sustained, centrifugal loads on the blades at elevated temperature give rise to creep damage, a time-dependent, permanent elongation. Cyclic loads associated with starting and stopping of the engine, coupled with the simultaneous changes in material temperature, produce thermomechanical fatigue (TMF) damage. Unlike creep damage, TMF damage and subsequent growth of TMF

cracks are directly dependent on the number of stress cycles the blades encounter, not on the total exposure time at elevated temperatures.

To withstand the high-temperature loads developed in turbine blades, nickel-base superalloys are used in modern-day engines. These blade alloys can be made as conventional castings or as directionally solidified castings. In the former instance, a random polycrystalline microstructure is produced, whereas, in the latter instance, an aligned polycrystalline microstructure is produced. The directionally solidified casting can also be produced such that the entire blade is a single grain or crystal. In all three forms, the superalloy derives much of its high-temperature strength from the γ' particles. Carbides are also present in the polycrystalline forms to enhance the creep strength of the grain boundaries.

Of the three forms of nickel-base superalloy blading materials mentioned, the single crystal form has the highest temperature, longest life capability because the detrimental effect of grain boundaries is eliminated. Further enhancement of single-crystal fatigue properties is attained by removal of carbides, which improve creep properties of grain boundaries, but also serve as initiation sites for fatigue cracks.

In the following pages I will discuss various aspects of creep and fatigue behavior of advanced single-crystal superalloys which have been the subject of recent research programs at Lewis Research Center.

CREEP BEHAVIOR OF SINGLE CRYSTALS

The typical heat-treated microstructure of modern single-crystal superalloys contains about 60 percent of the γ' precipitates dispersed in a continuous matrix of γ . The γ' particles are usually present as spheres or cubes after heat treatment, and an example of this microstructure is shown in figure 1. However, under an applied stress at elevated temperatures, these discrete γ' particles link up in certain alloys to form plates, which are commonly called γ' rafts. These γ' rafts have been shown to improve the creep life of single crystals at elevated temperatures.

The γ' rafts have a beneficial effect on creep life if they form rapidly and are relatively perfect (ref. 1). An example of a "perfect" rafted microstructure is shown in figure 2 for a single-crystal alloy containing 13.9 percent molybdenum. However, when the molybdenum content of the alloy was increased slightly to 14.6 percent, an additional phase forms which causes imperfections or gaps in the rafts. An example of this discontinuous rafted structure is also shown in figure 2. The degradation in raft perfection causes a dramatic decrease in the creep life. Thus, our research is aimed at understanding the mechanisms of this phenomenon to exploit the maximum benefit from rafted microstructures.

A major factor which influences γ' rafting behavior is the lattice mismatch. The magnitude of the lattice mismatch indicates the difference in lattice parameters (the dimensions of the atomic structure) between the γ and γ' phases. The sign of the mismatch is one factor which determines the orientation of the rafted structure. Superalloys with large, negative values of lattice mismatch form rafts perpendicular (P-type) to the applied tensile axis,

whereas alloys with large, positive values of mismatch form rafts parallel (N-type) to the applied tensile axis. However, the sign of the mismatch can actually change from positive to negative as temperature increases (ref. 2). Thus P-type rafts can form at elevated temperatures in some alloys which have a small positive mismatch at room temperature. It is therefore important to obtain lattice mismatch measurements at elevated temperatures in order to make accurate predictions of raft orientation.

To further our understanding of the rafting process, a field-oriented, microstructural lattice model (fig. 3) was developed (ref. 3). In this approach the microstructure is discretized onto a fine lattice. Each element in the lattice is labeled accordingly as γ or γ' . Diffusion, that is, physical transport of material at elevated temperatures, is simulated by allowing exchanges of neighboring elements if the exchange lowers the total energy of the system. A Monte Carlo approach is used to select the exchange site, whereas the change in energy associated with the stress fields, that is, precipitate misfit and external creep load, is computed by using a finite-element technique.

To date, simulations of the rafting phenomenon in single crystals agree with real-world behavior. The orientation of the rafted structure under tensile loads and its dependence on precipitate misfit is illustrated in figure 4. The two alloys shown have identical properties and starting microstructures, except that one has a negative misfit and the other has a positive misfit. Rafting simulations run on both alloys show that rafts develop which are perpendicular to the stress axis for negative misfit but parallel to the stress axis for positive misfit. This is consistent with the experimental results.

FATIGUE BEHAVIOR OF SINGLE CRYSTALS

Although the creep damage produced at high temperatures by sustained loads affects the life of single-crystal turbine blades, failure is often attributed to thermomechanical fatigue damage. This damage is produced by the application of cyclic loads during heating and cooling of the blade. The damage often starts as cracks in the oxidation-resistant coating applied to single-crystal turbine blades. These cracks grow into the single crystal and eventually cause failure of the blade (fig. 5).

Thermomechanical fatigue (TMF) is particularly harmful in cycles where tensile loads are applied at temperatures below 800 °C, where ductility of superalloys is lowest. A TMF cycle of this type is termed out-of-phase (OP) and is often encountered in real engine cycles. Here the load and temperature change in opposite directions at the same time. This cycle produces tensile mechanical strains at the minimum temperature and compressive mechanical strains at the maximum temperature. Analysis is complicated, since the mechanical strain due to the changing load is mixed with thermal strains due to the changing temperature.

A large body of knowledge exists on fatigue damage produced by cyclic loads at constant temperature. This understanding cannot be easily applied to the TMF problem, where cyclic loads produce damage at continuously changing temperatures. But the "bithermal" TMF cycle provides the means to apply this knowledge. In this simplified TMF cycle, equal amounts of inelastic mechanical strain, of opposite sign, are applied at the temperature extremes in the cycle.

The inelastic strain is a permanent, or nonrecoverable, strain which produces damage within the material (fig. 6).

The bithermal TMF cycle produces the same type of damage as the more realistic TMF cycle (ref. 4). In out-of-phase (OP) tests where the temperature is changed between 650 and 1050 °C, both cycles produce premature surface cracks. Surface cracking also occurs in constant-temperature fatigue tests at 650 °C, and, at high cyclic strains, all cycles have comparable life. But in tests at low cyclic strains, the OP TMF life is up to 10 times shorter than in tests at 650 °C, as shown in figure 7.

At low strains, foreshortening of cyclic life in the OP bithermal TMF test results in part from oxidation damage at 1050 °C. When these tests are performed in vacuum (fig. 8), the OP bithermal TMF test lives increase and are approximately equivalent to the constant-temperature tests at 650 °C. Early surface cracking occurs in all of these tests, the OP bithermal TMF tests and the constant-temperature tests at 650 °C in both air and vacuum. Therefore oxidation at 1050 °C apparently accelerates growth of surface cracks in the OP bithermal TMF test.

In figure 9 a simple model of the damage mechanism for the OP bithermal cycle is presented which explains life degradation at low strains. It is assumed that surface cracks appear early in all tests. The crack tips are oxidized and thereby embrittled at 1050 °C. In tests employing large cyclic strains, the crack grows far beyond the embrittled region during a single cycle. Therefore the crack growth resistance of the unoxidized superalloy controls life, and oxidation at 1050 °C has little effect. But in tests at small cyclic strains, crack growth in the superalloy is slow compared to the advance of the oxidized region. Fracture of this environmentally damaged zone requires little load at low temperatures, such as 650 °C, and therefore provides a faster crack growth rate and shorter life at lower cyclic strains.

CONCLUSIONS

In this paper various aspects of recent research programs, on advanced single-crystal superalloys, at Lewis Research Center have been discussed. The first part of this paper discussed creep behavior and the beneficial effects of the rafted microstructure in single crystals. In the second part of this paper, the thermomechanical fatigue behavior of coated single crystals was discussed with particular attention given to the deleterious effect of the environment. Both experimental and analytical aspects of these activities were highlighted.

REFERENCES

1. MacKay, R.A.; and Ebert, L.J.: Factors Which Influence Directional Coarsening of Gamma-Prime During Creep in Nickel-Base Superalloy Single Crystals. Superalloys 1984, J.F. Radavich, et al., eds., Metallurgical Society of AIME, 1984, pp. 135-144.

2. MacKay, R.A.; and Nathal, M.V.: Microstructure-Property Relationships in Directionally Solidified Single-Crystal Nickel-Base Superalloys. MICON 86: Optimization of Processing, Properties, and Service Performance Through Microstructural Control, B.L. Bramfitt, et al., eds., ASTM STP-979, ASTM, 1988, pp. 202-221.
3. Srolovitz, D.J.; Hassold, G.N.; and Gayda, J.: Monte Carlo Simulation of Modulated Phases. NASA TM-89654, 1987.
4. Gayda, J., et al.: Bithermal Low-Cycle Fatigue Behavior of a NiCoCrAlY-Coated Single Crystal Superalloy. Effects of Load and Thermal Histories on Mechanical Behavior of Materials, P.K. Liaw and T. Nicholas, eds., Metallurgical Society of AIME, 1987, pp. 179-198. (NASA TM-89831.)

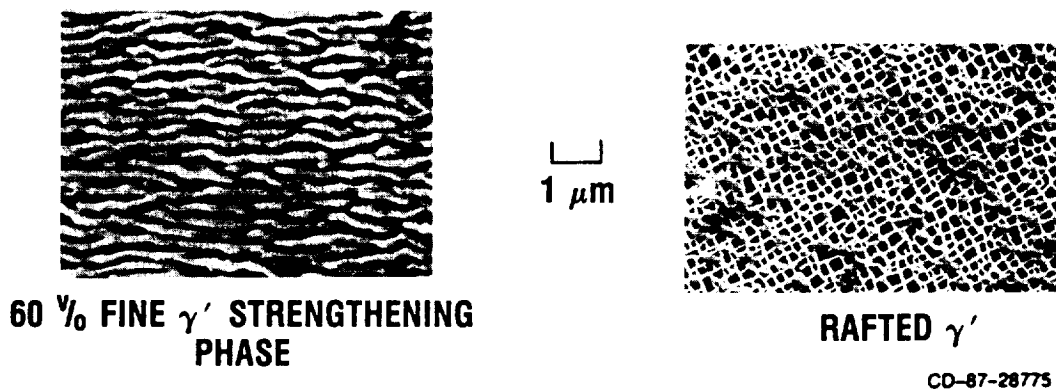
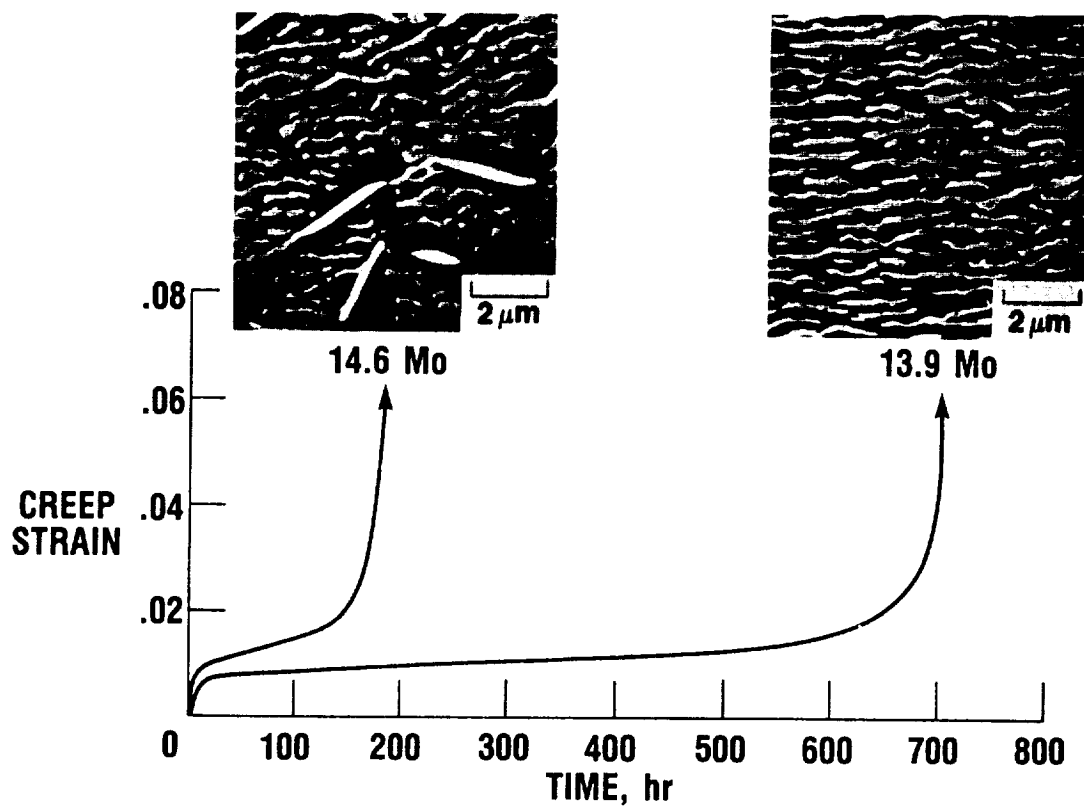


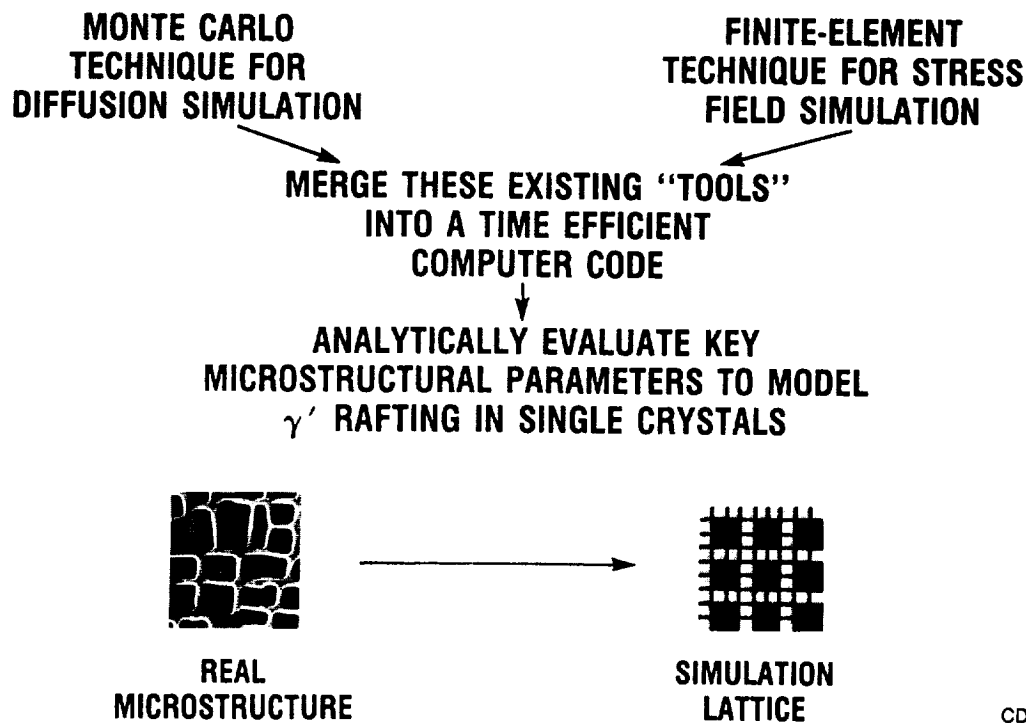
Figure 1. - Starting and rafted microstructure of single-crystal superalloy.

ORIGINAL PAGE
BLACK AND WHITE PHOTOGRAPH



CD-87-28776

Figure 2. - Effect of raft perfection on creep life.



CD-87-28778

Figure 3. - Schematic representation of microstructural lattice model used to analyze rafting phenomenon.

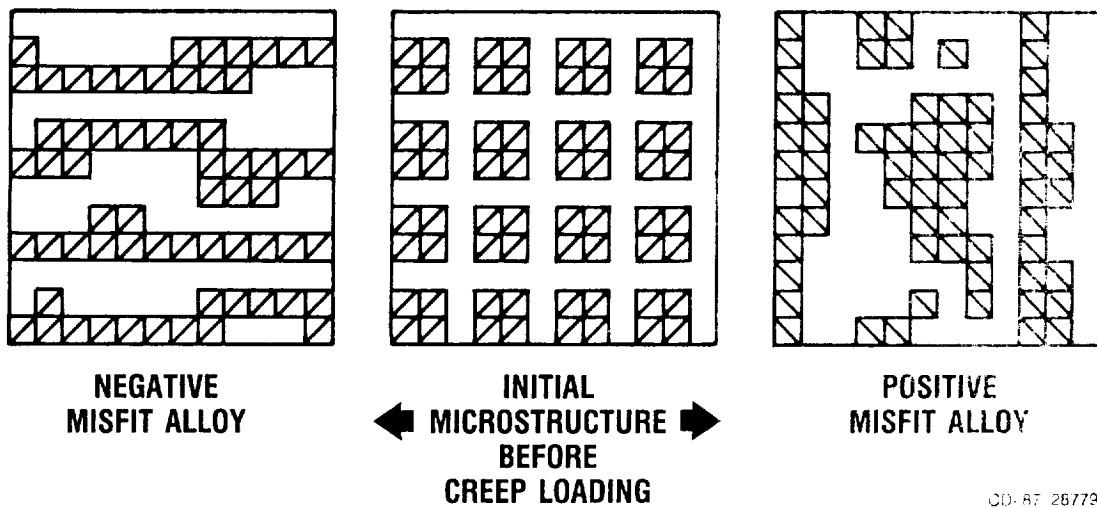


Figure 4. - Simulated rafting of positive and negative misfit alloys.

- **CYCLIC LOADS**
- **HEATING AND COOLING**

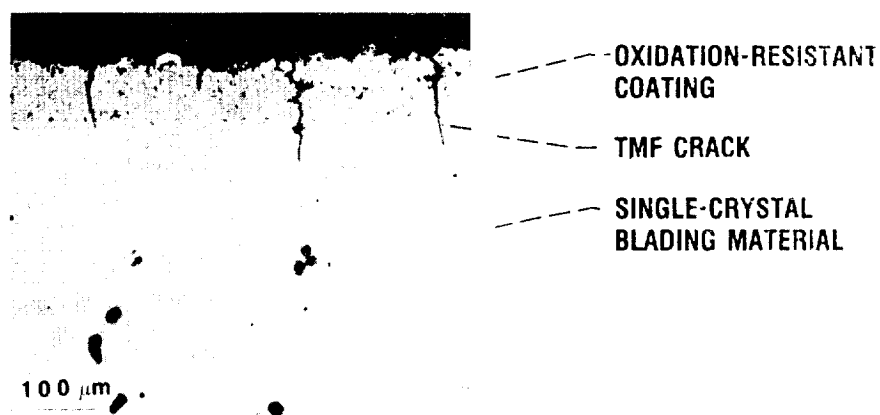


Figure 5. - TMF cracking in coated single-crystal alloy.

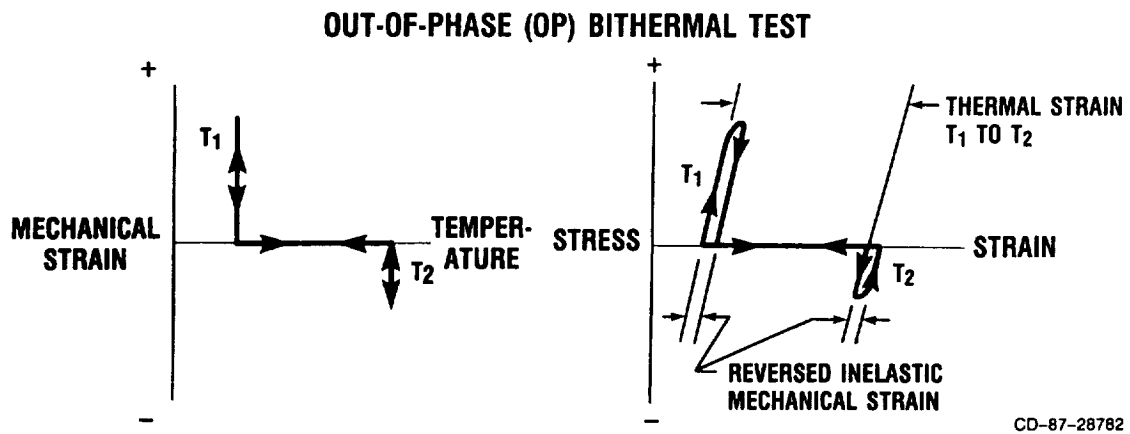


Figure 6. - Definition of bithermal fatigue cycle.

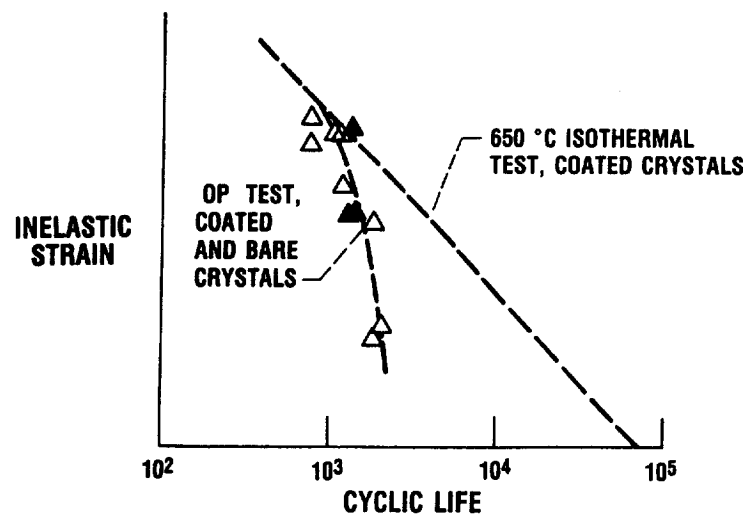


Figure 7. - Comparison of out-of-phase bithermal and 650 °C isothermal fatigue lives.

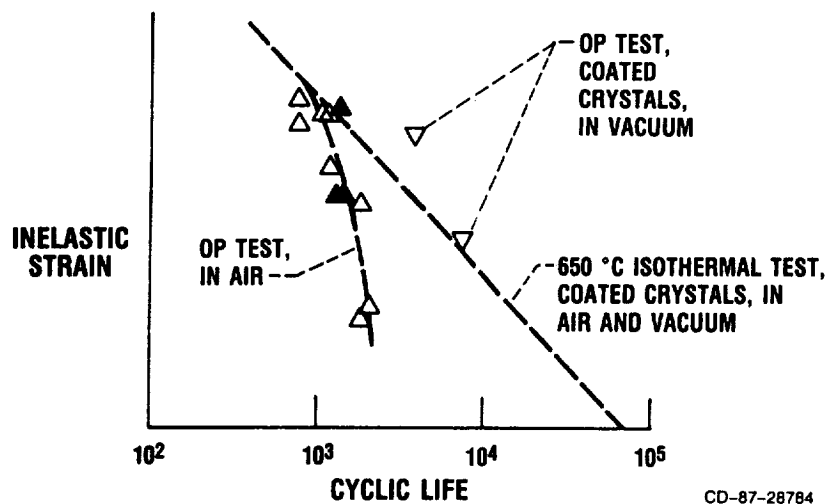


Figure 8. - Short life of bithermal out-of-phase tests largely associated with environmental effects.

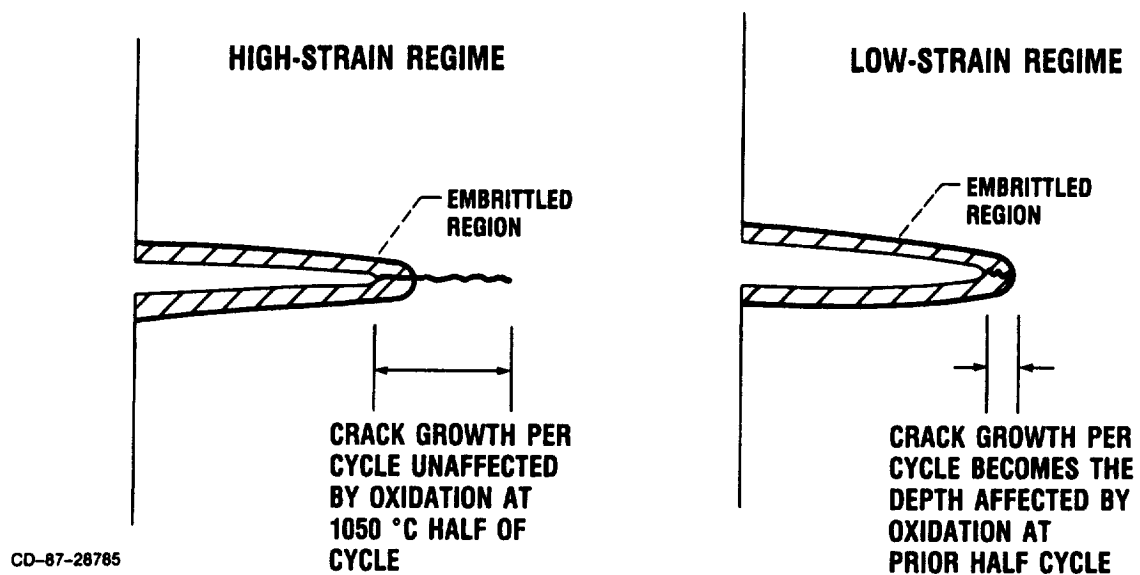


Figure 9. - Schematic representation of environmentally assisted crack growth mechanism for out-of-phase TMF tests.

DEVELOPMENT OF A NEW GENERATION OF HIGH-TEMPERATURE COMPOSITE MATERIALS

P.K. Brindley

SUMMARY

There are ever-increasing demands to develop low-density materials that maintain high strength and stiffness properties at elevated temperatures. Such materials are essential if the requirements for advanced aircraft are to be realized. Continuous fiber-reinforced metal matrix composites and inter-metallic matrix composites are currently being investigated at NASA Lewis Research Center for such applications because they offer potential increases in strength, stiffness, and use temperature at a lower density than that of super-alloys presently available.

A brief review of key contributions from past metal matrix composite investigations precedes the primary topic of this paper: intermetallic matrix composites proposed to meet advanced aeropropulsion requirements. The powder metallurgy fabrication process currently being used to produce these inter-metallic matrix composites will be presented, as will properties of one such composite, SiC/Ti₃Al+Nb (ref. 1). In addition, the direction of future research will be outlined, including plans for enhanced fabrication of inter-metallic composites by the arc-spray technique and fiber development by the floating-zone process.

PAST RESEARCH

NASA Lewis' involvement in composite materials development is shown pictorially in figure 1 with the appropriate composites listed alongside each area of interest. Much of the past composite work has been composed of model system studies to determine tensile and stress rupture properties (refs. 2 to 6) and the effect of fiber-matrix reaction on mechanical properties (ref. 7). The model composite systems studied were primarily W-reinforced Cu (W/Cu) (refs. 2 and 3), W/Cu alloys (refs. 4 and 7), and W/superalloys (refs. 5 and 6). A model developed during the generation of this data base is the well-known rule of mixtures, which is commonly used to predict baseline composite properties from the behavior of the constituents (ref. 3).

A series of W-reinforced matrices (FeCrAl, Incoloy 907, Waspaloy, and 316 stainless steel) were examined by Rocketdyne for NASA Lewis (ref. 8) to determine their potential as alternate materials for turbine and compressor blades in advanced versions of the space shuttle main engine (SSME). These composites have been screened through a series of tests including severe thermal shock (cryogenic to 2000 °F in 0.3 sec), thermal fatigue, and high and low

cycle fatigue. The most promising composite, W/Waspaloy, is continuing to be examined since it proved to have thermal fatigue properties equal to the currently used SSME blade material of directionally solidified Mar M 246 + Hf while being superior in thermal shock resistance and high and low cycle fatigue.

Another contribution in the area of metal matrix composites was a fabrication study performed by TRW for NASA Lewis (ref. 9) in which a W/superalloy composite turbine blade was made using a powder metallurgy approach. The composite blade, which is shown in figure 2, demonstrated both the feasibility of employing a continuous fiber composite to form a hollow blade and that the design requirements of a particular airfoil shape could be met. The airfoil of the W/superalloy blade has the external dimensions of a JT9D-7F first-stage, convection-cooled airfoil. The composite airfoil walls were designed to be thinner because of the increased strength and stiffness of the composite material. Designing thinner walls also reduced the composite blade weight to within 10 percent of the current Mar M 200 blade weight and allowed for more efficient cooling (ref. 10).

CURRENT RESEARCH

Our current efforts in advanced composites are also shown in figure 1 for aerospace applications. These endeavors center around the development of continuously reinforced aluminide matrix composites because of the potential these composites have to outperform existing superalloys. The primary properties required to realize advances toward hypersonic travel include lower density, improved strength at temperatures beyond 1800 °F, higher strength/density ratios, stiffness over the entire temperature range, enhanced oxidation resistance, and thermal barrier coating compatibility.

The densities of several aluminides targeted for development within NASA Lewis are compared in figure 3 with the nominal density of superalloys to show one advantage in pursuing aluminides. And, as expected, when aluminides are reinforced with SiC fiber, shown here at 40 vol % reinforcement, the density comparison is even more attractive. It is important to note that even though monolithic aluminides offer a weight savings, they typically are not competitive with superalloys on a strength basis unless they are reinforced. Thus, fiber-reinforced aluminide composites were chosen for examination. Three intermetallic matrix composite systems are currently under investigation with the following matrix materials: Fe-40 at. % Al (Fe-40Al), Ti-24 at. % Al-11 at. % Nb (Ti₃Al+Nb), and NiAl.

In any discussion of intermetallic materials it is important to note that limited ductility can be exhibited at low temperatures because their ordered atomic structures can limit the number of available, independent slip systems (ref. 11). This limited ductility in the matrix is one issue which needs to be overcome if intermetallics are to be successfully utilized in composites. In some cases ductility has been imparted to intermetallics by alloy addition to form a two-phase microstructure, as in the case of Ti₃Al+Nb (refs. 12 and 13), or by using an off-stoichiometric composition, as in the case of Fe-40Al (ref. 14). Thus, these aluminides were chosen as matrices for study because they exhibited ductility at room temperature and above, in addition to potential strength/density advantages over existing materials.

NiAl is also being pursued as a potential matrix material because of its high melting point of 2980 °F (ref. 15), and therefore high potential use temperature, and because it exhibits excellent oxidation resistance to 2012 °F (ref. 16). However, NiAl matrix composites are a longer term development than either Ti₃Al+Nb or Fe-40Al matrix composites because no means has yet been devised to achieve ductility in NiAl at low temperatures. Thus, NiAl is continuing to be researched to determine its potential as a suitable matrix material.

COMPOSITE DEVELOPMENT

A powder metallurgy approach is currently being used at NASA Lewis to fabricate intermetallic matrix composites, as illustrated in figure 4 for SiC/Ti₃Al+Nb. In this powder cloth technique, prealloyed aluminide powder is blended with Teflon powder and a solvent. The mixture is heated to drive off the excess solvent and to provide the proper consistency for the rolling operation from which a powder cloth is obtained. These metallic powder cloths are the matrix of the composite. Mats of full length SiC fibers are layered between the powder cloths until the desired number of reinforcement layers are achieved. These fiber layers can be oriented as desired to obtain maximum properties in particular directions. The entire layup is placed in a hot press and diffusion bonded, driving off the Teflon and remaining solvent in vacuum. The resultant SiC-reinforced intermetallic matrix composite is a 2- by 6-in. plate of desired thickness.

The microstructure of an actual SiC/Ti₃Al+Nb composite produced by the powder cloth technique is shown in figure 5. The lower magnification photomicrograph shows the three-fiber-layer composite, which is fully consolidated upon processing; no voids or cracks are evident in the matrix and the fiber-matrix interface appears to be well joined. The larger magnification view again shows the fiber-matrix interface to be fully consolidated. Other features include a two-phase Ti₃Al+Nb matrix, a small reaction zone between the fiber and matrix due to fabrication, and a zone surrounding the fiber and reaction zone that is depleted of second phase.

MECHANICAL PROPERTIES

Tensile properties at temperature for the AVCO SCS-6 SiC fiber, the Ti₃Al+Nb matrix material produced by the powder cloth technique, and the SiC/Ti₃Al+Nb composite tested in air are plotted in figure 6 (ref. 1). The fiber and the matrix-only data were used in the rule of mixtures (ROM) to calculate first-order composite properties. The ROM is a weighted average that predicts composite strength from the strength of the constituents (ref. 3). The data displayed here are for 40 vol % SiC fiber reinforcement. The actual composite strengths obtained were comparable to ROM in the intermediate temperature regime, but lower than expected at room temperature and at 1200 °F and above.

Consider first the room temperature results. It has previously been discussed that intermetallic compounds can be brittle at room temperature and that Nb has been successfully added to Ti₃Al to impart ductility at lower temperatures. It is also known that high levels of oxygen and carbon can negate the ductility benefits of Nb if present at levels of ~1000 ppm or greater. In this first generation of SiC/Ti₃Al+Nb composites, the oxygen level was ~1200 ppm.

It is therefore postulated that the oxygen was responsible for the low composite strengths obtained at room temperature resulting in cracking at low strains within the matrix and propagation through the brittle fibers such that the fibers were not able to attain their full strength potential. This proposed mode of failure was further supported by the lack of ductile features on the room temperature fracture surfaces as well as the overall flat fracture appearance of figure 8, in which the fibers and matrix failed in the same plane. It is hoped this room temperature strength difficulty can be solved by using matrix powder with lower oxygen contents. This is under investigation in the second generation of SiC/Ti₃Al+Nb composites in which powders with 480 to 620 ppm oxygen are being used.

With regard to the falloff in strength of SiC/Ti₃Al+Nb at 1200 °F and above, two features were observed on the fracture surfaces: debonding and fiber pullout. Figure 7 shows the presence and location of debonding which occurs at the fiber/fiber-coating interface and the fiber-coating/matrix interface after elevated-temperature tensile tests. At room temperature, the bond between the fiber and matrix appears to remain intact. However, at 1200 °F and above, the matrix separates from the C-rich coating of the fiber. Separation of the C-rich coating from the SiC fiber is sometimes observed in addition to the separation at the fiber coating/matrix interface, as shown here at 1200 °F.

Fiber pullout was also observed in the fracture surfaces of the SiC/Ti₃Al+Nb, as shown in figure 8. Note that very little fiber pullout was evident at room temperature but that increasing amounts of fiber pullout were obvious as test temperature was increased. These observations suggest that debonding and fiber pullout could have contributed to the deviation from ROM-predicted strengths at 1200 °F and above.

Fiber/matrix interface separations are not surprising when one considers the two- to five-fold differences in coefficient of thermal expansion (CTE) that exist between the currently available fibers for reinforcement and some of the candidate matrix materials, as shown in figure 9. Such large CTE mismatches are expected to be the most damaging under the thermal cycling and thermal mechanical fatigue conditions which these composites will surely encounter as components. Thus, it is imperative that thermal cycling and thermal mechanical fatigue characterization of these composites is performed. The need for new materials development to provide materials with higher CTE's is also clear, so as to minimize the damage induced in future generations of advanced composites during nonisothermal, cyclic conditions. The plans for new fiber development is discussed in the Future Composite Work section.

CHEMICAL COMPATIBILITY

Another area which requires characterization in any composite system is that of fiber-matrix chemical compatibility. In general, a large reaction zone between the fiber and matrix is unacceptable because it is accompanied by a decrease in mechanical properties (ref. 7). However, a small reaction zone may be acceptable. The first step in determining acceptable limits is to anneal coupons of the composite at various times and temperatures. Samples of SiC/Ti₃Al+Nb were annealed in vacuum at 1800 and 2200 °F for 1 to 100 hr to determine the rate of chemical reaction, as shown in figure 10. At short times,

the reaction was not extensive at either 1800 or 2200 °F. However, for long periods of time, the reaction at 2200 °F is especially damaging. After 10 hr at 2200 °F, the C-rich fiber coating has been depleted, and extensive reaction has occurred. After 100 hr at 2200 °F, large voids within the reacted zone were also observed. In contrast, after 100 hr at 1800 °F, the C-rich fiber coating was still present, and the reaction thickness was on the order of 10 μ m in thickness. These results indicated that fiber/matrix reaction will probably limit the use temperature of SiC/Ti₃Al+Nb to a maximum of 1800 °F. Direct measurements of strength with various quantities of reaction are required to determine the actual temperature and time limitations for applications of this composite.

Note also the matrix cracks which are present in the 1800 °F/100 hr photomicrograph of SiC/Ti₃Al+Nb in figure 10. These matrix cracks were induced during the several thermal cycles from room temperature to 1800 °F which were incurred during the accumulation of the 100 hr at 1800 °F. Again, these cracks most probably resulted because of the large CTE difference between the fiber and matrix combined with the low strain-to-failure of the composite components. This again points to the need for new fiber development of materials with larger CTE's, as discussed in the preceding section. One must also keep in mind that these data were from the high oxygen bearing material with low strain-to-failure. It is possible that the lower oxygen Ti₃Al+Nb being used in the second generation of composites may be able to accommodate more of the strain induced by the CTE mismatch. The amount of strain accommodation possible is under continued investigation.

To illustrate the potential of intermetallic matrix composites, the preliminary tensile properties of SiC/Ti₃Al+Nb were plotted on a strength/density basis versus temperature and compared with a range of wrought Ni-base superalloys and one single-crystal Ni-base superalloy in figure 11. These data show that the potential beyond superalloys anticipated for tensile properties of 0° fiber reinforced aluminide matrix composites is attainable.

FUTURE COMPOSITE WORK

Future work on intermetallic matrix composites includes investigating alternative processing techniques in order to obtain higher production rates and, more importantly, cleaner matrix materials. For this reason, we are presently pursuing the development of Ti₃Al+Nb in wire form to be used in our arc-spray facility (ref. 17), as shown schematically in figure 12. It is anticipated that the arc spray process will maintain a Ti₃Al+Nb matrix with a lower oxygen and carbon content than can be achieved by the powder cloth technique. Furthermore, the capabilities of the arc-spray process have been proven and documented in several composite systems including W/superalloys, W/Nb-1Zr, W/Cu, and SiC/Nb-1Zr, all of which displayed minimal oxygen and carbon pickup during processing.

New fiber development is also being pursued to investigate a wide range of materials which exhibit coefficients of thermal expansion similar to those of the intermetallics being considered as matrices. A floating-zone fiber drawing process (ref. 18), schematically shown in figure 13, is being procured and will be used to discern which materials are most promising on the basis of producibility, strength, and chemical compatibility. The most promising fibers

will then be processed on a large scale, possibly by chemical vapor deposition, and subsequently employed in composites for evaluation and characterization.

REFERENCES

1. Brindley, P.K.: SiC Reinforced Aluminide Composites. High-Temperature Ordered Intermetallic Alloys II, MRS Symp. Proc. vol. 81, N.S. Stoloff, ed., Materials Research Society, 1987, pp. 419-424.
2. McDanel, D.L.; Signorelli, R.A.; and Weeton, J.W.: Analysis of Stress-Rupture and Creep Properties of Tungsten-Fiber-Reinforced Copper Composites. NASA TN D-4173, 1967.
3. McDanel, D.L.; Jech, R.W.; and Weeton, J.W.: Stress-Strain Behavior of Tungsten-Fiber-Reinforced Copper Composites. NASA TN D-1881, 1963.
4. Petrusek, D.W.: Elevated-Temperature Tensile Properties of Tungsten Fiber Composites. AIME Trans., vol. 236, no. 6, June 1966, pp. 887-896.
5. Petrusek, D.W.: Effect of Rolling on the High Temperature Tensile and Stress-Rupture Properties of Tungsten Fiber Superalloy Composites. NASA TM X-71484, 1974.
6. Petrusek, D.W.; and Signorelli, R.A.: Stress-Rupture Strength and Microstructural Stability of W-Hf-C Wire Reinforced Superalloy Composites. NASA TM X-71529, 1974.
7. Petrusek, D.W.; and Weeton, J.W.: Effects of Alloying on Room-Temperature Tensile Properties of Tungsten-Fiber-Reinforced-Copper-Alloy Composites. AIME Trans., vol. 230, no. 5, Aug. 1964, pp. 977-990.
8. Petrusek, D.W.; and Signorelli, R.A.: Tungsten Fiber Reinforced Superalloys - A Status Review. NASA TM-82590, 1981.
9. Melnyk, P.; and Fleck, J.N.: Tungsten Wire/FeCrAl Matrix Turbine Blade Fabrication Study. (TRW-ER-8101, TRW Inc.; NASA Contract NAS3-20391) NASA CR-159788, 1979.
10. Petrusek, D.W.; and Signorelli, R.A.: Tungsten Fiber Reinforced Superalloys-A Status Review. Ceram. Eng. Sci. Proc., vol. 2, no. 7-8, July-Aug. 1981, pp. 739-786. (NASA TM-82590).
11. Stoloff, N.S.; and Davies, R.G.: The Mechanical Properties of Ordered Alloys. Prog. Mater. Sci., vol. 13, no. 1, 1966, pp. 3-84.
12. Sastry, S.M.L.; and Lipsitt, H.A.: Ordering Transformations and Mechanical Properties of Ti₃Al and Ti₃Al-Nb Alloys. Metall. Trans. A, vol. 8, no. 10, Oct. 1977, pp. 1543-1552.
13. Martin, P.L., et al.: The Effects of Alloying on the Microstructure and Properties of Ti₃Al and TiAl. Titanium '80 Science and Technology, vol. 2, H. Kimura and O. Izumi, eds., Metallurgical Society of AIME, Warrendale, PA, 1980, pp. 1245-1254.

14. Crimp, M.A.; Vedula, K.M.; and Gaydosch, D.J.: Room Temperature Tensile Ductility in Powder Processed B2 FeAl Alloys. High-Temperature Ordered Intermetallic Alloys II, MRS Symp. Proc. vol. 81, N.S. Stoloff, ed., Materials Research Society, 1987, pp. 499-504.
15. Hansen, M.; and Anderko, K.: Constitution of Binary Alloys. 2nd ed., McGraw-Hill, New York, 1958, p. 119.
16. Petit, F.S.: Oxidation Mechanisms for Nickel-Aluminum Alloys at Temperatures Between 900 and 1300 °C. AIME Trans., vol. 239, no. 9, Sept. 1967, pp. 1296-1305.
17. Westfall, L.J.: Tungsten Fiber Reinforced Superalloy Composite Monolayer Fabrication by an Arc Spray Process. NASA TM-86917, 1985.
18. Haggerty, J.S.: Production of Fibers by a Floating Zone Fiber Drawing Technique. (ADL-73235, Arthur D. Little Inc.; NASA Contract NAS3-14328) NASA CR-120948, 1972.

ORIGINAL PAGE
BLACK AND WHITE PHOTOGRAPH

W/Cu (-Zr)
W/FeCrAlY

MODEL SYSTEM STUDIES RULE OF MIXTURES

W/Nb (-1Zr)
Gr/Cu



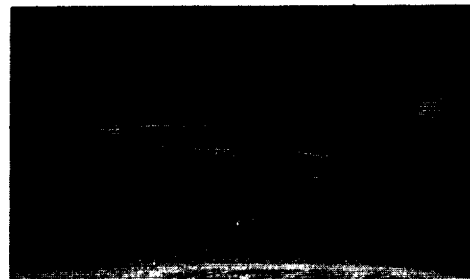
SPACE POWER COMPONENTS



SPACE SHUTTLE MAIN ENGINE COMPONENTS

W/FeCrAlY
W/INCOLOY 903 AND 907
W/WASPALLOY
W/316 STAINLESS
SiC/SUPERALLOY
B₄C-B/SUPERALLOY

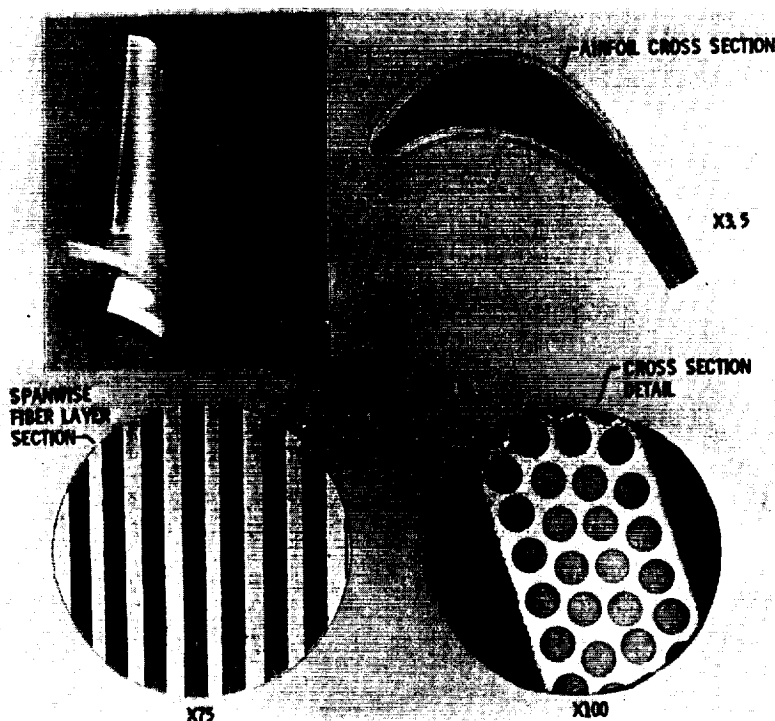
Gr/Cu
SiC/Fe-40Al
SiC/NiAl
SiC/Ti₃Al + Nb



PROPULSION SYSTEM COMPONENTS

CD-87-28877

Figure 1. - NASA Lewis involvement in composite materials development.



CD-87-28878

Figure 2. - Tungsten-fiber-reinforced superalloy blade formed using powder metallurgy (ref. 8).

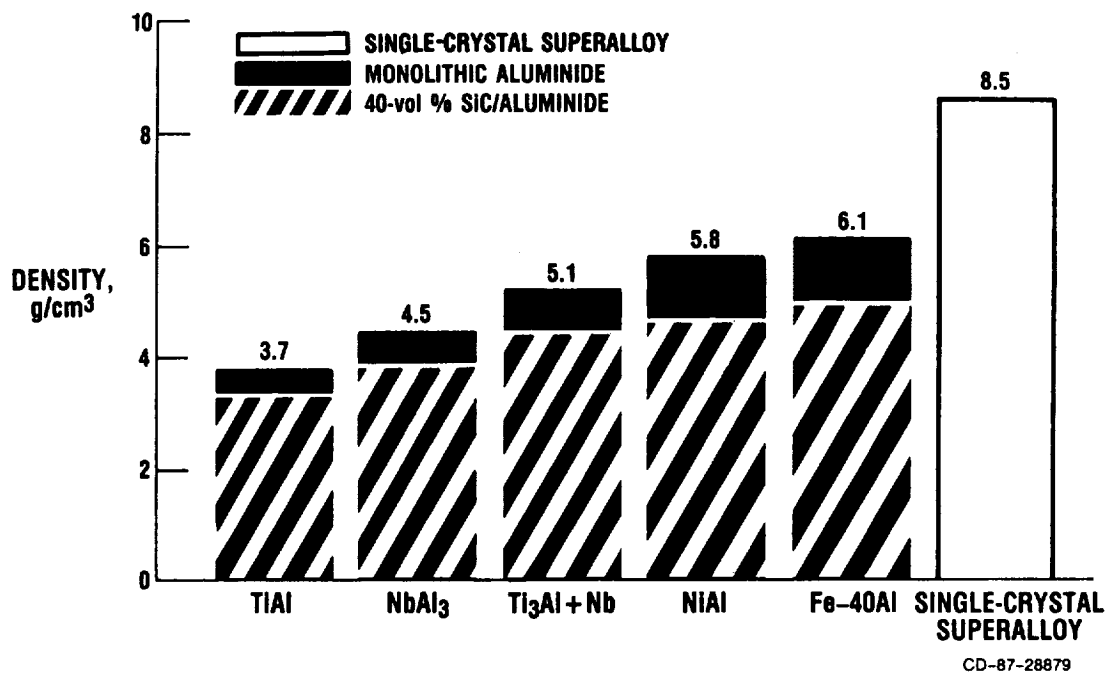


Figure 3. - Density comparison of superalloys, monolithic aluminides, and SiC-reinforced aluminides.

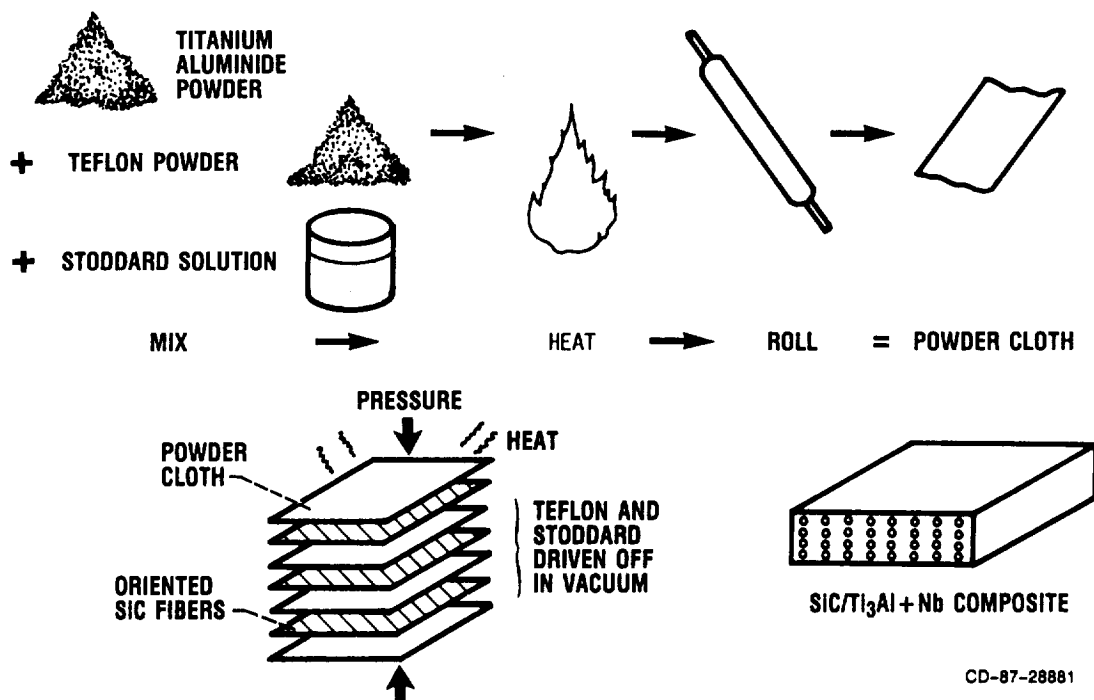


Figure 4. - Powder metallurgy approach currently being used at NASA Lewis to fabricate SiC/Ti₃Al+Nb intermetallic-matrix composite.

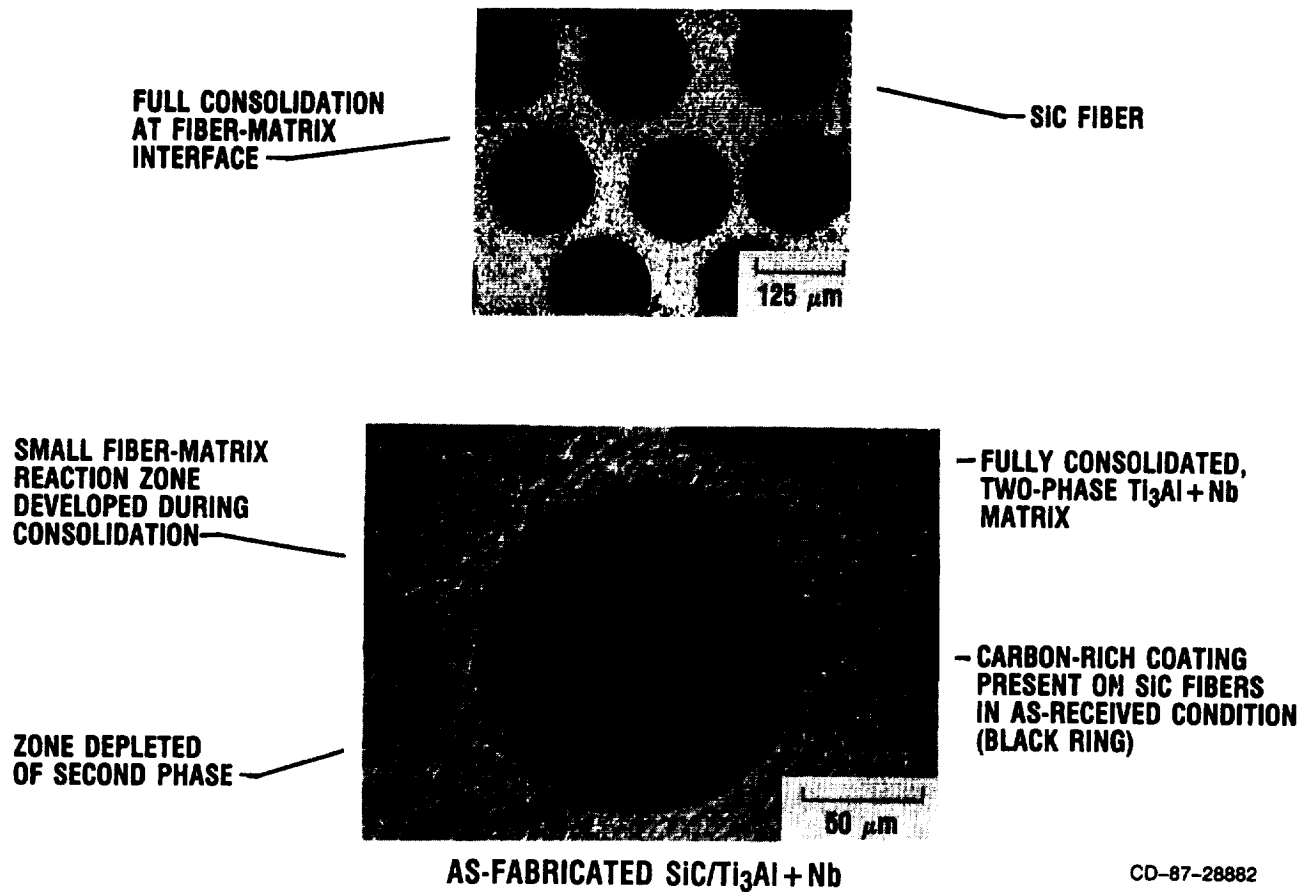


Figure 5. - Two views of $\text{SiC}/\text{Ti}_3\text{Al} + \text{Nb}$ composite fabricated by powder cloth technique.

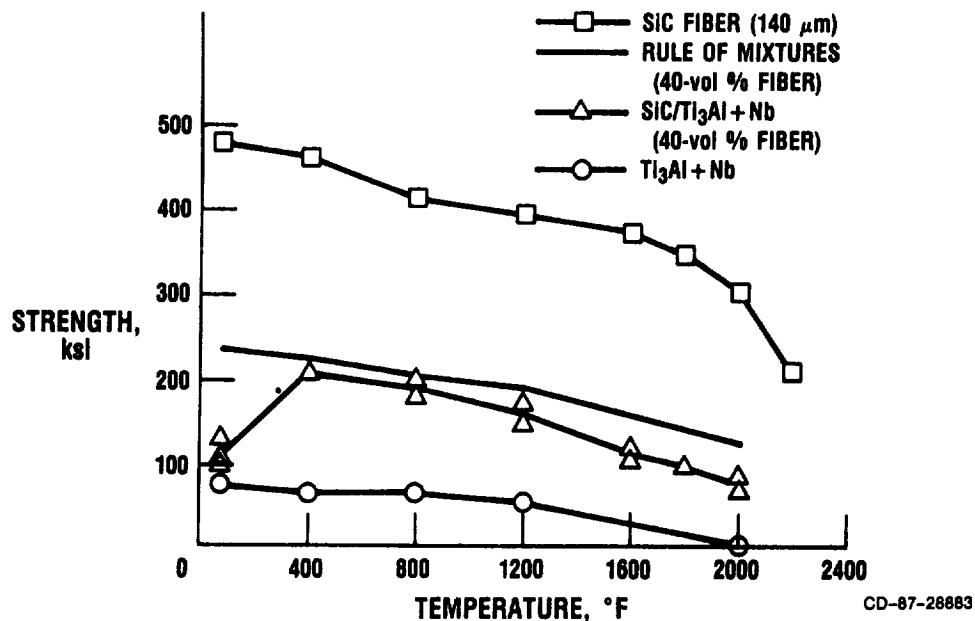
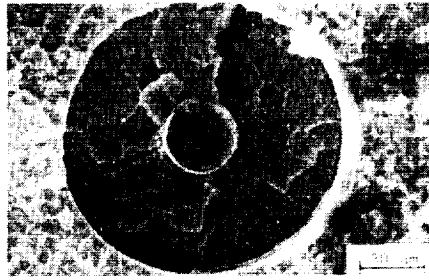
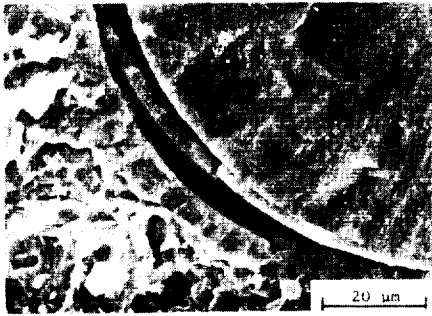


Figure 6. - Tensile properties at temperature for SCS-6 SiC fiber, $\text{Ti}_3\text{Al} + \text{Nb}$ matrix material produced by powder cloth technique, and $\text{SiC}/\text{Ti}_3\text{Al} + \text{Nb}$ composite tested in air. Fiber and matrix-only data were used in rule of mixtures (ROM) to determine first-order composite properties.

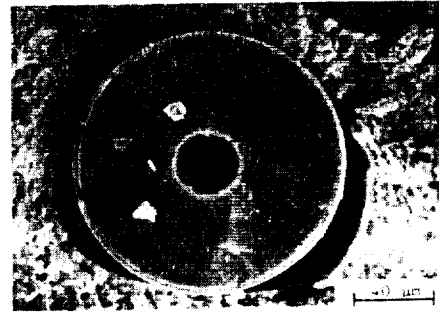
ORIGINAL PAGE
BLACK AND WHITE PHOTOGRAPH



23 °C (73 °F)



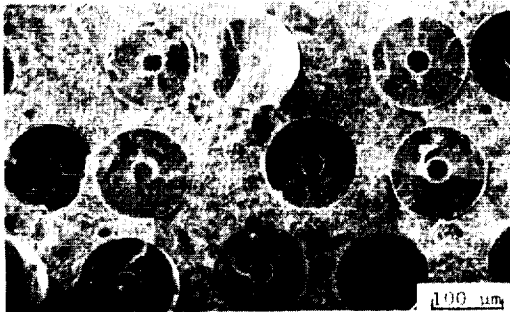
650 °C (1202 °F)



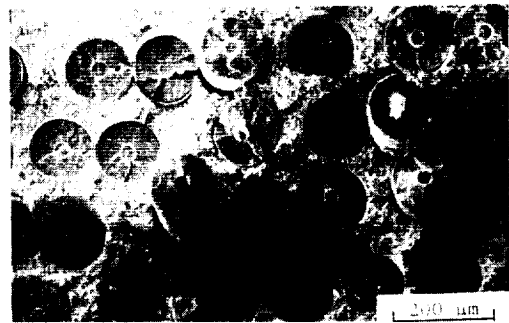
1100 °C (2012 °F)

CD-87-28884

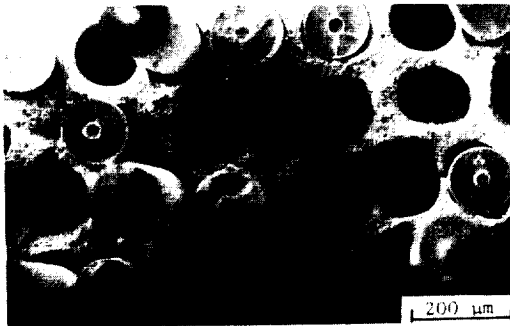
Figure 7. - Presence and location of debonding which occurred at fiber/fiber-coating interface and fiber-coating/matrix interface after elevated temperature tensile tests of SiC/Ti₃Al+Nb.



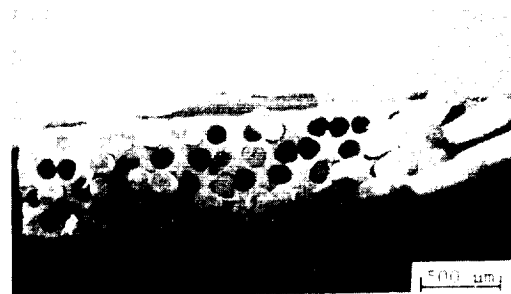
23 °C (73 °F)



425 °C (797 °F)



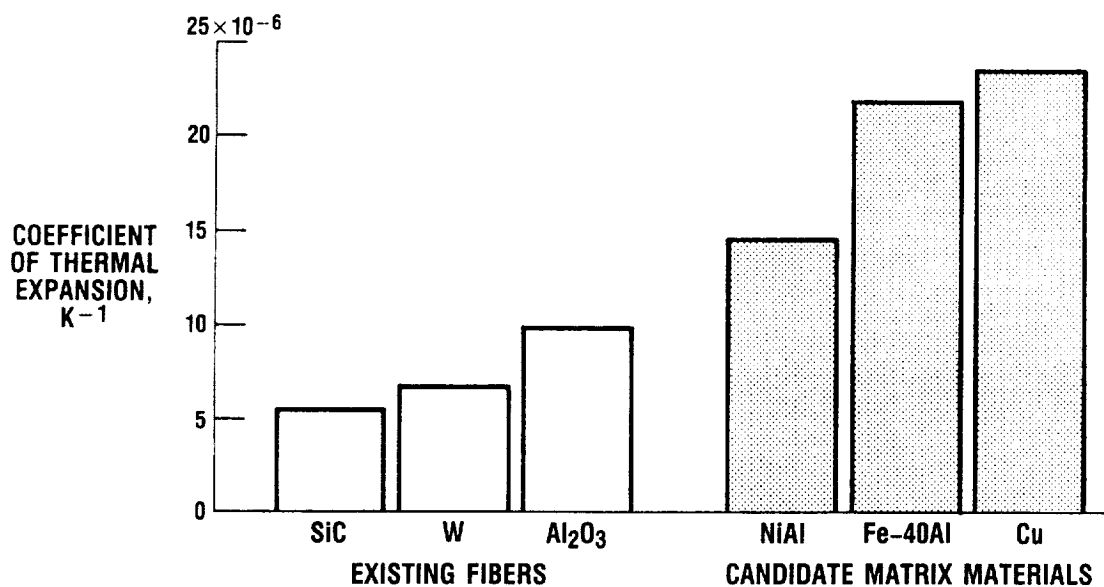
875 °C (1607 °F)



1100 °C (2012 °F)

CD-87-28885

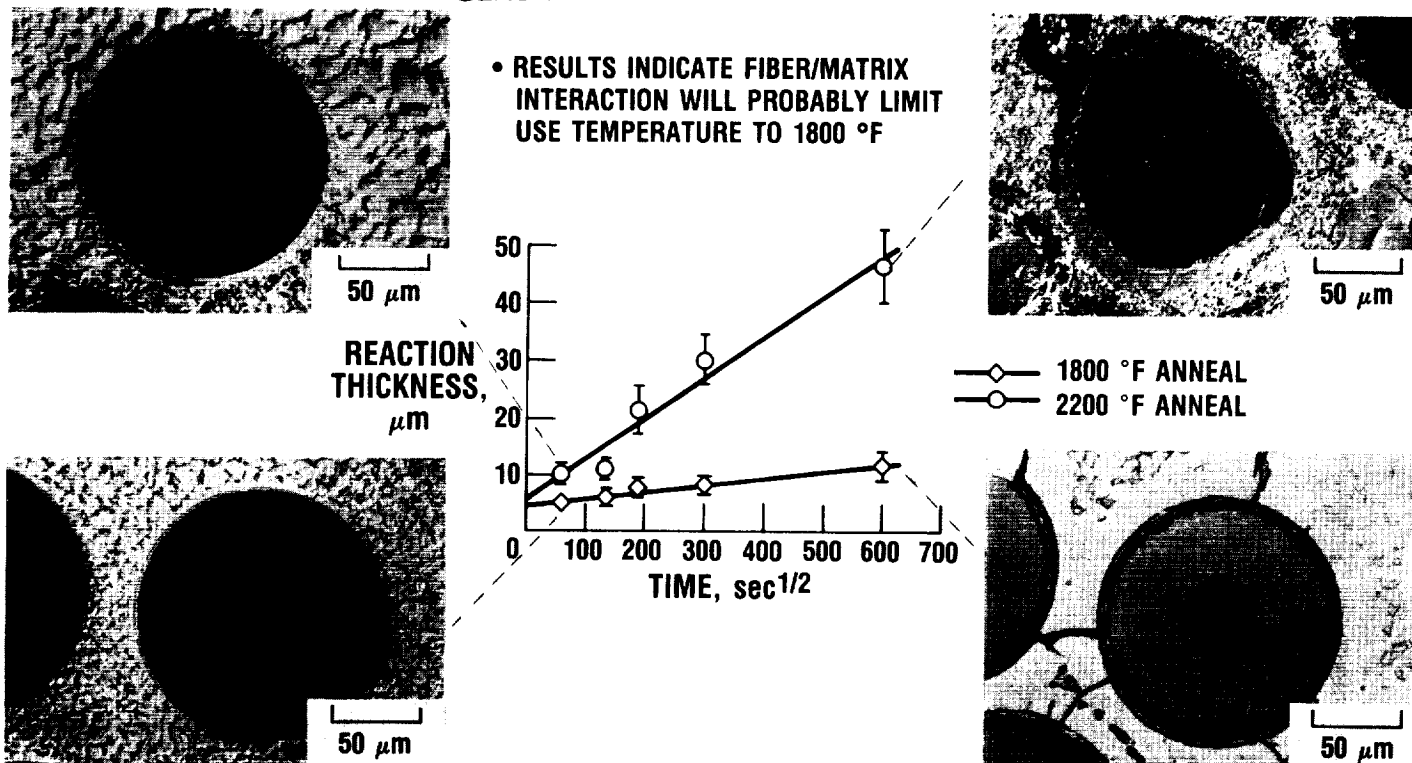
Figure 8. - Increased amount of fiber pullout observed as test temperature increased in tensile fracture surfaces of SiC/Ti₃Al+Nb.



CD-87-28889

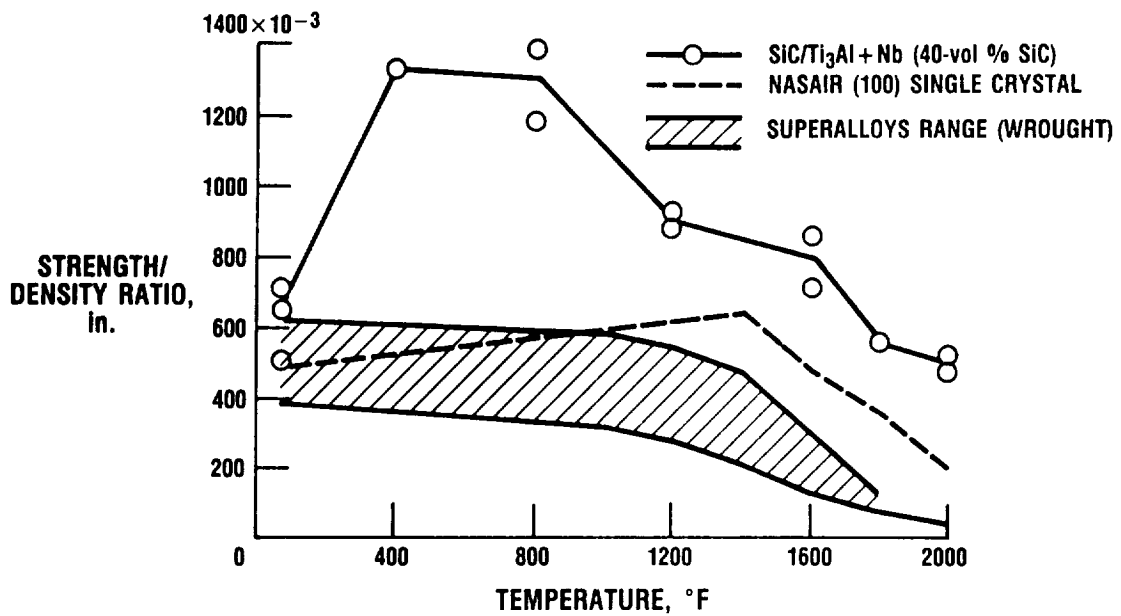
Figure 9. - The two- to five-fold difference in CTE that exists between currently available fibers for reinforcement and some candidate matrix materials point to need for new fiber development of materials with higher CTE's.

ORIGINAL PAGE
BLACK AND WHITE PHOTOGRAPH



CD-87-28886

Figure 10. - Fiber-matrix chemical compatibility results of SiC/Ti₃Al+Nb annealed in vacuum. Fiber-matrix reaction will probably limit use temperature of this composite to 1800 °F.

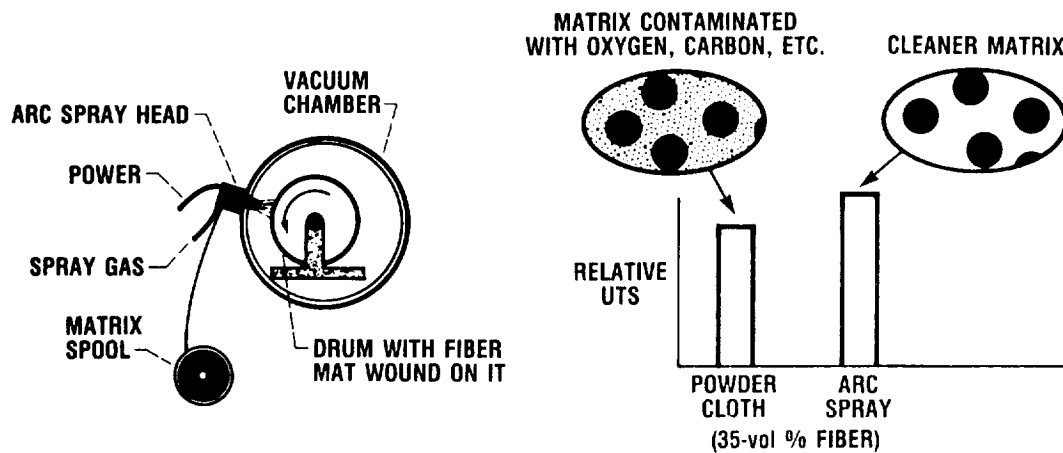


CD-87-28887

Figure 11. - Strength/density versus temperature comparison of SiC/Ti₃Al+Nb, range of wrought superalloys, and single-crystal superalloy.

BENEFITS

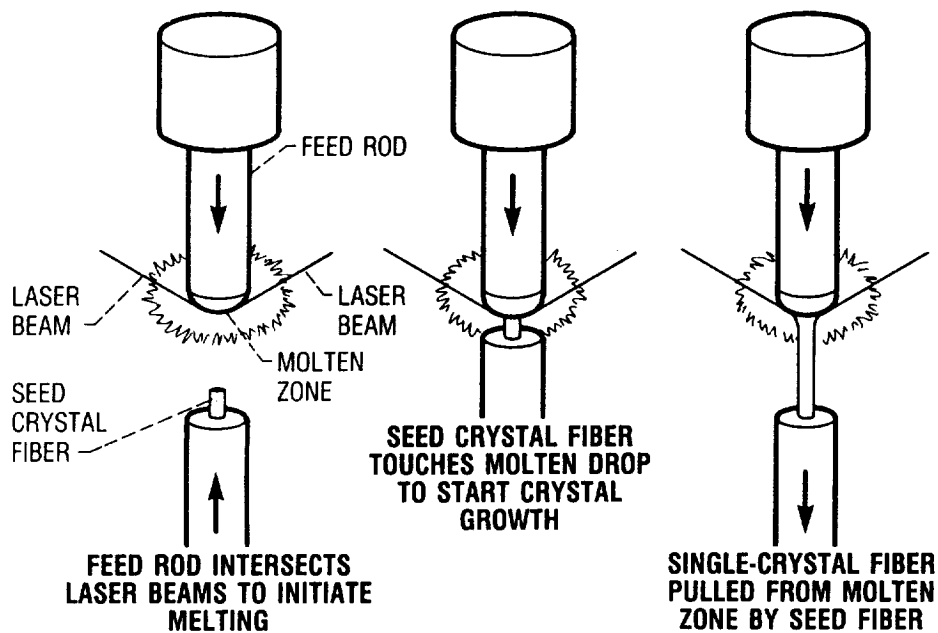
- HIGHER PRODUCTION RATES—AUTOMATED
- CLEANER MATRIX—ENHANCED DUCTILITY AND STRENGTH
- PROVEN PROCESS CAPABILITIES IN OTHER COMPOSITE SYSTEMS:
W/SUPERALLOYS, W/Nb-1Zr, W/Cu, AND SiC/Nb-1Zr



CD-87-28888

Figure 12. - Future SiC/Ti₃Al+Nb fabrication employing arc spray technique (ref. 17) in order to obtain cleaner matrix materials and higher production rates.

PROVEN PROCESS CAPABILITIES: Al_2O_3 , Y_2O_3 , TiC



CD-87-28890

Figure 13. - Floating-zone fiber drawing process (ref. 18) being procured to develop lab-scale quantities of fiber which exhibit CTE's similar to inter-metallics being considered as matrix materials.

SELF-LUBRICATING COATINGS FOR HIGH-TEMPERATURE APPLICATIONS

Harold E. Sliney

SUMMARY

Solid lubricants with maximum temperature capabilities of about 1100 °C are known. Unfortunately, none of the solid lubricants with the highest temperature capabilities are effective below about 400 °C. However, research at Lewis shows that silver and stable fluorides such as calcium and barium fluorides act synergistically to provide lubrication from below room temperature to about 900 °C. This paper describes plasma-sprayed composite coatings that contain these solid lubricants in combination with a metal-bonded chromium carbide. The lubricants control friction, and the carbide matrix provides wear resistance. Successful tests of these coatings as backup lubricants for compliant gas bearings in turbomachinery and as self-lubricating cylinder liners in a four-cylinder Stirling engine are discussed.

INTRODUCTION

Some present-day aeropropulsion systems already impose severe demands on the thermal and oxidative stability of lubricant, bearing, and seal materials. These demands will be much more severe for systems planned to be operational around the turn of the century. The complex gas turbine engines in modern aircraft contain many variable geometry components with load-bearing surfaces that must be self-lubricating at high temperatures and gas pressures. In hypersonic aircraft of the future, the propulsion systems will also incorporate variable-angle air inlet ramps that will need seal surfaces with the ability to slide with low friction and wear at very high temperatures. In addition, the airframe control surface bearings may see high temperatures and certainly will need to be protected by sliding-contact control surface seals that will be the first line of defense against the temperatures generated by aerodynamic heating at hypersonic velocities.

Conventional solid lubricants such as graphite and molybdenum disulfide (MoS_2) are a class of materials with a layer lattice crystal structure which is ideal for providing the low shear strength associated with low friction. However, these lubricants have very limited high-temperature oxidation resistance. Both graphite and MoS_2 oxidize in air well below 500 °C. Therefore, it is necessary to creatively screen other classes of candidate materials for chemical and physical properties that are likely to afford the necessary combination of chemical stability and lubricity.

A class of materials that possess this combination of properties consists of the fluorides of the alkali metals, especially lithium fluoride (LiF), and the fluorides of the alkaline earth metals, especially barium fluoride (BaF_2)

and calcium fluoride (CaF_2). These compounds are lubricious above their brittle-to-ductile transition temperatures (typically about 500 °C) to just below their melting points, which are LiF , 870 °C; BaF_2 , 1280 °C; and CaF_2 , 1410 °C. Unfortunately, these compounds do not lubricate below their brittle-to-ductile transition temperatures. However, our research shows that a combination of silver (Ag), which is lubricious as a thin film below 500 °C, with the $\text{BaF}_2/\text{CaF}_2$ eutectic acts synergistically to provide lubrication from below room temperature to 900 °C (ref. 1).

This paper describes plasma-sprayed composite coatings that contain these solid lubricants in combination with a Nichrome matrix or with a metal-bonded chromium carbide. Successful tests of these coatings as seal material, as backup lubricants for compliant gas bearings in turbomachinery, and as self-lubricating cylinder liners in a four-cylinder Stirling engine are discussed.

MATERIAL PROPERTIES CONSIDERATIONS

There is clearly a need for high-temperature lubricants in many advanced terrestrial and aerospace applications where the high temperature often precludes the use of conventional liquid lubrication. Figure 1 lists examples of some of these application areas and the associated bearing and seal temperatures.

Conventional solid lubricants such as molybdenum disulfide (MoS_2) and graphite have limited high-temperature capability because they oxidize in air at temperatures below 500 °C. The effect of oxidation on the friction coefficient of MoS_2 is illustrated in figure 2. The sharp rise in the friction coefficient of molybdenum disulfide as the temperature is increased above about 350 °C is caused by oxidation of the solid lubricant to solid molybdenum trioxide and gaseous sulfur oxides. It is therefore clear that a primary criterion for the survivability of high-temperature materials is thermochemical stability. Some physical properties of importance involve the hardness and ductility or plasticity of the candidate material. Properties that effective solid lubricants have in common are the following: (1) they are soft, (2) they have a high degree of plasticity (the plasticity must be associated with a low yield strength in shear for lubricity), and (3) they must exhibit adequate adhesion to the lubricated surfaces. (Obviously, no matter how desirable the other properties of a solid are, that material cannot lubricate if it is not retained at the sliding interface.)

We have used calcium fluoride, barium fluoride, and silver as solid lubricants in our high-temperature coatings. They satisfy all of the above criteria over specific ranges of temperatures. Thermochemical calculations indicate that these materials should be chemically stable to high temperatures in air or in hydrogen, and this has been experimentally verified. The hardness-temperature characteristics of these two fluorides and of metallic silver are given in figure 3(a) from reference 2. Silver is very soft at room temperature with a hardness of about 30 kg/mm^2 , and this continuously decreases to about 4 kg/mm^2 at 800 °C. Thin films of silver lubricate quite well at temperatures up to about 500 °C, but appear to have inadequate film strength to support a load at higher temperatures. The fluorides, on the other hand, are considerably harder than silver at the lower temperatures, but their hardness drops off rapidly with temperature, and at about 400 °C, their hardness is 30 kg/mm^2 or less. Also, brittle-to-ductile transition temperatures, at

high strain rates, of 300 to 400 °C have been reported for these fluorides (refs. 3 to 5). Since fluoride coatings have been shown to become lubricious at about 400 °C, but ineffective as lubricants at lower temperatures (ref. 1), there is an apparent correlation of hardness-temperature characteristics and of the brittle-to-ductile transition temperature with the friction-temperature characteristics.

Because silver films are lubricative at the lower temperatures and the fluorides discussed are lubricative at higher temperatures than silver, it is reasonable that a composite coating containing silver and the fluorides might be lubricious over a wide temperature range, and this has been demonstrated repeatedly in our research (refs. 1 and 6). Figure 3(b) from reference 1 illustrates this point. The friction-temperature characteristics of 0.02-mm-thick, fused fluoride coatings with and without silver, which were prepared by a process similar to porcelain enameling, are compared. The all-fluoride coatings were lubricous only above about 400 °C, while the coatings that also contained silver lubricated from room temperature to 900 °C. These results with relatively thin coatings led to research with plasma-sprayed coatings.

PLASMA-SPRAYED COATINGS

Researchers at Lewis have reported two series of plasma-sprayed coatings containing fluoride solid lubricant: the PS100 and the PS200 series (refs. 6 and 7). The first series contains stable fluorides and silver with a Nichrome binder; the second series contains the same lubricants and chromium carbide with a nickel-cobalt alloy binder. The proportions of the components can be varied to optimize the coatings for various uses. In general, the PS100 series, which is softer, has been useful in applications where a slightly compliant, but nongalling coating is needed. The friction and wear properties of PS100 and PS101 are illustrated in figure 4. The PS100 composition, which contained calcium fluoride as the only lubricant, lubricated above about 400 °C, but not at lower temperatures. The transition from high to low friction and wear corresponded to the brittle-to-ductile transition temperature of calcium fluoride at high shear rates. The addition of silver as the second lubricant in PS101 resulted in a coating with good lubricating properties from -60 to 900 °C. The Nichrome-based coatings exhibited moderate ductility. This property and their good lubricating properties have led to their application in high-temperature, lightly loaded shaft seals. An example of this type of application is the shaft seal shown in figure 5 from reference 8. Wear coefficients k for the PS100 series of coatings are on the order of 10^{-5} mm³/Nm, and the friction coefficient is typically 0.2.

When more wear-resistant coatings are needed, the PS200 series is preferable. The PS200 concept is summarized in figure 6. As the sketch indicates, the coating is a composite material with the lubricating solids distributed throughout a very wear-resistant chromium carbide/nickel alloy matrix. The solid lubricant content can be optimized for a particular set of operating conditions. A typical composition consists of 10 wt % each of silver and calcium fluoride/barium fluoride eutectic in the metal-bonded chromium carbide matrix. Results of friction and wear tests and applications of this coating are given in the following section. Wear coefficients are about one-tenth those of PS100.

APPLICATION TESTS OF PS200 GAS BEARINGS

Figure 7 is a gas bearing journal coated with PS200 and finished by diamond grinding. Start-stop tests of this journal in a foil bearing were conducted by using the test apparatus shown in figure 8 and reported in references 9 and 10. Torque profiles during start-stop cycles show that the highest torque occurs at the beginning and end of each cycle when the surface velocity is below the critical lift-off velocity for the bearing and the journal is in sliding contact with the bearing foils. Foil bearings with PS200 coated journals have routinely survived durability tests consisting of 9000 starts and stops (18 000 rubs) at preprogrammed bearing temperatures from 25 to 650 °C, and have not failed in long duration life tests of up to 30 000 start/stop cycles. Therefore, the bearing life is determined by the number of start/stop cycles it can survive before the lubricant coating fails or excessive foil wear occurs.

Typical wear data for Inconel X-750 bearing foils are given in figure 9. Data are compared for foils run against a journal coated with PS200 and one coated with metal-bonded chromium carbide with no solid lubricant additions. The foils run against the unmodified coating were worn excessively after 3000 start/stop cycles, while those run against PS200 easily survived a specified 9000 start/stops. The initial run-in wear rate against PS200 levels off to a very low steady-state value, thus providing much longer bearing life than could be predicted by a linear extrapolation of the wear rate during run-in.

STIRLING ENGINE CYLINDER LINER

PS200 was evaluated as a cylinder liner coating for an automobile Stirling engine. This was part of the DOE/NASA Automotive Stirling Engine Project. The lubrication of the piston ring/cylinder contacts in the Stirling engine is a challenging high-temperature tribological problem. Metal temperatures are as high as 600 to 1000 °C near the top of the cylinder walls. The working fluid in the engine thermodynamic cycle is hydrogen. The lubricant coating, therefore, must not only provide low friction and wear, but also must be thermochemically stable in a strongly reducing hydrogen atmosphere. Friction measurement, employing a pin-on-disk wear test machine, showed that a cobalt alloy, Stellite 6B, is a good counterface material in sliding contact with PS200. The friction coefficients for 6B on PS200 in helium and in hydrogen are summarized in figure 10. Friction coefficients were typically 0.2 in hydrogen from room temperature to 760 °C and considerably lower than measured for a baseline chromium carbide coating with no solid lubricant additions.

In current designs of the Stirling engine, the piston rings are made of reinforced polytetrafluoroethylene (PTFE). They are located in ring grooves near the bottom of the piston where the temperatures are relatively low and do not degrade the PTFE. This arrangement results in a long, annular gap from the top of the piston to the piston ring. This gap, known as the appendix gap, is the source of parasitic energy losses (ref. 11). It therefore would be desirable to minimize the appendix gap by locating the top ring in a groove near the top of the piston. A schematic of the ring locations in the baseline piston and in a piston with an added Stellite 6B hot ring are shown in figure 11.

A four-cylinder automotive Stirling engine was used in an engine test reported in reference 12 (fig. 12). The cylinders were bored out to allow for a PS200 coating thickness of 0.25 mm (0.010 in), and the pistons were modified to accept the hot piston rings. The coatings were sprayed on the cylinder walls to a thickness of about 0.35 mm (0.015 in), then were diamond ground to a final thickness of 0.25 mm. Engine tests were run at 700 °C heater head temperature and 5, 10, and 15 MPa mean operating pressures over a range of operating speeds. Tests were run both with the hot rings in place and without them to provide a baseline for comparison. At some operating conditions, efficiency as indicated by specific fuel consumption increased up to 7 percent compared to the baseline engine. Under other conditions, no significant differences in efficiency were measured. The overall average indicated about a 3-percent increase in efficiency with the hot rings over the baseline configuration. This increase was over and above the friction loss introduced by the hot rings. Seal leakage measurements showed a significant reduction in leakage with the hot ring in place. In addition, cylinder wall temperature measurements indicated less cylinder heating in the appendix gap area between the lower piston rings and the hot ring. Approximately 22 hr of ring-on-coating operation was recorded. After the initial break-in period, ring and coating wear were low. Although this application test involved an automobile engine, the results of this program are relevant to sliding contact seals and bearings in aeropropulsion systems. The results are especially relevant to the hydrogen-fueled engine being considered for hypersonic aircraft of the future.

CONCLUDING REMARKS

This paper reviews some of the tribological research at NASA Lewis Research Center that is relevant to the lubrication of high-temperature aeropropulsion sliding contact bearings and seals with solid lubricants. The most significant conclusions are

1. Certain materials properties can be used to establish a qualitative model for predicting whether or not a chemical element or compound is likely to have solid lubrication capability within a given temperature range. The required properties are plasticity, low yield strength in shear, low hardness, and thermochemical stability at the temperatures and in the environment of interest.
2. For solid materials that lubricate only at elevated temperatures, the onset of lubrication appears to correlate with their brittle-to-ductile transition temperatures.
3. Some combinations of two or more solid lubricants, each with different temperature capabilities, can be incorporated into composites with a broader temperature capability than that of any single solid lubricant.

A recently developed coating employing this concept is PS200. This is a plasma-sprayed composite coating in which silver and barium fluoride/calcium fluoride eutectic are dispersed throughout a matrix of metal-bonded chromium carbide. Silver alone is lubricative to about 500 °C, while the fluorides are lubricative from 400 to 900 °C. The combination in this coating lubricates from room temperature to 900 °C.

REFERENCES

1. Sliney, H.E.: The Use of Silver in Self-Lubricating Coatings for Extreme Temperatures. ASLE Trans., vol. 29, no. 3, July 1986, pp. 370-376.
2. Deadmore, D.L.; and Sliney, H.E.: Hardness of CaF_2 and BaF_2 Solid Lubricants at 25 to 670 °C. NASA TM-88979, 1987.
3. Phillips, W.L., Jr.: Deformation and Fracture Processes in Calcium Fluoride Single Crystals. J. Am. Ceram. Soc., vol. 44, no. 10, Oct. 1961, pp. 499-506.
4. Burn, R.; and Murray, G.T.: Plasticity and Dislocation Etch Pits in CaF_2 . J. Am. Ceram. Soc., vol. 45, no. 5, Nov. 1962, pp. 251-252.
5. Liu, T.S.; and Li, C.H.: Plasticity of Barium Fluoride Single Crystals. J. Appl. Phys., vol. 35, no. 11, Nov. 1964, pp. 3325-3330.
6. Sliney, H.E.: Wide Temperature Spectrum Self-Lubricating Coatings Prepared by Plasma Spraying. Thin Solid Films, vol. 64, 1979, pp. 211-217.
7. DellaCorte, C.; and Sliney, H.E.: Composition Optimization of Self-Lubricating Chromium-Carbide-Based Composite Coatings for Use to 760 °C. ASLE Trans., vol. 30, no. 1, Jan. 1987, pp. 77-83.
8. Sliney, H.E.: Status and New Directions for Solid Lubricant Coatings and Composite Materials. Tribology in the 80's, NASA CP-2300, Vol. 2, 1984, pp. 665-680.
9. Wagner, R.C.; and Sliney, H.E.: Effects of Silver and Group II Fluoride Solid Lubricant Additions to Plasma-Sprayed Chromium Carbide Coatings for Foil Gas Bearings to 650 °C. Lubr. Eng., vol. 42, no. 10, Oct. 1986, pp. 594-600.
10. DellaCorte, C.: Composition Optimization of Chromium Carbide Based Solid Lubricant Coatings for Foil Gas Bearings at Temperatures to 650 °C. NASA CR-179649, 1987.
11. Tomazic, W.A.: Stirling Engine Supporting Research and Technology. NASA TM-87175, 1985.
12. Allen, D.J.; and Tomazic, W.A.: Hot Piston Ring Tests. DOE/NASA/50112-72, NASA TM-100256, 1987.

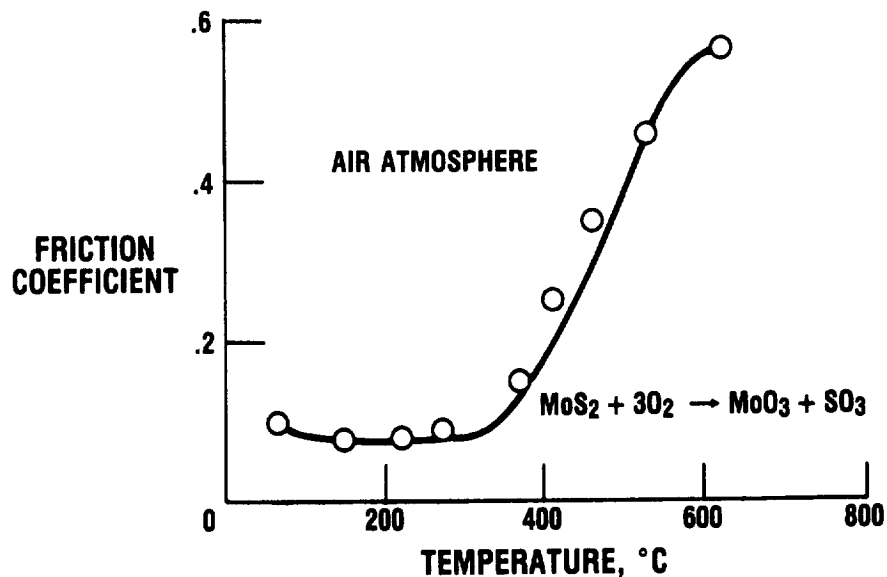
CURRENT AND FUTURE NEEDS FOR HIGH-TEMPERATURE SOLID LUBRICANTS

**TEMPERATURE,
°C**

• AIRCRAFT GAS TURBINE ENGINES	
VARIABLE STATOR-VANE BUSHINGS	
COMPRESSORS—CURRENT	350
TURBINES—NEAR FUTURE	1000
THRUST-REVERSAL BEARINGS	800
• SUPERSONIC AIRCRAFT (MACH 3-5)	
CONTROL-SURFACE BEARINGS	350
CONTROL-SURFACE RUB SEALS	650
• HYPERSONIC AIRCRAFT	
CONTROL-SURFACE RUB SEALS	500-2000
• ROTARY ENGINES FOR GENERAL AVIATION	
APEX SEALS	300-650
• ADIABATIC DIESEL CYLINDER LINERS	600-1100
• STIRLING ENGINES	760-1100
• AUTOMOTIVE GAS TURBINE ENGINES	
REGENERATOR WEAR FACE SEALS	260-1100
FOIL BEARINGS (MAIN SHAFT)	650

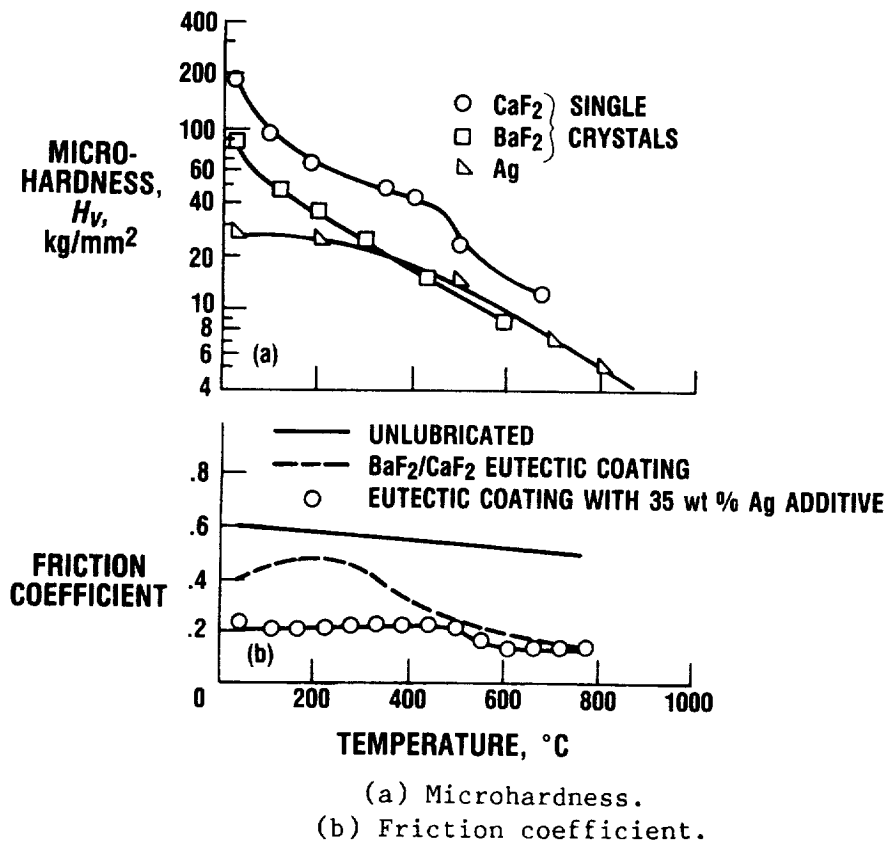
CD-87-28704

Figure 1. - Applications for high-temperature solid lubricants.



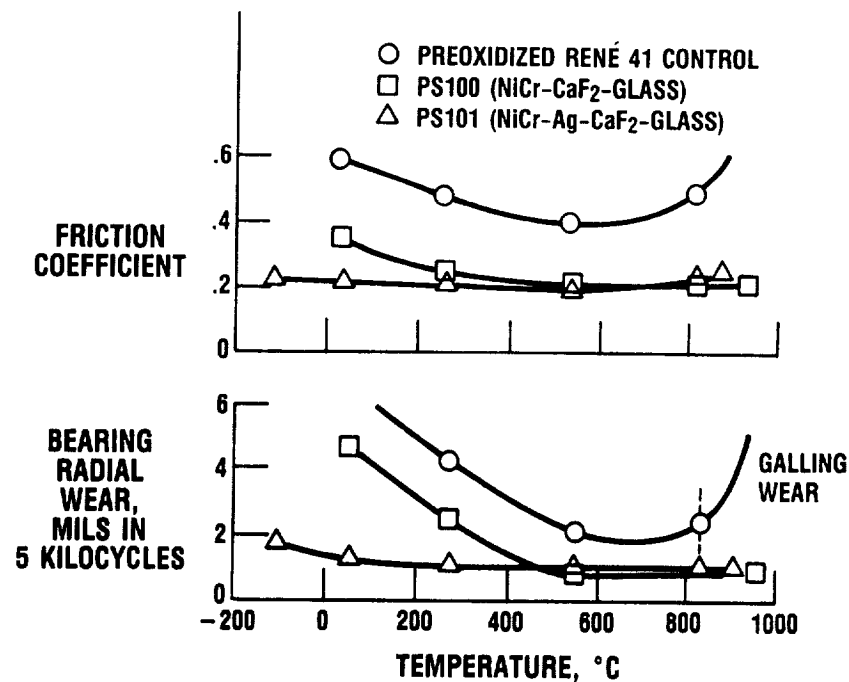
CD-87-28705

Figure 2. - Effect of oxidation on lubrication with molybdenum disulfide.



CD-87-28708

Figure 3. - Effect of temperature on microhardness and friction coefficients of coating materials.



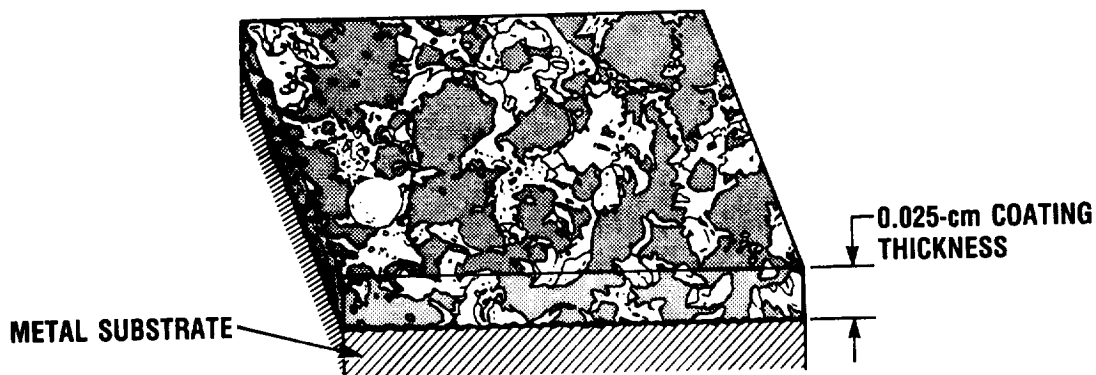
CD-87-28707

Figure 4. - Plasma-sprayed coatings for self-aligning oscillating bearings (34-MPa radial load).



CD-87-28706

Figure 5. - Compressor/turbine shaft seal operates at 650 °C.



COMPOSITION

FUNCTION

32% Ni ALLOY
48% Cr₃C₂

WEAR AND OXIDATION RESISTANCE

10% Ag

LOW-TEMPERATURE LUBRICATION

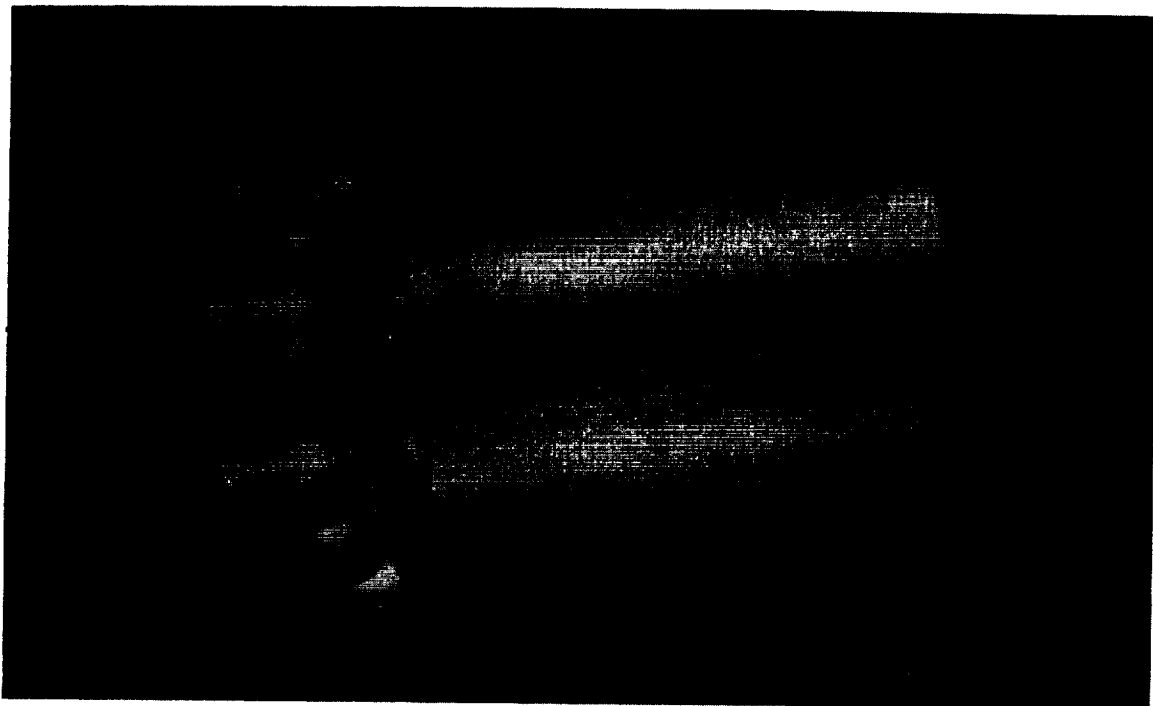
10% BaF₂/CaF₂
EUTECTIC

HIGH-TEMPERATURE LUBRICATION

• LUBRICATES IN AIR, HELIUM, OR HYDROGEN TO -900 °C

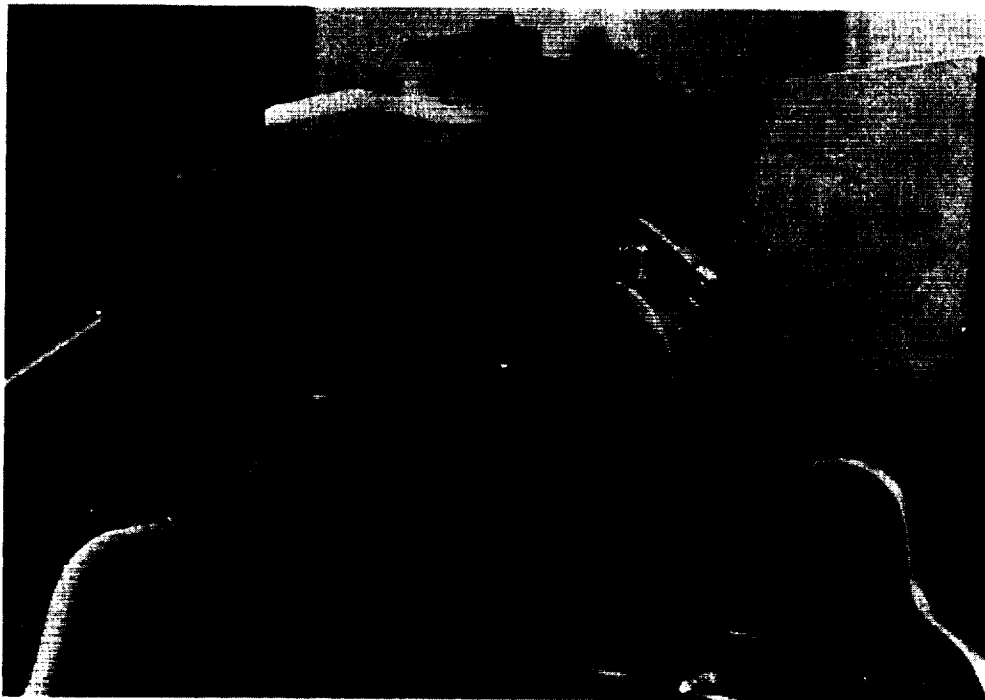
CD-87-28709

Figure 6. - The concept of PS200 - a plasma-sprayed composite solid lubricant coating.



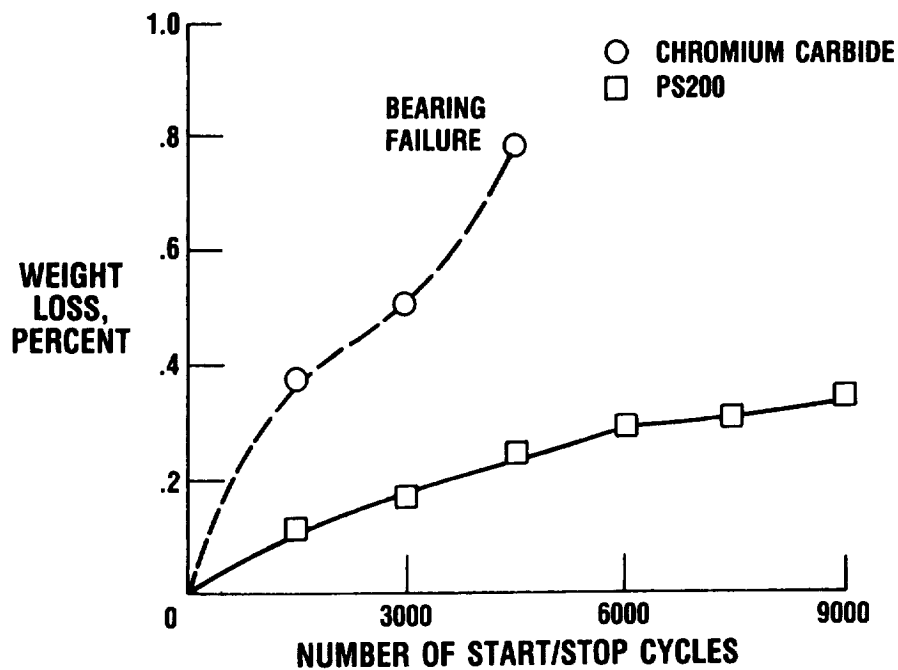
CD-87-28710

Figure 7. - Gas bearing journal coated with PS200 and finished by diamond grinding.



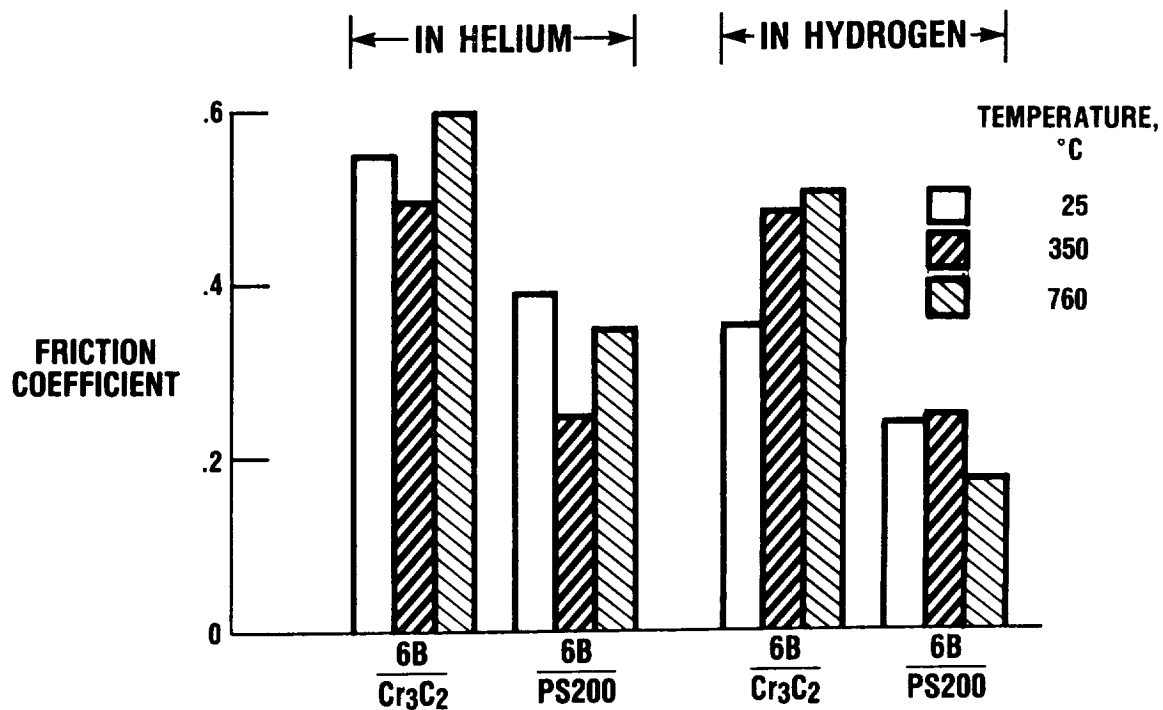
CD-87-28711

Figure 8. - Foil bearing under test at 700 °C.



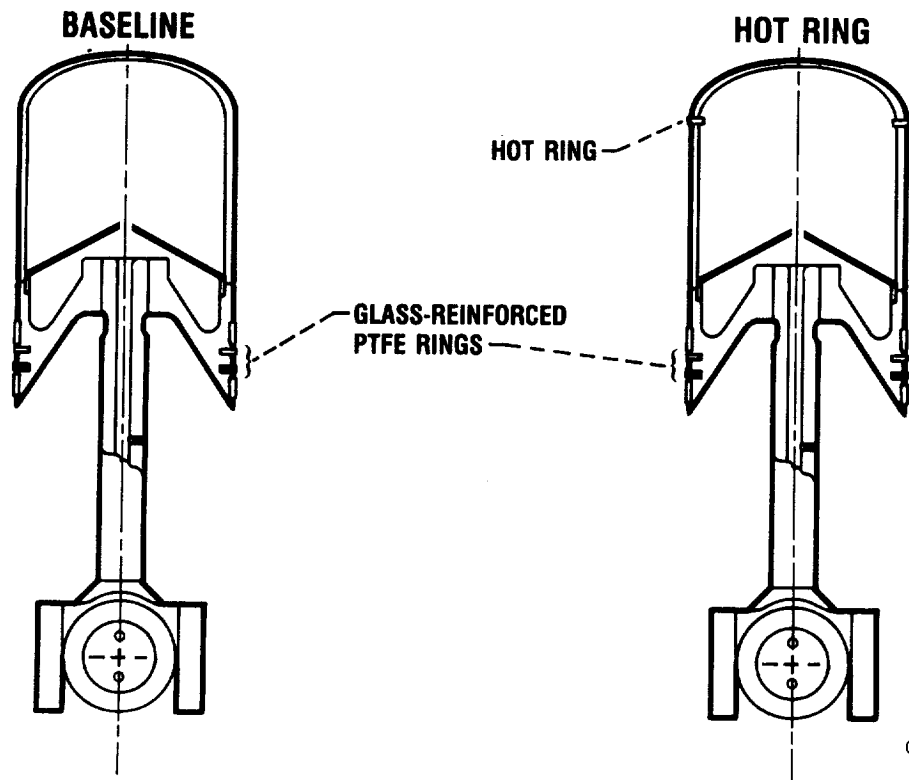
CD-87-28712

Figure 9. - Wear profiles of preoxidized Inconel X-750 foil bearings run against journals lubricated with plasma-sprayed chromium carbide or PS200.



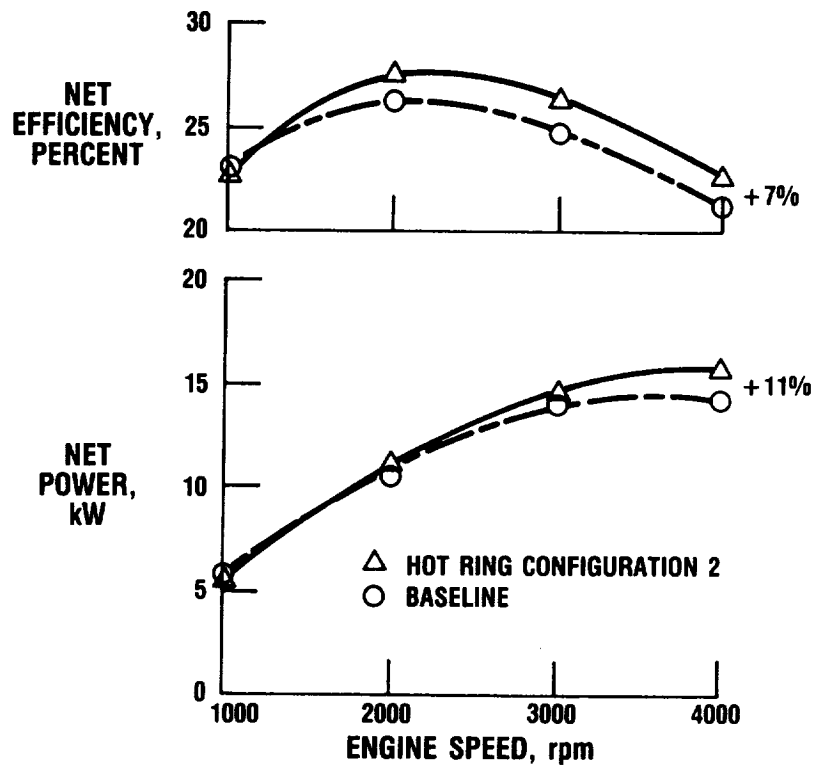
CD-87-28713

Figure 10. - Bonded chromium carbide and PS200 in Stirling engine atmospheres.



CD-87-28715

Figure 11. - Application example: Stirling engine hot piston ring tests.



CD-87-28714

Figure 12. - Results of hot piston ring tests.

CERAMICS FOR ENGINES

James D. Kiser,
Stanley R. Levine,
and
James A. DiCarlo

SUMMARY

The NASA Lewis Research Center's Ceramic Technology Program is focused on aerospace propulsion and power needs. Thus, emphasis is on high-temperature ceramics and their structural and environmental durability and reliability. The program is interdisciplinary in nature with major emphasis on materials and processing, but with significant efforts in design methodology and life prediction.

INTRODUCTION

Structural ceramics have been under nearly continuous development for various heat engine applications since the early 1970's (refs. 1 to 4). These efforts have been sustained by the unique properties that ceramics offer in the areas of high-temperature strength, environmental resistance, and low density, and the large benefits in system efficiency and performance that can result. The results of recent studies of potential ceramic applications in small aeropropulsion engines (ref. 5) have revealed that substantial benefits are possible over current engine technology. As shown in figure 1, small gains can be obtained via improved aerodynamic and cycle efficiency. Much larger benefits are possible by going to a regenerated cycle or by going to an uncooled hot section. Both of these approaches require ceramics (i.e., a ceramic regenerator for weight considerations and ceramic hot section components to overcome the need for hot section component cooling). An engine that uses both a regenerated cycle and an uncooled hot section would achieve optimum fuel efficiency.

But the promise of ceramics has not been realized because of their brittle nature, which results in high sensitivity to microscopic flaws and catastrophic fracture behavior. This has translated into low reliability for ceramic components and thus limited application in engines. For structural ceramics to successfully make inroads into the terrestrial heat engine market, further advances are necessary in net shape fabrication of components with greater reliability and lower cost (fig. 2). The cost constraint as well as technical constraints currently dictate use of monolithic or possibly particulate or whisker-toughened ceramics. Improvements in properties such as toughness, strength, lubricity, and durability may also be needed for specific applications. These advances in technology will lead to very limited use of ceramics in noncritical applications in aerospace engines. For critical

aerospace applications, an additional requirement is that the ceramics display markedly improved toughness and noncatastrophic (i.e., graceful) fracture.

STRUCTURAL CERAMICS APPLICATIONS

The engines shown in figure 3 contain ceramic components that were developed in the Advanced Gas Turbine (AGT) Development Project. This program was funded by the U.S. Department of Energy and managed by the NASA Lewis Research Center (refs. 6 and 7). These all-ceramic hot gas flowpath engines are being considered as alternatives to conventional piston engines in automobiles. Complex structural ceramic components were fabricated and tested, and improvements in the areas of design methodology and life prediction were achieved. The technology from this program (which was completed in 1987) and its continuation, the Advanced Turbine Technology Applications Program (ATTAP), will help make it possible for ceramics to ultimately be used in automotive engines and provide part of the technology base for some aerospace applications.

CERAMIC TECHNOLOGY PROGRAM

The Ceramic Technology Program at NASA Lewis is focused on aerospace propulsion and power needs. Thus, emphasis is on high-temperature use of ceramics and on their structural and environmental durability and reliability. The objective of our Ceramic Technology Program is to identify and develop ceramics and ceramic composites with strength, toughness, reliability, and durability sufficient for use at temperatures to 1650 °C (3000 °F) and above in future advanced aerospace propulsion and power systems. The program is interdisciplinary, with major emphasis on materials and processing, but with significant efforts in design methodology and life prediction:

- (1) Materials and processing
 - (a) Reliable, tough ceramics
 - (b) Fiber-reinforced ceramics
 - (c) Advanced ceramic fibers
 - (d) Wear-resistant and low friction coatings
- (2) Design methodology
 - (a) Brittle materials design code
 - (b) Friction and wear data
- (3) Life prediction
 - (a) Environmental effects
 - (b) Nondestructive evaluation
 - (c) Fracture and fatigue
 - (d) Time-dependent behavior

About 35 researchers in the Materials and Structures Divisions are involved in the project. Strong interactions between researchers involved in

materials efforts and nondestructive evaluation (NDE), corrosion, fracture, and design methodology have led to successful collaborations (refs. 8 to 13).

APPROACHES TO CERAMIC RELIABILITY

Two basic forms of reliability can be defined for ceramics. The first is a statistical reliability, as illustrated in figure 4. Ceramics typically display a broad distribution of strengths. In the inspection approach to reliability, we would separate unacceptable parts by NDE and proof testing and would reject them. A more efficient and cost effective approach lies in improved processing that increases strength and yields no defective parts.

We define the second form of reliability as functional reliability because it relates to how well a component performs its function during system assembly and service. Thus, factors such as fracture toughness, impact resistance, and failure mode (graceful versus catastrophic) need to be considered. Specific approaches to improved functional reliability include the addition of particulate and whisker phases which can improve fracture toughness, and the addition of continuous fibers which can both improve toughness and provide a noncatastrophic failure mechanism. This brings us into the realm of engineered microstructures (i.e., composites).

MONOLITHIC AND TOUGHENED CERAMICS

Current NASA Lewis materials, design, and life prediction research is focused on SiC and Si₃N₄, since these materials offer the desired combination of high-temperature strength, thermal shock resistance, and environmental durability. We are concluding efforts on monolithic SiC and Si₃N₄ reliability improvement. Future efforts are being focused on determining the potential of these materials for use in the 1300 to 1600 °C range. This requires improvements in strength and toughness and an understanding of how these improvements translate into use potential. These efforts are synergistic with our effort in fiber-reinforced ceramics, where our major emphasis is on SiC and Si₃N₄ materials (for matrix and fiber reinforcement applications).

Some recent progress at NASA Lewis in improving the strength of monolithic silicon carbide (ref. 14) is illustrated in figure 5. Materials fabricated by dry pressing or slurry pressing, followed by sintering at 2200 °C for 30 min have four-point flexural strengths of about 345 and 414 MPa, respectively. Hot-isostatic pressing tantalum-encapsulated, green, slurry-pressed specimens at 1900 °C for 30 min under 138 MPa argon pressure improves strength to about 552 MPa while achieving the same density. This densification at a much lower temperature yields a much finer grain size and a shift in the strength-limiting flaw from internal defects, such as pores and agglomerates, to surface machining defects. Improvements are being sought to reduce sensitivity to surface flaws. Annealing in air has proven successful, and improved fracture toughness from the addition of particulates or whiskers is expected to be beneficial.

In the area of monolithic silicon nitride processing, an improved NASA 6Y (6 wt % Y₂O₃) sintered Si₃N₄ composition was realized by iterative utilization of conventional x-radiography to characterize structural (density) uniformity as affected by systematic changes in powder processing and sintering parameters

(ref. 15). As shown in figure 6, four-point flexural strength was improved 56 percent, and the standard deviation was reduced by more than a factor of three. Correlated with these improvements were improved microstructures and a change in critical flaw character from processing flaws such as voids to large grains, as shown by the fractographs at the lower left and right of figure 6, respectively.

NASA has supported major contract research efforts to improve the statistical reliability and strength of silicon nitride (Garrett Ceramic Components Division) and silicon carbide (Ford Motor Co.) via improved processing centered about injection molding. Both efforts have made good progress toward the goals of 100-percent improvement in Weibull modulus and 20-percent improvement in strength (refs. 14 and 16). The effort at Garrett is essentially complete. One Garrett accomplishment, as shown in figure 7, was the development of material GN-10, which appears to have significantly advanced the state of the art for Si_3N_4 in terms of both room- and elevated-temperature strength.

An interdisciplinary toughened ceramics life prediction project has been initiated at NASA Lewis. The objective of this research is to understand the room- and high-temperature behavior of toughened ceramics, especially SiC whisker-toughened Si_3N_4 , as the basis for developing a life prediction methodology. A major goal is to determine material behavior as a function of time, temperature, and whisker content. A second major objective is to understand the relationship between microstructure and mechanical behavior. These results will be used in materials development and design methodology development. Resultant design codes will be verified.

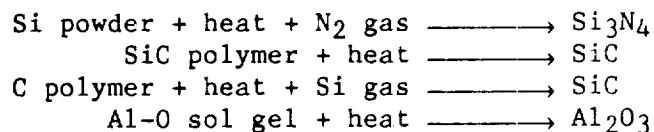
Fiber-Reinforced Ceramics

Improved strength, toughness, and reliability can be achieved by incorporating continuous ceramic fibers into a ceramic matrix. Reinforcing with ceramic fibers having a modulus and ultimate strength greater than the monolithic ceramic used as the matrix material yields ceramic composites with greater stiffness and greater strength at first matrix cracking. If small-diameter fibers are used, matrix crack propagation can be delayed by the bridging mechanism depicted in figure 8. This results in matrix failure for the composite at a stress and strain level higher than for the monolithic ceramic. If the fiber-matrix interfacial bonding is optimum, matrix cracks propagate around the fibers and not through them. Once matrix cracks start to form, they occur at a regular spacing. The ceramic is then held together by the load carrying capacity of the fibers until they begin to fracture in a statistical manner. The net result for a tough ceramic composite is that a metallike stress-strain curve is displayed with first-matrix cracking stress corresponding to the yield stress of metals and fiber fracture corresponding to the ultimate strength. Thus, fiber-reinforced ceramics fail in a graceful manner, rather than catastrophically.

The processing of fiber-reinforced composites is more difficult than the processing of monolithic ceramics. Also, available fibers for high-temperature (1400 °C) ceramic matrix composites are limited, and the proper fiber-matrix bond must be maintained in fabrication as well as during the life of the composite. Too strong a bond yields a loss in toughness and a reversion to

monolithic ceramic behavior, while too weak a bond yields loss in stiffness, strength, and toughness.

The focus of current NASA Lewis research in fiber-reinforced ceramics (FRC) is on the development of fabrication approaches that yield good matrix properties and can be carried out with minimal degradation of fiber strength. Four approaches that are being pursued are listed as follows:



Each process has a specific advantage. The reaction-bonded Si_3N_4 matrix has excellent strength, the use of SiC- or C-yielding polymers can provide low-cost processing (ref. 17) or tailorable matrix capability, and an Al_2O_3 matrix (with oxide fiber reinforcement) would provide excellent oxidation resistance. Extension of the capability of FRC via development of advanced fibers and fiber coatings is a second area of focus. Effort is focused on identifying and developing high-strength fibers (ref. 18), especially those with the potential for use at temperatures greater than 1650 °C (3000 °F). Environmental protection through coatings and control of the fiber-matrix bond are also being evaluated. The third area of focus is assessment of FRC capability to perform in applications such as NASP and rocket propulsion systems. These efforts thus focus on key issues associated with each application, such as process scale-up to enable component fabrication, compatibility with the environment, and resistance to thermal shock.

The fabrication sequence, microstructure, and mechanical properties of a strong and tough SiC fiber-reinforced, reaction-bonded silicon nitride composite recently developed at NASA Lewis are summarized in figure 9. Silicon and SiC fiber monotapes are interleaved and subjected to a mild hot-pressing step to burn out the binder and provide some green strength (ref. 19). The composite is then nitrided to convert the silicon to Si_3N_4 . The resultant composite microstructure contains high levels of porosity, particularly between fibers. In four-point flexural testing, the composite exhibits a first matrix cracking strength comparable to typical monolithic reaction-bonded silicon nitride (RBSN) even though the matrix density at 2.0 g/cm³ is far lower than that of monolithic RBSN. The ultimate strength of the composite is more than twice that of a typical RBSN at both 23 and 40 percent fiber loading. Further, the high-temperature strength of this SiC/RBSN composite exceeds that of various commercial ceramics. In figure 10, four-point bend strengths for the NASA Lewis SiC/RBSN composite at room temperature, 1200 °C (2200 °F), and 1400 °C (2550 °F) are compared with data for the following commercially available ceramic materials: fully dense, hot-pressed Si_3N_4 , reaction-bonded Si_3N_4 , and SEP SiC/SiC composite (one-dimensional). At elevated temperature, 23 vol % SiC/RBSN is stronger than both monolithics and more than twice as strong as the SEP SiC/SiC composite.

Tensile stress-strain data and fracture behavior of 30 vol % SiC/RBSN composites (ref. 20) are illustrated in figure 11. An additional strain occurs after matrix fracture at about 0.12 percent strain. The stress at failure is much higher than for first matrix cracking. The fracture surface exhibits the moderate fiber pullout required for achieving a strong, tough ceramic matrix composite. It is expected that with the development of high

strength, smaller diameter SiC fibers, the fracture properties of the SiC/RBSN will improve significantly.

An example of studies aimed at improved ceramic fibers is a recent in-house study of post-processing of Nicalon SiC fibers (ref. 21). This research involved high-temperature/high-pressure treatments of Nicalon in an attempt to determine if the fiber properties could be improved or stabilized. Results are summarized in figure 12. Treatment under 1360 atm argon results in about a 300 °C increase in the maximum exposure temperature (for avoiding excessive strength degradation). This effect is transitory in nature. Thus, exposure to high temperature at 1 atm after pressure treatment gives the same results as exposure of a virgin fiber. However, if high-temperature exposure is necessary only for processing of the composite, the pressure treatment approach may have significant merit.

CONCLUDING REMARKS

For ceramics to achieve their promise in advanced aerospace applications, reliable and economical fabrication processes must be developed for monolithic, whisker-toughened, and fiber-reinforced ceramics and their constituents. In addition, a basic understanding of the materials science of ceramics is required for the development of processing, design, and life prediction methodologies that will enable ceramics to be used. NASA Lewis is actively pursuing all of these goals through our integrated multidisciplinary Ceramics Technology Program.

REFERENCES

1. McLean, A.F.: Ceramics in Small Vehicular Gas Turbines. Ceramics For High Performance Applications, J.J. Burke, A.E. Gorum, and R.N. Katz, eds., Brook Hill Publishing Company, Chestnut Hill, MA, 1974, pp. 9-36.
2. Katz, R.N.: Ceramics For Vehicular Engines: State-of-the-Art. AMMRC-MS-80-2, June 1980. (Avail. NTIS, AD-A087589.)
3. Pascucci, M.R.: The Role of Ceramics in Engines - An Assessment. Metals and Ceramics Information Center, Current Awareness Bulletin, Issue 126, Aug. 1983, pp. 1-4.
4. Helms, H.E.: Ceramic Applications in Turbine Engines. Ceramics for High-Performance Applications III: Reliability, E.M. Lenoe, R.N. Katz, and J.J. Burke, eds. Plenum Press, New York, 1983, pp. 151-172.
5. Vanco, M.R.; Wintucky, W.T.; and Niedzwiecki, R.W.: An Overview of the Small Engine Component Technology (SECT) Studies. AIAA Paper 86-1542, June 1986. (NASA TM-88796.)
6. Helms, H.E.; Johnson, R.A.; and Grosseclose, L.E.: AGT 100 Advanced Gas Turbine Technology Project. Proceedings of the 22nd Automotive Technology Development Contractors' Coordination Meeting, Society of Automotive Engineers, Warrendale, PA, 1984, pp. 359-365.

7. Kidwell J.R.; and Kreiner, D.M.: AGT 101 Advanced Gas Turbine Technology Development Project. Proceedings of the 22nd Automotive Technology Development Contractors' Coordination Meeting, Society of Automotive Engineers, Warrendale, PA, 1984, pp. 345-357.
8. Klima, S.J.: NDE for Heat Engine Ceramics. NASA TM-86949, 1984.
9. Baaklini, G.Y.; Kiser, J.D.; and Roth, D.J.: Radiographic Detectability Limits for Seeded Voids in Sintered Silicon Carbide and Silicon Nitride. Adv. Ceram. Mater., vol. 1, no. 1, Jan. 1986, pp. 43-49.
10. Roth, D.J., et al.: Reliability of Void Detection in Structural Ceramics by Use of Scanning Laser Acoustic Microscopy. Mater. Eval. vol. 44, no. 6, May 1986, pp. 762-769.
11. Jacobson N.S.; and Smialek, J.L.: Hot Corrosion of Sintered α -SiC at 1000 °C. J. Am. Ceram. Soc., vol. 68, no. 8, Aug. 1985, pp. 432-439.
12. Fox, D.S.; Jacobson, N.S.; and Smialek, J.L.: The Molten Salt Corrosion of SiC and Si₃N₄. Proceedings of the 24th Automotive Technology Development Contractors' Coordination Meeting, SAE, 1986, pp. 163-172.
13. Smialek, J.L.; Fox, D.S.; and Jacobson, N.S.: Hot Corrosion Attack and Strength Degradation of SiC and Si₃N₄. Environmental Degradation of Materials III, M.R. Louthan, R.P. McNitt, and R.D. Sisson, eds., Pennsylvania State University, University Park, PA, 1987, pp. 69-80.
14. Levine, S.R., et al.: Improved Processing of SiC and Si₃N₄. Proceedings of the 24th Automotive Technology Development Contractors' Coordination Meeting, SAE, 1986, pp. 299-311.
15. Sanders, W.A.; and Baaklini, G.Y.: Correlation of Processing and Sintering Variables with the Strength and Radiography of Silicon Nitride. Ceram. Eng. Sci. Proc., vol. 7, no. 7-8, July-Aug. 1986, pp. 839-859. (NASA TM-87251.)
16. Yeh, H; Fang, H.; and Teng, K.: Process Improvement for Si₃N₄ for Heat Engine Applications. Ceram. Eng. Sci. Proc., vol. 9, no. 9-10, Sept.-Oct. 1988, pp. 1333-1342.
17. Hurwitz, F.I., et al.: Silsesquioxanes as Precursors to Ceramic Composites. Ceram. Eng. Sci. Proc., vol. 8, no. 7-8, July-Aug. 1987, pp. 732-743. (NASA TM-89893.)
18. DiCarlo, J.A.: Fibers for Structurally Reliable Metal and Ceramic Composites. J. Met., vol. 37, no. 6, June 1985, pp. 44-49.
19. Bhatt, R.T.: Mechanical Properties of SiC Fiber-Reinforced Reaction-Bonded Si₃N₄ Composites. NASA TM-87085, 1985.
20. Bhatt, R.T.; and Phillips, R.H.: Laminate Behavior for SiC Fiber-Reinforced Reaction-Bonded Silicon Nitride Matrix Composites. NASA TM-101350, 1988.
21. Jaskowiak, M.H.: Effects of High Pressure Nitrogen Treatment on the Thermal Stability of SiC Fibers. Presented at the Silicon Carbide Symposium, Columbus, OH, Aug. 2-5, 1987.

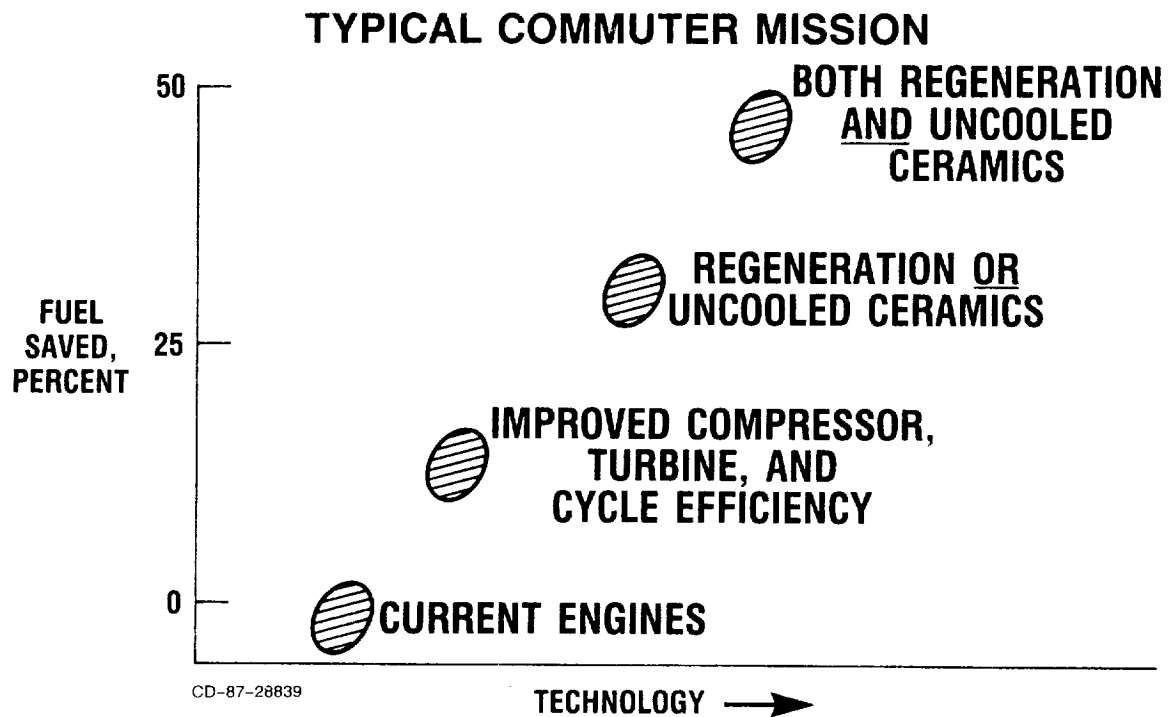


Figure 1. - Technology benefits from ceramics.

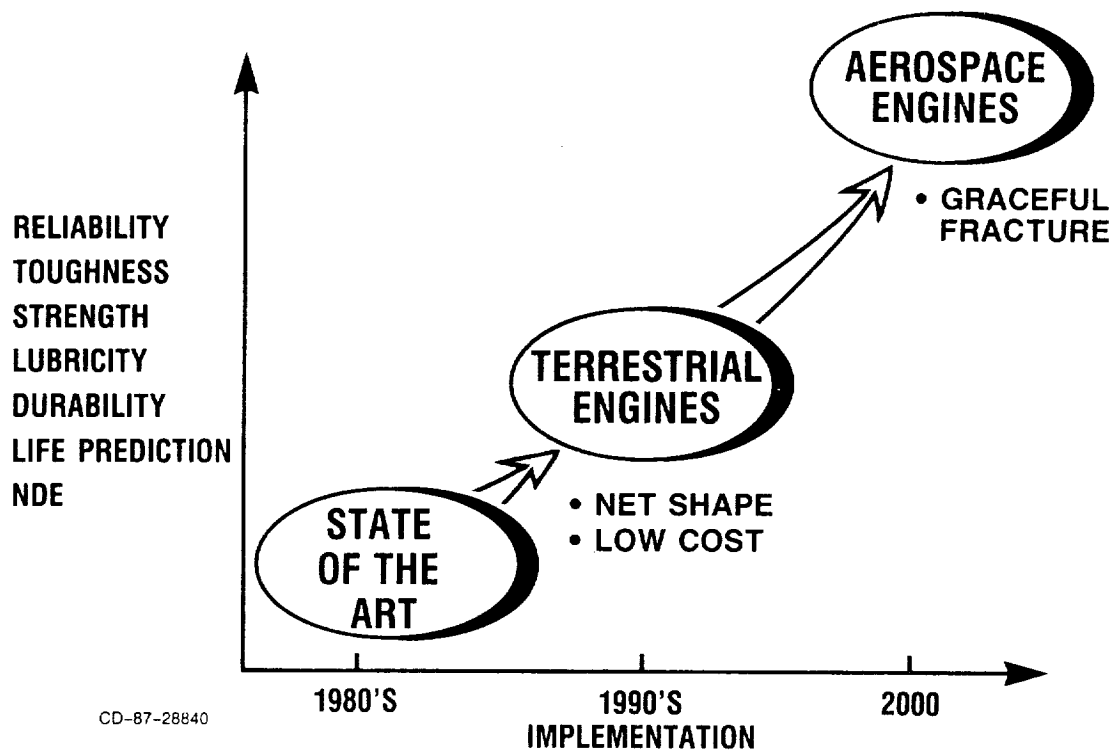
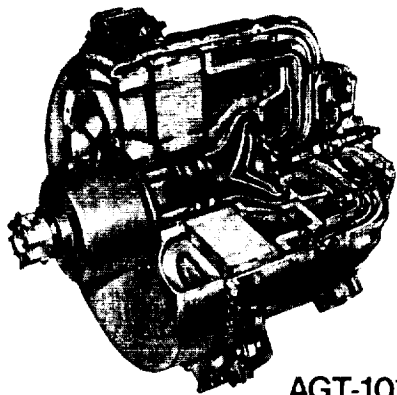


Figure 2. - Ceramic technology needs.



AGT-101



AGT-100

CD-87-28838

Figure 3. - All-ceramic hot gas flowpath engines are being considered as alternative to conventional piston engines in automobiles.

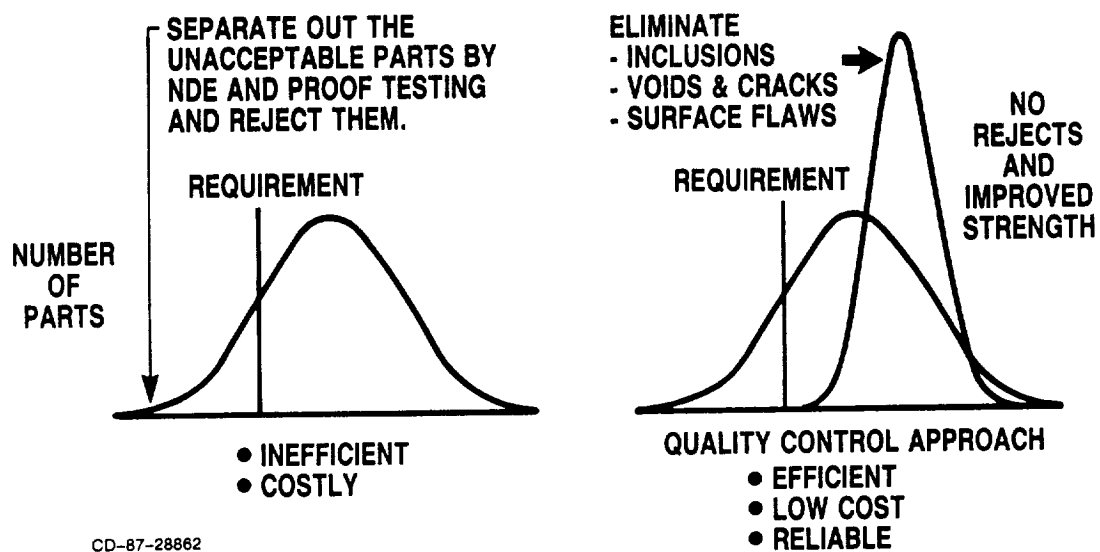
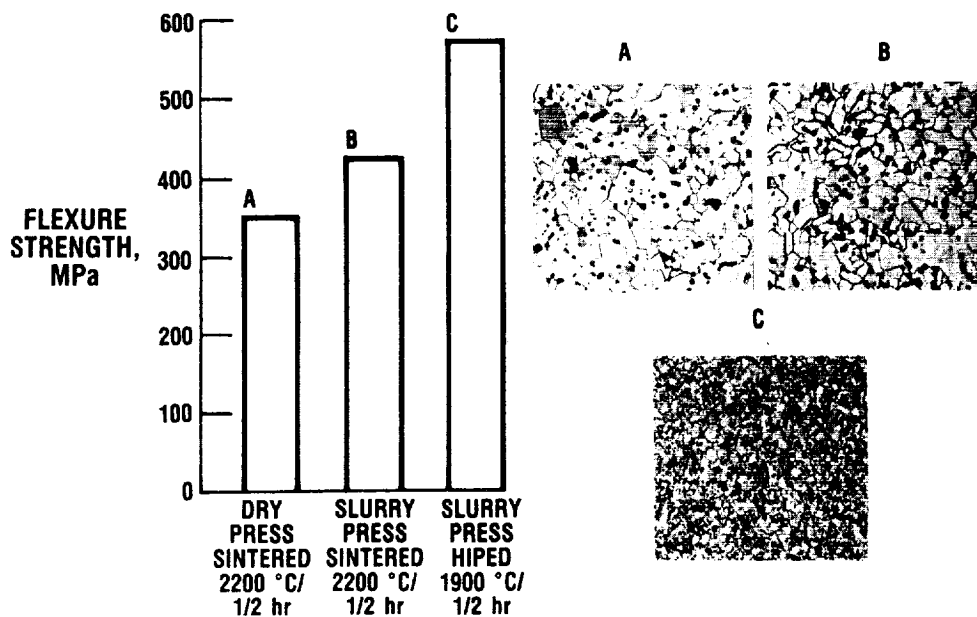
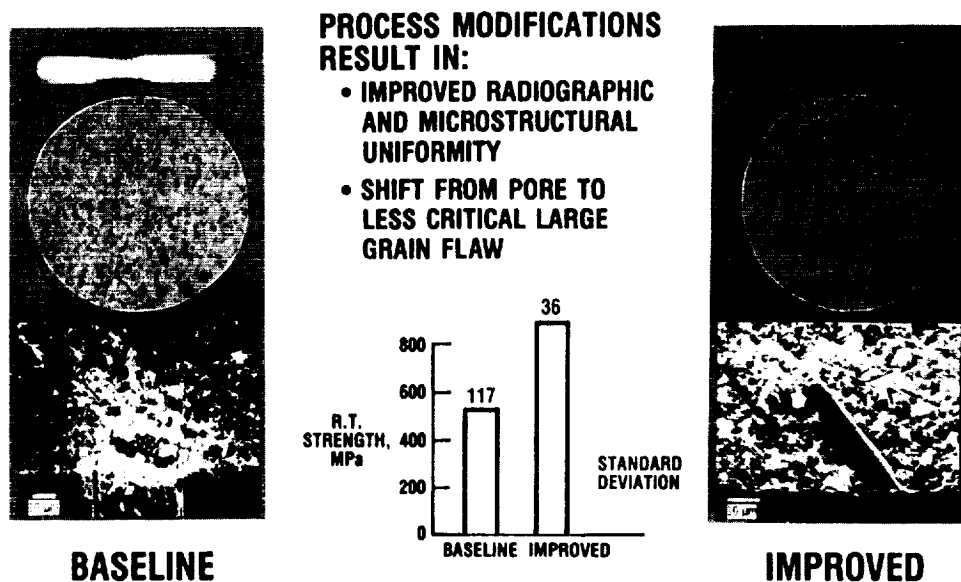


Figure 4. - Approaches to ceramic reliability.



CD-87-28864

Figure 5. - Improved silicon carbide by hot-isostatic pressing.



CD-87-28865

Figure 6. - NASA 6Y sintered silicon nitride improved by radiographically-guided processing changes.

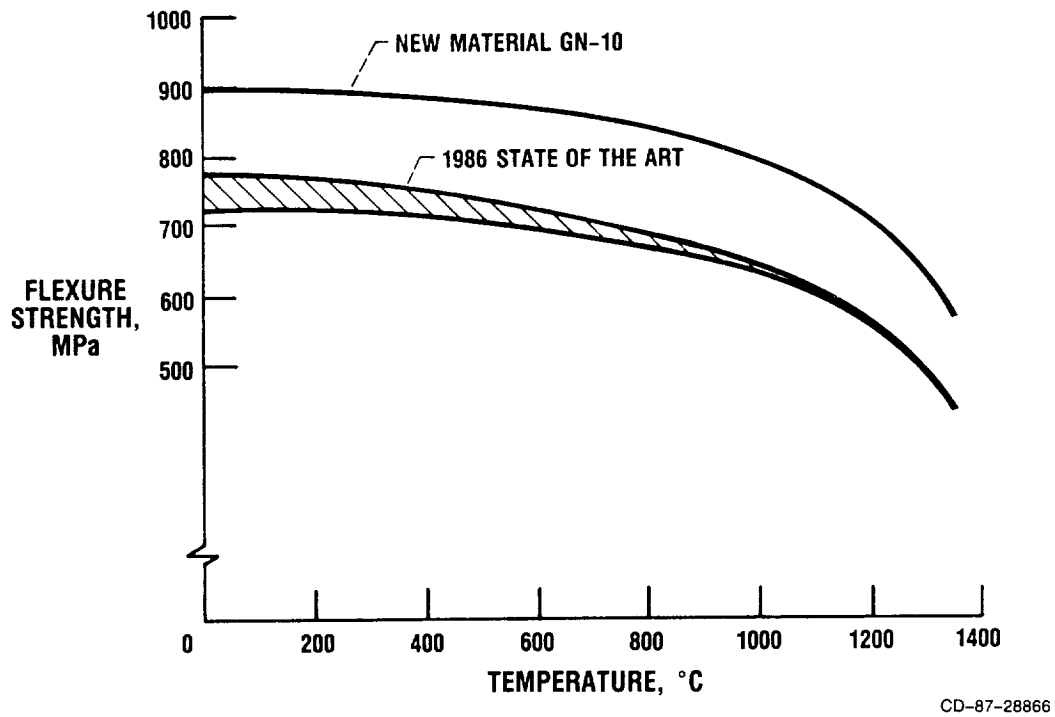


Figure 7. - Improvements in sintered silicon nitride.

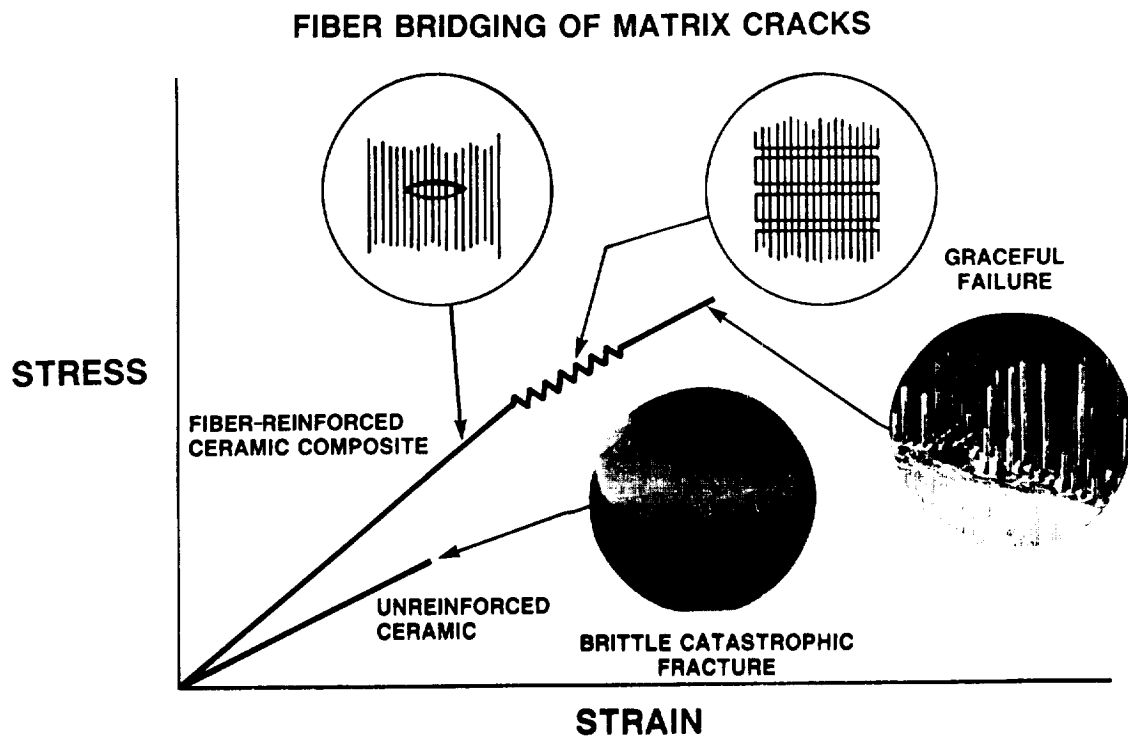


Figure 8. - Graceful failure of ceramic composites.

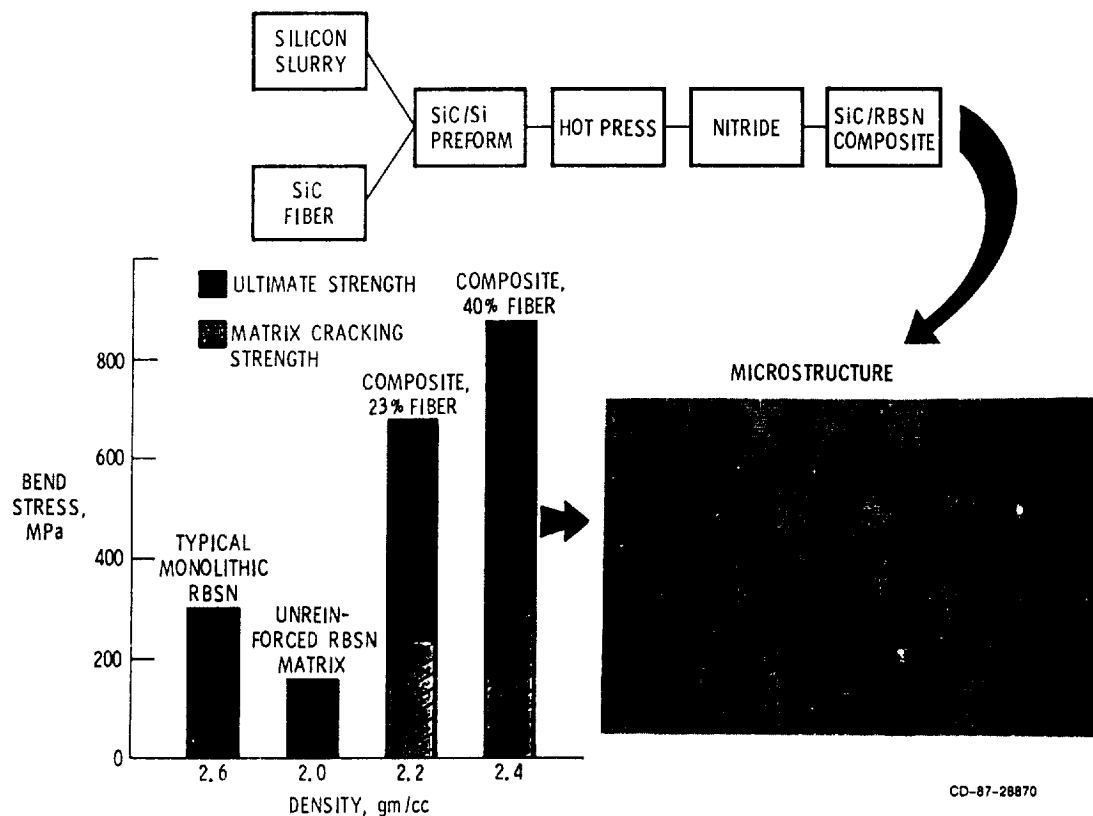


Figure 9. - SiC fibers strengthen and toughen reaction-bonded Si_3N_4 .

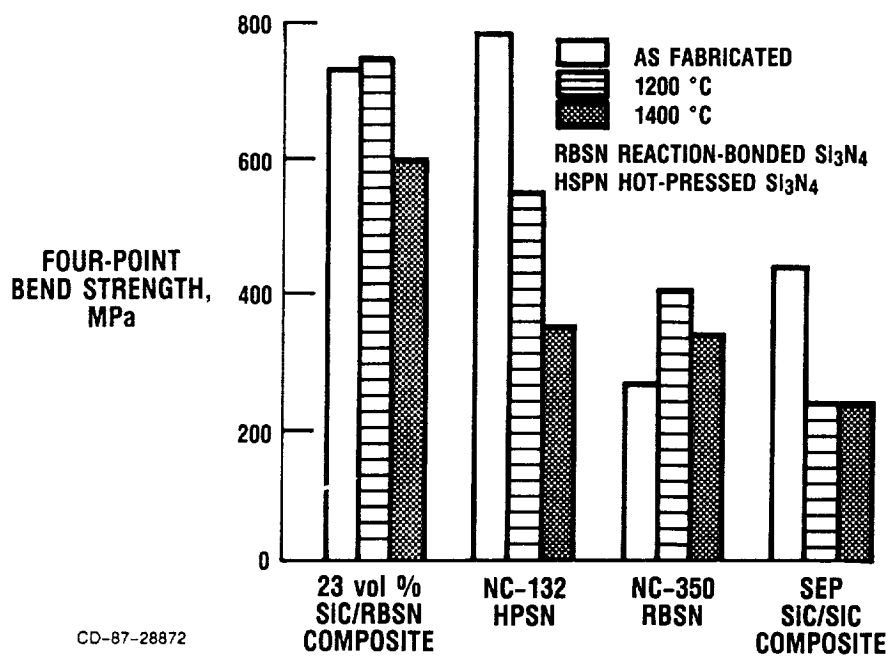
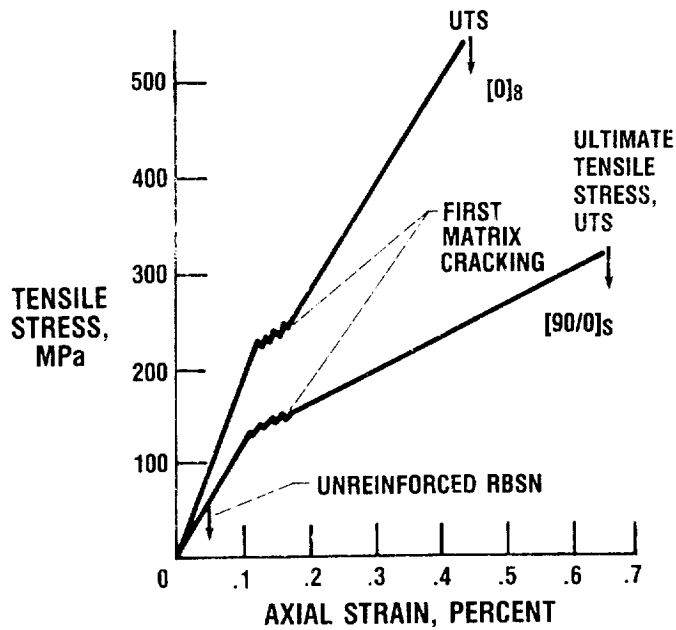


Figure 10. - High-temperature strength of SiC/RBSN composites is better than that of commercial ceramics.

**ROOM-TEMPERATURE TENSILE STRESS-STRAIN
BEHAVIOR FOR SiC/RBSN COMPOSITE LAMINATES
(VOLUME FRACTION FIBERS ≈ 0.3)**

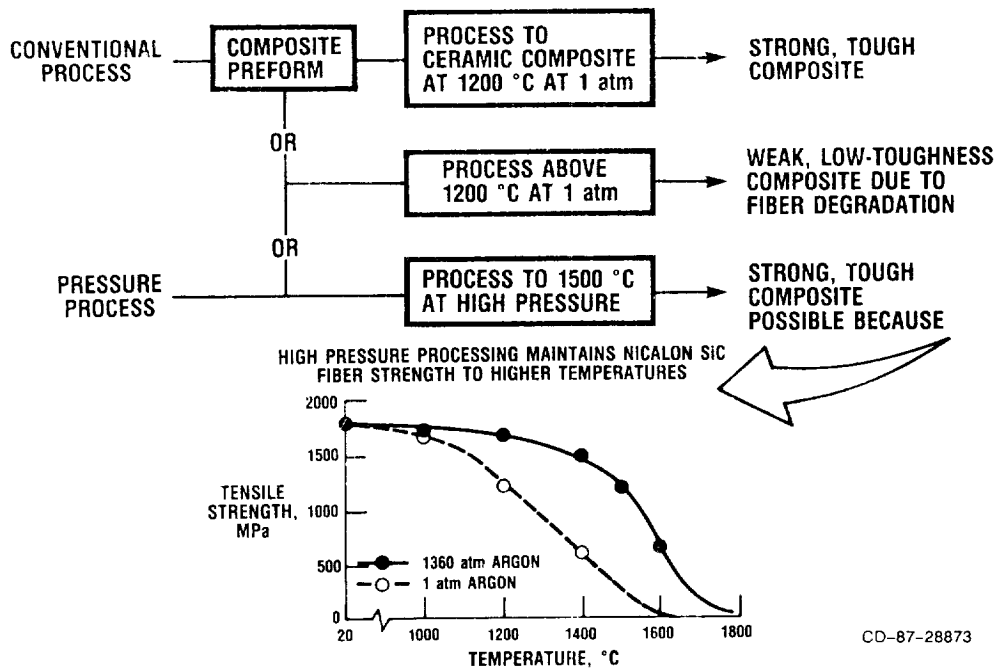


FRACTURED SPECIMEN



CD-87-28871

Figure 11. - SiC/RBSN composites fracture gracefully.



CD-87-28873

Figure 12. - High pressure extends processing window for ceramic matrix composites.

SESSION 2 - AEROPROPULSION STRUCTURES RESEARCH

AEROPROPULSION STRUCTURES

Lester D. Nichols

SUMMARY

Aeropropulsion systems present unique problems to the structural engineer. The extremes in operating temperatures, rotational effects, and behaviors of advanced material systems combine into complexities that require advances in many scientific disciplines involved in structural analysis and design procedures. This paper provides an overview of the complexities of aeropropulsion structures and the theoretical, computational, and experimental research conducted to achieve the needed advances.

STRUCTURES DIVISION

The Structures Division is engaged principally in developing validated analysis methods for predicting the performance of the structural components and systems of aerospace propulsion machinery (fig. 1). Performance here refers to a diversity of operating behavior characteristics, such as instantaneous or time-dependent stresses and deformations, structural dynamics, aeroelasticity, material behavior, and structural-life-related phenomena. Experiments are used both to validate methods and to understand complex structural and material behaviors in order to develop theoretical models that emulate them. The structures of aeronautical propulsion systems have a unique combination of complexities: they operate with long life in extremely harsh loading environments, have rotating components with complex dynamic behavior, and are constructed of lightweight advanced material systems with unique characteristics.

COMPLEX STRUCTURAL PROBLEMS OF AEROPROPULSION SYSTEMS

Propulsion systems present a number of complex structural problems from different sources (fig. 2). Because of the loading environment, materials exhibit two forms of nonlinear behavior: plasticity (considered to be instantaneous response), and creep (deformation and stress relaxation accumulating with time). Advanced material systems, because of their microstructures, represent local complexities that have to be included in global analysis methods. Single-crystal, directionally solidified, or fiber-reinforced materials result in anisotropic and nonhomogeneous local structures that must be mathematically characterized over wide ranges of nonlinear response and over the predicted structural life.

Another source of complexity is the large deflection associated with flexible structures such as fan blades and advanced turboprop blades. Large deflections introduce (a different kind of) nonlinearity into the calculations

that are geometric in nature and that are usually coupled with aerodynamic and thermal effects. Furthermore, descriptions of the loading environments and the material properties may not be available except in the form of a probability distribution. Phenomena related to structural integrity and life are among the most vexing and most important considerations. All these complexities and their possible interactions have to be considered in developing credible methods for predicting the structural behavior of propulsion systems.

PARTICIPATING DISCIPLINES

Research is needed in a number of scientific disciplines to solve the complex problems facing the structural designer of aeropropulsion systems. The nonlinearities of material behavior require major advances over conventional finite element or boundary element methods. These advances also have to reflect the new opportunities offered by the upcoming multiprocessor computer revolution.

Shortcomings in characterizing the material behavior under cyclic thermomechanical mission loads are major obstacles to improved accuracy and computational efficiency. Combining the required advances in constitutive modeling with the mechanics of fiber-reinforced composites adds to the complexity (fig. 3).

Nonlinear dynamics and aeroelasticity are needed to predict the operating characteristics of rotating, flexible bladed systems so that acceptable operating envelopes can be defined (fig. 4). Methods for predicting various structural-integrity-related behaviors of advanced material systems are needed in order to realize future aeropropulsion concepts with their demands for lighter structures operating in extremely hostile environments (fig. 5).

The final intent of the structural designer is not just to analyze trial design concepts, but also to approach an optimum design. Multidisciplinary design optimization methods are needed to guide the human designer through the complex interactions of the design variables toward an optimum design (fig. 6). Experimental capabilities are needed in dynamics and in high temperatures to study new phenomena and to validate theoretical models.

STRUCTURES WORK ELEMENTS

The three fundamental structures work areas are structural mechanics, structural dynamics, and life prediction methods:

- (1) Structural performance
 - (a) Constitutive relationships modeling and experiments
 - (b) Mechanics of composites
 - (c) Vibration control
 - (d) System dynamics
 - (e) Aeroelasticity
- (2) Structural life prediction
 - (a) Interactive effects on fatigue life
 - (b) Damage initiation modeling
 - (c) Crack growth
 - (d) Mechanics of fracture

The structural mechanics work is focused on the mechanics of materials in order to develop models for their behavior under cyclic thermomechanical mission load conditions. These models are needed in the advanced integrated structural analysis methods being developed. Under structural dynamics the aeroelasticity of flexible, rotating bladed systems is important for advanced propulsion design concepts. Developments in vibration control and systems dynamics are needed to ensure safe and efficient operation of rotating propulsion structures, particularly as they become lighter and operate at higher speeds.

The life prediction focus is on understanding, predicting, and controlling structural failures caused by fatigue and fracture. A wide range of advanced materials and material systems is being considered, many of them more brittle and therefore less forgiving.

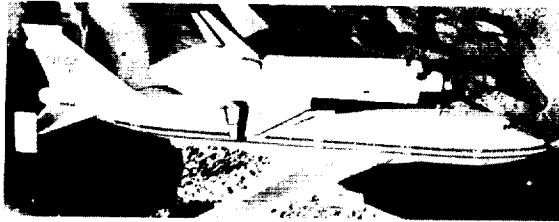
The structural designer needs input data from all disciplines in the interdisciplinary chain of activities during product design:

- (1) Integrated analysis and applications
 - (a) Computational mechanics
 - (b) Computational methods
 - (c) Probabilistic methods
 - (d) Optimization and tailoring
 - (e) Nondestructive evaluation
 - (f) Concept evaluation

- (2) Project support and consultation

Advanced computational mechanics analysis methods are being developed for cyclic thermomechanical mission loads. Under computational methods the program architectures and algorithms are being developed that best utilize advances in computer technology. Mission load environments and also the properties of advanced material systems can often be best described in probabilistic terms. This provides designers with more information on which to base designs. Integrated analysis methods are coupled with optimization methods for integrated multidisciplinary design optimization. Experimental methods are needed for two purposes: to study and understand phenomena and formulate models, and to test models for validation. The capabilities developed are distributed to users and are also employed in providing consultation to and participation in major NASA projects.

BUSINESS: AEROSPACE PROPULSION STRUCTURES

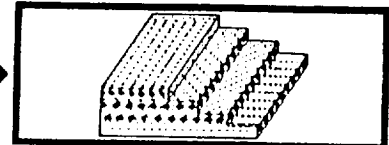
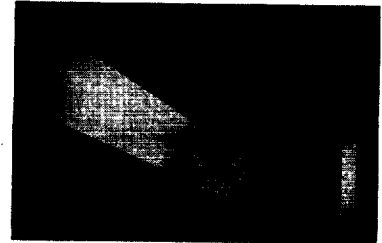
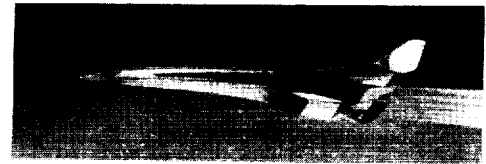


PRINCIPAL PRODUCT:

**VALIDATED METHODS TO PREDICT THE
STRUCTURAL PERFORMANCE OF AEROSPACE
PROPULSION SYSTEMS**

STRUCTURES OF PROPULSION SYSTEMS ARE UNIQUE:

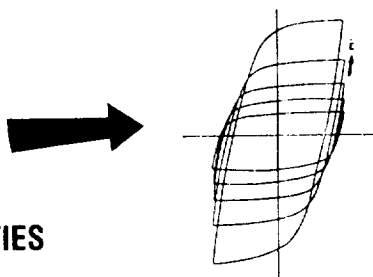
- **EXTREME LOADING ENVIRONMENTS**
- **HIGH-SPEED ROTATING STRUCTURES**
- **ADVANCED MATERIAL SYSTEMS**



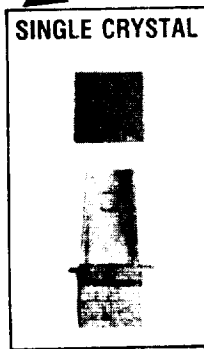
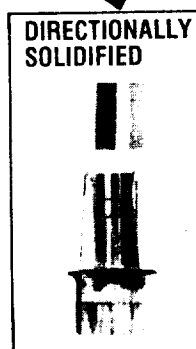
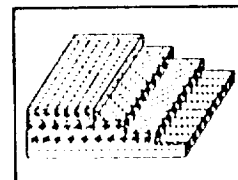
CD-87-28940

Figure 1. - Structures Division.

- MATERIAL NONLINEARITIES
 - PLASTICITY
 - CREEP



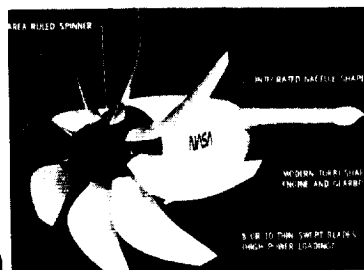
- COMPLEX MATERIAL PROPERTIES
 - ISOTROPIC/ANISOTROPIC
 - HOMOGENEOUS/NONHOMOGENEOUS



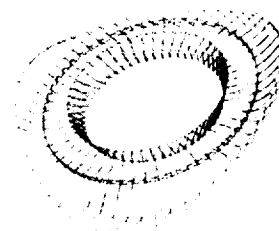
- SiC
- Al₂O₃
- Si₃N₄
- CARBON/CARBON

CD-87-28941

- GEOMETRIC NONLINEARITIES
 - LARGE DEFLECTIONS
 - ROTATIONAL EFFECTS

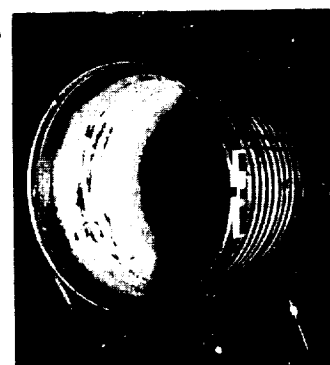
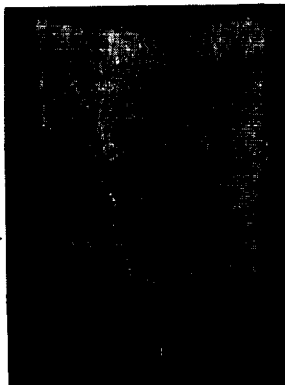
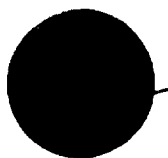
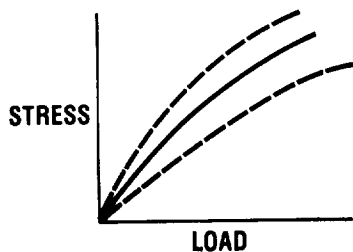


- COUPLED AERO-THERMO-STRUCTURAL EFFECTS



- STRUCTURAL INTEGRITY

- DETERMINISTIC/PROBABILISTIC DESCRIPTIONS



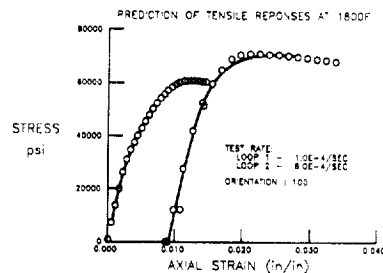
CD-87-28942

Figure 2. - Structural problem areas.

ORIGINAL PAGE
BLACK AND WHITE PHOTOGRAPH

- ADVANCED ANALYSIS METHODS
 - FINITE ELEMENT METHODS
 - BOUNDARY ELEMENT METHODS

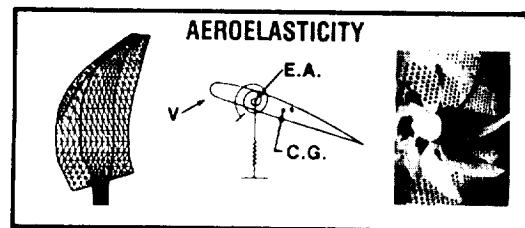
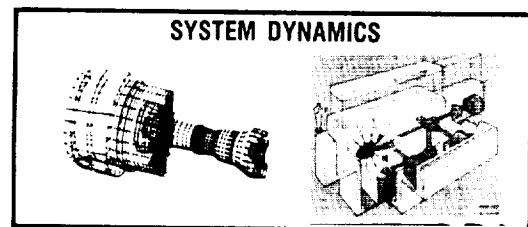
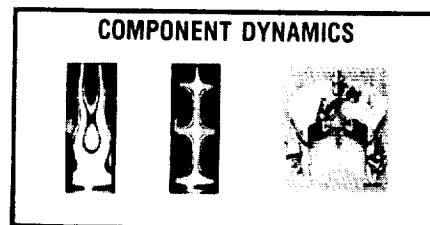
- MATERIAL BEHAVIOR MODELING
 - CONSTITUTIVE MODELING
 - MECHANICS OF COMPOSITES



CD-87-28943

Figure 3. - Advanced analysis methods.

- STRUCTURAL DYNAMICS
 - COMPONENT DYNAMICS
 - SYSTEM DYNAMICS
 - VIBRATION CONTROL
 - AEROELASTICITY

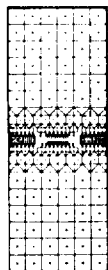
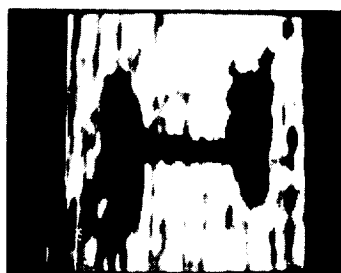


CD-87-28944

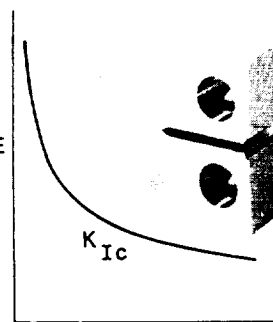
Figure 4. - Structural dynamics.

- **STRUCTURAL INTEGRITY PREDICTION**

- STRENGTH
- STATIC AND DYNAMIC STABILITY
- THERMOMECHANICAL FATIGUE AND FRACTURE
- COMPOSITES PHENOMENA



FRACTURE
STRESS



CRACK SIZE

CD-87-28945

Figure 5. - Structural integrity prediction.

- **INTEGRATED MULTIDISCIPLINARY ANALYSIS AND OPTIMIZATION**

- **EXPERIMENTAL METHODS**



ENGINE



FINITE ELEMENT MODEL



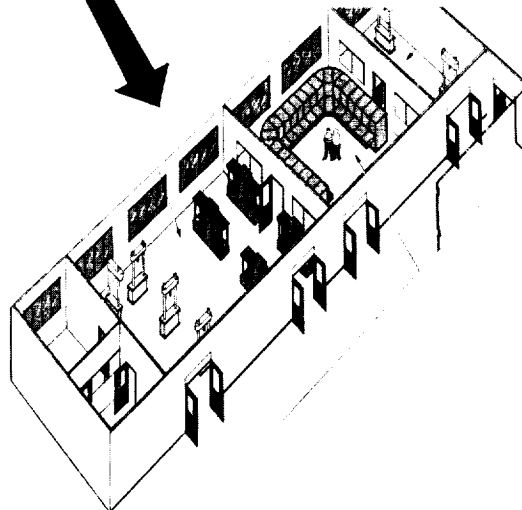
BLADE



ROTOR SECTOR



ROTOR STAGE



CD-87-28946

Figure 6. - Design optimization methods.

DETERMINING STRUCTURAL PERFORMANCE

Edited by Michael A. Ernst

SUMMARY

The objective of this paper is to give an overview of the methods and concepts developed to enhance and predict structural dynamic characteristics of advanced aeropropulsion systems. Aeroelasticity, vibration control, dynamic systems, and computational structural methods are four disciplines that make up the structural dynamic effort here at Lewis. The aeroelasticity program develops analytical and experimental methods for minimizing flutter and forced vibration of aerospace propulsion systems. Both frequency domain and time domain methods have been developed for applications on the turbofan, turbo-pump, and advanced turboprop. In order to improve life and performance, the vibration control program conceives, analyzes, develops, and demonstrates new methods for controlling vibrations in aerospace systems. Active and passive vibration control is accomplished with electromagnetic dampers, magnetic bearings, and piezoelectric crystals to control rotor vibrations. The dynamic systems program analyzes and verifies the dynamics of interacting systems, as well as develops concepts and methods for high-temperature dynamic seals. Work in this field involves the analysis and parametric identification of large, nonlinear, damped, stochastic system. The computational structural methods program exploits modern computer science as an aid to the solutions of structural problems.

INTRODUCTION

Overall, this paper will present (1) methods that have been developed to dynamically characterize the components of aeropropulsion systems, (2) advanced concepts that are being applied for the benefit of system and durability, and (3) test rigs and facilities that are used to validate the methodologies developed.

The editor wishes to acknowledge the following authors for their contributions to this paper.

Gerald Brown
Eliseo DiRusso
David Fleming
David Janetzke
Albert Kascak
Krishna Kaza
Robert Kielb

Louis J. Kiraly
Charles Lawrence
Oral Mehmed
Erwin Meyn
John Ramsey
Bruce Steinetz

ANALYTICAL METHODS

The turbomachinery aeroelastic effort at NASA Lewis Research Center includes unstalled and stalled flutter, forced response, and whirl flutter of propulsion systems. Even though the effort is currently focused on single-rotation and counterrotation propfans, the analytical models and the computer codes are applicable to turbofans with and without blade sweep and compressors. Because of certain unique features of propfans, it is not possible to directly use the existing aeroelastic technology of conventional propellers, turbofans, or helicopters. Therefore, reliable aeroelastic stability and response analysis methods for these propulsion systems must be developed.

The development of these methods for propfans requires specific basic technology disciplines, such as two-dimensional and three-dimensional, steady and unsteady (unstalled and stalled), aerodynamic theories in subsonic, transonic, and supersonic flow regimes; modeling of composite blades; geometric nonlinear effects; and passive or active control of flutter and response.

The computer program MISER (mistuned engine response) is a two-dimensional aeroelastic program that allows the user to explore the effects of mistuning on a series of blade cross sections in cascade (fig. 1). The computer program ASTROP (aeroelastic stability and response of propulsion systems) is a three-dimensional program that allows the user to predict the aeroelastic nature of propfan blades in cascade (fig. 2). Both programs have the capability of analyzing blades in both the subsonic and supersonic (subsonic leading-edge locus) flow regimes.

In order to improve the capability of both MISER and ASTROP, work is in progress to extend the unsteady aerodynamic packages in both programs. Currently, work is in progress to extend ASTROP into the stall and transonic flow regimes, while MISER's unsteady aerodynamic package is being extended to handle supersonic axial throughflow applications. For example, recent interest in supersonic and hypersonic flight has renewed interest in the development of propulsion systems that include a supersonic axial-flow fan (fig. 3). The supersonic axial-flow fan encounters supersonic flow normal to the plane of rotation as well as relative to the blades, and has supersonic flow through the entire blade passage. This fan is characterized by oblique shocks contained downstream of the locus of blade leading edges. Since the aeroelastic stability of the proposed single-stage fan is a concern, an analytical capability is needed to predict the unsteady aerodynamic loading. Consequently, a computer program was developed using Lane's equation for the unsteady pressure distribution in the case of supersonic axial flow. This code predicts the unsteady pressure distribution for an isolated airfoil, or a series of blades in cascade.

Over the past five years, both ASTROP and MISER have offered extensive insight into the aeroelastic behavior of propfans, as well as fan stages of turbofan engines.

Capabilities exist not only to dynamically characterize fan blades, but also to characterize the vibrations of entire rotor systems (fig. 4). Three nonlinear transient computer codes were developed to model complex aerospace structures. The code TRAN integrates the physical system of equations and is

used for short-term, high-frequency events. The programs ARDS and TETRA employ component modal synthesis methods using an appropriate set of modes and are, therefore, more applicable for longer transients. The ARDS code has been enhanced to provide shock spectrum analysis and automatic optimum rotor design. The TETRA code can use either modal data generated by NASTRAN or experimental data, and has been further enhanced by a steady-state analysis.

Deficiencies in existing modeling techniques, however, limit an analyst's ability to adequately model the connections between components. Connections between structural components are often mechanically complex, and hence very difficult to accurately model analytically. The effect that connections have on overall system behavior can be profound. Thus, to refine the prediction of overall system behavior, improved analytical models for connections are needed. An analytical and experimental program was carried out to develop improved methods for characterizing connections between structural components (fig. 5). Of particular interest was the identification of stiffness properties. The procedures developed in this program were evaluated with experimental vibration data obtained from the Rotating System Dynamics Rig.

The accuracy of modeling is improved through the use of optimization methods that reduce discrepancies between the measured characteristics of an actual structural system and those predicted by an analytical model of the system. The approach used in this work involves modeling the system components with either finite elements or experimental modal data and then connecting the components at their interface points. Experimentally measured response data for the overall system are then used in conjunction with optimization methods to make improvements in the connections between components. The improvements in connections are computed in terms of physical stiffness parameters so that the physical characteristics of the connections can be better understood.

As new methodologies are being developed and state-of-the-art programs become more cumbersome, there arises a critical need to be able to run these programs in a timely and efficient manner.

Computational methods research is directed toward finding new and more efficient ways of performing structural computations (fig. 6). There is a heavy emphasis on emerging parallel processing methods. Many different main-frame computers are used, as well as a 67-processor transputer system for most of the parallel methods research. This system is designed to be electronically reconfigured into a variety of different equivalent architectures so that the interplay between algorithms and architectures can be fully explored. This system is built with high-performance processors, but is not expected to perform as well as a dedicated computer.

In one approach, finite-element analyses are conducted by distributing stiffness matrices throughout the processor array. Multigrid analysis methods, which employ successive refinements of mesh sizes, have the refined meshes assigned to successive processors. Problems involving the management of global variables are being studied in order to distribute graphics primitives to a processor array to support high-speed animation. Eigenvalue solution routines that employ recursive, binary, tree-structured search algorithms are taking advantage of the transputer network's ability to reconfigure processor interconnections. When new methods are fully developed, they will be

transferred to larger dedicated computer facilities within the NASA computer network.

APPLICATIONS OF ADVANCED CONCEPTS

Research does not stop with the development of new methodologies. Advanced concepts are being applied to aeropropulsion systems to improve both performance and durability.

NASA Lewis, in conjunction with the General Electric Company, has developed a high-precision servomechanism for controlling turboprop aircraft blade angles (fig. 7.). The pitch-change mechanism can accurately control the variable pitch of large (13 000 hp) turboprop aircraft propellers over the complete spectrum of flight-operating conditions. It also helps attain advanced turboprop performance goals of improving propulsion system efficiency by 30 percent and reducing operating costs by 10 percent. Advanced design features include a fiber-optic data link, a high-speed electric motor/alternator combination, a high-mechanical-ratio blade-articulating mechanism, and an autonomous propeller that generates its own electrical power and has an independent self-contained control module. The key to minimizing noise with these large propeller systems is accurate synchrophasing (i.e., precise blade speed and phase synchronization of left and right propellers). The blade-angle resolution capabilities of this pitch-control mechanism have been theoretically shown to meet or exceed the requirements for minimizing blade noise that will be experienced by passengers on board aircraft flying in the 1990's.

Shown in figure 8 are examples of projects in passive control of blade vibration. The variable-normal-load friction-damper test fixture was developed to allow detailed study of friction dampers in a rotating environment. The data generated with this test fixture were used to fine-tune and verify advanced mathematical models of friction-damper behavior. The models were used to show that friction dampers have the potential to stabilize fluttering fan blades.

For example, the first-stage turbine blades of the space shuttle main engine (SSME) high-pressure oxygen pump (HPOTP) have experienced cracking problems due to excessive vibration. A solution is to incorporate a well-designed friction damper to attenuate blade vibration. An integrated experimental/analytical approach was used to evaluate a damper design. An optimized design resulted in a modest microslip damper.

An analytical study of impact dampers has been completed. The model predicts that the relatively light impactor (1 to 4 percent of the blade mass) produces substantial damping. In addition, the phenomenon of frequency tuning is not present for the impact damper. However, it is replaced by what might be called amplitude tuning. Experimental verification is now being planned.

Active control of rotor vibrations offers important advantages over passive control, especially in the matter of greater damping. This principle is illustrated in the center of figure 9. Shaft position sensors send signals to a controller which, guided by a control algorithm, operates actuators located at the bearings. The actuators oppose undesired shaft vibrational motion. Three types of actuators are illustrated. In the upper left is a research

rig with electromagnetic shakers. In the lower left is a group of three piezoelectric actuators, which change length when a voltage is applied to them. In the upper right is an electromagnetic device that both reduces vibration and replaces the conventional shaft bearings. Magnetic attraction between frame-mounted, fast-acting coils and iron disks mounted on and rotating with the shaft carries the weight of the shaft and exerts the vibration control forces. When sensors detect unwanted shaft movement, currents in the appropriate coils increase to pull the shaft back. This system permits higher shaft speed, automatic balancing, and better shaft positioning. Magnetic bearings need improvements in the speed and size of the electronics and in the actuator to meet flight requirements. Among the exciting possible advances in the actuator is the use of high-temperature superconductors that would make the windings more compact and eliminate the iron cores. The much more compact result is illustrated in the lower right.

TEST RIGS AND FACILITIES

Test rigs and facilities are employed for the experimental verification of the methodologies and advanced concepts that have been developed. For example, an experimental research program is being conducted in the 8- by 6-Foot Supersonic Wind Tunnel to understand the flutter and forced-response characteristics of advanced high-speed propellers or propfans (fig. 10). Flutter and forced-response data have been obtained from 2-ft-diameter single-rotation and counterrotation models. This has allowed researchers to compare measured and calculated flutter boundaries.

The Spin Rig is a facility that performs rotation dynamic spin tests of rotors in a vacuum to measure their vibratory and steady-state deflections and strains (fig. 11). The rotor wheel is contained in a armored test tank where it can be spun up to 18 000 rpm. The tank can be evacuated to 0.001 atm, reducing air friction and blade loads to near zero. Up to 50 strain gages can be bonded to the rotor blades at strategic locations. These signals can be recorded on two 14-channel tape recorders. Data from the strain gages can then be analyzed. A laser system is also available to facilitate the measurement of centrifugally produced deflections.

The Rotation System Dynamics (RSD) Rig is a general facility that is used for determining the dynamic characteristics of rotating systems (fig. 12). Instrumentation consists of (1) displacement measurement (9 channels), (2) acceleration and velocity measurement (18 channels), and (3) force measurement (4 channels). Fourteen channels of data can be recorded on tape, and all data can be monitored on oscilloscopes during testing. Four electrodynamic shakers, which are driven by a signal generator, provide forcing-function input to the system under test. The rotating shaft is driven by an air turbine. Maximum rotating is currently 10 000 rpm.

In conventional gas turbine engines, squeeze-film dampers are used to control nominal rotor unbalance. To control a transient blade-loss event, active damping may have to be used. Figure 13 shows a blade-loss test rig with piezoelectric actuators as active dampers. The object of the test was to investigate various algorithms to control the transient. A magnetic damper is being designed for this rig.

In the case of the National Aerospace Plane, cryogenic fluids could be used as the fuel. At cryogenic temperatures, there is no verified damper. There is a need for either passive or active dampers. Potential passive cryogenic dampers are elastomeric, curved-beam, hydrostatic, closed-cartridge, non-Newtonian fluid, and eddy current. Figure 14 shows the liquid nitrogen damper test rig. A liquid hydrogen test rig is available.

The High Load Thrust Rig, shown in figure 15, was designed to test engine dampers that carry a larger-than-normal radial load (e.g., due to blade loss). It can also apply a thrust load to the test damper, for testing radial dampers used at thrust-bearing locations. The damper is loaded by unbalancing the disk at the left end of the shaft. Eddy-current probes measure shaft and damper vibration, and quartz load washers measure the force applied to the damper. From these measurements, the stiffness and damping of the test damper can be calculated.

Figure 15 shows three dampers that may be tested in the rig. The dual squeeze-film damper has a conventional low-clearance film that provides the required damping at low imbalance levels. When the imbalance increases (as from a blade loss), a second, large-clearance film becomes active. This provides the damper amplitude needed to handle the higher imbalance.

The curve beam damper uses beam elements to provide stiffness. Fluid is forced through orifices to provide damping. This damper is inherently linear; stiffness and damping coefficients do not vary with vibration amplitude.

A magnetic damper applies a damping force to the rotor through electromagnets. The damper control system allows active control of rotor vibration, in which effective stiffness and damping are varied with speed and imbalance to optimize rotor performance.

CONCLUDING REMARKS

Programs such as ASTROP, TETRA, TRAN, and ARDS are state-of-the-art tools for the dynamic analysis of aeropropulsion components. Work involved in computational methods, and in the characterization of structural connections, is expected to add greatly to the efficiency and accuracy of many of the programs already developed. Advanced concepts, such as electrodynamic dampers or piezoelectric actuators, will continue to be explored in order to improve the life and performance of aeropropulsion systems. Test facilities such as the Spin Rig and the 8- by 6-Foot Supersonic Wind Tunnel will continue to be used by both government and industry for the experimental validation of the methodologies developed and of the advanced concepts applied.

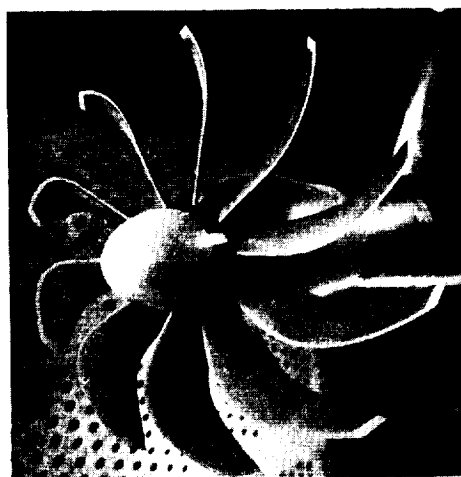
Lewis Research Center is committed to aeropropulsion excellence. In turn, the structural dynamic effort continues to be devoted to the development of new methodologies and the application of advanced concepts in order to meet this commitment.

BIBLIOGRAPHY

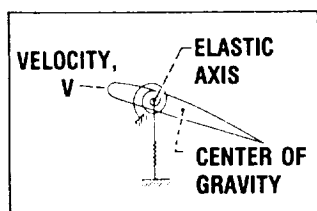
Brown, G.V.; and North, C.M.: The Impact Damped Harmonic Oscillator in Free Decay. NASA TM-89897, 1987.

- Brown, G.V., et al.: Lewis Research Center Spin Rig and Its Use in Vibration Analysis of Rotating Systems. NASA TP-2304, 1984.
- Cameron, T.M., et al.: An Integrated Approach for Friction Damper Design. The Role of Damping in Vibration and Noise Control, L. Rogers and J.C. Simonis, eds., ASME, 1987, pp. 205-212.
- DiRusso, E.: Active Suppression of Rotor Vibrations. NASA Tech Briefs, vol. 11, no. 6, June 1987, p. 64. (LEW-14488.)
- Favenesi, J.; Danial, A.; and Bower, M: Transputer Based Finite Element Solver, Phase I. Sparta Inc., Laguna Hills, CA, 1988. (NASA Contract NAS3-25126.)
- Gallardo, V.D.; and Black, G.: Blade Loss Transient Dynamics Analysis. Vol. I, Task II - TETRA 2 Theoretical Development. NASA CR-179632, 1986.
- Hirschbein, M., et al.: Structural and Aeroelastic Analysis of the SR-7L Propfan. NASA TM-86877, 1985.
- Hucklebridge, A.A.; and Lawrence, C.: Identification of Structural Interface Characteristics Using Component Mode Synthesis. Modal Testing and Analysis, T.G. Carne and J.C. Simonis, eds., ASME, 1987, pp. 121-129. (NASA TM-88960.)
- Kascak, A.F.; and Tomko, J.J.: Effects of Different Rub Models on Simulated Rotor Dynamics. NASA TP-2220, AVSCOM TR-83-C-8, 1984.
- Kascak, A.F: Direct Integration of Transient Rotor Dynamics. NASA TP-1597, AVRADCOM TR-79-42, 1980.
- Kascak, A.F.: The Response of Turbine Engine Rotors to Interference Rubs. NASA TM-81518, AVRADCOM TR-80-C-14, 1980.
- Kaza, K.R.V.: Turbomachinery Aeroelasticity at NASA Lewis Research Center. Presented at the Symposium on Transonic Unsteady Aerodynamics and Aeroelasticity, 1987, NASA Langley Research Center, May 20-22, 1987.
- Kaza, K.R.V.; and Kielb, R.E.: Flutter and Response of a Mistuned Cascade in Incompressible Flow. AIAA J., vol. 20, no. 8, Aug. 1982, pp. 1120-1127.
- Kaza, K.R.V., et al.: Analytical Flutter Investigation of a Composite Propfan Model. 28th Structures, Structural Dynamics and Materials Conference, Part 2A, AIAA, 1987, pp. 84-97. (NASA TM-88944.)
- Kaza, K.R.V., et al.: Analytical and Experimental Investigation of Mistuning in Propfan Flutter. 28th Structures, Structural Dynamics and Materials Conference, Part 2A, AIAA, 1987, pp. 98-110. (NASA TM-88959.)
- Kielb, R.E.; and Kaza, K.R.V.: Aeroelastic Characteristics of a Cascade of Mistuned Blades in Subsonic and Supersonic Flows. J. Vibration, Stress Reliability Design, vol. 105, no. 4, Oct. 1983, pp. 425-433.

- Kiraly, L.J.: Structural Dynamic Measurement Practices for Turbomachinery at the NASA Lewis Research Center. NASA TM-88857, 1986.
- Lawrence, C.: Identification of Differences Between Finite Element Analysis and Experimental Vibration Data. NASA TM-87336, 1986.
- Lawrence, C., et al.: A NASTRAN Primer for the Analysis of Rotating Flexible Blades. NASA TM-89861, 1987.
- Mehmed, O.; and Kaza, K.R.V.: Experimental Classical Flutter Results of a Composite Advanced Turboprop Model. NASA TM-88792, 1986.
- Mehmed, O., et al.: Bending-Torsion Flutter of a Highly Swept Advanced Turboprop. NASA TM-82975, 1982.
- Murthy, D.V.; and Kaza, K.R.V.: A Computational Procedure for Automated Flutter Analysis. NASA TM-100171, 1987.
- Ramsey, J.K.; and Kielb, R.E.: A Computer Program for Calculating Unsteady Aerodynamic Coefficients for Cascades in Supersonic Axial Flow. NASA TM-100204, 1987.
- Reddy, T.S.R.; and Kaza, K.R.V.: A Comparative Study of Some Dynamic Stall Models. NASA TM-88917, 1987.
- Sinha, A.; Griffin, J.H.; and Kielb, R.E.: Influence of Friction Dampers on Torsional Blade Flutter. J. Eng. Gas Turbines Power, vol. 108, no. 2, Apr. 1986, pp. 313-318.
- Steinetz, B.M., et al.: An Advanced Pitch Change Mechanism Incorporating a Hybrid Traction Drive. AIAA Paper 84-1383, June 1984. (NASA TM-83709.)
- Wu, J.C.; Kaza, K.R.V.; and Sankar, L.N.: A Technique for the Prediction of Airfoil Flutter Characteristics in Separated Flow. 28th Structures, Structural Dynamics and Materials Conference, Part 2B, AIAA, 1987, pp. 664-673.



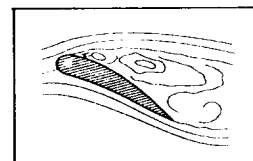
ASTROP CODE



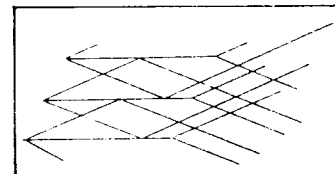
MISER CODE

CD-87-29578

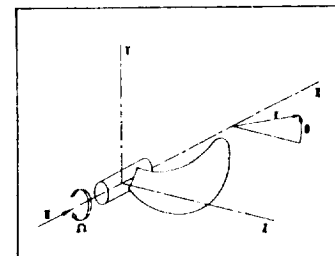
UNSTEADY
AERODYNAMIC
DEVELOPMENT



STALL

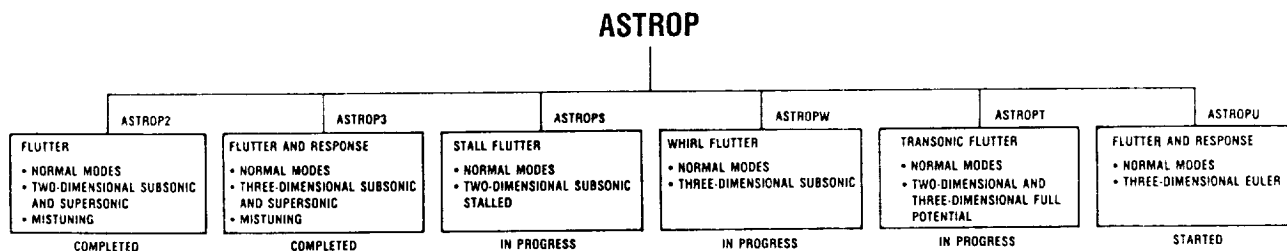


SUPERSONIC FLOWTHROUGH

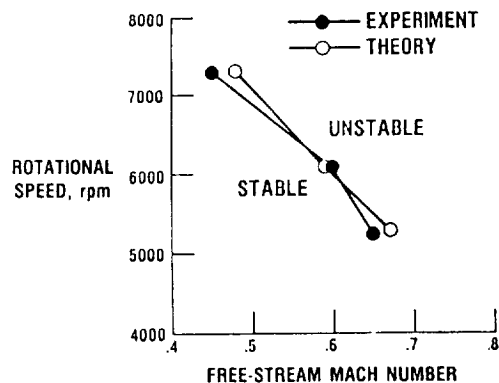


THREE-DIMENSIONAL SUBSONIC,
TRANSONIC, SUPERSONIC

Figure 1. - Aeroelastic methods.



COMPARISON OF EXPERIMENTAL AND
THEORETICAL FLUTTER BOUNDARY



PROPFAN
WIND TUNNEL MODEL



CD-87-29585

Figure 2. - Aeroelastic stability and response of propulsion systems (ASTROP).

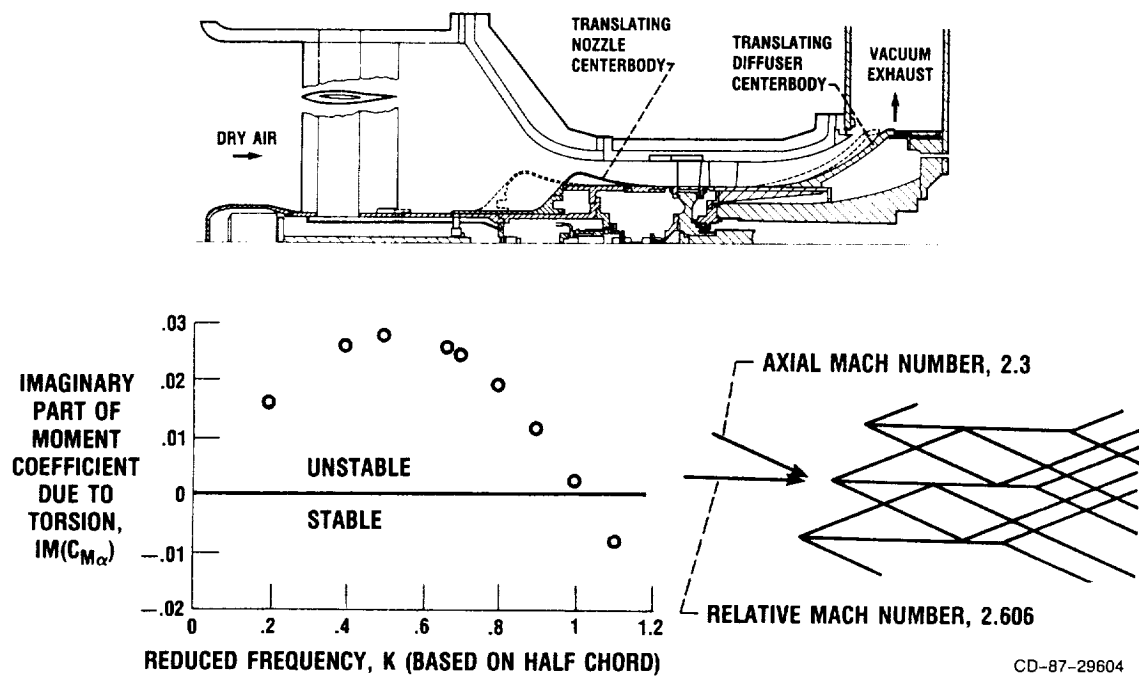
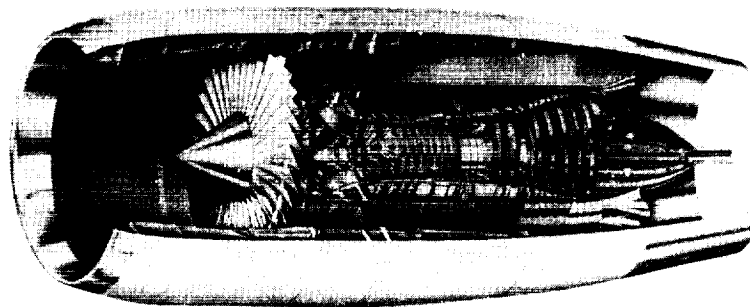


Figure 3. - Supersonic axial throughflow.



ENERGY EFFICIENT ENGINE (E³) SYSTEM (GENERAL ELECTRIC CONFIGURATION)

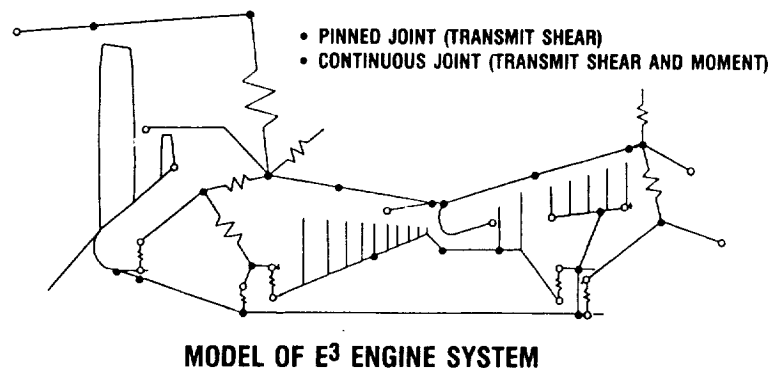
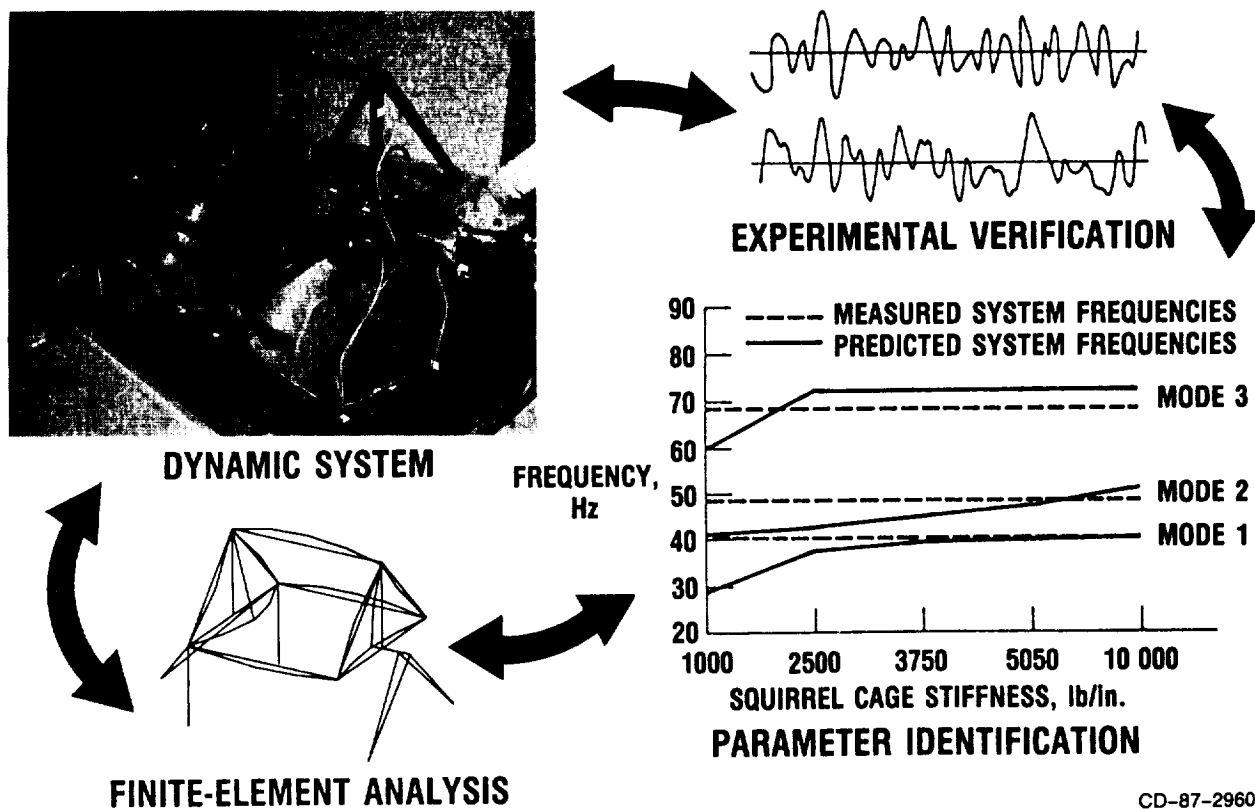


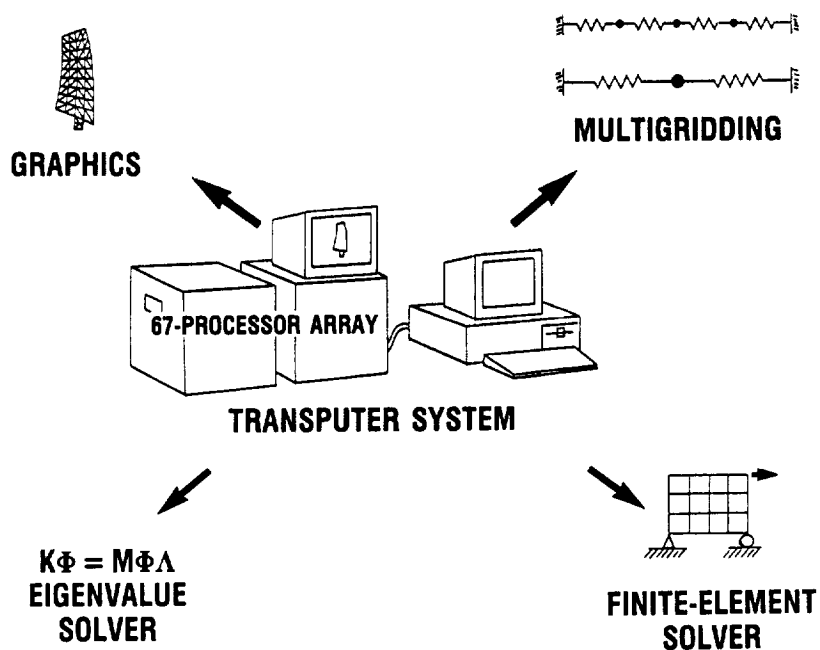
Figure 4. - Rotor systems modeling.

ORIGINAL PAGE
BLACK AND WHITE PHOTOGRAPH



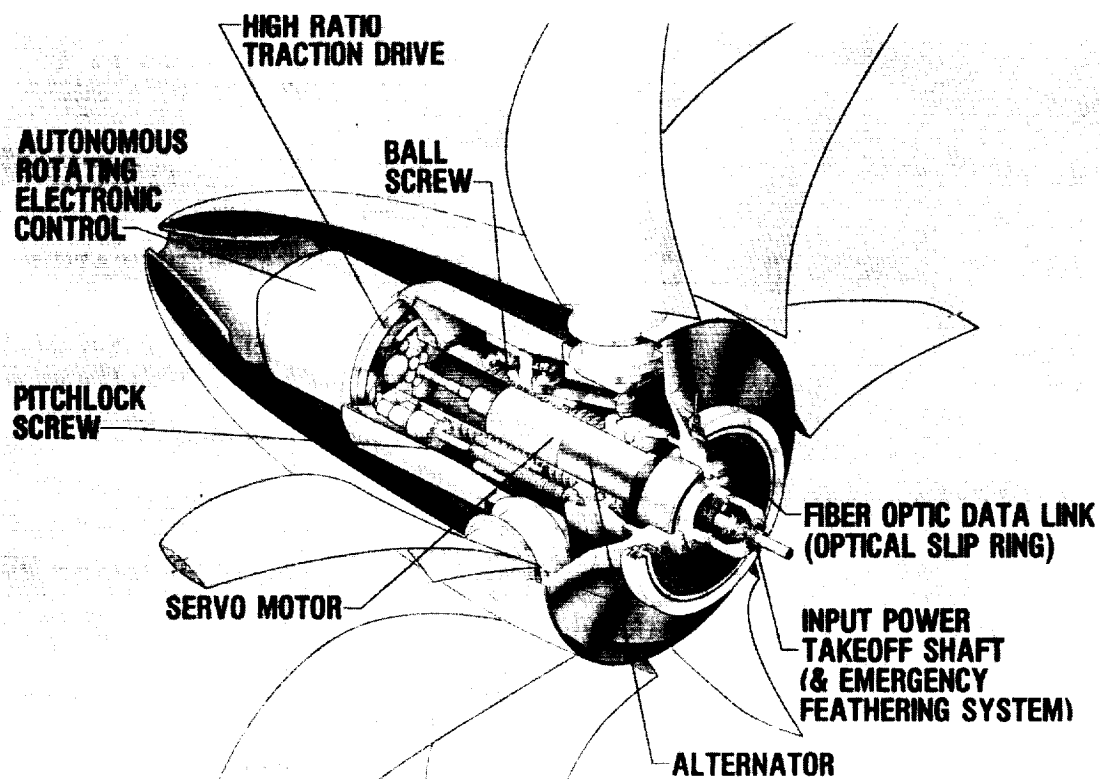
CD-87-29605

Figure 5. - Characterization of structural connections.



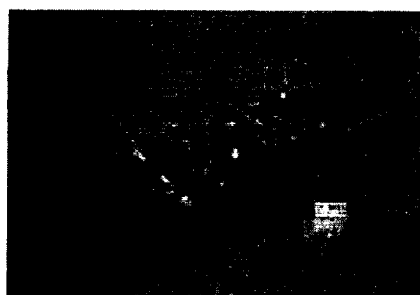
CD-87-29591

Figure 6. - Computational methods.

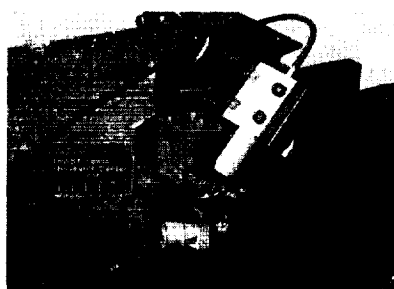


CD-87-29603

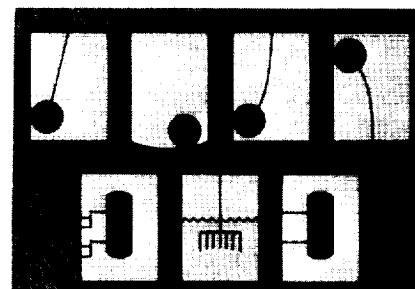
Figure 7. - Advanced turboprop pitch-change mechanism.



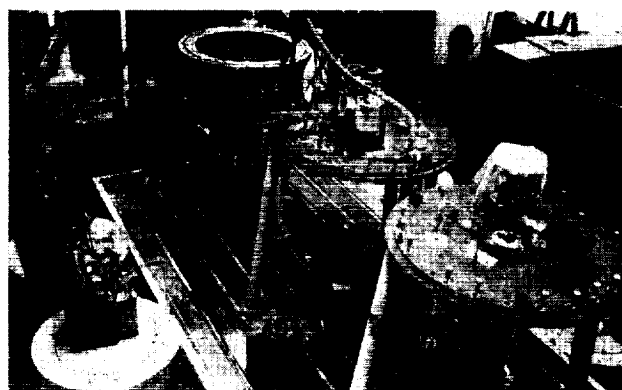
VARIABLE-NORMAL-LOAD
FRICTION DAMPER



SSME HIGH-PRESSURE OXYGEN
PUMP (HPOTP) FRICTION DAMPER



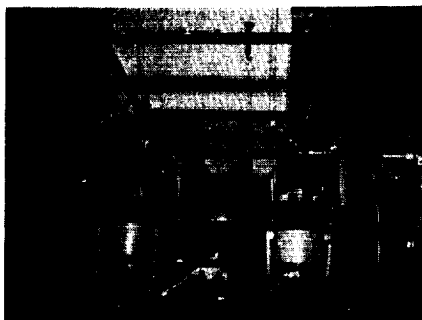
ADVANCED CONCEPT
IMPACT DAMPERS



SPIN RIG VERIFICATION

CD-87-29584

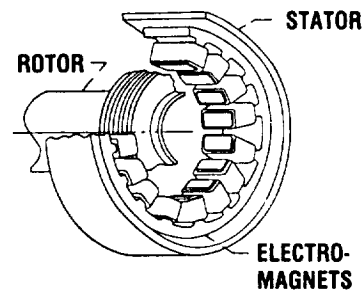
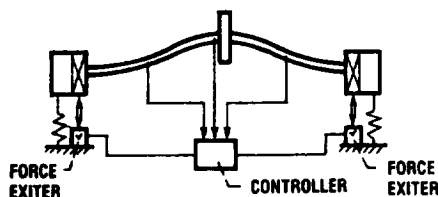
Figure 8. - Blade vibration control.



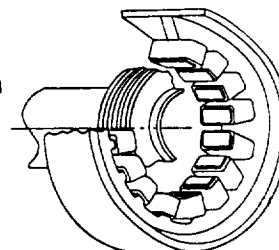
ACTIVE CONTROL TEST RIG



PIEZOELECTRIC ACTUATORS



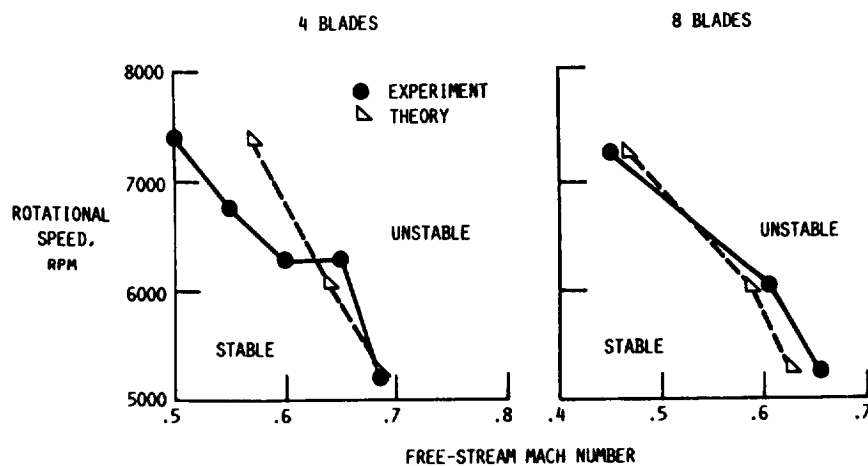
MAGNETIC BEARING



**MAGNETIC BEARING
WITH HIGH-TEMPERATURE
SUPERCONDUCTOR WINDINGS**

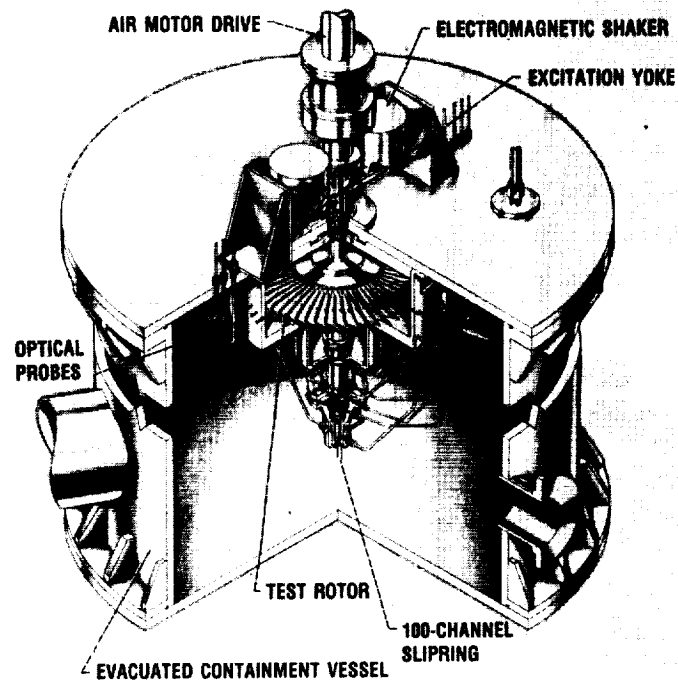
CD-87-29588

Figure 9. - Active rotor control.



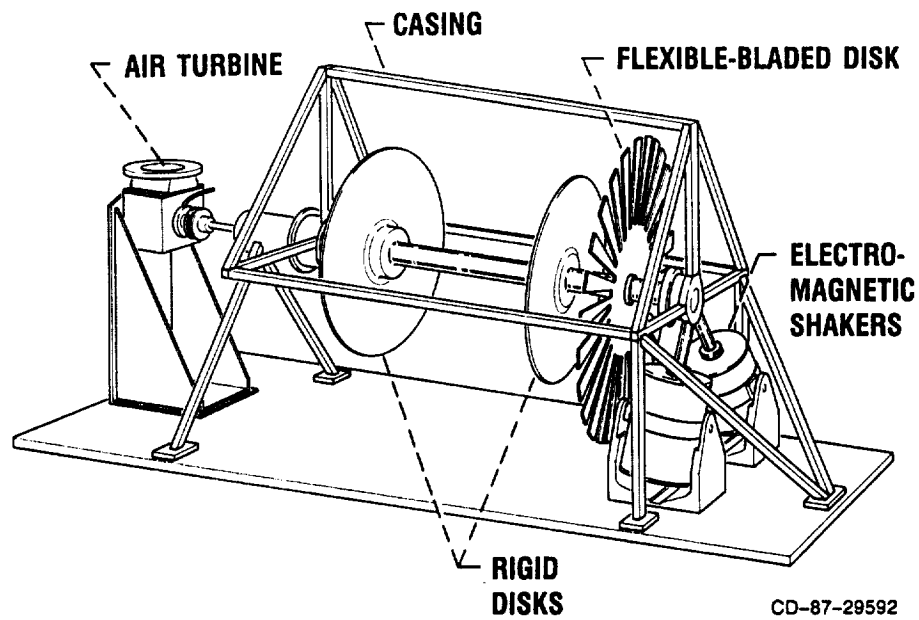
CD-87-29586

Figure 10. - Comparison of measured and calculated flutter boundaries (SR3C-X2 propfan model).



CD-87-29592

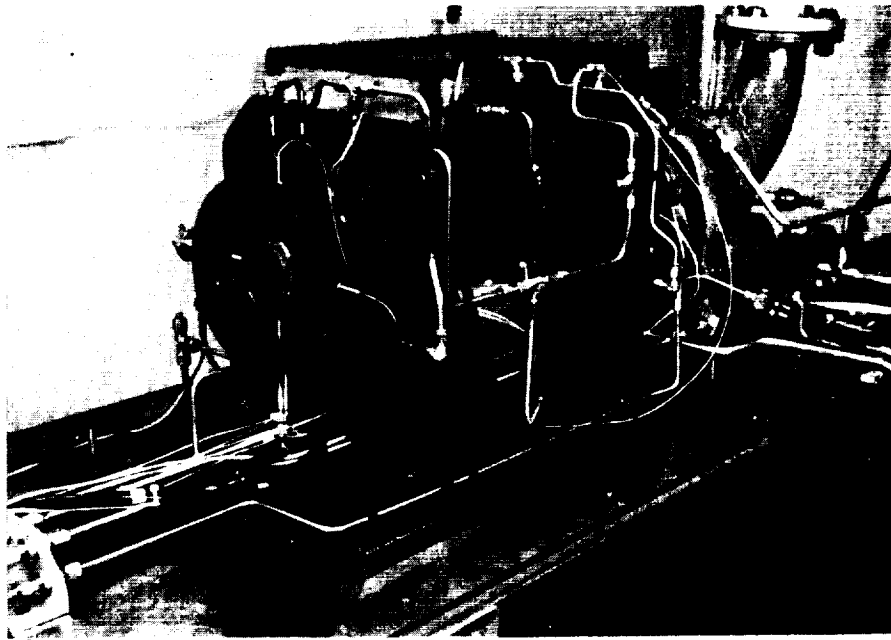
Figure 11. - Spin rig.



CD-87-29592

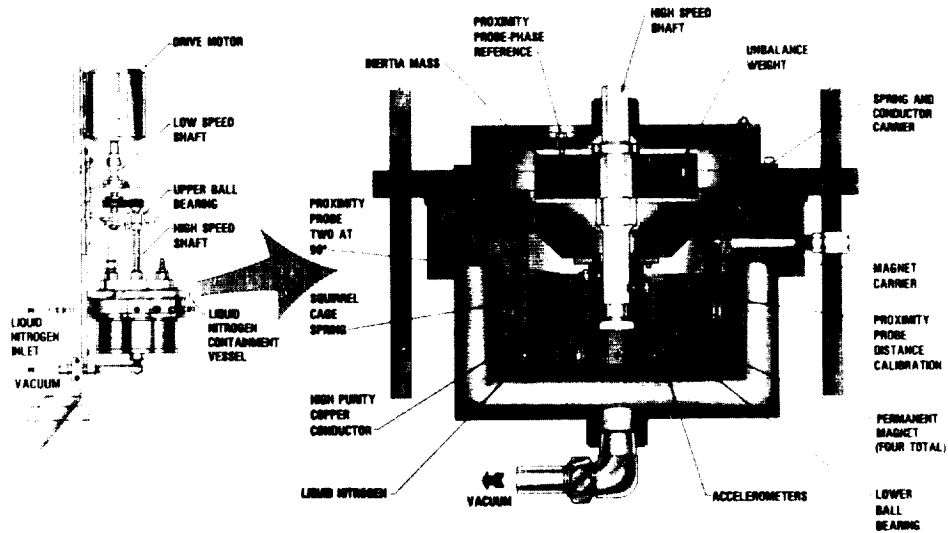
Figure 12. - Rotating systems dynamics rig.

ORIGINAL PAGE IS
BLACK AND WHITE PHOTOGRAPH



CD-87-29589

Figure 13. - Blade-loss test rig.



CD-87-29589

Figure 14. - Liquid nitrogen damper test rig.

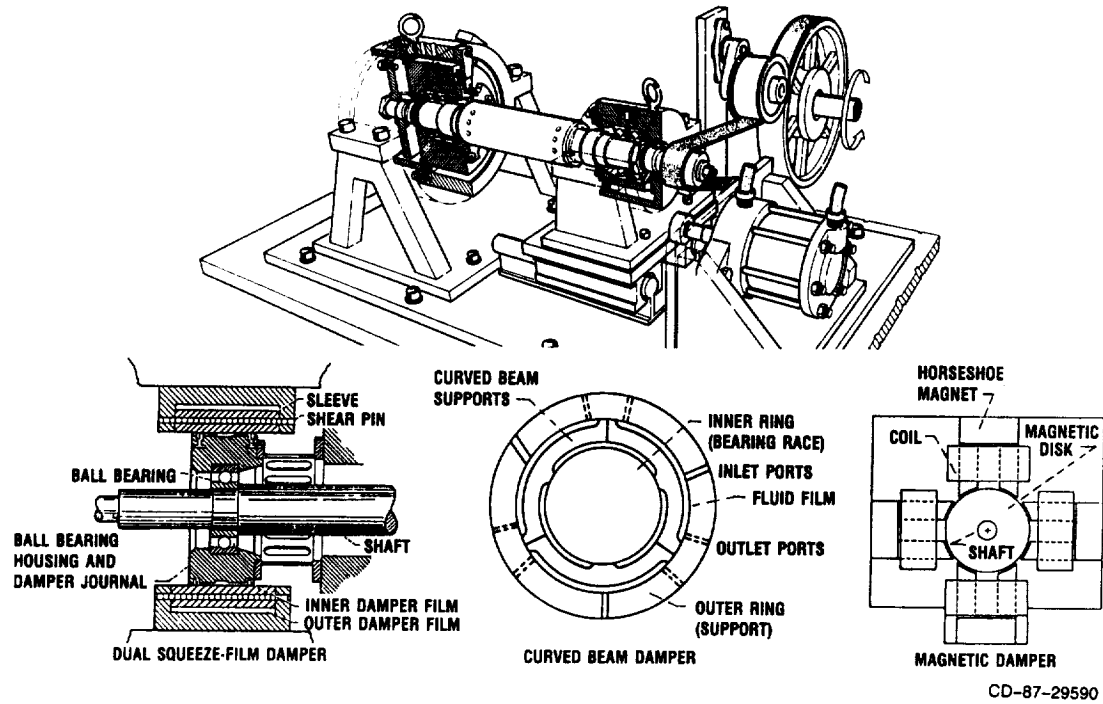


Figure 15. - High-load, thrust-bearing damper rig.

LIFE PREDICTION TECHNOLOGIES FOR AERONAUTICAL PROPULSION SYSTEMS

Michael A. McGaw

SUMMARY

Fatigue and fracture problems continue to occur in aeronautical gas turbine engines. Components whose useful life is limited by these failure modes include turbine hot-section blades, vanes, and disks. Safety considerations dictate that catastrophic failures be avoided, while economic considerations dictate that noncatastrophic failures occur as infrequently as possible. The decision in design is therefore making the tradeoff between engine performance and durability. The NASA Lewis Research Center has contributed to the aeropropulsion industry in the area of life prediction technology for over 30 years, developing creep and fatigue life prediction methodologies for hot-section materials. At the present time, emphasis is being placed on the development of methods capable of handling both thermal and mechanical fatigue under severe environments. Recent accomplishments include the development of more accurate creep-fatigue life prediction methods such as the total strain version of Lewis' strainrange partitioning (SRP) and the HOST-developed cyclic damage accumulation (CDA) model. Other examples include the development of a more accurate cumulative fatigue damage rule - the double damage curve approach (DDCA), which provides greatly improved accuracy in comparison with usual cumulative fatigue design rules. Other accomplishments in the area of high-temperature fatigue crack growth may also be mentioned. Finally, we are looking to the future and are beginning to do research on the advanced methods which will be required for development of advanced materials and propulsion systems over the next 10 to 20 years.

PERFORMANCE VERSUS DURABILITY

Fatigue and fracture problems continue to occur throughout aeronautical gas turbine engines. Safety considerations dictate that life-threatening catastrophic failures be avoided, and economic considerations dictate that noncatastrophic failures occur as infrequently as possible. The failure rate, however, can be related directly to the performance extracted from the machine. We thus have the perennial dichotomy: performance versus durability (fig. 1). Because the primary driver for aeropropulsion is performance, we must view lack of adequate durability as a constraint to the desired performance. Knowledge of both aspects is necessary to understand and quantify the tradeoffs between the two. Performance may take a variety of forms, including for example, higher thrust-to-weight ratio or better fuel efficiency. Similarly, durability is constrained by factors which include excessive deformation, thermomechanical fatigue, and fracture. Our ability to accurately predict the durability of a structure is much less sophisticated than our ability to accurately predict structural performance. This is due primarily to three factors. First, in the

case of structural performance, analytical solutions exist, in most cases, which can be applied with high accuracy. In the case of structural durability, analytic solutions for the majority of failure modes simply don't exist. Secondly, in the case of performance, verification of performance goals occurs early in the design and development cycle, whereas durability aspects generally require long-term testing for verification. Nowhere is the tradeoff more critical than in the turbine hot section, where multiple failure modes are present in varying degree.

Figure 2 illustrates typical components that have exhibited histories of limited durability. Compressor blades, combustor liners, guide vanes, turbine blades, disks, shafts, bearings, and spacers are just a few of the more common components that have exhibited cyclic crack initiation, propagation, and fracture phenomena. These failure phenomena arise because of repeated thermal and/or mechanical loading induced by the service cycle.

LEWIS RESEARCH CENTER CONTRIBUTIONS

At Lewis Research Center, we have aided the aeropropulsion industry by concentrating on developing fracture and elevated-temperature fatigue life methods (fig. 3). One of the earliest contributions was the development of the basic plastic strain-life fatigue law, discovered independently by Manson in 1953 (ref. 1) and by Coffin in 1954 (ref. 2). In an effort to provide a means of assessing the fatigue behavior of materials from data commonly assessable to engineers, the method of universal slopes was developed (ref. 3) in 1965. The universal slopes equation predicts the fatigue behavior of a metallic material based on the material's monotonic tensile properties, namely, the ultimate tensile strength and ductility.

In the development of high-temperature creep-fatigue life prediction techniques, a number of enhancements to creep-rupture parameters and to the time-and-cycle-fraction rule were made. One of the more highly developed methods included strainrange partitioning (SRP), a method which views the creep-fatigue problem in terms of an inelastic strain measure derived from four fundamental straining (or loading) cycles and employs a damage interaction rule to arrive at a life assessment. The ductility-normalized strainrange partitioning (DN-SRP) (ref. 4) provided designers a means of estimating creep-fatigue life from monotonic tensile and creep-rupture data. The total-strain version (TS-SRP) provided a means of predicting creep-fatigue life in terms of the total strains experienced by the structure (ref. 5). As aeropropulsion became more sophisticated and advanced materials were developed, we increased our level of intensity and degree of sophistication in life prediction modeling. At the present time, emphasis is placed on methods capable of dealing with both thermal and mechanical fatigue under severe environments. Life prediction methods under development include those designed to handle anisotropic materials such as directionally-solidified (DS) or single-crystal materials, as well as improvements addressing thermomechanical fatigue. The bithermal testing technique, originated and developed at Lewis, has shown considerable promise. The bithermal test is one which is substantially easier to perform as well as to interpret (ref. 6). Many of the first order behaviors of TMF are captured in the bithermal experiment. We are also looking to the needs of the future and are beginning to do research on the advanced methods that will be required of advanced materials and propulsion systems over the next 10 to 20 years. In this context, models

of damage evolution for composite materials and models which integrate crack initiation, crack growth and fracture models are being pursued.

HIGH-TEMPERATURE FATIGUE CRACK INITIATION

A comparison of the predictive accuracy of two relatively recent (1983, 1984) isothermal life prediction methods for fatigue crack initiation (0.030-in.-length surface crack): the HOST cyclic damage accumulation (CDA) model developed by Pratt & Whitney under contract to Lewis (ref. 7), and the total strain versions of Lewis' strainrange partitioning (TS-SRP) (ref. 5), is shown in figure 4. Note the rather sizeable factors of 3, and hence, our inability to predict the high-temperature, low-cycle fatigue lives of coupons of a cast nickel-base turbine alloy. Factors of safety of nearly an order of magnitude on average life would have to be applied if these methods were to be used in a design situation. While this appears to be a very large factor, it is considerably less than would be required by alternate methods.

COMPLEX LOADING AND CUMULATIVE DAMAGE

Mission profiles resolve into complex thermal and mechanical loading histories on many components (fig. 5). Components whose lives are limited as a result undergo creep and fatigue in varying and interacting degrees, which eventually lead to failure. One such typical component is a hot-section turbine blade.

When considering the life of components subjected to complex mechanical loading histories, it is common to use a fatigue crack initiation life criterion in conjunction with a suitable damage accumulation expression. Traditionally, the damage accumulation expression used is the classical linear damage rule (ref. 8). While this rule simplifies life prediction calculations, it can often lead to unconservative designs, especially under certain loading conditions. An advancement in increasing the accuracy of life predictions by using a nonlinear damage accumulation rule was made at Lewis recently. This new expression, called the double damage curve approach (ref. 9), accounts for loading level dependence in damage evolution. The resulting increase in predictive accuracy is substantial, as much as nearly an order of magnitude improvement over the linear damage rule (fig. 6).

HIGH-TEMPERATURE FATIGUE CRACK PROPAGATION

High- and low-temperature cyclic crack propagation life predictions based on the concepts of path-independent integrals and crack tip oxidation mechanisms have been developed under NASA Lewis sponsorship for turbine alloys (ref. 10, fig. 7). This life prediction method is the result of several years of research conducted by H. W. Liu of Syracuse University under the HOST program sponsorship of NASA Lewis. Note again the rather sizeable scatter of factors of 3 on crack propagation rate even for well-controlled laboratory coupon tests.

COMBUSTOR LINER STRUCTURAL AND LIFE ANALYSIS

An application of the Lewis-originated creep-fatigue life prediction method, strainrange partitioning (for crack initiation), is shown in figure 8. Pratt & Whitney modified the approach to suit their unique requirements and used the method in the design and evaluation of combustor liners in the JT9D high-bypass-ratio engine (ref. 11). Factors of about 2 in cyclic lifetime are noted. This remarkably good accuracy is obtained, in part, by the manner in which the Pratt & Whitney version of the method is calibrated to the failure behavior of real hardware. The variation in predicted lives results from different engine usage which can be accommodated by the predictive method.

TURBINE BLADE STRUCTURAL AND LIFE ANALYSIS

In another application of the Lewis-originated creep-fatigue life prediction method, strainrange partitioning, the General Electric Company analyzed an air-cooled turbine blade, making an assessment of expected service life (ref. 12). This particular blade, a first-stage, high-pressure turbine blade, is subjected to cyclic thermal straining in the tip cap region because of the service history involved (fig. 9). After conducting a thermal analysis and a nonlinear structural analysis of the cap region, an assessment of component life was performed. The analysis was supplemented by laboratory experiments on the blade alloy for the temperature-strain history calculated from the analysis. Strainrange partitioning was found to predict component life over a range which spanned the observed service life.

BRITTLE MATERIALS DESIGN METHOD

The design of brittle ceramics differs from that of ductile metals because of the inability of ceramic materials to redistribute high local stresses caused by inherent flaws. Random flaw size and orientation require that a probabilistic analysis employing the weakest link theory be performed if the component reliability is to be determined. The lack of adequate design technology, such as general purpose design programs, standards, nondestructive evaluation (NDE) expertise, and codes of procedure has prompted NASA Lewis to initiate research focused on ceramics for heat engines at the beginning of this decade. One of the early accomplishments of this effort has been the development of the unique, public-domain design program called Structural Ceramics Analysis and Reliability Evaluation (SCARE) (fig. 10). It is still under development, with new enhancements in improved fast fracture and time-dependent reliability analysis being added and validated.

NONDESTRUCTIVE EVALUATION (NDE) TECHNOLOGY

The need for nondestructive materials characterization is indicated where local properties are critical or where the presence, identity, and distribution of potentially critical flaws can only be assessed statistically. In the latter case, flaws can be so microscopic, numerous, and dispersed that it is impractical to resolve them individually. Large populations of nonresolvable flaws may interact with each other (e.g., surface versus volume flaws) or with morphological anomalies. These interactions would be manifested as degraded

bulk properties (e.g., deficiencies in strength and toughness). Although a structure may be free of discrete critical flaws, it may still be susceptible to failure because of inadequate or degraded intrinsic mechanical properties. This can arise from faulty material processing and/or degradation under aggressive service environments. It is important, therefore, to have nondestructive methods for quantitatively characterizing mechanical properties. Figure 11 describes the use of NDE methods.

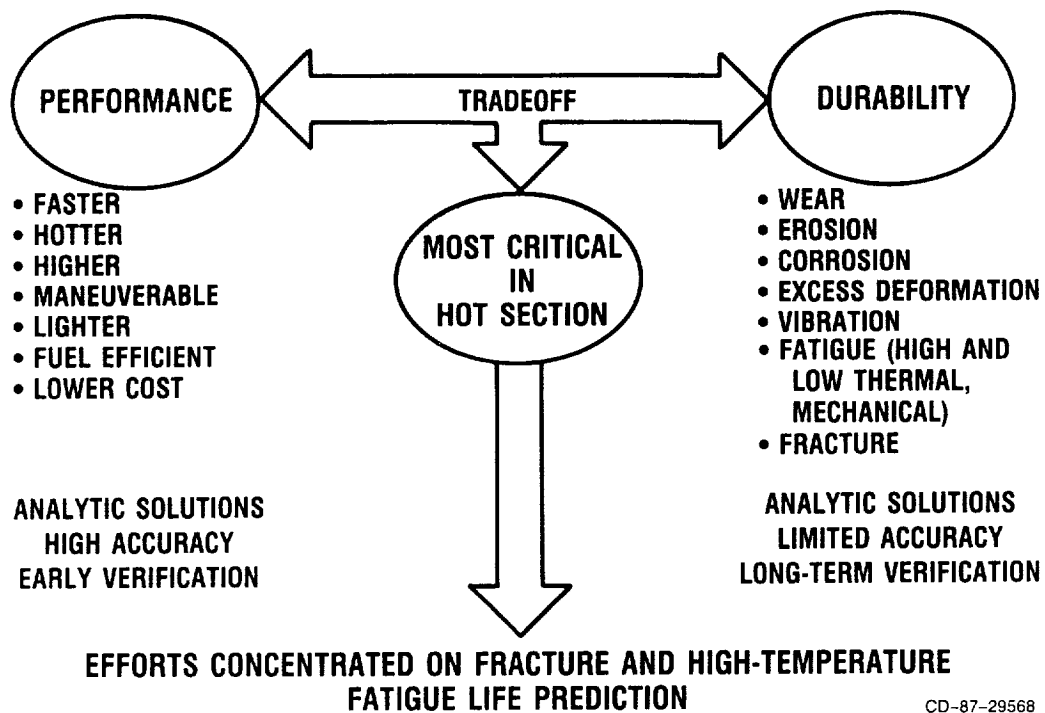
CONCLUDING REMARKS

The NASA Lewis Research Center has been actively involved in developing life prediction technology to address durability problems in aeronautical gas turbine engines. Current research programs are addressing the problem of thermal and mechanical fatigue, and a number of predictive methods have been developed which possess greater accuracy. As the aerospace field moves toward higher performance propulsion systems resulting in the introduction of new materials and configurations (e.g., composites), the Center is embarking on a program of research to address the unique problems these materials and their operating environments present.

REFERENCES

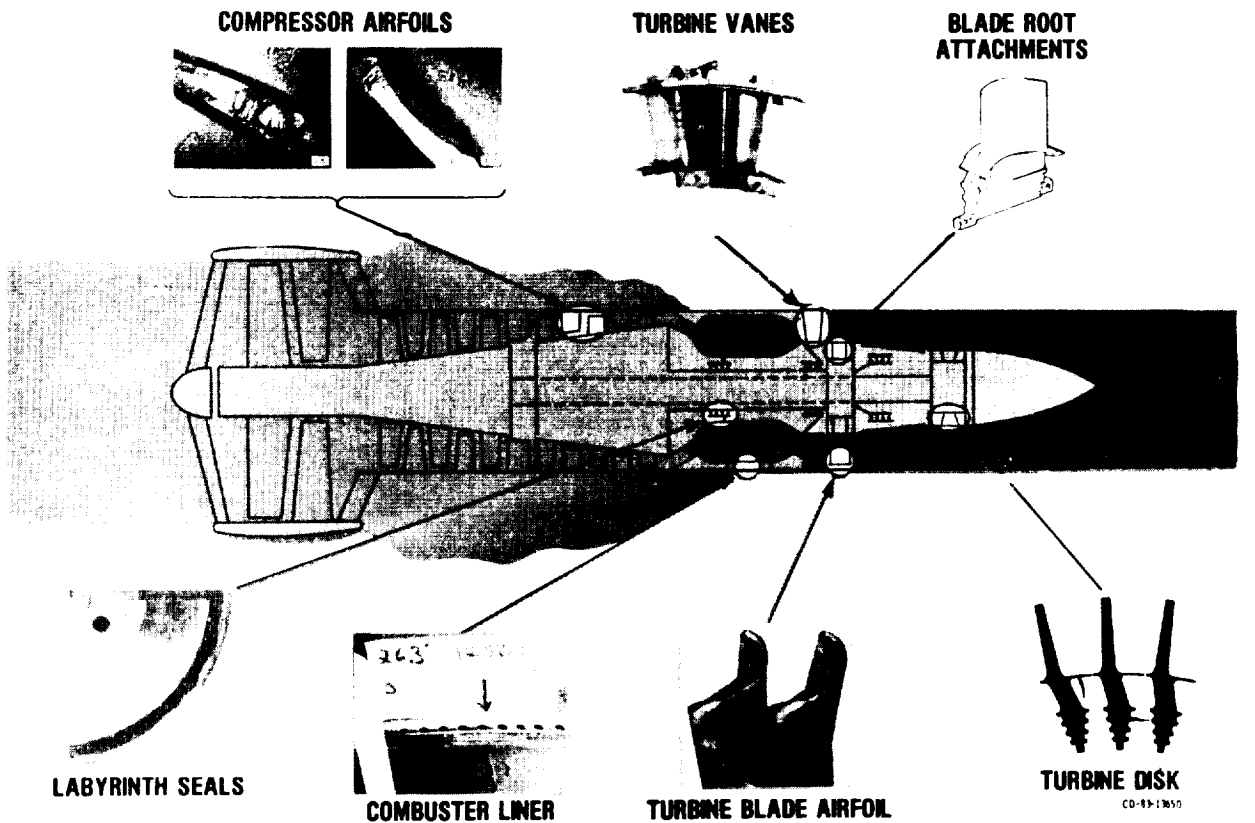
1. Manson, S.S.: Behavior of Materials Under Conditions of Thermal Stress. NACA TN-2933, 1953.
2. Coffin, L.F., Jr.: A Study of the Effects of Cyclic Thermal Stresses on a Ductile Metal. Trans. ASME, vol. 76, no. 6, Aug. 1954, pp. 931-950.
3. Manson, S.S.: Fatigue: A Complex Subject--Some Simple Approximations. Exper. Mech., vol. 5, no. 7, July 1965, pp. 193-226.
4. Halford, G.R.; Saltsman, J.F.; and Hirschberg, M.H.: Ductility Normalized-Strainrange Partitioning Life Relations for Creep-Fatigue Life Predictions. Environmental Degradation of Engineering Materials, M.R. Louthan, Jr., and R.P. McNitt, eds., Virginia Tech Printing Dept., V.P.I. and State University, Blacksburg, VA, 1977, pp. 599-612. (NASA TM-73737.)
5. Halford, G.R.; and Saltsman, J.F.: Strainrange Partitioning - A Total Strainrange Version. NASA TM-83023, 1983.
6. Halford, G.R., et al.: Bithermal Fatigue: A Link Between Isothermal and Thermomechanical Fatigue. Low Cycle Fatigue, ASTM STP 942, H.D. Solomon et al., eds., American Society for Testing and Materials, 1988, pp. 625-637.
7. Moreno, V., et al.: Application of Two Creep-Fatigue Life Models for the Prediction of Elevated Temperature Crack Initiation of a Nickel-Base Alloy. AIAA Paper 85-1420, July 1985.
8. Miner, M.A.: Cumulative Damage in Fatigue. J. Appl. Mechanics, vol. 12, no. 3, Sept. 1945, pp. 159-164.
9. Manson, S.S.; and Halford, G.R.: Re-Examination of Cumulative Fatigue Damage Analysis - An Engineering Perspective. Eng. Fract. Mech., vol. 25, no. 5/6, 1986, pp. 539-571. (NASA TM-87325).

10. Liu, H.W.; and Oshida, Y.: Grain Boundary Oxidation and Fatigue Crack Growth at Elevated Temperatures. Theoretical Appl. Fract. Mech., vol. 6, no. 2, Oct. 1986, pp. 85-94.
11. Moreno, V.: Combustor Liner Durability Analysis. (PWA-5684-19, Pratt and Whitney Aircraft Group's NASA Contract NAS3-21836) NASA CR-165250, 1981.
12. McKnight, R.L., et al.: Turbine Blade Nonlinear Structural and Life Analysis. J. Aircraft, vol. 20, no. 5, May 1983 ,pp. 475-480.



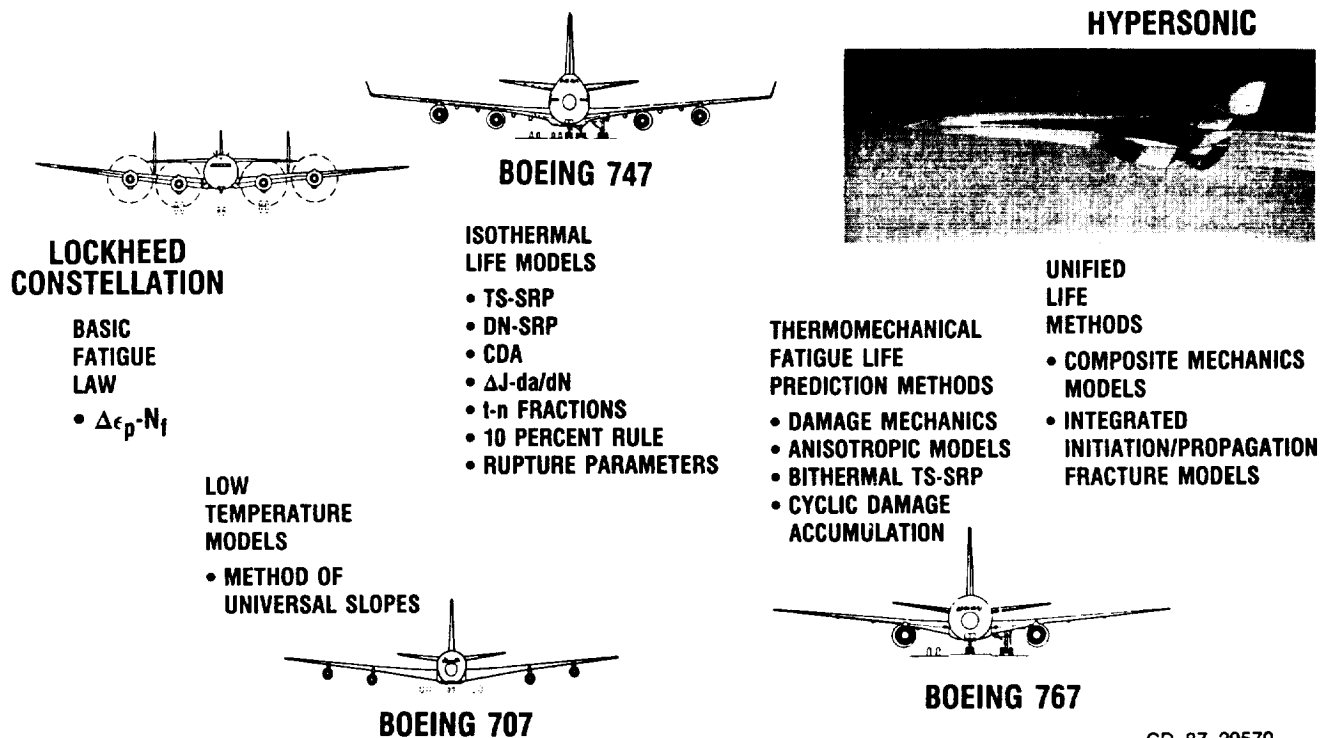
CD-87-29568

Figure 1. - Performance versus durability.



CD-87-29569

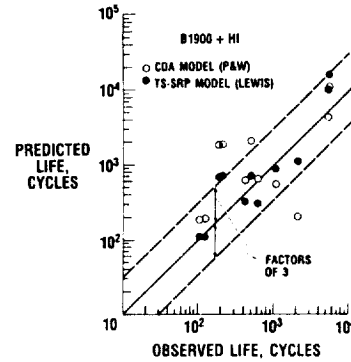
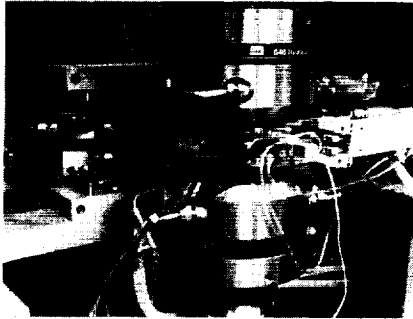
Figure 2. - Gas turbine fatigue and fracture problem areas.



CD-87-29570

Figure 3. - Lewis Research Center has contributed to fatigue research since the 1950's.

ISOTHERMAL VERIFICATION



CYCLIC DAMAGE ACCUMULATION (CDA) MODEL

$$\dot{\epsilon}_{Pnet} - \left[\frac{dD}{dN} \right]_{Ref} \times \left\{ \left(\frac{\sigma_t}{\sigma_{tRef}} \right) \left(\frac{\Delta\sigma}{\Delta\sigma_{Ref}} \right) + \left[\left(\frac{\Delta\sigma_{Ref}}{\Delta\sigma} \right) \left(\frac{\sigma_t}{\sigma_{tRef}} \right) \right]^b \times \left[\left(\frac{t}{t_{Ref}} \right)^c - 1 \right] \right\} dN = 0$$

TOTAL STRAIN, STRAINRANGE PARTITIONING (TS-SRP)

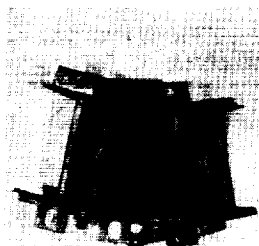
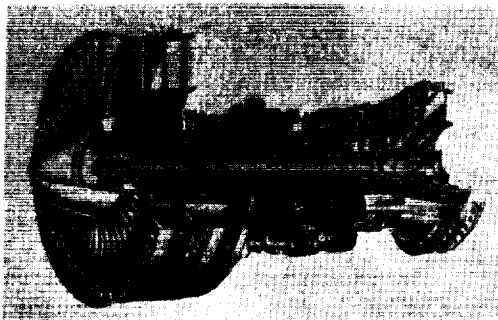
$$\Delta\epsilon = K_{ij} (C')^n N_f^b + C' N_f^c$$

$$C' = \left[\sum F_{ij} (C_{ij})^{uc} \right]^c$$

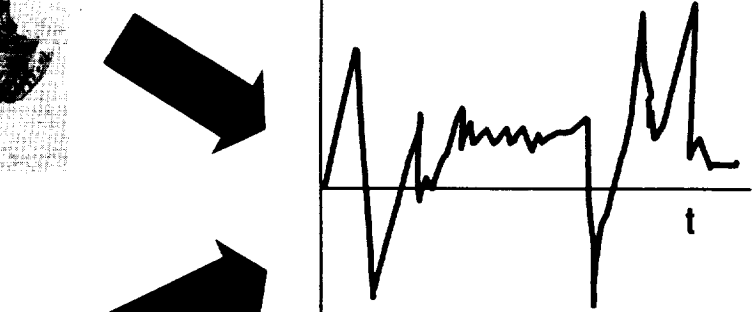
CD-87-29571

Figure 4. - High-temperature fatigue crack initiation.

ENGINE



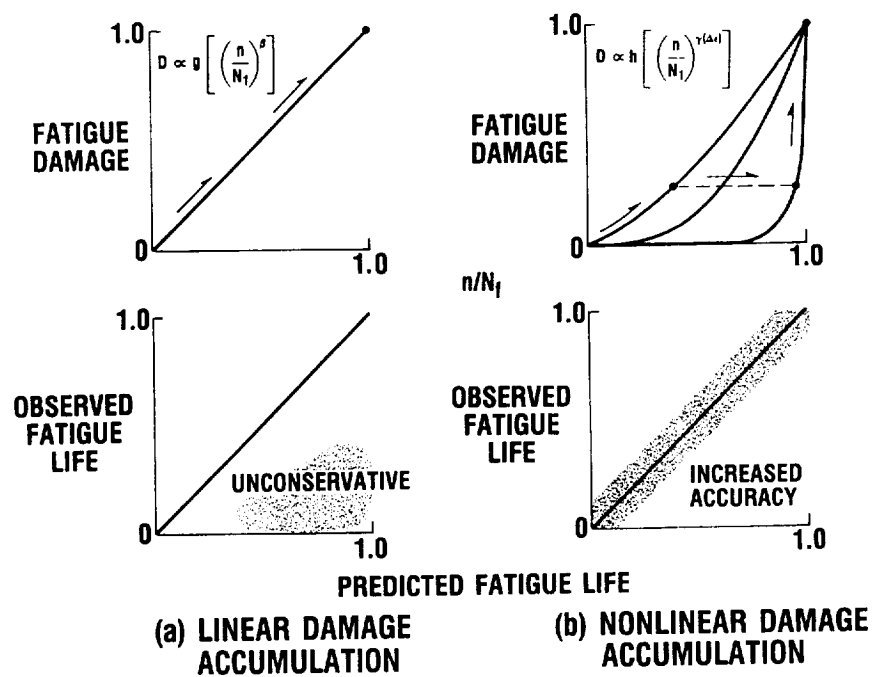
TURBINE COMPONENT



MISSION HISTORY AS SEEN
BY TURBINE COMPONENT

CD-87-29572

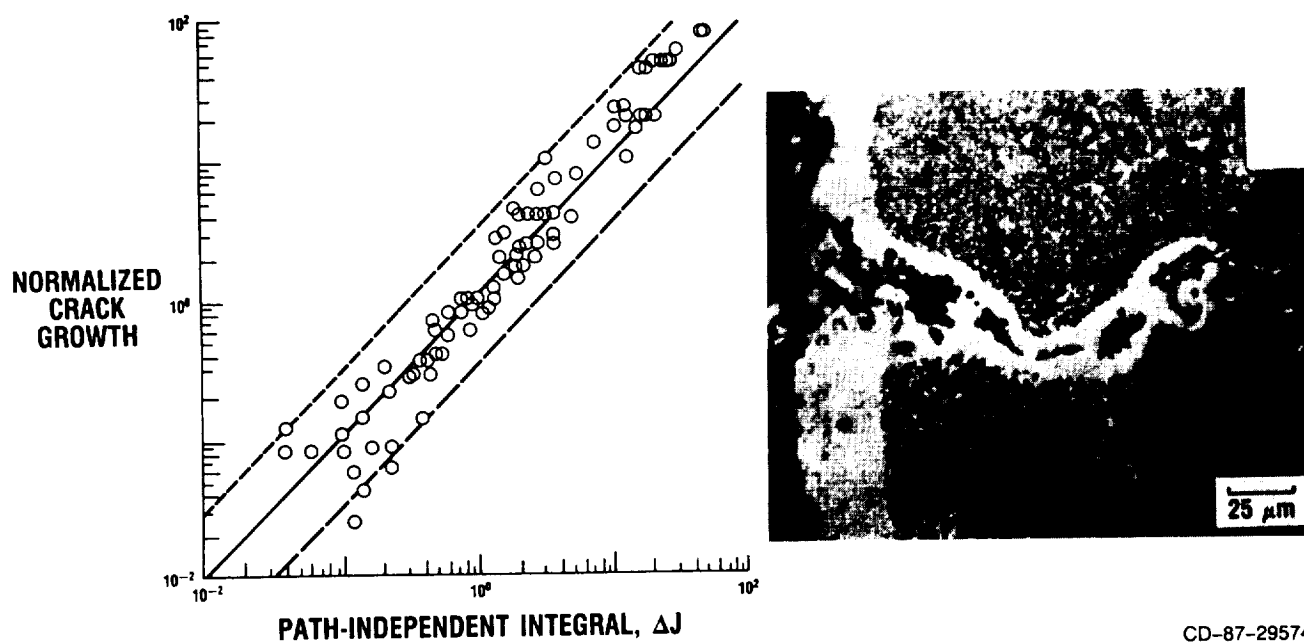
Figure 5. - Mission history produces complex component loading histories.



CD-87-29573

Figure 6. - Lewis nonlinear damage accumulation theories accurately model cumulative fatigue.

ΔJ PARAMETER FOR LOW TEMPERATURE OXIDATION MODEL FOR HIGH TEMPERATURE



CD-87-29574

Figure 7. - Isothermal fatigue crack propagation model.

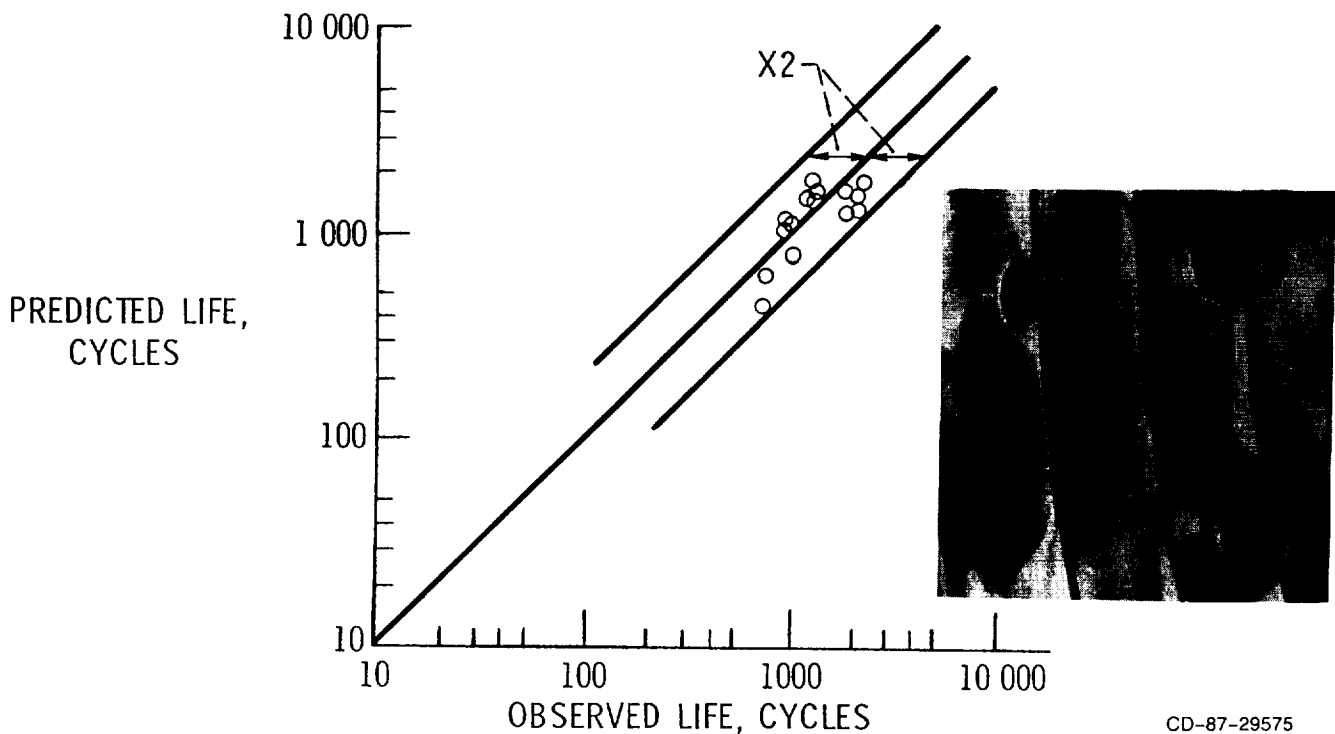


Figure 8. - Accuracy of Pratt & Whitney's version of ductility normalized strain-range partitioning in predicting combustor liner life in high-bypass-ratio engines.

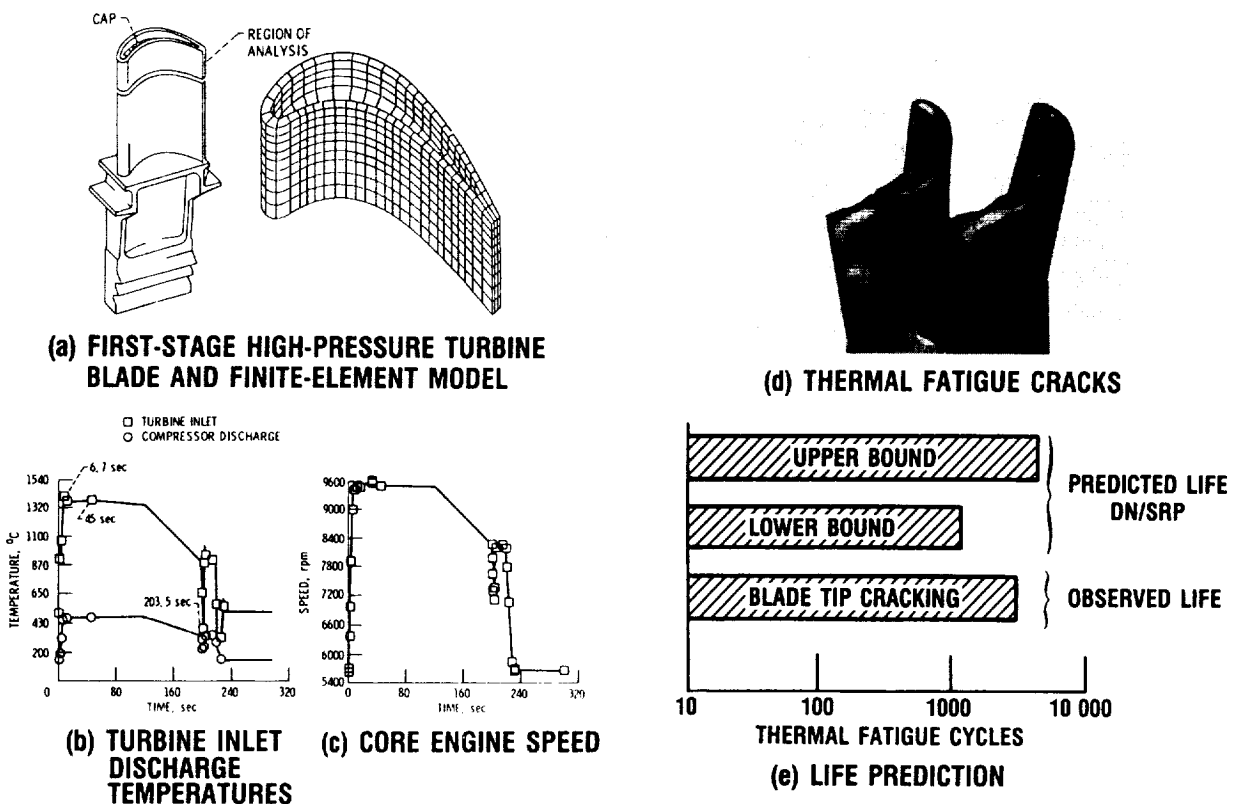
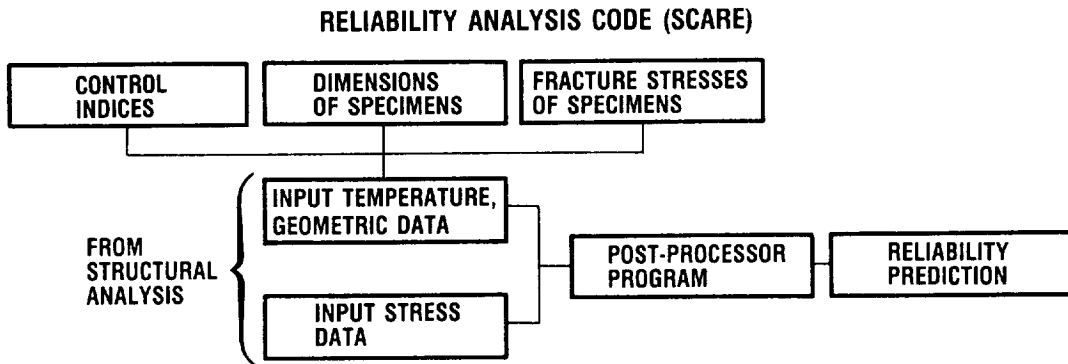


Figure 9. - Turbine blade structural and life analysis.

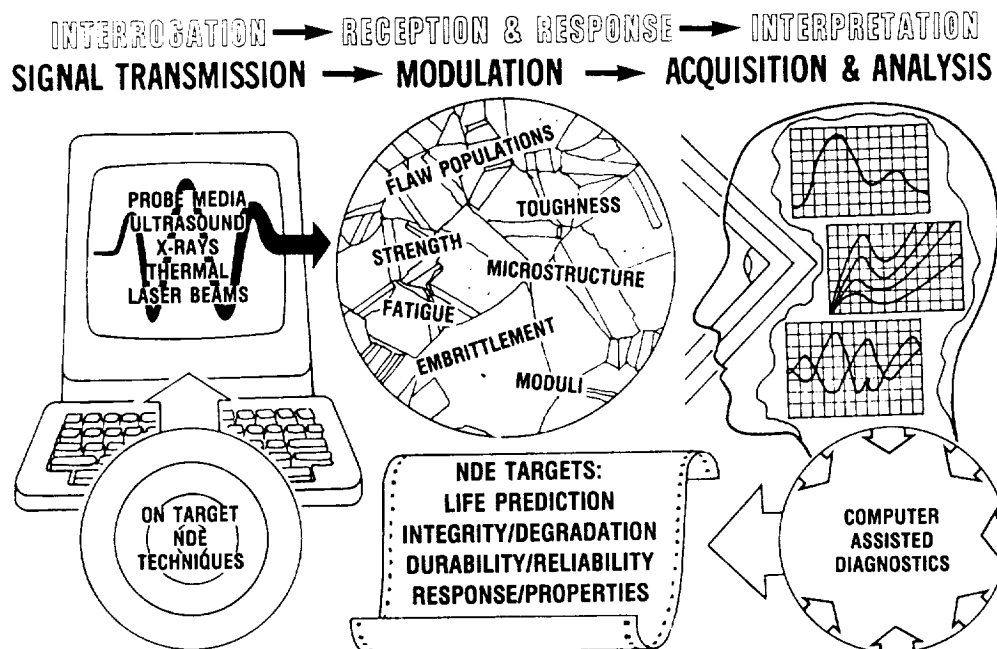
MATERIAL BRITTLENESS AND PRESENCE OF DEFECTS REQUIRE

- **PROBABILISTIC APPROACH ALLOWING FOR STRENGTH DISPERSION**
- **USE OF WEAKEST LINK THEORY TO TREAT SIZE EFFECT**
- **REFINED THERMAL AND STRESS ANALYSIS—FIELD SOLUTIONS**



CD-87-29577

Figure 10. - Ceramics/brittle materials life prediction technology.



CD-87-30079

Figure 11. - Nondestructive evaluation (NDE) technology.

INTEGRATED ANALYSIS AND APPLICATIONS

Dale A. Hopkins

SUMMARY

An overview is presented of current research activities which, in a broad context, are focused on the development and verification of integrated structural analysis and optimal design capabilities for advanced aerospace propulsion and power systems. The overview encompasses a variety of subject areas including (1) composite materials, (2) advanced structural analysis, (3) constitutive modeling, (4) computational simulation, (5) probabilistic analysis, and (6) multidisciplinary optimization. Typical results are presented which illustrate the benefit and utility of the emerging technologies as applied to propulsion and power system structures.

INTRODUCTION

The perpetual "ideology" of propulsion system design is to achieve increasingly higher levels of performance and, at the same time, longer life cycles. This presents difficult challenges for the structural engineer to provide, in the most cost-effective manner possible, designs that are lightweight, fuel-efficient, durable, and reliable. Successful accomplishment of these tasks depends on the availability of structural analysis and design tools that are capable of accurately and efficiently representing the complex geometries, material responses, loading histories, and boundary conditions typical of propulsion system structures.

With an objective to address these needs, the Structures Division of NASA Lewis Research Center is conducting a variety of research and development activities. It is the purpose here to provide an executive overview of a sample of those efforts from which particularly promising technologies have recently emerged or which represent the most current programmatic emphasis. The overview encompasses a variety of subject areas including

- (1) Composite materials - analytical models (composite mechanics), integrated computational capabilities, and experimental characterization of composite structural behavior and durability for polymer, metal, and ceramic matrix systems
- (2) Advanced structural analysis - algorithms and numerical schemes for more accurate and efficient inelastic analyses
- (3) Constitutive modeling - theoretical model formulation and experimental characterization of thermoviscoplastic material behavior

- (4) Computational simulation - engine structures from single components to assemblies and up to an entire engine system subjected to simulated test-stand and mission load histories
- (5) Probabilistic structural analysis - quantification of uncertainty in geometry, material, load, and boundary conditions on structural response for reliability assessment
- (6) Structural optimization - implementation of mathematical optimization and multidisciplinary analyses to provide streamlined, autonomous optimal design systems

In some instances, typical results are presented which illustrate the benefit and utility of these emerging technologies as applied to propulsion system structures.

INTEGRATED COMPOSITES ANALYZER

The numerous properties needed for composite structural analysis and design, combined with the difficulty and expense of obtaining experimental measurements of these properties, has motivated development of the Integrated Composites Analyzer (ICAN) computer code (refs. 1 and 2). The ICAN code incorporates the necessary composite mechanics to perform point analysis of multilayered fiber composite laminates subjected to arbitrary hygrothermal environments. Input variables to ICAN include constituent material system(s), laminate configuration, fabrication conditions, and service environment. The ICAN code predicts virtually all composite hygral, thermal, and mechanical properties necessary to perform structural analysis and has proven to be an effective tool for preliminary design of composite structures. Confidence in the predictive capabilities of ICAN has been established through favorable comparisons with experimental data obtained for a variety of composite systems in extreme hygrothermal environments (fig. 1).

COMPUTATIONAL SIMULATION OF COMPOSITE SANDWICH STRUCTURE

A recent enhancement of the ICAN computer code has extended its applicability to composite sandwich structural configurations. This new feature of ICAN was demonstrated recently in the preliminary design of composite antenna reflector structure for the Advanced Communications Technology Satellite (refs. 3 and 4). In this application, parametric studies were conducted to determine desirable face sheet and honeycomb core configurations necessary to provide thermal distortion-free structure in the simulated space environment. A critical variable of interest in the investigation was the effective thermal expansion coefficient for a candidate configuration and its variation over the range of simulated hygrothermal conditions representative of the space environment (fig. 2). The approximate methodology developed to simulate thermostructural behavior of sandwich composites has been demonstrated to be highly effective for preliminary design purposes (ref. 5).

COMPREHENSIVE EVALUATION OF COMPOSITE DURABILITY

In an effort to characterize durability and damage tolerance of composite structures, a comprehensive research program is ongoing to develop analytical models with experimental verification. The analytical models including composite mechanics, composite failure theories, and cumulative damage models are incorporated into the Composite Durability Structural Analyzer (CODSTRAN) computer code (refs. 6 and 7). The CODSTRAN code assesses durability in terms of defect growth and damage progression on a ply-by-ply basis through an incremental/iterative solution scheme. The companion experimental program is conducted by using the unique Real-Time Ultrasonic C-Scan (RUSCAN) facility where sequential graphic images are created from acoustic emissions taken in real time of a specimen as it is incrementally loaded to fracture. The excellent correlation achieved between the CODSTRAN predictions and experimental observations (fig. 3) enhances confidence in the ability to analytically assess durability of composite structures.

STRUCTURAL ANALYSIS FOR HIGH-TEMPERATURE COMPOSITES

The mechanical performance and structural integrity of high-temperature composites is ultimately governed by the behavior of the constituents (i.e., fiber, matrix, and interphase) locally. This local constituent behavior is dynamic and complex because of various nonlinearities associated with, for example, (1) large excursions in stress/strain, (2) temperature-dependent material properties, and (3) time-dependent effects. In the analysis/design of a composite structure, then, it is essential to be able to track this local behavior and to relate its effects on global structural response. An integrated approach has been developed to provide this capability by incorporating constituent material models and cumulative damage models, composite mechanics (micro and macro), and global structural analysis (fig. 4). The cyclic arrangement depicts the computational effort for each load increment of a nonlinear structural analysis. Material nonlinearity is treated at the constituent level, where the present material model defines a time-temperature-stress dependence of a constituent's mechanical and thermal properties at a given instant in its "material history space." Characteristic properties of the composite, at the various levels of simulation, are approximated on the basis of the instantaneous constituent properties by using composite mechanics models. This process termed "synthesis" results in a point description of equivalent pseudohomogeneous properties for the composite which can be used for subsequent global structural analysis. In a similar manner global response variables can be decomposed into localized response, again at the various levels of simulation. This integrated approach has recently been implemented into the Metal Matrix Composite Analyzer (METCAN) computer code (ref. 8). An example of the type of information obtained from METCAN is the nonlinear stress-strain response to monotonic loading at room temperature for tungsten/copper composites (unidirectional) of two different fiber volume fractions (fig. 5). Exhibited in the results is the excellent correlation between METCAN predicted response and experimental observations.

METAL MATRIX COMPOSITE TECHNOLOGY DEVELOPMENT

Through a cooperative effort between the Structures and Materials Divisions, Lewis Research Center is providing a unique contribution to the

development of metal matrix composite (MMC) technology (fig. 6). The Materials Division is capable of fabricating thin-walled tubular MMC specimens (ref. 9), which are then tested by the Structures Division under multiaxial conditions at elevated temperatures (ref. 10). From these tests the necessary material functions and parameters can be determined to support theoretical formulation of viscoplastic constitutive models (ref. 11). The constitutive models, in turn, are implemented into advanced structural analysis computer codes to predict the response of MMC components subjected to complex thermomechanical loading histories. These analyses provide important information to aid the engineer in making design decisions for actual aerospace propulsion system applications.

ADVANCED INELASTIC STRUCTURAL ANALYSIS METHODS

The desire for increased performance and efficiency of gas turbine engines has led to designs having more severe operating cycles (i.e., higher pressures and temperatures). The general result has been an exhibited decrease in engine durability with associated increase in maintenance costs, particularly in the hot section, where more hostile environments accelerate component wear and damage. Reliable, cost-effective design to achieve prescribed durability requires effective (i.e., accurate and efficient) structural analysis tools that account for the complex geometries, loading conditions, and forms of non-linear material response that are characteristic of these components in their operating environment (fig. 7). A broad spectrum of structures technology development carried out under the Hot Section Technology (HOST) Program (ref. 12) is addressing these needs. These efforts encompass three key elements: (1) constitutive modeling, which includes theoretical formulation of viscoplastic constitutive models for both isotropic and anisotropic materials to improve the stress-strain prediction of structures subjected to cyclic thermomechanical loads, (2) experimentation to aid in the development and verification of analytical models as well as the development and evaluation of advanced instrumentation, and (3) computations to develop algorithms, advanced numerical techniques, and self-adaptive solution strategies.

ADVANCED COMBUSTOR LINER STRUCTURAL CONCEPT EVALUATION

Advanced combustor liner structural concepts and materials are being tested and analyzed as part of a cooperative program between NASA Lewis Research Center and Pratt & Whitney Aircraft (ref. 12). The integrated and interdisciplinary test/analysis program is conducted for advanced "floatwall" or paneled combustor liner segments. The cyclic tests, conducted in the Structural Component Response Rig, simulate the taxi, ascent, cruise, and descent temperature transients of an engine flight profile by using a computer-controlled quartz lamp heating system. High-quality data bases of liner temperatures and distortions are obtained for calibration and verification of analytical models and computational tools used for predicting the structural response and life of representative liners (fig. 8).

METHODOLOGY OF LEADING EDGE CONCEPT EVALUATION

Leading edges on hypersonic aircraft are subjected to high-heat-flux loads induced by aerodynamic friction. To accommodate this requires advanced

high-temperature materials and structural cooling. In response, the Cowl Lip Technology Program is underway to evaluate materials and actively cooled leading edge concepts (ref. 13). The problem is approached through an integrated program of design, analysis, fabrication, and testing (fig. 9). Leading edge concepts are designed, and representative test articles are fabricated from candidate materials including metal and ceramic matrix composites. The articles are tested in a high-heat-flux facility to obtain experimental data for comparison with analytical predictions. The data and analytical predictions provide the basis for assessing the design concept.

ENGINE STRUCTURES COMPUTATIONAL SIMULATOR

A major element of the Computational Structural Mechanics Program (ref. 14) is the development of the Engine Structures Computational Simulator (ESCS). The ESCS, which incorporates discipline-specific methodology and computer codes developed under several research and technology programs, is intended to simulate the structural behavior and performance under test-stand or flight-mission conditions or both. The simulation can be for subcomponents (airfoil), components (turbine blade), subassemblies (rotor sector), assemblies (rotor stage), and up to the entire engine (fig. 10). New design concepts, materials, mission requirements, and so on, can be simulated and their potential benefits evaluated prior to final design and certification testing. Local or component damage effects on engine structural performance can be assessed, and engine structural durability and integrity can be determined. With the availability of this information, the probability of unanticipated failures can be established, and the safety of the engine structure can be assessed.

PROBABILISTIC STRUCTURAL ANALYSIS AND DESIGN METHODOLOGY

The variables of the structural design process (i.e., geometry, material properties, loads, and boundary conditions) are known only with some uncertainty. Although risk necessarily accompanies this uncertainty, an assessment of the degree of risk associated with a design is usually not determined. Rather, the traditional approach is to rely on deterministic design methodology which incorporates some sort of safety factor in an attempt to simply avoid risk altogether. Eliminating risk in a design increases safety and reliability but only at some expense, either in the form of direct cost of production or indirect cost of reduced performance efficiency. In the interest of both safety and economy, then, it is desirable to quantify the effects of uncertainty in a design, and probabilistic design methodology provides the means to accomplish this. This philosophy (fig. 11) is especially pertinent to the design of high-performance, high-energy propulsion systems where mission economy and safety requirements of human-rated vehicles are the two primary (and generally competing) design drivers. In this case the ability to accurately quantify risk is essential to establish an acceptable balance between performance and safety. With this motivation the Structures Division is conducting a comprehensive research program to develop probabilistic analysis and design methodology for propulsion system structures (refs. 15 and 16).

STRUCTURAL TAILORING OF ADVANCED TURBOPROP BLADES

The traditional approach to propeller design has been to satisfy requirements on aerodynamic performance and structural integrity independently through numerous manual design iterations. This process, often conducted by different design groups, is time consuming (expensive), cumbersome (error-prone) and highly subjective (potentially unsuccessful). As a result the process is usually carried out only to the point where a satisfactory design, but not likely the best design, is achieved. The Structural Tailoring of Advanced Turboprops (STAT) computer code (ref. 17) was developed to streamline, automate, and formalize the turboprop design process by incorporating multidisciplinary analysis methodology (aerodynamic, acoustic, and structural) together with numerical optimization techniques, into a computationally effective design system. The system has demonstrated its utility in successful optimizations of large-scale advanced propfan designs to achieve reductions of several percent in aircraft direct operating cost (fig. 12).

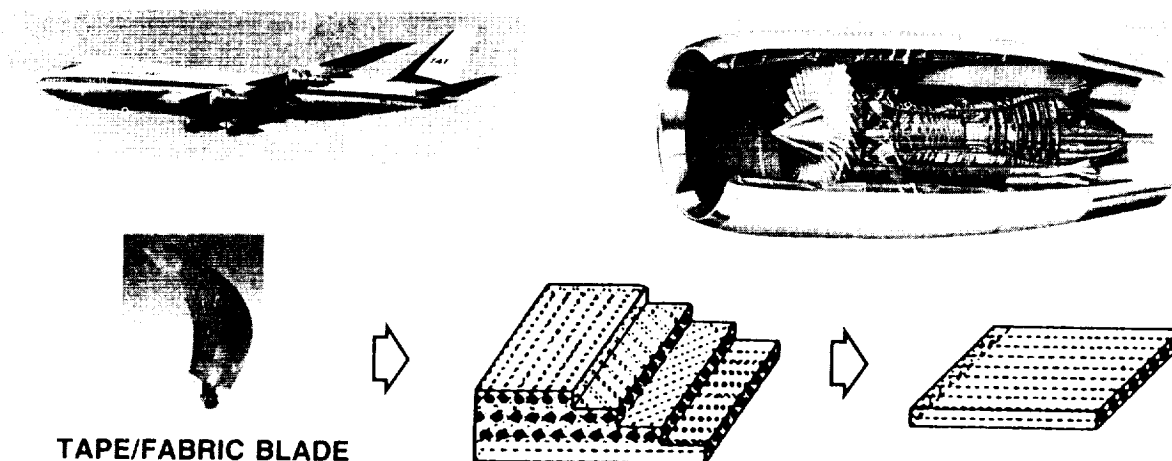
CONCLUDING REMARKS

A cursory overview has been presented of several research activities currently underway in the Structures Division of the NASA Lewis Research Center. From these efforts, promising technologies are emerging which will better enable the structural engineer to conduct the complex analyses required to provide improved designs for aerospace propulsion system structures.

REFERENCES

1. Murthy, P.L.N.; and Chamis, C.C.: ICAN - Integrated Composites Analyzer. AIAA Paper 84-0974, May 1984. (NASA TM-83700.)
2. Ginty, C.A.; and Chamis, C.C.: ICAN - A Versatile Code for Predicting Composite Properties. NASA TM-87334, 1986.
3. Ginty, C.A.; and Chamis, C.C.: Select Fiber Composites for Space Applications - A Mechanistic Assessment. Technology Vectors, SAMPE, 1984, pp. 979-993. (NASA TM-83631.)
4. Ginty, C.A.; and Endres, N.M.: Composite Space Antenna Structures - Properties and Environmental Effects. Proceedings of the 18th International SAMPE Technical Conference, J.T. Hoggatt, S.G. Hill, and J.C. Johnson, eds., SAMPE, 1986, pp. 545-560. (NASA TM-88859.)
5. Chamis, C.C.; and Aiello, R.A.: Composite Sandwich Thermostructural Behavior - Computational Simulation. 27th Structures, Structural Dynamics, and Materials Conference, Part 1, AIAA, 1986, pp. 370-381. (NASA TM-88787.)
6. Irvine, T.B.; and Ginty, C.A.: Progressive Fracture of Fiber Composites. J. Compos. Mater., vol. 20, Mar. 1986, pp. 166-184.
7. Murthy, P.L.N.: Computational Simulation Methods for Composite Fracture Mechanics. Lewis Structures Technology 1988, Vol. 2, Structural Mechanics, NASA CP-3003-VOL-2, 1988, pp. 157-169.

8. Hopkins, D.A.; and Murthy, P.L.N.: METCAN - The Metal Matrix Composite Analyzer. Lewis Structures Technology 1988, Vol. 2. Structural Mechanics, NASA CP-3003-VOL-2, 1988, pp. 141-156.
9. Westfall, L.J.: Tungsten Fiber Reinforced Superalloy Composite Monolayer Fabrication by an Arc-Spray Process. NASA TM-86917, 1985.
10. Bartolotta, P.A.: Experiments Investigating Advanced Materials Under Thermomechanical Loading. Lewis Structures Technology 1988, Vol. 2, Structural Mechanics, NASA CP-3003-VOL-2, 1988, pp. 27-35.
11. Robinson, D.N.: Unified Constitutive Model Development for Metal Matrix Composites at High Temperature. Lewis Structures Technology 1988, Vol. 2, Structural Mechanics, NASA CP-3003-VOL-2, 1988, pp. 49-56.
12. Thompson, R.L.: HOST Structural Analysis Program Overview. Turbine Engine Hot Section Technology 1987, NASA CP-2493, 1987, pp. 13-24.
13. Melis, M.E.; and Gladden, H.J.: Thermostructural Analysis with Experimental Verification in a High Heat Flux Facility of a Simulated Cowl Lip. 29th Structures, Structural Dynamics, and Materials Conference, Part I, AIAA, 1988, pp. 106-115.
14. Chamis, C.C.: Computational Structural Mechanics for Engine Structures. Lewis Structures Technology 1988, Vol. 2, Structural Mechanics, NASA CP-3003-VOL-2, 1988, pp. 189-203.
15. Burnside, O.H.: NESSUS/Expert and NESSUS/FPI in the Probabilistic Structural Analysis Methods (PSAM) Program. Structural Integrity and Durability of Reusable Space Propulsion Systems, NASA CP-2471, 1987, pp. 139-143.
16. Newell, J.F.: Composite Loads Spectra for Select Space Propulsion Structural Components. Structural Integrity and Durability of Reusable Space Propulsion Systems, NASA CP-2471, 1987, pp. 175-188.
17. Brown, K.W.; Harvey, P.R.; and Chamis, C.C.: Structural Tailoring of Advanced Turboprops. 28th Structures, Structural Dynamics, and Materials Conference, Part I, AIAA, 1987, pp. 827-837.



ICAN COMPARISON

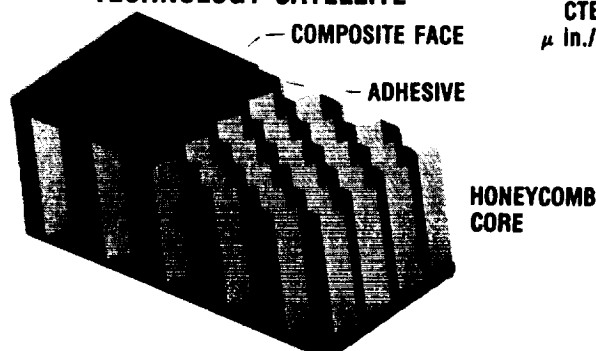
LAMINATE MATERIAL	LONGITUDINAL ELASTIC MODULUS, ksi					
	EXPERIMENTAL			ICAN PREDICTIONS		
	-300 °F	70 °F	200 °F	-300 °F	70 °F	200 °F
7781E-GLASS CLOTH	4600	4370	3970	4589	4251	4076
7576E-GLASS CLOTH	6540	6020	6050	5587	5395	5457
REPRESENTATIVE	5320	4370	4150	4440	4114	3948

CD-87-28951

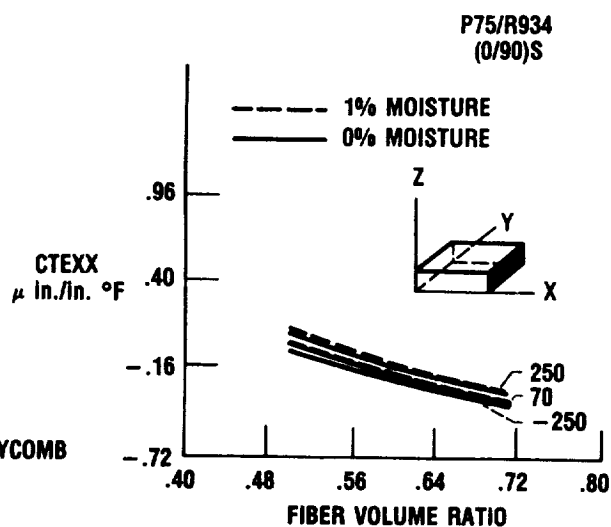
Figure 1. - Integrated Composites Analyzer (ICAN).



ACTS ADVANCED COMMUNICATION TECHNOLOGY SATELLITE



COMPUTER-GENERATED MODEL OF THE STRUCTURE USED FOR THE ANALYSIS



CD-87-28957

Figure 2. - Composite sandwich structural simulation for satellite antenna reflectors.

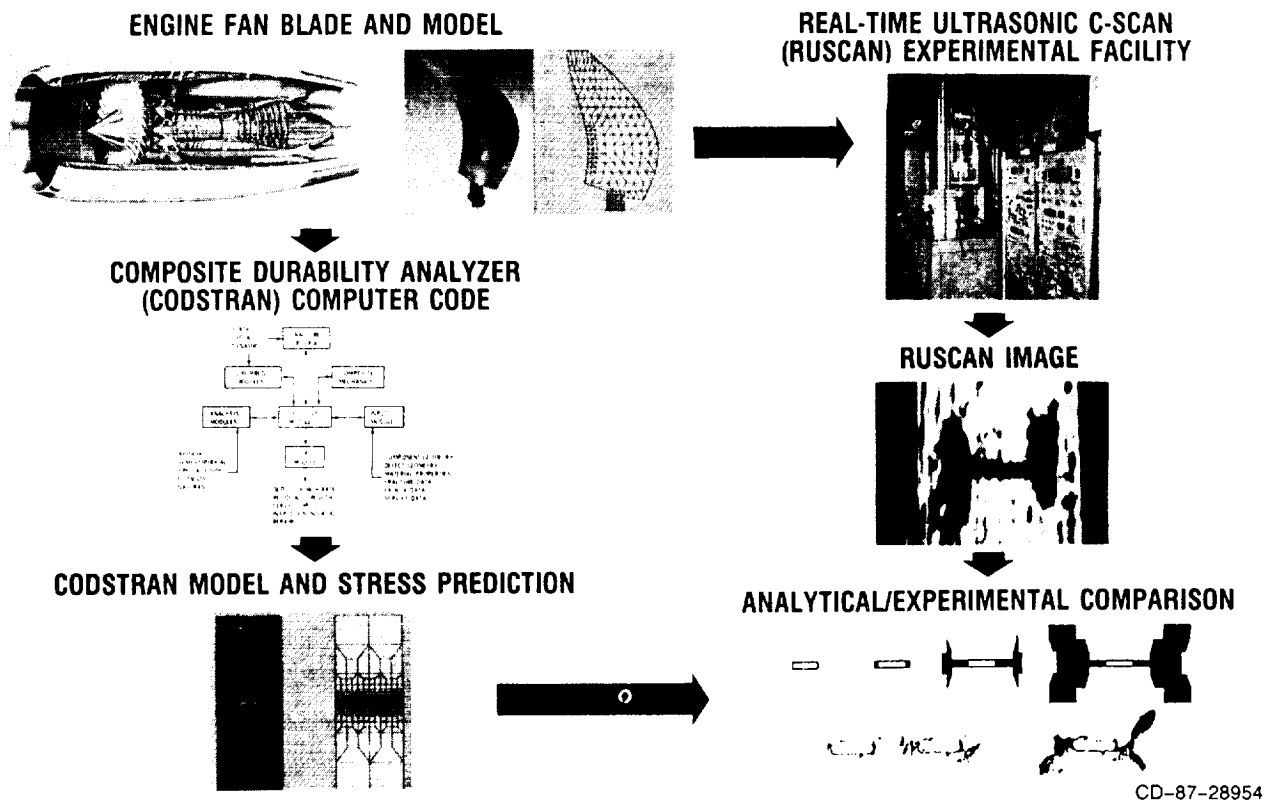


Figure 3. - Comprehensive analytical/experimental evaluation of composite durability.

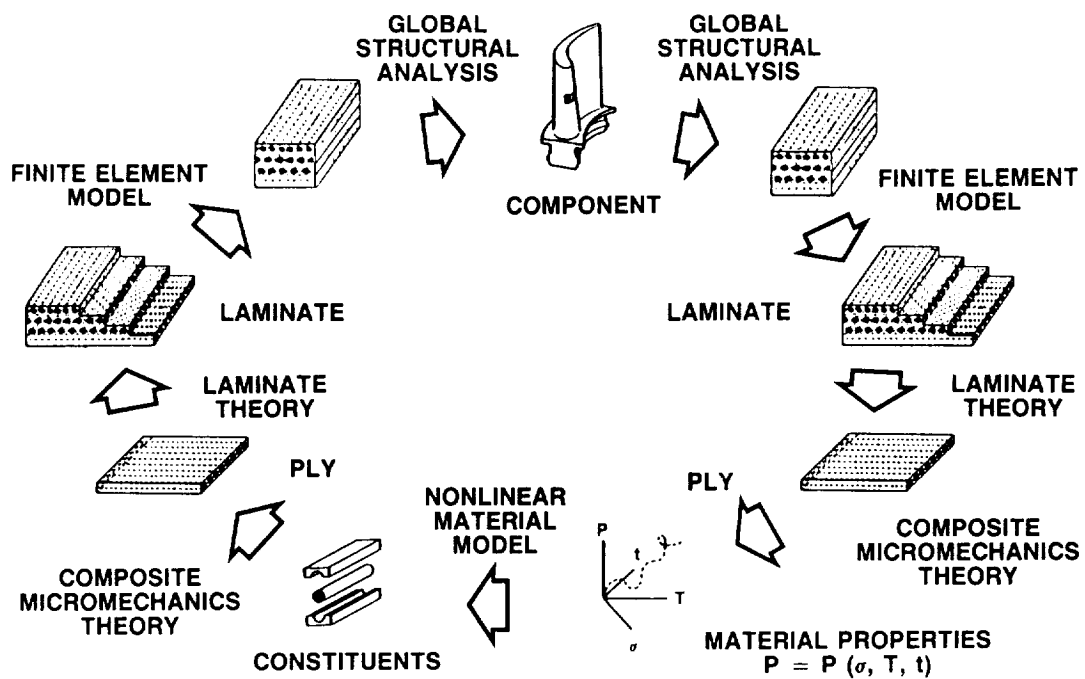
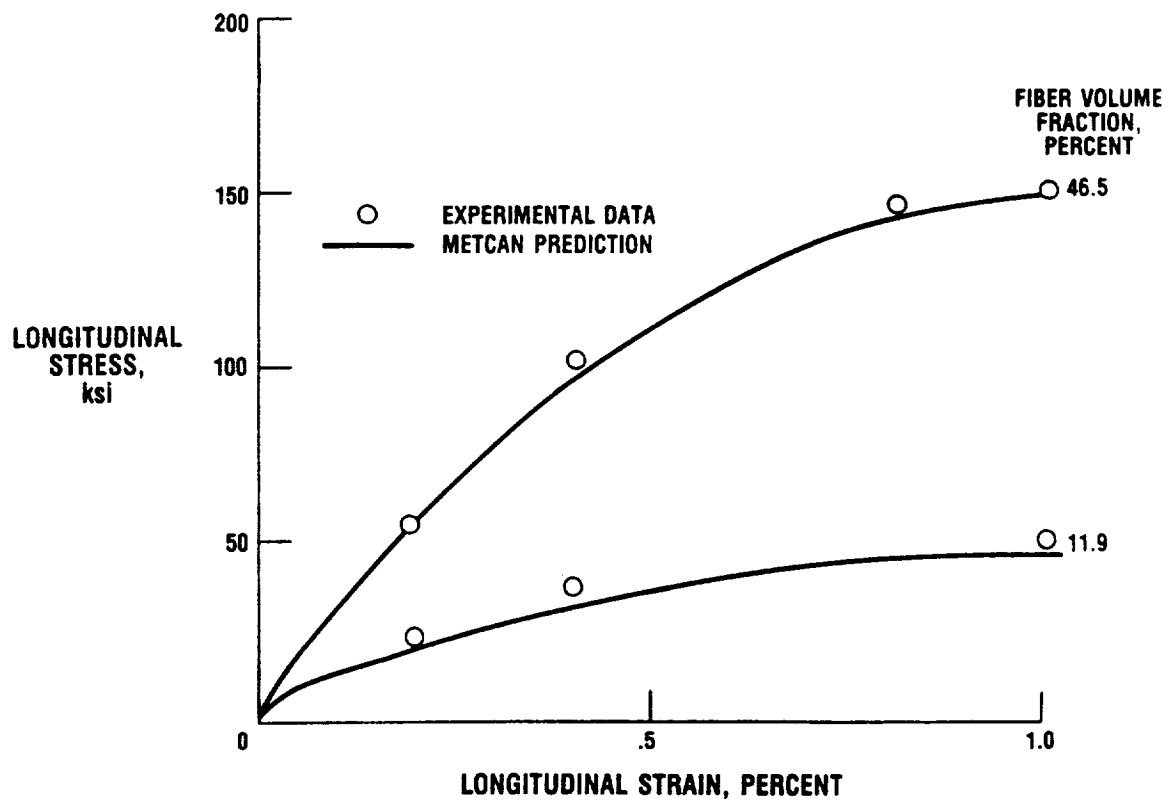
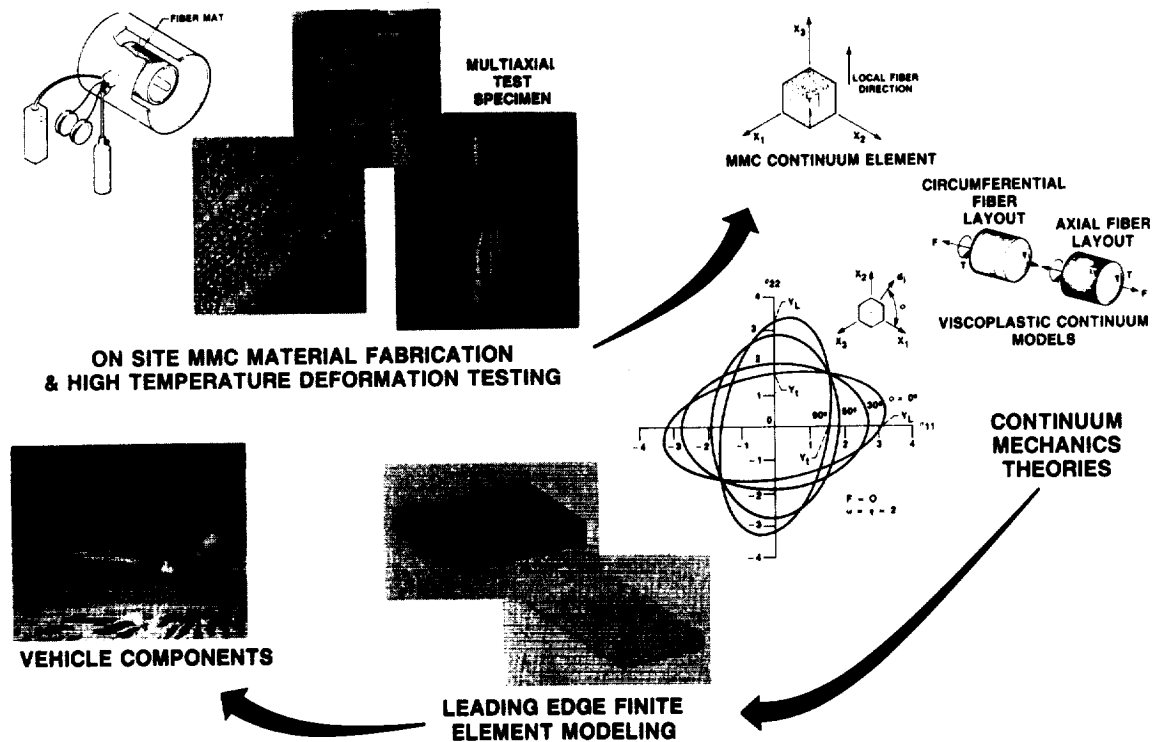


Figure 4. - Integrated approach to structural analysis for high-temperature composites.



CD-88-32587

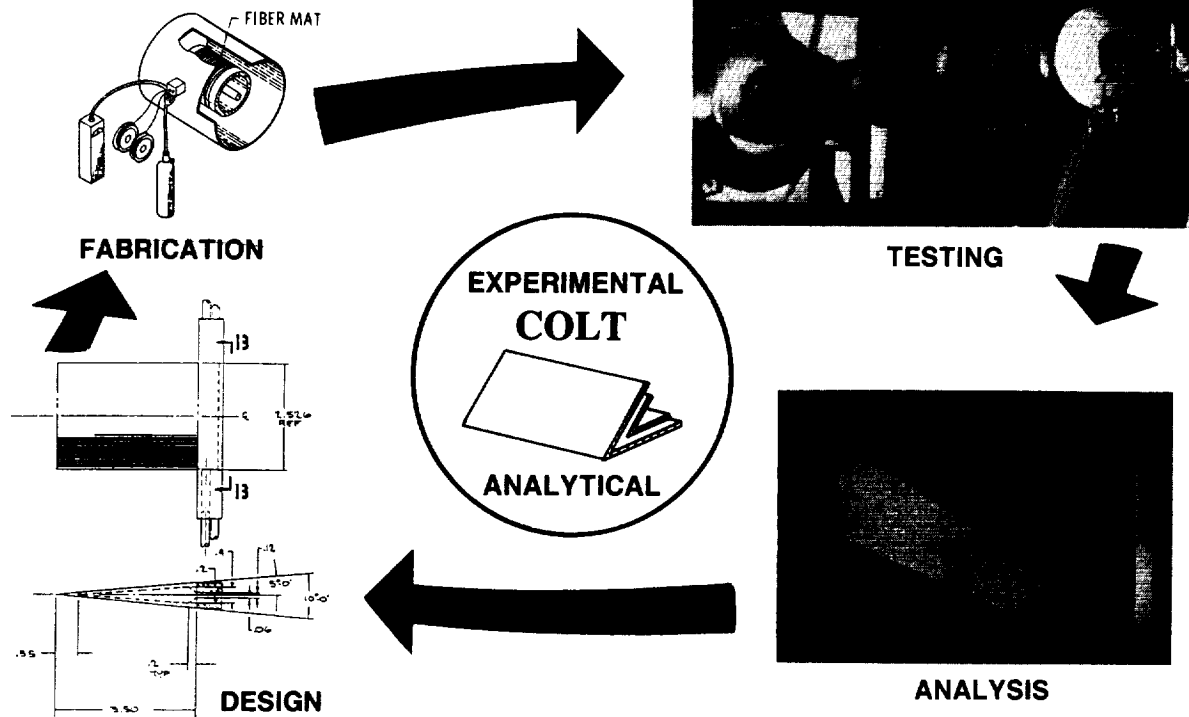
Figure 5. - Nonlinear, monotonic stress-strain response of unidirectional tungsten/copper composite.



CD-87-28050

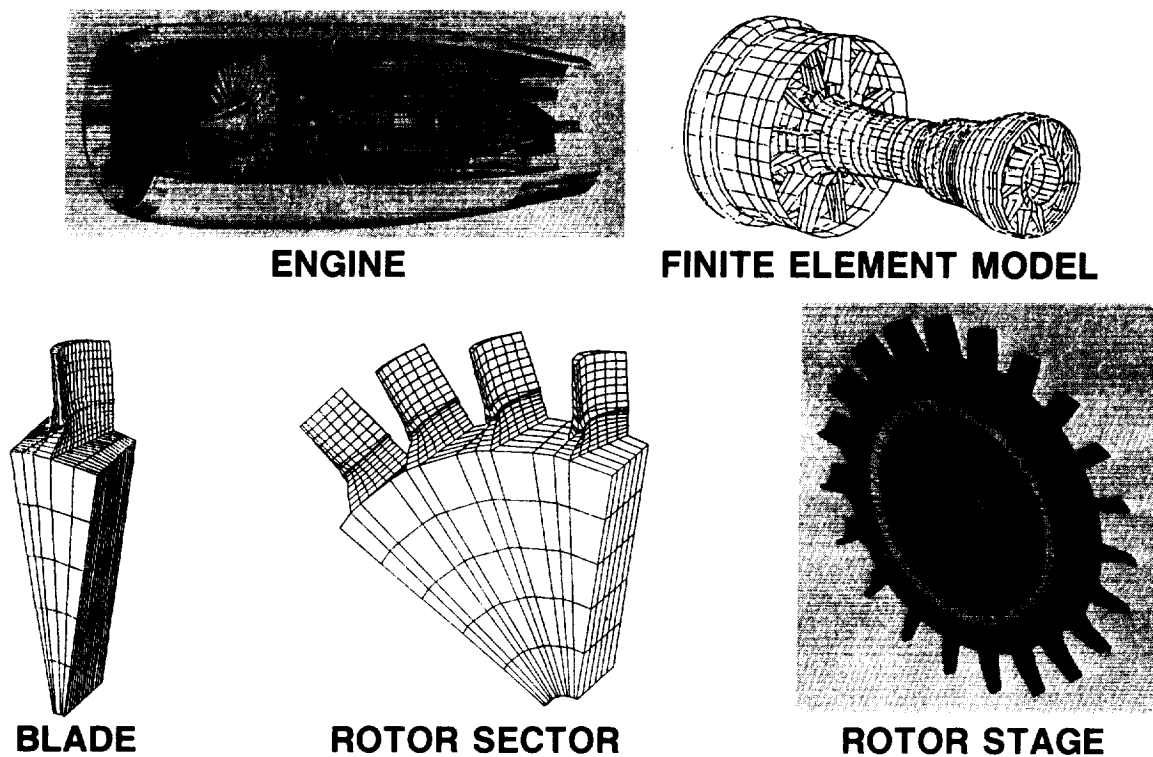
Figure 6. - Lewis' unique role in metal matrix composite technology development.

ARC SPRAY MONOTAPE FABRICATION UNIT



CD-87-29511

Figure 9. - Methodology of leading edge concept evaluation.



CD-87-28953

Figure 10. - Engine Structures Computational Simulator.

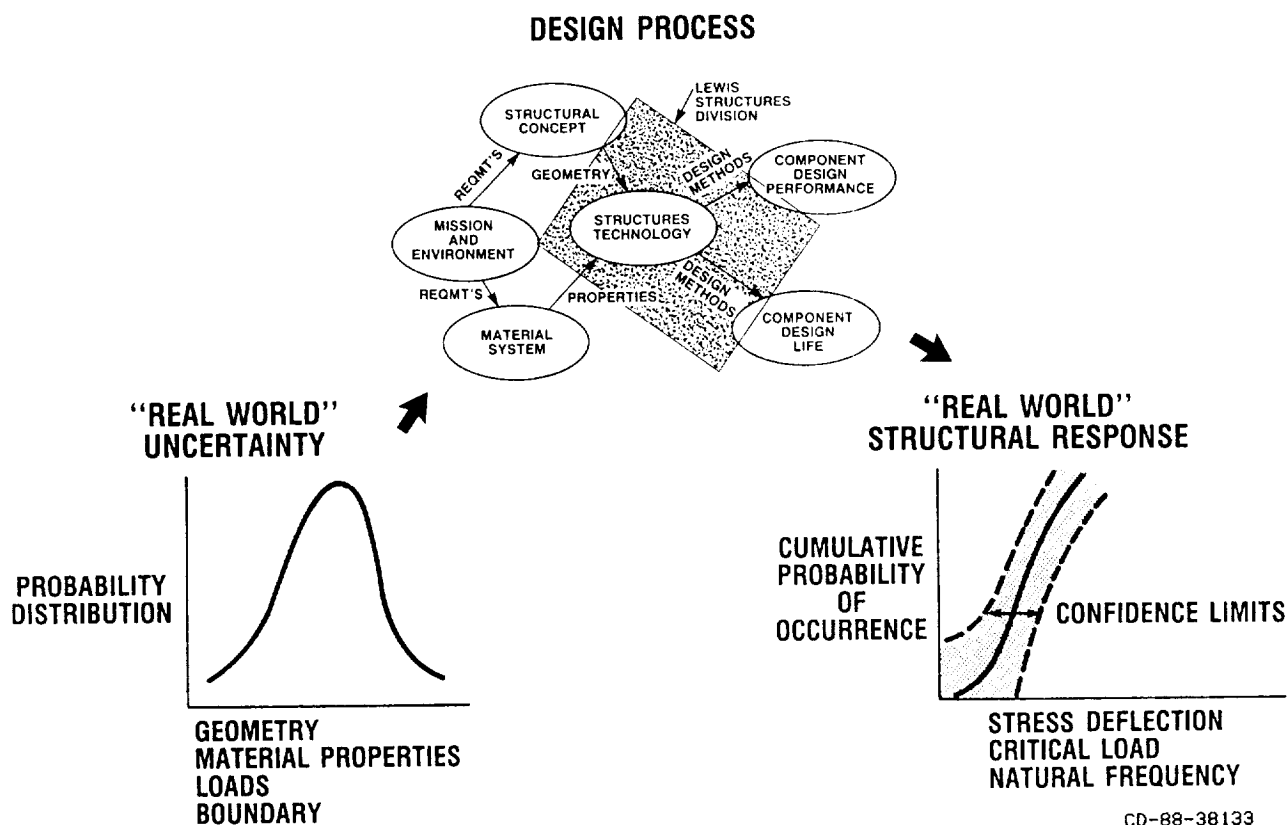
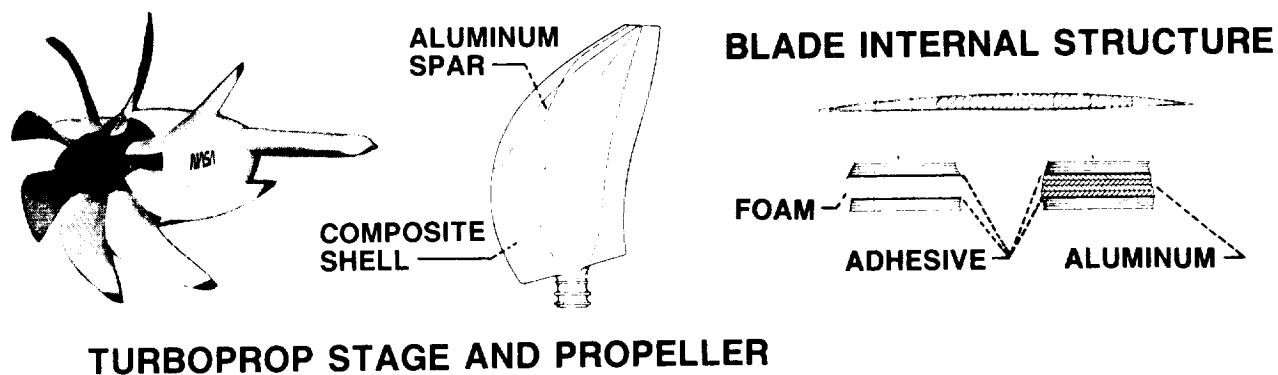


Figure 11. - Probabilistic Structural Analysis/Design methodology.



MULTIDISCIPLINARY ANALYSIS MODULES

- ADS OPTIMIZER
- BLADE MODEL GENERATION
- AERODYNAMIC ANALYSIS
- ACOUSTIC ANALYSIS
- STRESS AND VIBRATIONS ANALYSIS
- FLUTTER ANALYSIS
- 1 P FORCED REPONSE

TYPICAL ANALYSIS RESULTS

	<u>INITIAL</u>	<u>FINAL</u>
EFFICIENCY, %	82.86	83.17
NEAR-FIELD NOISE, DB	143.8	137.3
WEIGHT, LB	41.1	41.2
DOC	-.853	-4.201

CD-87-28956

Figure 12. - Structural tailoring of advanced turboprops.

SESSION 3 - INTERNAL FLUID MECHANICS RESEARCH

INTRODUCTION TO THE INTERNAL FLUID MECHANICS RESEARCH SESSION

Brent A. Miller
and
Louis A. Povinelli

Internal fluid mechanics research at Lewis is directed toward an improved understanding of the important flow physics affecting aerospace propulsion systems, and applying this improved understanding to formulate accurate predictive codes. To this end, research is conducted involving detailed experimentation and analysis. The following three papers summarize ongoing work and indicate future emphasis in three major research thrusts: inlets, ducts, and nozzles; turbomachinery; and chemical reacting flows.

The underlying goal of the research in each of these areas is to bring internal computational fluid mechanics to a state of practical application for aerospace propulsion systems. Achievement of this goal requires that carefully planned and executed experiments be conducted in order to develop and validate useful codes. It is critical that numerical code development work and experimental work be closely coupled. The insights gained are represented by mathematical models that form the basis for code development. The resultant codes are then tested by comparing them with appropriate experiments in order to ensure their validity and determine their applicable range. The ultimate user community must be a part of this process to assure relevancy of the work and to hasten its practical application.

Propulsion systems are characterized by highly complex and dynamic internal flows. Many complex, three-dimensional flow phenomena may be present, including unsteadiness, shocks, and chemical reactions. By focusing on specific portions of a propulsion system, it is often possible to identify the dominant phenomena that must be understood and modeled for obtaining accurate predictive capability. In the following papers of this section, research emphasis is placed on inlets, ducts, and nozzles, on turbomachinery, and on chemical reacting flows. These three research thrusts serve as a focus leading to greater understanding of the relevant physics and to an improvement in analytical tools. This in turn will hasten continued advancements in propulsion system performance and capability.

PRECEDING PAGE BLANK NOT FILMED

INLETS, DUCTS, AND NOZZLES

John M. Abbott,
Bernhard H. Anderson,
and Edward J. Rice

SUMMARY

The internal fluid mechanics research program in inlets, ducts, and nozzles consists of a balanced effort between the development of computational tools (both parabolized Navier-Stokes and full Navier-Stokes) and the conduct of experimental research. The experiments are designed to better understand the fluid flow physics, to develop new or improved flow models, and to provide benchmark quality data sets for validation of the computational methods.

The inlet, duct, and nozzle research program is described according to three major classifications of flow phenomena: (1) highly three-dimensional flow fields, (2) shock - boundary-layer interactions, and (3) shear layer control. Specific examples of current and future elements of the research program are described for each of these phenomenon. In particular, the highly three-dimensional flow field phenomenon is highlighted by describing the computational and experimental research program in transition ducts having a round-to-rectangular area variation. In the case of shock - boundary-layer interactions, the specific details of research for normal shock - boundary-layer interactions are described. For shear layer control, research in vortex generators and the use of aerodynamic excitation for enhancement of the jet mixing process are described.

Future research in inlets, ducts, and nozzles will include more emphasis on three-dimensional full Navier-Stokes methods and corresponding experiments designed to concentrate on the appropriate three-dimensional fluid flow physics.

INTRODUCTION

The internal fluid mechanics research program in inlets, ducts, and nozzles is described according to three types of fluid flow phenomena: highly three-dimensional flow fields, shock - boundary-layer interactions, and shear layer control. The importance of each of these flow phenomena is a result of the drivers listed in figure 1. For example, highly three-dimensional internal flow fields result from unconventional engine locations where twisting and turning inlets, ducts, and nozzles must be designed to deliver the airflow to and from the free stream. Aircraft thrust vectoring requirements quite often lead to the transitioning of nozzle cross-sectional geometries from round to rectangular with resultant three-dimensional flows. Aircraft maneuverability requirements can lead to significant three-dimensional flow fields entering

the propulsion system inlet and ducting system. The push toward higher flight speeds, for both military and civilian applications, leads to the importance of research in shock - boundary-layer interactions within inlets, ducts, and nozzles. The desire to design inlets, ducts, and nozzles to be as short and light as possible points to the importance of shear layer control as a means for "stretching" the limits of the geometry while avoiding internal flow separations. Shear layer control in another sense, that is, the use of aerodynamic excitation to control the formation and development of a mixing layer, offers the potential for enhancing the mixing process in external nozzle flows.

Specific elements of the inlet, duct, and nozzle research program are listed in figure 2 for each of the three flow field phenomena. The four elements underlined in the figure will be expanded upon in the remainder of the paper. Specifically, highly three-dimensional flow fields will be illustrated by describing the transition duct research program. The shock - boundary-layer interaction phenomenon will be illustrated with a description of the normal shock - boundary-layer interaction research program. Shear layer control research will be illustrated with two examples of current programs: vortex generator research and enhanced jet mixing research. The remaining four elements of the overall program, that is, offset ducts, oblique shock - boundary-layer interactions, glancing sidewall shock - boundary-layer interactions, and boundary-layer bleed, will not be described in this paper, although they are also key elements of the overall program.

As illustrated in figure 3, the approach to the research program in inlets, ducts, and nozzles consists of a balance between computational and experimental research. Computationally, much of the emphasis up until recently has been on the development and validation of parabolized Navier-Stokes methods. More recently and for the future, more emphasis is being placed on three-dimensional full Navier-Stokes methods. Shown on the right-hand side of the figure are the elements of the experimental program in inlets, ducts, and nozzles. They are aligned with the respective computational method and point out the close linkage between the computational and experimental elements of the program. Note that each of the program elements listed in figure 2 under the three different flow phenomena also appear here in figure 3 as specific experiments.

HIGHLY THREE-DIMENSIONAL FLOW FIELDS

Transition Ducts

Highly three-dimensional flow field research is illustrated by describing the transition duct research program.

Transition ducts are characterized by a cross-sectional geometry that transitions from round to rectangular (ref. 1). A sample three-dimensional parabolized Navier-Stokes (PNS) computation for a specific transition duct geometry is illustrated in figure 4. (Details of the computational method are given in refs. 2 and 3.) The geometry is described by a rectangular exit having an aspect ratio (width/height) of 3.0. The duct is 1.5 inlet diameters long and has an exit-to-inlet area ratio of 1.0. The figure shows near-wall velocity vectors on the left, with a display of the secondary velocity vectors in the rectangular exit plane shown below it. The three-dimensional character of

the flow field is clear. On the right side of the figure are contours of surface shear stress on the duct. Zero shear stress corresponds to the onset of flow separation on the duct surface. Note that the computation indicates that this particular geometry has a small localized separation zone about halfway down the duct. The flow reattaches just downstream of this zone and remains attached for the remainder of the duct length. The separation is apparent in both the near-wall velocity vectors and in the surface shear stress contours.

As an illustration of how the computational results shown in the previous figure can be used, figure 5 shows the internal flow separation bounds for a class of transition duct geometries. Each duct geometry has the same area ratio of 1.0, but the length ratio and the exit aspect ratio are varied. Specifically, for four different aspect ratios, the length ratio was decreased from a value where the internal flow was completely attached to a value where the flow just began to separate. This series of computations then resulted in the separation bound shown in the figure. For geometries above the curve, the flow is attached; for geometries below the curve, the flow is separated. One experimental data point is spotted on the figure as a case where the flow was massively separated within the duct.

To develop a more detailed understanding of the flow physics within transition ducts, to improve models of the flow physics, and to validate computations like those shown in the previous two figures, experiments are underway using the model and facility shown in figure 6. The model was machined to match exactly one of the geometries for which the three-dimensional PNS method had been applied. Shown in this figure is a photo of the model during the final machining stage together with a superimposed display of the computational surface. Also shown is the test facility. Special care was taken to condition the transition duct inflow properly to provide the desired levels of inflow turbulence, flow angularity, and boundary-layer profile. Modifications to the facility are currently underway whereby the inflow tank is being connected to a high-pressure supply system to provide higher Reynolds number test capability.

Experimental results are shown in figure 7 at a one-dimensional duct Mach number of 0.5. On the left side of the figure, surface static pressure measurements are shown along the centerline of the duct. On the right side of the figure are shown results from a surface oil streak flow visualization experiment. These oil streaks agree quite well qualitatively with the computational near wall velocity vectors. Although not shown here, experimental measurements have just been made of flow direction in the duct exit plane. Efforts are currently underway to compare those results with the corresponding three-dimensional PNS computations. Future experiments will include detailed probing of the flow field within this duct and others, and direct measurement of surface shear stress using an advanced laser measurement technique.

In addition to conducting aerodynamic experiments with the highly three-dimensional flow fields of transition ducts, heat-transfer experiments are also being conducted. Heat transfer is of particular concern for these types of flow fields because of applications where the three-dimensional flows may result in high-temperature flow streams (i.e., engine core flow) finding their way to the transition duct (nozzle) surfaces. Figure 8 shows a square-to-rectangular transition duct model which was tested in the facility shown on the right (ref. 4). To measure the surface heat-transfer characteristics of the

duct, the surface was coated with a liquid-crystal material. After establishing the desired amount of airflow through the duct, the duct surface was heated so that the resulting color bands (isotherms) on the liquid-crystal surface could be interpreted in terms of local heat transfer coefficient (refs. 5 to 7).

Results from the liquid-crystal heat-transfer experiment are illustrated in figure 9. Different colors on the liquid-crystal surface correspond to different surface temperatures, which, when combined with the known level of surface heat input, lead to experimentally determined values of surface heat-transfer coefficient. Regions of high and low heat transfer are pointed out in the figure. By photographing the surface and then digitizing the photographic image, quantitative values of surface heat-transfer coefficient are obtained over the entire surface.

SHOCK - BOUNDARY-LAYER INTERACTIONS

Normal Shock - Boundary-Layer Interaction

Shock - boundary-layer interaction research is illustrated by describing the normal shock - boundary-layer interaction research program. Other shock - boundary-layer interaction work is described in references 8 to 12.

Figure 10 illustrates the nature of the normal shock - boundary-layer interaction. The interaction is shown at two Mach numbers, 1.3 and 1.6, and the nature of the interaction is illustrated with a schlieren photograph and a surface oil streak photograph at each Mach number. The photographs were obtained in the Lewis 1- by 1-Foot Supersonic Wind Tunnel. The schlieren photographs give a view of the interaction integrated across the full width of the test section, while the surface oil streaks illustrate the details of the flow field along the sidewall of the test section. At both Mach numbers, the schlieren photographs show the shock being bifurcated into a "lambda shock" in the interacting region. The sidewall surface oil streaks indicate a significant difference in the structure of the flow field for the two cases. At Mach 1.3 the flow along the sidewall remains uniform and passes through the shock structure with no major alteration. At Mach 1.6, the adverse pressure gradient across the shock is strong enough to force the boundary layer to separate from the tunnel walls and form the closed separation bubble shown in the figure. Note that this is a two-dimensional slice through a highly three-dimensional flow field that exists in the corner region.

Both the Mach 1.3 and 1.6 shock - boundary-layer interaction flow fields were surveyed in detail using nonintrusive laser anemometry (ref. 13). Results are shown in figure 11 for the Mach 1.6 case in two different planes within the flow field. The top set of Mach contours illustrates the nature of the flow field in a cross plane downstream of the shock. The lower set of Mach contours shows the development of the flow field within a vertical plane passing through the centerline of the test section. The separated region in the vicinity of the initial interaction causes the actual flow area to contract downstream of the initial shock, leading to a reacceleration of the flow to supersonic Mach numbers. The flow then shocks down again, reaccelerates again because of the thickened boundary layer, and finally shocks down one last time.

In the lower portion of figure 12, the lower portion of figure 11 is repeated, that is, Mach contours as measured with laser anemometry in a vertical plane passing through the centerline of the test section at Mach 1.6. The upper portion of figure 12 is a two-dimensional Navier-Stokes computation of the same flow field. Although the computation captures fairly well the initial portions of the flow in the vicinity of the first shock, in the downstream regions, none of the flow physics are adequately represented in the computation. This result is expected, of course, since the experimental results have shown the strong three-dimensional character of the flow. This comparison points out the need for three-dimensional computational methods for computing such flow fields.

Figure 13 is a frame from a film that illustrates the additional insight and understanding that can be obtained from setting in motion a three-dimensional contour representation of the flow field. The graphics package used to generate the film was actually developed for presenting computational results. The experimental laser anemometry data sets were modified to a format that was acceptable to the graphics software. The researcher can rotate the image, adjust the rate of rotation, and select the axis of rotation while sitting at the display console. One gains a perspective from these rotating images much more quickly than one would by looking at a series of two-dimensional or even three-dimensional plots.

SHEAR LAYER CONTROL

Vortex Generators

The first aspect of shear layer control, boundary layer control, is illustrated by describing the vortex generator research program.

Figure 14 illustrates a research model and facility that were used in an experiment to assess the performance of vortex generators in a diffusing offset duct (ref. 14). The duct had a length-to-diameter ratio of 5.0, an offset-to-diameter ratio of 1.34, and an exit-to-inlet area ratio of 1.50. Initial experiments with the duct identified the location of a separated flow region as shown by the surface oil streak photograph. Vortex generators were then added to the duct surface just upstream of the separated region to control the separation.

A comparison of total pressure contours at various locations down the length of the duct with the vortex generators in place is shown in figure 15. The experimental data were obtained by surveying the flow field with a total pressure probe. The computational results are from the three-dimensional PNS method. The method includes a model for the vortex generators that allows one to position the individual generators anywhere within the duct and permits an adjustment to the strength of the vortex based on an empirical relationship with the vortex generator angle of attack (ref. 15).

Enhanced Jet Mixing

Another aspect of the shear layer control, the use of aerodynamic excitation to control the development and evolution of large-scale structures in a

shear layer, is illustrated by describing the enhanced jet mixing research program. Other shear layer control work, using aerodynamic excitation, is described in references 16 to 31.

The mixing process between a jet and the surrounding air flow can be enhanced through use of aerodynamic excitation as illustrated in figure 16. The naturally occurring flow structure of the jet mixing process is shown in the left-hand schlieren photograph. By applying an excitation signal at the proper frequency, here by use of acoustic drivers upstream of the jet exit plane, the naturally occurring large-scale structures within the mixing layer are regularized and enhanced and lead to a more rapid mixing process as illustrated in the right-hand photograph.

Results of an axisymmetric Navier-Stokes computation of a jet flow exiting into a quiescent region are shown in figure 17 (ref. 32). The jet exit Mach number is 0.3, and the results are shown in terms of vorticity contours. Two cases are shown - an unexcited case on the left side, and an excited case on the right side. For the excited case, the excitation signal is applied at a frequency chosen to maximize the development and growth of the large-scale structures. In both cases, results of the computation are shown at three different times. Also for both cases, lines are drawn through the centers of the large-scale vortices to illustrate how they propagate downstream. Note that with excitation applied at the proper frequency, adjacent vortices combine or pair to form a single larger vortex, which, in turn, has the effect of more rapidly mixing the jet flow with the surrounding quiescent flow.

The effect of excitation on the jet mixing process for a jet having an exit Mach number of 0.3 and an initial turbulence level of 0.15 percent is shown in figure 18. The results were obtained in an experiment wherein both the frequency and the level of the excitation signal could be varied (ref. 33). The results show how the ratio of centerline velocity for the excited case to that of the unexcited case varies as the level of the excitation is increased at a fixed frequency. The measurements are made nine jet diameters downstream of the nozzle exit plane. As in the previous figure, the excitation frequency has been selected to provide the maximum degree of mixing enhancement. As indicated, the effect of the excitation is quite significant with, in this case, a reduction in centerline velocity of about 16 percent at the maximum available excitation level of 130 dB.

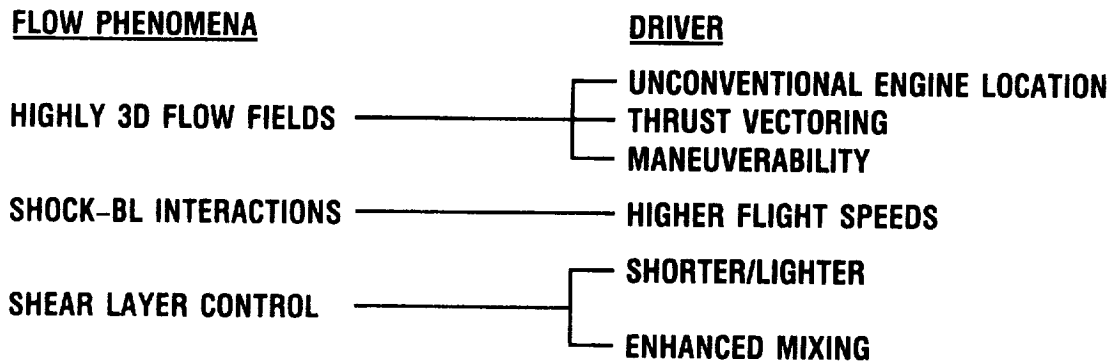
The internal fluid mechanics research program in inlets, ducts, and nozzles is a balanced effort between the development of computational tools and the conduct of experimental research. The program has been briefly described by highlighting research efforts in highly three-dimensional flow fields, shock - boundary-layer interactions, and shear layer control. Much of the computational focus up until now has been on the development and validation of parabolized Navier-Stokes methods. More recently, and in the future, more emphasis will be placed on the development and validation of three-dimensional Navier-Stokes methods. The experimental element of the program will continue to provide a fundamental understanding of the fluid flow physics, develop new and/or improved flow models, and to provide benchmark data sets for computational method validation of both the parabolized and full Navier-Stokes methods.

REFERENCES

1. Patrick, W.P.; and McCormick, D.C.: Circular-to-Rectangular Duct Flows, A Benchmark Experimental Study. SAE Paper 871776, Oct. 1987.
2. Briley, W.R.; and McDonald, H.: Analysis and Computation of Viscous Subsonic Primary and Secondary Flows. AIAA Paper 79-1453, July 1979.
3. Briley, W.R.; and McDonald, H.: Three-Dimensional Viscous Flows With Large Secondary Velocity. J. Fluid Mech., vol. 144, July 1984, pp. 47-77.
4. Jones, T.V.; and Hippensteele, S.A.: High-Resolution Heat-Transfer-Coefficient Maps Applicable to Compound-Curve Surfaces Using Liquid Crystals in a Transient Wind Tunnel. Developments in Experimental Techniques in Heat Transfer and Combustion, R.O. Warrington, Jr., M.M. Chen, and J.D. Felske, eds., ASME, 1987, pp. 1-9.
5. Hippensteele, S.A.; Russell, L.M.; and Stepka, F.S.: Evaluation of a Method for Heat Transfer Measurements and Thermal Visualization Using a Composite of a Heater Element and Liquid Crystals. ASME Paper 81-GT-93, Mar. 1981 (NASA TM-81639).
6. Hippensteele, S.A.; Russell, L.M.; and Torres, F.J.: Local Heat-Transfer Measurements on a Large, Scale-Model Turbine Blade Airfoil Using a Composite of a Heater Element and Liquid Crystals. NASA TM-86900, 1985.
7. Hippensteele, S.A.; Russell, L.M.; and Torres, F.J.: Use of a Liquid-Crystal, Heater-Element Composite for Quantitative, High-Resolution Heat Transfer Coefficients on a Turbine Airfoil, Including Turbulence and Surface Roughness Effects. NASA TM-87355, 1987.
8. Hingst, W.R.; and Tanji, F.T.: Experimental Investigation of a Two-Dimensional Shock-Turbulent Boundary Layer Interaction with Bleed. AIAA Paper 83-0135, Jan. 1983 (NASA TM-83057).
9. Jurkovich, M.S.: Flow Visualization Studies of 3-D Shock/Boundary-Layer Interaction in the Presence of a Non-Uniform Approach Boundary Layer. AIAA Paper 84-1560, June 1984.
10. Skebe, S.A.; Greber, I.; and Hingst, W.R.: Investigation of Two-Dimensional Shock-Wave/Boundary-Layer Interactions. AIAA J., vol. 25, no. 6, June 1987, pp. 777-783.
11. Barnhart, P.J.; Greber, I.; and Hingst, W.R.: Glancing Shock Wave-Turbulent Boundary Layer Interaction with Boundary Layer Suction. AIAA Paper 88-0308, Jan. 1988.
12. Benhachmi, D.; Greber, I.; and Hingst, W.R.: Experimental and Numerical Investigation of the Effect of Distributed Suction on Oblique Shock Wave/Turbulent Boundary Layer Interaction. NASA TM-101334, 1988.
13. Chriss, R.M., et al.: An LDA Investigation of Three-Dimensional Normal Shock-Boundary Layer Interactions in a Corner. AIAA Paper 87-1369, June 1987.

14. Vakili, A.D., et al.: Flow Control in a Diffusing S-Duct. AIAA Paper 85-0524, Mar. 1985.
15. Kunik, W.G.: Application of a Computational Model for Vortex Generators in Subsonic Internal Flows. AIAA Paper 86-1458, June 1986.
16. Stone, J.R.; and McKinzie, D.J., Jr.: Acoustic Excitation - A Promising New Means of Controlling Shear Layers. NASA TM-83772, 1984.
17. Rice, E.J.; and Zaman, K.B.M.Q.: Control of Shear Flows by Artificial Excitation. AIAA Paper 87-2722, Oct. 1987.
18. Lepicovsky, J., et al.: Acoustically Excited Heated Jets. I-Internal Excitation, II-In Search of a Better Understanding, III-Mean Flow Data, NASA CR-4129-PT-1,-2,-3, 1988.
19. Zaman, K.B.M.Q.; Bar-Sever, A.; and Mangalam, S.M.: Effect of Acoustic Excitation on the Flow Over a Low-Re Airfoil. J. Fluid Mech., vol. 182, Sept. 1987, pp. 127-148.
20. Mangalam, S.M., et al.: Transition and Separation Control on a Low-Reynolds Number Airfoil. Aerodynamics at Low Reynolds Numbers Re Greater Than 10^4 and Less Than 10^6 , Vol. 1, Royal Aeronautical Society, London, 1986, pp. 10.1-10.19.
21. Raman, G.; Ghorashi, B.; Rice, E.J.; and Miles, J.H.: Enhanced Mixing in Free Shear Layers by Acoustic Excitation. Presented at the AIChE Annual Meeting, Nov. 10-15, 1985.
22. Raman, G.: Enhanced Mixing of an Axisymmetric Jet by Aerodynamic Excitation. NASA CR-175059, 1986.
23. Ghorashi, B.; Raman, G.; Rice, E.J.; and Miles, J.H.: Upstream Excitation of an Axisymmetric Jet. Presented at the AIChE Annual Meeting, Miami, FL, Nov. 3-7, 1986.
24. Ghorashi, B.; and Raman, G.: Measurements in an Acoustically Excited Jet. Proceedings of the 4th Miami International Symposium on Multi-Phase Transport and Particulate Phenomena, Clean Energy Research Institute, University of Miami, Coral Gables, FL, Dec. 15-17, 1986.
25. Raman, G.; Rice, E.J.; and Mankbadi, R.R.: Saturation and the Limit of Jet Mixing Enhancement by Single Frequency Plane Wave Excitation: Experiment and Theory. National Fluid Dynamics Congress, 1st, Pt. 2, AIAA, 1988, pp. 1000-1007 (NASA TM-100882).
26. Raman, G.; Zaman, K.B.M.Q.; and Rice, E.J.: Controlled Excitation of a Round Jet at Various Levels of Initial Turbulence. Bull. Am. Phys. Soc., Division of Fluid Dynamics, Nov. 23-25, 1986.
27. Raman, G.; and Rice, E.J.: Excitation of an Axisymmetric Jet at Fundamental and Subharmonic Frequencies. Presented at the 41st Annual Meeting of the American Physical Society, Nov. 20-22, 1988.

28. Mankbadi, R.R.; Raman, G.; and Rice E.J.: Effects of Core Turbulence on Jet Excitability. Presented at the 41st Annual Meeting of the American Physical Society, Nov. 20-22, 1988.
29. Taghavi, R.; Rice, E.J.; and Farokhi, S.: Controlled Excitation of a Cold Turbulent Swirling Free Jet. J. Vibration, Acoustics, Stress, Reliability Design, vol. 110, no. 2, Apr. 1988, pp. 234-237.
30. Farokhi, S.; Taghavi, R.; and Rice E.J.: Effect of Initial Tangential Velocity Distribution on the Mean Evolution of a Swirling Turbulent Free Jet. National Fluid Dynamics Congress, 1st, Pt. 2, AIAA, 1988, pp. 947-954 (NASA TM-100934).
31. Taghavi, R.; and Farokhi, S.: Turbulent Swirling Jets With Excitation, NASA CR-180895, 1988.
32. Scott, J.N.: Numerical Simulation of Self-Sustained and Forced Oscillations in Jet Shear Layers. Forum on Unsteady Flow Separation, K.N. Ghia, ed., ASME 1987, pp. 123-130.
33. Raman, G.; Zaman, K.B.M.Q.; and Rice, E.J.: Initial Turbulence Effects on Jet Evolution With and Without Tonal Excitation. AIAA Paper 87-2725, Oct. 1987 (NASA TM-100178).



CD-87-29854

Figure 1. - Flow phenomena of interest in inlets, ducts, and nozzles together with interest drivers.

- HIGHLY 3D FLOW FIELDS
 - TRANSITION DUCTS
 - OFFSET DUCTS
- SHOCK-BOUNDARY-LAYER INTERACTIONS
 - NORMAL SHOCK-BOUNDARY LAYER
 - OBLIQUE SHOCK-BOUNDARY LAYER
 - GLANCING SIDEWALL SHOCK-BOUNDARY LAYER
- SHEAR LAYER CONTROL
 - VORTEX GENERATORS
 - BOUNDARY-LAYER BLEED
 - ENHANCED JET MIXING

CD-87-29855

Figure 2. - Elements of inlet, duct, and nozzle research program.

COMPUTATIONAL METHODS

3D PARABOLIZED
NAVIER-STOKES (PNS)

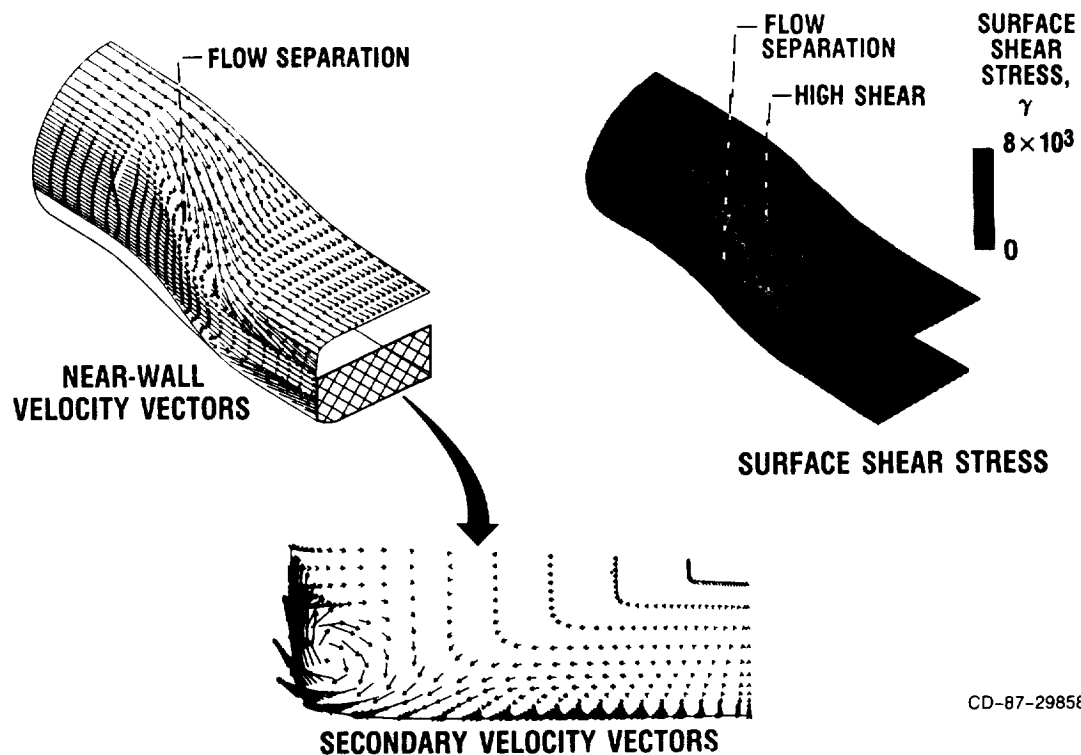
3D NAVIER-STOKES (NS)

EXPERIMENTS

- (1) TRANSITION DUCTS
- (2) OFFSET DUCTS
- (3) SHOCK-BOUNDARY-LAYER
INTERACTION
- (4) VORTEX GENERATORS
- (5) BOUNDARY-LAYER BLEED
- (6) EXPERIMENTS (1) TO (5)
- (7) SEPARATION FLOW PHYSICS
- (8) NONORTHOGONAL SURFACES
- (9) JET MIXING

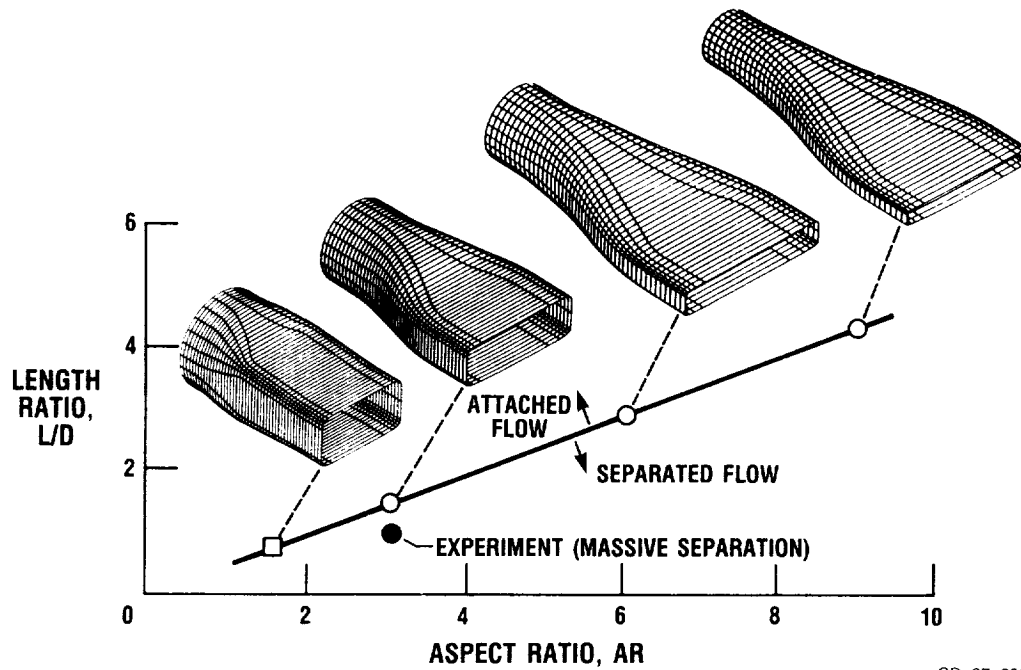
CD-87-29856

Figure 3. - Approach to research program in inlets, ducts, and nozzles.



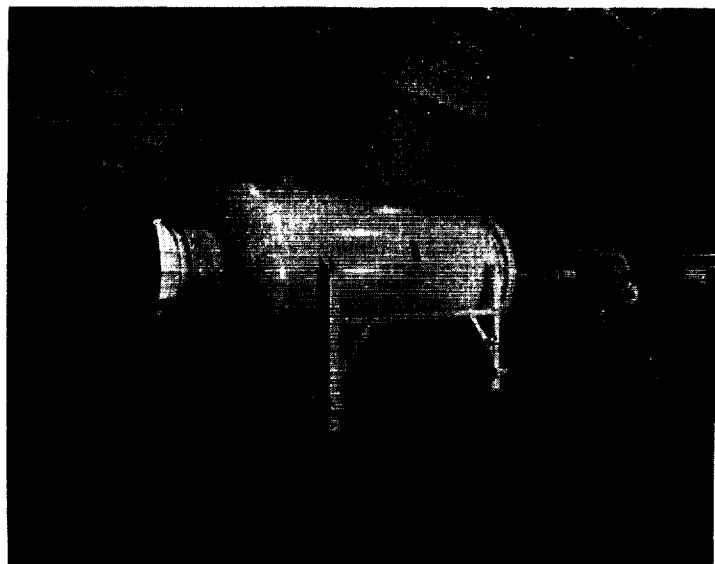
CD-87-29858

Figure 4. - Three-dimensional PNS computational results for transition duct (duct exit aspect ratio (width/height), 3.0; duct length to inlet diameter ratio, 1.5; duct exit-to-inlet area ratio, 1.0).



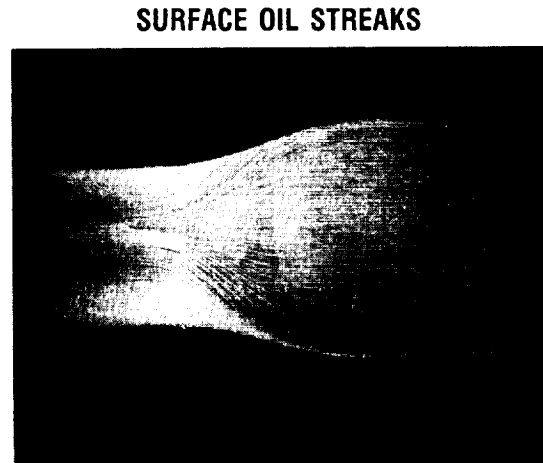
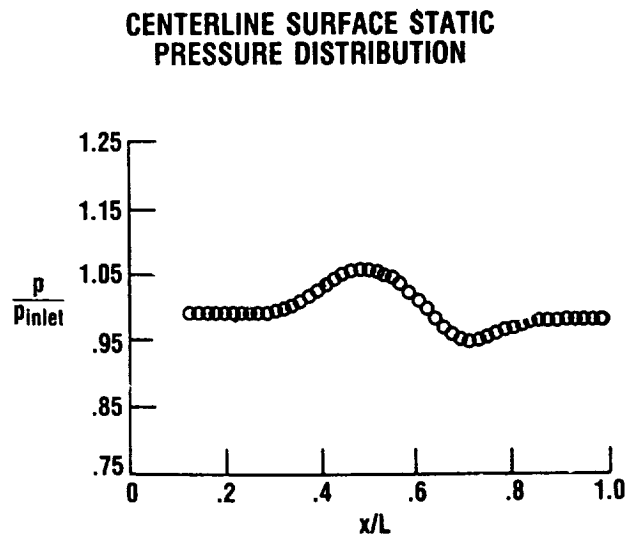
CD-87-29859

Figure 5. - Three-dimensional PNS computations of transition duct separation characteristics (transition duct exit-to-inlet area ratio, 1.0).



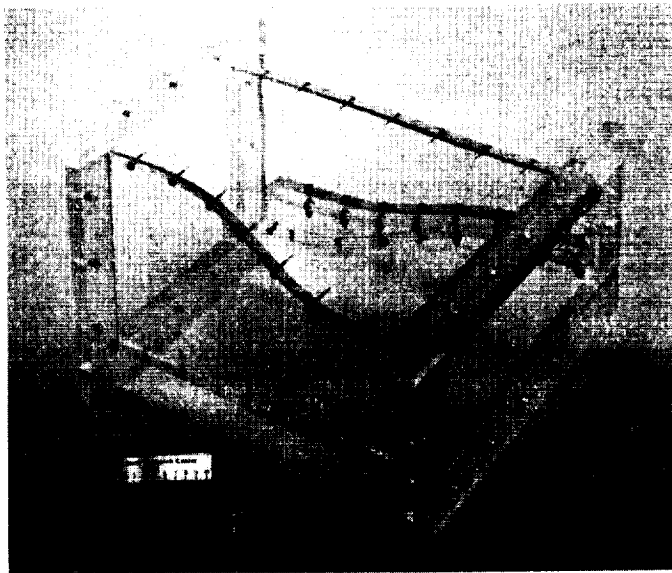
CD-87-29860

Figure 6. - Transition duct aerodynamic experiments.



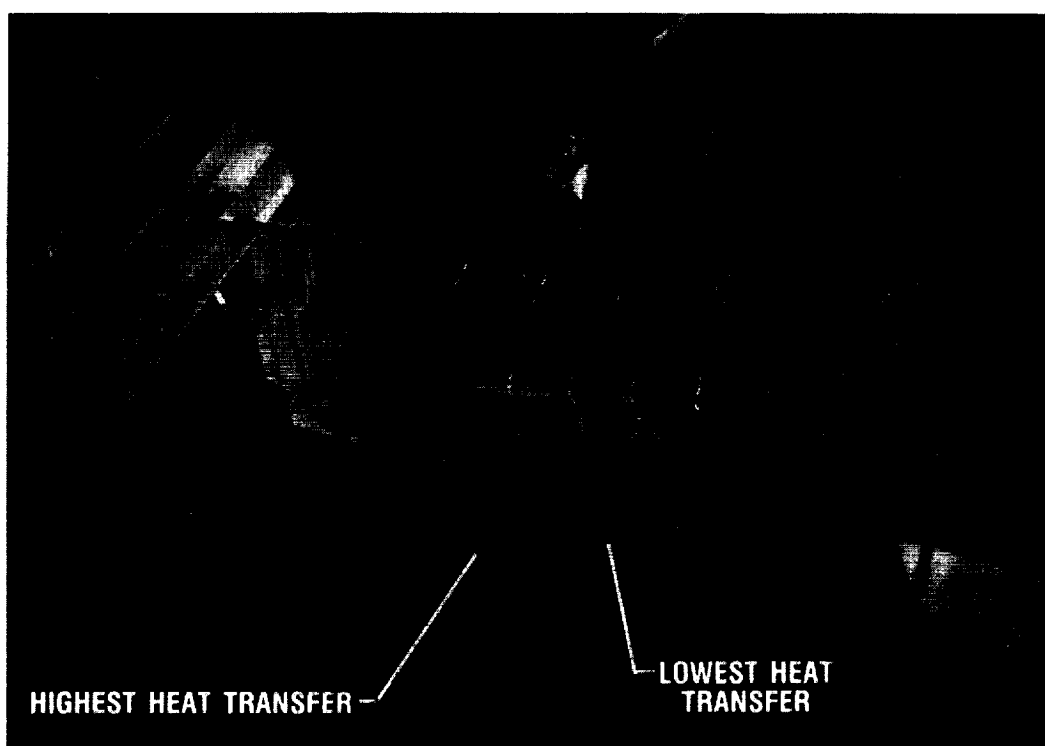
CD-87-29861

Figure 7. - Transition duct aerodynamic results (duct Mach number, 0.5).



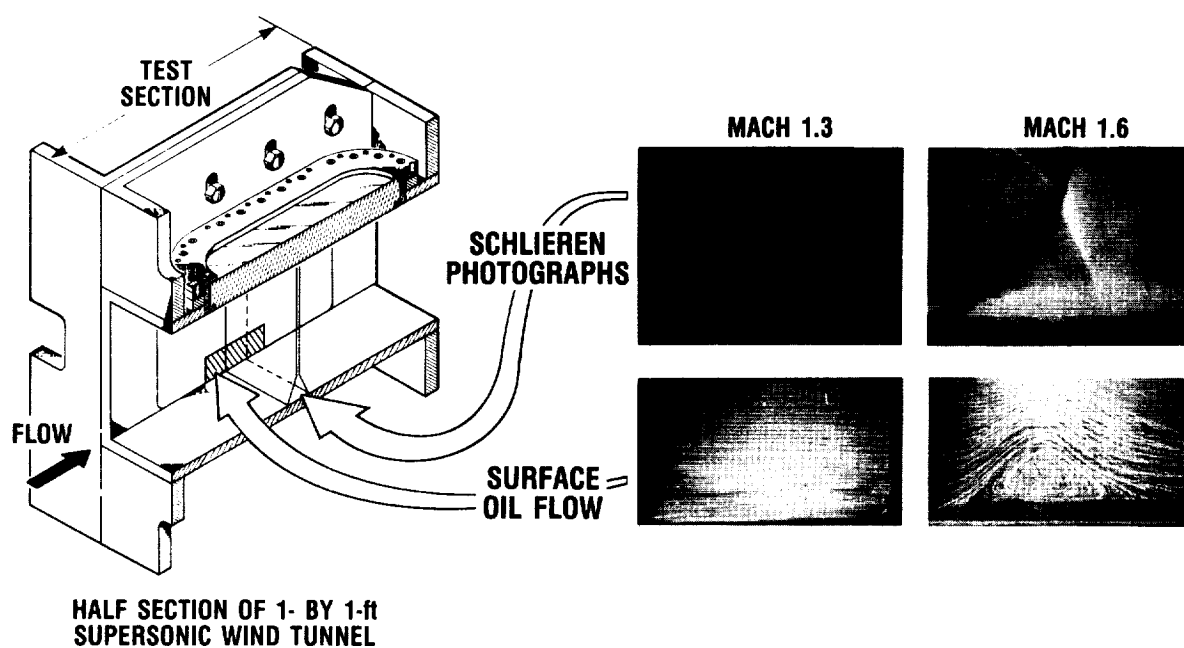
CD-87-29862

Figure 8. - Transition duct heat-transfer experiments.



CD-87-29863

Figure 9. - Transition duct heat-transfer results.



CD-87-29864

Figure 10. - Normal shock - boundary-layer interaction experiments.

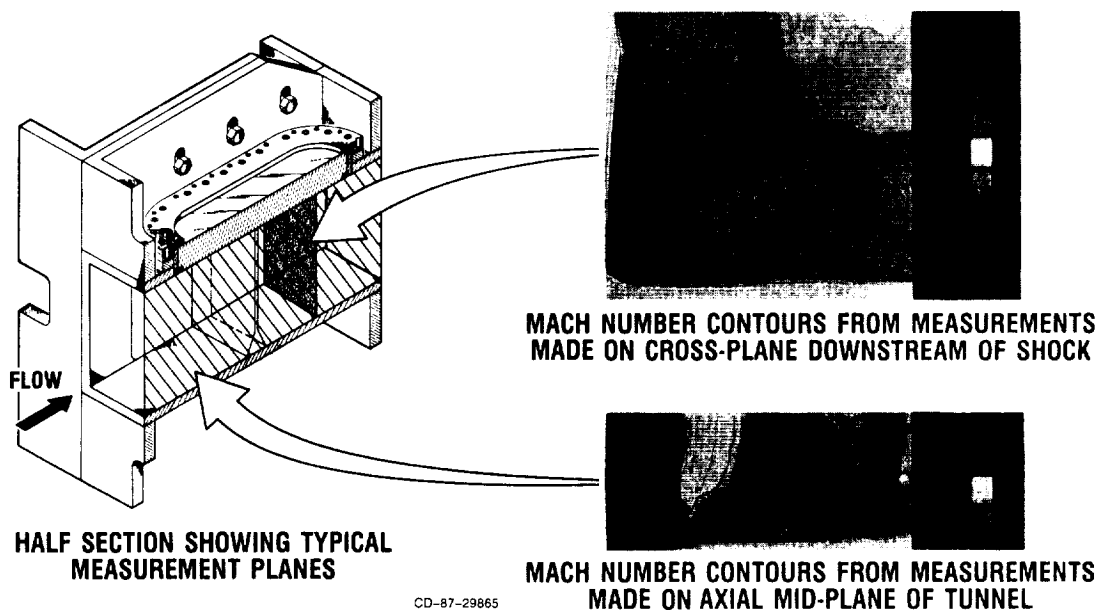


Figure 11. - Results of laser anemometer measurements for normal shock - boundary-layer interaction at Mach 1.6.

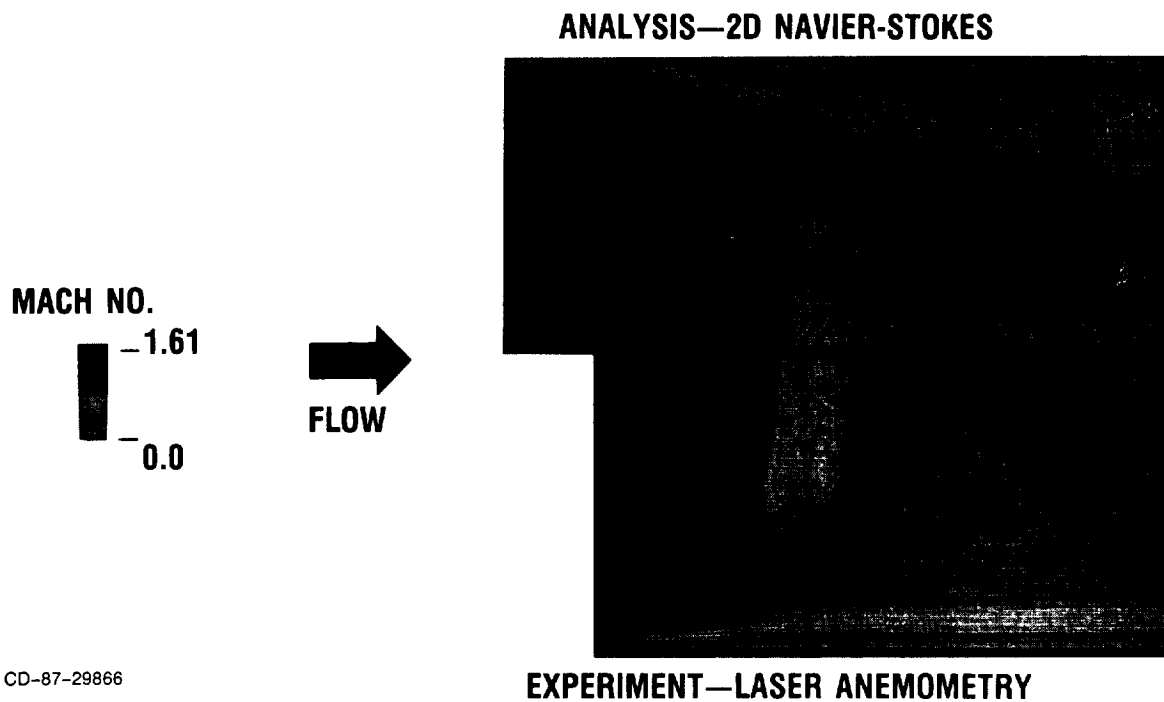
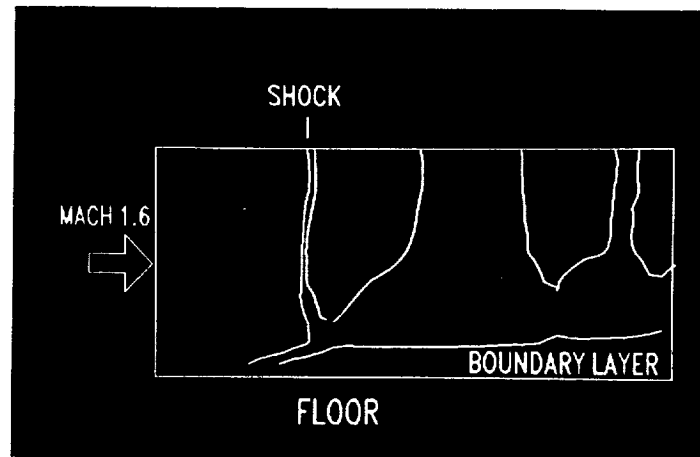


Figure 12. - Comparison of LDV experiment and two-dimensional Navier-Stokes calculation for Mach 1.6 normal shock - boundary-layer interaction.

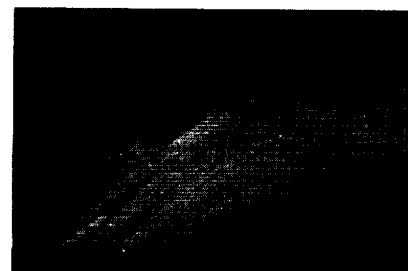


CD-87-29867

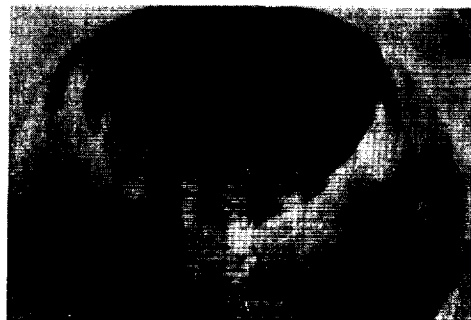
Figure 13. - Frame from film showing laser anemometry results of normal shock - boundary-layer interaction.



EXPERIMENT SETUP



**SURFACE OIL STREAKS
WITHOUT VORTEX GENERATORS**



VORTEX GENERATORS

CD-87-29868

Figure 14. - Vortex generators in diffusing offset duct (duct length-to-diameter ratio, 5.0; duct offset-to-diameter ratio, 1.34; duct exit-to-inlet area ratio, 1.50).

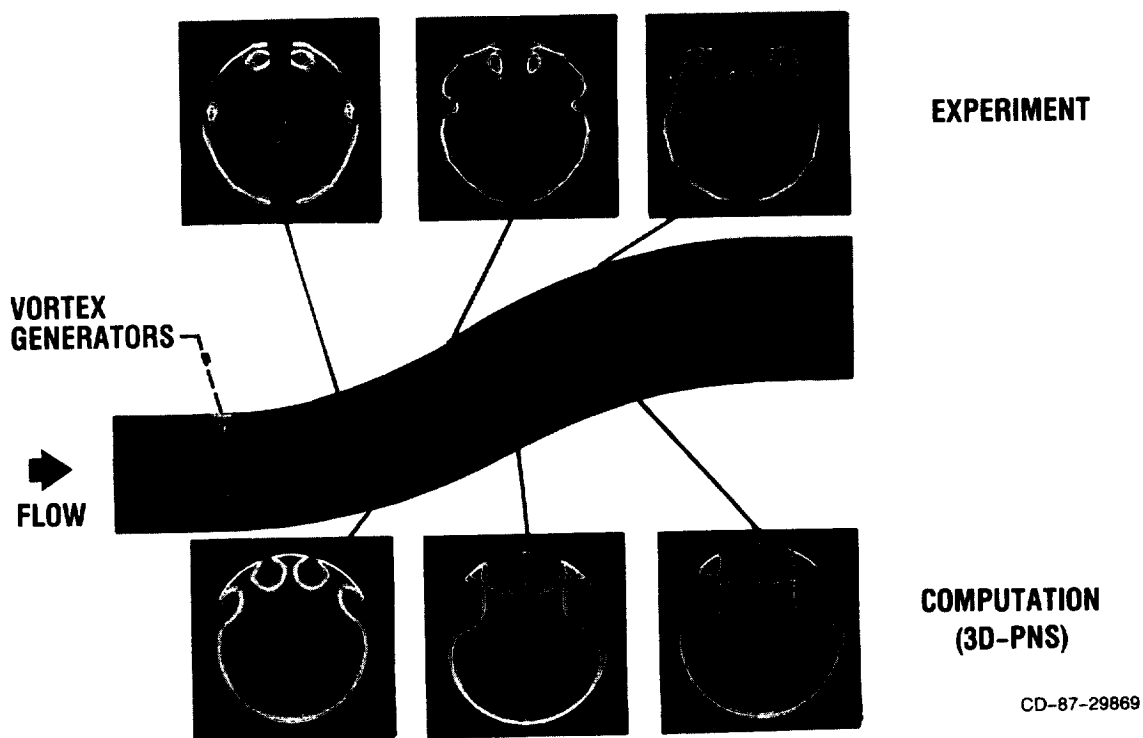


Figure 15. - Comparison of analysis and experiment for vortex generators in diffusing offset duct (total pressure contours at duct Mach number of 0.6).

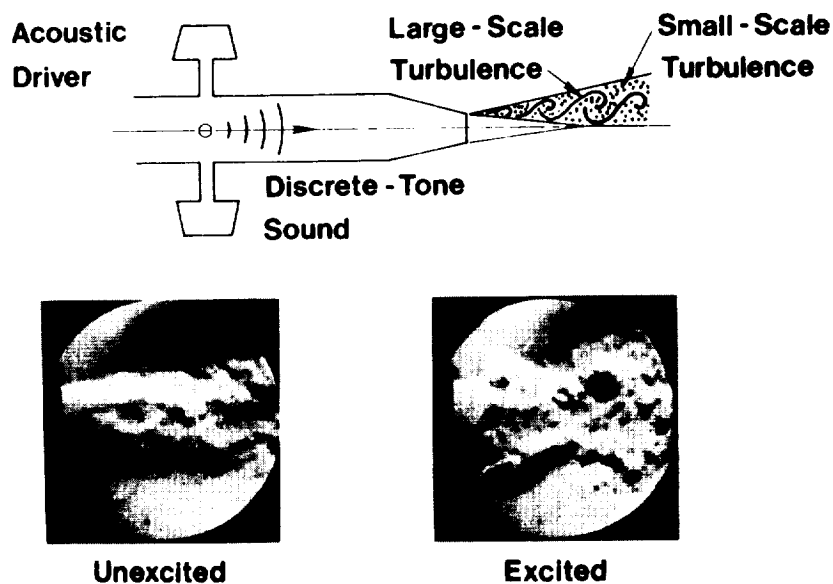


Figure 16. - Enhanced jet mixing through excitation of coherent large-scale turbulence.

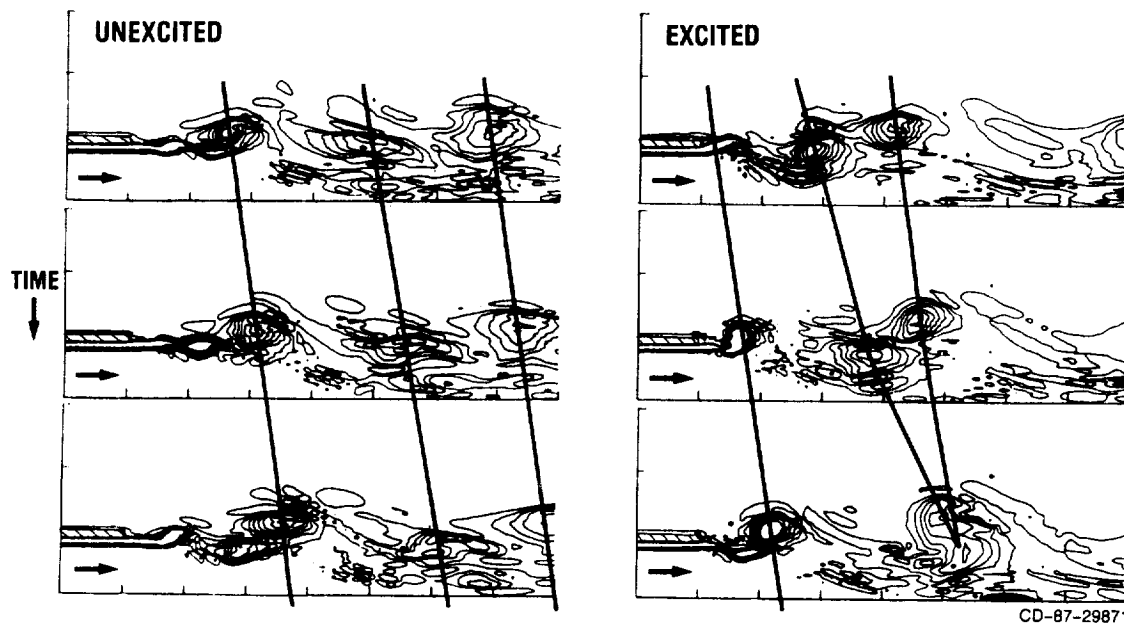


Figure 17. - Navier-Stokes computational results showing effect of excitation on jet shear layer evolution (vorticity contours at jet Mach number of 0.3).

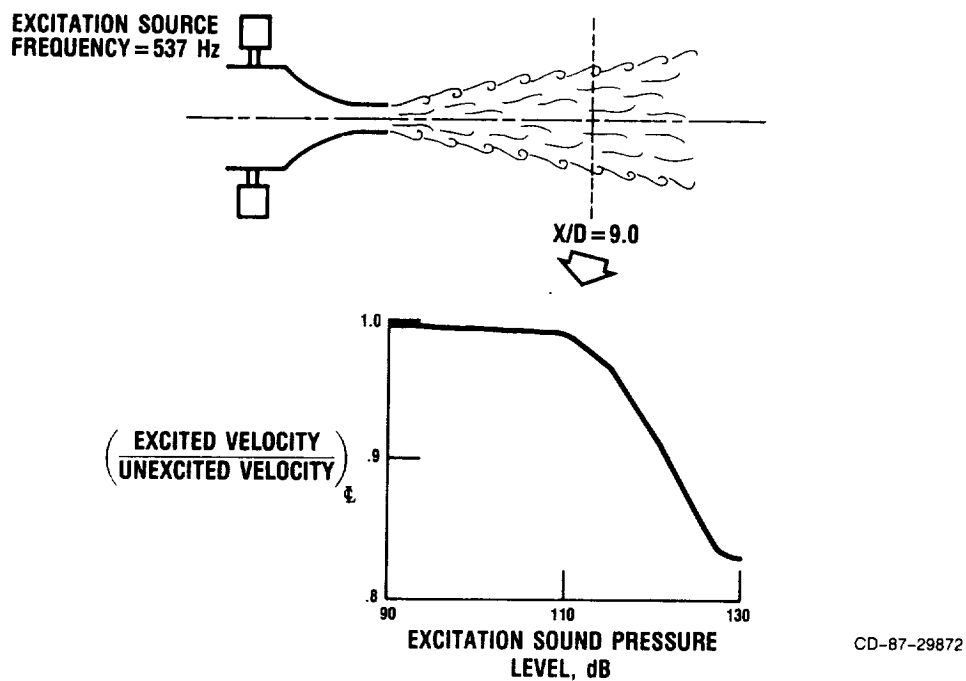


Figure 18. - Experimental results showing effect of excitation on jet mixing (jet exit Mach number, 0.3; jet exit turbulence, 0.15 percent).

TURBOMACHINERY

Robert J. Simoneau, Anthony J. Strazisar,
Peter M. Sockol, Lonnie Reid,
and John J. Adamczyk

SUMMARY

The discipline research in turbomachinery, which is directed toward building the tools needed to understand such a complex flow phenomenon, is based on the fact that flow in turbomachinery is fundamentally unsteady or time dependent. Success in building a reliable inventory of analytic and experimental tools will depend on how we treat time and time-averages, as well as how we treat space and space-averages. The challenge is to develop a set of computational and experimental tools which genuinely increase our understanding of the fluid flow and heat transfer in a turbomachine. Examples of the types of computational and experimental tools under current development, with progress to date, are examined. The examples include work in both the time-resolved and time-averaged domains.

INTRODUCTION

Because flow in turbomachinery is fundamentally unsteady or time dependent, the discipline research in turbomachinery is directed toward building the tools needed to understand such a complex flow phenomenon. Success in building a reliable inventory of analytic and experimental tools will depend on how we treat time and time-averages, as well as how we treat space and space-averages. The raw tools at our disposal - both experimental and computational - are truly powerful, and their numbers are growing at a staggering pace. As a result of this power, a case can be made that we are currently in a situation where information is outstripping understanding. The challenge is to develop a set of computational and experimental tools which genuinely increase our understanding of the fluid flow and heat transfer in a turbomachine. References 1 to 7 provide some background on the state of the art in developing these tools.

This paper outlines a philosophy based on working on a stairstep hierarchy of mathematical and experimental complexity to build a system of tools that will enable one to aggressively design the turbomachinery of the next century. Examples of the types of computational and experimental tools under current development at Lewis, with progress to date, are examined. The examples include work in both the time-resolved and time-averaged domains.

A CENTRAL THEME OF THE TURBOMACHINERY RESEARCH PROGRAM

The long-range goal of the turbomachinery research program at NASA Lewis is to establish a validated three-dimensional viscous analysis capability for

multistage turbomachinery, including unsteady effects and surface heat transfer. A full range of experimental and computational tools are being brought to bear on this problem in order to genuinely increase our understanding of the fluid flow and heat transfer in a turbomachine. The key to this understanding is the selection and successful application of the right tools for the right job.

A central theme of the turbomachinery research program, illustrated in figure 1, is that everything in a turbomachine is fundamentally unsteady (i.e., time dependent). This time dependency is further complicated by strong random disturbances. We have a choice. We can work in the time domain, which is expensive and time consuming; or we can work in the time-averaged domain, which is cheaper but yields less information. Furthermore, it is not simply an on/off, unsteady/steady situation. The averaging is by steps. Some of the time dependent nature can be averaged out, while some can remain. It is a matter of the time scale (or for that matter the length scale) over which the averaging is performed. Time average does not necessarily mean time independent or "steady". Thus, the question becomes both when and when not to average, and also how to average. A proper balance is required. Ultimately the engineer/designer is most interested in average information, but to get there one must properly handle time.

The levels of complexity associated with the handling are illustrated in figures 2 and 3. The time-accurate, unsteady Navier-Stokes and energy equations, which are capable of resolving all relevant time scales, describe the flow in a turbomachine. These are at the top of the stairs in figure 2. They are the easiest set to formulate, but the most difficult set to solve because they require enormous computer power for the simplest cases. To ease the solution a variety of averages are taken. The critical step is to average properly by using the proper time and length scales. Each averaging step results in a loss of information or resolution in the equations, introduces more unknowns, and requires external input (obtained by experiment and by solving the exact equations for simpler cases). One can use engineering judgement to determine how much information is needed to complete the mathematical description of the particular problem at hand. The averaged equations allow this introduction of engineering judgement. The pure unaveraged Navier-Stokes equations must be solved in their entirety.

Similarly in the experimental arena, as illustrated in figure 3, both time-resolved and time-averaged measurements are essential to a full understanding of turbomachinery flow and heat-transfer characteristics. As with analysis, the problem is in determining which technique to apply and when to apply it. Frequently, an average result offers more insight than time-accurate detail. A qualitative visual observation may be crucial to understanding the essential physics. At other times, such a measurement may bury the essential physics. Traditionally, dynamic measurements have provided less accurate absolute measurements than average measurements. Recent improvements suggest that averaging time-resolved measurements may be more accurate than making average measurements, especially in heat transfer. Laser anemometry, in addition to offering the well-known nonintrusive advantage, has an especially nice feature of providing ensemble averages of the random statistics while retaining and identifying the deterministic time dependency. Ultimately, all levels are needed to do the job. The challenge is to choose the right tool for the right job.

The average passage equation system, developed by Adamczyk and coworkers (refs. 8 to 10), is an example of averaging the Navier-Stokes equations. The three momentum equations and the energy equation are subjected to three averaging steps: one to remove random unsteadiness, a second to remove unsteadiness associated with blade-passing frequency and, finally, one to account for the uneven airfoil count from row to row. At its most fundamental level the averaging process introduces 11 unknowns in the axial momentum equation alone, as shown below. The advantage is that the resulting equation set is much easier to solve mathematically. It will be necessary to conduct physical and/or numerical experiments to provide the correlations which bring closure to these equations. The properly averaged equations provide the framework for a large research effort into understanding the physics of fluid flow and heat transfer in turbomachines.

AXIAL MOMENTUM EQUATION:

$$\begin{aligned}
 & \frac{\partial}{\partial t} \lambda_1 \bar{\bar{\bar{\rho}}} \bar{\bar{\bar{r}}} \bar{\bar{\bar{V}}}_z + \frac{\partial}{\partial r} \lambda_1 \bar{\bar{\bar{r}}} \bar{\bar{\bar{\rho}}} \bar{\bar{\bar{V}}}_r \bar{\bar{\bar{V}}}_z + \frac{\partial}{\partial \theta} \lambda_1 \bar{\bar{\bar{\rho}}} \bar{\bar{\bar{V}}}_\theta \bar{\bar{\bar{V}}}_z + \frac{\partial}{\partial z} \lambda_1 \left(\bar{\bar{\bar{r}}} \bar{\bar{\bar{\rho}}} \bar{\bar{\bar{V}}}_r \bar{\bar{\bar{V}}}_z + \bar{\bar{\bar{r}}} \bar{\bar{\bar{\rho}}} \bar{\bar{\bar{V}}}_\theta \bar{\bar{\bar{V}}}_z \right) \\
 & \left. \begin{aligned}
 &= \frac{\partial}{\partial r} \lambda_1 \left(\bar{\bar{\bar{r}}} \bar{\bar{\bar{\rho}}} \bar{\bar{\bar{V}}}_r \bar{\bar{\bar{V}}}_z - \bar{\bar{\bar{r}}} \bar{\bar{\bar{\rho}}} \bar{\bar{\bar{V}}}_r \bar{\bar{\bar{V}}}_z - \bar{\bar{\bar{r}}} \bar{\bar{\bar{\rho}}} \bar{\bar{\bar{V}}}_r \bar{\bar{\bar{V}}}_z - \bar{\bar{\bar{r}}} \bar{\bar{\bar{\rho}}} \bar{\bar{\bar{V}}}_r \bar{\bar{\bar{V}}}_z \right) \\
 &+ \frac{\partial}{\partial \theta} \lambda_1 \left(\bar{\bar{\bar{\rho}}} \bar{\bar{\bar{V}}}_\theta \bar{\bar{\bar{V}}}_z - \bar{\bar{\bar{\rho}}} \bar{\bar{\bar{V}}}_\theta \bar{\bar{\bar{V}}}_z - \bar{\bar{\bar{\rho}}} \bar{\bar{\bar{V}}}_\theta \bar{\bar{\bar{V}}}_z - \bar{\bar{\bar{\rho}}} \bar{\bar{\bar{V}}}_\theta \bar{\bar{\bar{V}}}_z \right) \\
 &+ \frac{\partial}{\partial z} \lambda_1 \left(\bar{\bar{\bar{r}}} \bar{\bar{\bar{\rho}}} \bar{\bar{\bar{V}}}_r \bar{\bar{\bar{V}}}_z - \bar{\bar{\bar{r}}} \bar{\bar{\bar{\rho}}} \bar{\bar{\bar{V}}}_r \bar{\bar{\bar{V}}}_z - \bar{\bar{\bar{r}}} \bar{\bar{\bar{\rho}}} \bar{\bar{\bar{V}}}_r \bar{\bar{\bar{V}}}_z - \bar{\bar{\bar{r}}} \bar{\bar{\bar{\rho}}} \bar{\bar{\bar{V}}}_r \bar{\bar{\bar{V}}}_z \right)
 \end{aligned} \right\} \\
 & + F_{IN}^{(2R)} + F_V^{(2R)} + F_{IN}^{(2S)} + F_V^{(2S)}
 \end{aligned}$$

CONVECTIVE TERMS

DIFFUSIVE TERMS

THE SUCCESSIVE OVERBARS REPRESENT AVERAGING OUT:
(1) RANDOM UNSTEADINESS
(2) PERIODIC UNSTEADINESS
(3) UNEQUAL BLADE COUNT

An example of a calculation using the average passage system of equations (ref. 10) depicts the evolution of a total-temperature distortion through the space shuttle main engine (SSME) fuel pump turbine, as shown in figure 4. The total-temperature profiles are color coded, with red denoting regions of hot gas and blue denoting regions of cold gas. At this stage in the development of the average passage equation system, many of the unknown viscous correlations remain to be determined and are set equal to zero for this calculation. The equations do, however, properly account for the interaction between blade rows. These results show that inviscid mixing as a result of streamwise vorticity generation can produce significant temperature differences between the suction and pressure side of a blade. This difference can lead to local regions of high thermal stress which can cause blade failure. The ability to capture the physics associated with this inviscid mixing process is a key element in increasing the durability of turbine blading.

Similarly the proper experimental tools must be developed and applied. High-speed turbomachinery research facilities are characterized by high-speed rotating machines, small blade-passage heights, three-dimensional flows, transonic velocity levels, high noise and vibration levels, and restricted mechanical access. Because of its high spatial and temporal resolution and nonintrusive nature, laser anemometry has become the measurement method of

choice for obtaining the detailed data required to assess the accuracy and sensitivity of flow analysis codes. In order to overcome the long measurement times required by laser anemometers and to capitalize on the detailed nature of the data which they generate, computer control of data acquisition and real-time data reduction and display, as illustrated in figure 5, are required. NASA Lewis is recognized as a world leader in the development and application of computer-controlled laser anemometer systems for use in both rotating and nonrotating turbine and compressor research applications. The work is summarized in reference 11.

Karman vortex streets are known to exist in blunt-body wakes over a wide flow regime. However, the existence of vortex streets in transonic fan and compressor-blade wakes was not generally anticipated since these blades have thin trailing edges. Laser anemometer measurements obtained in the wake of a transonic fan blade indicated two distinct states of the flow in the central portion of the blade wake - a high-velocity state and a low-velocity state. This behavior is consistent with that which would be displayed by a Karman vortex street. A simple vortex street model was constructed in an attempt to explain the experimental measurements. The model qualitatively agreed with the bimodal character of the velocity measurements. The model was also used to explain, for the first time, the highly unsteady nature of high-response pressure measurements made in the same wake flowfield. This research, which was a cooperative effort with MIT, typifies the manner in which advanced measurements coupled with simple modeling improve our understanding of complex flow phenomena. This work is summarized in figure 6, with details available in reference 12.

RESEARCH IN THE TIME-RESOLVED DOMAIN

Referring back to figure 1, a few examples of research in the time-resolved domain are presented to illustrate the physics which can be identified with time-resolved measurements and analyses. Measurements of the unsteady flowfield within a compressor stator operating downstream of a transonic fan rotor have been obtained using laser anemometry (refs. 13 to 15). Figure 7 shows a contour plot of the ensemble-averaged unresolved unsteadiness in the stator (which includes unsteadiness due to both turbulence and vortex shedding) for one rotor/stator relative position. Areas of high unresolved unsteadiness contain fluid which is in the rotor-blade wake. As the rotor blades rotate past the stator blades, the rotor wakes are convected through the stator row by the absolute flow velocity and, subsequently, chopped by the stator blades. Data obtained at additional times during the blade-passing cycle have been used to produce a movie sequence which illustrates the ensemble-averaged wake dynamics and its effect on the stator flowfield. We have the tools to measure temporal behavior in generic equivalents of a real machine.

A simulation was performed by Whitfield et al. (ref. 16) of the flow through a supersonic throughflow fan stage. This machine differs from today's machinery in that the axial Mach number is supersonic. For supersonic cruise, it offers an improvement in performance over transonic machinery. The three-dimensional simulation highlighted the rotor-stator interaction which occurs at design operating conditions. One of the interactions under study is the formation of "hot spots" at the leading edge of the stator, shown in figure 8. An animation illustrating the processes has also been made. The "hot spots" are at a temperature which exceeds the instantaneous total temperature

(absolute) of the flow stream exiting the rotor. Their formation is believed to be caused by the motion of the shock wave emanating from the pressure surface of the stator. We have the tools to compute temporal behavior in a real machine.

NASA is also developing rotor/stator interaction viscous flow codes (refs. 17 and 18). A quasi-three-dimensional viscous code used to solve for the flow in an isolated turbomachinery blade row was modified to handle equal pitch stator/rotor interaction computations (ref. 17). The solution procedure has been applied to the first-stage turbine rotor of the space shuttle main engine (SSME) fuel turbopump. For this calculation, shown in figure 9, the upstream stator was scaled so that its pitch matched that of the rotor, and the pitch-to-chord ratio remained unchanged. A converged periodic solution was obtained after the stator had seen 10 passing rotor blades or 10 pitch rotations of the rotor, which takes about 2.5 hr on the Cray. Mach contours are shown in the figure for an equal pitch stator/rotor configuration. The average inlet Mach number to the upstream stator is 0.15. The wake region that develops behind the stator passes through the grid interface and is seen in the rotor computational domain. Currently, the analysis is being applied to multiple passages of a single-stage turbine. The stage airfoil configuration is two upstream stators followed by three rotors. The airfoil geometries are taken from the first stage of the SSME fuel turbopump and are scaled to 2:3 from their actual 41:63 airfoil ratio. The details of such interactions are important to our understanding of turbomachinery flows.

EFFECT OF WAKES ON LAMINAR-TURBULENT TRANSITION IN A TURBINE STAGE

Detailed phase-resolved heat-flux data have been obtained on the blade of a full-stage rotating turbine by Dunn (refs. 19 and 20) for Teledyne Corp. in conjunction with a Vane-Blade Interaction program sponsored by the Air Force. A shock tube is used as a short-duration source of heated air, and platinum thin-film gages are used to obtain the heat-flux measurements. Some thin-film gages can be seen figure 10(a) in a leading-edge insert. Heat-flux results are presented in figure 10(b) for the midspan at several locations along the suction surface from stagnation point to 78-percent wetted distance. Each phase-resolved plot represents the ensemble-average of about four to five vane-wake (or passage) crossings. The rapid decrease in heat flux level from stagnation point to trailing edge is evident, as well as the fluctuating laminar-to-turbulent (and back to laminar) component, as the rotor cuts the stator wakes. This high-frequency oscillation from laminar to turbulent flow has important implications for turbine heat-transfer analysis and can only be identified with sophisticated sensors, electronics, and dynamic signal analysis.

As a result of several recent studies, the nature and significance of wake-related flow unsteadiness in turbomachinery blading and its profound effect on heat transfer are beginning to be recognized. In particular, the enhancement of heat transfer to the stagnation region is of interest because of the critical importance of heat transfer in this region. The effect of free-stream turbulence on time-average stagnation region heat transfer has been well documented. However, very few measurements have been obtained of the time-resolved effects of wake passage on heat transfer and the relationship of these effects to the corresponding velocity fluctuations. Current efforts (refs. 21 and 22 and unpublished work by J.E. O'Brien and S.P. Capp are aimed

at obtaining such measurements and performing statistical analysis to determine correlations between the unsteady velocity and heat-flux records. Figure 11 shows a schematic of the rotor-wake rig and representative fluctuating velocity measurements. In addition, stagnation region unsteady heat-flux records are shown which reveal the high degree of heat-transfer enhancement associated with each wake-passing event.

Since gas-side heat-transfer coefficients can vary by an order of magnitude within the transition region, a detailed understanding of boundary-layer transition is critical to the design of effective turbine-airfoil cooling schemes. This is particularly important when one realizes that such events can occur at blade-passing frequency. The present research (ref. 23) is aimed at understanding the fundamental differences between the "classical" boundary-layer transition process and the "bypass" transition process which occurs when a laminar boundary layer is perturbed by large free-stream disturbances. The time-resolved hot wire velocity measurements obtained at a grid-generated free-stream turbulence level of only 0.7 percent, shown in figure 12, indicate a bypass of small disturbances and the rapid development of a turbulent boundary layer as the flow progresses down the plate.

RESEARCH IN THE TIME-AVERAGED DOMAIN

Again, referring to figure 1, a few examples of research in the time-averaged domain are presented to illustrate the composite results which can be obtained from averaged measurements and analyses. As an example (refs. 24 to 26), a photograph of the experimental color temperature patterns of high-resolution, liquid-crystal thermography (figure 13) shows complex contours of constant temperature obtained from an experimental technique in which a uniformly heated turbine-vane cascade endwall surface is operated in an air flow. The resulting isotherms on the test surface are also lines of constant heat-transfer coefficient. The photographic data are then digitized for computer-based processing and display to show color contours of Stanton Number (nondimensional heat-transfer coefficient). The highest heat transfer rates occur in the vane stagnation region (shown in red). This computer-generated display can be used for direct comparison with code-generated predictions. Complex phenomena such as these require complex analyses - the three-dimensional Navier-Stokes codes.

A three-dimensional Navier-Stokes analysis code (RVC3D) is being developed for turbomachinery blade rows (ref. 27). The Navier-Stokes equations are written in a body-fitted coordinate system rotating about the x-axis. Streamwise viscous terms are neglected by using the thin-layer assumption, and turbulence effects are modeled with the Baldwin-Lomax eddy viscosity. The equations are discretized by using finite differences, and solved by using a multistage Runge-Kutta algorithm with a spatially varying time step and implicit residual smoothing. Calculations have been made of a horseshoe vortex formed at the junction of a turbulent endwall boundary layer and a blunt fin, as shown in figure 14. This geometry is to be tested experimentally later this year in an experiment described in the next paragraph. The calculations were done on 65 by 33 by 25 grid (lower figure) at the nominal tunnel operating conditions (Mach number, 0.6; fin thickness Reynolds number, 260 000; inlet boundary-layer thickness, 1 in.). Total pressure contours, 0.025 in. above the endwall, show the primary vortex core (center figure). Vector plots on the upstream symmetry plane (upper left) and on a downstream cross-channel plane (upper right) show the development of a double vortex system. The calculations

required about 1 million words of storage and 10 min of CPU time on a Cray X-MP.

A new facility for fluid mechanics and heat-transfer research, shown in figure 15, will provide benchmark quality experimental data for internal flow code validation. Focus will be on the three-dimensional interaction of the intersecting model with the surface plate (i.e., the horseshoe vortex). The facility will have the following capabilities: (1) maximum Mach number of 0.6, (2) no tunnel side-wall boundary layers, (3) controllable boundary layer on top and bottom walls of the tunnel, and (4) low inlet turbulence (less than 0.5 percent). The first phase of the experiment will consist of three parts: (1) fluid mechanics measurements will be taken by using a five-hole probe and hot film shear-stress gauges, (2) various flow visualization techniques will be used to define the flow path at the intersecting surfaces, and (3) heat transfer data will be recorded by the liquid crystal technique. The second phase of the work, to be conducted in about two years, will include full flow-field measurements by laser anemometry. This experiment and the RVC3D code development form a critical partnership to the successful development of a turbomachinery analysis capability.

Another complex geometry, the centrifugal compressors feature large surface area and small exit-passage heights. Viscous flow effects, therefore, have a major impact on the flowfield within centrifugal compressors. The inability to accurately predict and measure these flows contributes in large part to the inherently lower efficiency of centrifugal compressors relative to axial-flow compressors.

The large low-speed centrifugal compressor shown in the background of figure 16 has been designed (ref. 28) specifically to provide flow modeling and viscous code-validation data for centrifugal compressors. The impeller was designed to be aerodynamically similar to high-performance, high-speed centrifugal compressors such as the small 6:1 pressure-ratio impeller shown in the photograph. The low-speed impeller has a tip diameter of 60 in. and a design rotational speed of 1920 rpm. Inlet and exit blade heights are 8.70 and 5.4 in., respectively. The large size and low speed of the new impeller generate viscous flow regions (such as blade and endwall boundary layers) and tip clearance flows which are large enough to measure in detail with laser anemometry.

To analyze such geometries an efficient Navier-Stokes analysis code (RVCQ3D) (ref. 5) has been developed for turbomachinery. The effects of radius change, stream surface thickness, and rotation are included, which allows calculations of centrifugal impellers, radial diffusers, and axial machines with contoured endwalls. The unsteady Navier-Stokes equations are solved in finite-difference form by using an explicit Runge-Kutta algorithm with a spatially varying time step and multigrid convergence acceleration. The flow in the 6:1 pressure-ratio centrifugal impeller of figure 16 has been calculated on a 161 by 33 grid. Relative Mach number contours (figure 17(a)) show a supersonic bubble on the leading edge terminated by a shock. Rotational effects make the suction-surface boundary layer thin, the pressure-surface boundary layer thick, and they cause the wake to leave the trailing edge in a spiral. The calculations required about 3 million words of storage and 1.5 min of CPU time on a Cray X-MP. The flow in the new, large low-speed rig has also been calculated and is shown in figure 17(b). The ability to validate this

and other codes in the large low-speed rig will generate confidence in the high-speed calculations where validation is near to impossible.

In order to fully validate the codes, they must be shown capable of capturing real physics in real machines. An example is the shock behavior in a transonic fan. Many axial fan and compressor design systems currently in use do not account for passage shock three-dimensionality. In addition, preliminary blade designs are often performed as two-dimensional calculations on blade-to-blade stream surfaces. An assessment of the shock three-dimensionality in transonic rotors is therefore necessary in order to properly account for three-dimensional effects in the design process. Shock locations determined from laser anemometer measurements (ref. 29) are shown on blade-to-blade surfaces of revolution in the upper half of figure 18. Three different views of the same data, as displayed on a graphics workstation, are shown in the lower half of figure 18. A significant spanwise lean of the shock surface is evident in these three-dimensional views.

Increased emphasis on sustained supersonic cruise or hypersonic cruise has revived interest in the supersonic throughflow fan as a possible component in advanced propulsion systems. Use of a fan that can operate with a supersonic inlet axial Mach number is attractive from the standpoint of reducing the inlet losses incurred in diffusing the flow from a supersonic flight Mach number to a subsonic one at the fan face. The data base for components of this type is practically nonexistent, and design of any experiment to study feasibility of this concept must rely heavily on advanced computational tools to enhance the possibility of success. Computer codes that have been developed for design and analysis of transonic turbomachines were modified to allow calculations of blade rows with supersonic inlet Mach numbers (refs. 30 and 31). An inviscid/viscous code and a parabolized viscous code were used to design and analyze the variable nozzle and variable diffuser necessary for the experiment. Off-design analysis of the various components of the experiment indicated that all components would operate as expected over the flow and speed range of the experiment. Figure 19 shows the results obtained for the inlet variable nozzle which sets up the inlet flowfield, the fan rotor, and the variable diffuser, which decelerates the flow toward the collector inlet. All components were analyzed with two different codes in order to give increased confidence in the computed results. This is the ultimate goal of the turbomachinery program - to develop the tools which allow us to push beyond our experience with confidence.

CONCLUDING REMARKS

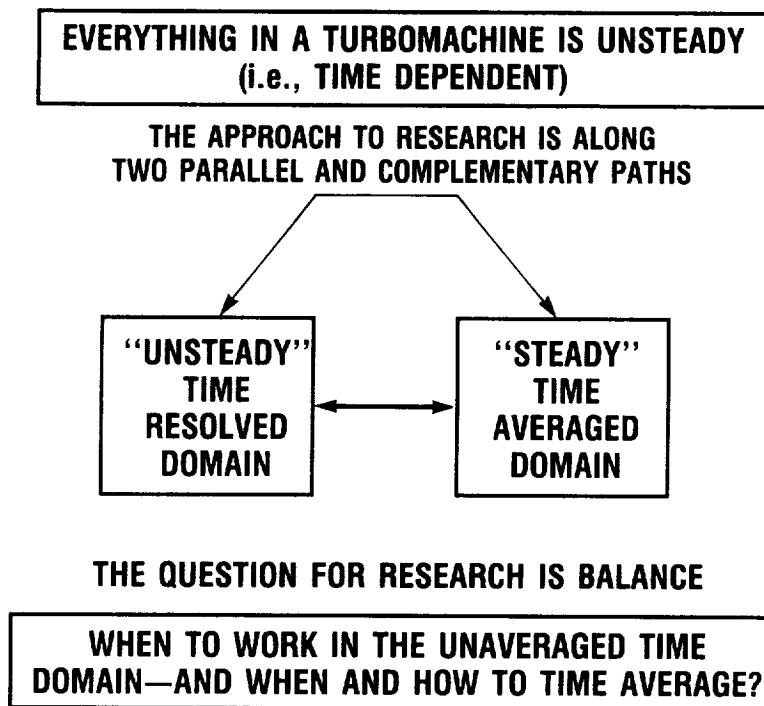
A complete and mature program has research at all levels along the computational and experimental paths. In the NASA Lewis turbomachinery program, special emphasis is placed on the analytic range from the ensemble (Reynolds) averaged Navier-Stokes equations to the average passage equations. The experimental emphasis is on high-response time-resolved measurements and on real machinery laser anemometry measurements. It is important to emphasize that the successful application of these tools will require a strong interaction between the computational and experimental paths. This concept for developing the tools we need is illustrated in figure 20.

REFERENCES

1. Simoneau, R.J.: Heat Transfer in Aeropropulsion Systems. Heat Transfer in High Technology and Power Engineering, W.J. Yang and Y. Mori, eds., Hemisphere Publishing Corp., Washington, D.C., 1985, pp. 285-319. (NASA TM-87066.)
2. McNally, W.D.; and Sockol, P.M.: Computational Methods for Internal Flows with Emphasis on Turbomachinery. J. Fluids Eng., vol. 107, no. 1, Mar. 1985, pp. 6-22.
3. Povinelli, L.A.: Assessment of Three-Dimensional Inviscid Codes and Loss Calculations for Turbine Aerodynamic Computations. J. Eng. Gas Turbines Power, vol. 107, no. 2, Apr. 1985. pp. 265-275.
4. Rai, M.M.: Navier-Stokes Simulations of Rotor/Stator Interaction Using Patched and Overlaid Grids. J. Propulsion Power, vol. 3, no. 5, Sept.-Oct. 1987, pp. 387-396.
5. Chima, R.V.: Explicit Multigrid Algorithm for Quasi-Three-Dimensional Viscous Flows in Turbomachinery. J. Propulsion Power, vol. 3, no. 5, Sept.-Oct. 1987, pp. 397-405.
6. Davis, R.L.; Ni, R.H.; and Carter, J.E.: Cascade Viscous Flow Analysis Using the Navier-Stokes Equations. J. Propulsion Power, vol. 3, no. 5, Sept.-Oct. 1987, pp. 406-414.
7. Hah, C.: Calculation of Three-Dimensional Viscous Flows in Turbomachinery with an Implicit Relaxation Method. J. Propulsion Power, vol. 3, no. 5, Sept.-Oct. 1987, pp. 415-422.
8. Adamczyk, J.J.; Mulac, R.A.; and Celestina, M.L.: A Model for Closing the Inviscid Form of the Average-Passage Equation System. J. Turbomachinery, vol. 108, no. 2, Oct. 1986, pp. 180-186.
9. Adamczyk, J.J.: A Model Equation for Simulating Flows in Multistage Turbomachinery. ASME Paper 85-GT-226, Mar. 1985.
10. Mulac, R.A., et al.: The Utilization of Parallel Processing in Solving the Inviscid Form of the Average-Passage Equation System for Multistage Turbomachinery. AIAA Paper 87-1108, June 1987. (NASA TM-89845.)
11. Strazisar, A.J.: Laser Fringe Anemometry for Aero Engine Components. Advanced Instrumentation for Aero Engine Components, AGARD CP-399, AGARD, Neuilly-Sur-Seine, France, 1986, pp. 6-1 to 6-32. (Avail. NTIS, AD-A182954.)
12. Hathaway, M.D., et al.: Rotor Wake Characteristics of a Transonic Axial-Flow Fan. AIAA J., vol 24, no. 11, Nov. 1986, pp. 1802-1810.
13. Hathaway, M.D.: Unsteady Flows in a Single-Stage Transonic Axial-Flow Fan Stator Row. NASA TM-88929, 1986.
14. Suder, K.L., et al.: Measurements of the Unsteady Flow Field Within the Stator Row of a Transonic Axial-Flow Fan. I - Measurement and Analysis Technique. ASME Paper 87-GT-226, May 1987.

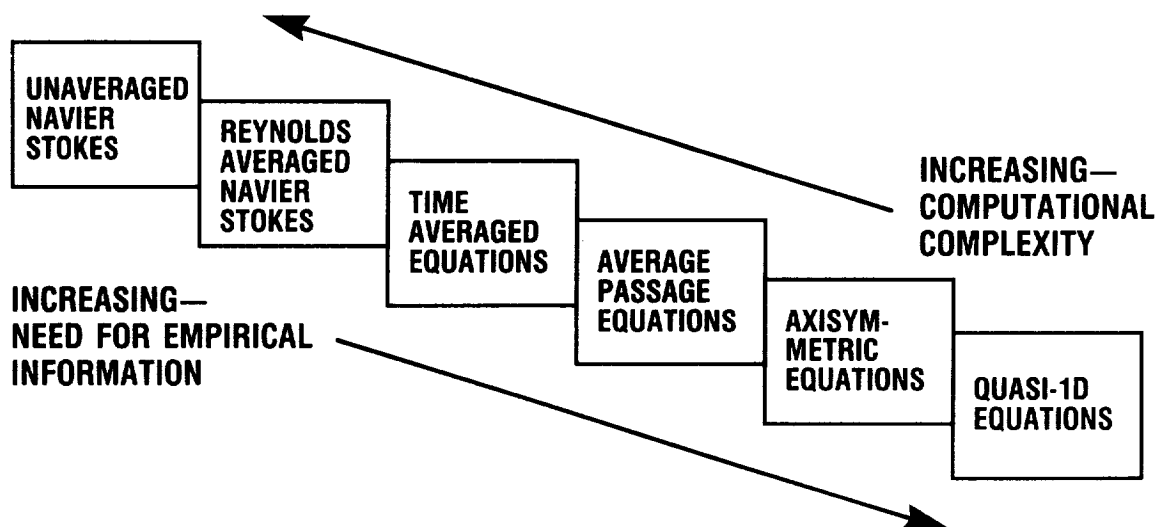
15. Hathaway, M.D., et al.: Measurements of the Unsteady Flow Field Within the Stator Row of a Transonic Axial-Flow Fan. II - Results and Discussion," ASME Paper 87-GT-227, May 1987.
16. Whitfield, D.L., et al.: Three-Dimensional Unsteady Euler Solutions for Propfans and Counter-Rotating Propfans in Transonic Flow. AIAA Paper 87-1197, June 1987.
17. Jorgenson, P.C.E.; and Chima, R.V.: An Explicit Runge-Kutta Method for Unsteady Rotor/Stator Interaction. AIAA Paper 88-0049, Jan. 1988. (NASA TM-100787.)
18. Rai, M.M.: Unsteady Three-Dimensional Navier-Stokes Simulations of Turbine Rotor-Stator Interaction. AIAA Paper 87-2058, June 1987.
19. Dunn, M.G.; and Hause, A.: Measurement of Heat Flux and Pressure in a Turbine Stage. J. Eng. Power, vol. 104, no. 1, Jan. 1982, pp. 215-223.
20. Dunn, M.G., et al.: Phase-Resolved Heat-Flux Measurements on the Blade of a Full-Scale Rotating Turbine. ASME Paper 88-GT-173, June 1988.
21. O'Brien, J.E., et al.: Unsteady Heat Transfer and Direct Comparison to Steady-State Measurements in a Rotor-Wake Experiment. Heat Transfer 1986, Vol. 3, C.L. Tien et al., eds., Hemisphere Publishing Corp., Washington, D.C., 1986, pp. 1243-1248.
22. O'Brien, J.E.: Effects of Wake Passing on Stagnation Region Heat Transfer. Heat Transfer in Gas Turbine Engines and Three-Dimensional Flows, E. Elovic, J.E. O'Brien, and D.W. Pepper, eds., ASME, 1988, pp. 17-28.
23. Suder, K.L.; O'Brien, J.E.; and Reshotko, E.: Experimental Study of Bypass Transition in a Boundary Layer. NASA TM-100913, 1988.
24. Hippensteele, S.A.; Russell, L.M.; and Stepka, F.S.: Evaluation of a Method for Heat Transfer Measurements and Thermal Visualization Using a Composite of a Heater Element and Liquid Crystals. J. Heat Trans., vol. 105, no. 1, Feb. 1983, pp. 184-189.
25. Hippensteele, S.A.; and Russell, L.M.: High Resolution Liquid-Crystal Heat-Transfer Measurements on the Endwall of a Turbine Passage with Variations in Reynolds Number. NASA TM-100827, 1988.
26. Boyle, R.J.; and Russell, L.M.: Experimental Determination of Stator End-wall Heat Transfer. ASME Paper 89-GT-219, June 1989, NASA TM-101419.
27. Chima, R.V.; and Yokota, J.W.: Numerical Analysis of Three-Dimensional Viscous Internal Flows. NASA TM 100878, 1988.
28. Wood, J.R.; Adam, P.W.; and Buggele, A.E.: NASA Low-Speed Centrifugal Compressor for Fundamental Research. AIAA Paper 83-1351, June 1983. (NASA TM-83398.)

29. Wood, J.R.; Strazisar, A.J.; and Simonyi, P.S.: Shock Structure Measured in a Transonic Fan Using Laser Anemometry. Transonic and Supersonic Phenomena in Turbomachines, AGARD CP-401, AGARD, Neuilly-Sur-Seine, France, 1987, pp. 2-1 to 2-14. (Avail. NTIS, AD-A182996.)
30. Wood, J.R., et al.: Application of Advanced Computational Codes in the Design of an Experiment for a Supersonic Through-Flow Fan Rotor. ASME Paper 87-GT-160, June 1987. (NASA TM-88915.)
31. Schmidt, J.F., et al.: Supersonic Through-Flow Fan Design. AIAA Paper 87-1746, June 1987. (NASA TM-88908.)



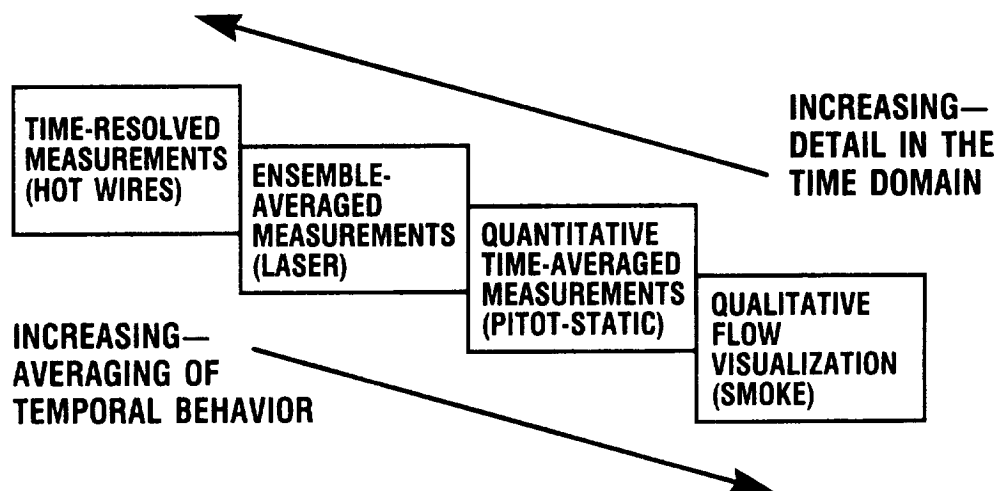
CD-87-28978

Figure 1. - Central theme for turbomachinery research.



CD-87-28979

Figure 2. - Levels of complexity along the path of computational analysis.



CD-87-28980

Figure 3. - Levels of a complexity along the path of experimental measurements.

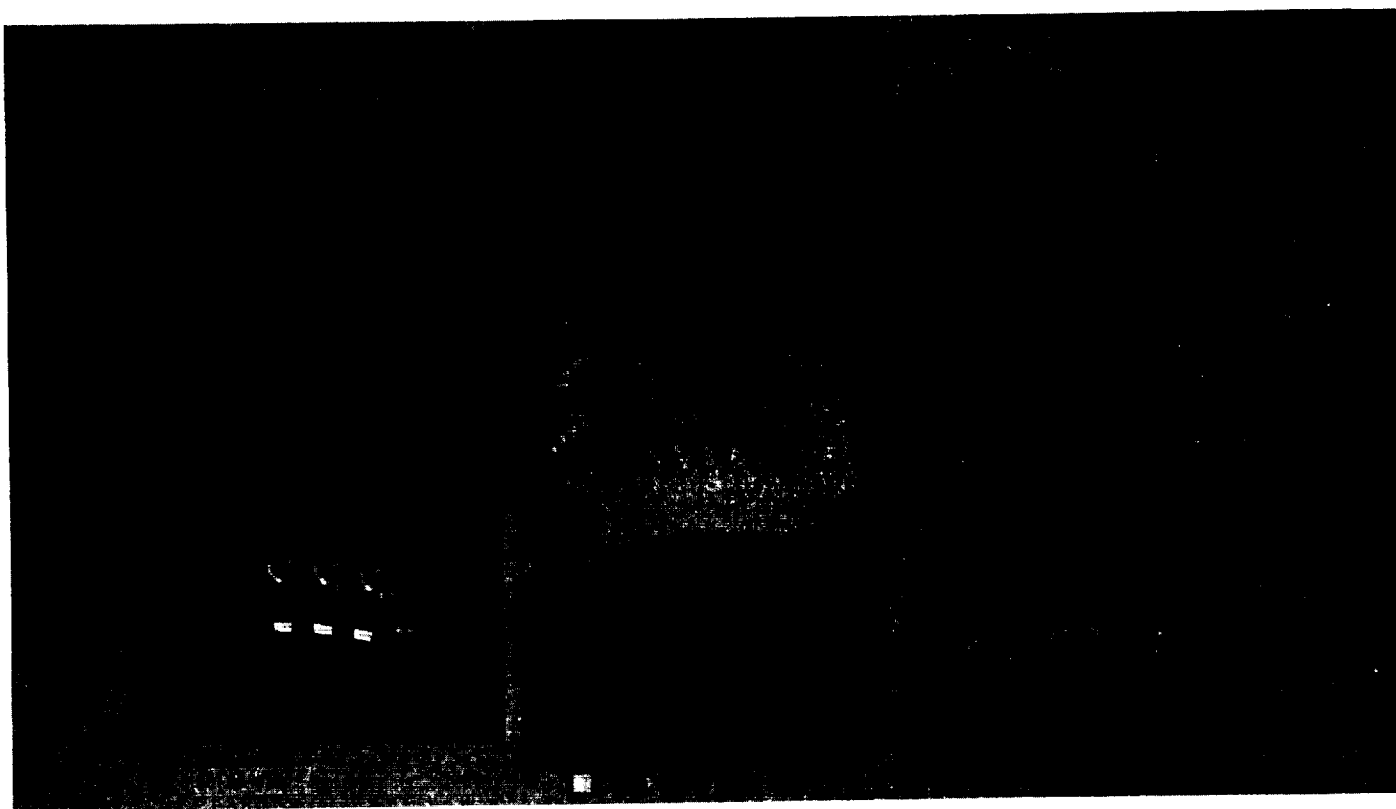
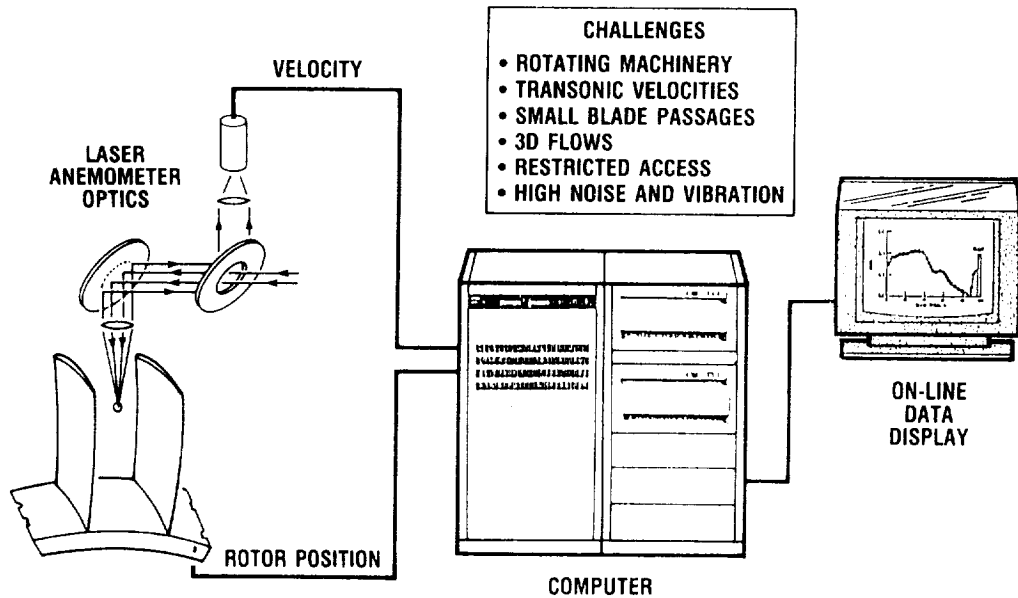
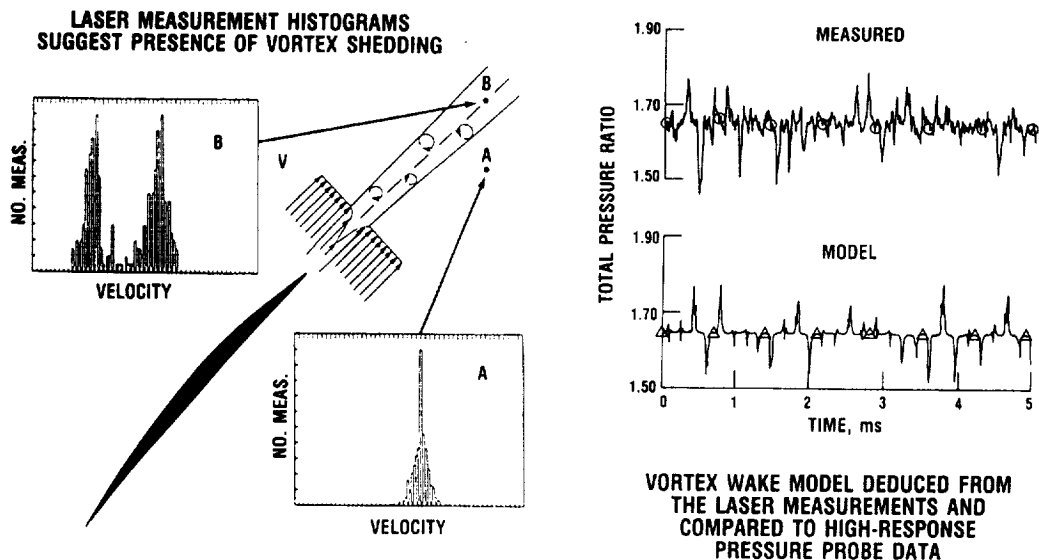


Figure 4. - Evolution of total temperature field within SSME fuel turbine.



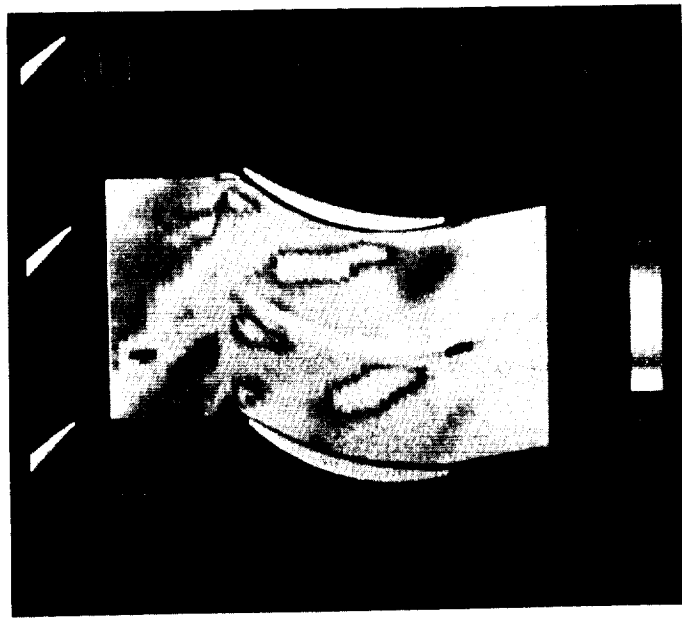
CD-87-28983

Figure 5. - Turbomachinery laser anemometry systems.



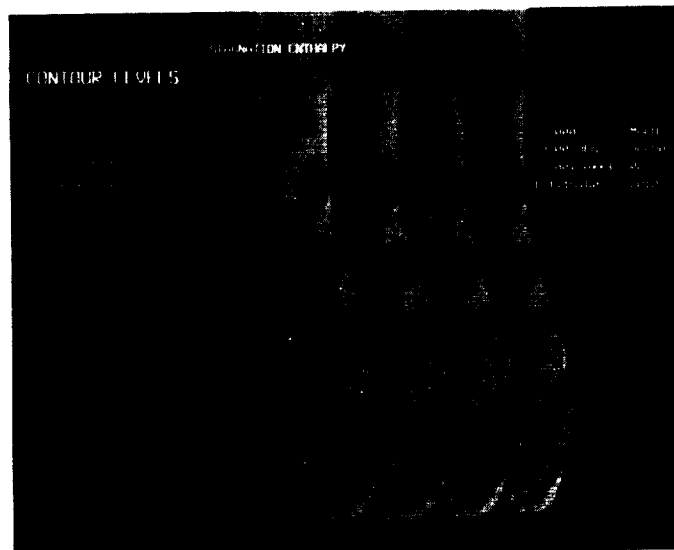
CD-87-28984

Figure 6. - Developing models to explain flow physics.



CD-87-28986

Figure 7. - Compressor "turbulent" kinetic energy distribution (one frame from data movie showing progress of wake through stator passage downstream of rotor).



CD-87-28987

Figure 8. - Unsteady Euler calculation for a supersonic throughflow fan (one frame from computational movie showing progress of supersonic rotor exit total temperature through downstream stator).

TIME ACCURATE 2D NAVIER-STOKES
CALCULATION, SHOWING THE MACH
CONTOUR DISTRIBUTION AT ONE
INSTANT OF TIME IN A BLADE-
PASSING PERIOD



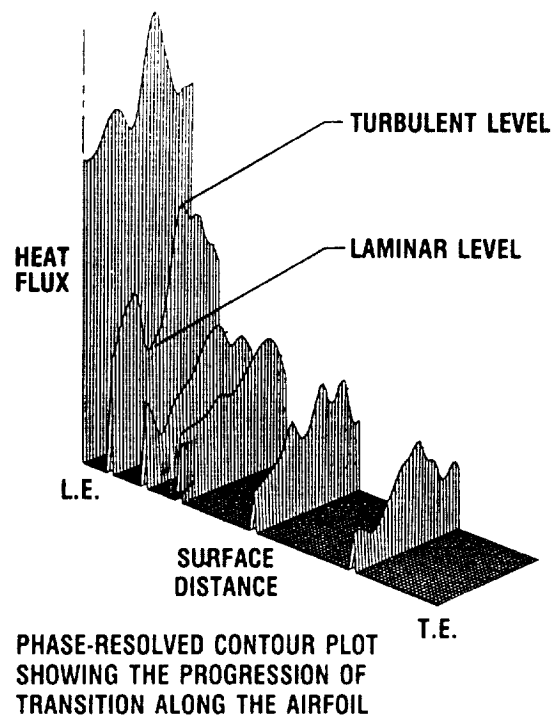
CD-87-28988

Figure 9. - Rotor/stator interaction calculation - SSME fuel turbine.



PHOTO OF A ROTOR BLADE INSTRUMENTED
WITH THIN-FILM SENSORS

CD-87-28989



PHASE-RESOLVED CONTOUR PLOT
SHOWING THE PROGRESSION OF
TRANSITION ALONG THE AIRFOIL

Figure 10. - Effect of wakes on laminar-turbulent transition in a turbine stage.

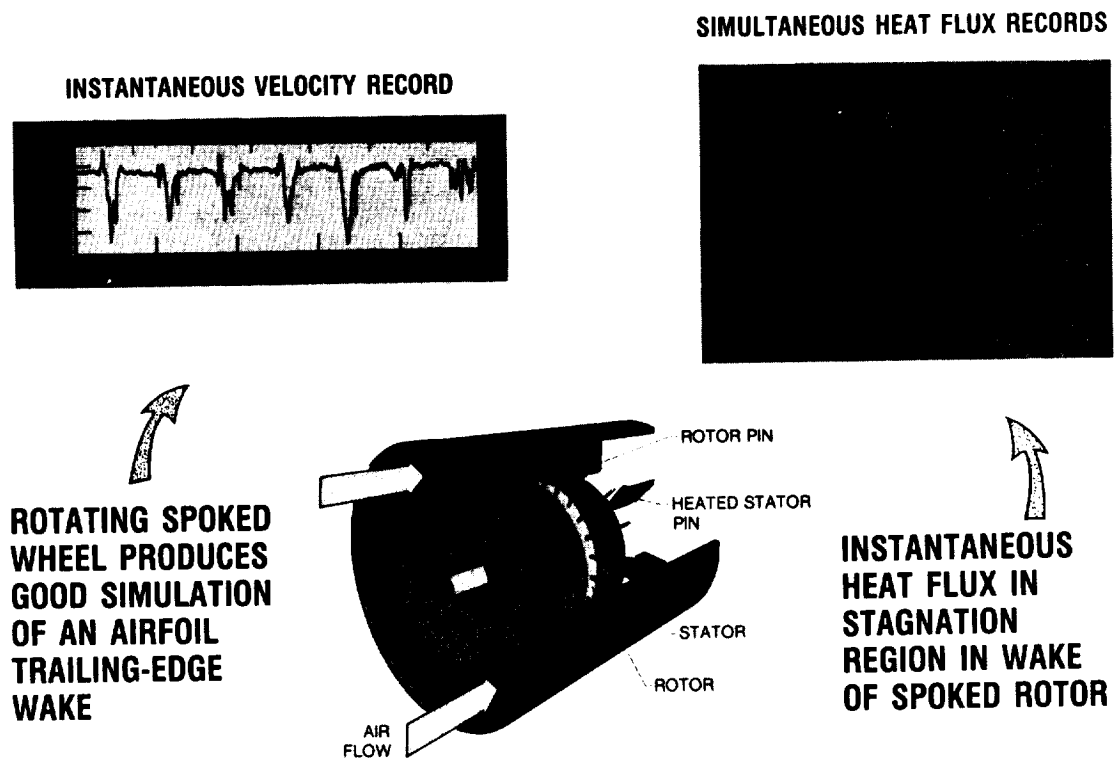
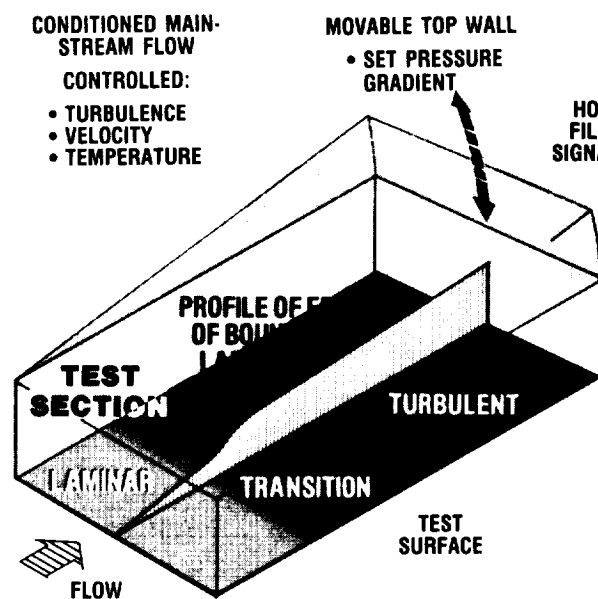
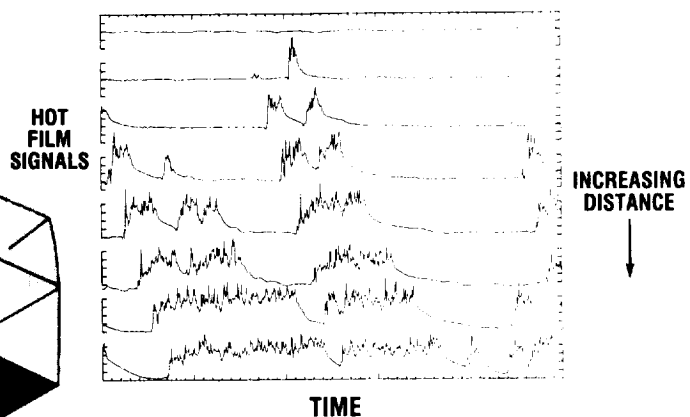


Figure 11. - Unsteady heat transfer in rotor-wake flows.

SKETCH OF TEST SECTION SHOWING MAJOR FEATURES OF FACILITY



FREE-STREAM TURBULENCE LEVEL 0.77%

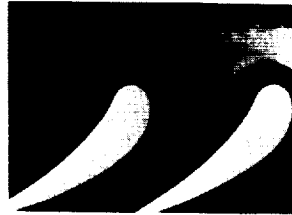


CARPET PLOT OF SIMULTANEOUS HOT FILM RECORDS, SHOWING PROGRESSION AND GROWTH OF TURBULENCE ALONG THE PLATE SURFACE

CD-87-28991

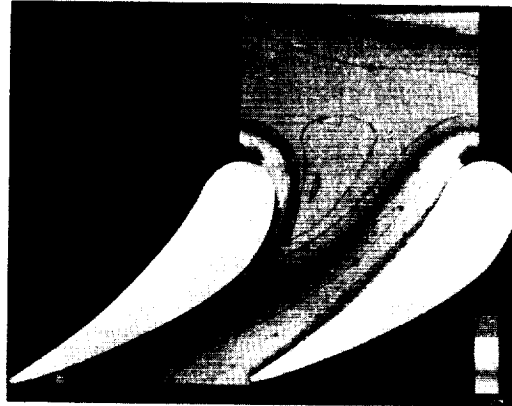
Figure 12. - Boundary-layer transition research - a study of intermittent behavior.

**EXPERIMENTAL LIQUID-
CRYSTAL COLOR
TEMPERATURE PATTERNS**



**(ISOTHERMS
AT CONSTANT
HEAT FLUX)**

**COMPUTER-BASED COLOR CONTOURS OF THE
ENDWALL HEAT TRANSFER DISTRIBUTION**

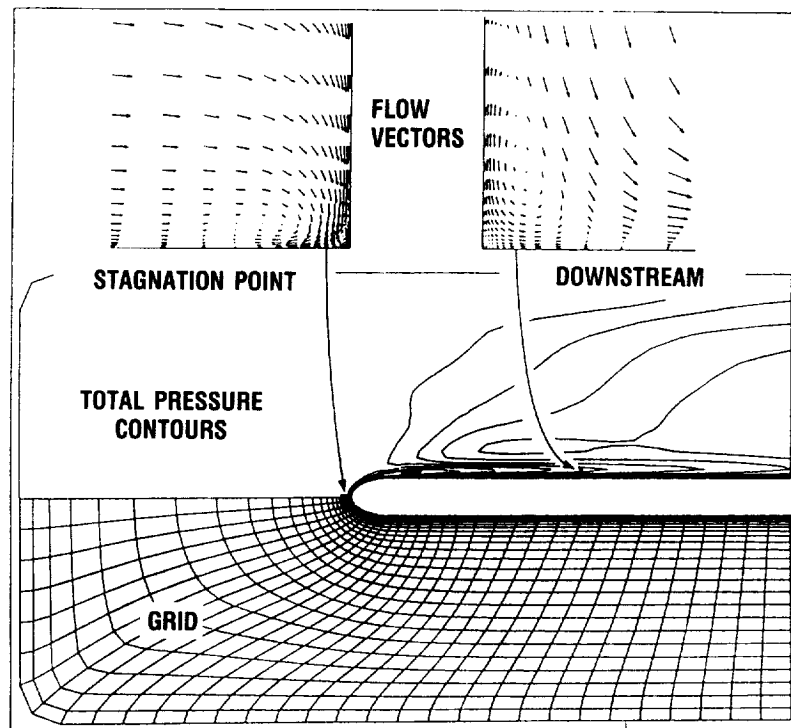


**(DIGITIZED COMPOSITE
OF EXPERIMENTAL DATA)**

CD-87-28993

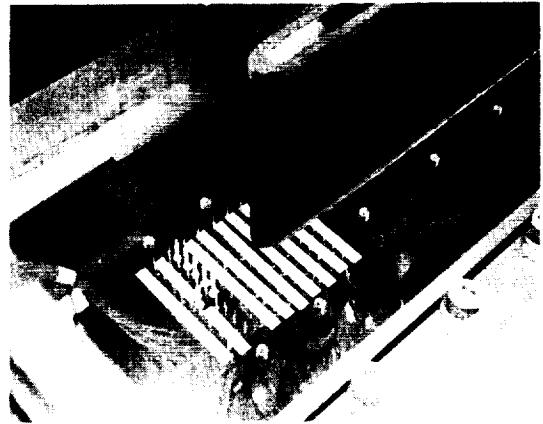
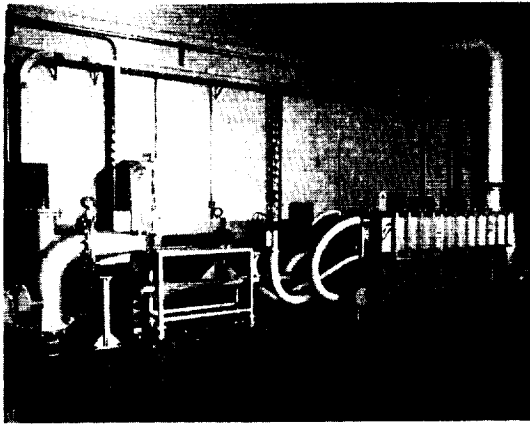
Figure 13. - High-resolution, liquid-crystal turbine endwall heat-transfer data.

**CALCULATION OF
HORSESHOE VORTEX
FOR SAME GEOMETRY
AND CONDITIONS OF
THE COMPRESSIBLE
FLOW TUNNEL
(SEE FIG. 15.)**



CD-87-28994

Figure 14. - Three-dimensional Navier-Stokes code analysis of turbulent horseshoe vortex.



OBJECTIVE

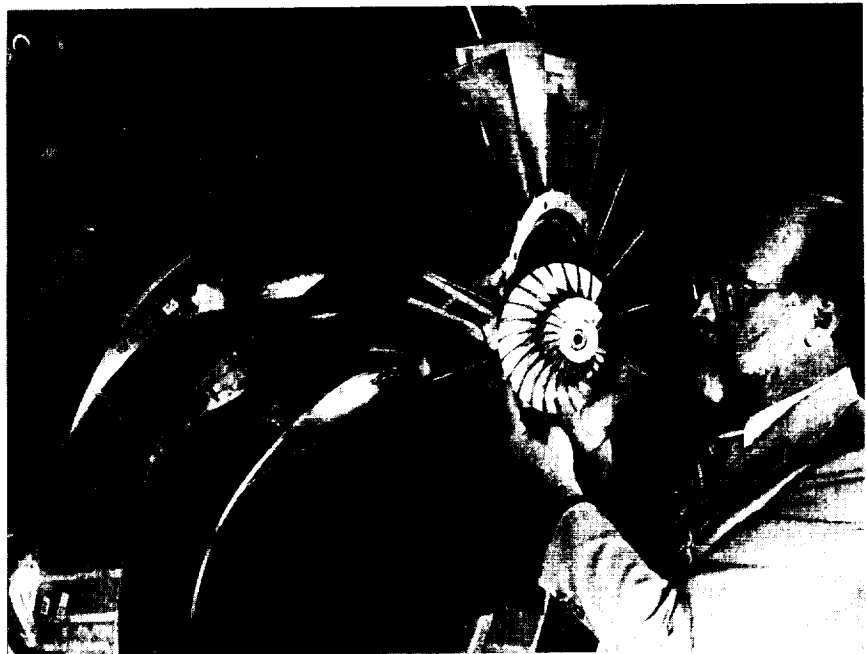
TO OBTAIN DATA TO VERIFY COMPUTATIONAL FLUID MECHANICS COMPUTER CODES THAT ARE CAPABLE OF SOLVING FULLY 3D FLOWS INCLUDING HEAT TRANSFER

CD-87-28995

Figure 15. - Three-dimensional compressible flow tunnel.

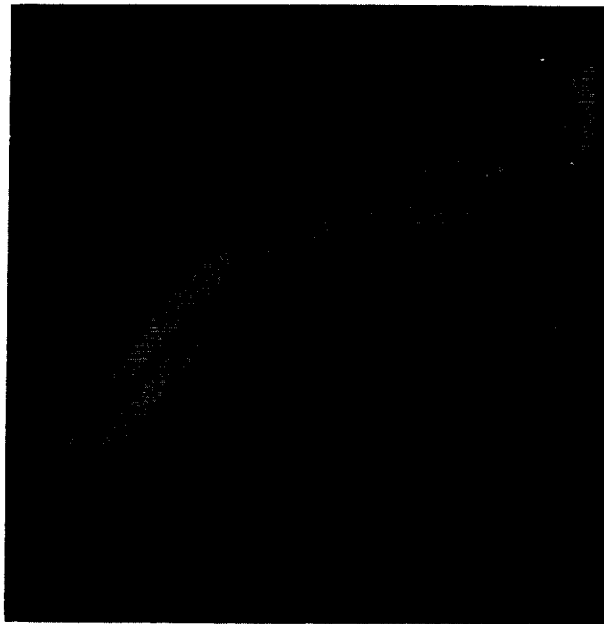
UNDERSTANDING THE FLOW
PHYSICS AND THE VALIDATION
OF COMPLEX TURBOMACHINERY
3D NAVIER-STOKES CODES
REQUIRES VERY LARGE ROTA-
TING MACHINERY IN ORDER TO
BE ABLE TO EXAMINE THE
VISCIOUS BOUNDARY LAYERS

SIZE COMPARISON BETWEEN
LOW-SPEED IMPELLER AND
2-LB/S HIGH-SPEED IMPELLER

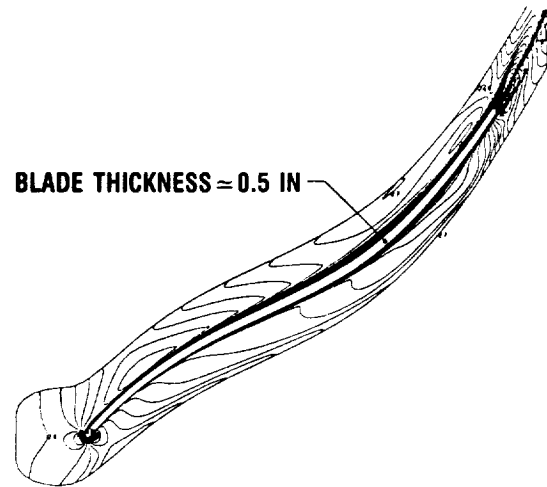


CD-87-28996

Figure 16. - Large low-speed centrifugal compressor - new flow physics and code validation rig.



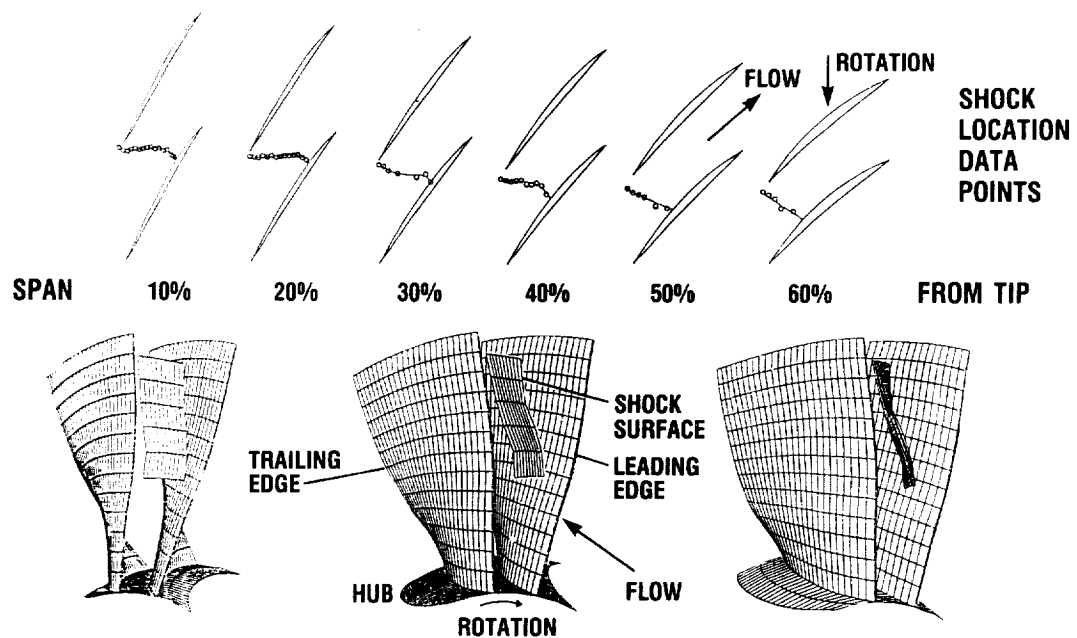
ANALYSIS OF HIGH-SPEED 6:1
CENTRIFUGAL IMPELLER



ANALYSIS OF LARGE LOW-SPEED
CENTRIFUGAL IMPELLER

CD-87-28997

Figure 17. - Quasi-three-dimensional Navier-Stokes code for turbomachinery analysis.



CD-87-28998

DATA ENHANCEMENT AND 3D VIEWING ROTATION

Figure 18. - Measurement of three-dimensional shock structure in transonic axial-flow fan.

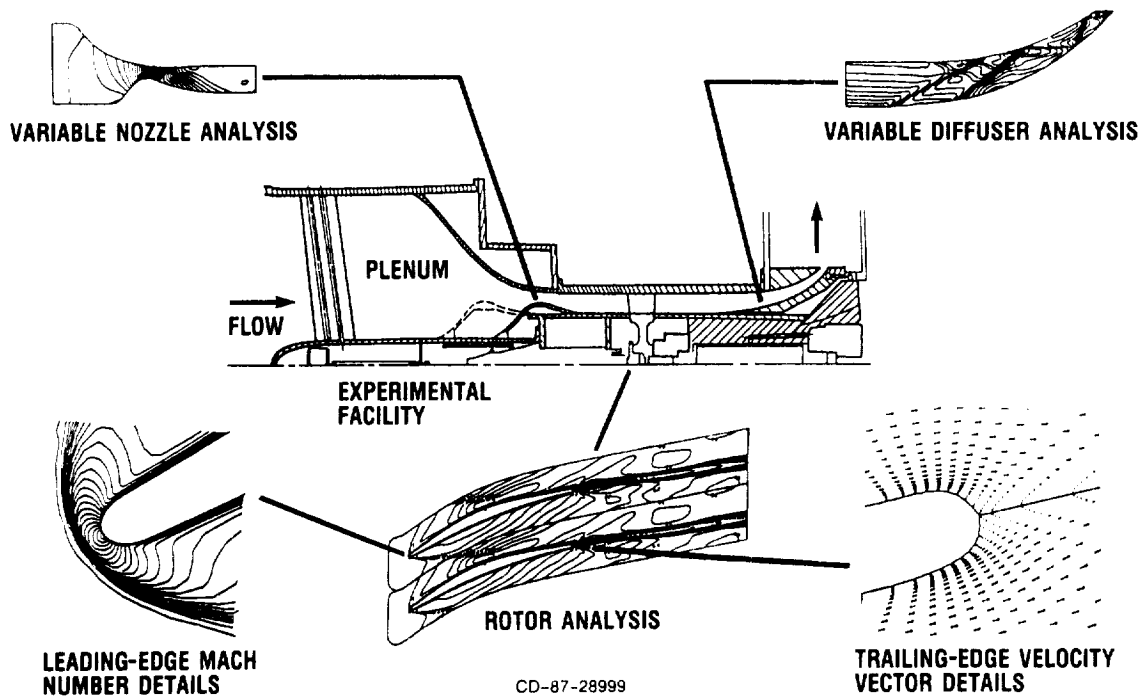


Figure 19. - Application of advanced codes for design of supersonic throughflow fan experiment.

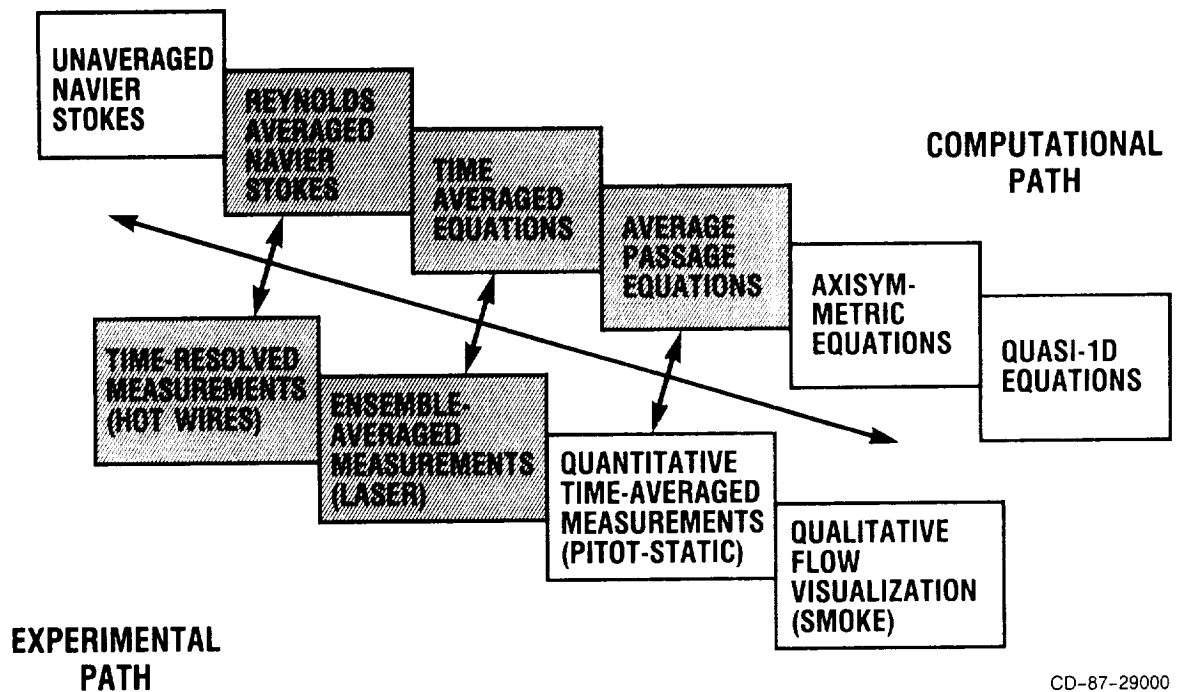


Figure 20. - Position of turbomachinery research program on computational and experimental paths.

CHEMICAL REACTING FLOWS

Edward J. Mularz
U.S. Army Aviation Research and
Technology Activity - AVSCOM

and

Peter M. Sockol

SUMMARY

Future aerospace propulsion concepts involve the combustion of liquid or gaseous fuels in a highly turbulent internal airstream. Accurate predictive computer codes which can simulate the fluid mechanics, chemistry, and turbulence-combustion interaction of these chemical reacting flows will be a new tool that is needed in the design of these future propulsion concepts. Experimental and code development research is being performed at Lewis to better understand chemical reacting flows with the long-term goal of establishing these reliable computer codes.

Our approach to understanding chemical reacting flows is to look at separate, more simple parts of this complex phenomenon as well as to study the full turbulent reacting flow process. As a result we are engaged in research on the fluid mechanics associated with chemical reacting flows. We are also studying the chemistry of fuel-air combustion. Finally, we are investigating the phenomenon of turbulence-combustion interaction. This presentation will highlight research, both experimental and analytical, in each of these three major areas.

INTRODUCTION

Chemical reacting flows of aerospace propulsion systems have features similar to internal flows in ducts, nozzles, and turbomachinery. The flows are typically highly turbulent, with large secondary flows and three-dimensional flow characteristics. Flow oscillations and unsteadiness are usually prevalent in these flows. However, there are additional features unique to flows with combustion that add a great deal of complexity to the process. This includes a substantial increase in temperature as the flow moves downstream, and a significant change in fluid properties due to fluid species changes. In addition, the time scale for combustion is often orders of magnitude different from the fluid flow time, and there is often a strong interaction between the turbulent flow and the combustion process. These complex features not only make experimental studies difficult but also significantly affect the methods for simulating these flows on the computer.

The research activities in chemical reacting flows are divided into three areas, as shown in figure 1:

(1) Fluid mechanics, which looks at the fluid flow phenomena associated with combustion without the added complexity of including heat release. Research includes studying the multiphase processes of fuel sprays, and the highly three-dimensional and time varying flows that typically exist in real propulsion systems.

(2) Combustion chemistry, which concentrates on the combustion of fuel and oxidizer without including the fluid mechanics. Research is seeking to understand the ignition process of fuel and oxidizer and to probe the detailed chemistry to obtain an accurate combustion model for future fluid codes. Catalytic combustion is also being studied as a fuel processor for high-speed propulsion.

(3) Turbulence-combustion interaction, which looks at both the fluid mechanics and the chemistry of combustion and their effects on each other. Work is being done to understand the dominant physics of turbulent reacting flow and to construct accurate computer codes to simulate this flow. Also, as a useful "numerical experiment," the technique of direct numerical simulation is being used to better understand chemical reacting flows.

These three major areas of activities are all being performed to achieve the long-term goal of obtaining an accurate predictive code with coupled fluid mechanics and chemistry which will be needed in the design of future aerospace propulsion systems. This paper will look at an example of the research in each of these three areas.

FLUID MECHANICS

In this area, an important research activity is the study of the multiphase flows of liquid fuel sprays in air. The fuel-spray process is extremely important in terms of engine efficiency, durability, and operability. The ultimate objective of the research is to develop a computer code that can accurately model the fuel and air mixing with subsequent combustion. Since these processes are very complicated, the model is being approached in a series of steps of increasing complexity. Particle-laden jets were initially studied in order to assess the capability of current two-phase flow models (refs. 1 to 4). Evaporating liquid sprays and combusting sprays are now being studied.

Figure 2 shows the arrangement of the particle-laden jet experimental study. An air jet containing solid glass beads ($39\text{ }\mu\text{m}$, Sauter mean diameter) discharged downward into a still environment. Particle-laden jets with three swirl numbers were studied. Nonintrusive measurements of velocity were obtained with a two-channel laser velocimeter. Particle size and velocity were measured with a phase/doppler particle anemometer. The gas phase was seeded with nominal $1\text{-}\mu\text{m}$ -diameter aluminum oxide powder to measure gas-phase velocities.

Figures 3 and 4 present typical results from the particle-laden jet study. A contour plot of experimentally measured axial velocity of the gas phase (left side) and particle phase (right side) is illustrated in figure 3. It is evident that, initially, the gas phase has a higher velocity than the particle phase. The particles are initially accelerated by the gas phase, and then their velocity begins to decay. Because of their inertia, the rate of decay of axial velocity is slower for the particles than the gas. Shown in figure 4 are predictions from the SSF model at 10 diameters downstream of the tube exit.

This model tracks particle trajectories in the computed gas-phase flowfield and allows momentum exchange between phases. The model also considers effects of gas-phase turbulence on particle trajectories. Predictions from the model show reasonable agreement with the data. More details on these experiments and a full description of the computer code and model can be found in references 1 to 4.

Future directions for multiphase flow research include evaporating liquid sprays and combusting liquid sprays. Evaporating sprays are currently being studied under contract at the University of California, Irvine, and Allison Gas Turbine as part of the HOST Program. Results have been reported in references 5 to 9. The test cell where the particle-laden jets were studied is currently being modified to study liquid fuel sprays with combustion.

COMBUSTION CHEMISTRY

An example of the research in the area of combustion chemistry is the study of the chemical kinetics of hydrogen-air combustion.

In a supersonic ramjet (scramjet) propulsion system, the time required between the injection of fuel into the airstream and its combustion point is very important with regards to the length of the engine and its weight. These high-speed propulsion concepts will be tested in wind tunnels where the air has been heated to simulate the temperatures and velocities of the air that would be ingested into the engine as the vehicle flies at high Mach numbers in the atmosphere. Research is underway to determine the combustion delay time of hydrogen fuel and air and to determine the effects of air contaminants in the wind tunnel on this combustion delay time.

Shown in figure 5 is a schematic of a scramjet engine. Air at supersonic velocity enters the engine where fuel is injected. At a position downstream from this injection point, the fuel will burn with the air. The information which we are seeking is to determine how far from the fuel injection point will a stable flame exist in a supersonic airstream of various Mach numbers. Also, since heated wind tunnels have small amounts of contaminants or additives in the air, we are studying the effects of these contaminants on this combustion delay time.

Shown in table I are the levels of four major air contaminants which exist in the two U.S. hypersonic wind tunnels when they are simulating a Mach 7 flight speed. Carbon dioxide and water vapor are known to lengthen the combustion delay time. Nitric oxide and nitrogen dioxide, although orders of magnitude smaller in concentrations, would tend to shorten the combustion delay time.

Stoichiometric H_2-O_2 ignition delay times were measured behind reflected shock waves at 1.1 atm pressure over the temperature range 1300 to 950 K by using a chemical shock tube. A picture of the facility is shown in figure 6. A chemical kinetic model was then constructed, and the data from the shock tube experiments were compared with model predictions. The proposed chemical

kinetic model predicted ignition delay times in excellent agreement with the experimental data, as shown in figure 7.

Applying the chemical kinetic computer model to the prediction of combustion delay time for a scramjet flying at a Mach 7 flight condition yielded a 70-cm distance between the fuel injection point and the flame front, as shown in figure 8(a). When the wind tunnel contaminants were taken into account, this distance was significantly shorter: only 13 cm between the fuel injection point and the flame front (fig. 8(b)). Thus, the small concentration of contaminants (nitric oxide and nitrogen dioxide) resulted in over 80 percent reduction in combustion length. Not only is this effect important in evaluating wind tunnel experiments of propulsion concepts, but it also indicates that trace additives into the flow could significantly shorten the required engine length and thereby considerably reduce weight.

Preliminary results of this work have been reported in reference 10. This work is continuing to explore the effects of these trace contaminants or additives and to better quantify their potential benefit to future scramjet designs.

TURBULENCE-COMBUSTION INTERACTION

While it is important and quite useful to look at the fluid mechanics and the combustion chemistry aspects of chemical reacting flows independently, to get a full understanding of the dominant phenomena of these flows, we must examine the interaction of turbulent flow with combustion. Activities in this area include both numerical code development work and experimental research.

TURBULENT REACTING FLOW

The objective of this work is to understand the coupling between fluid dynamics and combustion and to establish an accurate computer code which simulates the dominant features of turbulent reacting flow. Existing combustion data sets are incomplete for validating computational computer codes. Especially lacking are the inlet and exit boundary conditions, as pointed out in a review report, reference 11. An experiment is being constructed which focuses on many of these features of turbulent reacting flow, both steady state and unsteady. This experiment is to examine a plane free shear layer with combustion. Turbulent reacting flow computer codes, both steady state and time accurate, are also being developed concurrently, and the database from the experiment will serve as a means to validate these new computer codes.

Excellent free shear layer experiments have been carried out, and are reported in the literature (e.g., ref. 12). The data are incomplete, however, for validation of advanced combustion models (ref. 13), and more experimental information is required.

The objectives of the planar reacting shear layer experiment, shown as a schematic in figure 9, are (1) to understand the coupling between fluid dynamics and combustion and (2) to establish a data set to validate computer codes which simulate the physics and chemistry of high-speed chemical reacting flow. A complete description of this experiment is presented in reference 14. Two

gas streams, one of hydrogen and nitrogen, the other of air, will mix downstream of a plane splitter plate. Combustion will occur where the fuel and air have properly mixed. Pressure oscillations in this closed duct will exist because of the dynamic features of the flow, and the interactions between these pressure oscillations and the combustng shear layer will be examined. The unique features of this experiment are (1) a continuous flow capability, (2) flow velocities of both the air and the hydrogen-nitrogen mixture which are in the high subsonic range, (3) the air will be heated ahead of the mixing shear layer without any contamination effects, and (4) the heat release in this experiment will be quite high, typical of propulsion systems. The experiment is in fabrication, and nonintrusive instrumentation is being purchased. Experiments are expected to begin in spring of 1989.

In the numerical code development area, two activities are highlighted. In the first code development effort, a time-accurate version of a two-dimensional finite volume code has been used to calculate forced shear flows (ref. 15). The code is fully second-order accurate in time and space. QUICK differencing is used for the convective terms, and block correction combined with Stone's strongly implicit algorithm is used to solve the pressure correction equation. A two-equation turbulence model is used to represent three-dimensional, small-scale turbulent motions. The large, two-dimensional scales of motion are calculated exactly.

Shown in figure 10 are vorticity contours for a two-dimensional, numerical calculation of a forced shear layer at a Reynolds number of about 100 000. The positive and negative vorticity contours originate at the boundary layers, specified at the inlet of the computational domain. Forcing is applied at a long wavelength, and smaller scale vorticities spontaneously develop as a result of the natural instability of the layer. These small-scale vorticities cluster on the scale of the longer, forced wavelength. Small pockets of positive vorticity persist as remnants of the low-speed boundary layer. The collective interaction of these small-scale vortices, merging into larger scale structures, largely controls the dynamics of the shear layer. These calculations were performed on the NAS Cray 2 computer.

In the second code development effort, a new computational fluid dynamics (CFD) code, the RPLUS code, has been developed for the study of mixing and chemical reactions in the flowfields of the ramjets and scramjets. The code employs an implicit finite-volume, lower-upper symmetric successive overrelaxation scheme (LU-SSOR) (refs. 16 and 17) for solving the complete two-dimensional Navier-Stokes and species transport equations. The RPLUS code is written in generalized curvilinear coordinates and therefore can handle any arbitrary two-dimensional geometry. The implicit LU-SSOR scheme requires only scalar diagonal inversions while most other implicit schemes require block matrix inversions. The use of scalar diagonal inversions offers order-of-magnitude efficiency improvement over conventional implicit schemes, which require the inversion of block matrices, when large systems of partial differential equations must be solved, such as the reacting flows in ramjets and scramjets.

The validity of the code has been demonstrated by comparing the numerical calculations with both experimental data and previous numerical results over a wide range of flow conditions (ref. 17). The code was then used to calculate the mixing and chemical reactions of a hydrogen jet transversely injected into a supersonic airstream. Figure 11 illustrates the inflow conditions and the

static pressure contours. The injected high-pressure hydrogen expands rapidly and yields large pressure gradients along the jet path. This figure indicates that the jet partially blocks the axial flow and yields a strong bow shock just ahead of the injector. The two bow shocks resulting from the two hydrogen jets at top and bottom walls intersect at the center plane and yield a large pressure rise. This code is continuing to be developed, including expanding to three dimensions, in order to be applied to practical complex problems of interest.

CONCLUDING REMARKS

Research in the area of chemical reacting flow will lead to an understanding of this complex flow and accurate predictive computer codes. Activity in this topic is focused on three areas: fluid mechanics, combustion chemistry, and turbulence-combustion interaction. Results from this research will provide important technical tools we need to develop new aerospace propulsion systems for the year 2000 and beyond.

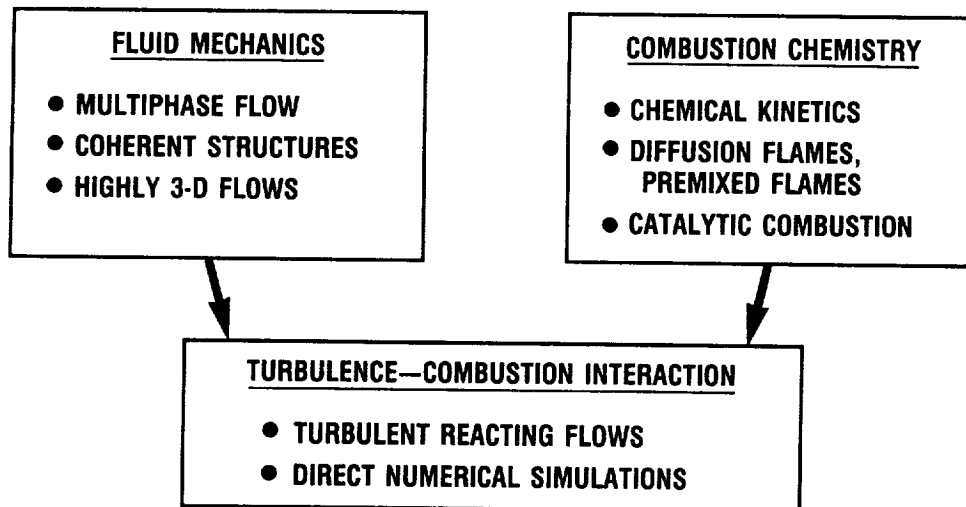
REFERENCES

1. Shuen, J.S., et al.: A Theoretical and Experimental Study of Turbulent Particle-Laden Jets. NASA CR-168293, 1983.
2. Bulzan, D.L.; Shuen, J.S.; and Faeth, G.M.: Particle-Laden Swirling Free Jets: Measurements and Predictions. AIAA Paper 87-0303, Jan. 1987. (NASA TM-88904.)
3. Bulzan, D.L.; Shuen, J.S.; and Faeth, G.M.: Particle-Laden Weakly Swirling Free Jets: Measurements and Predictions. NASA TM-100920, 1988.
4. Bulzan, D.L.; Shuen, J.S.; and Faeth, G.M.: Particle-Laden Weakly Swirling Free Jets: Measurements and Predictions. AIAA Paper 88-3138, July 1988.
5. Mostafa, A.A., et al.: On the Evolution of Particle-Laden Jet Flows: A Theoretical and Experimental Study. AIAA Paper 87-2181, June 1987.
6. Mostafa, A.A., et al.: On the Evolution of Particle-Laden Coaxial Jet Flows: A Theoretical and Experimental Study. AIAA Paper 88-0239, Jan. 1988.
7. Turbine Engine Hot Section Technology 1985, NASA CP-2405, 1985.
8. Turbine Engine Hot Section Technology 1986, NASA CP-2444, 1986.
9. Turbine Engine Hot Section Technology 1987, NASA CP-2493, 1987.
10. Brabbs, T.A., et al.: Hydrogen Oxidation Mechanism with Applications to (1) The Chaperon Efficiency for Carbon Dioxide and (2) Vitiating Air Testing. NASA TM-100186, 1987.

11. Strahle, W.C.; and Lekoudis, S.G.: Evaluation of Data on Simple Turbulent Reacting Flows. AFOSR-TR-85-0880TR, Sept. 1985. (Avail. NTIS, AD-A170071.)
12. Mungal, M.G.; Hermanson, J.C.; and Dimotakis, P.E.: Reynolds Number Effects on Mixing and Combustion in a Reacting Shear Layer. AIAA J., vol. 23, no. 9, Sept. 1985, pp. 1418-1423.
13. Farshchi, M.: Prediction of Heat Release Effects on a Mixing Layer. AIAA Paper 86-0058, Jan. 1986.
14. Marek, C.J.; Wey, C.; Miles, J.H.; and Fricker, D.: Experimental Study of a Planar Reacting Shear Layer with Pressure Interactions. Twenty-Second Symposium (International) on Combustion, The Combustion Institute, Pittsburgh, PA, Aug. 1988, to be published.
15. Claus, R.W.; Huang, P.G.; and MacInnes, J.M.: Time-Accurate Simulations of a Shear Layer Forced at a Single Frequency. AIAA Paper 88-0061, Jan. 1988. (NASA TM-100836.)
16. Yoon, S.; and Jameson, A.: An LU-SSOR Scheme for the Euler and Navier-Stokes Equations. AIAA Paper 87-0600, Jan. 1987.
17. Shuen, J.S.; and Yoon, S.: Numerical Study of Chemically Reacting Flows Using an LU Scheme. AIAA Paper 88-0435, Jan. 1988.

TABLE I. - HEATED WIND TUNNEL AIR CONTAMINANTS

Carbon dioxide, percent . . .	6 to 10
Water vapor, percent	13 to 17
Nitric oxide, percent	0.9
Nitrogen dioxide, percent	0.025

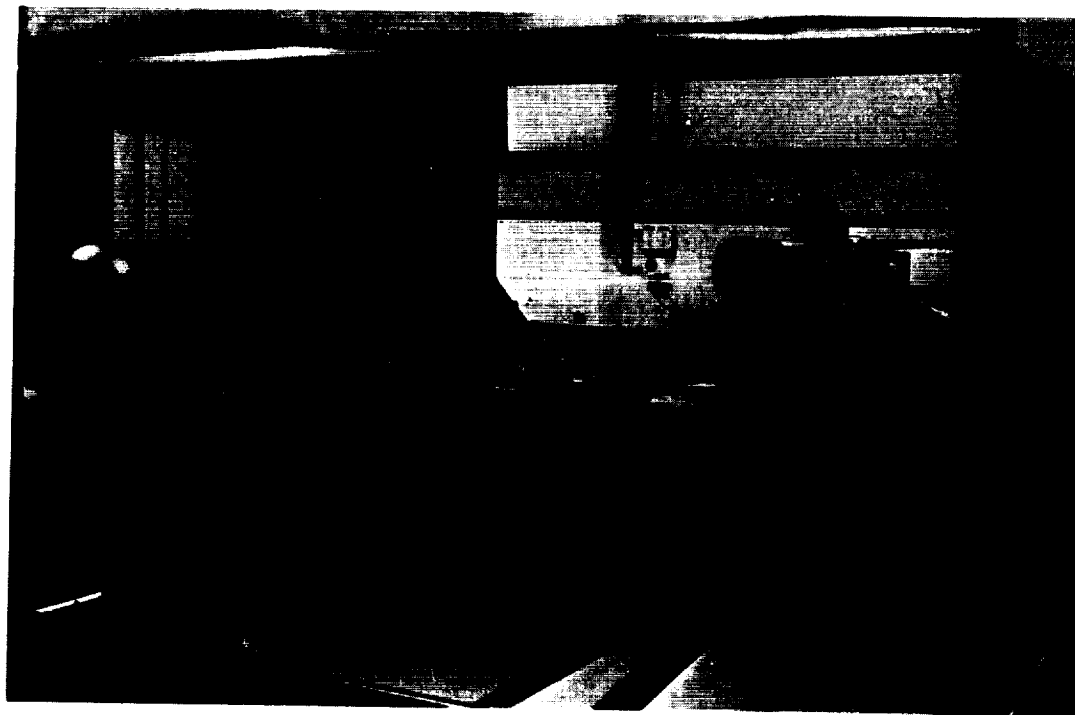


**LONG TERM GOAL: ACCURATE PREDICTIVE CODE WITH COUPLED FLUID MECHANICS
AND CHEMISTRY FOR FUTURE AEROSPACE PROPULSION**

CD-87-28755

Figure 1. - Major areas of research for chemical reacting flows which focus on common long-term goal.

ORIGINAL PAGE
BLACK AND WHITE PHOTOGRAPH



CD-87-28757

Figure 2. - Particle-laden swirling flow experiment.

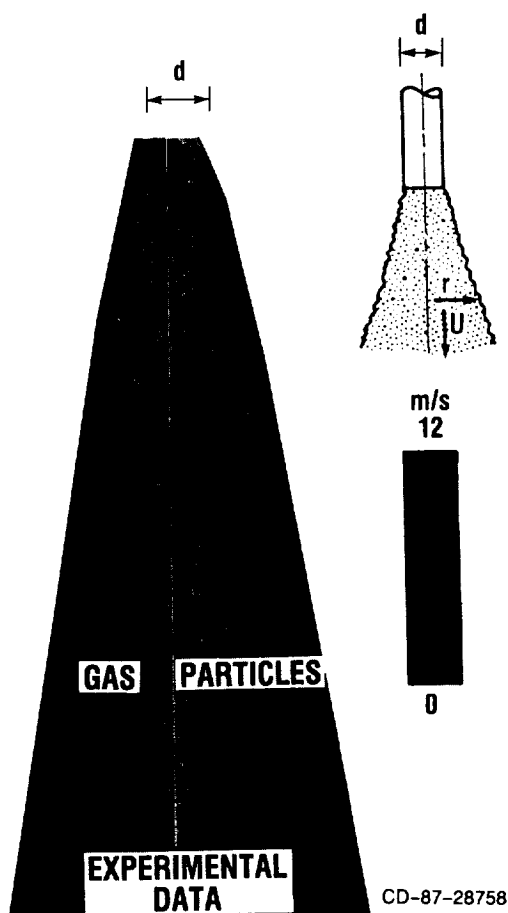


Figure 3.- Measured gas and particle axial velocities of particle-laden swirling jet (nonswirling case).

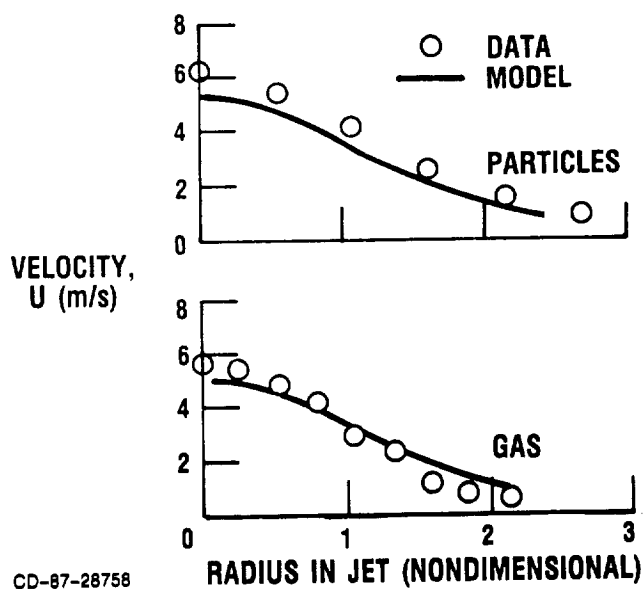
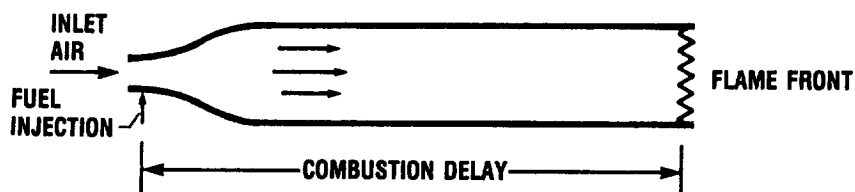


Figure 4. - Radial profiles of axial velocity for particle-laden swirling jet at $x/d = 10$ (nonswirling case; particle diameter, $39 \mu\text{m}$ (SMD)).

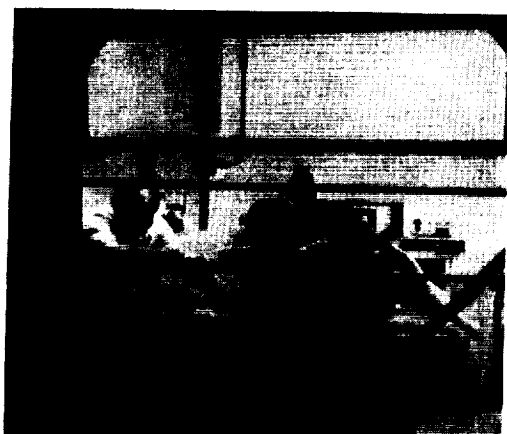


- HOW FAR WILL STABLE FLAME BE FROM FUEL INJECTION POINT?
- WHAT IS EFFECT OF AIR CONTAMINANTS OR ADDITIVES ON THIS COMBUSTION DELAY?

CD-87-28761

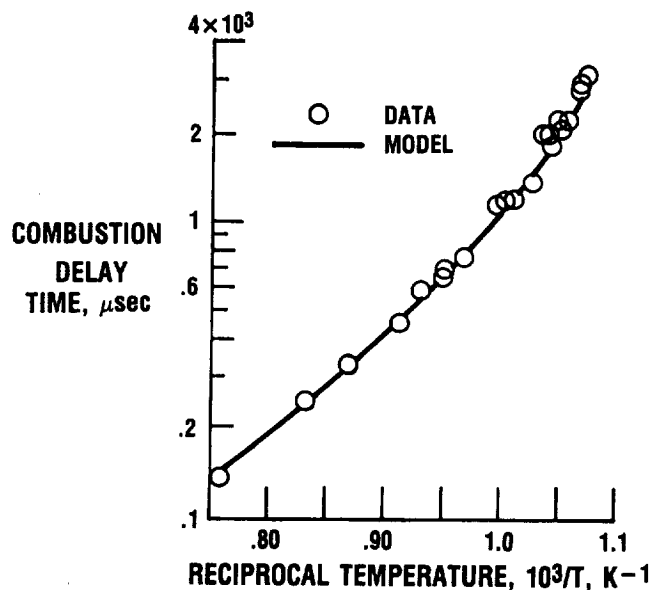
Figure 5. - Schematic of scramjet engine, used to define combustion delay time.

ORIGINAL PAGE
BLACK AND WHITE PHOTOGRAPH



CD-88-31310

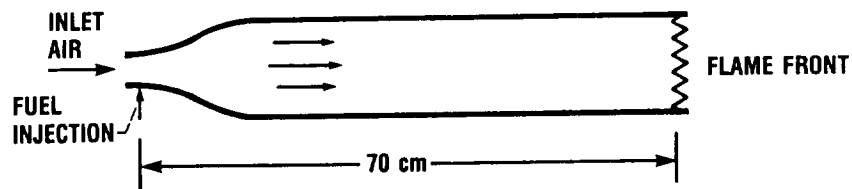
Figure 6. - NASA Lewis Chemical Shock Tube Facility.



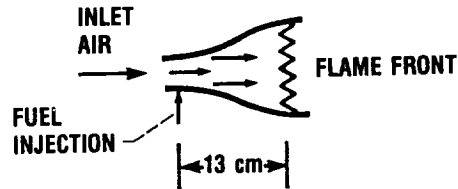
CD-88-31310

Figure 7. - Comparison between predictions of combustion delay time using hydrogen-oxygen chemical kinetic model and measured combustion delay time from shock tube experiments.

CALCULATED COMBUSTION DELAY FOR MACH 7 SCRAMJET FLIGHT CONDITION:



(A) BASED ON PURE DRY AIR.



(B) BASED ON PURE AIR WITH CONTAMINANTS OR ADDITIVES.

CD-87-28763

Figure 8. - Calculated comparison between wind tunnel and pure dry air effects of combustion time delay in scramjet engine at Mach 7 flight condition.

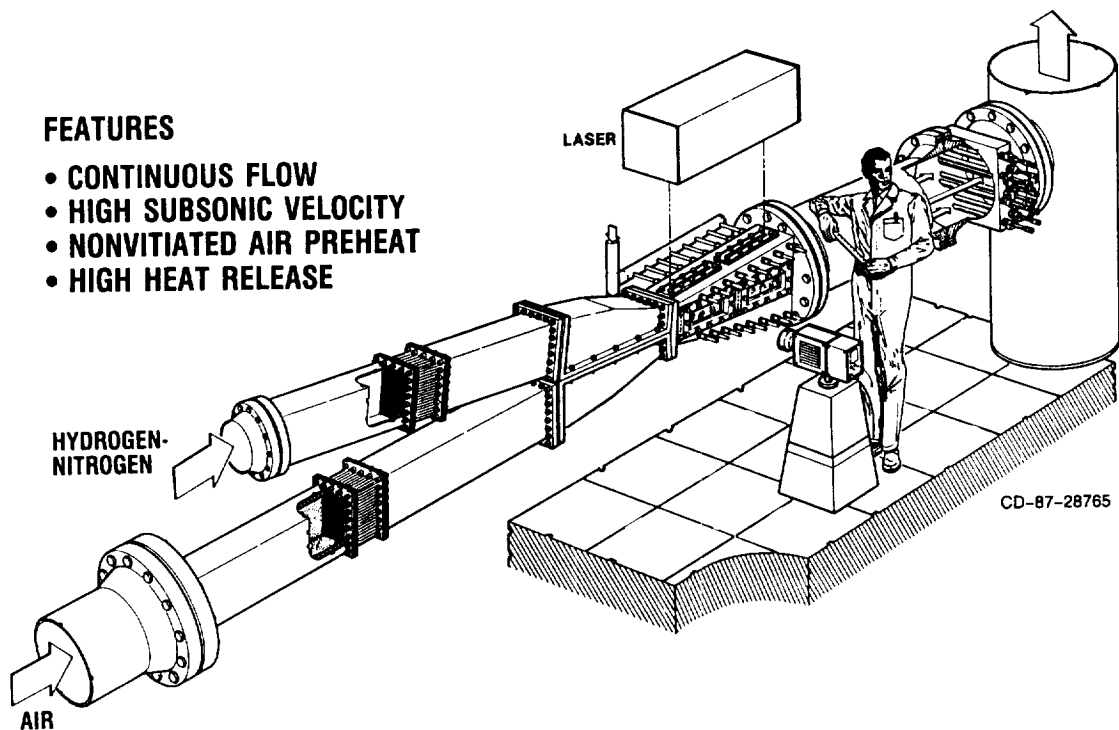


Figure 9. - Schematic of planar reacting shear layer experiment.

ORIGINAL PAGE
BLACK AND WHITE PHOTOGRAPH

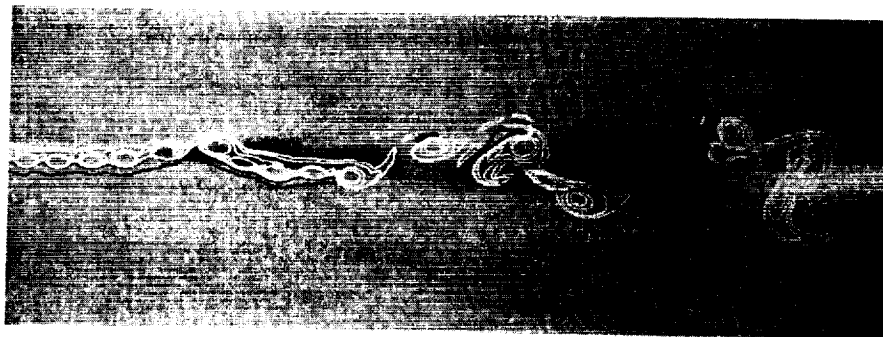
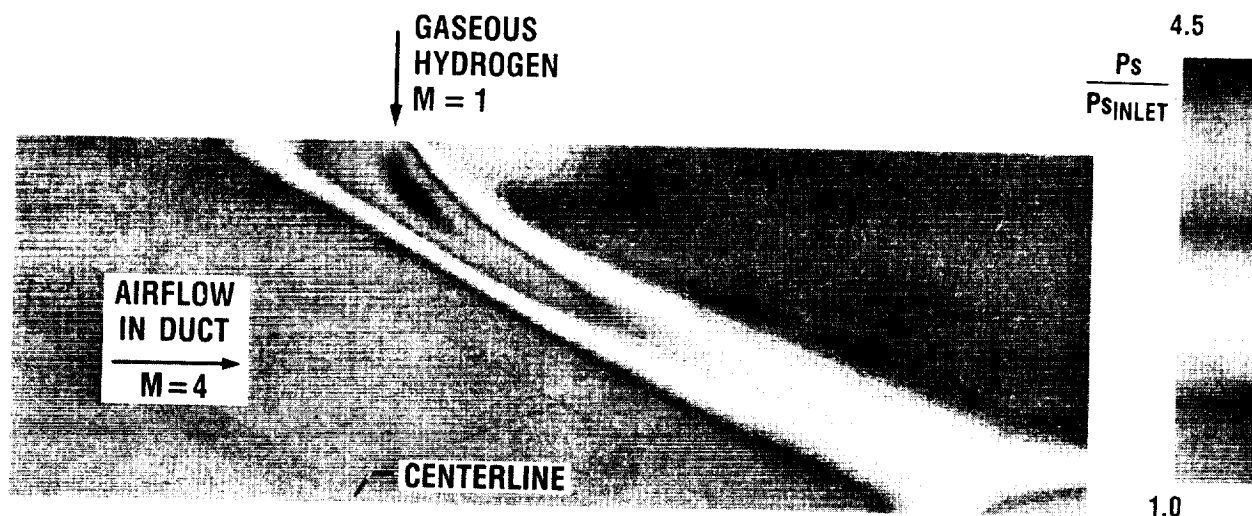


Figure 10. - Spatially evolving shear layer: instantaneous vorticity against background of averaged Reynolds stresses.

STEADY STATE FLUID MECHANICS COMPUTER CODE:

**COMPUTER CODE RESULTS OF GASEOUS FUEL JET—AIR MIXING AND COMBUSTION IN
INTERNAL DUCT FLOW, SHOWING STATIC PRESSURE CONTOURS**



CD-87-28769

Figure 11. - Static pressure contours for hydrogen injection into Mach 4 airflow calculated using RPLUS code.

CONCLUDING REMARKS TO THE INTERNAL FLUID MECHANICS

RESEARCH SESSION

Brent A. Miller
and
Louis A. Povinelli

The internal fluid mechanics research program at NASA Lewis is a balanced effort between the conduct of experimental research and the development of computational tools. The program has been briefly described by highlighting research efforts in three areas: inlets, ducts, and nozzles; turbomachinery; and chemically reacting flows. Much of the computational focus of the inlets, ducts, and nozzles area has been on the development and validation of parabolized Navier-Stokes codes. In the future, more emphasis will be placed on three-dimensional Reynolds averaged Navier-Stokes methods. The experimental effort will continue to provide a fundamental understanding of the fluid flow physics to develop new and/or improved flow models, and to provide benchmark datasets for validation of both parabolized and Reynolds averaged Navier-Stokes methods.

In the turbomachinery area, the program encompasses a variety of computational and experimental approaches. Special emphasis is placed on the Reynolds averaged Navier-Stokes equations, the unsteady Euler equations, and the average passage equations. The experimental emphasis is on high response time--resolved measurements and on measurements within rotating machinery blade passages.

Activity in chemical reacting flow research is focused on fluid mechanics, combustion chemistry, and turbulence/combustion interaction. Emphasis is placed on Reynolds averaged Navier-Stokes solvers and direct numerical simulation. The experimental activity includes unsteady reacting flows, shock tube kinetics, and multiphase flow phenomena.

In conclusion, it is noted that as numerical methods are improved and the ability to compute complex fluid physics is enhanced, it is critical that the users be aware of the code validity and limitations. These limitations can only be established by a careful systematic evaluation of each numerical scheme. It is by this systematic approach and the involvement of the ultimate user community that internal computation fluid mechanics will grow in importance as a practical tool for the analysis and design of aerospace propulsion systems.

SESSION 4 - INSTRUMENTATION AND CONTROLS RESEARCH

INSTRUMENTATION AND CONTROLS RESEARCH SUMMARY

This paper presents an overview of current and recently completed aeropropulsion instrumentation and controls research at NASA Lewis Research Center. The focus of the aeropropulsion instrumentation research is on miniature sensors and optical measurement systems that are needed for aeropropulsion research. The controls research is focused on the development of fiber-optic-based hardware necessary to implement a "fly-by-light" control system as well as on the development of advanced control methods that are needed for propulsion systems of increasing complexity and highly coupled aircraft and propulsion systems. Also included in this paper is an overview of the Lewis high-temperature electronics program. This program is directed toward developing silicon carbide solid-state electronic technology in order to produce electronic devices with a temperature capability of 400 °C and higher.

I - INTRODUCTION

Norman C. Wenger

NASA Lewis has a long history of research and technology programs in instrumentation and controls for propulsion. These programs are motivated by the many specialized needs for instrumentation in propulsion research that could not be met by standard commercially available instrumentation, and in the case of controls, by the need to develop techniques and hardware for maximizing the performance of increasingly more complex propulsion systems. This paper will present a few of the recent highlights from the Lewis program as well as provide insight on future program directions.

The Lewis instrumentation and controls program has been focused on satisfying the needs of the aeropropulsion industry and on taking maximum advantage of newly emerging technological opportunities. There are numerous drivers that impact the Lewis program. The major program drivers for aeropropulsion research instrumentation are as follows:

- Experimental research
- Performance validation
- Reduced cost of testing
- Computer code validation
- More hostile measurement environments
- New materials (e.g., ceramics, composites)

Experimental research, namely the exploration of fundamental phenomena and development of a basic understanding of propulsion system performance, and performance validation of both components and entire systems have always been the traditional roles for instrumentation.

The reduction of propulsion system testing costs, while always an important factor, grew extremely important in the early 1970's when both utility and labor costs began to escalate rapidly. Considerable effort was initiated back then and continues to the present to design and operate experiments, facilities, and instrumentation to acquire the required information at minimum cost.

Computer code validation is probably today's major instrumentation program driver because of the strong emphasis being placed on computational efforts. Code validation typically requires large amounts of data with not only high accuracy but with a high degree of spatial resolution and with minimal disturbance of the measurand by the instrument. These requirements have provided a great impetus in the development of today's nonintrusive-laser-based instrumentation.

The need for instrumentation to operate in more hostile measurement environments has always been a strong program driver, but the need has increased in recent years because of strong emphasis on hot section durability enhancement. Improving the ability to predict the life of turbine engine hot section components was the primary goal of the recently completed Lewis-managed program in turbine engine hot section technology, which was also known as the HOST Program. Many of the instrumentation highlights in the following sections are a result of the HOST Program.

Today's instrumentation research program is being strongly driven by the needs to make measurements on and around propulsion system components made from ceramics and ceramic-composite materials. These new materials not only allow the propulsion system environments to become even more hostile, but they present difficulties and limitations in our ability to install sensors on these materials. Sensors and lead wires can no longer be installed into grooves cut into the component surfaces. With ceramic components, all measurements must be made either with miniature surface-mounted sensors or via remote sensing techniques.

The Lewis instrumentation research program has always been geared to readily adapt opportunities and techniques from other research activities in order to continue the advancement in measurement capability. Some of the major technologies that have impacted instrumentation are listed as follows:

- Computers (minicomputers, microcomputers)
- Lasers
- Electro-optical devices/fiber optics
- Thin-film technology
- Solid-state electronics (e.g., sensor/electronics integration)

As expected, computers head this list. Computer technology is the basic enabling technology that has permitted the automation of instrument systems and the development of "smart" instruments. Modern instrument systems normally include a high degree of automation not only with respect to data acquisition, but also with respect to calibration, instrument health monitoring, and aids to servicing and maintenance.

Lasers, electro-optic devices, and fiber optics have opened up the field of nonintrusive measurements. The laser anemometer is perhaps the best example of where these impacting technologies have permitted a major new measurement capability to emerge.

Thin-film technology has opened up the field of minimally intrusive surface sensors. It is now possible, in some cases, to sputter-deposit, through a series of masks, a complete sensor directly on the surface of a component. Much work must be done in this area before thin-film sensors are widely used on aeropropulsion system components.

Solid-state electronics has made a significant impact on instrumentation in many areas. However, since virtually all solid-state electronic devices available today are silicon based and since silicon devices are temperature limited, most solid-state electronic devices associated with instrumentation are found on the control room end of the measurement systems and not on the

sensor end. There are many advantages to integrating the electronics with the sensor, and indeed much research is underway nationally to develop a variety of these integrated sensors. However, since the basis for this work is silicon technology, there is going to be a definite upper limit on the temperature capabilities for these devices. The upper limit for silicon-based devices is about 300 °C (575 °F). Thus, there is a need to investigate semiconductor materials that have higher temperature capabilities than that of silicon if the needs for integrated sensors in advanced propulsion systems are to be met. A subsequent section of this paper, High-Temperature Electronics, describes the Lewis program to develop high-temperature solid-state devices.

Some of the major drivers in the Lewis controls research and technology program are listed as follows:

- Propulsion system performance
- Integration of engine, inlet, nozzle, and aircraft control systems
- Durability/maintainability of propulsion system (condition monitoring/diagnostics)

First and foremost on the list is propulsion system performance. Propulsion system complexity is increasing at a rapid rate and presents a major challenge to the controls engineer. The number of measured parameters and controlled variables has been increasing almost linearly with time since the 1950's for both military and commercial engines. The controls engineer has been forced to deal not only with this increasing system complexity but also with greatly expanded mission requirements which require operation over increasingly larger flight envelopes.

One approach toward increased aircraft capability is through greater integration of the various propulsion and flight control systems. This integration of controls can give worthwhile benefits in conventional takeoff and landing aircraft, and is virtually mandatory in STOVL aircraft if the pilot is to perform any other functions than operating the aircraft. The control is the critical link between the propulsion and flight systems and the pilot. The controls engineer is faced with the task of designing a system that can meet all of the technical requirements mandated by flight and propulsion systems and, at the same time, providing a manageable interface for the pilot.

As control system functionality continues to increase, greater demands can and will be placed on the control system. One of these is the issue of durability and maintainability of the propulsion system. Information being acquired by today's aircraft control system is sufficient, with proper interpretation, to tell a great deal about the current health and condition of the propulsion system. Such monitoring systems are, of course, in current use. As knowledge increases as to the relationship between component life and the operating environmental history of that component, a significant future capability will be the prediction of remaining component life. The role of the propulsion control system, in the future, will change from its current reactive role, where it strives to maintain the engine at some prescribed operating point in the face of random disturbances, to where with its greater system intelligence it will operate the engine on the basis of more global considerations such as overall mission requirements, current system health, and remaining component life.

The opportunities and technologies that have made a major impact in aeropropulsion controls are as follows:

- Computers
- Solid-state electronics (e.g., sensor/electronics integration)
- Fiber optics
- Expert systems

Here also, computers head the list. The development of lightweight, high-speed, reliable digital computers has greatly enhanced control system capability compared to the previous hydromechanical technology.

Solid-state electronics, embodied in many forms, has made and continues to make significant impacts in the control sensor area. One dramatic improvement, discussed previously in this section, will come with the availability of solid-state devices that are capable of operating at high temperatures, so that the sensor and electronics can be integrated.

Fiber optics holds the promise of lighter weight control systems with greater immunity to electromagnetic interference. With today's rapid increase in avionic systems on board all types of aircraft, it is extremely important that these systems do not interfere with each other nor exhibit susceptibility to external interference. In stealth applications it is also important that these systems not radiate. Fiber-optic-based control systems hold the promise of meeting these requirements.

Expert systems are beginning to make inroads into many areas, including aeropropulsion controls. The final section of this paper will present insight to how Lewis envisions the use of expert systems as essential building blocks in an intelligent control system.

II - RESEARCH SENSORS

David R. Englund

The Lewis program in research sensors is directed at development of sensors and sensing techniques for research applications on turbine engines and propulsion systems. In general, the sensors are used either to measure the environment at a given location within a turbine engine, or to measure the response of an engine component to the imposed environment. Locations of concern are generally within the gas path and, for the most part, are within the hot section of the engine. Since these sensors are used for research testing as opposed to operational use, a sensor lifetime of the order of 50 hr is considered sufficient. The following discussion will present a sample of this work, describing programs to develop a dynamic gas temperature measuring system, total heat flux sensors, a variety of thin-film sensors, and high-temperature strain measuring systems.

DYNAMIC GAS TEMPERATURE MEASURING SYSTEM

One of the most important parameters in a turbine engine hot section is gas temperature. Normally only time-averaged temperature is measured. Fluctuations in gas temperature are, however, of great concern for hot section durability and combustor modeling activities. The dynamic gas temperature measuring system uses a probe (fig. II-1) with two wire thermocouples of different diameters, typically 75 and 25 μm (0.01 and 0.003 in.). The thermocouple junctions are butt welded and are located midway between the supporting posts. The thermocouples are within 1 mm of each other so that they are measuring essentially the same gas sample. This probe provides dynamic signals with limited frequency response. By comparing these signals over a range of frequencies, a compensation spectrum can be generated sufficient to provide compensated temperature data over an extended frequency range. The target frequency response for this system was 1000 Hz. This is probably higher than necessary for questions of durability loss due to thermal cycling, but if one is interested in modeling combustor processes or the flow in a combustor, 1000 Hz is a reasonable target. The upper limit in achievable frequency response for such a system is determined by the signal-to-noise ratio.

This system has been developed and used to measure fluctuating temperatures in both combustors and engines (refs. II-1 to II-4). Figure II-2 shows dynamic temperature data obtained from a probe at the turbine inlet of a PWA F-100 engine operating at an intermediate power setting and with an average turbine inlet temperature of 925 °C (1700 °F). The plot on the left is the dynamic signal from the 25- μm -diameter (0.003-in.-diam) wire thermocouple with no frequency compensation. The rms value of the temperature fluctuation is 41 °C (74 °F). The plot on the right is the compensated signal from the same

thermocouple. The rms value of the temperature fluctuation is 218 °C (390 °F) and the peak-to-peak fluctuation is over 1000 °C (1800 °F). Such a large temperature fluctuation implies that there are filaments of primary combustion gas and dilution gas within the combustor exhaust stream.

TOTAL HEAT FLUX SENSORS

Another environmental parameter of interest for hot section durability is total heat flux. We have developed miniature total heat flux sensors (refs. II-5 to II-10) which can be welded into combustor liners and built into cooled turbine airfoils. Figure II-3 shows one sensor configuration based on the Gardon gage design as it would be built into an airfoil. In this case, the airfoil must be opened so that the sensor can be installed from the cooled wall side. A cylindrical cavity 1.5 mm in diameter (0.06 in.) is cut in the wall leaving a thin membrane at the hot side surface. ISA type K thermocouple wires are located in the cavity as shown, and then the cavity is filled with ceramic cement. With this sensor, the temperature difference between the center of the membrane and the side wall is a measure of heat flux. This temperature difference is measured with the Alumel-bladewall-Alumel differential thermocouple. The use of the burner liner or airfoil material as part of a differential thermocouple circuit is an innovation that considerably simplifies construction, but it requires calibration of the materials involved. Calibration tests showed that this technique could provide acceptable signals. These miniature heat flux sensors must be calibrated over the temperature range in which they will be used because of the nonstandard differential thermocouple and because of the uncertainty in positioning the thermocouple junctions.

Total heat flux sensors have been used in tests on combustor liners and on turbine airfoils. Figure II-4 shows a segment of a combustor liner which has been instrumented with five total heat flux sensors. The sensors are 7.5-mm-diameter (0.3-in.-diam) disks with thermocouple leads radiating from the edge of the disk. The actual sensor part of the unit is at the center of the disk and is only 1.5 mm (0.06 in.) in diameter. The sensors are individually calibrated and then welded into holes cut in the liner. Tests on combustors such as this one have produced useful heat flux data over a range of combustor operating conditions. Similar sensors built into turbine airfoils have been less successful because of the sensitivity of these sensors to temperature and/or heat flux gradients, which are more prevalent in turbine airfoils.

As noted previously in this section, calibration of total heat flux sensors over the range of temperatures and heat fluxes that will be encountered is a requirement. Figure II-5 shows a photograph of a heat flux sensor calibration system developed at Lewis. The heat source is a 100-kW arc lamp. A reflector is used to focus the energy from the arc onto a ceramic sensor holder. This system can supply a maximum flux of 6 MW/m² (500 Btu/ft²-sec), which is higher than the heat fluxes in present-day turbine engines. The system can operate in both steady-state and transient modes. Two other roughly comparable calibration facilities exist in this country; efforts to cross-compare calibration of test sensors have been started. This is especially important since a national standard for heat flux sensor calibration does not exist for these high levels of heat flux.

THIN-FILM SENSORS

Lewis has been the major advocate and sponsor for development of thin-film sensors for turbine engine applications (refs. II-11 to II-19). Thin-film sensors applicable to turbine engines include temperature sensors, strain gages, and heat flux sensors. Thin-film sensors are formed directly on the component to be instrumented (fig. II-6) by first depositing a suitable insulating film and then depositing sensor and protective films as required. A stable, adherent, pinhole-free insulating film is the base for the whole structure and is the most critical element of the sensor.

An excellent application for thin-film thermocouples is the measurement of the surface temperature of a cooled turbine vane such as shown in figure II-7. The surface of the vane is covered with Al_2O_3 thermally grown from an anticorrosion coating and augmented with sputtered Al_2O_3 . Pt and Pt-Rh films are sputter-deposited with thermocouple junctions formed by overlapping the two films at the desired spot. The films extend to the base of the vane where leadwires are connected. Typical thicknesses are 3 μm for the Al_2O_3 and 5 μm for each of the thermocouple alloy films; in this case, no cover film was used. The advantage of this technique over the previous technology, which required swaged thermocouple wires to be buried into grooves cut into the surface, should be obvious.

The present state of the thin-film sensor technology is sufficiently advanced that dynamic strain gages have been used on compressor blades, and thermocouples have been used to measure turbine airfoil surface temperatures in some turbine engine test facilities in the United States. Thin-film, high-temperature static strain gages and thin-film heat flux sensors are still under development. In addition, work is continuing on the basic thin-film sensor technology with the goals of simplifying and improving sensor processing and adapting the presently used techniques to other substrate and sensor materials.

One of our goals is to make the thin-film sensor technology available to the whole U.S. turbine engine community. Impediments to wider usage of this technology are many. One problem is that sensor fabrication is material specific; technology has not been established for a wide variety of materials. Another problem is that the investment required to establish a thin-film sensor fabrication capability is considerable, and commercial services for custom fabrication of thin-film sensors are not yet available.

HIGH-TEMPERATURE STRAIN MEASURING SYSTEMS

The most ambitious goal of the research sensor program is development of 980 °C (1800 °F) strain measuring systems. Approaches being followed in this work include both wire and thin-film resistance strain gages and remote strain measuring systems. The resistance strain gage work involves development of new strain gage materials and extensive testing of available strain gages. Work on remote strain measuring systems has involved three different system concepts based on laser speckle patterns.

A major part of our work in resistance strain gages has been the development of a new palladium-based strain gage alloy (refs. II-20 and II-21). The

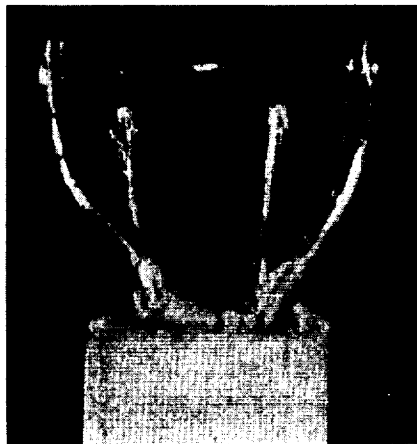
outstanding property of this alloy is its repeatability of resistance over the temperature range up to 980 °C (1800 °F). Repeatability of resistance over the temperature range within a few hundred parts per million is a fundamental requirement for a high-temperature strain gage alloy. Work is now underway to develop thin-film and wire strain gage systems using this alloy. Work with other strain gages has involved high-temperature evaluation testing (refs. II-22 to II-24) including a 700 °C (1300 °F) strain gage available from the People's Republic of China.

Resistance strain gages are not the only approach to high-temperature strain measurements. Attractive alternatives are found in a variety of remote optical strain measuring systems, many of which use the laser speckle pattern as a basis for measurements of in-plane surface deformation. We have worked with two laser speckle systems: a photographic system in which speckle pattern photographs are analyzed in an interferometric photocomparator, and an electronic system in which strain is determined from the shift in the speckle pattern falling on a linear photodiode array. This work has included both laboratory development and evaluation in test cell environments (refs. II-23 and II-25 to II-27). A fundamental problem with remote optical systems in test cell environments is interference generated within the viewing path; methods for minimizing or eliminating this problem are being studied.

FUTURE THRUSTS IN RESEARCH SENSORS

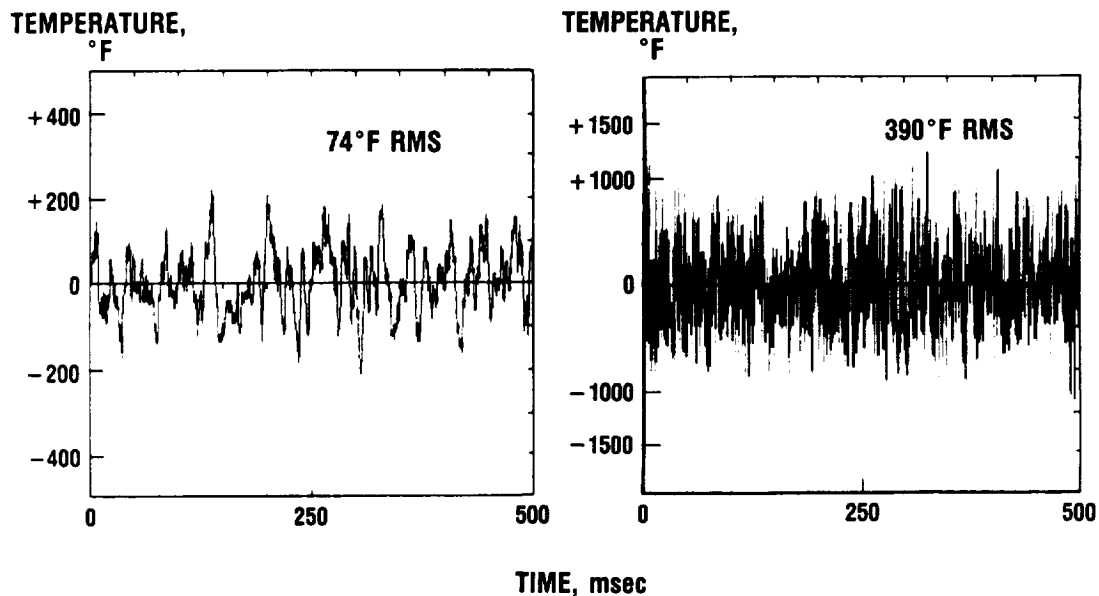
Future work in research sensors will be strongly influenced by programs to develop new materials for turbine engines which will permit significantly higher hot section temperatures. These materials are expected to be in the forms of metallic or intermetallic and ceramic matrix composites. The impact of such developments will be twofold. First, these new materials will have markedly different properties compared to the metals involved in the sensors developments already described. The emphasis for surface-mounted sensors will be on thin films, and extensive development of fabrication procedures for these new substrate materials will be required. For remote sensors, there will be requirements to adapt or develop new sensing techniques suitable for these new materials.

The second area of impact is the higher temperatures that will be encountered. Higher temperatures may require new sensor materials and may ultimately require abandonment of surface-mounted sensor techniques. Work is already in progress on development of sensors and sensing techniques for ceramic components for turbine engines. Results of studies on applicable sensor techniques for measurements of surface temperature, strain, and heat flux are available (refs. II-28 and II-29).



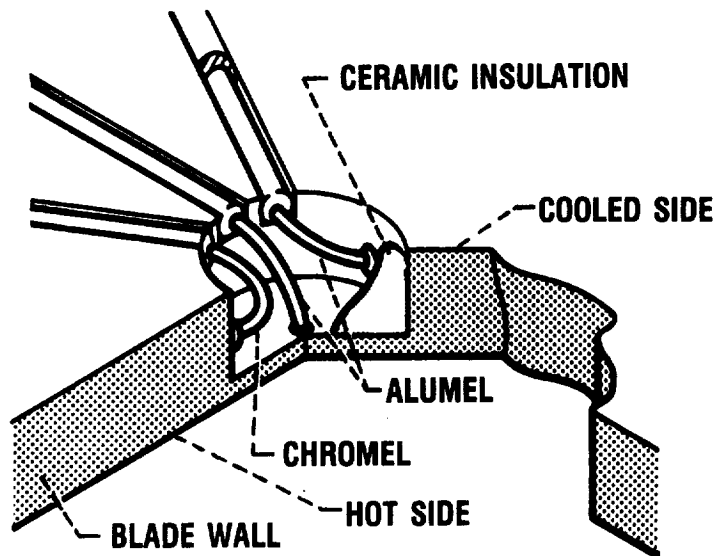
CD-87-29397

Figure II-1. - Dynamic gas temperature probe.



CD-87-29398

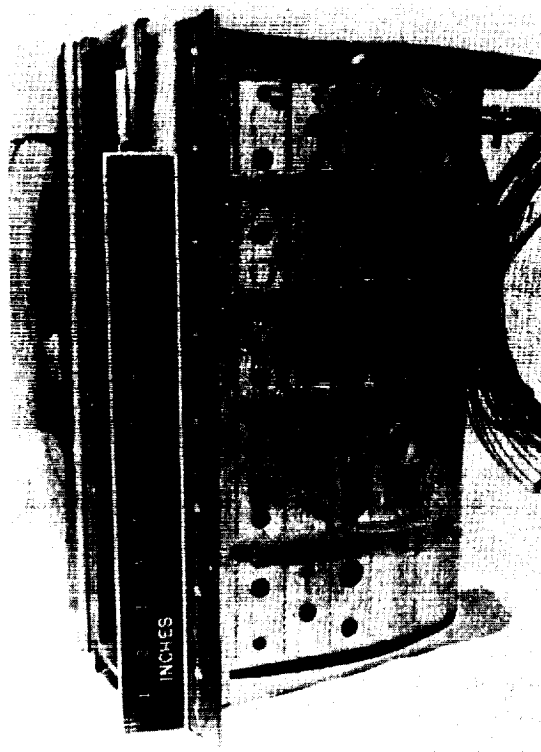
Figure II-2. - Fluctuating gas temperature measured at turbine inlet of PWA F-100 engine. Left plot shows as-recorded data from 25- μ m-diameter (0.003-in.-diam) wire thermocouple with no compensation; right plot shows same data compensated for flat frequency response to 1000 Hz.



CD-87-29399

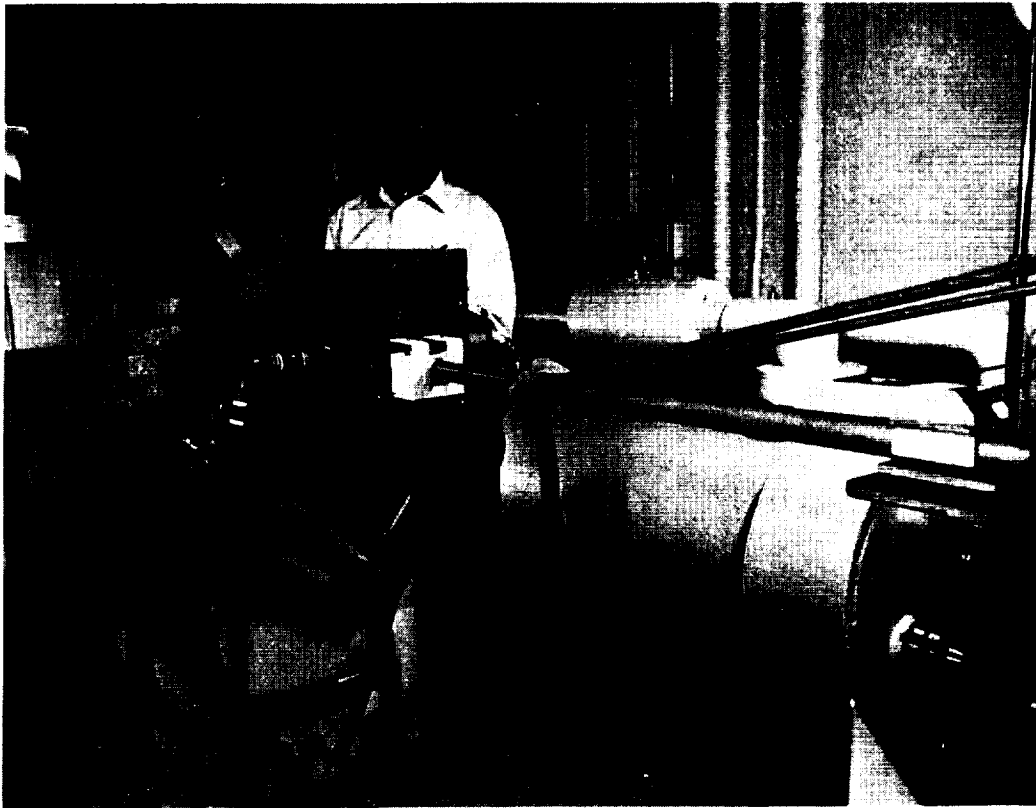
Figure II-3. - High-temperature heat flux sensor based on Gardon gage design.

ORIGINAL PAGE
BLACK AND WHITE PHOTOGRAPH



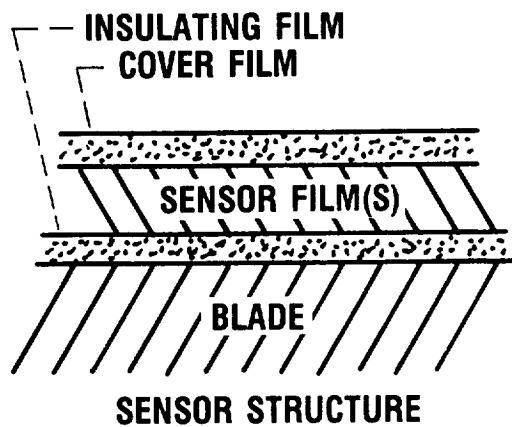
CD-87-29400

Figure II-4. - Segment of combustor liner instrumented with heat flux sensors.



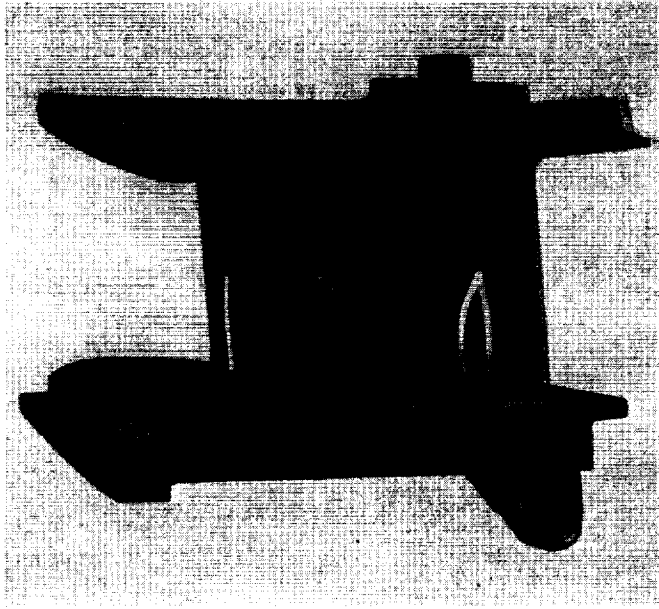
CD-87-29401

Figure II-5. - Heat flux sensor calibration system at Lewis Research Center.



CD-87-29402

Figure II-6. - Cross section of thin-film sensor on blade.



CD-87-29403

Figure II-7. - Cooled turbine vane instrumented with four thin-film thermocouples.

III - OPTICAL MEASUREMENT SYSTEMS

Daniel J. Lesco

This section of the report describes some of the areas of research conducted at the Lewis Research Center on optical measurement techniques for propulsion systems research. Most of the optical techniques used to measure gas parameters depend on very inefficient light scattering principles and therefore require the high light intensities provided by lasers. Significant advances in laser technology, together with the availability of sensitive photodetection systems, provide much of the impetus for research in optical diagnostic techniques.

These nonintrusive measurement systems are needed in applications where traditional sensors would excessively disturb the measured parameter or where an intrusive sensor could not survive the environmental conditions under which the measurement must be made. As the operating temperatures of propulsion systems increase and the size of engine components and flow passages decreases, the need for optical measurement systems becomes increasingly important.

The goal of the research described here is to enhance the capabilities of nonintrusive research instrumentation to meet the special needs of aeropropulsion research. Optical techniques are being used to validate analytical codes and to verify the performance of aeropropulsion components and systems.

Listed in table III-I are some important areas of current research, together with two recently completed efforts, the rainbow schlieren and the hot section viewing system. The fluid and structural parameters measured by the listed techniques are also shown. Several of the areas will be described in more detail in this paper to illustrate the aeropropulsion instrumentation needs we are trying to fill. Other research areas are discussed in references III-1 to III-3.

Applying laser anemometry to aeropropulsion research facilities presents many challenges for the instrumentation research (refs. III-4 and III-5). Desired characteristics include the ability to measure flow along three axes through a very limited viewport, to make velocity measurements near surfaces, and to make measurements efficiently in a turbulent or highly accelerating flow. Both the enabling technology required to achieve these capabilities and the development of new systems are being addressed in Lewis's instrumentation program. As an example of the former research, the use of fiber optics in laser anemometry systems is currently being investigated to meet the problems of high vibration and acoustic noise levels, which are commonly encountered in aeropropulsion research and test facilities (ref. III-6). Two new laser anemometer (LA) systems developed to meet specific needs are the three-axis LA and the four-spot LA. The three-axis LA system (ref. III-7) was designed to measure

the radial component of flow in addition to the axial and circumferential components through a single optical viewing port in a turbine stator cascade facility. The system uses a Fabry-Perot interferometer technique in conjunction with the more common dual-beam fringe configuration. The annular vane ring shown in figure III-1 has a contoured hub to enhance the radial velocity component. Velocity data for each axis and total velocity are shown in figure III-1(c) and compared with the predicted values obtained with a computer code. Total mean velocity and the three components (ratioed to a Mach 1 velocity parameter) are plotted for the passageway between two vanes.

The four-spot LA system (refs. III-8 and III-9) was developed at Lewis in conjunction with Case-Western Reserve University. It is a laser transit anemometer (LTA) wherein velocity is determined by measuring the time required for seed particles to cross the gap between closely spaced laser beams. The four-spot system has the feature of wide flow acceptance angle (necessary for measurements in turbulent flows) while retaining the LTA advantages of close-to-wall measurements and small seed particle compatibility. The use of orthogonally polarized optics in generating the probe volume (which results in the four-beam configuration named here as "four spot") more precisely defines the time of crossing of a seed particle and hence improves the accuracy of the measurement over a wide range of velocities.

The four-spot LA has been tested in a small facility capable of generating hot (1000 K) turbulent flows, as shown in figure III-2. Velocity surveys were obtained to within 200 μm of a turbine vane surface inserted into the test flow, as compared with a typical value of about 1 mm obtained with fringe-type LA systems. Other tests demonstrated velocity measurements to Mach 1.3 with 0.5- μm seed particles.

Two paths to higher performance engines are to increase the operating temperatures in the combustor and to decrease the weight of engine components. The combustor viewing system (ref. III-10) was designed as a diagnostic tool for use in studying internal processes in high-temperature, high-pressure combustors. One of the primary goals was to study the onset of combustor liner failures such as cracking. Images of the combustor interior are transmitted to a photographic or video camera through a coherent bundle of 75 000 10- μm -diameter fibers. Also included are two 1-mm-diameter fibers to provide illumination from a laser or arc lamp, for those applications where there is no natural illumination or where the natural radiation is unsuitable and is replaced as the illumination source by pulsed illumination and subsequent synchronous detection. The rotatable, retractable probe is purged with N_2 to keep the tip clean and water cooled to allow operation at environmental temperatures above 2000 K.

In the figure III-3 photograph of the combustor viewing system probe, the two illumination-carrying fibers and the angled tip of the imaging bundle can be identified by the backlighting. The probe is 1.25 cm in diameter. The photograph shown in figure III-4 of a combustor fuel nozzle in a PW 2037 engine was recorded through the combustor viewing system while the engine was operating at full power. Operating experience was also obtained in a high-pressure turbine component test facility at Lewis and at a hot gas facility at the Naval Air Propulsion Center.

Not all of the optical systems under research at Lewis involve laser excitation. The rainbow schlieren system (refs. III-11 to III-13), developed at Lewis, uses a bull's-eye color filter to add a continuous color spectrum to the classic black-and-white, "knife-edge" flow visualization technique in order to enhance index-of-refraction gradients such as those accompanying shock waves. Not only does the color aid the eye's sensitivity in perceiving minor flow features, it adds a potential for quantitative flow analysis by color coding the magnitude of refractive index changes in those flows exhibiting simple geometries. This schlieren system has been installed in the Lewis 10- by 10-Foot Supersonic Wind Tunnel. The black-and-white copy of a color photograph shown in figure III-5 illustrates the flow visualization for a supersonic side inlet tested in the tunnel. Color gradations across the shocks (visible here as different shades of gray) can be used to evaluate shock strengths and geometries.

In many areas of measurement technology, the available commercial instrument systems satisfy research needs. Optical droplet sizing systems appear to be adequate for most aeropropulsion-related applications such as fuel-spray and icing research. But important questions remain on the proper use and calibration of these instruments. We are conducting comparison tests on the most useful systems to better define their operating regimes (droplet size, droplet concentration, droplet velocity, etc.) and are also developing adequate calibration tools and techniques (refs. III-14 to III-17).

Shown in figure III-6 is a cloud droplet sizing instrument used on the Lewis Twin Otter aircraft during icing research. This instrument measures the size of single droplets (from about 2 to 50 μm) as they pass through a small probe volume defined by a laser beam and the collection optics contained in the cylindrical extensions at the front. Techniques to better calibrate this and similar optical instruments are being developed and evaluated. Shown in figure III-7 is a rotatable calibration reticle with precisely-sized spots used to simulate droplets passing through the probe volume of the instrument. The effects of droplet velocity and trajectory within the probe volume can be determined. In addition to the development of calibration techniques and hardware, a comprehensive computer analysis of several light-scattering based instruments has been undertaken to enable a thorough understanding of the limits to accuracy and operating regimes. These analyses have led to the design of applications-specific corrective optics to extend the usable operating range of commercial instruments.

Our present program in optical instrumentation research is driven by the needs of the aeropropulsion researcher and aided by the advances in optical and electronic technology. Prevalent needs are dynamic data, including time correlation between two or more parameters, and rapidly acquired whole-field data maps. The need to obtain data rapidly, always important in high-operating-cost facilities, becomes critical in some aeropropulsion research areas (e.g., limited run-time hypersonic blowdown facilities). Fiber optics and new solid-state lasers are two of the important ingredients for rugged diagnostic systems to be used in aeropropulsion facilities. The use of fiber optics as a light-carrying conduit in instrumentation systems is already widespread; solid-state lasers are just starting to mature enough to be considered as components in instrumentation systems. Laser spectroscopy, including the techniques of laser-induced fluorescence and various Raman spectroscopy configurations, has been extensively researched in the laboratory and will be moving into increasingly

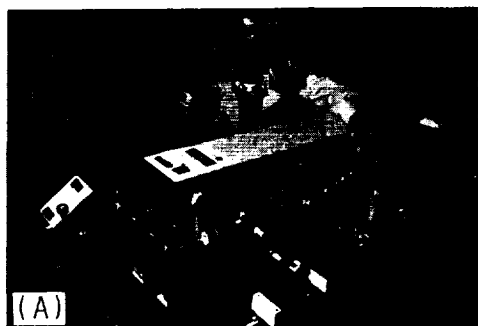
harsh facility environments as the supporting technology matures. There is also a strong potential for the application of artificial intelligence to complex optical diagnostic systems, both for the interpretation of whole-field data and for the alignment, both initial and corrective, of these systems.

A brief review of recent and future research at Lewis on optical measurement techniques for aerospace propulsion research has been presented. Although the techniques being investigated can be applied to meet measurement needs in many fields of research, the goals of this instrumentation research are to satisfy the very demanding measurement needs necessary to advance aeropropulsion technology.

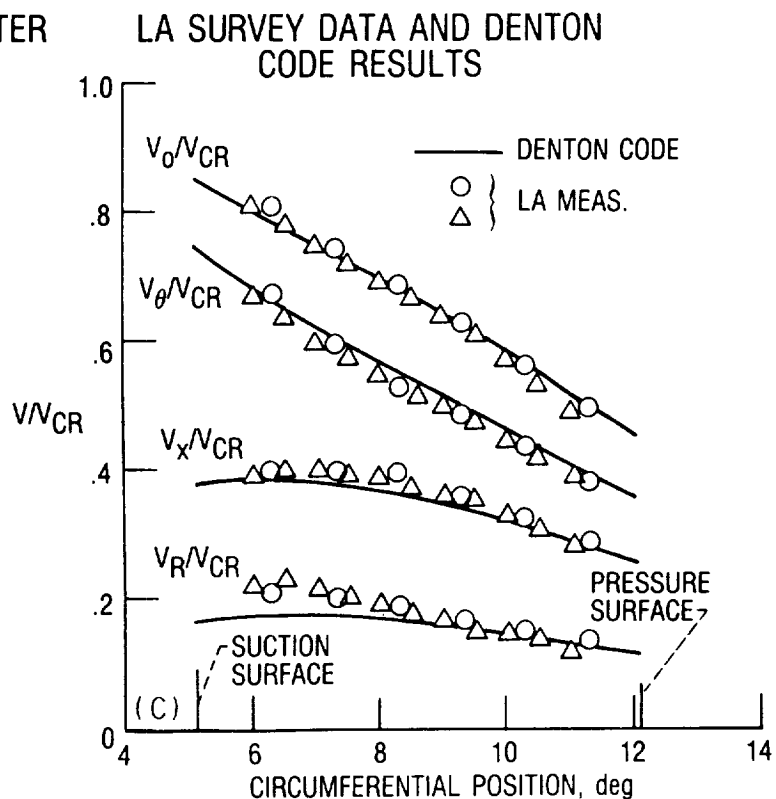
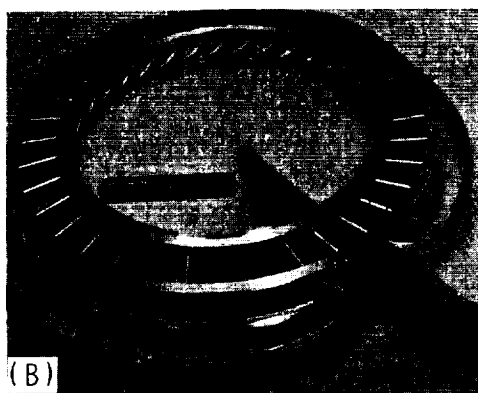
TABLE III-I. - NONINTRUSIVE RESEARCH INSTRUMENTATION
FOR AEROPROPULSION SYSTEMS

Technique	Parameters
Laser anemometry	For average flow velocity, flow angle, turbulence intensity
Holographic interferometry	For gas density changes, surface displacements
Laser spectroscopy	For gas temperature, constituents, velocity, pressure
Particle sizing	For fuel spray and cloud droplet diameters
Laser speckle systems	For surface strain
Rainbow schlieren	For flow visualization
Hot section viewing system	For monitoring hot section phenomena

THREE COMPONENT LASER ANEMOMETER

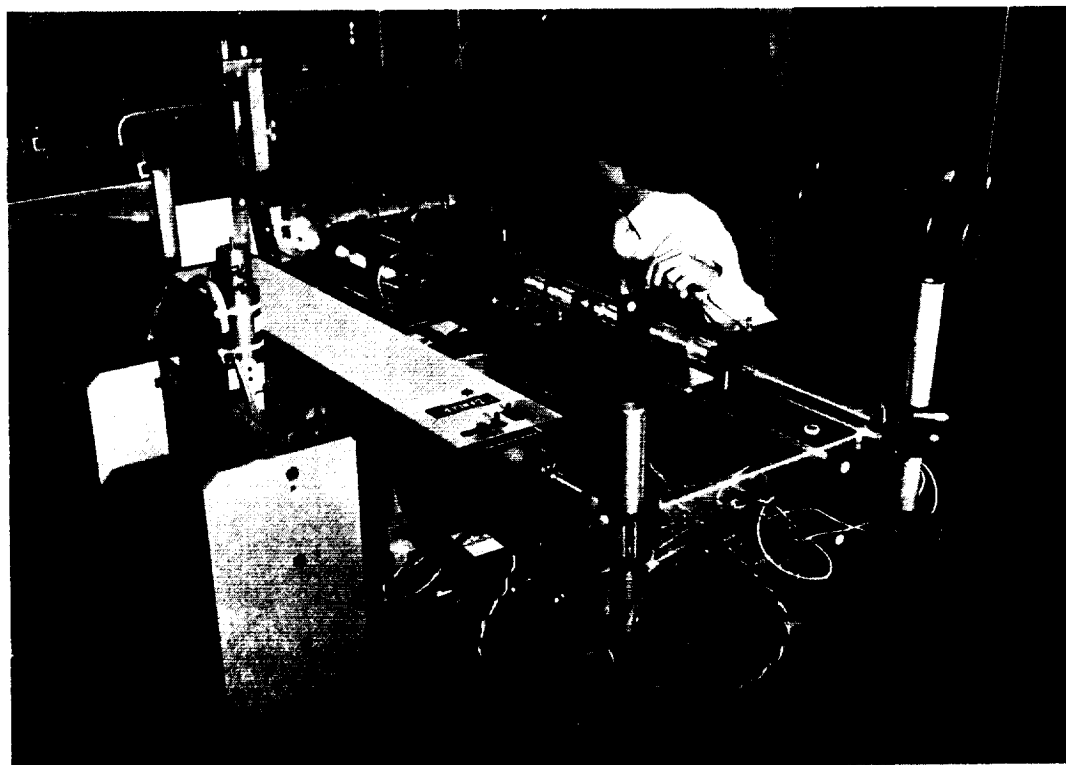


ANNULAR VANE RING



CD-87-29410

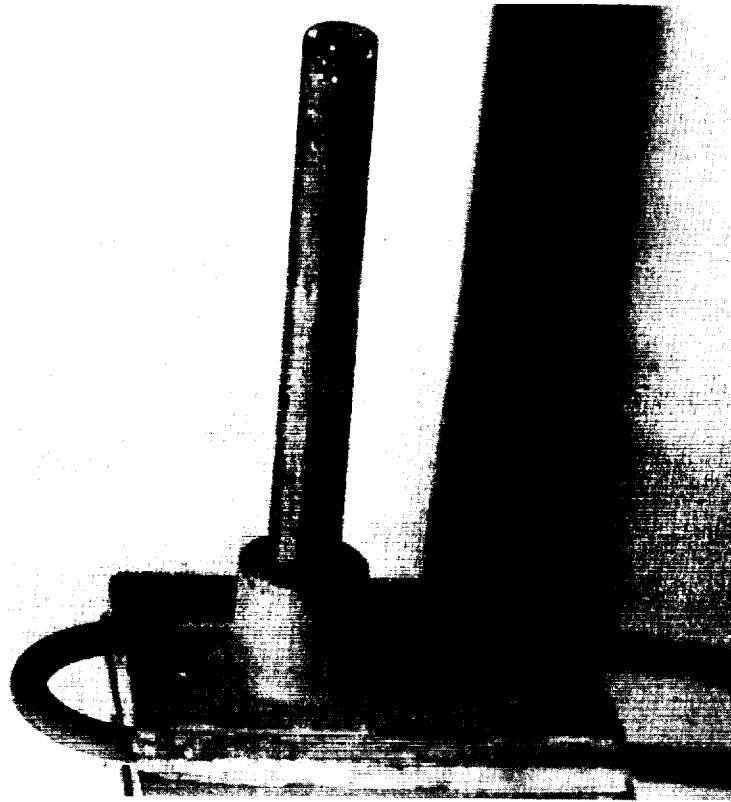
Figure III-1. - Three-component laser anemometry system.



CD-87-29412

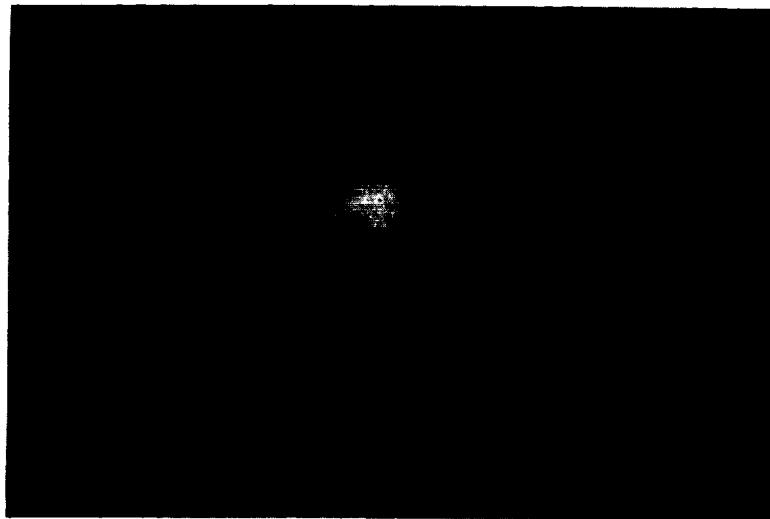
Figure III-2. - Testing of four-spot laser anemometry in open jet burner facility.

ORIGINAL PAGE
BLACK AND WHITE PHOTOGRAPH



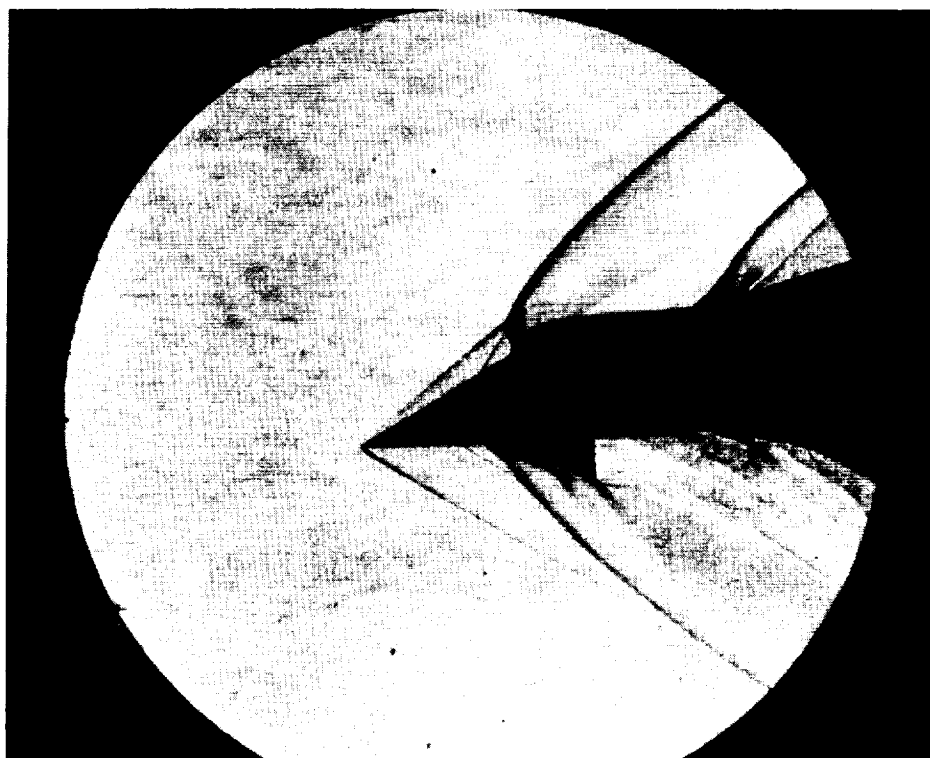
CD-87-29417

Figure III-3. - Combustor viewing system probe.



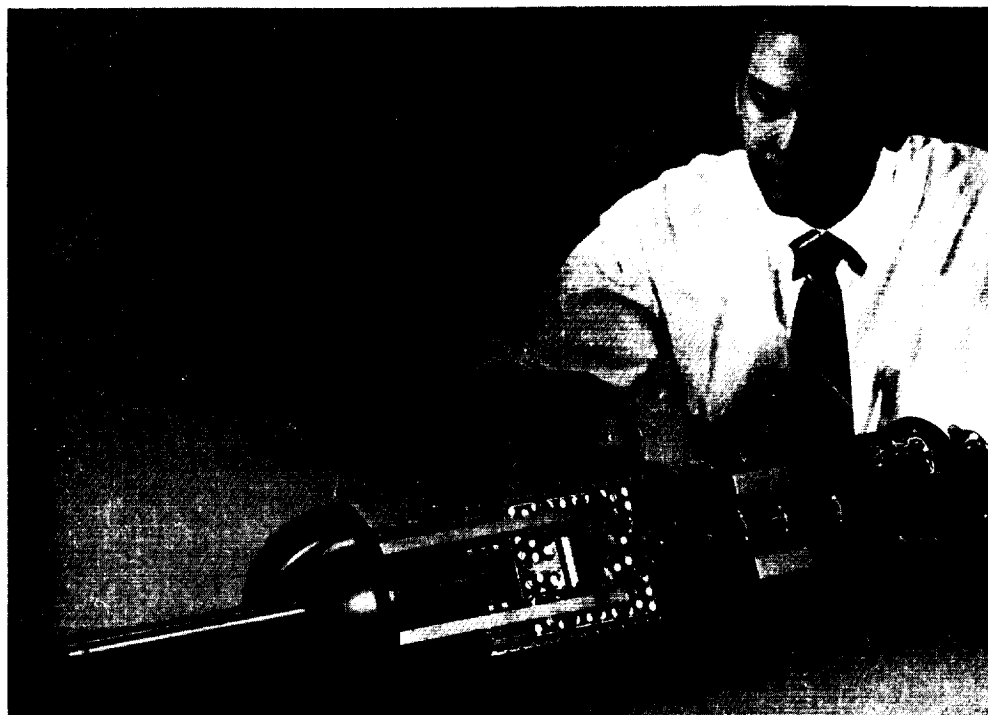
CD-87-29418

Figure III-4. - PW 2037 engine fuel nozzle at full power.



CD-87-29415

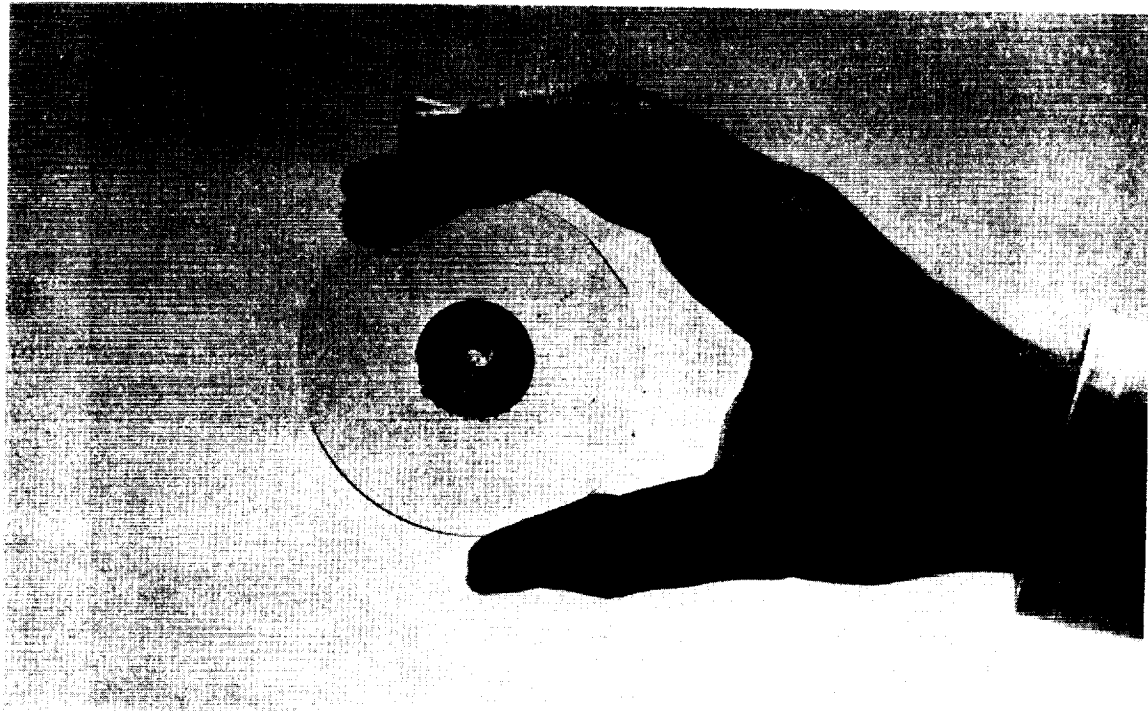
Figure III-5. - Rainbow schlieren photograph of supersonic inlet tested in 10- by 10-ft wind tunnel at Lewis.



CD-87-29420

Figure III-6. - Droplet sizing instrument used in icing flight research.

ORIGINAL PAGE
BLACK AND WHITE PHOTOGRAPH



CD-87-29421

Figure III-7. - Calibration reticle for droplet sizing instrument.

IV - HIGH-TEMPERATURE ELECTRONICS

Lawrence G. Matus and Gary T. Seng

In recent years, the aerospace propulsion and space power communities have acknowledged the growing need for electronic devices that are capable of sustained high-temperature operation. Applications for high-temperature electronic devices include engine ground test instrumentation such as multiplexers, analog-to-digital converters, and telemetry systems capable of withstanding hot section engine temperatures in excess of 600 °C. Similarly, engine-mounted integrated sensors could reach temperatures which exceed 500 °C, while uncooled operation of control and condition monitoring systems in advanced supersonic aircraft would subject electronic devices to temperatures in excess of 300 °C (ref. IV-1). Hypersonic vehicles will ultimately pose even more severe demands on electronic devices and sensors.

In addition to aeronautics, there are many other areas that would benefit from the existence of high-temperature electronic devices. Space applications include power electronic devices for the Freedom space station, space platforms, and satellites. Since power electronics require radiators to shed waste energy, electronic devices that operate at higher temperatures would allow a reduction in radiator size. Other applications on earth include deep-well drilling instrumentation, power electronics, and nuclear reactor instrumentation and control.

To meet the needs of the applications mentioned previously, the high-temperature electronics program at the Lewis Research Center is developing silicon carbide (SiC) as a high-temperature semiconductor material. This program supports a major element of the Center's mission: to perform basic and developmental research aimed at improving aerospace propulsion systems. Research is focused on developing the crystal growth, characterization, and device fabrication technologies necessary to produce a family of SiC devices.

BENEFITS OF SILICON CARBIDE AS A SEMICONDUCTOR MATERIAL

Since the desired operating temperature for some of the applications mentioned approaches 600 °C, it is clear that a new semiconductor material will need to be developed. On the basis of the inherent solid-state properties of silicon, the maximum temperature at which a silicon device could theoretically operate is about 300 °C. Gallium arsenide could theoretically operate at 460 °C, but has not proven operationally stable at this temperature. In comparing potential candidate materials for high-temperature semiconductor devices, SiC stands out not only because of its excellent high-temperature electronic properties but also because it is a very stable ceramic material up to temperatures of 1800 °C. The maximum operating temperature for a semiconductor is determined by the forbidden bandgap energy. The temperature limit is reached when

the number of intrinsic carriers, thermally excited across the energy gap, approaches the number of extrinsic carriers. This temperature (when expressed as the absolute temperature) is roughly proportional to the energy bandgap.

By using the same criteria as applied to silicon, SiC could theoretically be employed at temperatures as high as 1200 °C. A more reasonable, shorter term goal is to produce electronic devices capable of 600 °C operation. SiC is characterized by excellent physical and chemical stability making it suitable for long-term use in high temperature, corrosive environments. The combination of the material's high thermal conductivity and high breakdown field provides the potential for improved power system electronics and for increasing the number of devices per unit area. Those properties which determine the high-frequency characteristics of semiconductor devices also appear to be excellent for SiC and superior to those of silicon or gallium arsenide. The properties and benefits of SiC are summarized in table IV-I.

SILICON CARBIDE CRYSTAL GROWTH

Until recently, there was no process whereby single crystals of SiC with sufficient size, purity, and perfection could be grown reproducibly. SiC does not melt at any reasonable temperature and pressure, so this rules out the growth-from-melt technique commonly used to obtain other semiconductor single crystals such as silicon and gallium arsenide. Historically, vapor phase growth processes have proven to be the most successful method for producing SiC crystals. Early research was done on SiC crystals that were a by-product of the industrial process for making abrasives. In the industrial process, SiC is formed at 2500 °C by the reaction of silica and coke. At this temperature, gas pockets form within the SiC reaction product. The SiC sublimes and then condenses on the walls of pockets located at cooler parts of the reaction product. Occasionally, isolated SiC crystals are produced within these pockets during the production process. The larger and better crystals were selected for research purposes.

In 1955, Lely developed a laboratory version of the industrial sublimation process and was able to produce rather pure SiC crystals. Encouraged by the Lely process, NASA Lewis and other laboratories pursued the development of SiC semiconductor devices during the 1960's and early 1970's (refs. IV-2 to IV-6). Though SiC devices were demonstrated above 400 °C, by the early 1970's the Lely process and other processes had not matured to the point where high-quality large-area crystals could be grown reproducibly. Since crystal substrates are crucial to device fabrication, interest in SiC waned. From 1973 to 1980, there was very little effort in the U.S. on SiC. However, research did continue in Japan and in Europe during this period.

In 1980, because of the increased need for high-temperature electronics in advanced turbine engines, NASA Lewis again embarked on a high-temperature electronics program. The emphasis again has been on developing SiC. The problem regarding the crystal growth of SiC is rooted in the fact that SiC crystals can take on many different structural forms called polytypes. In most cases, SiC crystals grown by sublimation techniques are a mixture of different polytypes. Since each SiC polytype has its own electronic properties, sublimation-grown SiC crystals usually contain heterojunctions and possess unpredictable electronic properties. To favor growth of a single polytype of SiC, epitaxial growth on a host crystalline substrate from gases containing silicon and carbon was hypothesized. The host crystal imparts its crystalline regularity to the

thin growing layer. Since silicon is available in perfect, large, and low-cost crystals, many attempts at the heteroepitaxial growth of SiC on Si were made. These efforts were largely unsuccessful because of the large lattice mismatch that exists between Si and SiC. (The SiC lattice is 20 percent smaller than the Si lattice.)

Large-area heteroepitaxial growth of cubic SiC on Si was finally achieved at the NASA Lewis Research Center in 1983 by using a chemical vapor deposition (CVD) process (ref. IV-7). In recognition of this achievement, an IR-100 award was presented to NASA Lewis. Recently, a research program utilizing the NASA Lewis SiC crystal growth process has been established at Howard University (ref. IV-8).

Crystal growth takes place at atmospheric pressure in a fairly conventional horizontal CVD system. A complete system description is given in reference IV-9. The chemical vapor deposition reaction system is illustrated schematically in figure IV-1. To grow single-crystal cubic SiC, first an electronic-grade silicon substrate is placed on an rf-heated graphite susceptor. The essential step in the growth process is a rapid temperature ramp from near room temperature to a growth temperature of 1360 °C in the presence of a hydrocarbon gas. The NASA Lewis process uses propane as the carbon-containing gas. During the first 2 min of growth, a single-crystal cubic SiC film about 20 nm thick is produced on the Si substrate. After this initial SiC growth, silane gas is added to provide a silicon source and to initiate the final step, the bulk growth of cubic SiC to the desired thickness. During this time, the cubic SiC layer grows at a rate of 3 to 4 $\mu\text{m/hr}$.

A photograph of the chemical vapor deposition system is shown in figure IV-2. The reaction tube and associated plumbing are in the hood (center). The control valves and flow controllers reside in the vented area directly to the right. In the right foreground are the manual and computer control systems, while in the left foreground is a mass spectrometer used to monitor system gases. The rf generator is not shown.

Cubic SiC is a transparent, yellow crystal which fractures into regular rectangular pieces. In the photograph of figure IV-3, the silicon substrate has been chemically removed from a 16- μm -thick crystal. Although visually, the material appears to be of relatively good quality, in actuality a high density of defects exists in the crystal. Certain defects can adversely affect the electrical properties of SiC devices. During the past five years, much progress has been made in understanding problems associated with crystal growth, but much research remains to be done in this area.

CHARACTERIZATION OF SiC FILMS

Initially, the transition from the Si substrate to the SiC epitaxial layer was thought to occur by means of a thin buffer layer or transition layer of the order of 20 nm thick (ref. IV-7). However, high-resolution transmission electron microscopy (TEM) has demonstrated that the SiC/Si interface is abrupt with no transition region (ref. IV-10). The cubic SiC films do contain a large

density of defects that include interfacial twins, stacking faults, and anti-phase disorder (ref. IV-11). The defect density in the films is greatest near the SiC/Si interface and decreases with distance away from the interface.

A particular type of lattice defect, called antiphase boundaries (APB's), was reported to be present in all SiC films grown on Si at NASA Lewis (ref. IV-12). The APB's can be decorated by chemical etching, sputter etching, wet oxidation, or cubic SiC growth in the presence of diborane (ref. IV-13) and have the appearance of irregular-shaped boundaries as shown in figure IV-4(a). APB's form in the initial stages of growth on the Si substrate when SiC islands of opposite phase nucleate and grow together. Across the APB, the chemical bonding is between like atoms (i.e., Si-Si or C-C), instead of the normal Si-C bond between neighboring atoms.

Normally, in epitaxial growth on Si, the surface of the Si substrate is oriented precisely parallel to an atomic plane, for example, the (001) plane. It has been found in the growth of gallium arsenide on Si that APB's are eliminated by orienting the substrate slightly off-axis from the (001) plane. This technique was applied to SiC growth at NASA Lewis with the following results: for Si substrates that were tilted 1° to 4° from the (001) plane, all APB's were eliminated from the subsequent films grown. In addition, the resultant SiC films were smoother by a factor of 2 to 3 than the films grown on on-axis substrates (ref. IV-13). The micrograph in figure IV-4(b) shows the results of using an off-axis Si substrate for SiC growth. Further work is needed to determine the effect on electrical properties and the performance of devices fabricated from these films. Also, the optimum tilt angle and the direction of optimum tilt have yet to be determined.

Additional SiC material characterization is provided by photoluminescence, Raman, Rutherford backscattering, cathodoluminescence, and DLTS techniques (refs. IV-14 to IV-17).

Electrical characterization to determine electrical properties of the cubic SiC films is an important and necessary evaluation step if high-quality SiC films are to be achieved. Room-temperature Hall measurements were made on cubic SiC films grown at NASA Lewis using the van der Pauw configuration (ref. IV-18). Ohmic electrical contacts consisted of sputtered tantalum followed by sputtered gold. Detailed analysis of the Hall measurements indicated that unintentionally doped films were always n-type and that the films were heavily compensated. It is believed that all present-day cubic SiC films grown at NASA Lewis and elsewhere are compensated. The significance of compensation is the degradation of device quality. Compensated semiconductors have many ionized impurities (positive for donors and negative for acceptors) embedded in the crystal lattice, and these ions serve as scattering centers for the moving charge carrier. This increases the impurity scattering and reduces the total mobility of the charge carrier compared to uncompensated material with the same density of free carriers. Identification and eventual elimination of the compensating impurities remains a research goal.

SiC DEVICE FABRICATION TECHNOLOGY

Devices fabricated from NASA Lewis-grown SiC have been characterized and compared to conventional silicon devices. Shown in figure IV-5 are the current-voltage curves for ion-implanted SiC and Si diodes. Note that at 300 °C the Si diode is rendered useless (shorted) while the SiC retains its rectification

properties. The poorer quality of the SiC diode characteristics at room temperature is due to the unoptimized design of the device, the fabrication process, and the crystal quality (ref. IV-19).

The availability of SiC substrates now allows NASA Lewis to place increasing emphasis on device fabrication. In-house research is pursuing the fabrication of an in situ grown junction diode. Device technology is also being developed through outside activities at two separate research laboratories.

North Carolina State University (NASA grant NAG3-782) is concentrating on fundamental SiC device fabrication utilizing, when possible, technology compatible with the silicon industry. Three device structures are being pursued at NCSU: Schottky barrier diodes, ion implanted diodes, and a metal-insulator-semiconductor field effect transistor (MISFET). The National Bureau of Standards (Contract C-30007-K) is developing a device quality insulating layer, oxide or nitride, for SiC. A quality insulating layer is of paramount importance for integrated circuit technology. Earlier research had examined the quality of an oxide insulating layer deposited onto the SiC surface (refs. IV-20 and IV-21).

Although SiC can easily survive the 600 °C temperature requirement for the NASA Lewis program, an electrical contact material must be developed which also can survive. Successful metallization (i.e., electrical contact) requires a metal that adheres well to the SiC surface and possesses a chemically stable metal/SiC interface. Additionally, low contact resistance and chemical stability of the metallization scheme at high temperatures are also necessary. In the study of SiC metallization, extensive information concerning the SiC surface properties has been learned (refs. IV-22 and IV-23). Methods to create a carbon-rich or silicon-rich SiC surface prior to metallization have been developed (refs. IV-24 and IV-25). Metals that are refractory carbide-formers or silicide-formers are currently being tested at 600 °C for long periods of time (refs. IV-26 and IV-27).

FOCUS OF CURRENT AND FUTURE SiC RESEARCH

Current and future program plans are outlined in figure IV-6. Near-term studies will be performed primarily through in-house and grant research efforts. Computer modeling of the chemical vapor deposition process for SiC crystal growth has been initiated as an in-house project based on a recently completed SBIR contract, NAS3-23891 (ref. IV-28). The goal is to improve the SiC crystal growth through the identification and understanding of the important chemical reactions involved in the growth process.

Ultimately, to achieve our goals of integrated circuits and sensors, the scope of the high-temperature electronics program must be expanded into the area of device packaging. At the same time, however, the basic crystal growth and characterization research must continue to receive appropriate attention.

CONCLUDING REMARKS

The development of semiconductor materials does not occur overnight. First germanium, then silicon and then gallium arsenide, for example, have come to the marketplace after years in the laboratory and countless dollars spent for development costs. The history of SiC as a high-temperature semiconductor has been one of high expectations followed by disappointment. Recent advances in the crystal growth of SiC and the increased knowledge of the bulk material properties of the grown SiC are cause for renewed enthusiasm. It should be noted that foreign research programs are more aggressively pursuing the development of SiC technology than are those in the U.S., and although the development of SiC falls into the category of high-risk research, the future looks promising and the potential payoffs are tremendous. SiC now appears ready to emerge as a useful semiconductor material.

TABLE IV-I. - BENEFITS OF SILICON CARBIDE AS SEMICONDUCTOR MATERIAL

Property	Benefit
High operating temperature	600 °C electronics
Excellent stability	Sustained use in hostile environment
High thermal conductivity and high breakdown field	Improved power electronics and increased device packing density
Excellent high-frequency properties	Superior high-frequency devices

CHEMICAL VAPOR DEPOSITION REACTION SYSTEM

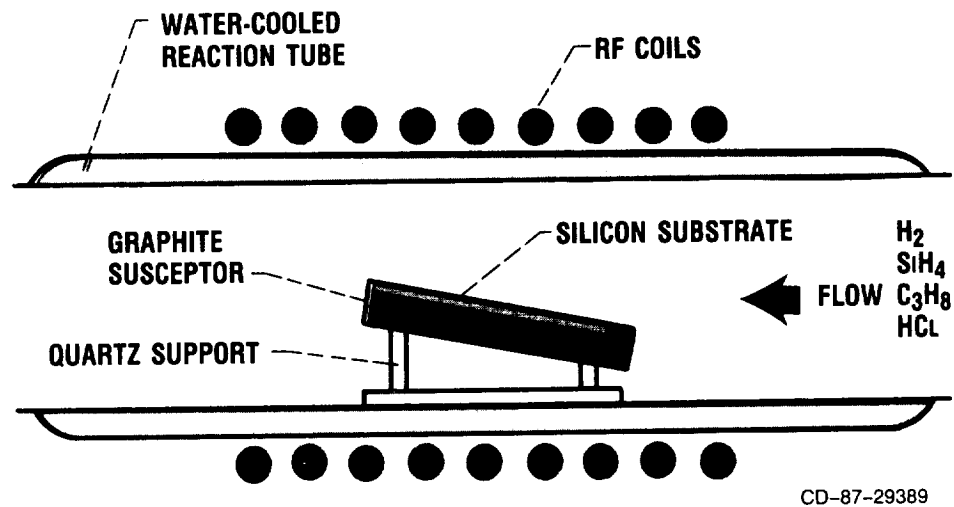
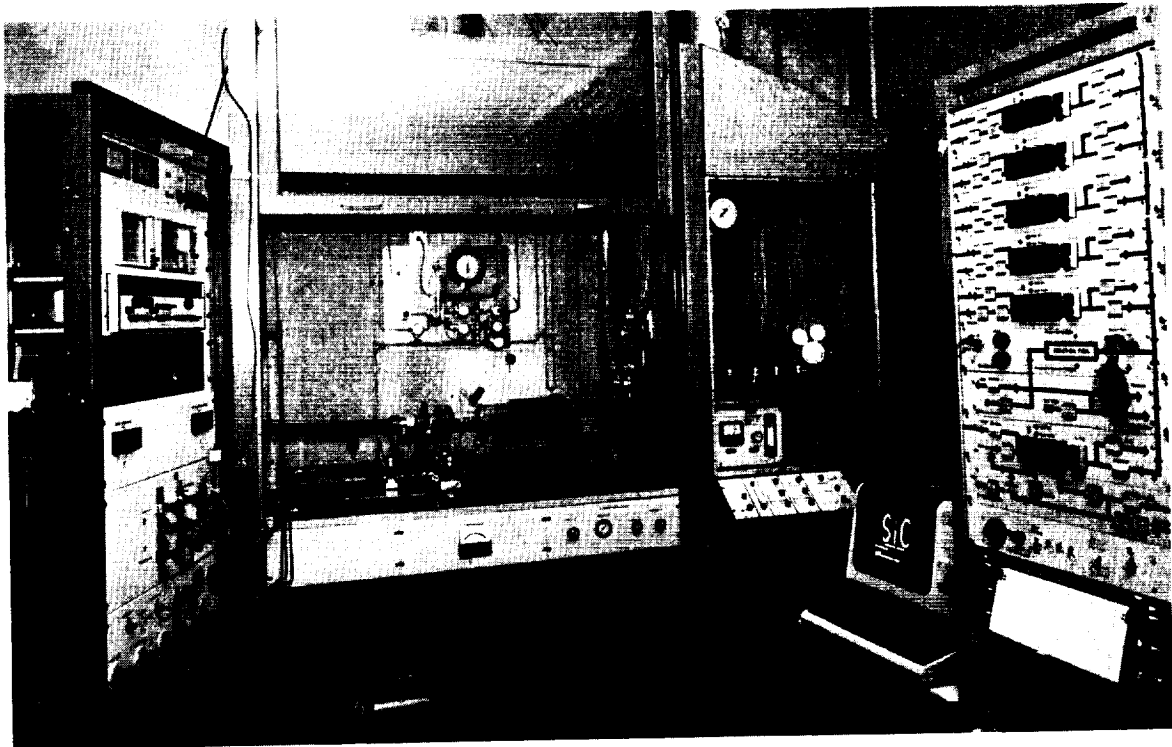
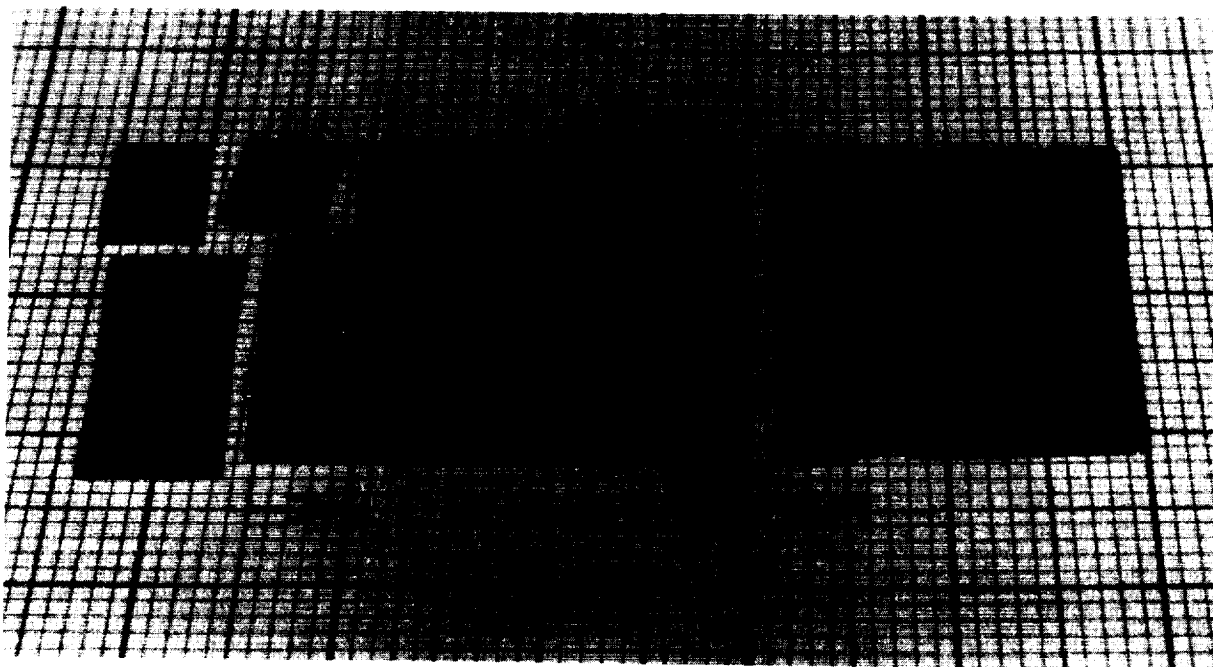


Figure IV-1. - Chemical vapor deposition reaction system.



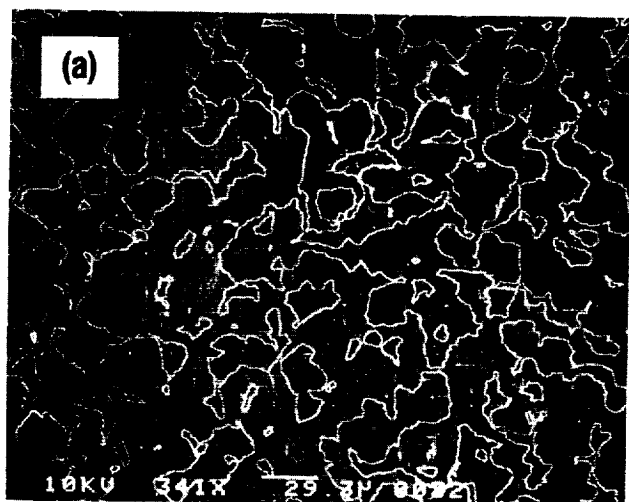
CD-87-29390

Figure IV-2. - Chemical vapor deposition system.

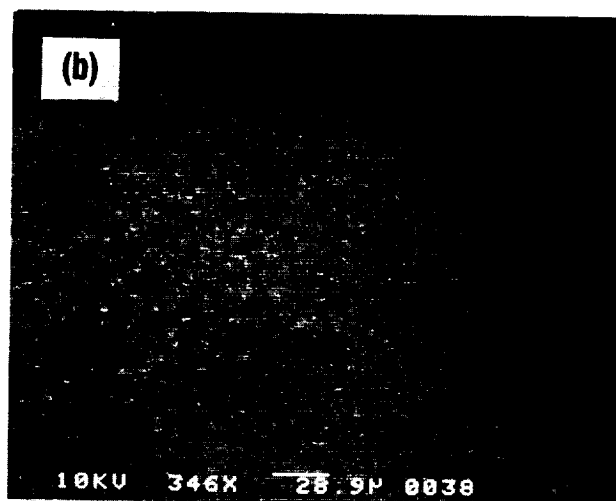


CD-87-29391

Figure IV-3. - Silicon carbide crystal.



ON-AXIS (001) Si SHOWING
DEFECT (ANTIPHASE BOUNDARIES)



OFF-AXIS (001) Si SHOWING
ELIMINATION OF DEFECT

CD-87-29631

Figure IV-4. - Scanning electron micrographs of SiC grown on silicon (Si).

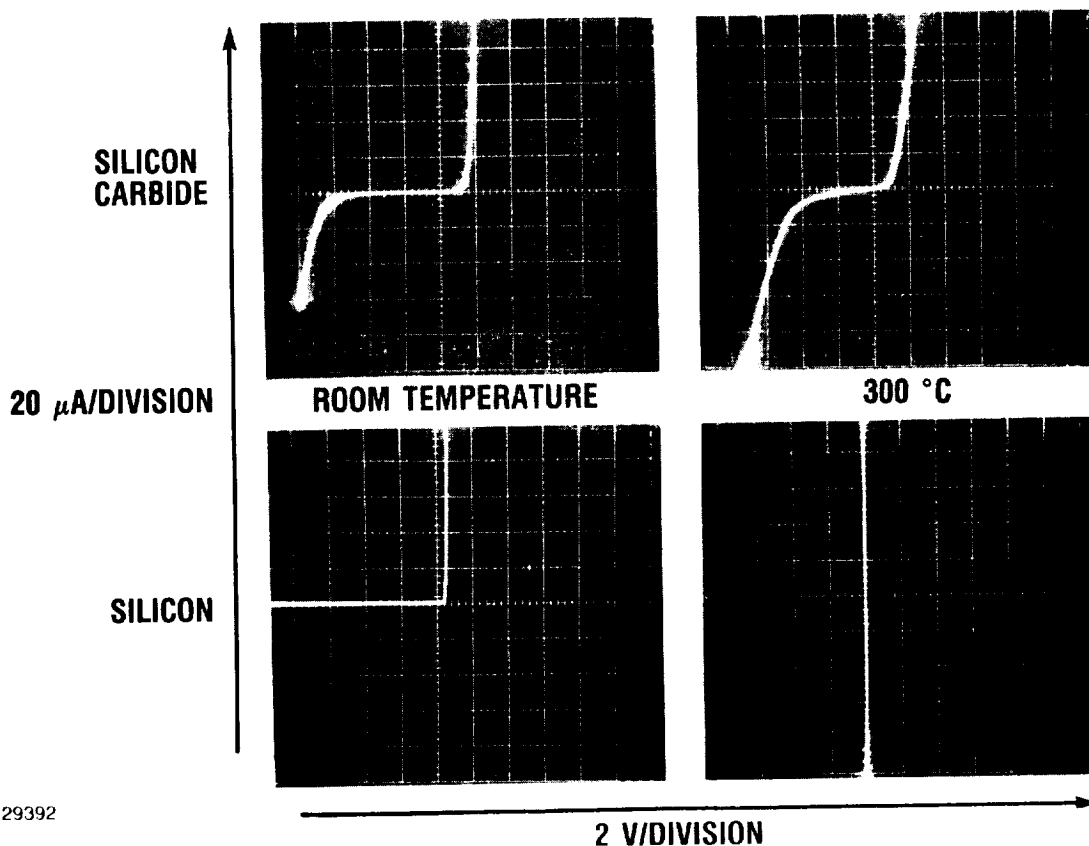


Figure IV-5. - Temperature characteristics of SiC and Si diodes.

CURRENT:

- CONTINUE PRESENT CVD STUDIES TO IMPROVE CRYSTAL QUALITY
- STUDY ALTERNATE CRYSTAL GROWTH METHODS
- CONTINUE DETAILED CHARACTERIZATION STUDIES
- CONTINUE DISCRETE DEVICE FABRICATION TECHNOLOGY RESEARCH
- CONTINUE CVD MODELING STUDIES

FUTURE:

- STUDY ALTERNATE CRYSTAL GROWTH METHODS
- CONTINUE DETAILED CHARACTERIZATION STUDIES
- DEMONSTRATE SIMPLE INTEGRATED-CIRCUIT TECHNOLOGY
- DEVELOP DEVICE METALIZATION AND PACKAGING TECHNIQUES
- DEMONSTRATE INTEGRATED-SENSOR TECHNOLOGY

CD-87-29393

Figure IV-6. - Focus of current and future Lewis SiC research.

V - FIBER OPTICS FOR CONTROLS

Gary T. Seng

The challenge of those involved in aircraft-control-system hardware development is to accommodate an ever-increasing complexity in aircraft control, while limiting the size and weight of the control system components and improving system reliability. A technology that displays promise towards this end is fiber optics. The application of fiber-optic/electro-optic technology to aircraft control systems boasts a number of inherent advantages over current wire-based systems. Replacing the propulsion and flight control system electrical wiring with optical fibers results in a substantial weight and volume savings. For example, in an F-15 fighter, the weight reduction is estimated to be 57 kg (125 lb) while for transport aircraft, weight savings could reach as high as 680 kg (1500 lb). Because optical fibers are dielectric, problems with electromagnetic interference, and electromagnetic pulse and lightning susceptibility are eliminated. This, in turn, eliminates the need for shielding and surge-quenching circuits. This is particularly advantageous as modern aircraft move towards the use of composite structures, which provide little inherent shielding. The high bandwidth capability is advantageous for data bus lines and offers the potential for all avionics data to be transmitted over a single line. Fiber optics also eliminates the threat of fires due to insulation failures or short circuits which could cause inadvertent actuation of control hardware.

Figure V-1 shows an artist's conception of a fly-by-light aircraft. In this greatly simplified diagram, the engine control and flight control computers are linked to their respective set of optical sensors and optical actuators using fiber optic cables and an electro-optic interface (not shown).

FIBER-OPTIC CONTROL SYSTEM INTEGRATION PROGRAM (FOCSI)

The design, development, and testing of a fiber-optic integrated propulsion/flight control system for an advanced supersonic dash aircraft (flies at supersonic speeds for short periods of time) is the goal of the joint NASA and DOD Fiber-Optic Control System Integration (FOCSI) program. Phase I, which assessed current technology and provided system design options, was completed early in fiscal year 1987 (Oct. 1986) (refs. V-1 and V-2). Phase I provided a comparison of electronic and optical control systems, identified the status of current optical sensor technology, defined the aircraft sensor/actuator environment, proposed architectures for fully optical control systems, and provided schedules for development. Overall, it was determined that there are sufficient advantages in employing a fiber-optic-based control system to warrant

continued efforts to develop such a system. It was also determined that it is feasible to build a fiber-optic control system for the development of a data base for this technology, but that further work is necessary in sensors, actuators, and components to develop an optimum-design, fully fiber-optic integrated control system compatible with advanced aircraft environments.

Phase II, which is to design, construct, and ground-test a fly-by-light control system, has been initiated, with the first task aimed at providing a detailed design of the electro-optic architecture required.

A phase III program for flight test of the system is currently under consideration to establish an initial data base on the performance, reliability, and maintainability of fly-by-light control systems.

FIBER-OPTIC SENSORS PROGRAM

As indicated in the previous section, to implement a fiber-optic control system requires the development of passive optical sensors and optically controlled or powered actuators capable of surviving aircraft environments. Table V-I provides a preliminary list of the set of control and condition monitoring sensors being considered for incorporation into the FOCSI control system. The entire control system must be flight qualified to withstand a supersonic dash aircraft environment. It must perform reliably with repeated temperature cycling and vibration. The most severe overall environments occur in the engine bay areas. For current-generation fighters, the highest soaking temperature a sensor may see is 473 K (200 °C) and the lowest is 218 K (-55 °C), while the highest gas stream temperature that the sensing element may see is 1370 K (1100 °C) (in the hot section, ref. V-1). Fiber-optic cables and connectors in the engine bay area are exposed to a temperature range of 218 K to in excess of 373 K (100 °C). The electro-optics are contained within the protected engine control computer environment and must operate reliably in a temperature range of 218 to 358 K (-55 to 85 °C), although flight qualification requires military specification components which are tested to 398 K (125 °C). Currently, actuators would most likely be of the optically-controlled variety, able to operate reliably in a temperature environment from 218 to 423 K (-55 to 150 °C)

NASA Lewis has addressed this critical area of technology since 1975 by developing a wide variety of optical sensors and a high-temperature electro-optic switch through in-house, contract, and grant efforts (refs. V-3 to V-11). A list of accomplishments in this area is presented in table V-II.

Currently, work is continuing to improve methods for temperature, pressure, and position measurements; and work has been initiated to develop referencing techniques for intensity modulated sensors, optical sensor multiplexing schemes, and shock position sensors (refs. V-12 to V-30). Two examples which will be discussed further are a wavelength division multiplexed (WDM) optical encoder and a semiconductor-etalon temperature sensor (refs. V-31 to V-34).

A diagram of the wavelength division multiplexed optical encoder is shown in figure V-2. It uses a micro-optical wavelength multiplexer/demultiplexer in conjunction with a reflective code plate. This approach results in a compact, rugged, and potentially inexpensive device. The multiplexer unit consists of a 5-mm-diameter graded index (GRIN) rod lens epoxied to a prism/grating assembly.

Broadband light from two LED's enters the transducer via the encoder input/output fiber. The multiplexer disperses the broadband spectrum across the channels of a reflective code plate. Those wavelengths directed to a channel in the logic zero state are absorbed by the code plate. Those wavelengths directed to a channel in the logic 1 state are reflected by the code plate and retransmitted to the input/output fiber. At the receiver of the WDM optical encoder, demultiplexing is performed by a second grating assembly which disperses the spectrum onto a photodiode array. The pattern of "on"-peaks (logic 1) and "off"-valleys (logic 0) defines the position of the actuator to 10-bit resolution. Currently, a prototype encoder is being constructed for future engine and flight tests. Figure V-3 is a photograph of the current prototype.

A schematic diagram of a semiconductor-etalon temperature sensor is presented in figure V-4. The sensing element is a silicon carbide (SiC) etalon on silicon (Si). Light incident on the etalon is partially reflected from both of its surfaces. Interference patterns from these reflected beams can be related to the optical thickness of the etalon which, in turn, is a function of the temperature. An optical fiber delivers light to the sensor. A graded index (GRIN) rod microlens collimates this light and directs it towards the sensing etalon. Light reflected by the etalon is recoupled into the fiber by the GRIN lens. A dual interferometer (not shown) system is employed to determine the optical thickness. An alumina tube positions the sensing etalon a distance of 5 cm from the GRIN rod lens to permit the measurement of temperatures significantly higher than can be withstood by the fiber and GRIN rod lens. The sensing etalon is a single-crystal film of silicon carbide (SiC) with a thickness of 18 μm . A silicon substrate provides mechanical support to the SiC and serves to protect its surface. A smaller, more advanced version of the sensor is currently being constructed. Figure V-5 is a photograph of an earlier, larger prototype.

CONCLUDING REMARKS

NASA intends to continue to aggressively pursue all the areas of fiber-optic technology presented. Future directions in the program are described as follows:

- (1) Continue efforts aimed at achieving FOCSI objectives
- (2) Continue development of novel fiber-optic sensor concepts
- (3) Develop engine test prototypes of promising fiber-optic sensor systems
- (4) Study innovative approaches to actuation device design
- (5) Serve as focus for achieving consensus on fiber-optic component specifications for aircraft

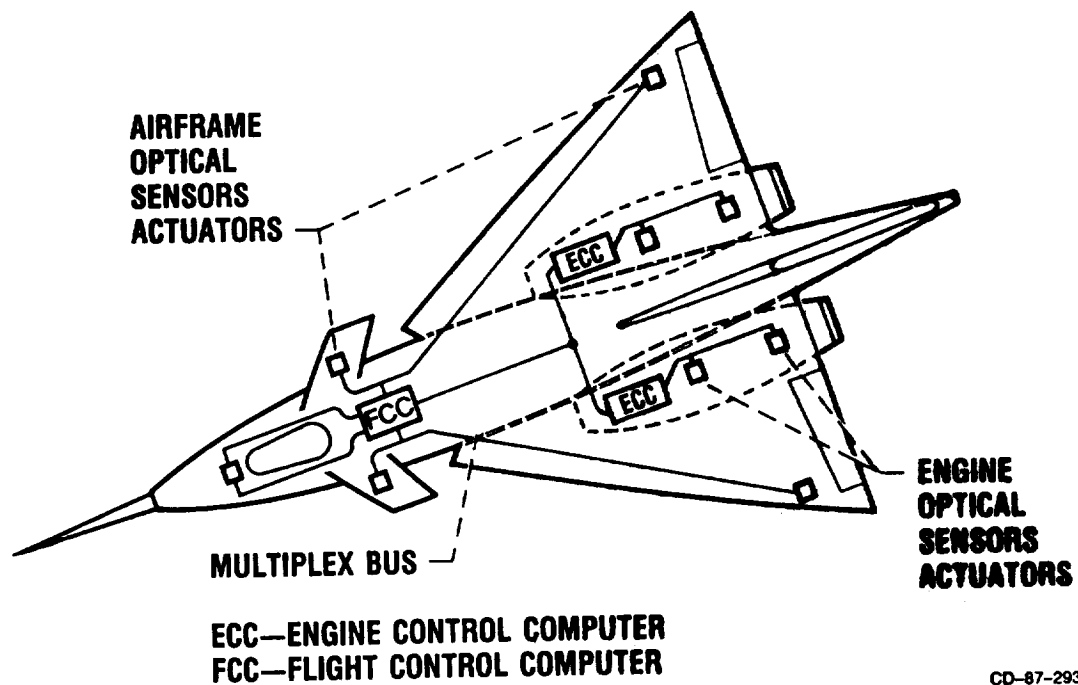
One area which deserves attention in the near term is fly-by-light control systems for future generation fighter aircraft and high-speed aircraft such as those flying in sustained supersonic or hypersonic regimes. Such control systems will require fiber-optic components capable of much higher temperature operation than was reported here.

TABLE V-I. - PRELIMINARY FOCSI SENSOR SET

Propulsion	Flight
Control sensors	
Pressure Compressor inlet, discharge Turbine discharge Speed Fan Core Temperature Compressor, turbine inlet Turbine blade Actuator positions Fuel flow Light-off detector	Actuator positions Pressure (total, static) Mach number Angle of attack Total temperature Interface with flight guidance
Condition monitoring sensors	
Oil temperature, level, debris Vibration Fuel temperature	Hydraulic pressure, temperature, level Fuel level

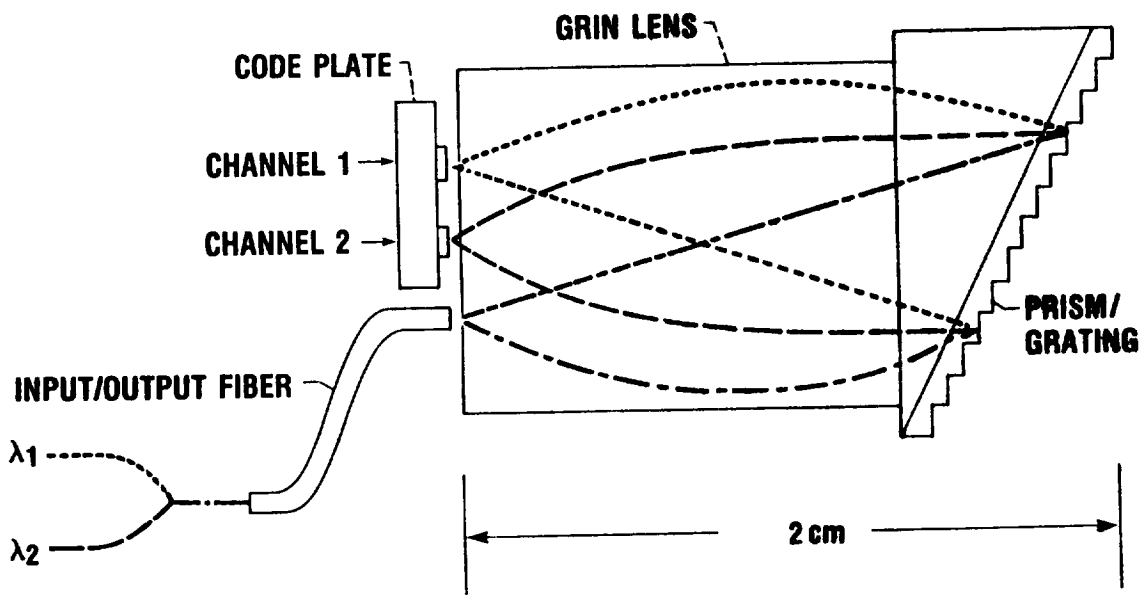
TABLE V-II. - FIBER-OPTIC SENSORS PROGRAM ACCOMPLISHMENTS

Accomplishment	Date
Tachometer demonstrated on engine	1976
Position encoder demonstrated on compressor guide vane	1976
Tip clearance sensor demonstrated on compressor stage	1980
800 °C temperature sensor developed (absorption)	1980
1000 °C temperature sensor developed (Fabry-Perot)	1983
Gallium arsenide photoswitch developed (260 °C operation)	1985
High-temperature pressure sensor developed (microbend)	1985
1700 °C gas temperature sensor developed (blackbody)	1986
Intensity sensor referencing techniques developed	1987



CD-87-29375

Figure V-1. - Fly-by-light aircraft.



CD-87-29380

Figure V-2. - Wavelength division multiplexed (WDM) optical encoder.

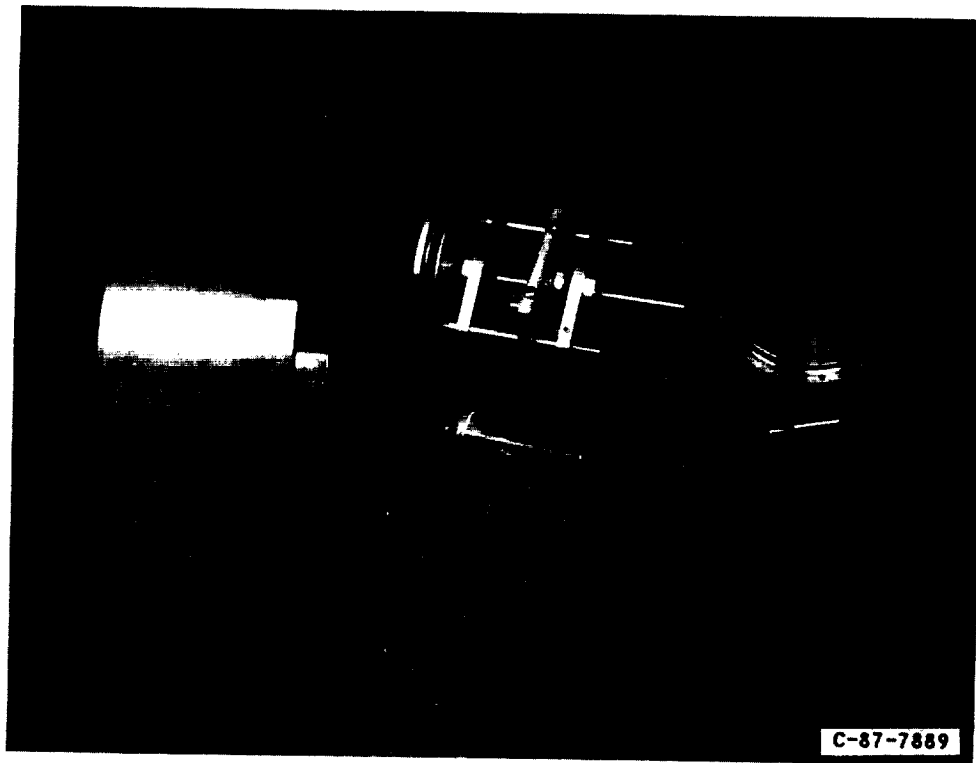
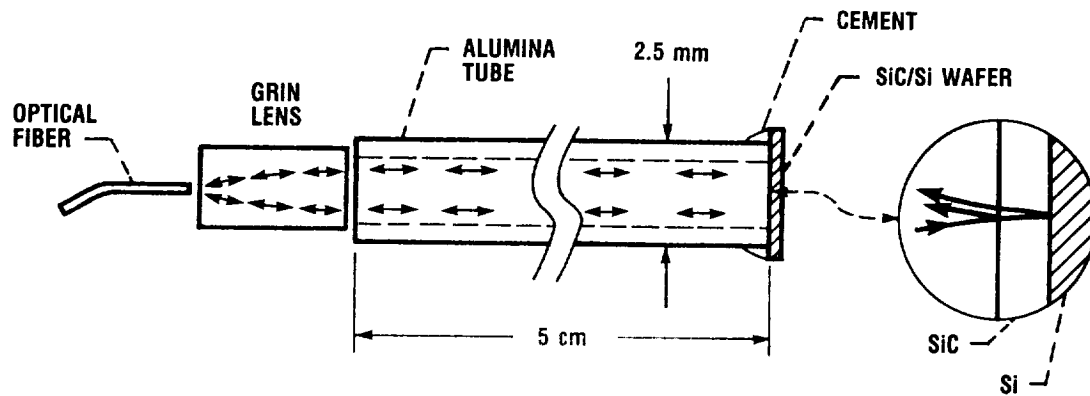


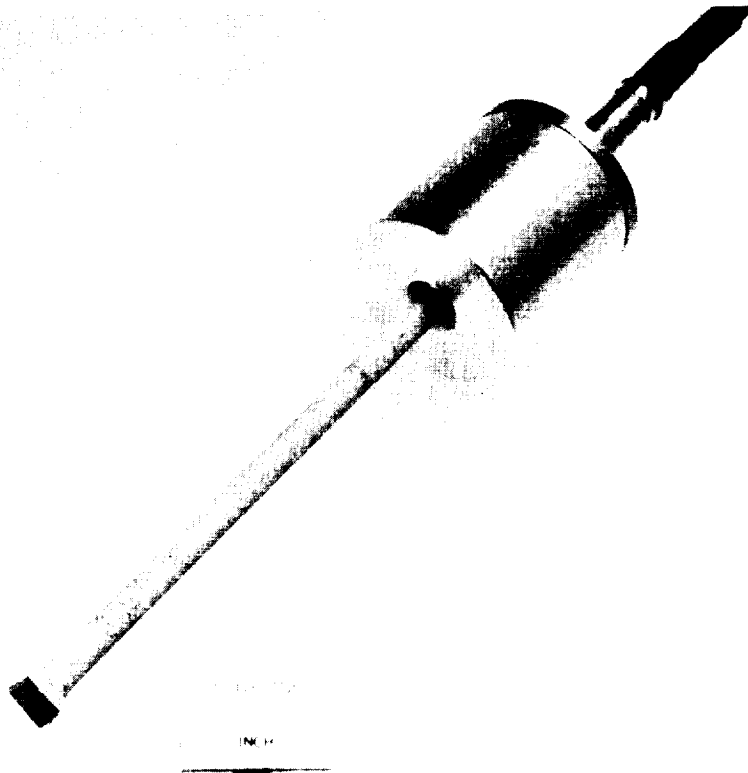
Figure V-3. - Prototype WDM optical encoder.



CD-87-29382

Figure V-4. - Semiconductor-etalon temperature sensor.

ORIGINAL PAGE
BLACK AND WHITE PHOTOGRAPH



CD-87-29383

Figure V-5. - Prototype temperature sensor.

VI - DIRECTIONS IN PROPULSION CONTROL

Carl F. Lorenzo

This section discusses research at NASA Lewis in the area of propulsion controls as driven by trends in advanced aircraft. The objective of the Lewis program is to develop the technology for advanced reliable propulsion control systems and to integrate the propulsion control with the flight control for optimal full-system performance.

CONTEMPORARY PROPULSION CONTROLS ISSUES

The primary drivers seen for propulsion control research are a continuing increase in aircraft and propulsion system complexity, increased dynamic coupling between the aircraft and the propulsion system, and a continuing need to reduce control system weight while increasing reliability.

The demand for increased functionality for future aircraft and the desire to optimize aircraft and propulsion systems as an integrated entity has led to a large increase in the physical complexity of the aircraft/propulsion systems. The new functionalities can include vertical and short-takeoff-and-landing capabilities coupled with high-speed cruise. To achieve these capabilities special-purpose aircraft are being designed with a high degree of dynamic coupling between aircraft and propulsion systems. This is a dramatic departure from traditional aircraft design where such coupling was minimized. The effect of large dynamic coupling is to increase pilot work load. Advanced controls can help alleviate the problem of pilot work load and allow optimal aircraft performance to be achieved; however, this necessitates that the unified or integrated design approach to aircraft flight controls and propulsion control be evolved.

Control weight as a percentage of propulsion system weight is significant in spite of gains made by conversion to digital systems. Previous sections of this paper have discussed our efforts in fiber optics and high-temperature electronics (using silicon carbide), which should help reduce control system weight. Further efforts are perhaps best approached by industry as part of the design process and by applying new materials technologies.

COMPLEXITY ISSUE

Airbreathing engine complexity is reflected by the number of primary control variables managed for a given engine (fig. VI-1). This is an important measure, since it indicates the number of sensors required as well as the amount of actuation, and it is a general indicator of propulsion system complexity. The trend has shown a steady increase in controlled variables over

the years. With this trend has come the use of full-authority digital electronic controllers, which have helped in dealing with the complexity issue. The increase in control components implies a corresponding decrease in control reliability unless specific measures are taken to deal with the issue.

DYNAMIC COUPLING

Typical of aircraft with significant dynamic coupling are supersonic short takeoff and vertical landing aircraft (STOVL) (fig. VI-2), advanced high-speed x-wing rotor craft, and even hypersonic aircraft where engine air capture and aircraft pitch control are tightly coupled. Vertical lift aircraft flight control at low forward speed and through transition are typically dominated by propulsion control considerations. These aspects provide strong motivation for research in the area of flight/propulsion control integration.

PROPULSION CONTROLS

Current activities of the NASA Lewis controls research program are indicated as follows:

- (1) Hypersonic propulsion dynamics and control
- (2) Reconfigurable control
- (3) Controls networking
- (4) Sensor failure detection, isolation, and accommodation

The hypersonic propulsion control work includes hypersonic engine dynamic modeling, propulsion control, and control instrumentation keyed to the NASP technology maturation program. Dynamic models of the various NASP components are being developed (refs. VI-1 to VI-4) and integrated into full engine models for study of dynamic ramjet/scramjet stability and control. Several dynamic inlet models, which include inlet unstart studies, have been implemented, and combustor models consistent with real-time simulation have been formulated.

The reconfigurable control effort seeks to create expert system intelligence which, in real time, can "redesign" a control system to account for significant changes in aircraft or engine behavior. In this process (fig. VI-3) an on-line recursive identifier will monitor the plant variables to detect changes in the plant. When such a change occurs an expert system (ref. VI-5) will be invoked to manage a control redesign using one of several design approaches. The new design will be impressed on the plant controller. If necessary, a second expert system (yet to be developed) will tune the control for desired performance.

Efforts in controls networking aim to develop high-performance communications systems tailored specifically to distributed integrated aircraft flight/propulsion controls. The magnitude and the time variability of network-induced delay directly impacts control system stability. Thus, network performance, that is, end-to-end delay as a function of offered load and communications packet size, for various configurations has been both simulated and measured directly from network systems for various configurations (refs. VI-6 to VI-12). Further, to improve control tolerance of delay, the use of filters and observers, and control synchronization across the distributed control system are being studied (refs. VI-13 to VI-16).

FAILURE DETECTION ISOLATION AND ACCOMMODATION

The Sensor Failure Detection and Accommodation program (refs. VI-17 to VI-28) strives to attain control system reliability through the application of analytical redundancy instead of hardware redundancy (multiple sensors for each measurement). Analytical redundancy uses available sensor information and reference models of the engine to detect sensor failures and to generate accurate estimates which replace failed sensor information to the controller (fig. VI-4).

Sensor failure accommodation logic has been developed that uses sensed signals from the engine and actuators together with analytical models of the engine to create (Kalman filter based) estimates of the engine parameters. These estimates (fig. VI-5) are used by the multivariable control as representing the actual engine variables. Failed sensors are detected by "hypothesis testing" a series of hypothesis filters, each of which uses all available signals but one. Likelihood statistics are generated and compared to detect the failed sensor(s). The failed sensors are then removed from the calculation of the estimates.

The sensor failure accommodation algorithm and multivariable controller are implemented (fig. VI-6) in a triple-microprocessor-based control system (ref. VI-24). The computers calculate (1) the multivariable control laws, (2) the detection and accommodation logic, and (3) the isolation logic to determine which sensors have failed. The processors are Intel 80186/80187 based hardware which allow a 40-msec update time while processing the algorithms in a high-level language (FORTRAN). This computer implementation was used to validate the detection and accommodation logic both for real-time simulations and with an actual engine.

To validate the analytical formulation and practical implementation of the sensor failure algorithm, full-scale tests were performed (ref. VI-22) with the Pratt & Whitney F-100 engine in the Lewis Propulsion System Laboratory (fig. VI-7). The tests were conducted over a wide range of altitude/Mach number conditions.

In the tests, various forms of sensor failure were electronically imposed on the control sensors. Actual engine performance in response to an imposed drift failure in the nozzle pressure sensor signal is shown in figure VI-8. Such small drift failures are very difficult to detect, and thus the time of detection is not immediate. It can be seen, however, that the actual engine thrust loss is quite small. In the figure the "sensed" variable is the signal that would be normally seen by the control. The "actual" is the "sensed" variable without the imposed drift failure, and the "estimated" is nozzle pressure as determined by the Kalman filter.

The major events are as follows: at point A, a slow drift is introduced into the sensed signal, so that sensed signal would begin to deviate at a rate of 1 psi/sec. From point A to point B, the control tries to accommodate what is going on. It senses the pressure rising and opens up the nozzle area. In response to that the actual pressure begins to fall, until a loss of control authority at point B. At that point the sensed pressure begins to deviate at the 1 psi/sec rate. At point C the logic has determined that failure has occurred and removes the faulty sensed variable, in this case, nozzle pressure,

from the estimator calculation. Then the actual signal and the estimate begin to come back together as the control returns to a normal mode operation. At point E, without sensor failure accommodation, engine shutoff occurs.

The results of the sensor failure accommodation testing on the F-100 engine are summarized as follows:

- (1) High-performance failure detection (120 different failure scenarios, 11 engine operating conditions, both subsonic and supersonic conditions)
- (2) Good post-failure accommodation performance (no significant loss of performance power transients with accommodated failures)
- (3) Sequential failure detection and accommodation
- (4) Simultaneous failure detection and accommodation
- (5) Engine control with all feedback sensors failed

One hundred and twenty different failure scenarios were run. Demonstrated capabilities include the detection, isolation, and accommodation of drift, in-range step, noise, and large-scale "hard" failures. Failure testing was done at 11 Mach number/altitude operating conditions over the flight envelope. Also demonstrated was the capability to detect sequential sensor failures as well as simultaneous failures. The algorithm worked satisfactorily for all tests. Excellent post-failure control performance was demonstrated including full-range operation with single sensor failure.

As a demonstration case the F-100 engine was run with all feedback sensors failed. (The input sensors Pt_2 and Tt_2 were not failed.) Under the condition of all engine control sensors failed, the controller correctly detected each failure and accommodated all failures by using the computed estimates for all the signals. While in this condition the engine was smoothly accelerated and decelerated as shown in figure VI-9.

The NASA Lewis new thrusts in propulsion control are focused on the areas of supersonic STOVL integrated control and intelligent system control.

INTEGRATED FLIGHT/PROPULSION CONTROL

The supersonic STOVL aircraft (fig. VI-10) typifies the trend toward complex aircraft with large dynamic coupling between the aircraft and propulsion system. A NASA Lewis and NASA Ames program will develop advanced integrated controls methodologies and designs for this application. Current plans focus on the F-16 aircraft and the F-110 engine with vectorable nozzles and an ejector as the vertical thrust effector. The integration problem is to evolve controls designs and methodologies which integrate subsystem controls in a manner to achieve optimal aircraft performance. Nonlinear simulation models of both aircraft and propulsion system are being created. Linear control models will be abstracted from these to be used as a basis for control design. Validation tests at NASA Lewis will incorporate a piloted simulator and actual engine/ejector firing together with a simulated aircraft to evaluate developed control laws. Final validation is planned to be done with the NASA Ames Vertical Motion Simulator.

INTELLIGENT SYSTEM CONTROL

The block diagram in figure VI-11 indicates an expansion of the traditional control function into a broad system intelligence (ref. VI-29). This will be initially applied to reusable space propulsion systems. The inner control loop will be designed with life-extending methodologies (yet to be developed) which will combine controls technologies with those of structure and material sciences. The new interdisciplinary technology will be applied to state-of-the-art engines such as space shuttle main engine or hypersonic propulsion systems where transient effects on engine life are important, and where transient performance must be controlled.

Artificial intelligence concepts will likely be used for the highlighted functions. An on-board diagnostic/prognostic expert system will identify impending hardware failures using information from component condition monitoring instruments, and engine dynamics monitor and performance information. A high-level coordinator will determine the required remedial action; for example, change control request or if necessary invoke a control adapter that will reconfigure (redesign) the control in flight. This research is expected to greatly enhance vehicle and propulsion performance, and substantially improve life, reliability, and maintainability.

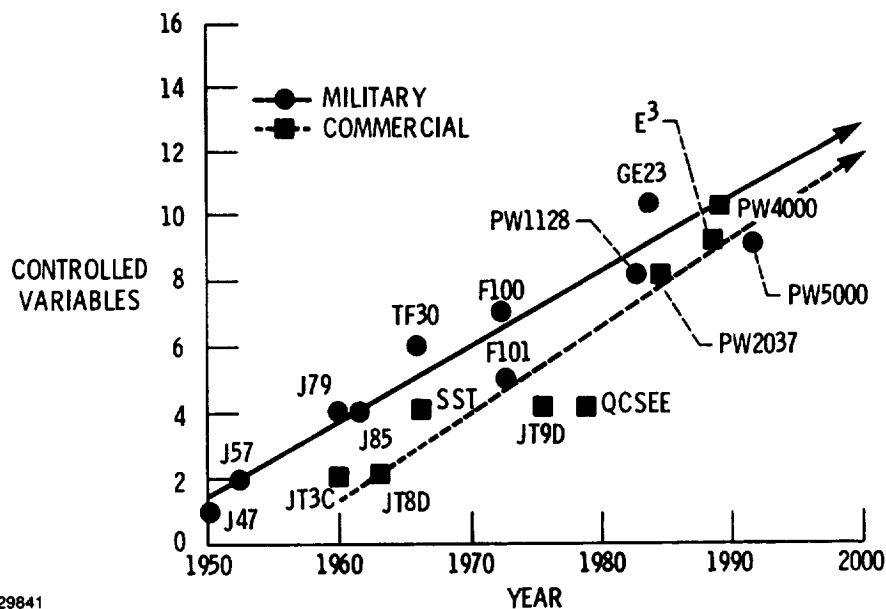
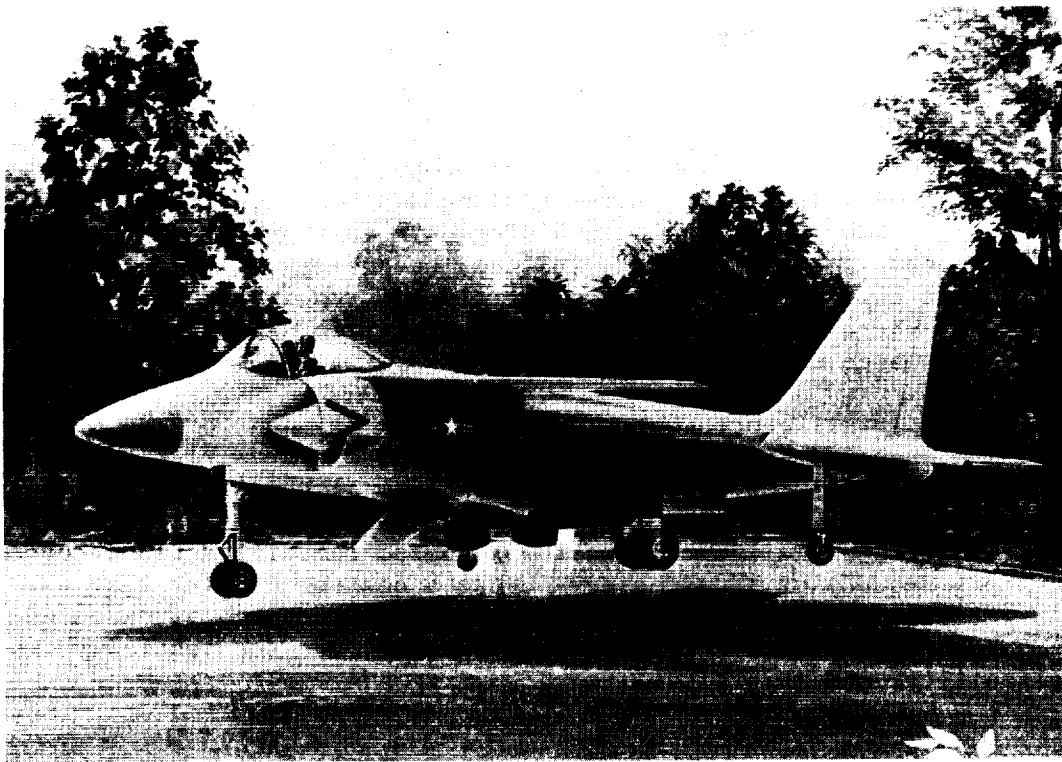


Figure VI-1. - Trends in control complexity of aircraft turbine engines.



CD-87-29842

Figure VI-2. - Supersonic short takeoff and vertical landing aircraft.

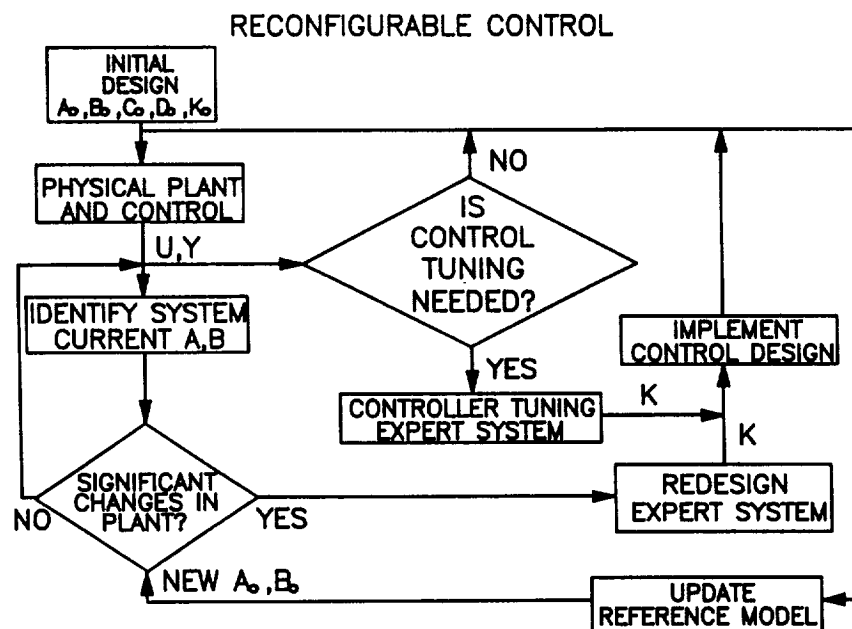


Figure VI-3. - Block diagram of reconfigurable control system.

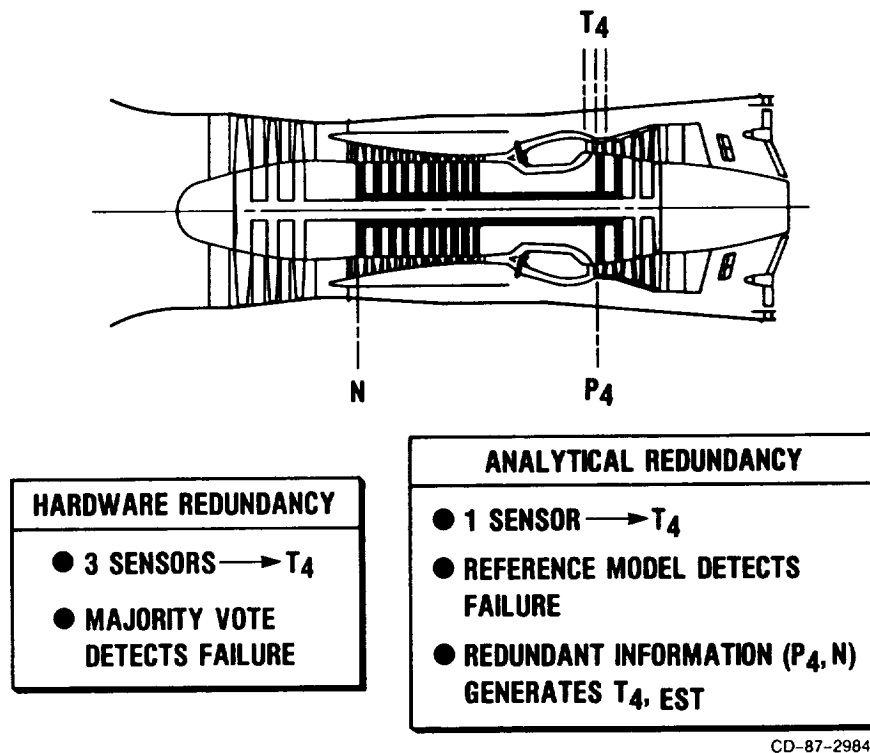
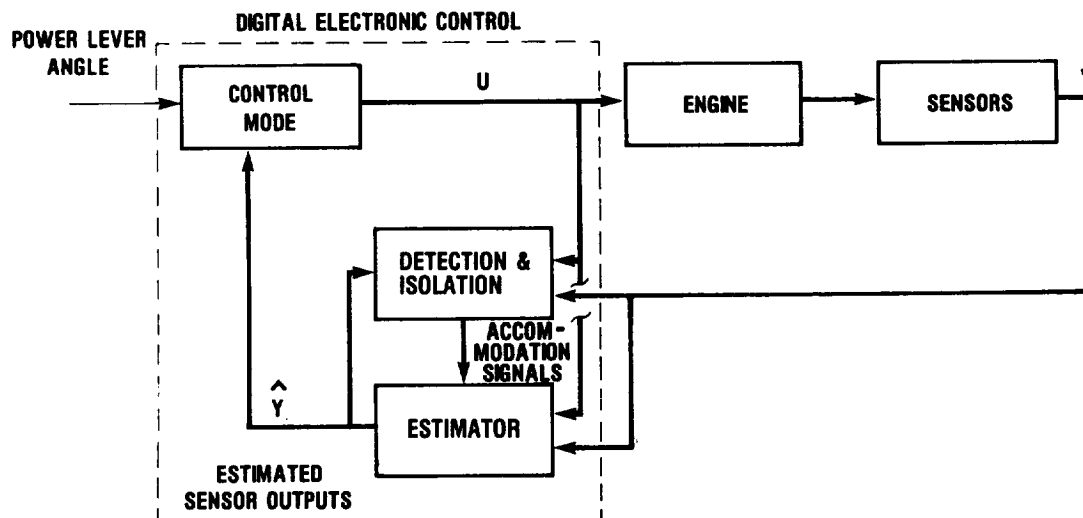
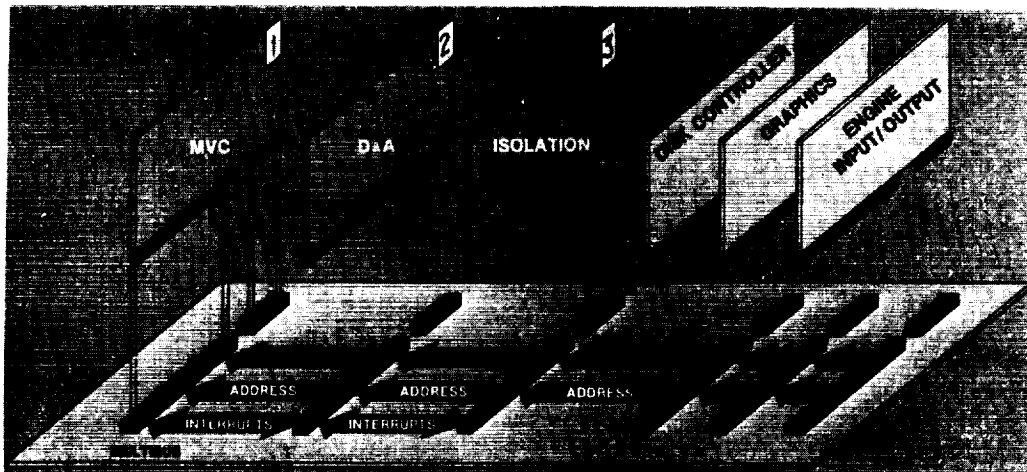


Figure VI-4. - Analytical redundancy.



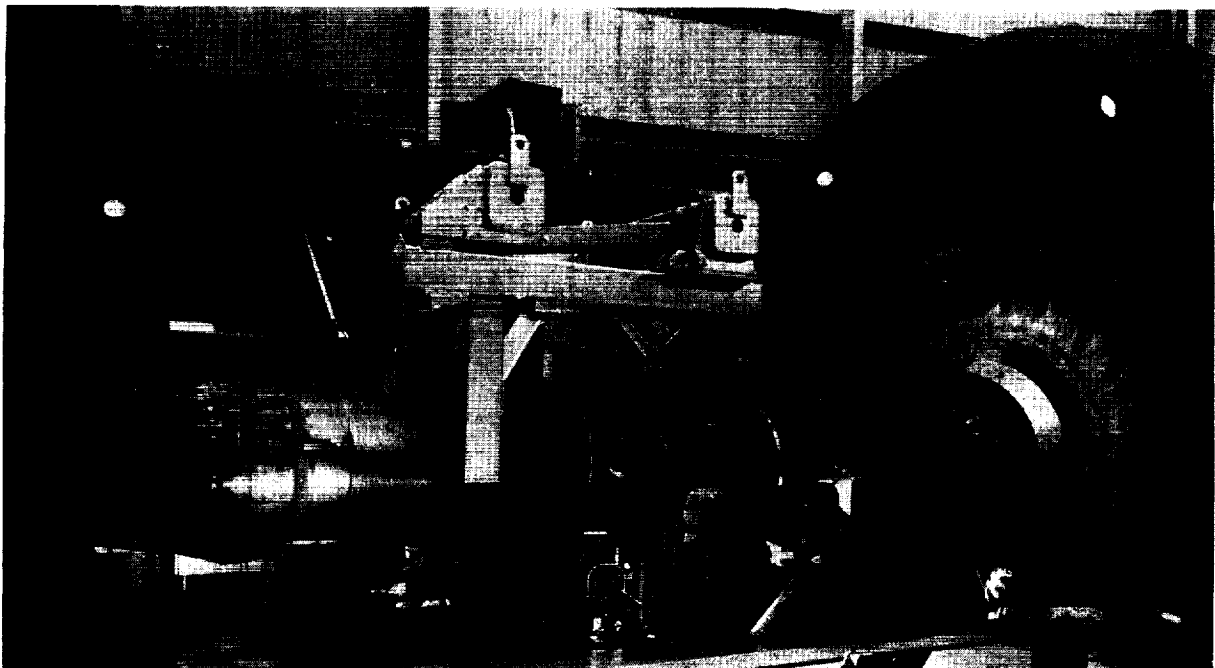
CD-87-29845

Figure VI-5. - Simplified block diagram for sensor failure accommodation system.



CD-87-29846

Figure VI-6. - Hardware implementation for sensor failure accommodation system.



CD-87-29847

Figure VI-7. - Pratt & Whitney F-100 as used in sensor failure accommodation program in Propulsion Systems Laboratory.

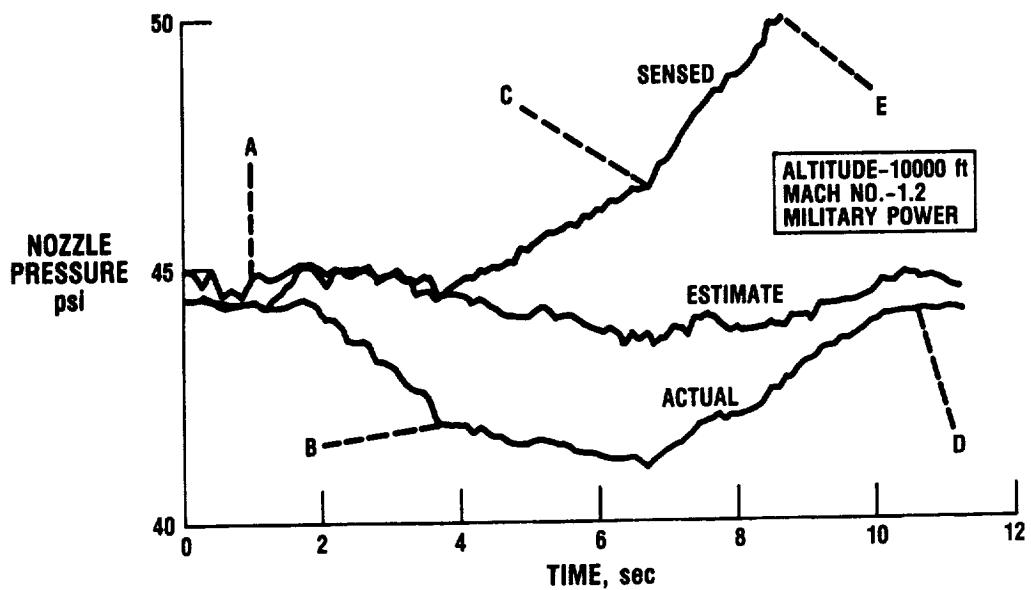


Figure VI-8. - F-100 engine drift failure on nozzle pressure.

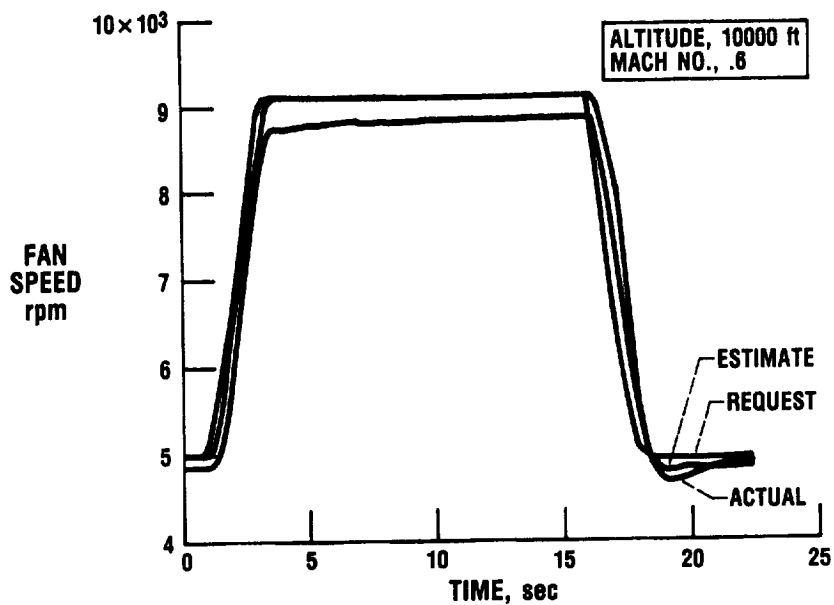


Figure VI-9. - Engine response to throttle transient with all sensors failed.

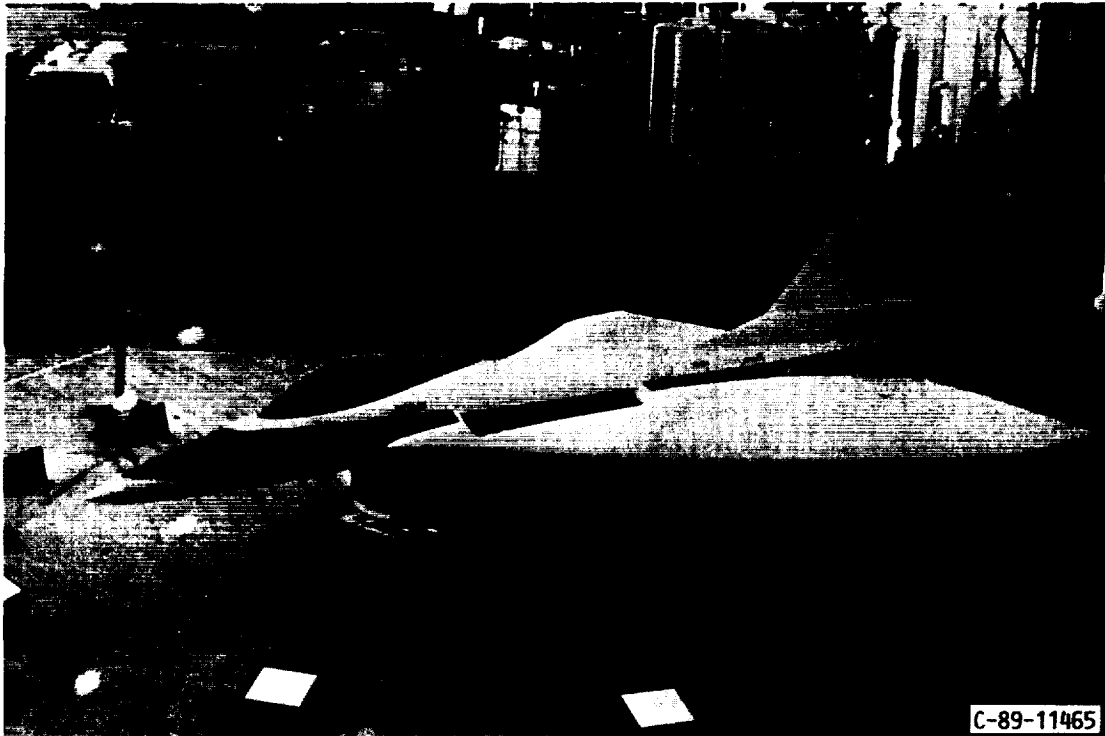


Figure VI-10. - Supersonic STOVL ground test aircraft to be used in integrated controls studies.

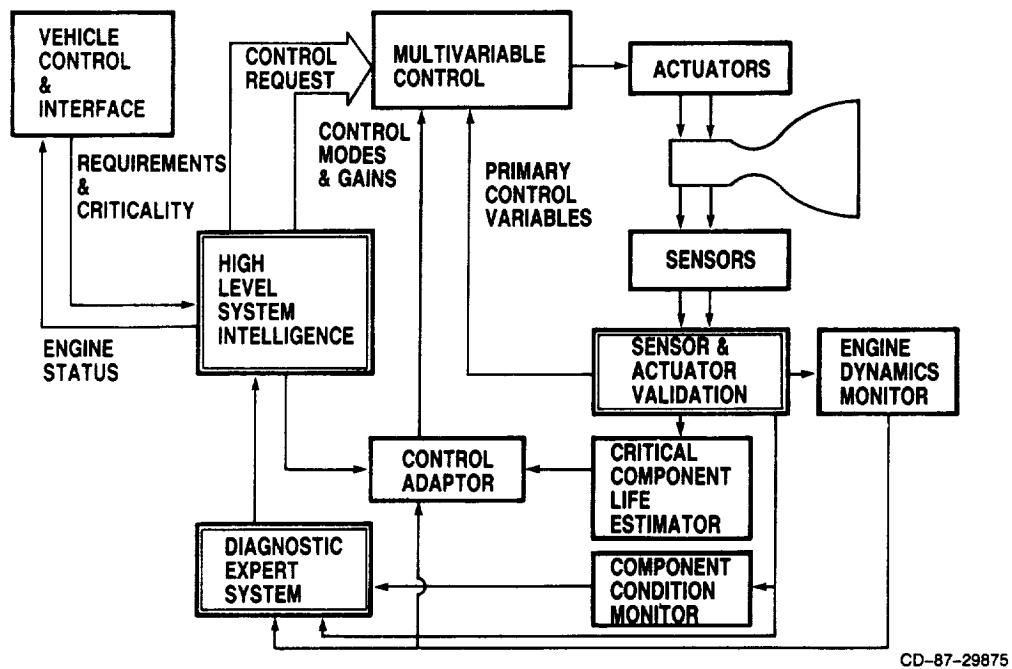


Figure VI-11. - Block diagram of intelligent system control.

VII - INSTRUMENTATION AND CONTROLS RESEARCH REFERENCES

Research Sensors

- II-1. Elmore, D.L.; Robinson, W.W.; and Watkins, W.B.: Dynamic Gas Temperature Measurement System. Instrumentation in the Aerospace Industry, Vol. 30, Advances in Test Measurements, Vol. 21, Instrument Society of America, Research Triangle Park, NC, 1984, pp. 289-302.
- II-2. Elmore, D.L.; Robinson, W.W.; and Watkins, W.B.: Dynamic Gas Temperature Measurement System, Vol. I, Technical Efforts. (PWA/GPD-FR-17145-VOL-1, Pratt and Whitney Aircraft; NASA Contract NAS3-23154) NASA CR-168267-VOL-1, 1983.
- II-3. Elmore, D.L.; Robinson, W.W.; and Watkins, W.B.: Further Development of the Dynamic Gas Temperature Measurement System, Volume I, Technical Efforts. (P&W/GPD FR-19381-VOL-1, Pratt and Whitney; NASA Contract NAS3-24228) NASA CR-179513-VOL-1, 1986.
- II-4. Stocks, D.R.; and Elmore, D.L.: Further Development of the Dynamic Gas Temperature Measurement System, Vol. II, Computer Program User's Manual. (P&W/GPD-FR-19381-VOL-2, Pratt and Whitney Aircraft; NASA Contract NAS3-24228) NASA CR 179513-VOL-2 (Also listed as NASA CR-179604), 1986.
- II-5. Atkinson, W.H.; Hobart, H.F.; and Strange, R.R.: Advanced High Temperature Heat Flux Sensors. Advances in Instrumentation, Vol. 38, Part 2, Instrument Society of America, Research Triangle Park, NC, 1983, pp. 1457-1479.
- II-6. Atkinson, W.H.; and Strange, R.R.: Development of Advanced High-Temperature Heat Flux Sensors. (PWA-5723-27, Pratt and Whitney Aircraft; NASA Contract NAS3-22133) NASA CR-165618, 1982.
- II-7. Atkinson, W.H.; Cyr, M.A.; and Strange, R.R.: Development of High-Temperature Heat Flux Sensors, Phase II, Verification Testing. (PWA-5914-39, Pratt and Whitney Aircraft; NASA Contract NAS3-22133) NASA CR-174973, 1985.
- II-8. Atkinson, W.H.; Cyr, M.A.; and Strange, R.R.: Turbine Blade and Vane Heat Flux Sensor Development, Phase 1. (PWA-5914-21, Pratt and Whitney Aircraft; NASA Contract NAS3-23529) NASA CR-168297, 1984.
- II-9. Atkinson, W.H.; Cyr, M.A.; and Strange, R.R.: Turbine Blade and Vane Heat Flux Sensor Development, Phase 2. (PWA-5914-39, Pratt and Whitney Aircraft; NASA Contract NAS3-23529) NASA CR-174995, 1985.
- II-10. Holanda, R.: Analysis of Thermoelectric Properties of High-Temperature Complex Alloys of Nickel-Base, Iron-Base, and Cobalt-Base Groups. NASA TP-2278, 1984.

- II-11. Grant, H.P.; and Przybyszewski, J.S.: Thin Film Temperature Sensor. (PWA-5526-31, Pratt and Whitney Aircraft; NASA Contract NAS3-20768) NASA CR-159782, 1980.
- II-12. Grant, H.P.; Przybyszewski, J.S.; and Claing, R.G.: Turbine Blade Temperature Measurements Using Thin Film Temperature Sensors. (PWA-5604-31, Pratt and Whitney Aircraft; NASA Contract NAS3-20831) NASA CR-165201, 1981.
- II-13. Grant, H.P., et al.: Thin Film Temperature Sensors, Phase III for Engine-Test Evaluation (PWA-5708-26, Pratt and Whitney Aircraft; NASA Contract NAS3-22002) NASA CR-165476, 1982.
- II-14. Liebert, C.H., et al.: High Temperature Thermocouple and Heat Flux Gage Using a Unique Thin Film-Hardware Hot Junction. J. Eng. Gas Turbines Power, vol. 107, no. 4, Oct. 1985, pp. 938-944 (NASA TM-86898).
- II-15. Kreider, K.G.; Semancik S.; and Olson, C.: Advanced Thin Film Thermocouples. (NBSIR 84-2949, National Bureau of Standards) NASA CR-175541, 1984.
- II-16. Kreider, K.G.; and Semancik, S.: Thermal and Sputtered Aluminum Oxide Coatings for High Temperature Electrical Insulation. J. Vac. Sci. Technol. A, vol. 3, no. 6, Nov./Dec. 1985, pp. 2582-2587.
- II-17. Prakash, S., et al.: Pretreatment Effects on the Morphology and Properties of Aluminum Oxide Thermally Grown on NiCoCrAlY. J. Vac. Sci. Technol. A, vol. 3, no. 6, Nov./Dec. 1985, pp. 2551-2556.
- II-18. Budhani, R.C.; Prakash, S.; and Bunshah, R.F.: Thin-Film Temperature Sensors for Gas Turbine Engines: Problems and Prospects. J. Vac. Sci. Technol. A, vol. 4, no. 6, Nov./Dec. 1986, pp. 2609-2617.
- II-19. Budhani, R.C., et al.: Oxygen Enhanced Adhesion of Platinum Films Deposited on Thermally Grown Alumina Surfaces. J. Vac. Sci. Technol. A, vol. 4, no. 6, Nov.-Dec. 1986, pp. 3023-3024.
- II-20. Hulse, C.O.; Bailey, R.S.; and Lemkey, F.D.: High Temperature Static Strain Gage Alloy Development Program. (R85-915952-13, United Technologies Research Center; NASA Contract NAS3-23169) NASA CR-174833, 1985.
- II-21. Hulse, C.O., et al.: High Temperature Static Strain Gage Development Contract, Tasks 1 and 2. (R87-916527-1, United Technologies Research Center; NASA Contract NAS3-23722) NASA CR-180811, 1987.
- II-22. Hulse, C.O., et al.: Advanced High Temperature Static Strain Sensor Development. (R86-995875-28, United Technologies Research Center; NASA Contract NAS3-22126) NASA CR-179520, 1987.
- II-23. Stetson, K.A.: Demonstration Test of Burner Liner Strain Measuring System. (R84-926376-15, United Technologies Research Center; NASA Contract NAS3-23690) NASA CR-174743, 1984.
- II-24. Hobart, H.F.: Evaluation Results of the 700°C Chinese Strain Gages for Gas Turbine Engines. NASA TM-86973, 1985.

- II-25. Stetson, K.A.: The Use of Heterodyne Speckle Photogrammetry to Measure High-Temperature Strain Distributions. Holographic Data Nondestructive Testing, D. Vukicevic, ed., SPIE Proc. Vol. 370, Society of Photo-Optical Instrumentation Engineers, Bellingham, WA, 1983, pp. 46-55.
- II-26. Lant, C.T.; and Qaqish, W.: Optical Strain Measurement System Development-Phase I. NASA CR-179619, 1987.
- II-27. Lant, C.T.; and Qaqish, W.: Optical Strain Measurement System Development. NASA CR-179646, 1987.
- II-28. Atkinson, W.H.; Cyr, M.A.; and Strange R.R.: Development of Sensors for Ceramic Components in Advanced Propulsion Systems. (PWA-6113-12, Pratt and Whitney Aircraft; NASA Contract NAS3-25141) NASA CR-182111, 1988.
- II-29. Bennethum, W.H.; and Sherwood, L.T.: Sensors for Ceramic Components in Advanced Propulsion Systems. NASA CR-180900, 1988.

Optical Measurement Systems

- III-1. Decker, A.J.: Advanced Optical Measuring Systems for Measuring the Properties of Fluids and Structures. NASA TM-88829, 1986.
- III-2. Decker, A.J.; Beam-Modulation Methods in Quantitative and Flow-Visualization Holographic Interferometry. NASA TM-87306, 1986.
- III-3. Decker, A.J.; and Stricker, J.: A Comparison of Electronic Heterodyne Moire Deflectometry and Electronic Heterodyne Holographic Interferometry for Flow Measurements. SAE Paper 851896, 1985 (NASA TM-87071).
- III-4. Seasholtz, R.G.; Oberle, L.G.; and Weikle, D.H.: Optimization of Fringe-Type Laser Anemometers for Turbine Engine Component Testing. AIAA Paper 84-1459, June 1984 (NASA TM-83658).
- III-5. Seasholtz, R.G.: Application of Laser Anemometry in Turbine Engine Research. NASA TM-83513, 1983.
- III-6. Pelaccio, D.G.: Investigation of Laser Anemometry for Space Shuttle Main Engine Model Verification Experiments. (RI/RD86-163, Rockwell International; NASA Contract NAS3-24356) NASA CR-179470, 1986.
- III-7. Seasholtz, R.G.; and Goldman, L.J.: Combined Fringe and Fabry-Perot Laser Anemometer for Three-Component Velocity Measurements in Turbine Stator Cascade Facility. NASA TM-87322, 1986.
- III-8. Wernet, M.P.; and Edwards, R.V.: Implementation of a New Type of Time-of-Flight Laser Anemometer. Appl. Opt., vol. 25, no. 5, Mar. 1, 1986, pp. 644-648.
- III-9. Wernet, M.P.; and Oberle, L.G.: Laser Anemometry Techniques for Turbine Applications. ASME Paper 87-GT-241, 1987 (NASA TM-88953).
- III-10. Morey, W.W.: Hot Section Viewing System. (R84-925830-33, United Technologies Corp.; NASA Contract NAS3-23156) NASA CR-174773, 1984.

- III-11. Howes, W.L.: Rainbow Schlieren. NASA TP-2166, 1983.
- III-12. Howes, W.L.: Rainbow Schlieren and Its Applications. Appl. Opt., vol. 23, no. 14, July 15, 1984, pp. 2449-2460.
- III-13. Howes, W.L.: Rainbow Schlieren vs Mach-Zehnder Interferometer: A Comparison. Appl. Opt., vol. 24, no. 6, Mar. 15, 1985, pp. 816-822.
- III-14. Hovenac, E.A.: Performance and Operating Envelope of Imaging and Scattering Particle Sizing Instruments. Focus on Electro-Optic Sensing and Measurement (ICALEO 1987), G. Kychakoff, ed., Springer-Verlag, 1988.
- III-15. Hovenac, E.A.: Calibration of Droplet Sizing and Liquid Water Content Instruments: Survey and Analysis. (FAA/CT-86-19, Sverdrup Technology Inc.; NASA Contract NAS3-24105) NASA CR-175099, 1986.
- III-16. Hovenac, E.A.: Use of Rotating Reticles for Calibration of Single Particle Counters. The Changing Frontiers of Optical Techniques for Industrial Measurement and Control (ICALEO 1986), C.M. Penney and H.J. Caulfield, eds., Springer-Verlag, 1987, pp. 129-134.
- III-17. Hovenac, E.A.; Hirleman, E.D.; and Ide, R.F.: Calibration and Sample Volume Characterization of PMS Optical Array Probes. 3rd International Conference on Liquid Atomisation and Spray Systems (ICLASS 1985), P. Eisenklam and A. Yule, eds., Institute of Energy, London, England, 1985.

High-Temperature Electronics

- IV-1. Nieberding, W.C.; and Powell, J.A.: High Temperature Electronic Requirements in Aeropropulsion Systems. IEEE Trans. Industrial Electronics, vol. 29, no. 2, May 1982, pp. 103-106.
- IV-2. Powell, J.A.: Crystal Growth of 2H Silicon Carbide. J. Appl. Phys., vol. 40, no. 11, Oct. 1969, pp. 4660-4662.
- IV-3. Powell, J.A.: Refractive Index and Birefringence of 2H Silicon Carbide. J. Opt. Soc. Am., vol. 62, no. 3, Mar. 1972, pp. 341-344.
- IV-4. Powell, J.A.; and Will, H.A.: Low-Temperature Solid-State Phase Transformations in 2H Silicon Carbide. J. Appl. Phys., vol. 43, no. 4, Apr. 1972, pp. 1400-1408.
- IV-5. Powell, J. A.; and Will, H. A.: Epitaxial Growth of 6H SiC in the Temperature Range 1320^o-1390^oC. J. Appl. Phys., vol. 44, no. 11, Nov. 1973, pp. 5177-5178.
- IV-6. Powell, J.A.; and Will, H.A.: Process for Fabricating SiC Semiconductor Devices. U.S. Patent No. 3,956,032, May 11, 1976.
- IV-7. Nishino, S.; Powell, J.A.; and Will, H.A.: Production of Large-Area Single-Crystal Wafers of Cubic SiC for Semiconductor Devices. Appl. Phys. Lett., vol. 42, no. 5, Mar. 1, 1983, pp. 460-462.

- IV-8. Harris, G.L., et al.: Low-Pressure Growth of Single-Crystal Silicon Carbide. *Mater. Lett.*, vol. 4, no. 2, Feb. 1986, pp. 77-80.
- IV-9. Powell, J.A.; Matus, L.G.; and Kuczmarski, M.A.: Growth and Characterization of Cubic SiC Single-Crystal Films on Si. *J. Electrochem. Soc.*, vol. 134, no. 6, June 1987, pp. 1558-1565.
- IV-10. Chorey, C.M., et al.: TEM Investigation of Beta-SiC Grown Epitaxially on Si Substrate by CVD. *Semiconductor-Based Heterostructures: Interfacial Structure and Stability*, M.L. Green, et al., eds., The Metallurgical Society, Warrendale, PA, 1986, pp. 115-125.
- IV-11. Pirouz, P., et al.: Lattice Defects in Beta-SiC Grown Epitaxially on Silicon Substrates. *Heteroepitaxy on Silicon II*, J.C.C. Fan, J.M. Phillips, B.-Y. Tsaur, eds., MRS Symp. Proc. Vol. 91, Materials Research Society, Pittsburgh, PA, 1987, pp. 399-404.
- IV-12. Pirouz, P.; Chorey, C.M.; and Powell, J.A.: Antiphase Boundaries in Epitaxially Grown Beta-SiC. *Appl. Phys. Lett.*, vol. 50, no. 4, Jan. 26, 1987, pp. 221-223.
- IV-13. Powell, J.A., et al.: Improved Beta-SiC Heteroepitaxial Films Using Off-Axis Si Substrates. *Appl. Phys. Lett.*, vol. 51, no. 11, Sept. 14, 1987, pp. 823-825.
- IV-14. Choyke, W.J.; Feng, Z.C.; and Powell, J.A.: Low Temperature Photoluminescence Studies on Chemical-Vapor-Deposition-Grown 3C-SiC on Si. *J. Appl. Phys.*, vol. 64, no. 6, Sept. 15, 1988, pp. 3163-3175.
- IV-15. Feng, Z.C., et al.: Raman Scattering Studies of Chemical-Vapor-Deposited Cubic SiC Films on (100)Si. *J. Appl. Phys.*, vol. 64, no. 6, Sept. 15, 1988, pp. 3176-3186.
- IV-16. Feng, Z.C.; Choyke, W.J.; and Powell, J.A.: Raman Determination of Layer Stresses and Strains for Heterostructures and its Application to the Cubic SiC/Si System. *J. Appl. Phys.*, vol. 64, no. 12, Dec. 15, 1988, pp. 6827-6835.
- IV-17. Zhou, P.Z., et al.: Observation of Deep Levels in Cubic Silicon Carbide. *Appl. Phys. Lett.*, vol. 50, no. 19, May 11, 1987, pp. 1384-1385.
- IV-18. Segall, B., et al.: Compensation in Epitaxial Cubic SiC Films. *Appl. Phys. Lett.*, vol. 49, no. 10, Sept. 8, 1986, pp. 584-586.
- IV-19. Avila, R.E.; Kopanski, J.J.; and Fung, C.D.: Behavior of Ion-Implanted Junction Diodes in 3C-SiC. *J. Appl. Phys.*, vol. 62, no. 8, Oct. 15, 1987, pp. 3469-3471.
- IV-20. Fung, C.D.; and Kopanski, J.J.: Thermal Oxidation of 3C Silicon Carbide Single Crystal Layers on Silicon. *Appl. Phys. Lett.*, vol. 45, no. 7, Oct. 1, 1984, pp. 757-759.
- IV-21. Avila, R.E.; Kopanski, J.J.; and Fung, C.D.: Behavior of Inversion Layers in 3C Silicon Carbide. *Appl. Phys. Lett.*, vol. 49, no. 6, Aug. 11, 1986, pp. 334-336.

- IV-22. Dayan, M.: AES and LEED Study of the Zinc Blende SiC(100) Surface. J. Vac. Sci. Technol. A, vol. 3, no. 2, Mar.-Apr. 1985, pp. 361-366.
- IV-23. Wheeler, D.R.; and Pepper, S.V.: Angle-Resolved X-Ray Photoelectron Spectroscopy of Epitaxially Grown (100) Beta-SiC to 1300°C", Surf. and Interface Anal., vol. 10, no. 2-3, Mar. 1987, pp. 153-162.
- IV-24. Bellina, J.J., Jr.; and Zeller, M.V.: Stoichiometric Changes in the Surface of (100) Cubic SiC Caused by Ion Bombardment and Annealing. Appl. Surf. Sci., vol. 25, 1986, pp. 380-390.
- IV-25. Bellina, J.J., Jr.; Ferrante, J.; and Zeller, M.V.: Surface Modification Strategies for (100)3C-SiC. J. Vac. Sci. Technol. A, vol. 4, no. 3, May-June 1986, pp. 1692-1695.
- IV-26. Bellina, J.J., Jr.; and Zeller, M.V.: Thermally Activated Reactions of Titanium Thin Films with (100) 3C-SiC Substrates. Novel Refractory Semiconductors, D. Emin, T.L. Aselage, and C. Wood, eds., MRS Symp. Proc. Vol. 97, Materials Research Society, Pittsburgh, PA, 1987, pp. 265-270.
- IV-27. Zeller, M.V., et al.: AES Studies of the M/SiC Interface with Metal Carbide Formers. Novel Refractory Semiconductors, D. Emin, T.L. Aselage, and C. Wood, eds, MRS Symp. Proc. Vol. 97, Materials Research Society, Pittsburgh, PA, 1987, pp. 283-288.
- IV-28. Stinespring, C.D.; and Wormhoudt, J.C.: Gas Phase Kinetics Analysis and Implications for Silicon Carbide Chemical Vapor Deposition. J. Cryst. Growth, vol. 87, no. 4, Mar. 1988, pp. 481-493.

Fiber Optics for Controls

- V-1. Poumakis, D.J.; and Davies, W.: Fiber Optic Control System Integration. NASA CR-179569, 1986.
- V-2. Poppel, G.L.; Glasheen, W.M.; and Russell, J.C.: Fiber Optic Control System Integration. (R87AEB111, General Electric Co.; NASA Contract NAS3-24624) NASA CR-179568, 1987.
- V-3. Baumbick, R.J.: Fiber Optic Sensors for Measuring Angular Position and Rotational Speed. NASA TM-81454, 1980.
- V-4. Baumbick, R.J.: Fiber Optics for Aircraft Engine/Inlet Control. NASA TM-82654, 1981.
- V-5. Poppel, G.L.; Marple, D.T.F.; and Kingsley, J.D.: Analysis, Design, Fabrication and Testing of an Optical Tip Clearance Sensor. (R81AEG215, General Electric Co.; NASA Contract NAS3-21843) NASA CR-165265, 1981.
- V-6. Design, Fabrication and Testing of an Optical Temperature Sensor for High Temperature Control Applications. (United Technologies Research Center, NASA Contract NAS3-22774) NASA CR-174698, 1983.

- V-7. James, K.; and Quick, B.: Fiber-Optic, Fabry-Perot Temperature Sensor. NASA CR-174712, 1984.
- V-8. Berak, J.M.; Grantham, D.H.; and Eder, M.: Optical Switching of High Temperature GaAs Devices for Digital Control of Aircraft Direct-Drive Actuators. (UTRC-R86-926733-27, United Technologies Corp.; NASA Contract NAS4-24219) NASA CR-179465, 1986.
- V-9. Mossey, P.W.; Shafferknocker, W.M.; and Mulukutla, A.R.: 1700°C Optical Temperature Sensor. (R86AEB267, General Electric; NASA Contract NAS3-24085) NASA CR-175108, 1986.
- V-10. Glenn, W.H.; Morey, W.W.; and Snitzer, E.: Analysis and Preliminary Design of Optical Sensors for Propulsion Control. (R79-924112-14, United Technologies Research Center; NASA Contract NAS3-21004) NASA CR-159468, 1979.
- V-11. Baumbick, R.J., et al.: Optical Sensors for Aeronautics and Space. NASA TM-81407, 1980.
- V-12. Fritsch, K.; and Adamovsky, G.: Simple Circuit for Feedback Stabilization of a Single-Mode Optical Fiber Interferometer. Rev. Sci. Instrum., vol. 52, no. 7, July 1981, pp. 996-1000.
- V-13. Carome, E.F.; and Adamovsky, G.: High Kilohertz Frequency Fiber Optic Phase Modulators. Fiber-Optic Rotation Sensors and Related Technologies, Springer Series in Optical Sciences, Vol. 32, S. Ezekiel and H.J. Arditty, eds., Springer-Verlag, 1982, pp.157-162.
- V-14. Adamovsky, G.: All-Fibre Sensing Loop Using Pulse-Modulated Light-Emitting Diode. Electron. Lett., vol. 21, no. 20, Sept. 25, 1985, pp. 922-923.
- V-15. Adamovsky, G.: Time Domain Referencing in Intensity Modulation Fiber Optic Sensing Systems. Optical Testing and Metrology, C.P. Grover, ed., SPIE Proc. Vol. 661, Society of Photo-Optical Instrumentation Engineers, Bellingham, WA, 1986, pp. 145-151.
- V-16. Adamovsky, G.; and Piltch, N.D.: Fiber-Optic Thermometer Using Temperature Dependent Absorption, Broadband Detection, and Time Domain Referencing. Appl. Opt., vol. 25, no. 23, Dec. 1, 1986, pp. 4439-4443.
- V-17. Adamovsky, G.: Referencing in Fiber Optic Sensing Systems. Optical Techniques for Sensing and Measurement in Hostile Environments, C.H. Gillespie and R.A. Greenwell, eds., SPIE Proc. Vol. 787, SPIE, 1987, pp. 17-23.
- V-18. Adamovsky, G.: Amplitude Spectrum Modulation Technique for Analog Data Processing in Fiber Optic Sensing System with Temporal Separation of Channels. Fiber Optic and Laser Sensors V, R.P. De Paula and E. Udd, eds., SPIE Proc. Vol. 838, Society of Photo-Optical Instrumentation Engineers, Bellingham, WA, 1987, pp. 264-270.
- V-19. Adamovsky, G.: Fiber Optic Displacement Sensor with Temporally Separated Signal and Reference Channels. Appl. Opt., vol. 27, no. 7, Apr. 1, 1988, pp. 1313-1315.

- V-20. Adamovsky, G.; and Maitland, D.J.: Fiber Optic Sensors with Internal Referencing. Optical Testing and Metrology II, C.P. Grover, ed., SPIE Proc. Vol. 954, Society of Photo-Optical Instrumentation Engineers, Bellingham, WA, 1989, pp. 647-651. (NASA TM-100893.)
- V-21. Adamovsky, G.; and Maitland, D.J.: Fiber Optic Sensing Systems Using High Frequency Resonant Sensing Heads with Intensity Sensors. NASA TM-101318, 1988.
- V-22. Beheim, G.; and Fritsch, K.: Remote Displacement Measurements Using a Laser Diode. Electron. Lett., vol. 21, no. 3, Jan. 31, 1985, pp. 93-94.
- V-23. Beheim, G.; and Fritsch, K.: Range Finding Using Frequency-Modulated Laser Diode. Appl. Opt., vol. 25, no. 9, May 1, 1986, pp. 1439-1442.
- V-24. Beheim, G.; and Anthan, D. J.: Loss-Compensation of Intensity-Modulating Fiber-Optic Sensors. NASA TM-88825, 1986.
- V-25. Beheim, G.: Fiber-Optic Interferometer Using Frequency-Modulated Laser Diodes. Appl. Opt., vol. 25, no. 19, Oct. 1, 1986, pp. 3469-3472.
- V-26. Beheim, G.: Loss-Compensation Technique for Fiber-Optic Sensors and Its Application to Displacement Measurements. Appl. Opt., vol. 26, no. 3, Feb. 1, 1987, pp. 452-455.
- V-27. Beheim, G.; and Anthan, D.J.: Fiber-Optic Photoelastic Pressure Sensor with Fiber-Loss Compensation. Opt. Lett., vol. 12, no. 3, Mar. 1987, pp. 220-222.
- V-28. Beheim, G.; Fritsch, K.; and Poorman, R.N.: Fiber-Linked Interferometric Pressure Sensor. Rev. Sci. Instrum., vol. 58, no. 9, Sept. 1987, pp. 1655-1659.
- V-29. Mercer, C.R.; and Beheim, G.: Active Phase-Compensation System for Fiber Optic Holography. NASA TM-101295, 1988.
- V-30. Beheim, G., et al.: Modulated-Splitting-Ratio Fiber Optic Temperature Sensor. NASA TM-101332, 1988.
- V-31. Fritsch, K.; and Beheim, G.: Wavelength-Division Multiplexed Digital Optical Position Transducer. Opt. Lett., vol. 11, no. 1, Jan. 1986, pp. 1-3.
- V-32. Beheim, G.; and Fritsch, K.: Spectrum-Modulating Fiber-Optic Sensors for Aircraft Control Systems. NASA TM-88968, 1987.
- V-33. Beheim, G.: Fiber-Optic Thermometer Using Semiconductor-Etalon Sensor," Electron. Lett., vol. 22, no. 5, Feb. 27, 1986, pp. 238-239.
- V-34. Beheim, G.; Fritsch, K.; and Anthan, D.J.: Fiber-Optic Temperature Sensor Using a Spectrum-Modulating Semiconductor Etalon. NASA TM-100153, 1987.

Directions in Propulsion Control

- VI-1. Hartley, T.T.; Melcher, K.J.; and Bruton, W.M.: Near Real-Time, Large Perturbation Simulation of Internal Fluid Flows, NASP TM-1062, 1989.
- VI-2. Wenzel, L.M.; Melcher, K.J.; and Bruton, W.M.: Experimental and Analytical Investigation of Special System Dynamic Behavior, NASP TM-1068, 1989.
- VI-3. Lorenzo, C.F.; and Cole, G.L.: Dynamics and Controls Aspects of Hypersonic Propulsion, First National Aerospace Plane Symposium, May 20-22, 1986, Langley Research Center, Hampton, VA.
- VI-4. Melcher, K.J.: Small Perturbation Dynamic Inlet Model for Real Time Simulation, NASP TM-1037, 1988.
- VI-5. Litt, J.S.: An Expert System for Restructurable Control. NASA TM-101378, 1988.
- VI-6. Weaver, A.C.; and Colvin, M.A.: A Real-Time Messaging System for Token Ring Networks. Software - Pract. Experience Mag., vol. 17, no. 12, Dec. 1987, pp. 885-897.
- VI-7. Peden, J.H.; and Weaver, A.C.: Are Priorities Useful in an 802.5 Token Ring? IEEE Trans. Ind. Electron., vol. 35, no. 3, Aug. 1988, pp. 361-365.
- VI-8. Peden, J.H.; and Weaver, A.C.: An Analytic Model of Priority Traffic on the IEEE 802.5 Token Ring. University of Virginia, Dept. Computer Science, Aug. 1987.
- VI-9. Peden, J.H.; and Weaver, A.C.: A Performance Model for Token Rings Using Reservation Priorities. University of Virginia, Dept. Computer Science, July 1987.
- VI-10. Colvin, A.; Donnelly, T.; Simoncic, R.; and Weaver, A.C.: Ethernet Performance Analysis. University of Virginia Computer Science Report RM-86-01, Mar. 1986.
- VI-11. Smith, M.; and Weaver, A.: Real-Time Communications on CSMA/CD Networks. University of Virginia, Dept. Computer Science, Dec. 1984.
- VI-12. Weaver, A.C.; and Summers, C.F.: Performance Measurement for Local Area Networks. University of Virginia, Computer Science Report RM-85-05, Oct. 1985.
- VI-13. Luck, R.; and Ray, A.: Observer Design for Compensations of Network-Induced Delays in Integrated Communication and Control Systems. Recent Advances in Control of Nonlinear and Distributed Parameter Systems, Robust Control, and Aerospace Control Applications, J. Bentsman and S. Joshi, eds., American Society of Mechanical Engineers, New York, 1988, pp. 175-182.
- VI-14. Halevi, Y.; and Ray, A.: Integrated Communication and Control Systems: Part I - Analysis. J. Dyn. Syst. Meas. Control, vol. 110, no. 4, Dec. 1988, pp. 367-373.

- VI-15. Ray, A.; and Halevi, Y.: Integrated Communication and Control Systems: Part II - Design Considerations. J. Dyn. Syst. Meas. Control, vol. 110, no. 4, Dec. 1988, pp. 374-381.
- VI-16. Ray, A.: Introduction to Networking for Integrated Control Systems. IEEE Control Syst. Mag., vol. 9, no. 1, Jan. 1989, pp. 76-79.
- VI-17. Merrill, W.C.: Sensor Failure Detection for Jet Engines Using Analytical Redundancy, J. Guid., Control Dyn., vol. 8, no. 8, Nov.-Dec. 1985, pp. 673-682.
- VI-18. Merrill, W.C.: HYTESS II - A Hypothetical Turbofan Engine Simplified Simulation with Multivariable Control and Sensor Analytical Redundancy. NASA TM-87344, 1986.
- VI-19. Merrill, W.C.; and DeLaat, J.C.: A Real-Time Simulation Evaluation of An Advanced Detection, Isolation and Accommodation Algorithm for Sensor Failures in Turbine Engines. NASA TM-87289, 1986.
- VI-20. Melcher, K.J., et al.: A Sensor Failure Simulator for Control System Reliability Studies. NASA TM-87271, 1986.
- VI-21. Merrill, W.C.; DeLaat, J.C.; and Bruton, W.M.: Advanced Detection, Isolation, and Accommodation of Sensor Failures - Real-Time Evaluation. NASA TP-2740, 1987.
- VI-22. Merrill, W.C.; et al.: Full-Scale Engine Demonstration of an Advanced Sensor Failure Detection, Isolation, and Accommodation Algorithm - Preliminary Results. AIAA Paper 87-2259, Aug. 1987 (NASA TM-89880).
- VI-23. Litt, J.S.; DeLaat, J.C.; and Merrill, W.C.: A Microprocessor-Based Real-Time Simulator of a Turbofan Engine. NASA TM-100889, 1988.
- VI-24. DeLaat, J.C.; and Merrill, W.C.: Advanced Detection, Isolation, and Accommodation of Sensor Failures - Real Time Microprocessor Implementation. NASA TP-2925, 1989 (to be published).
- VI-25. Brown, H.; Corley, R.C.; Elgin, J.A.; and Spang, H.A.: Sensor Failures, Detection and Isolation in Multi-Engine Aircraft. (R84AEB359, General Electric Co.; NASA Contract NAS3-23692) NASA CR-174846, 1985.
- VI-26. Akhter, M.M.; and Rock, S.M.: Modification and Evaluation of the HYTESS Model. NASA Contract NAS3-23724, 1987.
- VI-27. Emami-Naeini, A.; Akhter, M.M.; and Rock, S.M.: Robust Detection, Isolation and Accommodation for Sensor Failures. (SCT-85-5449, Systems Control Technology; NASA Contract NAS3-24079) NASA CR-174825, 1986.
- VI-28. Weiss, J.L., et al.: Robust Detection-Isolation-Accommodation for Sensor Failures. NASA CR-174797, 1985.
- VI-29. Merrill, W.C.; and Lorenzo, C.F.: A Reusable Rocket Engine Intelligent Control. AIAA Paper 88-3114, July 1988 (NASA TM-100963).

SESSION 5 - SUBSONIC PROPULSION TECHNOLOGY

OVERVIEW OF THE SUBSONIC PROPULSION
TECHNOLOGY SESSION

G. Keith Sievers

INTRODUCTION

NASA is conducting aeronautical research over a broad range of Mach numbers. In addition to the generic and high-speed propulsion research described in separate sessions of this conference, the Lewis Research Center is continuing its substantial efforts towards propulsion technology for a broad range of subsonic flight applications. This session reviews some of the results from that program, including small engine technology, rotorcraft, icing research, hot section technology, and the Advanced Turboprop Project as major elements.

SUBSONIC PROPULSION TECHNOLOGY

Small Engine Technology Programs

Ongoing small engine programs are indicated in figure 1. The Automotive Gas Turbine (AGT) program is sponsored by the Department of Energy (DOE), and the Compound Cycle Turbine Diesel (CCTD) program is sponsored by the Army. There is a strong element of synergism between the various programs in several respects.

All the programs include research in high-temperature structural ceramics. This research tends to be generic in nature and has broad applications. The rotary technology and the CCTD programs are examining approaches to minimum heat rejection, or "adiabatic" systems employing advanced materials. The AGT program is also directed toward applications of ceramics to gas turbine hot-section components.

Turbomachinery advances in the gas turbine programs will benefit advanced turbochargers and turbocompounders for the internal combustion (IC) system, and the fundamental understandings and analytical codes developed in the research and technology (R&T) programs will be directly applicable to the system projects.

The chart in figure 2 shows opportunities for future major thrusts in small engine technology. Advanced cycles will be examined which offer the potential of large reductions in specific fuel consumption (SFC). New and enhanced computational tools will be developed, verified, and applied to advanced concepts to provide highly advanced, efficient, durable components. Advanced materials, such as ceramics and metal-matrix composites, will be applied to achieve maximum performance and life from the advanced engine concepts.

Rotorcraft Transmissions

Ongoing efforts involve computer code development and validation as well as analysis and optimization of components and full-scale transmissions (fig. 3). New tooth forms and gear materials are being investigated for operation at higher temperatures and loads. Advanced transmission concepts (split-torque, bearingless planetary) are being explored for reduced weight and noise as well as increased life and reliability.

Aircraft Icing Research Program

The NASA aircraft icing research program (fig. 4) has two major technology thrusts: (1) development of advanced ice protection concepts and (2) development and validation of icing simulation techniques (both analytical and experimental). Technology is being developed that is applicable to both fixed and rotary wing aircraft.

Engine Hot Section Technology

The activities of the NASA Turbine Engine Hot Section Technology (HOST) Project (fig. 5) are directed toward durability needs, as defined in industry, and a more balanced approach to engine design. The HOST efforts will improve the understanding and prediction of thermal environments, thermal loads, structural responses, and life by focused experimental and analytical research activities. The overall approach is to assess existing analysis methods for strengths and deficiencies, to incorporate state-of-the-art improvements into the analysis methods, and finally to verify the improvements by benchmark quality experiments.

Advanced Turboprop Project

Figure 6 shows the overall content of the Advanced Turboprop Project in the areas of single rotation, gearless counterrotation, and geared counterrotation, and the flow into the area of advanced concepts. Figure 7 shows the major contractual elements of the Advanced Turboprop Project: the Large-Scale Advanced Propeller Project, the Propfan Test Assessment Project, the Unducted Fan Project, and the Advanced Gearbox Technology Project.

The four current flight test programs with advanced turboprops are shown in figure 8, and an artist's conception of potential near-term applications in commercial and military aircraft is shown in figure 9.

Propeller Research

Figure 10 shows the ongoing propeller research program of analysis and scale-model wind tunnel test verification leading to aerodynamic, acoustic, and structural code development. Advanced concepts of a single-rotation propfan with stator vane swirl recovery and a high-bypass-ratio ducted-fan configuration are illustrated.

High-Bypass Engines

Figure 11 shows the potential reduction of SFC for propulsion systems using ducted props and propfans as compared to high-bypass turbofans. Although the ducted props will not have the efficiency of unducted propfans, they are more suitable for "packaging" on large aircraft such as the B-747.

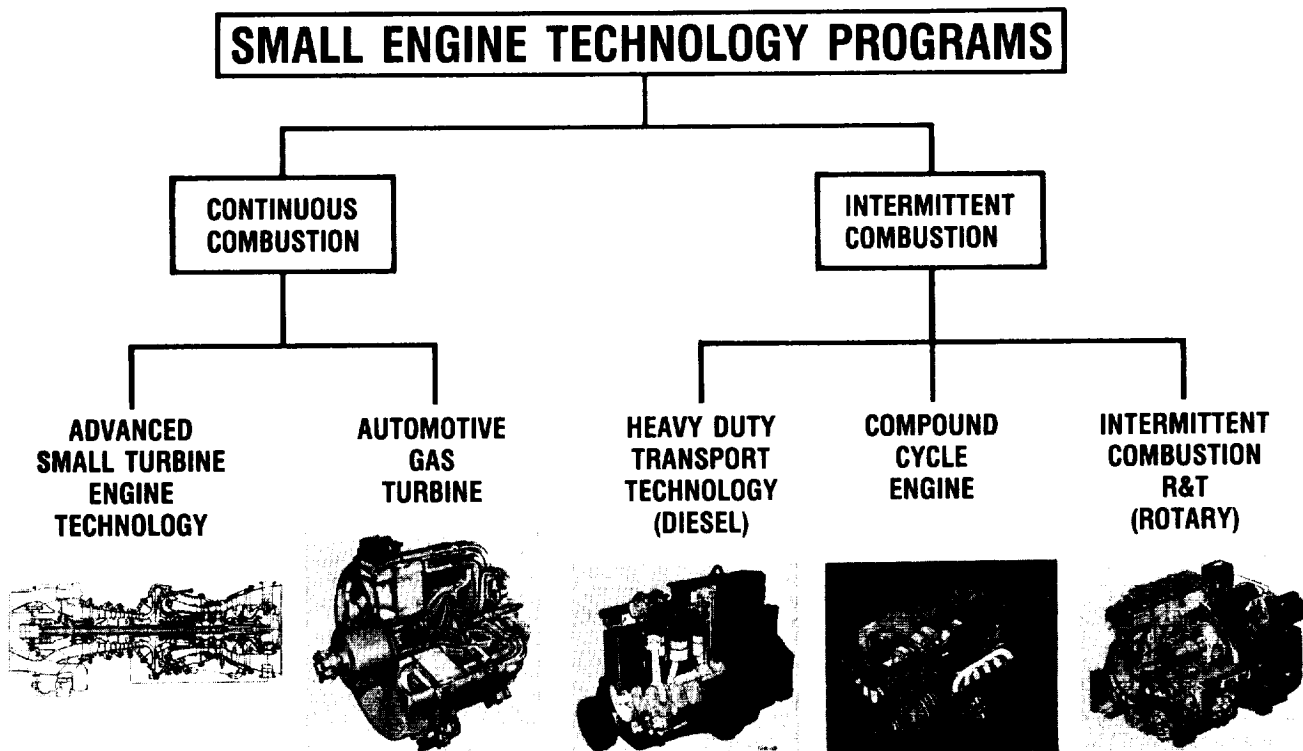


Figure 1. - Small engine technology programs.

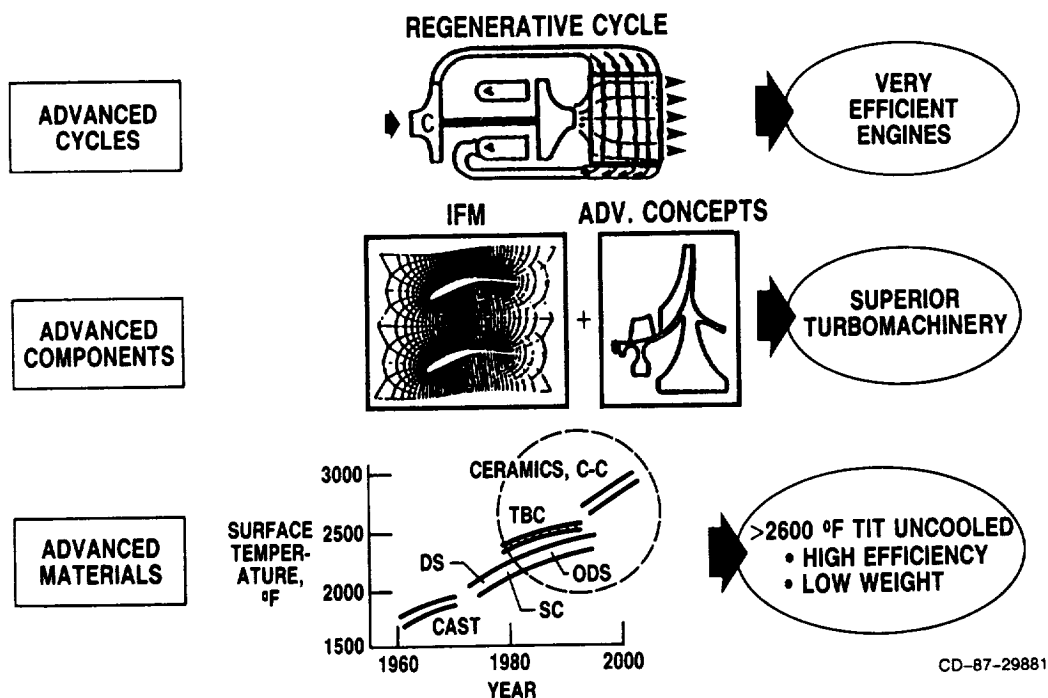
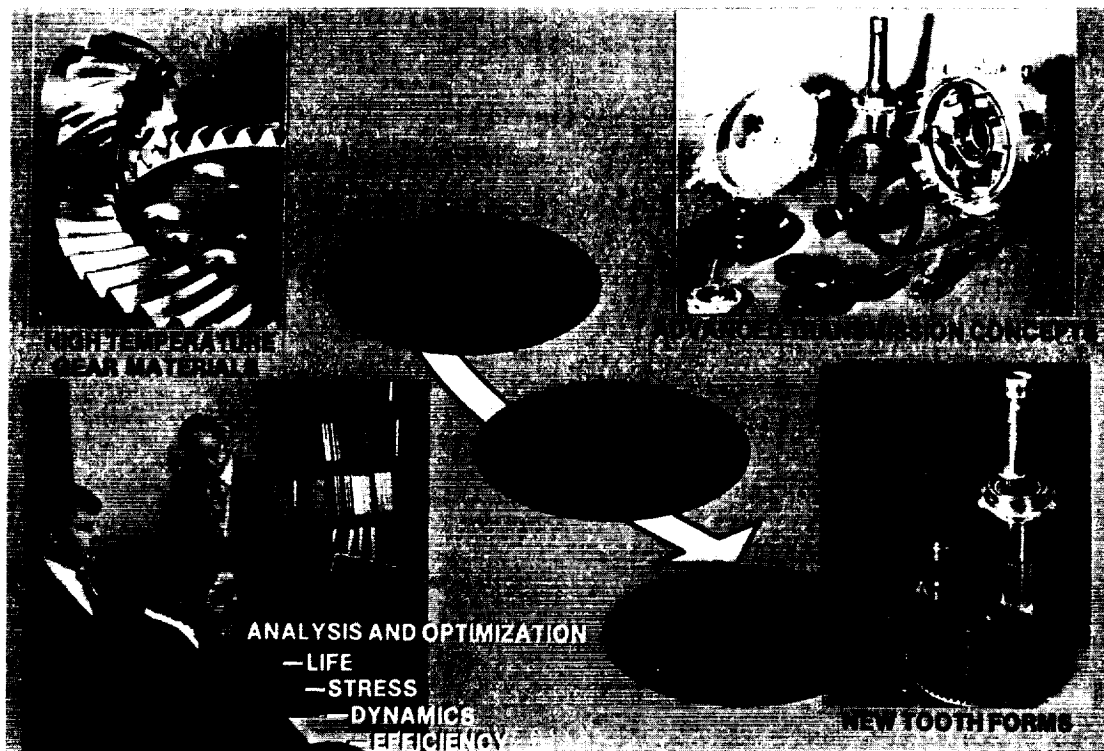
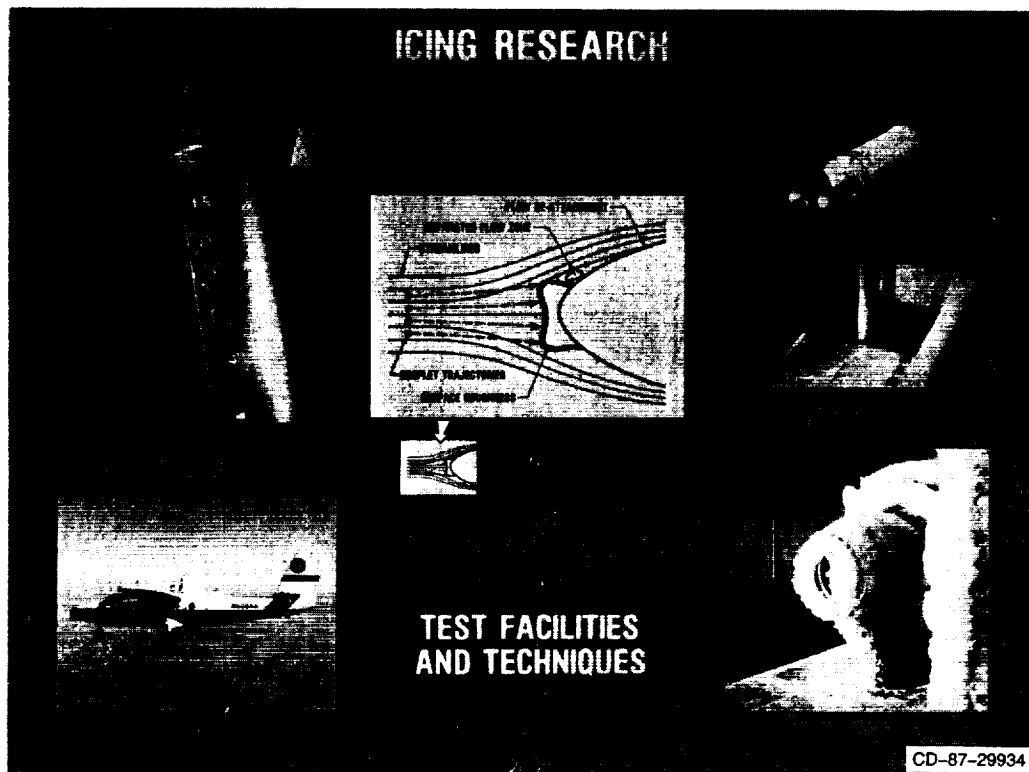


Figure 2. - Small engine technology thrusts.



CD-87-29883

Figure 3. - Rotorcraft transmissions.



CD-87-29934

Figure 4. - Aircraft icing research program.

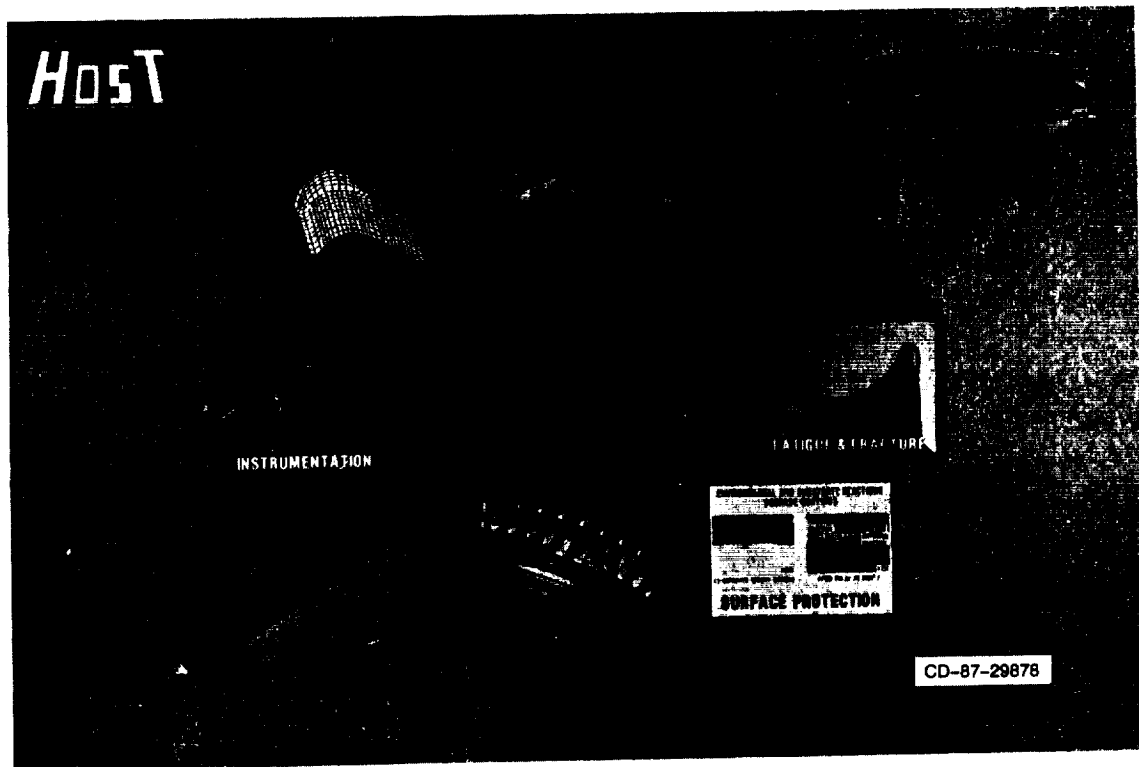


Figure 5. - Engine hot section technology.

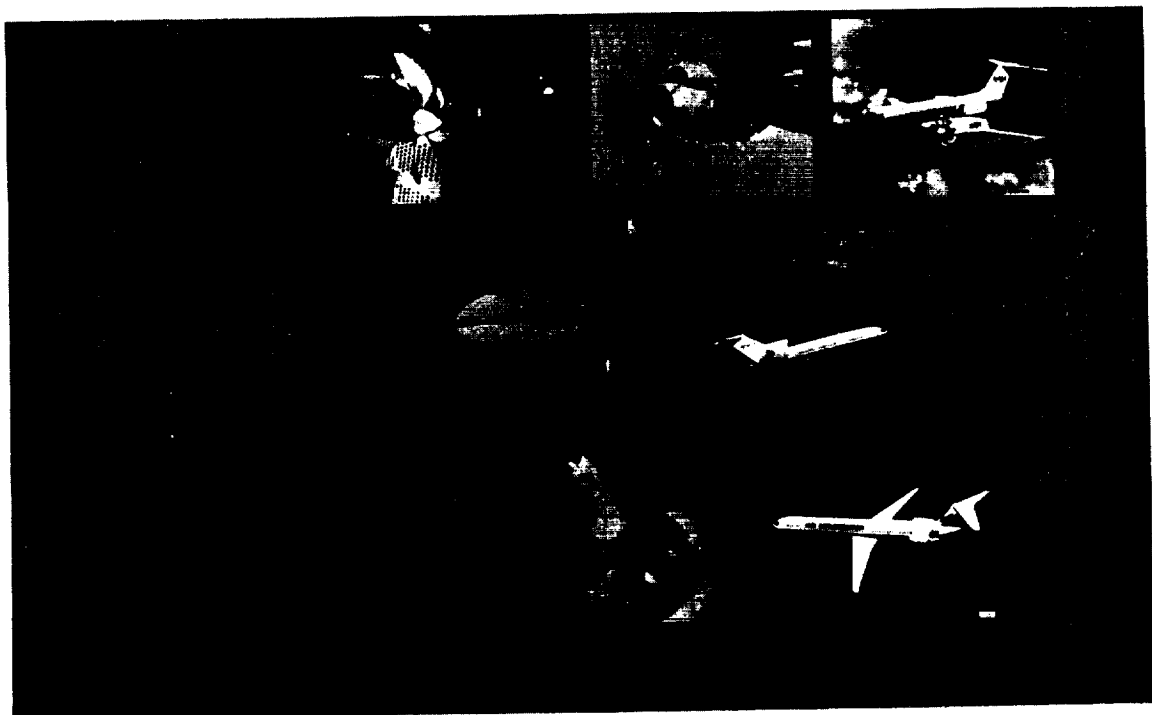


Figure 6. - Advanced Turboprop Project.

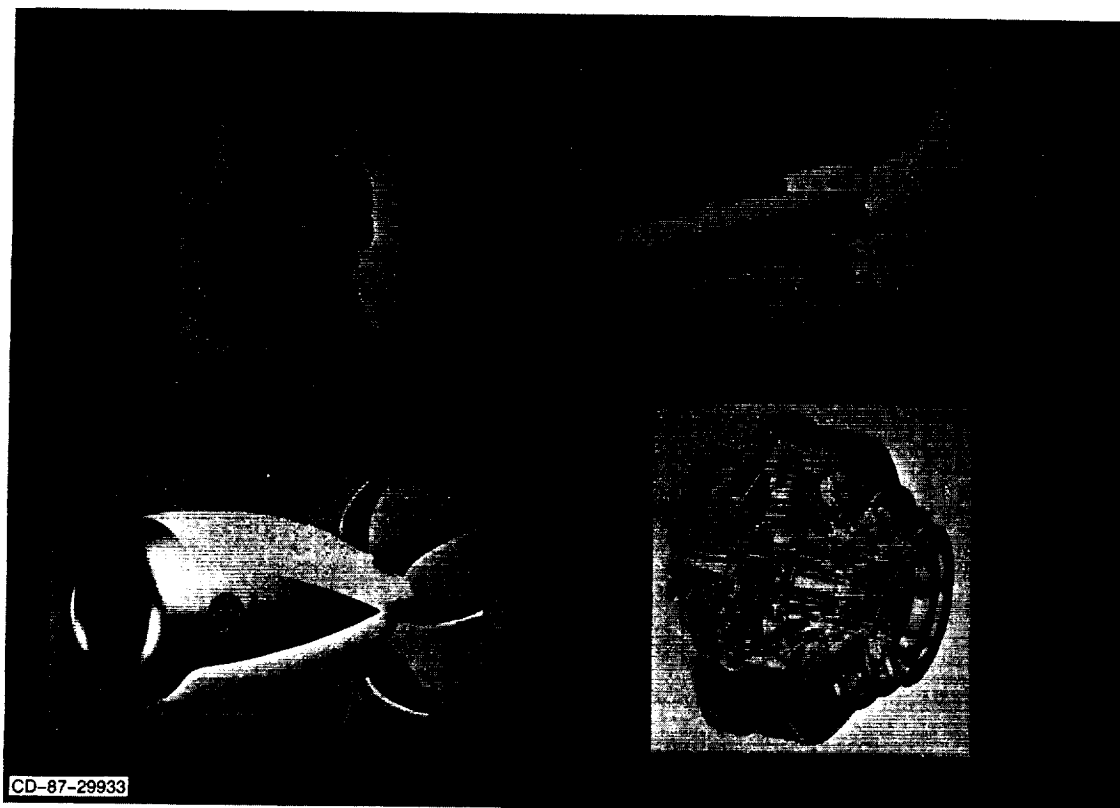


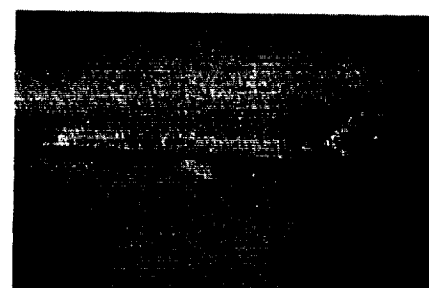
Figure 7. - Major contractual elements of the Advanced Turboprop Project.



PTA/GULFSTREAM GII



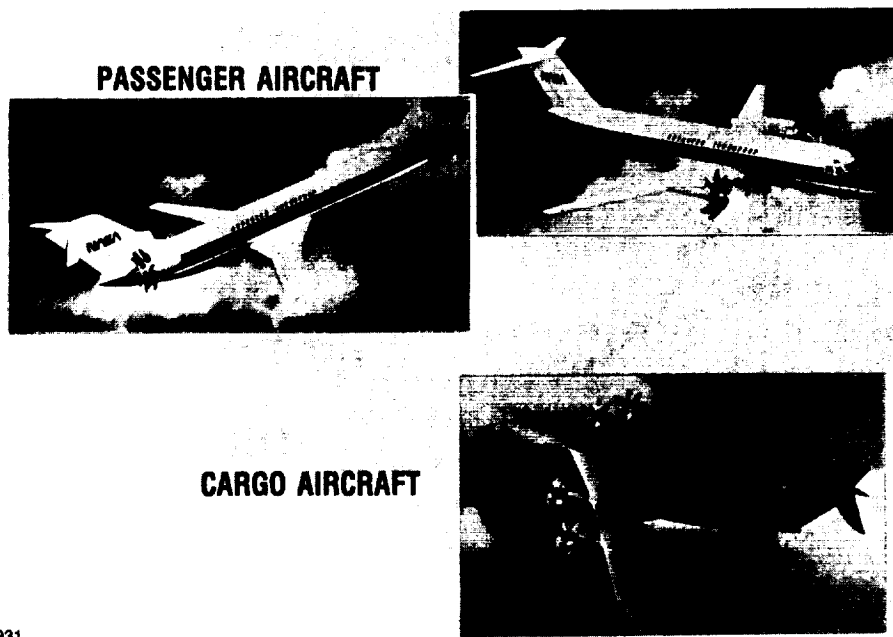
UDF/BOEING 727



**UDF/MD-80
578DX/MD-80**

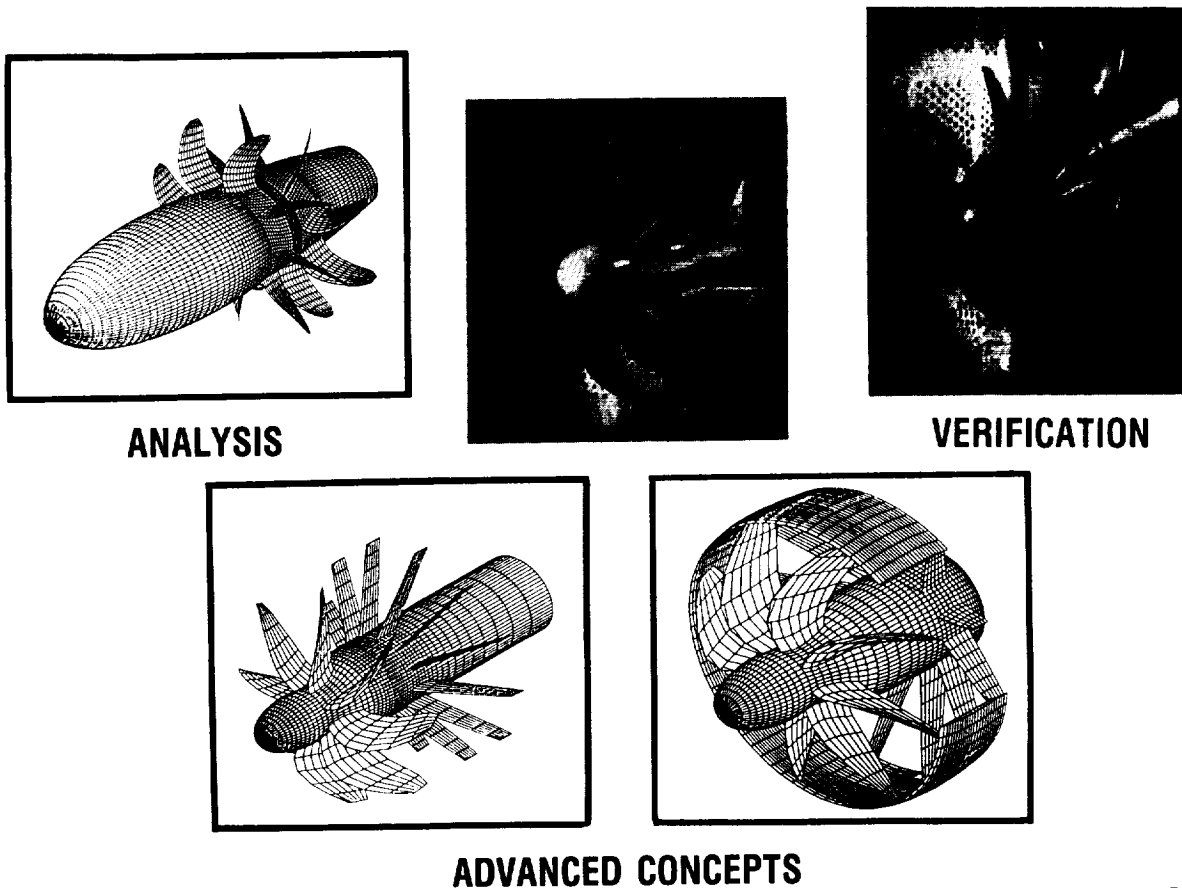
Figure 8. - Flight testing of advanced turboprops.

CD-87-29932



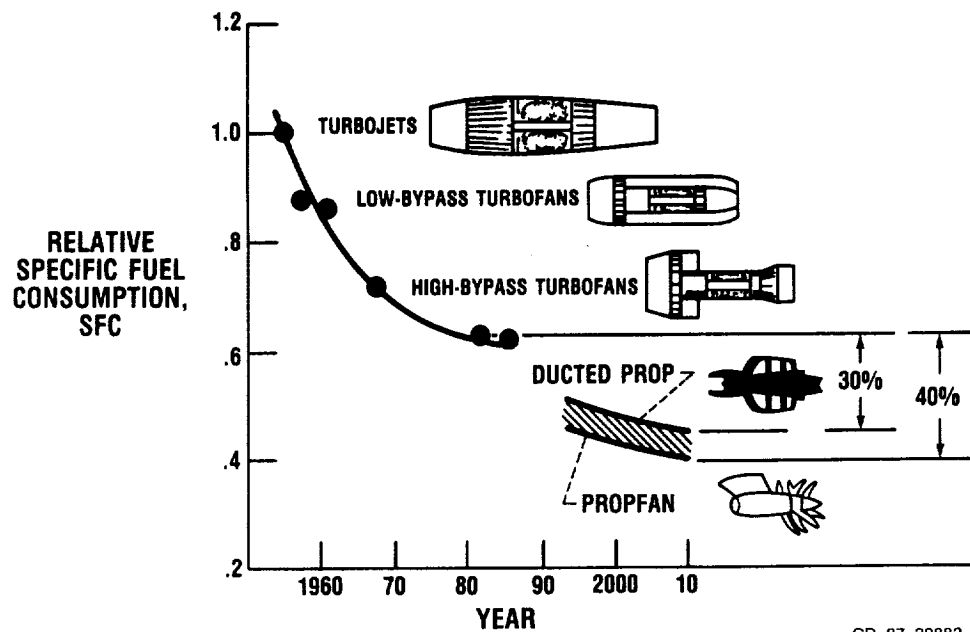
CD-87-29931

Figure 9. - Advanced turboprop applications.



CD-87-29930

Figure 10. - Propeller research.



CD-87-29882

Figure 11. - Specific fuel consumption for various propulsion systems.

SMALL ENGINE TECHNOLOGY PROGRAMS

Richard W. Niedzwiecki

SUMMARY

This paper describes small engine technology programs being conducted at the NASA Lewis Research Center. Small gas turbine research, cosponsored by NASA and the Army, is aimed at general aviation, commutercraft, rotorcraft, and cruise missile applications. The Rotary Engine program is aimed at supplying fuel flexible, fuel efficient technology to the general aviation industry, but also has applications to other missions. The Automotive Gas Turbine (AGT) and Heavy-Duty Diesel Transport Technology (HDTT) programs are sponsored by the Department of Energy (DOE). The Compound Cycle Engine program is sponsored by the Army. There is a strong element of synergism between the various programs in several respects. All of the programs are aimed towards highly efficient engine cycles, very efficient components, and the use of high-temperature structural ceramics. This research tends to be generic in nature and has broad applications. The HDTT, rotary technology, and the compound cycle programs are all examining approaches to minimum heat rejection, or "adiabatic" systems employing advanced materials. The AGT program is also directed towards ceramics application to gas turbine hot section components. Turbomachinery advances in the gas turbine programs will benefit advanced turbochargers and turbocompounders for the intermittent combustion systems, and the fundamental understandings and analytical codes developed in the research and technology programs will be directly applicable to the system projects.

INTRODUCTION

Ongoing and proposed small engine programs are indicated in figure 1. The Automotive Gas Turbine (AGT) and Heavy-Duty Diesel Transport Technology (HDTT) programs are sponsored by DOE, and the Compound Cycle Turbine Diesel (CCTD) by the Army. There is a strong element of synergism between the various programs in several respects.

All of the programs presently include or will include research in high-temperature structural ceramics. This research tends to be generic in nature and has broad applications. The HDTT, the rotary technology, and the CCTD are all examining approaches to minimum heat rejection, or "adiabatic" systems employing advanced materials. The AGT program is also directed towards ceramics application to gas-turbine hot-section components.

Turbomachinery advances in the gas turbine programs will benefit advanced turbochargers and turbocompounders for the intermittent combustion systems, and the fundamental understandings and analytical codes developed in the R&T programs will be directly applicable to the system projects.

SMALL ENGINE EFFICIENCY

Previous investments in technology have led to significant efficiency gains for large engines. These gains have resulted from improved cycles, components, and materials. However, much of these technologies has not been transferable to smaller engines (fig. 2). As engine power size decreases, performance decreases because of the combined effects of increased relative clearances, lower Reynolds number, increased relative surface roughness, and other factors. These adverse effects are particularly noticeable below 200 shaft horsepower (shp). Small engines employ different component configurations such as centrifugal compressors, reverse flow combustors, and radial turbines to minimize these effects. Future large turbofan engines designed for ultrahigh bypass ratios and higher cycle pressure ratios (greater than 50:1) will be limited in performance by some of the same size related problems which presently limit the performance of the small engines. This is a result of the inherent reduction in core engine flow size associated with the higher bypass ratio and the higher core pressure ratio, all of which reduces the turbomachinery size and the combustor length and volume. To counter the losses associated with the small turbomachinery blading, such things as replacing the back stages of the typically all-axial compressors with a centrifugal stage is now being considered, following the same trends as for small engines.

SMALL ENGINE TECHNOLOGY OPPORTUNITIES

Small engines are used in a broad spectrum of aeronautical applications including helicopters, commuters, general aviation airplanes, and cruise missiles. In exploring engine types to satisfy these applications it has been determined that all of the engine types being researched have the potential of significantly improved efficiency. Shown in figure 3 is a plot of thermal efficiency and shaft horsepower. Gas turbines are considered prime candidates for horsepower ranges of 500 shp and higher. Their potential in efficiency improvement, over current engines, is of the order of 50 percent. The sources of this improvement will be presented later. The rotary engine is considered a prime candidate for missions up to 500 shp, but is not limited to that size range. Their potential for efficiency improvement is similar to the gas turbine. The compound cycle diesel is being considered for missions requiring engines in the 750 to 2000 shp class. Their potential for improvement is comparable to the other engine types being researched. The chart in figure 4 illustrates the reasons for the keen military interest in substantially reducing specific fuel consumption (SFC) of their engines.

Many programs proposed previously have tended to be "evolutionary," focused on incremental improvements in component capabilities. This objective reflects our intent to establish a program which will lead to a major advance in small engine technology. Our target is to improve fuel consumption by 40 percent and to reduce DOC by 10 percent through the use of improved materials and design concepts. We believe that "revolutionary" powerplant improvements will have a truly significant impact, and will lead to a new generation of airframes with greatly expanded capabilities.

SMALL ENGINE COMPONENT TECHNOLOGY (SECT) STUDIES

The Small Engine Component Technology (SECT) studies were conducted, under joint NASA/Army funding, to provide a critical assessment by the small turbine industry on the technology needs for the year 2000 engines. The results of the studies will have a significant impact on the technology to be pursued in future programs. Study contractors were Allison, Avco Lycoming, Garrett, Teledyne CAE, and Williams International. General Electric and Pratt & Whitney also conducted parallel studies and made the results available for the technology assessments. Missions studies included rotorcraft in the 500 to 1000 hp size; general aviation/commuter missions in the 500 to 1000 hp size; auxiliary power units in the 300 to 500 hp size; and cruise missiles in the 200 to 1000 lb T size.

Study results in terms of benefits, high-payoff research areas, and national benefits achieved from the evolved research are shown in the chart in figure 5 for the various missions. Other component technologies identified as critical to achieving significant fuel savings and DOC/LCC reductions include bearings, shafts, seals, gearboxes, and slurry fuel combustion for the cruise missile engines.

IMPACT OF ADVANCED TECHNOLOGY ON CYCLE PERFORMANCE

Figure 6 presents two engine performance maps. The top map presents the performance for a state-of-the-art (SOA) 800-shp (uninstalled) simple-cycle gas turbine. It is used as a reference for comparison to advanced cycles. A turbine inlet temperature of 2200 °F and a pressure ratio of 14:1 were assumed as representative for the SOA engine. In addition, SOA component efficiencies and combustor/turbine cooling requirements were assumed. The brake specific fuel consumption (BSFC) for these conditions is approximately 0.43 lb/shp-hr and specific power approximately 180 shp/lb/sec.

The bottom engine map presents the performance for an advanced simple cycle for comparison to the SOA. For the advanced engine, advanced component efficiencies were assumed, together with higher operating pressures to 24:1, higher temperatures to 2600 °F, and uncooled ceramics. The advanced BSFC of 0.36 lb/hp-hr is 17 percent less than the SOA, and its specific power is 55 percent higher. Of the 17 percent improvement, 8 percent is attributed to advanced component efficiencies, 4 percent is due to the higher cycle pressure, temperature, and reduced turbine coolant penalty, and 5 percent results from totally eliminating the coolant penalty by using uncooled ceramics. Uncooled ceramics also have the potential for reducing costs.

Figure 7 presents the performance for an advanced regenerated cycle in comparison with the state-of-the-art simple cycle and the advanced simple cycle. Again, advanced component efficiencies were assumed, together with the high turbine inlet temperature of 2600 °F and uncooled ceramics. In terms of BSFC, the advanced regenerated cycle provides the potential for a very significant 37 percent reduction over the state-of-the-art simple cycle and some increase in specific power. Note, however, that the optimum cycle pressure ratio for the regenerated cycle is much lower than that for the advanced simple

cycle and results in fewer compression stages required. Regenerative cycles could utilize either a rotary regenerator or a stationary recuperator.

Although these potential performance gains are quite large, they must be examined in a representative mission model, taking into consideration projected changes in engine size, weight, cost, and other factors before the real benefit of the advanced small engine technology program can be assessed. Because of the diversity of small engine applications, several representative missions have been selected for study.

COMPRESSOR EFFICIENCY

The curve in figure 8 was derived from actual data. It is a plot of compressor polytropic efficiency as a function of compressor exit corrected flow in pounds per second. The solid line represents advanced, current technology. The 10-lb/sec efficiency value of 92 percent is energy efficient engine data. As shown, reducing flow size causes significant decreases in efficiency, until at 1 lb/sec the efficiency drops to approximately 78 percent. Identifying the causes for the efficiency falloff and minimizing their effects are major thrusts of the compressor program. Aggressive program goals are indicated by the dashed line.

COMPRESSOR TECHNOLOGY PROGRAM

Major thrusts of the compressor technology program are the following (fig. 9):

- (1) Doing axial and centrifugal compressor research to achieve higher pressure ratios, increased efficiency, and reduced number of stages with higher loading per stage
- (2) Quantifying and minimizing performance degradation factors accruing with reductions in flow size
- (3) Evolving improved design techniques through the development of improved analytical models and codes
- (4) Verifying and improving analytical models through the use of advanced diagnostics including laser anemometry

The Scaled Centrifugal Compressor program described in figure 10 was conducted to determine performance degradation with flow size. A 25-lb/sec centrifugal compressor was scaled down to a 10-lb/sec size. It was then attempted to scale the 10-lb/sec compressor down to a 2-lb/sec size. This was not possible, principally because of the wall thickness. A 2-lb/sec "doable" compressor was then designed and scaled to the 10-lb/sec size. Research was then conducted with thin- and thick-blade 10-lb/sec compressors and the thick-blade 2-lb/sec compressor wheels. The performance degradation factors shown in figure 11 were quantified for the three compressor wheels. Results were reported at the San Diego AIAA meeting.

Figure 12 shows the peak efficiency loss that occurs as the Reynolds number is varied for the 2-lb/sec and 10-lb/sec centrifugal compressors. The data from both compressors fall along a straight line. This indicates that the scaling laws hold within this size range. One of the problems in designing efficient small compressors is that they operate at lower Reynolds numbers which inherently produce increased inefficiency.

TURBINE EFFICIENCY

Figure 13 is a plot of turbine efficiency as a function of turbine inlet corrected flow. Figure 13(a) is for gas generator turbines. The dashed line represents current gas generator turbine technology for axial turbines. Actual data were used to construct this plot, with the higher flow rate incorporating energy efficient engine data. As can be seen, an efficiency dropoff of over 4 percent occurs as size is reduced. The top, shaded-in curve represents program goals for axial turbines. It also represents radial turbine data. Although they are very efficient, radial turbines are not currently on flying engines because other technologies they require have not evolved. The prime technology need for radial turbines is a method for satisfactorily cooling them. Figure 13(b) represents the current state of the art for axial power turbines (dashed line). Program goals are shown by the solid line.

SMALL TURBINE ENGINE TECHNOLOGY PROGRAM

Figure 14 displays the principal thrusts of the turbine program. Both axial and radial turbine research are being pursued, with the emphasis on radial turbines. The general approach of identifying, quantifying, and minimizing loss mechanisms (which occur with decreasing size, evolution of improved analytical codes for turbine design, and verification of the improved codes through the implementation of advanced diagnostics) is similar to that described previously for compressors.

Figure 15 summarizes progress achieved under a joint NASA/DOE project. The work consisted of an advanced structural analysis code applicable to the design of high-temperature structural ceramic engine components. Currently, the code is in the process of being verified. However, even at this early stage, the code has been applied to radial turbine wheels with the results being used to identify the most promising concepts.

Small Warm Turbine Test Facility

The modern facility shown in figure 16 can evaluate the aerodynamic and cooling performance of small and medium size axial, radial, or mixed-flow turbines while duplicating all significant similarity parameters. Unique instrumentation includes onboard rotor measurements of pressure and temperature, flow surveys between blade rows during stage operation, and a high-speed in-line torque meter. The main facility operating parameters are as follows: inlet temperature, 800 °F; coolant temperature, -50 °F; inlet pressure, 125 psig; flow rate, 10 lbm/sec; speed, 60 000 rpm; and power absorption, 1250 hp.

NASA/Allison Cooled Radial Turbine

A cooled high-temperature radial turbine (fig. 17) will be experimentally evaluated in a warm turbine test facility at the NASA Lewis Research Center. The turbine is designed with an uncooled ceramic stator with an inlet temperature of 2500 °F and mass flow of 4.56 lbm/sec. The rotor is designed with 4.5 percent cooling air, a work level of 185 Btu/lbm, and an efficiency of 86 percent. Three-dimensional heat transfer and aerodynamic analyses were performed on the turbine. These predictions will be verified by comparison with experimental results. Detailed measurements of temperature and pressure will be made on the rotor surface and within the cooling channel. Verifying the region of separation along the hub of a radial turbine and predicting rotor blade temperatures are of particular importance in future turbine designs.

SMALL COMBUSTOR TECHNOLOGY

Small gas turbine combustors currently operate at efficiencies near 100 percent at all landing-takeoff cycle operating conditions - efficiency is not a problem. However, advanced cycle engines will require increased temperature and pressure capability, reduced air coolant requirements for liners, and increased durability of injectors and liners. The research program in place is addressing all of those needs. Also required will be combustion systems which produce uniform exit temperature distributions - approximately twice the uniformity currently achievable.

Numerous small combustor types are employed. Three are shown in figure 18. Axial combustors are scaled-down versions of large combustors. Flow proceeds axially through the combustor. Reverse flow combustors are the most common variety. Compressor discharge air exhausts into a plenum, which then feeds the various combustor zones according to a preset schedule. This combustor design is popular because it packages well in small engines. However, it also has the greatest amount of hot-section surface area, liners, and reverse flow turn, and is thus the most difficult to cool. Radial outflow combustors are reverse flow types but contain several significant differences. They usually increase in volume radially, and fuel is injected through the spinning shaft. Thus fuel injectors are not required. This combustor type is used in cruise missile engines.

A recent combustion research accomplishment is shown in figure 19. An advanced combustor liner, the ceramic matrix, was developed. This combustor utilizes only backside cooling air - no chargeable air injected through the liner is required for keeping the liner within temperature limits. The concept employs a thick ceramic coating impregnated on a pliable felt metal. The pliable metal reduces stresses imposed on the ceramic, and supplies a heat shield to confine combustion temperatures. Short-duration performance tests of this concept were conducted to over 2600 °F, which is 300 to 400 °F hotter than current combustor temperatures. Current activities are underway in-house and under an Army contract to optimize the implementation of this concept.

DOE/NASA ADVANCED GAS TURBINE TECHNOLOGY

The Automotive Gas Turbine (AGT) program (fig. 20) began in 1980. Fiscal year 1986 was the final funding year, though funds were expended through fiscal year 1987. Also in fiscal year 1987 a new program was initiated; this will be described later in this section.

Figure 21 illustrates the Allison AGT 100 test bed engine. This regenerated, two-shaft engine has a maximum rotor speed to 86 000 rpm and has been operated to 2100 °F for 6 hour.

Figure 22 illustrates the ceramic components incorporated in the Allison engine. Similar components were also fabricated and tested in the Garrett engine. Ceramic materials used were silicon carbides, silicon nitrides, aluminum silicates and zirconias. Numerous contractors, both U.S. and foreign, were used to supply ceramic parts. Some of the contractors were Standard Oil, Norton, GTE Labs, AiResearch Casting, Corning, Coors, Pure Carbon, and AC Spark Plug. Development of new technologies and capabilities has been restricted to U.S. corporations. This approach, which will be continued in the future, has led to a significant improvement in national production capability. This capability is essential in applying ceramics of sufficiently high quality for both automotive and aeronautical missions.

In addition to providing viable alternatives to the automotive industry, much of the technology evolved is also applicable to aeronautical missions. This is especially true of the ceramics and composites research, the analytical design tools, and the component fabrication processes and procedures.

Figure 23 shows an all-ceramic Garrett AGT 101 engine that has been operated for 85 hours at 2200 °F. At that point, rotor damage was sustained. These results illustrated both the promise of ceramic components as well as the need for future research to develop long-life components.

The FY 1987 new start program, the Advanced Turbine Technology Applications Project (ATTAP), focuses on ceramic technology development. Major technological thrusts of the program are high-temperature structural ceramics, high-temperature heat exchangers, low-emission combustors, high-temperature bearings, and small, efficient turbomachinery. The goal of this program, which includes 5-year cost share contracts with Allison and Garrett, is to develop and demonstrate structural ceramic components in an automotive turbine engine environment up to 2500 °F peak temperature conditions.

ROTARY ENGINES

The target of the rotary engine program (fig. 24) is to improve fuel consumption by 40 percent, and to reduce engine weight while providing multifuel (jet fuel) for general aviation and other small engine aeronautical missions.

Rotary engines offer several advantages over piston engines for small engine aircraft applications. These include the following:

(1) They are potentially more fuel efficient.

(2) They are inherently more fuel flexible. Their implementation and operation with jet A fuel could make aviation gasoline obsolete.

The rotary program includes large contractual activities with John Deere Co. as well as grants and contracts with MCI, MTU, ADAPCO, Adiabatics, PDA Engineering, and MIT. Understanding the combustion processes and evolving the technology for advanced combustion systems are the key to advanced, high-performance rotary engines.

Advanced, fuel-efficient rotary engines will require evolution of lightweight rotors and housing, adiabatic components, and turbocompounding. Figure 25 summarizes recent progress with the NASA/Deere stratified-charge rotary engine and indicates program goals. The parameter used is brake specific fuel consumption. In 1986, initial tests with a high-speed electronic fuel control produced BSFC values to 0.51. In fiscal year 1987, BSFC was reduced to 0.46 through application of validated combustor cones and optimization of the electronic fuel control system. The overall BSFC goal is 0.35 at 160 hp and 8000 rpm. To achieve this goal turbocompounding, adiabatic components, and a lightweight rotor, with reduced friction, will be required.

COMPOUND CYCLE ENGINE

The Compound Cycle Engine (fig. 26) program is planned in three parts:

(1) Part 1, currently in progress, is aimed at establishing the technology base for a long-life diesel core. Activities focus on single-cylinder diesel research.

(2) Part 2 is aimed at validating life, minimizing heat rejection losses, optimizing intercylinder dynamics, and verifying diesel performance predictions.

(3) Part 3 will demonstrate the integrated turbine/diesel system concept and performance.

Since the program is in its initial phases, no engine currently exists. Figure 27 is a sketch illustrating main features of an application of the technology. It is anticipated that the gas turbine components technologies will be available from the small gas turbine program. The flow diagram illustrates the features of the integrated cycle.

Planned operation is as follows. Flow goes into the compressor (10.6:1) and through an aftercooler. The aftercooler reduces the air temperature to the cylinder thus lowering ring reversal and exhaust valve temperatures. (Most importantly, it will enhance life.) The exhaust from the diesel cylinder then goes to the gas generator and power turbines. Approximately one-fourth of the power is generated by the turbomachinery and three-fourths by the diesel.

DOE/NASA HEAVY-DUTY TRANSPORT TECHNOLOGY PROJECT

The Heavy-Duty Transport Technology Project (fig. 28) is DOE funded and technically managed by NASA. Program activities are being performed almost entirely under grant and contract. Key problem areas requiring research are exhaust gas heat recovery, adequate piston seals, low emission performance, engine friction and wear, and thermal insulation implementation.

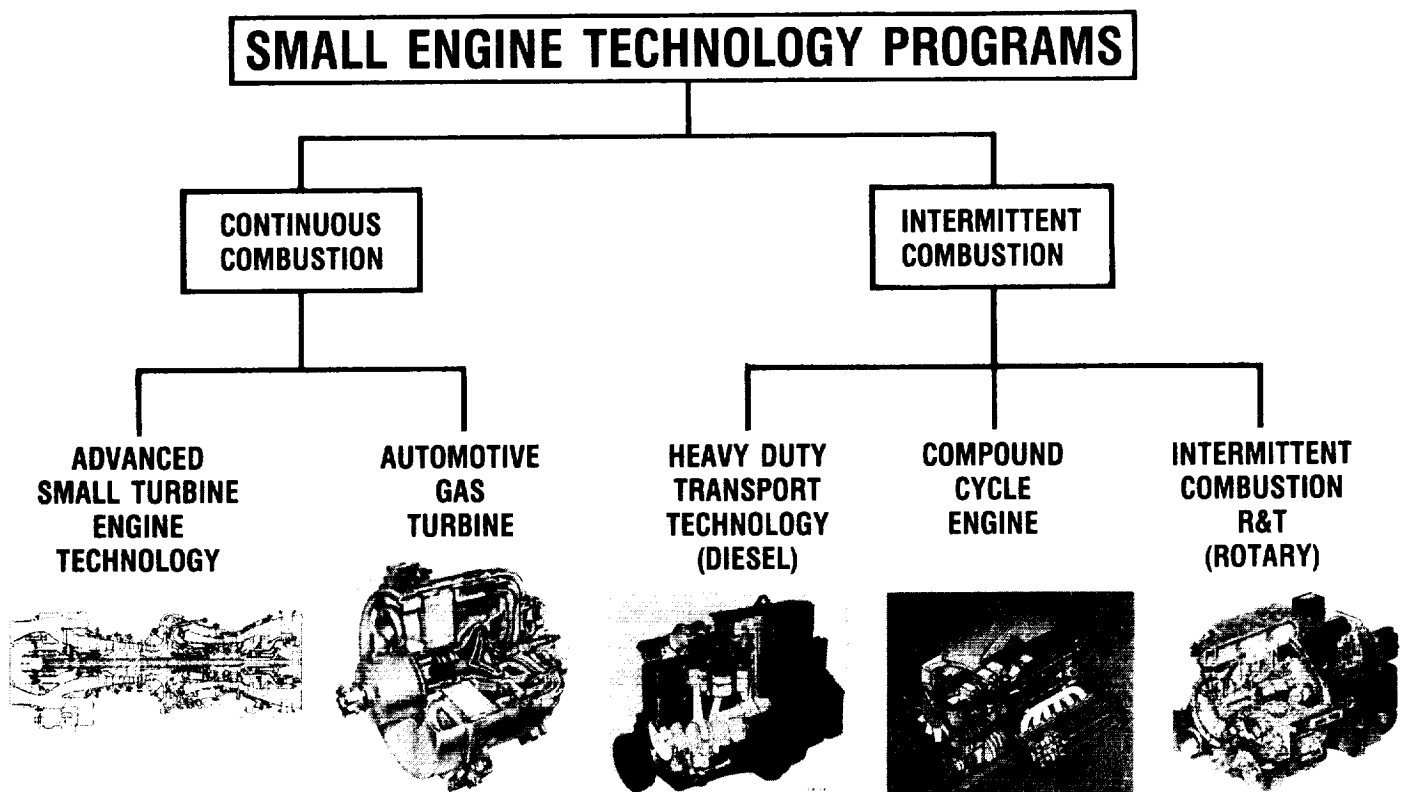
There exists much synergism between this program and the aeronautics programs - especially the Compound Cycle Engine program. Areas where much technology transfer is expected to occur are as follows:

(1) Thermal barrier coatings for heavy-duty diesel engines. Preliminary results indicate that plasma-sprayed coatings are viable alternatives to monolithic ceramics for in-cylinder insulation in the adiabatic diesel of the future.

(2) Evolution of piston ring/cylinder liner materials for advanced diesel engines. Ten candidate materials have been evaluated to date. Of those, K-162B and TIC had the lowest wear rates. They generated pseudo-lubricants. K-162B had the lowest dynamic friction coefficient.

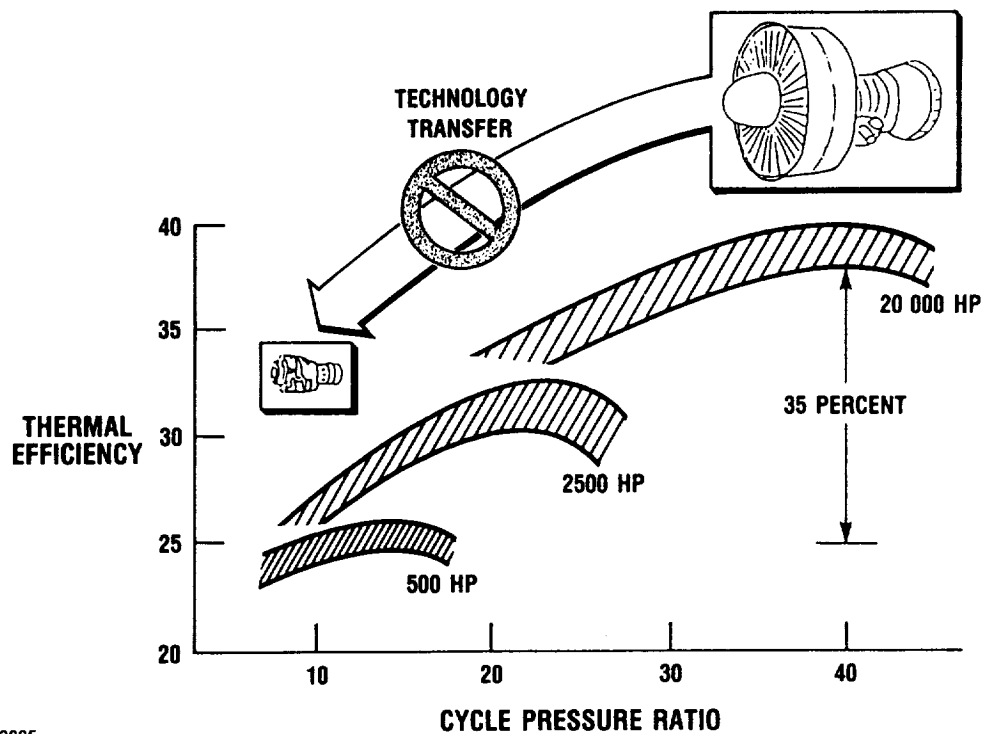
SMALL ENGINE RESEARCH SUMMARY

A summary of the small engine programs being conducted at Lewis Research Center is given in figure 29. Although each of these programs has specific objectives, there is a strong element of synergism between the various programs in several respects. All of the programs presently include or will include research in high-temperature structural ceramics. This research tends to be generic in nature and has broad applications. The HDTT, the rotary technology and the CCTD are all examining approaches to minimum heat rejection, or "adiabatic" systems employing advanced materials. The AGT program is also directed towards ceramics application to gas turbine hot-section components. Turbomachinery advances in the gas turbine programs will benefit advanced turbochargers and turbocompounders for the intermittent combustion systems, and the fundamental understandings and analytical codes developed in the R&T programs will be directly applicable to the system projects.



CD-87-29880

Figure 1. - Small engine technology programs.



CD-87-29885

Figure 2. - Small engine efficiency.

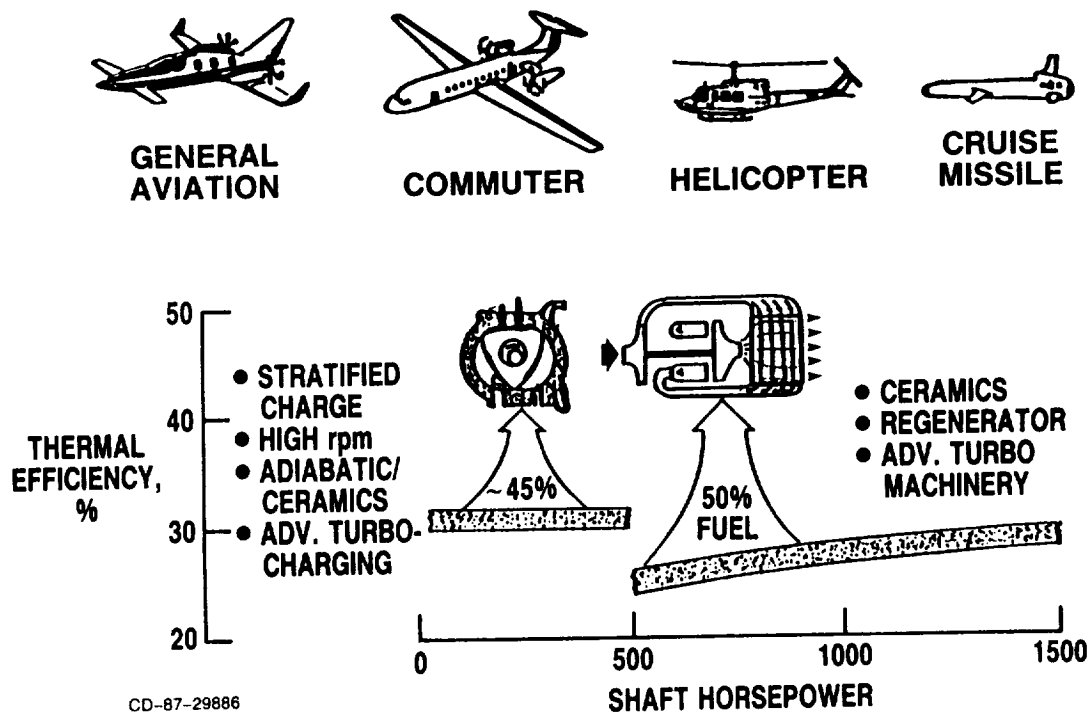


Figure 3. - Small engine technology opportunities.

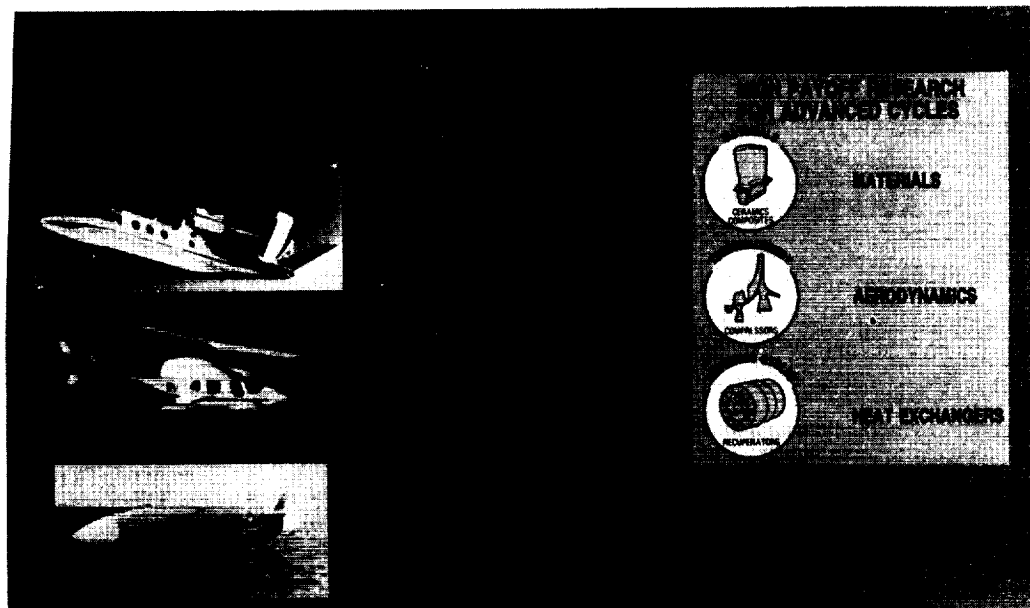
- FUEL IS 70 PERCENT OF TONNAGE SHIPPED
- ARMOR/MECH/INF DIVISIONS
 - AVIATION: 100,000 GAL/DAY PER DIV
 - GROUND: 50,000 GAL/DAY PER DIV
 - FOR 15,000 MAN DIVISION, 10 GAL/DAY/MAN PER DIV
- AIR ASSAULT DIVISION
 - AVIATION: 320,000 GAL/DAY PER DIV
 - GROUND: 20,000 GAL/DAY PER DIV
 - FOR 15,000 MAN DIVISION, 22 GAL/DAY/MAN PER DIV

• A 50 PERCENT SAVINGS IN AVIATION FUEL CAN SIGNIFICANTLY REDUCE TOTAL TONNAGE SHIPPED, THUS INCREASING MISSION CAPABILITY AND FLEXIBILITY.

CD-87-29887

Figure 4. - Impact of fuel on military mission flexibility from battlefield scenarios.

ORIGINAL PAGE
BLACK AND WHITE PHOTOGRAPH

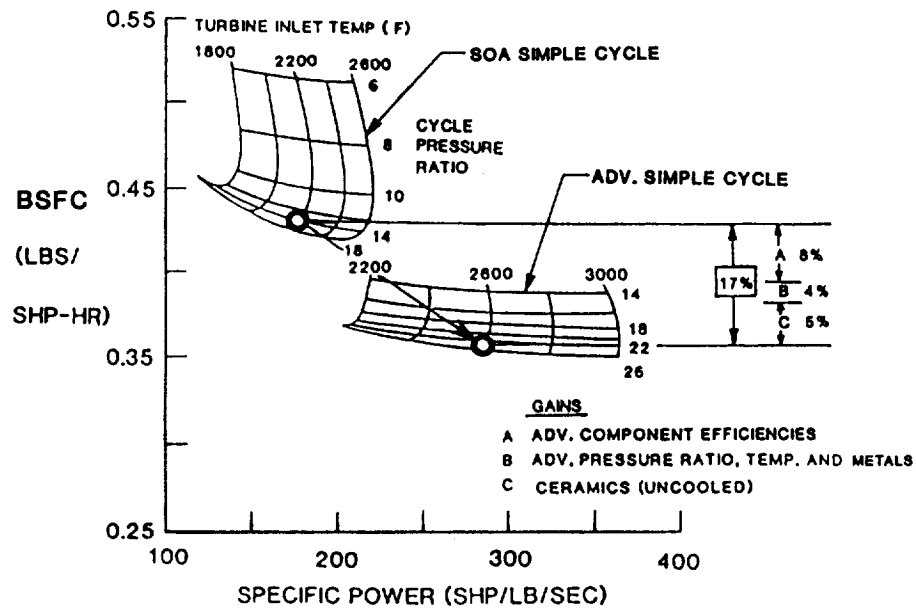


NATIONAL BENEFITS

- \$1-\$3 BILLION SAVINGS IN OPERATING COSTS IN 15 YEARS.
- 2-3 YEAR PAYBACK FOR R&D INVESTMENT.
- SIGNIFICANT MILITARY ADVANTAGES.
- STRENGTHEN U.S. COMPETITIVE EDGE IN FUTURE WORLD MARKET.

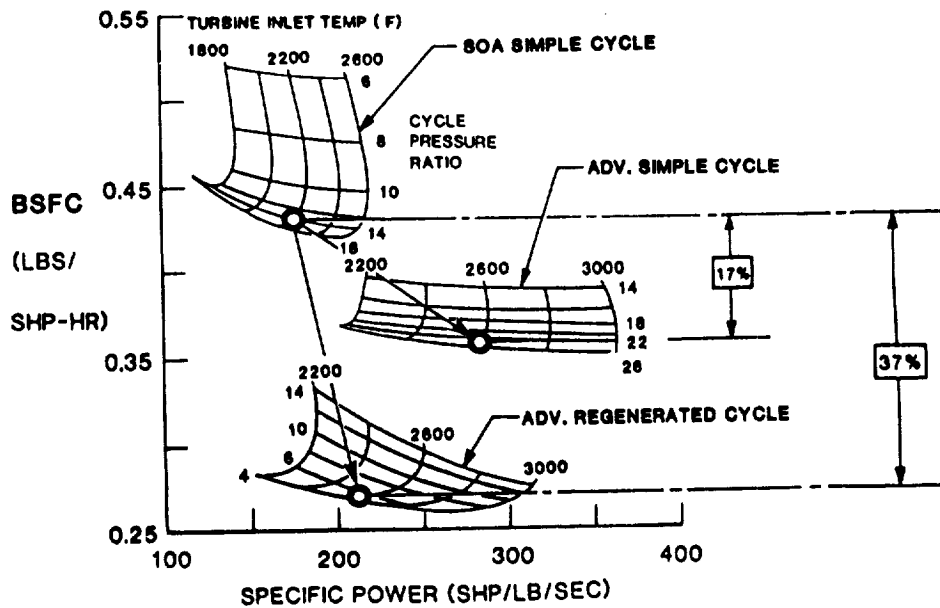
CD-87-29889

Figure 5. - Small engine component technology (SECT) studies (joint NASA/Army program).



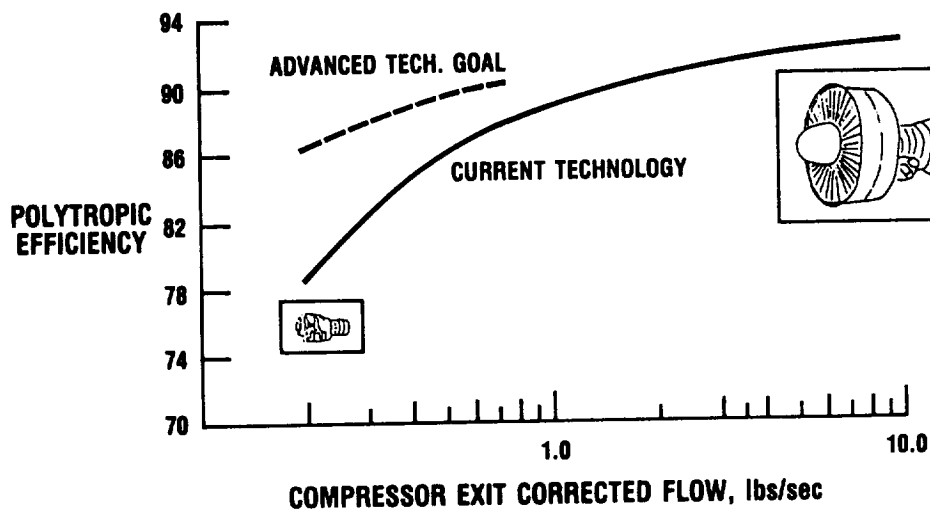
CD-87-29890

Figure 6. - Comparison of engine performance maps for state-of-the-art and advanced simple-cycle engines.



CD-87-29891

Figure 7. - Performance of advanced regenerated cycle in comparison with state-of-the-art and advanced simple cycles.



CD-87-29892

Figure 8. - Compressor efficiency.

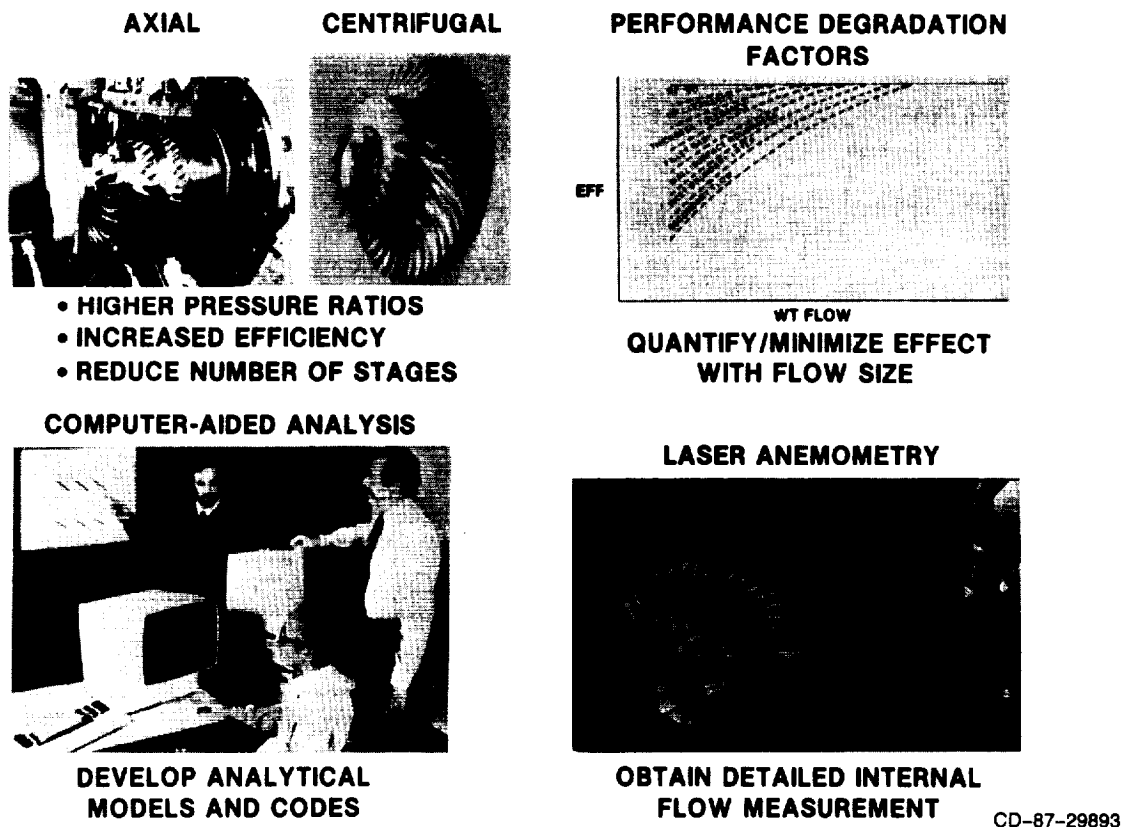


Figure 9. - Compressor technology.

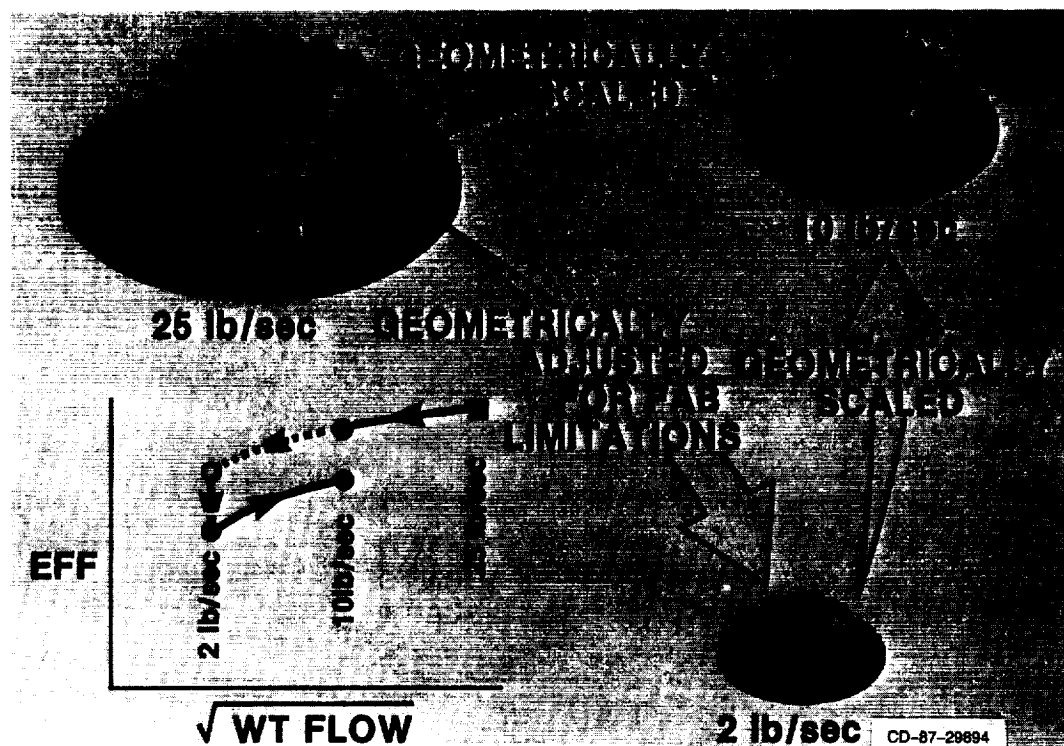
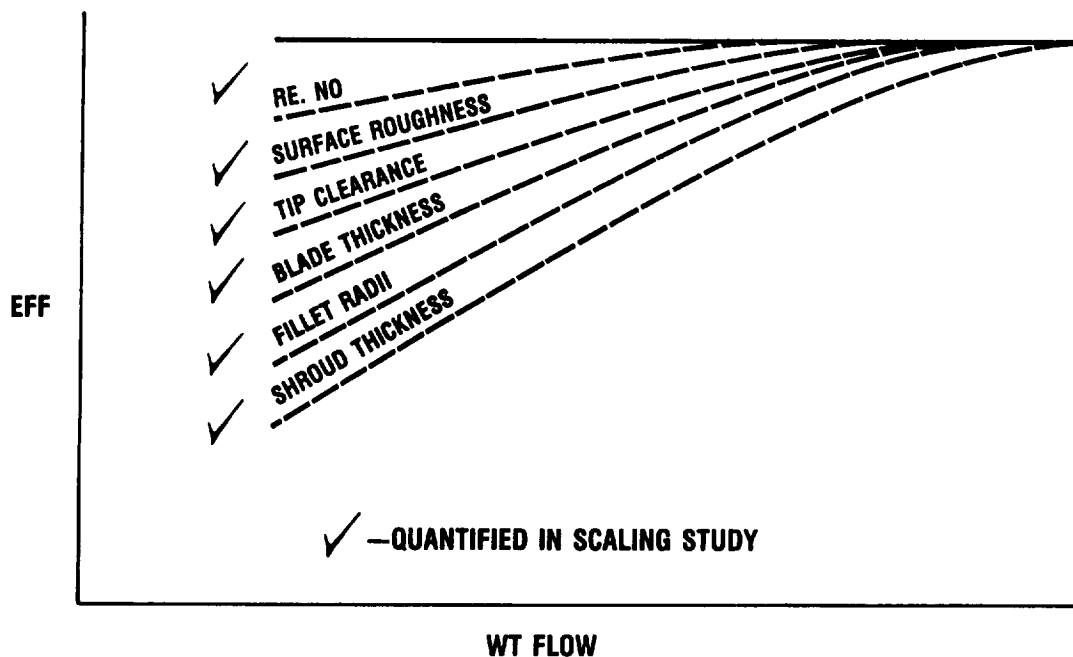
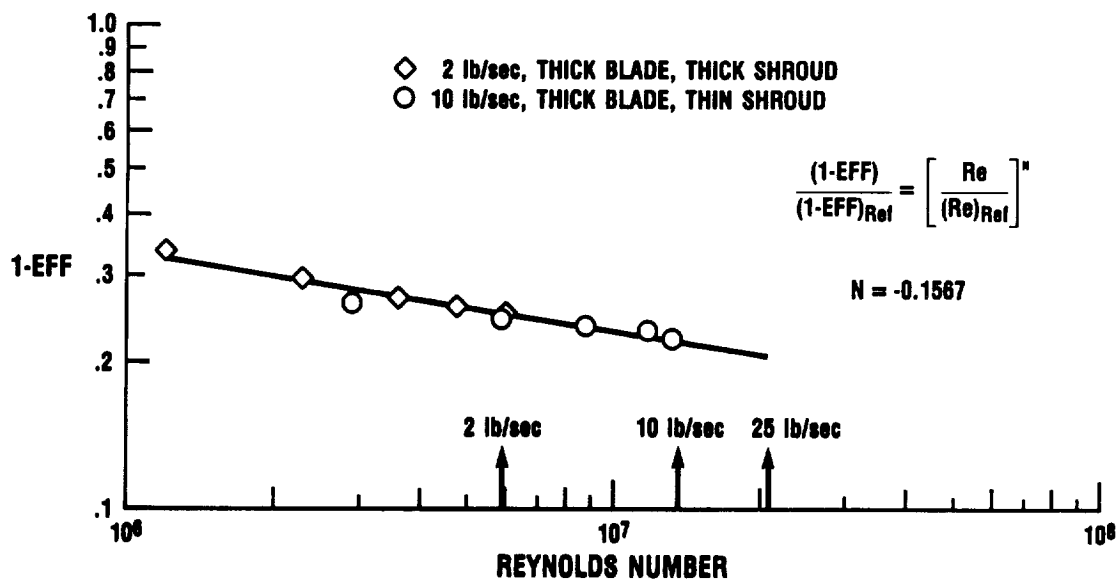


Figure 10. - Scaled centrifugal compressor program.



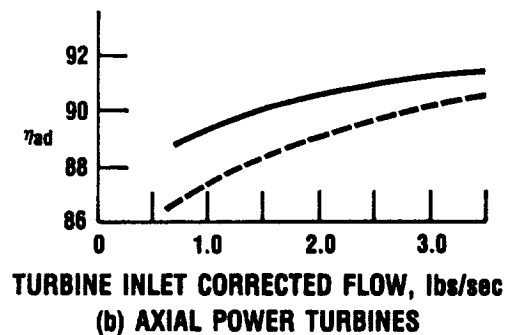
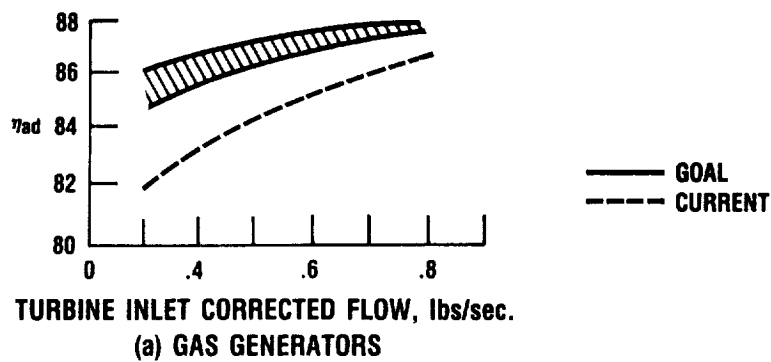
CD-87-29895

Figure 11. - Performance degradation factors.



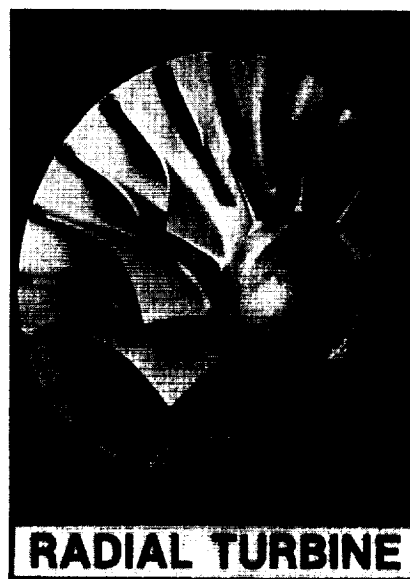
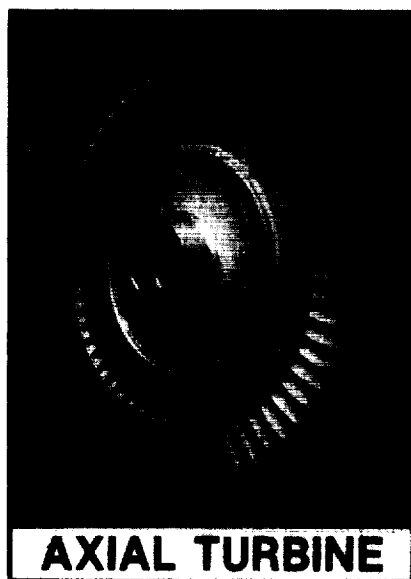
CD-87-29896

Figure 12. - Effect of scaling on centrifugal compressor performance.



CD-87-29897

Figure 13. - Turbine efficiency.

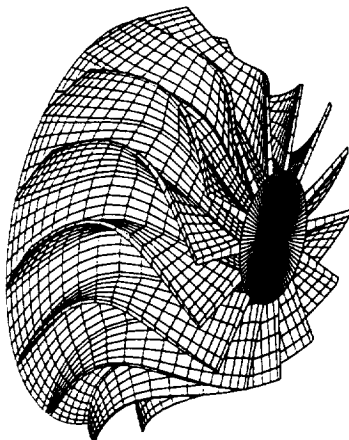


- ENDWALL EFFICIENCY IMPROVEMENT
- LOW ASPECT RATIO AERODYNAMICS
- ENGINE ENVIRONMENT EFFECTS
- SMALL SIZE PENALTIES
- HIGHLY LOADED STAGES
- VARIABLE GEOMETRY
- MANIFOLDS & DUCTS
- COOLING AERODYNAMICS
- VALIDATION OF COMPUTATIONAL METHODS

CD-87-30040

Figure 14. - Small turbine aerodynamics.

- APPLIED, FOR FIRST TIME, A NEW ADVANCED STRUCTURAL ANALYSIS CODE FOR PREDICTION OF FAST FRACTURE FAILURE PROBABILITY OF MONOLITHIC CERAMIC COMPONENTS. THE CODE COMBINES FINITE-ELEMENT STRUCTURAL ANALYSIS CAPABILITY (NASTRAN) WITH WEIBULL STATISTICAL AND FAILURE CRITERIA FROM FRACTURE MECHANICS.



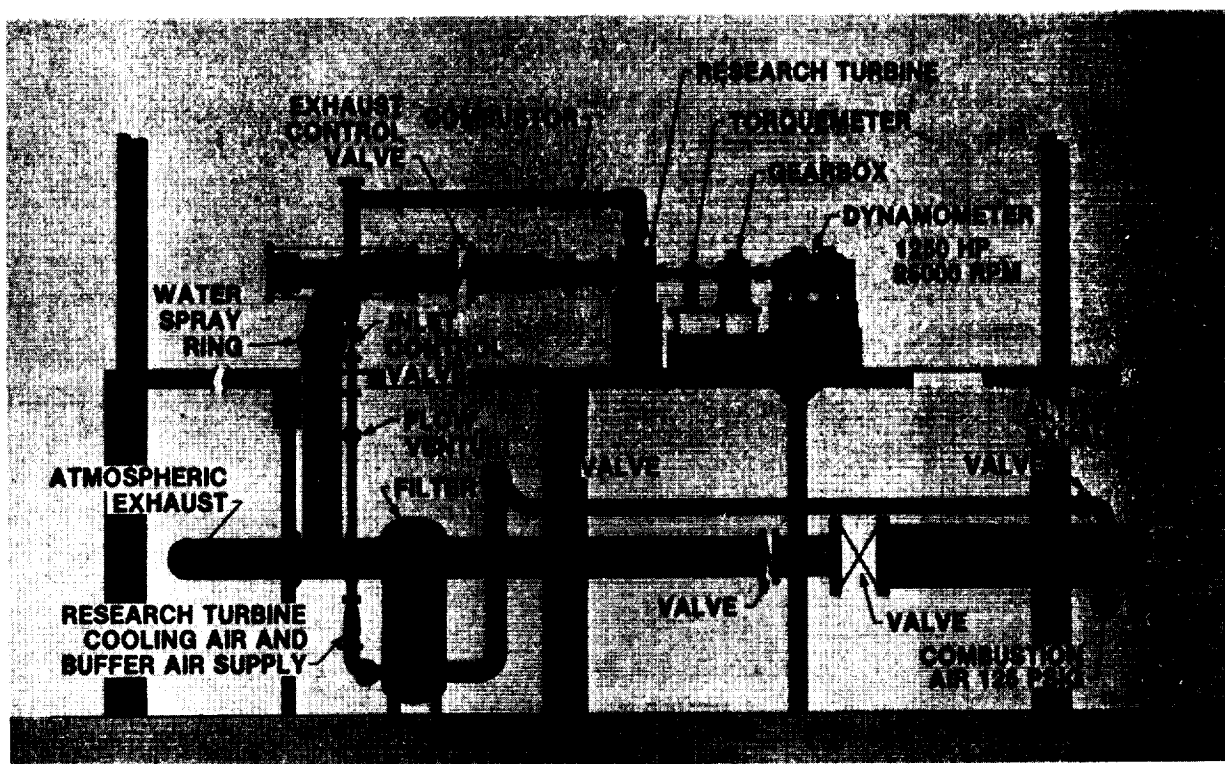
CERAMIC MIXED FLOW TURBINE

CD-87-29987

- COMPLETED THE AERODYNAMIC DESIGN OF HIGH WORK HIGH TEMPERATURE MIXED FLOW TURBINE.
- COMPLETED STRUCTURAL ANALYSIS OF FIRST DESIGN. INDICATED NEED FOR IMPROVED MATERIALS.
- CODE NEEDS FURTHER VALIDATION.

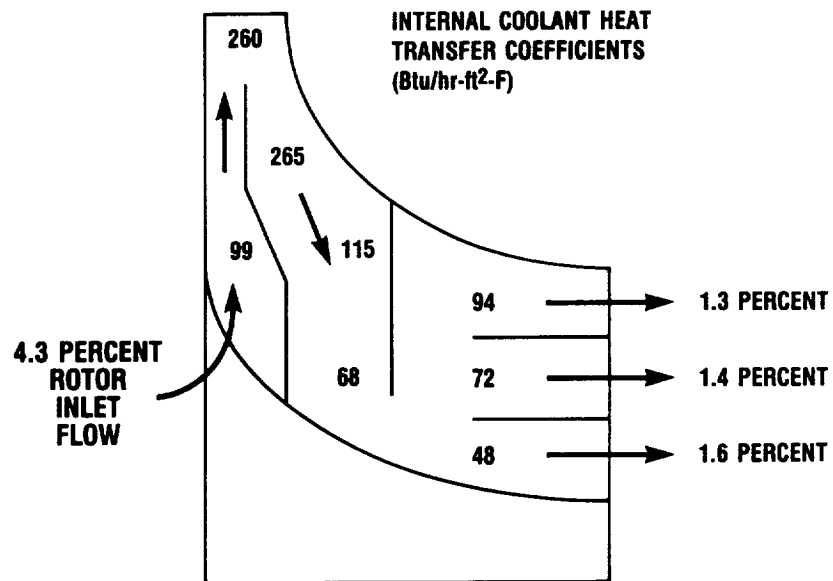
LEWIS IS THE ONLY GOVERNMENT FACILITY WITH AN IN-HOUSE CAPABILITY TO DESIGN CERAMIC COMPONENTS.

Figure 15. - Small turbine engine technology program.



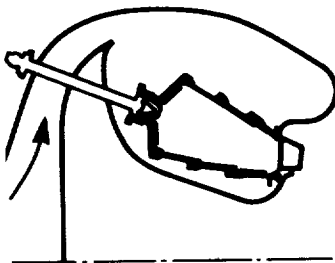
CD-87-29899

Figure 16. - Small Warm Turbine Test Facility.



CD-87-29900

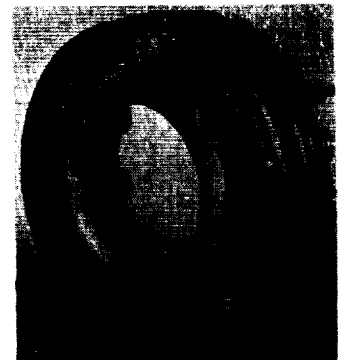
Figure 17. - NASA/Allison cooled radial turbine.



AXIAL FLOW

TECHNOLOGY NEEDS

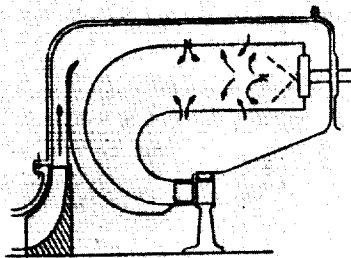
- INCREASED TEMP/PRESSURE CAPABILITY
- REDUCED AIR COOLANT REQUIREMENTS
- INCREASED DURABILITY/RELIABILITY



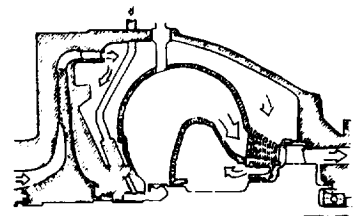
PRIMARY ZONE DESIGN METHODS



ADVANCED LINER COOLING



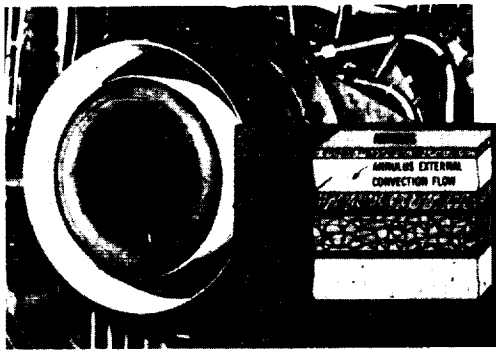
REVERSE FLOW



RADIAL OUTFLOW

CD-87-29901

Figure 18. - Small combustor technology.



CERAMIC MATRIX BENEFITS

- SIGNIFICANT PERFORMANCE IMPROVEMENTS EXPERIMENTALLY VERIFIED AT ADVANCED CYCLE CONDITIONS- 300 °F HOTTER THAN CURRENT ENGINES
- ADDITIONAL COOLANT NOW AVAILABLE FOR OTHER ENGINE USES

CD-87-29902

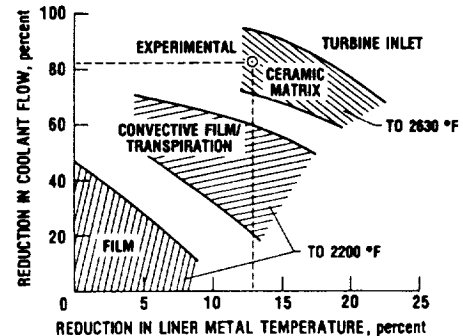
Figure 19. - Ceramic matrix combustor liner (joint NASA/Army program).

COMBUSTOR LINER COOLING COMPARISON (SIMULATED 16:1 ENGINE CYCLE)

OBJECTIVE: REDUCE COOLING REQUIREMENTS AND EXTEND LINER LIFE AT HIGHER TEMPERATURES THROUGH USE OF CERAMICS

- CERAMIC THERMAL BARRIER-YTTRIA STABILIZED ZIRCONIA WITH COMPLIANT METALLIC BACKING
- METAL SUBSTRATE SUPPORT STRUCTURE
- BACKSIDE CONVECTIVE COOLING ONLY

LINER COMPARISON (CYCLE 16:1)

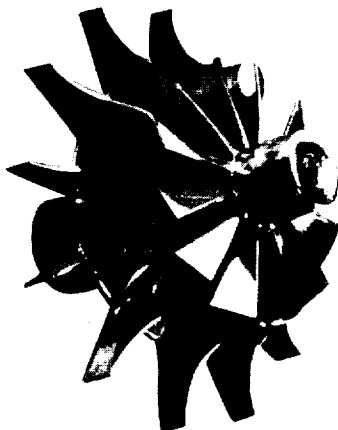
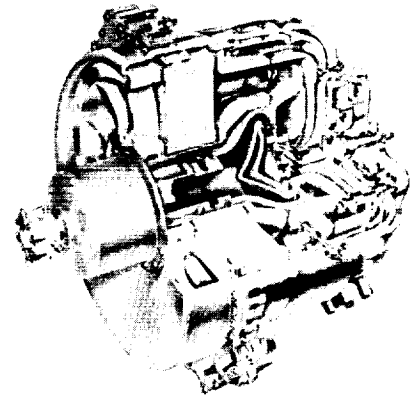


OBJECTIVE:

- DEVELOP A TECHNOLOGY BASE APPLICABLE TO A COMPETITIVE AUTOMOTIVE GAS TURBINE ENGINE

TECHNOLOGY FOCUS:

- HIGH TEMPERATURE CERAMIC COMPONENT TECHNOLOGY



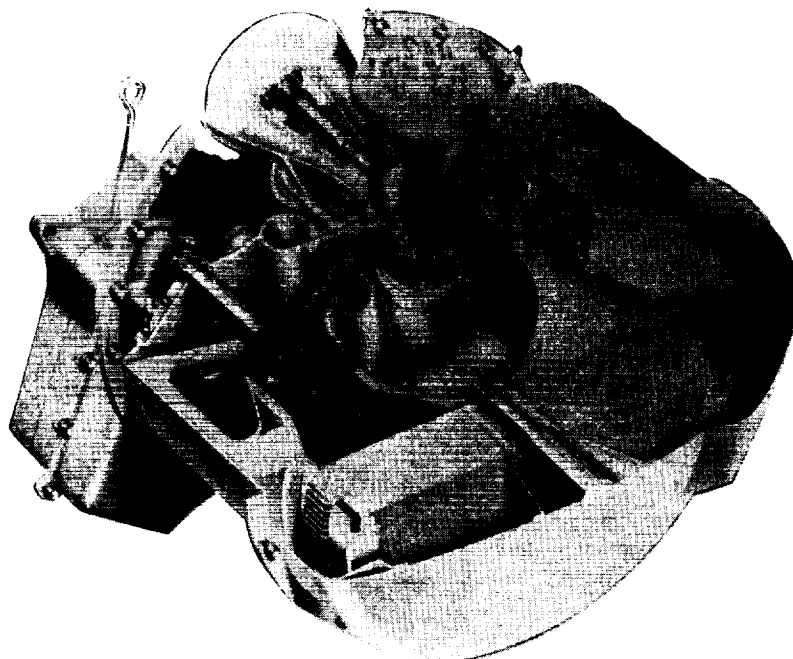
APPROACH:

- DEVELOP IMPROVED
 - ANALYTICAL DESIGN TOOLS
 - COMPONENT FABRICATION PROCESSES
 - PROCEDURES FOR EVALUATING CERAMIC COMPONENTS

CD-87-29903

Figure 20. - DOE/NASA advanced gas turbine technology.

AGT 100 TEST-BED ENGINE



DESCRIPTION

- REGENERATED TWO SHAFT
- TURBINE INLET TEMPERATURES UP TO 2350 °F
- MAXIMUM ROTOR SPEED 86,000 RPM

CD-87-29904

Figure 21. - DOE/NASA advanced gas turbine ceramic component technology.

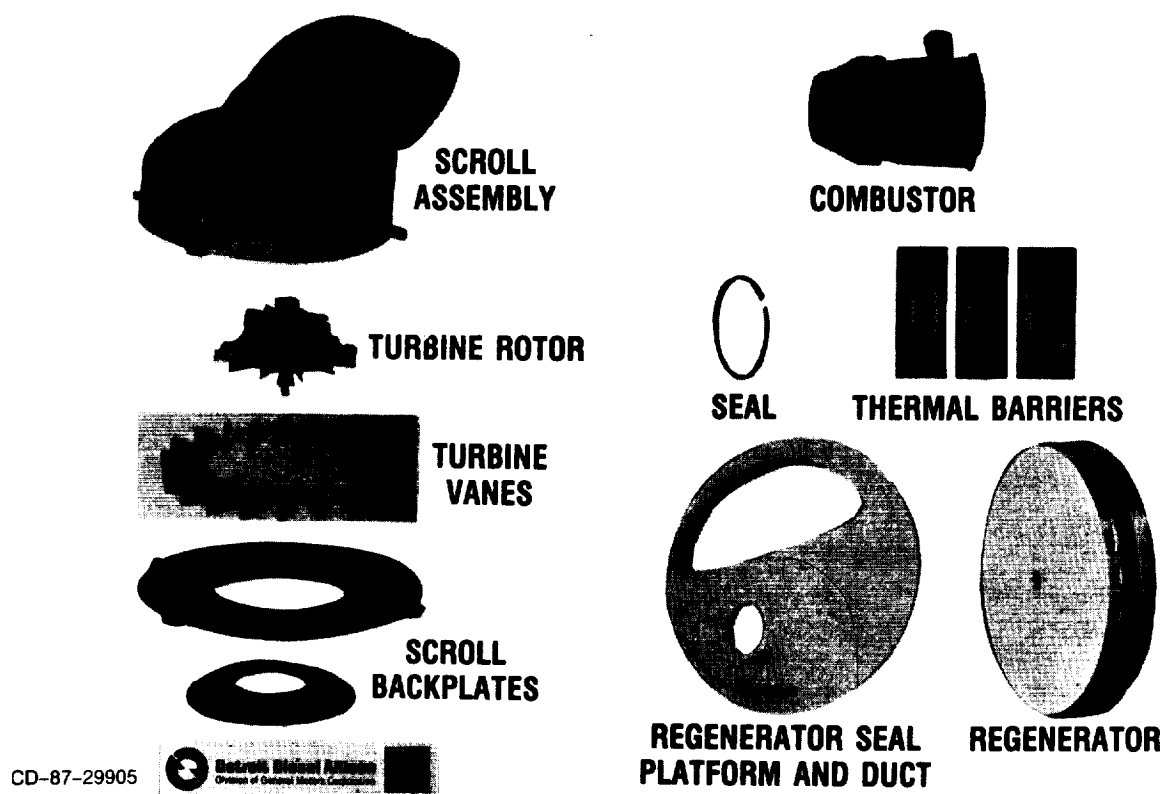
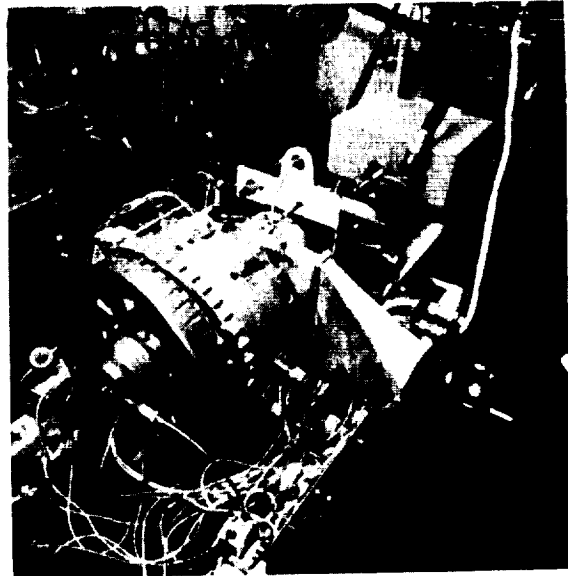


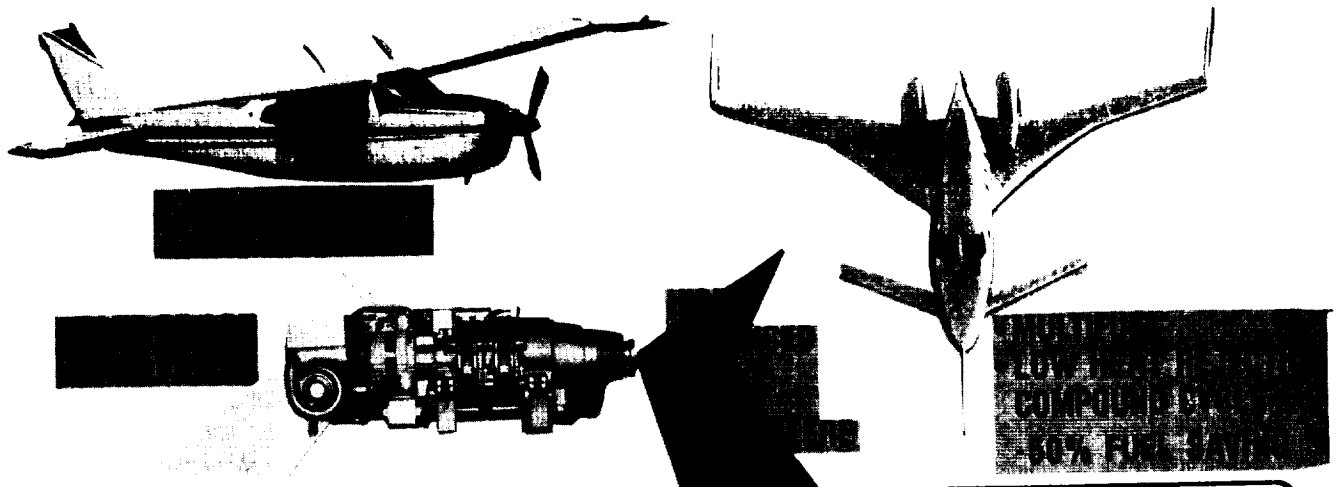
Figure 22. - AGT 100 ceramic components.

- **TURBINE INLET TEMPERATURE:**
2000-2200 °F
- **OPERATING SPEED:**
60,000-70,000 RPM
- **STARTS: 5**
- **SAME STRUCTURES FROM**
PREVIOUS TEST
- **TEST STOPPED DUE TO**
TURBINE ROTOR DAMAGE



CD-87-29906

Figure 23. - All-ceramic engine operated for 85 hr at 2200 °F.



**NASA-INDUSTRY
TECHNOLOGY
INVESTMENT**

PAST AND CURRENT

FUNDAMENTAL R & T

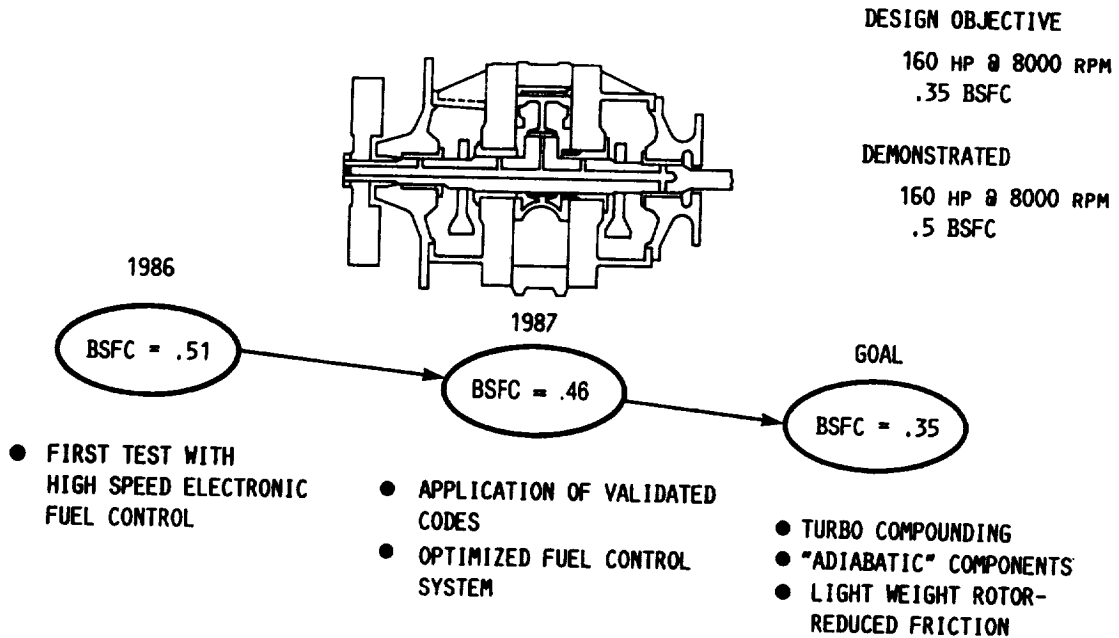
- COMBUSTION, THERMAL, MECHANICAL MODELS
- VALIDATION OF CODES
- LOW HEAT REJECTION TECHNOLOGY
- TRIBOLOGY AND TURBOCOMPOUNDING

TECHNOLOGY ASSESSMENT

- ADVANCED COMPONENT AND SYSTEMS TESTS

CD-87-29908

Figure 24. - Rotary engines.



CD-87-29909

Figure 25. - NASA/Deere stratified-charge rotary engine.

OBJECTIVE: ENLARGE DIESEL TECHNOLOGY BASE FOR WIDE RANGE OF AIR AND LAND VEHICLE APPLICATIONS

SIZE RANGE: 500 TO 2000 HP

APPROACH:

- FOCUS ON HIGH SPEED AND HIGH PRESSURE TO REDUCE SIZE
- RESUME PREVIOUS DARPA-SPONSORED PROGRAM WITH GARRETT
- BROADEN PROGRAM TO INCLUDE MORE OF ENGINE INDUSTRY
- ESTABLISH BASE FOR DEMONSTRATOR

EXPECTED RESULT:

- FUEL SAVINGS OF 40 PERCENT
- COMPACT, COMPOUND CYCLE
- BROAD APPLICATIONS



HELICOPTER
FIXED WING/PROPELLOR
TILT ROTOR

HIGH MOBILITY VEHICLE
LANDING CRAFT
AIR CUSHIONED VEHICLE

CD-87-29910

Figure 26. - Compound Cycle Engine program.

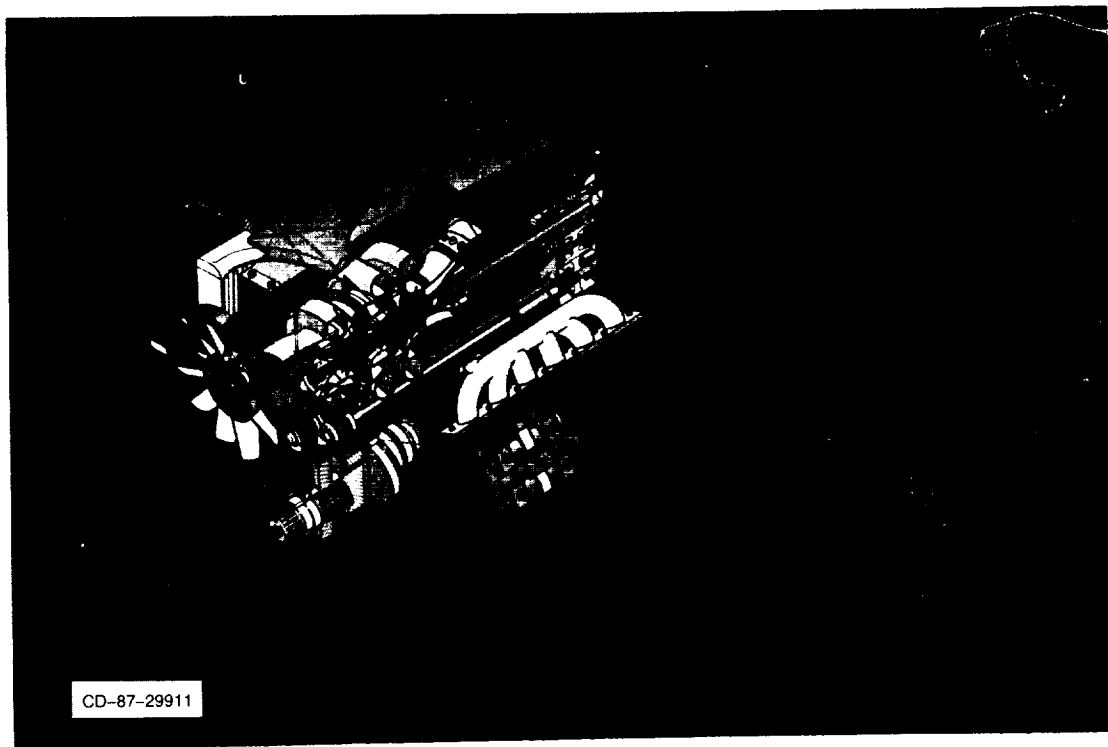


Figure 27. - Compound cycle engine.

OBJECTIVE:

**DEVELOP A TECHNOLOGY BASE APPLICABLE TO THE
ADVANCED "ADIABATIC" DIESEL ENGINE OF THE FUTURE**

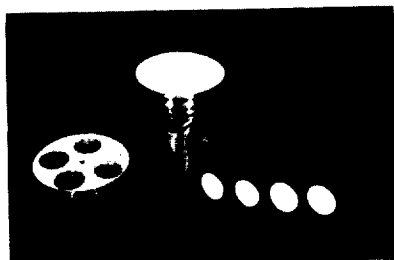
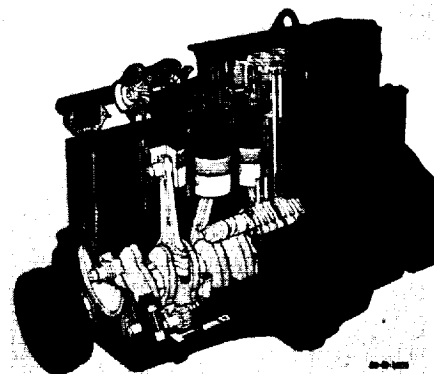
GOALS:

FUEL ECONOMY

**30% IMPROVEMENT OVER CONVENTIONAL
DIESEL ENGINES**

ECONOMIC & SOCIAL ACCEPTANCE

**COMPETITIVE CAPITAL & MAINTENANCE COSTS
MEET NOISE & EMISSIONS STANDARDS
FUEL TOLERANCE**

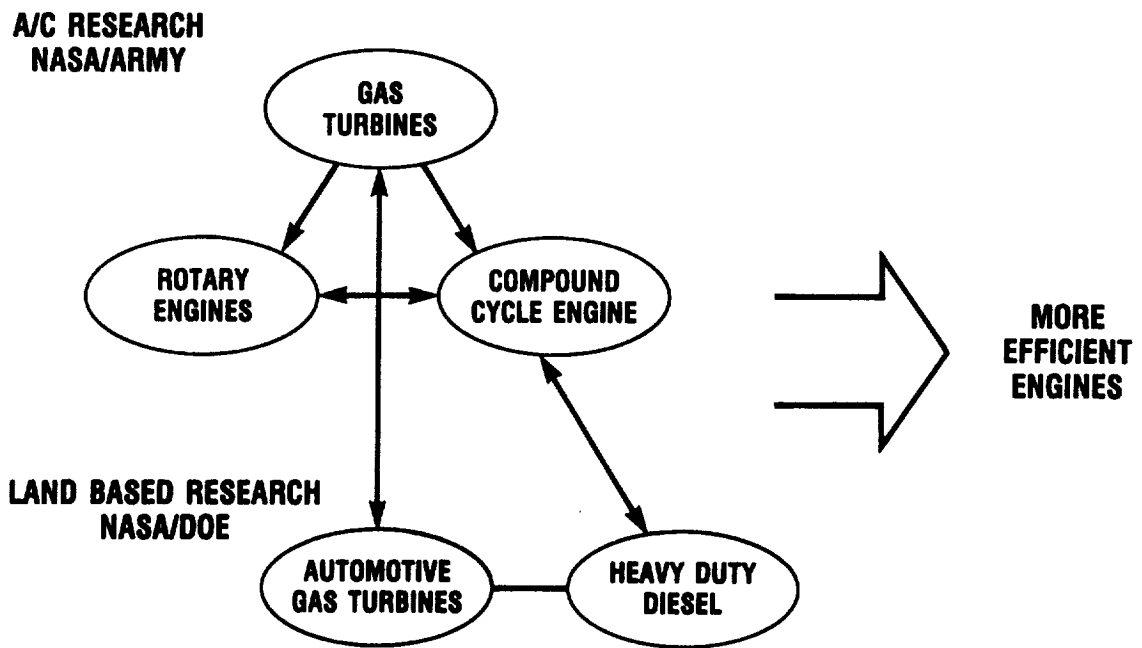


APPROACH:

**ELIMINATE WATER COOLING
CERAMIC INSULATING MATERIALS
HIGH TEMPERATURE TRIBOLOGY
WEAR COATINGS, PISTON SEALS, LUBRICATION
EXHAUST GAS HEAT RECOVERY
ADVANCED TURBOCOMPOUND, BOTTOMING CYCLE**

CD-87-29912

Figure 28. - DOE/NASA Heavy Duty Transport Technology Project.



CD-87-29915

Figure 29. - Small engine research summary.

ROTORCRAFT TRANSMISSIONS

John J. Coy

SUMMARY

The NASA Lewis Research Center and the U.S. Army Aviation Systems Command share an interest in advancing the technology for helicopter propulsion systems. In particular, this paper presents highlights from that portion of the program in drive train technology and the related mechanical components. The major goals of the program are to increase life, reliability, and maintainability, to reduce weight, noise, and vibration, and to maintain the relatively high mechanical efficiency of the gear train. The current activity emphasizes noise reduction technology and analytical code development followed by experimental verification. Selected significant advances in technology for transmissions are reviewed, including advanced configurations and new analytical tools. Finally, the plan for transmission research in the future is presented.

INTRODUCTION

Since 1970 the NASA Lewis Research Center and the U.S. Army Aviation Systems Command have shared an interest in advancing the technology for helicopter propulsion systems. The major goals of the program are to increase life, reliability, and maintainability, to reduce weight, noise, and vibration, and to maintain the relatively high mechanical efficiency of the gear train (fig. 1, ref. 1). Highlights from the current research activity are presented next.

ANALYSIS

The current activity emphasizes analytical code development and validation with emphasis on noise reduction technology for drive systems (fig. 2). There is a gear technology effort which supports advances in life, higher power density, and lubrication for gears.

On the basis of experimental, analytical, and design studies conducted under the transmission technology program, some advanced transmission concepts were evolved, including the advanced 500-hp transmission, the bearingless planetary transmission, and the split-torque transmission.

An extensive data base has been established for two sizes of helicopter transmissions. The Army's UH-60 Blackhawk transmission has been run in the Lewis test stand to determine thermal, vibration, stress, and efficiency information for a matrix of operating conditions (ref. 2). This information is

being used to compare with computer code predictions for code validation and to provide a baseline from which to assess the promised advantages of future designs and concepts. Information of a similar nature and purpose was collected for the OH-58 transmission (refs. 3 and 4). The Lewis test stands are currently operational and available for use in experimental transmission work.

The NASA/Army program has produced some very useful computer programs for designing and analyzing rolling element bearings (refs. 5 to 8). Generally, the computer program can predict performance characteristics including Hertz stress, load distribution, lubrication film thickness, component kinematics, fatigue life, heat generation, operating temperature, and power loss as a function of input parameters such as bearing geometry, speed, and load. The programs permit better designs and eliminate much trial-and-error testing prior to selection of a final design.

Analyses and computer codes have also been developed for gears to provide the following types of calculations: (1) power loss and efficiency, (2) bevel gear contact geometry, (3) gear dynamic analysis, (4) weight minimization, (5) life prediction, (6) lubrication, and (7) temperatures.

An in-house and university grant effort continues to develop computer programs for analysis and design of transmission systems. The unique facilities and hardware at Lewis are being used to validate the computer codes and to collect additional data for use in developing the codes. A library of computer codes and subroutines for transmission system analysis is being assembled. The goal is to develop a comprehensive computer program library for transmission system modeling (fig. 3).

GEAR AND TRANSMISSION LIFE

Pitting fatigue is a natural wearout mode of gear failure and occurs even under ideal operating conditions with proper lubrication and stress levels. For each hour of operation there is a reliability level which can be calculated. Early work at NASA provided an analytical methodology for calculating life and reliability for gears by assuming a quasi-static load on the gear teeth (ref. 9). It was desired, therefore, to improve on this methodology by replacing the assumed quasi-static load with a calculated dynamic load in the life and reliability model.

TELSGE, a NASA gear dynamic load prediction program (ref. 10), was modified, a pitting-fatigue-life prediction analysis was added, and parametric studies were performed. The study identified contact ratio and operating speed as the two most influential parameters among those studied (ref. 11). As a result, gear life can be increased through the improved analytical life prediction method.

Drive system life and reliability are important issues during the design, development, and field operation of helicopters. Analytical tools are needed for design and for comparing competing and alternate designs.

To meet this need, a versatile computer program was developed to predict helicopter transmission life (fig. 4, ref. 12). The program can analyze a variety of configurations composed of spiral bevel gears and planetary gears.

The program determines the forces on each bearing and gear for a given transmission configuration and applied load. The life of each bearing and gear is determined. Program output includes component and total system lives and load capacity for a given mission profile. The program predicts mean time between failures (MTBF) and can be used to evaluate proposed new designs and to project spare parts requirements for helicopter fleet operations.

GEAR NOISE

Historically, helicopters have been plagued by internal noise problems. Noise levels range from 100 to 120 dBA in the cabin. The sound can be from many sources, such as the transmission gear noise, the turbine engine compressor and exhaust noise, the rotor blades, and air turbulence. The transmission is a particularly troublesome source and is believed to be the main source of annoying noise in the helicopter cabin. The noise from the transmission enters the cabin following two paths: structure-borne radiation and direct radiation (fig. 5). The magnitude of the direct radiation is a function of the acoustic power radiated from the transmission case, transmitted acoustically to the cabin outer walls, and transferred through to the cabin. Of course if there are any small openings in the wall between the transmission compartment and the cabin, the sound will directly enter the cabin. The structure-borne path is particularly hard to block because the transmission case and its mounts are an integral part of the lift-load bearing path. The transmission mounts must be strong enough to support the entire helicopter by transferring the lift-load from the rotor blades to the air frame, and rigid enough for stable control of the helicopter. The stiff mounts pass the gear vibrations exceedingly well to the airframe, and the sound transmits to the cabin directly.

The major portion of our program in transmissions is devoted to finding solutions to this problem.

Spiral bevel gears are used in helicopters to transmit power "around the corner" from a horizontal engine output shaft to the vertical rotor shaft. Vibration from spiral bevel gears is a strong source of transmission noise (fig. 6, ref. 13).

The goal of a recent study was to relate gear noise to physical factors such as deviations of tooth surfaces and gear shaft centerlines from their ideal positions, tooth and gear body stiffness, bearing and housing support flexibility, and input shaft torque. Equations have been developed for computing the vibration and noise of the gear drive system. The work completed (1) provides the first detailed mathematical understanding of generalized transmission error in spiral bevel gears, (2) allows prediction of vibration excitation based on gear tooth measurements, and (3) relates gear noise to physical design parameters and therefore provides a basis for future improvements in spiral bevel gear design (ref. 14).

ADVANCED TRANSMISSIONS

Advancements in transmissions can come from either improved components or improved designs of the transmission system (fig. 7). The split-torque arrangement is in the second category. The figure shows a split-torque design which is compatible with the Blackhawk (UH-60A) helicopter. The fundamental

concept of the split-torque design is that the power from the engine is divided into two parallel paths prior to recombination on a single gear that drives the output shaft. Studies have shown that replacement of the planetary gear reduction stage with a split torque results in weight savings and increased reliability (ref. 15). There can be many pinions driving the output gear, but in the case of the UH-60A application it was found that four pinions gave the optimum design on the basis of least overall weight, reduced power losses, comparable total parts count compared to the existing UH-60 design, and least number (one) of nonredundant gears. The advantage of split torque over planetary is greatest for the larger sized helicopters.

The engineering analysis showed that the following performance benefits can be achieved for a 3600-hp split-torque transmission compared with the conventional transmission with a planetary gear stage: (1) weight is reduced 15 percent, (2) drive train power losses are reduced by 9 percent, (3) reliability is improved and vulnerability is reduced because of redundant power paths, and (4) the number of noise generation points (gear meshes) is reduced.

The transmission has potential for installation in the Blackhawk helicopter. The design study has carried the transmission to the detail design stage for a test model to be used for validation studies in the NASA Lewis 3000-hp helicopter transmission facility, but a test model has not been built. For the transmission to be used in the Blackhawk, a separate detail design and installation study would be required first.

The design emphasis for the NASA/Bell Helicopter Textron (BHT) 500-hp advanced technology demonstrator transmission was placed on a 500-hp version of the OH-58C, 317-hp transmission that would have a long, quiet life with a minimum increase in the cost, weight, and space that usually increases along with power increases. This was accomplished by implementing advanced technology that has been developed during the last decade and making improvements dictated by field experience (ref. 16).

These advanced technology components, concepts, and improvements, and their effect on the 500-hp transmission are as follows:

(1) High contact ratio planetary gear teeth reduce the noise level and increase life.

(2) Improved spiral bevel gears made of vacuum carburized gear steels, shot peened for increased gear tooth pitting fatigue life, as well as gear tooth bending fatigue strength, and lubricated with Aeroshell 555 oil save weight and space and increase transmission life.

(3) Improved bearings, made of cleaner steels and designed with improved analytical tools, save weight and space and increase reliability.

(4) Improved design of the planet carrier, made of two-piece construction with straddle mounting of the planet gears, improves gear alignment and power capacity.

(5) The cantilever-mounted planetary ring gear has no working spline to generate wear debris; it isolates the meshing teeth from the housing to reduce

noise, and it provides a flexible mount for a more uniform load distribution among the planets.

(6) The sun gear now has an improved spline (crown hobbled and hardened) running submerged in a bath of flowthrough oil, which prevents the spline from wearing.

(7) The straddle-mounted bevel gear allows higher torque to be transmitted without detrimental shifting of the tooth contact pattern.

In summary, the improved 500-hp design has a weight/horsepower ratio of 0.26 lb/hp, compared to 0.37 lb/hp for the 317-hp OH-58C transmission. This transmission is the basis for the transmission in the Army's improved OH-58D model helicopter.

One recent development in the area of high-performance power transmissions is the self-aligning, bearingless planetary (SABP) (ref. 17). This transmission arrangement can be generically classified as a quasi-compound planetary which uses a sun gear, planet spindle assemblies, ring gears, and rolling rings.

The design study projects a weight savings of 17 to 30 percent and a reliability improvement factor of 2:1 over the standard transmission. The benefits of using an SABP transmission are most effective when one uses reduction ratios between 16:1 and 26:1. It permits high reduction in two compound stages of high efficiency, providing sufficient flexibility and self-centering to give good load distribution between planet pinions, while effectively isolating the planetary elements from housing deflections.

This new transmission concept offers advantages over transmissions that use conventional planetary gears: higher reduction ratio, lighter weight, increased reliability, and decreased vulnerability. Since it has no planet bearings, there is a weight savings, and power losses and bearing failures commonly associated with conventional-design transmissions are nonexistent.

In conventional-design transmissions, planet bearings are heavily loaded and are the weak link when the lubricant is interrupted. The SABP transmission has decreased vulnerability because of increased operating time after loss of lubricant since there are no planet bearings.

One SABP transmission with a 17.44:1 ratio is currently being tested in the 500-hp transmission facility at NASA Lewis, and another variant with a ratio of 101:1 is being fabricated for testing.

FUTURE PLANS

Rotorcraft for the 1990's and beyond require extremely light, long-lived, quiet drive systems. The NASA/Army research, together with the helicopter builders' careful designs, has provided reliable and strong drive systems for civilian and Army helicopters. This paper has reviewed significant research in drive systems and their components.

The critical issues are (1) to achieve significant advances in power-to-weight ratio, (2) to increase reliability, and (3) to reduce the transmission

noise. New concepts to achieve these goals have been investigated. The advanced 500-hp transmission has explored an increased power-to-weight ratio by using advanced design techniques, component improvements, and advanced materials. The value of this kind of research activity was realized during the upgrading of the Army's OH-58 helicopter to the D model, when the research on the advanced 500-hp transmission laid the ground work for the transmission in the D model. The bearingless planetary transmission with helical gears offers advantages in reliability and reduced noise. The split-torque concept offers significant weight savings for large-size helicopters.

Our plan for future NASA/Army transmission research calls for increased emphasis on noise reduction, an aggressive development of computer-aided design codes for transmissions, and the design and construction of demonstrator transmissions in large and small size categories (fig. 8).

An important new initiative in transmissions by the Army will be conducted through the Propulsion Directorate, Aviation Research and Technology Activity (ARTA). A 6-year program, beginning in 1987, will develop advanced concept demonstrator transmissions for two categories of helicopters: the Advanced Cargo Aircraft (ACA) and the Future Attack Rotorcraft (FAR). The program will parallel the concept offered by engine demonstrator programs, and provide a way for the industry to develop advanced concepts and trial designs well in advance of critical needs. This is a first time for such a program for transmissions.

The program will address the issues of weight, noise and reliability, reducing weight by 25 percent, reducing noise by 10 decibels, and increasing MTBR (mean time between removal) to 5000 hr. For the program to be successful, it depends on the continued Army/NASA expertise and cooperation at Lewis Research Center. The transmission program will build on the strong technology base from the joint NASA/Army programs as well as NASA's noise reduction research.

REFERENCES

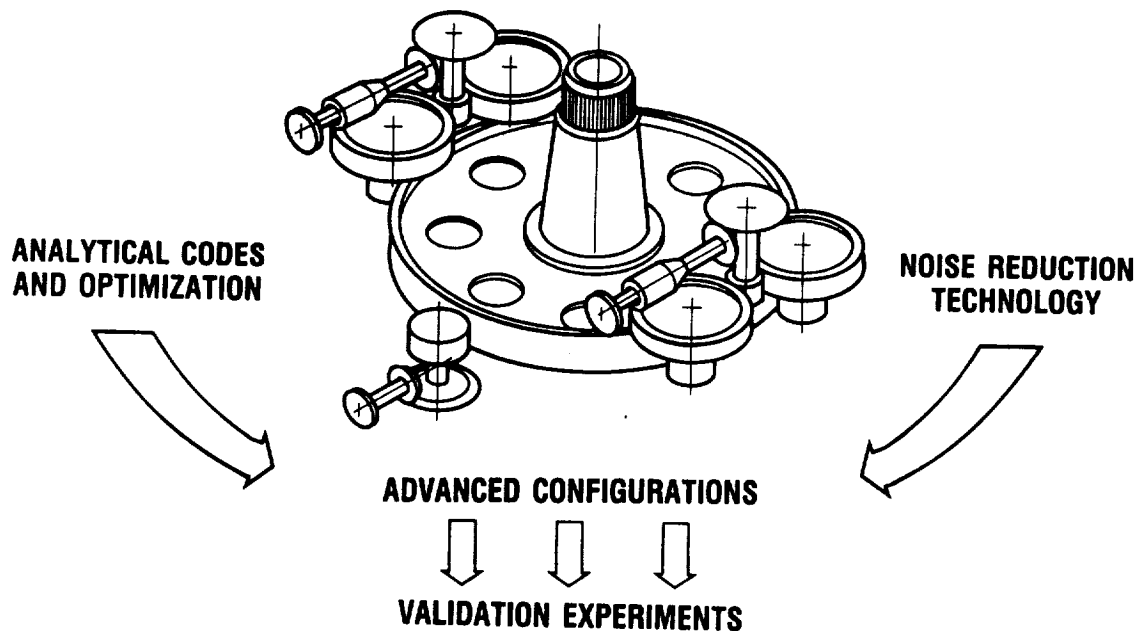
1. Coy, J.J.; Townsend, D.P.; and Coe, H.H.: Results of NASA/Army Transmission Research. NASA/Army Rotorcraft Technology, Vol. 2 - Materials and Structures Propulsion and Drive Systems, Flight Dynamics and Control, and Acoustics, NASA CP-2495-VOL-2, 1987, pp. 769-801.
2. Mitchell, A.M.; Oswald, F.B.; and Coe, H.H.: Testing of UH-60A Helicopter Transmission in NASA Lewis 2240-kW (3000-hp) Facility. NASA TP-2626, 1986.
3. Coy, J.J.; Mitchell, A.M.; and Hamrock, B.J.: Transmission Efficiency Measurements and Correlations with Physical Characteristics of the Lubricant. NASA TM-83740, USAAVSCOM-TR-84-C-11, 1984. (Avail. NTIS, AD-A149179.)
4. Lewicki, D.G.; and Coy, J.J.: Vibration Characteristics of the Oh-58A Helicopter Main Rotor Transmission. NASA TP-2705, USAAVSCOM-TR-86-C-42, 1987. (Avail. NTIS, AD-A180364.)

5. Hadden, G.B., et al.: User's Manual for Computer Program AT81Y003 SHABERTH. (SKF-AT81D040, SKF Technology Services; NASA Contract NAS3-22690) NASA CR-165365, 1981.
6. Dyba, G.J.; and Kleckner, R.J.: High Speed Cylindrical Roller Bearing Analysis, SKF Computer Program CYBEAN, Vol. 2 - User's Manual. (SKF-81ATD049-VOL-2, SKD Technology Services; NASA Contract NAS3-22690) NASA CR-165364, 1981.
7. Kleckner, R.J.; Dyba, G.J.; and Ragen, M.A.: SKF Computer Program SPHERBEAN, Vol II - User's Manual. (AT81D007, SKF Technology Services; NASA Contract NAS3-22807) NASA CR-167859, 1982.
8. Hadden, G.B., et al.: User's Manual for SKF Computer Program AT81Y005, PLANETSYS. (SKF-AT81D044, SKF Technology Services; NASA Contract NAS3-22690) NASA CR-165366, 1981.
9. Coy., J.J.; Townsend, D.P.; and Zaretsky, E.V.: Analysis of Dynamic Capacity of Low-Contact-Ratio Spur Gears using Lundberg-Palmgren Theory, NASA TN D-8029, 1975.
10. Wang, K.L.; and Cheng, H.S.: Thermal Elastohydrodynamic Lubrication of Spur Gears. NASA CR-3241, 1980.
11. Lewicki, D.G.: Predicted Effect of Dynamic Load on Pitting Fatigue Life for Low-Contact-Ratio Spur Gears, NASA TP-2610, AVSCOM-TR-86-C-21, 1986. (Avail. NTIS, AD-A170906.)
12. Savage, M.; and Brikmanis, C.K.: System Life and Reliability Modeling for Helicopter Transmissions. NASA CR-3967, 1986.
13. Coy, J.J., et al.: Identification and Proposed Control of Helicopter Transmission Noise at the Source. NASA/Army Rotorcraft Technology Conference, Vol. 2 - Materials and Structures, Propulsion and Drive Systems, Flight Dynamics and Control, and Acoustics, NASA CP-2495-VOL-2, 1987, pp. 1045-1065.
14. Mark, W.D.: Analysis of the Vibratory Excitation Arising from Spiral Bevel Gears. NASA CR-4081, 1987.
15. White, G.: 3600-hp Split Torque Helicopter Transmission. NASA CR-174932, 1985.
16. Braddock, C.E.; and Battles, R.A.: Design of an Advanced 500 HP Helicopter Transmission. Advanced Power Transmission Technology, G.K. Fischer, ed., NASA CP-2210, AVRADCOM-TR-82-C-16, 1983, pp. 123-139.
17. Folenta, D.J.: Design Study of Self-Aligning Bearingless Planetary (SABP). (TTC-80-01R, Transmission Technology Co. Inc.; NASA Contract NAS3-21604) NASA CR-159808, 1980.

REQUIREMENT	GOAL	BENEFIT
LIGHTER STRONGER	DRIVE TRAIN SPECIFIC WEIGHT 0.3 TO 0.5 lb/hp (CURRENTLY 0.4 TO 0.6 lb/hp)	INCREASED RANGE AND PAYLOAD
MORE RELIABLE	5000-hr MEAN TIME BETWEEN OVERHAULS (MTBO) (CURRENTLY 500 TO 2000 hrs)	LOWER OPERATING COST AND SAFER OPERATION
QUIETER	70 TO 80 dB IN CABIN (CURRENTLY 100 TO 110 dB)	GREATER USE FOR COMMER- CIAL COMMUTER SERVICE INCREASED PASSENGER AND PILOT COMFORT

CD-87-28719

Figure 1. - Transmission technology required for 1990's.



CD-87-28720

Figure 2. - Current research activity in transmissions.

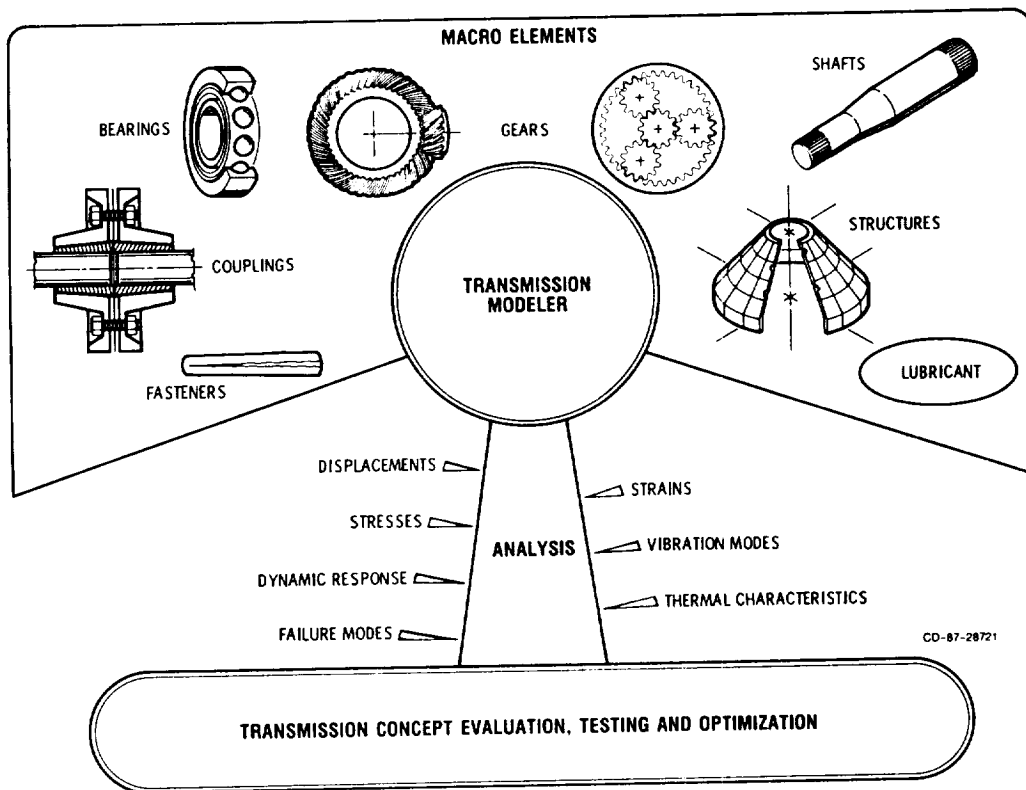
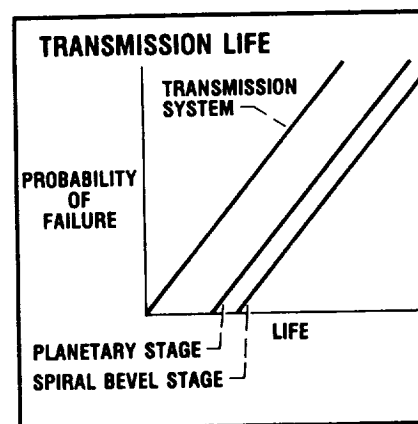
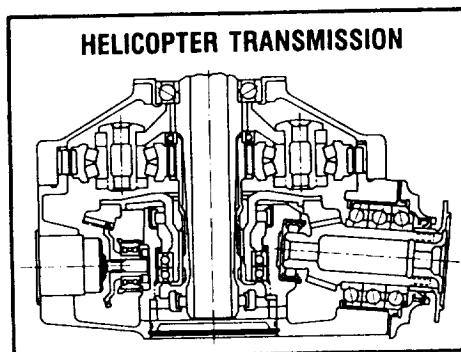


Figure 3. - Comprehensive transmission and modeling system.

SIGNIFICANCE:

- VERSATILE COMPUTER PROGRAM FOR PREDICTING TRANSMISSION LIFE AND RELIABILITY
- TOOL FOR EVALUATING PRELIMINARY AND COMPETING DESIGNS
- PROVIDES INFORMATION THAT CAN BE USED TO PLAN SPARE PARTS REQUIRED



FEATURES:

- INPUTS: TRANSMISSION CONFIGURATION, LOAD, AND SPEED
- OUTPUTS: TRANSMISSION COMPONENTS AND SYSTEM LIVES

CD-87-28722

Figure 4. - Helicopter transmission life and reliability computer program.

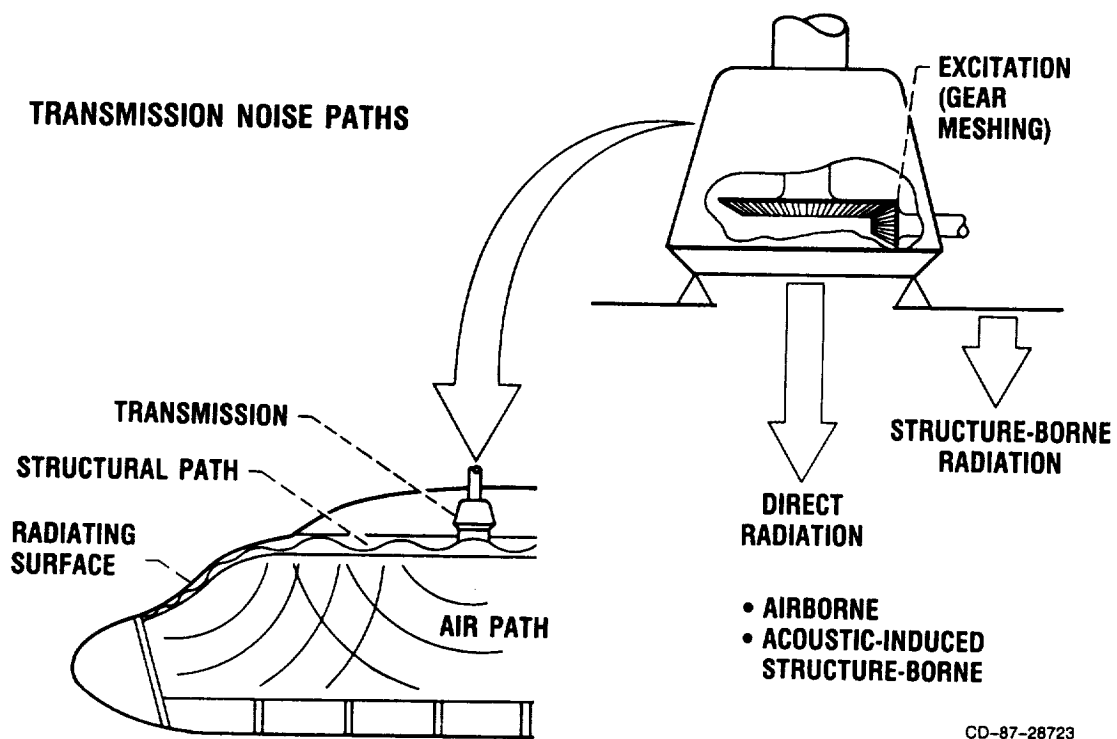
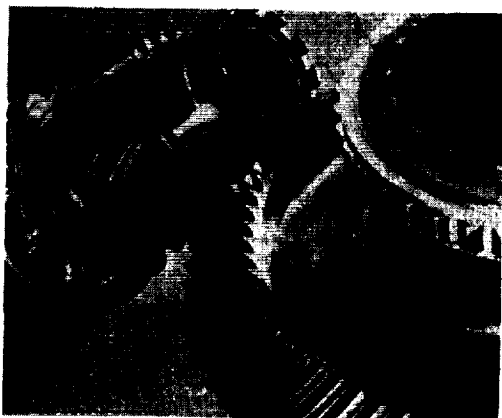
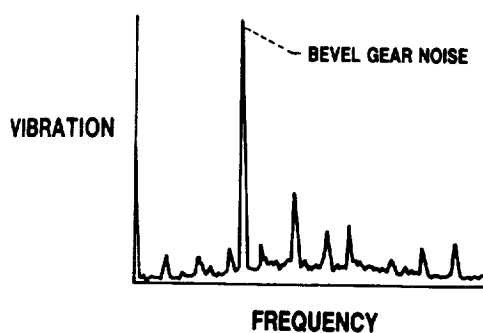


Figure 5. - Transmission noise reduction technology for rotorcraft.



SPIRAL BEVEL GEARS

MILESTONES COMPLETED:

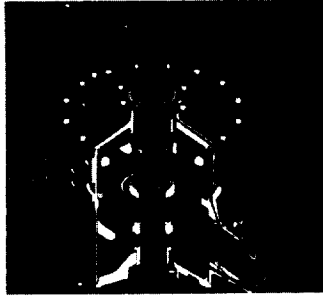
- MATHEMATICAL MODEL OF ZONE OF TOOTH CONTACT FOR SPIRAL BEVEL GEARS
- NEW UNDERSTANDING OF THREE-DIMENSIONAL NATURE OF TOOTH MESHING
- TIME AND FREQUENCY DOMAIN ANALYSIS FOR NOISE EXCITATION FUNCTION
- NASA CR 4081

SIGNIFICANCE:

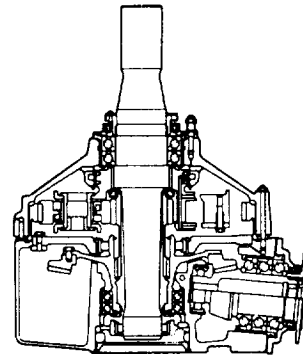
- ALLOWS PREDICTION OF VIBRATION FROM GEAR MEASUREMENTS
- PROVIDES BASIS FOR FUTURE IMPROVEMENTS IN SPIRAL BEVEL GEAR DESIGN

CD-87-28724

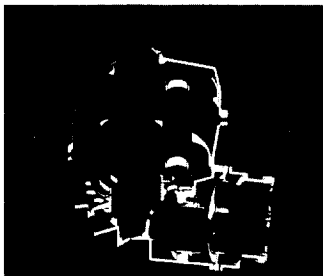
Figure 6. - Spiral bevel gear noise modeling.



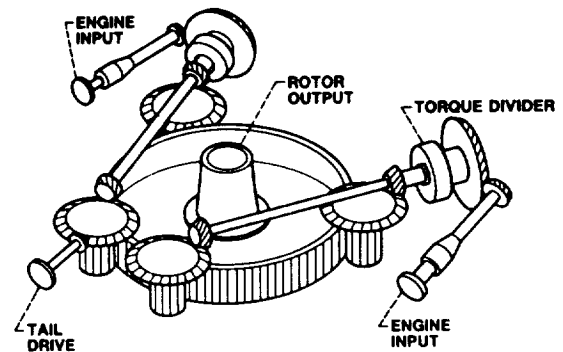
**500-hp BEARINGLESS PLANETARY
(LOW-RATIO)**



500-hp/ADVANCED COMPONENTS



**500-hp BEARINGLESS PLANETARY
(HIGH-RATIO)**



3600-hp SPLIT TORQUE

CD-87-28725

Figure 7. - Advanced transmissions.

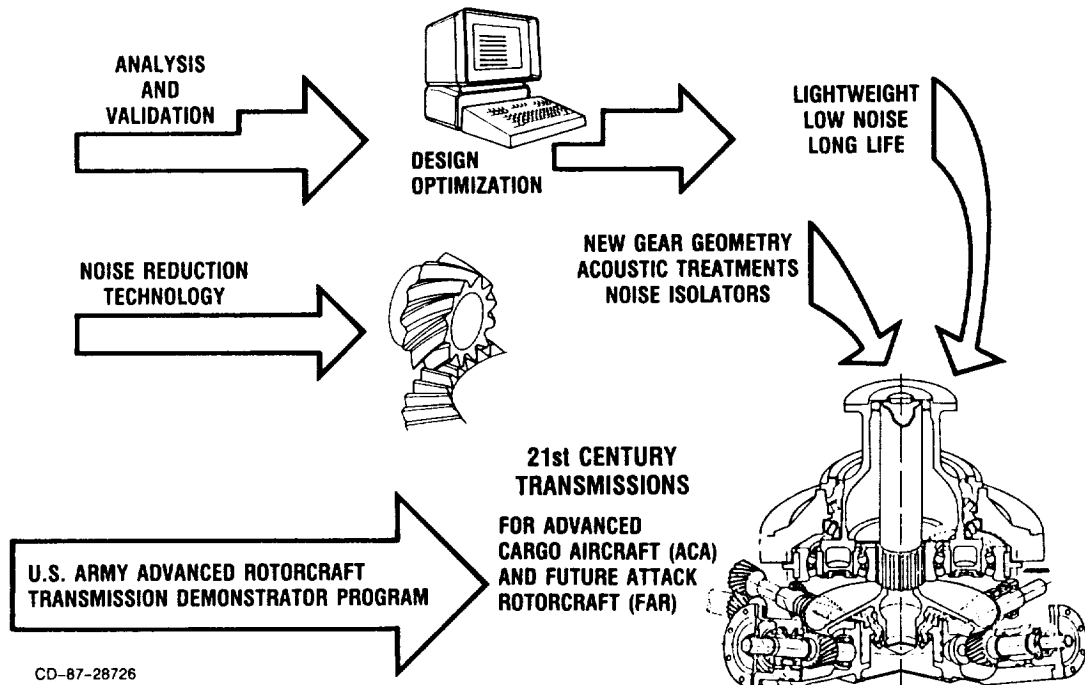


Figure 8. - Future thrust.

THE NASA AIRCRAFT ICING RESEARCH PROGRAM

Robert J. Shaw
and
John J. Reinmann

SUMMARY

The objective of the NASA aircraft icing research program is to develop and make available to industry icing technology to support the needs and requirements for all-weather aircraft designs. Research is being done for both fixed- and rotary-wing applications. The NASA program emphasizes technology development in two key areas: advanced ice protection concepts and icing simulation (analytical and experimental). This paper reviews the computer code development/validation, icing wind tunnel testing, and icing flight testing efforts which have been conducted to support the icing technology development.

PROGRAM OVERVIEW

The major areas of emphasis of the NASA icing research program are shown in figure 1. The program has a generic portion which is devoted to developing the required fundamental technology. The basic technology is applied with appropriate modifications and alterations to fixed- and rotary-wing specific icing problems. The icing research program is a balanced effort (fig. 2) in that it contains analysis code development/validation, wind tunnel testing, and icing flight research activities. These elements of the program are closely coordinated since all are conducted within the icing research group. In addition, close coordination exists with industry and universities through formal contracts and grants as well as through collaborative and cooperative programs.

Some recent accomplishments of the icing research program will be reviewed by looking at some past activities in two technology areas: ice protection concepts, and analytical and experimental icing simulation. The first area to be reviewed will be ice protection concepts, where the goal is to develop concepts which will result in lighter, more efficient ice protection systems for advanced military and civilian aircraft.

In fiscal year 1987, a 5-year NASA/industry/university program was completed to develop the technology data base for the electromagnetic impulse deicer concept (or EIDI) which shows great promise for providing highly efficient deicing with low power requirements. The major phases of this program are shown in figure 3.

The technology was developed through many different Icing Research Tunnel (IRT) tests of various general aviation and commercial transport components which require ice protection. The hardware was provided by the many aerospace companies that were part of the consortium. Complimentary analytical modeling

(structural and electrodynamic) and laboratory tests were conducted at Wichita State University to better understand the key physics associated with EIDI. Natural icing flight tests were conducted with the NASA icing research aircraft to which was affixed a leading edge glove or cuff with the EIDI system installed. Excellent deicing performance was documented in natural icing conditions. As a result of this program, the technology is now in hand for both the general aviation and transport manufacturers to consider EIDI for main wing/tail deicing for future applications.

The electrothermal deicing system has become the de facto standard for the helicopter industry, but the weight, power requirements, and complexity of electrothermal deicing systems has caused the industry to seek alternative concepts. In a joint program with the Army and industry (Bell Helicopter Textron and B.F. Goodrich), a pneumatic boot deicer was applied to the UH1H rotor and highly acceptable deicing capability was demonstrated (fig. 4). Deicing performance was demonstrated in both forward flight conditions behind the Army's spray tanker and near hover conditions at the Canadian NRC's Ottawa Spray rig. Prior to the icing flight tests, tests were conducted in the IRT on a full-scale, fixed-position UH1H rotor section. These tests were used to screen various pneumatic boot configurations and led to the selection of the configuration shown. Two of the attractive features of the pneumatic boot deicer system is that it had relatively few components and the UH1H system weight was only about 40 lb.

As a result of this program, the Army has qualified the UH1H helicopter with pneumatic deicers to fly into forecast icing conditions up to the "moderate" level. Future activities are being conducted by the Army and B.F. Goodrich to acquire the needed field experience especially as related to rain and sand erosion characteristics and the frequency of field repair/replacement required.

The second icing technology area to be reviewed will be analytical and experimental icing simulation. The following activities are included in this technology area:

- (1) Developing/validating codes to predict aircraft performance, stability, and control in icing
- (2) Improving/validating icing simulation facilities
- (3) Conducting natural/artificial icing flight tests
- (4) Improving icing instrumentation

First, the development and validation of icing analysis computer codes will be discussed. Figure 5 attempts to show the many codes required to form a comprehensive icing analysis methodology as well as some of the many interfaces required. The individual computer codes currently being developed and validated are as follows:

- (1) Trajectory analyses, both two dimensional and three dimensional
- (2) Airfoil ice accretion

- (3) Aerodynamic performance-in-icing, including airfoil, propeller, rotor (approximate), and complete aircraft (approximate)
- (4) Ice protection systems, including electrothermal, electroimpulse, fluid freezing point depressant, and pneumatic boot.

This set of codes forms a core analysis capability which can be used to build a more comprehensive icing analysis capability. Some examples of the various codes being developed and the supporting fundamental and validation experiments being conducted will be given.

A number of two- and three-dimensional trajectory analysis codes have been developed which can calculate water droplet paths around bodies ranging from simple, single-element airfoils to complete aircraft configurations. Appropriate data are required to validate the code accuracies, and one aspect of this experimental research as shown in figure 6. This is a joint NASA/FAA program to measure local water impingement rates (often called local collection efficiencies) on various airfoil, wing, and inlet configurations.

These curves are determined by collecting water mixed with a known concentration of blue dye on blotter strips affixed to the models like the Boeing 737-300 1/4-scale inlet shown. A He-Ne laser system measures the local reflectance of the blotter paper which can be converted to local collection efficiency. The first phase of this joint program has been completed, and additional tests are planned in order to acquire a comprehensive data base for code validation.

Figure 7 shows a computer graphics representation of the NASA icing research aircraft, a deHavilland DHC6 Twin Otter. This computer model is being used to calculate three-dimensional trajectories of water droplets about the aircraft to help in interpreting icing cloud instrument data. Selected results of trajectory analysis studies of the laser spectrometer droplet sizing instrument are shown in figure 8. The results show that significant errors can occur when the instrument is mounted beneath the main wing of the NASA icing research aircraft. This error is attributed to the three-dimensional flowfield effects on the trajectories of the water droplets. The curves indicate that, for the droplet sizes of interest (10 to 100 μm), the instrument will sense that fewer droplets per cubic meter exist than actually do exist in the "free stream" icing cloud. Similar results would be expected for any other aircraft configuration which had icing instruments located in close proximity to the aircraft surface.

A first-generation code has been developed to predict the growth of ice on a single-element airfoil. A typical comparison of the predictions of this code (called LEWICE) with data taken in the IRT on a 21 in. chord NACA 0012 airfoil is shown in figure 9. Currently evaluation studies of LEWICE are being conducted by NASA, FAA, and several companies under cooperative programs.

The LEWICE code uses a simple control volume approach for calculating local mass and energy balances which lead to local ice growth rate predictions. Such a global approach is necessary because the fundamental physics of aircraft icing are not that well understood. Fundamental in-house and university research efforts are under way to improve the basic physics understanding and incorporate this knowledge into later versions of LEWICE to improve the ice shape predictions. One example of this research is shown in figure 10.

Closeup flash pictures were taken of droplet impingement in the stagnation region of a circular cylinder. Individual cloud droplet streaks can be seen as well as water coalescence into much larger droplets and resulting movement on the surface prior to freezing.

Improved values for impact ice structural properties as well as adhesion strengths are required inputs to computer models of mechanical and thermal deicing systems. Fundamental experiments are being conducted to acquire such data, and a representative sample of the data being acquired is shown in figure 11. The figure shows adhesive shear stress as a function of airstream temperature. One important point to be gained from the figure is the considerable amount of scatter which exists with this type of data. Similar levels of data scatter have been observed by other researchers.

The current emphasis in predicting aerodynamic performance degradation due to icing is to extend and validate state-of-the-art airfoil analysis codes to predict "iced airfoil" performance. Detailed flowfield data are required to evaluate these codes, and the current approach being taken is shown in figure 12. A 21-in. NACA 0012 airfoil model was fabricated with an idealized leading edge ice accretion as shown. This initial ice accretion shape tested was meant to be generally like an ice accretion but to have well-defined cross-sectional characteristics and smooth continuous coordinates. This model was tested in the Ohio State University 4- by 5-ft low-speed wind tunnel. As the figure indicates, force and moment data were acquired as well as detailed surface pressure distributions, boundary layer profiles on both surfaces, concentrating in the vicinity of the separation reattachment zones, and flow visualization data. These data were used to compare with two state-of-the-art analysis codes - the ARC two-dimensional Navier-Stokes analysis code of NASA Ames and the Interactive Boundary Layer (IBL) code of Cebeci (California State, Long Beach). The lift and drag coefficient variations with angle of attack as predicted by the codes are compared in figure 13 to the data previously shown. Generally, the agreement is judged to be good for both codes although the IBL code tends to underpredict drag at the higher angles of attack. The activity is continuing, and, in particular, measurements and comparisons are being made with more realistic ice shape geometries.

Icing instrument research is an important part of the NASA icing research program. Figure 14 shows droplet size measurements made in the Icing Research Tunnel (IRT) using various laser spectrometer probes compared with the volume median droplet sizes determined from the facility calibration developed by NACA. The wide spread of the data away from the line of perfect agreement suggests the need for improvements in the accuracy of droplet sizing instrumentation. The data taken in this test program suggested current instrumentation accuracies of no better than $\pm 4 \mu\text{m}$ (on a volume median diameter (VMD) basis). The effect of a $\pm 4 \mu\text{m}$ variation of VMD on ice accretion shape and resulting airfoil drag increase are shown in figure 15. The figure suggests that the effects can be significant and that the accuracy of droplet sizing instrumentation must be improved.

A more accurate measurement of icing cloud properties (i.e., liquid water content and droplet size distribution) is necessary for many icing R&D purposes. Currently it is felt that the most severe problems exist for those instruments that measure droplet sizes. As indicated, the accuracy of current optical systems appears to be no better than $\pm 4 \mu\text{m}$ out of 20 (on a VMD basis).

The current research activities to improve current drop sizing instruments (fig. 16) include the following:

- (1) Improved calibration devices
- (2) Theoretical modeling of the optical characteristics of the instruments and complimentary fundamental research
- (3) Comparisons of available instruments in a simple, well-documented spray

The NASA Icing Research Tunnel (IRT) is the largest refrigerated icing wind tunnel in the world (fig. 17). It has played a key role in developing technology to solve aircraft icing problems since it became operational in June of 1944. As an indication of its importance and contributions, the American Society of Mechanical Engineers (ASME) recently designated the IRT to be an international mechanical engineering landmark facility, one of only 21 such facilities in the world. A \$3.6 million upgrade to the facility was recently completed to ensure that the IRT will continue to play a key role in the future in developing aircraft icing technology. Some of the key features of the new IRT are shown here. Of particular interest to the research community is the new spray bar system, which will allow a wider range of icing conditions to be provided to users. The final goal is to be able to provide complete coverage of the FAA/Icing envelopes.

Natural icing flight testing is also a key part of the aircraft icing research program. Currently, the aircraft being used for these tests is a deHavilland DHC6 Twin Otter. The prime emphasis of the flight tests has been to acquire an icing simulation data base, as indicated in figure 18. The primary parts of this data base are (1) the icing cloud properties (liquid water content (LWC) and droplet size spectra) measured by using the vast array of instruments on the aircraft, (2) main wing ice accretion shapes documented with a stereo photography system, and (3) wing section drag measured with a heated wake survey probe. This data being acquired over a wide range of natural icing conditions will be compared with IRT results from tests of a full-scale Twin Otter wing section and with icing analysis code predictions.

Studies of aircraft performance/stability and control changes due to icing are also being conducted with the Twin Otter. Representative performance and stability and control data are shown in figures 19 and 20. These data are also being compared with computer predictions.

Emphasis in the aircraft icing research program will eventually shift from the fixed wing to the rotary wing since some of the most difficult icing problems are faced by the rotorcraft community. Currently, the rotorcraft icing activities are focused on evaluating the model rotor icing test technique, that is, determining what use can be made of testing scale-model rotors in a large icing wind tunnel such as the IRT. To date, no such tests have been conducted in the U.S., and U.S. manufacturers must rely primarily on artificial/natural icing flight testing which is extremely costly and time consuming. In order to evaluate the model rotor test technique, NASA has teamed with the four major U.S. helicopter manufacturers and Texas A&M University to carry out all the activities required to test in the IRT a fully instrumented, powered-force model provided by Sikorsky and shown in figure 21. Prior to this test, several

supporting test techniques must be developed, and for these preliminary activities, an OH58 tail rotor rig shown here will be used. The OH58 is a much sturdier rig and therefore should be more forgiving to any unexpected surprises which might be encountered during the initial IRT test.

Once this initial evaluation is completed, it is envisioned that follow-on tests will be conducted, especially for comparison with full-scale, natural icing flight test results. Initial full-scale rotor icing test results were acquired in the recent NASA/Army Helicopter Icing Flight Test Program. The various activities in this multiphase program are shown in figure 22. This test program was a multiphase effort to acquire unprotected helicopter rotor ice accretion and aerodynamic performance data for both hover and forward flight conditions. The techniques developed will be used in proposed future programs to acquire flight data for comparison with the scale-model rotor data which will be acquired in follow-on IRT Tests.

Now that some highlights of the NASA aircraft icing research program have been reviewed, it is appropriate to consider figure 1 and indicate the future directions of the program.

The generic activities will continue as indicated:

- (1) The icing analysis codes will become more robust and sophisticated as to the problems which can be analyzed.

- (2) New instrumentation concepts will be investigated which will offer improved accuracy levels over current instruments.

- (3) Research will continue to look for alternate ice protection concepts which look attractive from weight, power requirement, and efficiency standpoints.

Future emphasis as related to fixed-wing aircraft will be to couple the codes together to form more comprehensive icing-effects-simulation computer models. Such models, once validated against icing flight data, could be used in pilot training simulators, for preliminary design studies, and possibly as part of certification/qualification programs.

- (1) Investigations will be conducted of potential icing problems for unique military aircraft configurations of the future with emphasis on the ice protection design requirements for such aircraft.

- (2) NASA is also developing jointly with the major U.S. airframe and engine manufacturers a proposed research program to investigate the ice protection requirements for the advanced propfan engine configurations which will be flying in the early 1990's. A major component of this proposed program would be natural icing flight tests of a propfan configuration, and it is felt that the so-called PTA aircraft would be the ideal research aircraft to conduct these studies.

The longer term emphasis of the NASA icing research program will shift to the helicopter, with the areas of emphasis shown in figure 1. In the shorter term, the majority of activities will be to evaluate the model rotor icing test technique.

A bibliography of icing reports generated by the NASA Aircraft Icing Research Program is included in the appendix.

APPENDIX - AIRCRAFT ICING RESEARCH PROGRAM BIBLIOGRAPHY

1980

Norment, H.G.: Calculation of Water Drop Trajectories To and About Arbitrary Three-Dimensional Bodies in Potential Airflow. NASA CR-3291, 1980.

1981

Bragg, M.B.; Gregorek, G.M.; and Shaw, R.J.: An Analytical Approach to Airfoil Icing. AIAA Paper 81-0403, Jan. 1981.

Breeze, R.K.; and Clark, G.M.: Light Transport and General Aviation Aircraft Icing Research Requirements. (NA-81-110, Rockwell International Corp.; NASA Contract NAS3-22186) NASA CR-165290, 1981.

Evanich, P.L.: NASA Lewis Research Center's Icing Research Program. Proceedings: Fifth Annual Workshop on Meteorological and Environmental Inputs to Aviation Systems, NASA CP-2192, D.W. Camp, W. Frost, and P.D. Parsley, eds., 1981, pp. 64-75.

Koegeboehn, L.P.: Commercial Aviation Icing Research Requirements. NASA CR-165336, 1981.

Kohlman, D.L., et al.: Icing Tunnel Tests of a Glycol-Exuding Porous Leading Edge Ice Protection System on a General Aviation Airfoil. (KU-FRL-464-1, Kansas University; NASA Grant NAG3 71) NASA CR-164377, 1981.

Kohlmann, D.L.; Schweikhard, W.G.; and Evanich, P.: Icing Tunnel Tests of a Glycol-Exuding Porous Leading Edge Ice Protection System on a General Aviation Airfoil. AIAA Paper 81-0405, Jan. 1981.

Olsen, W.: Survey of Aircraft Icing Simulation Test Facilities in North America. NASA TM-81707, 1981.

Peterson, A.A.; Dadone, L.; and Bevan, D.: Rotorcraft Aviation Icing Research Requirements: Research Review and Recommendations. (D210-11662-1, Boeing Vertol Co.; NASA Contract NAS3-22384) NASA CR-165344, 1981.

Reinmann, J.J., ed.: Selected Bibliography of NACA-NASA Aircraft Icing Publications. NASA TM-81651, 1981.

1982

Bragg, M.B.: Rime Ice Accretion and Its Effect on Airfoil Performance. NASA CR-165599, 1982.

Bragg, M.B.; and Gregorek, G.M.: Aerodynamic Characteristics of Airfoils With Ice Accretions. AIAA Paper 82-0282, Jan. 1982.

Bragg, M.B.; Gregorek, G.M.; and Shaw, R.J.: Wind Tunnel Investigation of Airfoil Performance Degradation Due to Icing. AIAA Paper 82-0582, Mar. 1982.

Bragg, M.B.; Zaguli, R.J.; and Gregorek, G.M.: Wind Tunnel Evaluation of Airfoil Performance Using Simulated Ice Shapes. NASA CR-167960, 1982.

DeWitt, K.J.; and Baliga, G.: Numerical Simulation of One-Dimensional Heat Transfer in Composite Bodies With Phase Change. NASA CR-165607, 1982.

Korkan, K.D.; Dadone, L.; and Shaw, R.J.: Performance Degradation of Propeller Systems Due to Rime Ice Accretion. AIAA Paper 82-0286, Jan. 1982. (J. Aircraft, vol. 21, no. 1, Jan. 1984, pp. 44-49).

MacArthur, C.D.; Keller, J.L.; and Luers, J.K.: Mathematical Modeling of Ice Accretion on Airfoils. AIAA Paper 82-0284, Jan. 1982.

Magenheim, B.; and Rocks, J.: A Microwave Ice Accretion Measurement Instrument (MIAMI). AIAA Paper 82-0285, Jan. 1982.

Magenheim, B.; and Rocks, J.K.: Development and Test of a Microwave Ice Accretion Measurement Instrument (MIAMI). NASA CR-3598, 1982.

Reinmann, J.J.; Shaw, R.J.; and Olsen, W.A., Jr.: Aircraft Icing Research at NASA. Proceedings of the First International Workshop on Atmospheric Icing of Structures, CRREL SR-83-17, L.D. Minsk, ed., Electric Power Research Institute, 1982, pp. 103-116. (Avail. NTIS, AD-A131869 and AD-E850387). (NASA TM-82919.)

Shaw, R.J.: The NASA Aircraft Icing Research Program. Sixth Annual Workshop on Meteorological and Environmental Inputs to Aviation Systems, NASA CP-2274, W. Frost, D.W. Camp, and L.W. Hershman, eds., 1982, pp. 50-56.

Shaw, R.J.; Sotos, R.G.; and Solano, F.R.: An Experimental Study of Airfoil Icing Characteristics. NASA TM-82790, 1982.

1983

Bragg, M.B.; and Gregorek, G.M.: An Analytical Evaluation of the Icing Properties of Several Low and Medium Speed Airfoils. AIAA Paper 83-0109, Jan. 1983.

Bragg, M.B.; and Gregorek, G.M.: Predicting Aircraft Performance Degradation Due to Ice Accretion. SAE Paper 830742, 1983.

Chang, K., et al.: Influence of Multidroplet Size Distribution on Icing Collection Efficiency. AIAA Paper 83-0110, Jan. 1983.

Chao, D.F.K.: Numerical Simulation of Two-Dimensional Heat Transfer in Composite Bodies With Application to De-Icing of Aircraft Components. NASA CR-168283, 1983.

DeWitt, K.J., et al.: Numerical Simulation of Electrothermal Deicing Systems. AIAA Paper 83-0114, Jan. 1983.

Flemming, R.J.; and Lednicer, D.A.: High Speed Ice Accretion on Rotorcraft Airfoils. Proceedings, 39th Annual Forum, American Helicopter Society, 1983, pp. 44-57.

Kohlman, D.L.; and Albright, A.E.: A Method of Predicting Flow Rates Required to Achieve Anti-Icing Performance With A Porous Leading Edge Ice Protection System. (KU-FRL-464-5 REV-A, Kansas University; NASA Grant NAG3-71) NASA CR-168213, 1983.

Korkan, K.D.; Dadone, L.; and Shaw, R.J.: Performance Degradation of Helicopter Rotor Systems in Forward Flight Due to Rime Ice Accretion. AIAA Paper 83-0029, Jan. 1983.

MacArthur, C.D.: Numerical Simulation of Airfoil Ice Accretion. AIAA Paper 83-0112, Jan. 1983.

Marano, J.J.: Numerical Simulation of an Electrothermal Deicer Pad. NASA CR-168097, 1983.

Miller, T.L.; Korkan, K.D.; and Shaw, R.J.: Statistical Study of an Airfoil Glaze Ice Drag Correlation. SAE Paper 830753, 1983.

Olsen, W.; Takeuchi, D.; and Adams, K.: Experimental Comparison of Icing Cloud Instruments. AIAA Paper 83-0026, Jan. 1983. (NASA TM-83340.)

Palko, R.L.; and Cassady, P.L.: Photogrammetric Analysis of Ice Buildup on a U.S. Army UH-1H Helicopter Main Rotor in Hover Flight. AEDC-TR-83-43, Oct. 1983. (Avail. NTIS, AD-B077844.)

Reinmann, J.J.; Shaw, R.J.; and Olsen, W.A., Jr.: NASA Lewis Research Center's Program on Icing Research. AIAA Paper 83-0204, Jan. 1983. (NASA TM-83031.)

Takeuchi, D.M., et al.: Comparison of Modern Icing Cloud Instruments. (MRI-82-FR-1862, Meteorology Research Inc.; NASA Contract NAS3-22760) NASA CR-168008, 1983.

1984

Albright, A.E.: Experimental and Analytical Investigation of a Freezing Point Depressant Fluid Ice Protection System. NASA CR-174758, 1984.

Albright, A.E.; and Kohlman, A.E.: An Improved Method of Predicting Anti-Icing Flow Rates for a Fluid Ice Protection System. AIAA Paper 84-0023, Jan. 1984.

Arimilli, R.V.; Keshock, E.G.; and Smith, M.E.: Measurements of Local Convective Heat Transfer Coefficients on Ice Accretion Shapes. AIAA Paper 84-0018, Jan. 1984.

Bernhart, W.D.; and Zumwalt, G.W.: Electro-Impulse Deicing: Structural Dynamic Studies, Icing Tunnel Tests and Applications. AIAA Paper 84-0022, Jan. 1984.

Bragg, M.B.: Predicting Airfoil Performance With Rime and Glaze Ice Accretions. AIAA Paper 84-0106, Jan. 1984.

Bragg, M.B.; Gregorek, G.M.; and Lee, J.D.: Experimental and Analytical Investigations Into Airfoil Icing. 14th Congress of the International Council of the Aeronautical Sciences, Vol. 2, B. Laschka and R. Staufenbiel, eds., AIAA, 1984, pp. 1127-1138.

Flemming, R.J.; and Lednicer, D.A.: Experimental Investigation of Ice Accretion on Rotorcraft Airfoils at High Speeds. AIAA Paper 84-0183, Jan. 1984.

Gregorek, G.M.; Bragg, M.B.; and Shilling, J.B.: Performance Analyses for Aircraft in Icing Conditions. AIAA Paper 84-0180, Jan. 1984.

Ide, R.F.; and Richter, G.P.: Comparison of Icing Cloud Instruments for 1982-83 Icing Season Flight Program. AIAA Paper 84-0020, Jan. 1984. (NASA TM-83569.)

Keith, T.G., Jr., et al.: Predicted Electrothermal Deicing of Aircraft Blades. AIAA Paper 84-0110, Jan. 1984.

Korkan, K.D.; Cross, E.J., Jr.; and Cornell, C.C.: Experimental Study of Performance Degradation of a Model Helicopter Main Rotor With Simulated Ice Shapes. AIAA Paper 84-0184, Jan. 1984.

Korkan, K.D.; Cross, E.J., Jr.; and Miller, T.L.: Performance Degradation of a Model Helicopter Main Rotor in Hover and Forward Flight With a Generic Ice Shape. AIAA Paper 84-0609, Mar. 1984.

Korkan, K.D.; Dadone, L.; and Shaw, R.J.: Helicopter Rotor Performance Degradation in Natural Icing Encounter. J. Aircraft, vol. 21, no. 1, Jan. 1984, pp. 84-85.

Lee, J.D.: Aerodynamic Evaluation of a Helicopter Rotor Blade With Ice Accretion in Hover. AIAA Paper 84-0608, Mar. 1984.

Lee, J.D.; Harding, R.; and Palko, R.L.: Documentation of Ice Shapes on the Main Rotor of a UH-1H Helicopter in Hover. NASA CR-168332, 1984.

Olsen, W.A., Jr.; Shaw, R.J.; and Newton, J.: Ice Shapes and the Resulting Drag Increase for a NACA 0012 Airfoil. AIAA Paper 84-0109, Jan. 1984.

Olsen, W.A., Jr.; Walker, E.D.; and Sotos, R.G.: Microscopic High Speed Movies Showing the Droplet Freezing Process of Icing. AIAA Paper 84-0019, Jan. 1984.

Palko, R.L., et al.: Initial Feasibility Ground Test of a Proposed Photogrammetric System for Measuring the Shapes of Ice Accretions on Helicopter Rotor Blades During Forward Flight. NASA TM-87391, 1984.

Potapczuk, M.G., et al.: Evaluation of Iced Airfoil Performance Using a Navier-Stokes Equation Solver With a Body-Fitted Curvilinear Coordinate System. AIAA Paper 84-0107, Jan. 1984.

Ranaudo, R.J., et al.: Performance Degradation of a Typical Twin Engine Commuter Type Aircraft in Measured Natural Icing Conditions. AIAA Paper 84-0179, Jan. 1984.

Schrag, R.L.; and Zumwalt, G.W.: Electro-Impulse Deicing: Concept and Electrodynamic Studies. AIAA Paper 84-0021, Jan. 1984.

Shaw, R.J.: Experimental Determination of Airfoil Performance Degradation Due to Icing. AIAA Paper 84-0607, Mar. 1984.

Shaw, R.J.: Progress Toward the Development of an Aircraft Icing Analysis Capability. AIAA Paper 84-0105, Jan. 1984. (NASA TM-83562.)

VanFossen, G.J., et al.: Heat Transfer Distributions Around Nominal Ice Accretion Shapes Formed on a Cylinder in the NASA Lewis Research Tunnel. AIAA Paper 84-0017, Jan. 1984.

Zaguli, R.J.: Potential Flow Analysis of Glaze Ice Accretions on an Airfoil. NASA CR-168282, 1984.

Zaguli, R.J.; Bragg, M.B.; and Gregorek, G.M.: Results of an Experimental Program Investigating the Effects of Simulated Ice on the Performance of the NACA-63A415 Airfoil With Flap. (AARL-TR-83-2, Ohio State Univ.; NASA Grant NAG3-28) NASA CR-168288, 1984.

Zumwalt, G.W.; and Mueller, A.A.: Flight and Wind Tunnel Tests of an Electro-Impulse De-Icing System. AIAA Paper 84-2234, July 1984.

1985

Albright, A.E.: A Summary of NASA's Research on the Fluid Ice Protection System. AIAA Paper 85-0467, Jan. 1985.

Bragg, M.B.; and Coirier, W.J.: Detailed Measurements of the Flowfield in the Vicinity of an Airfoil with Glaze Ice. AIAA Paper 85-0409, Jan. 1985.

Flemming, R.J.; and Lednicer, D.A.: Correlation of Airfoil Icing Relationships with Two-Dimensional Model and Full Scale Rotorcraft Icing Test Data. AIAA Paper 85-0337, Jan. 1985.

Flemming, R.J.; Shaw, R.J.; and Lee, J.D.: The Performance Characteristics of Simulated Ice on Rotorcraft Airfoils. Proceedings, 41st Annual Forum, American Helicopter Society, 1985, pp. 743-757.

Gregorek, G.M., et al.: NASA Twin Otter Flight Test Program - Comparison of Flight Results with Analytic Theory. SAE Paper 850924, Apr. 1985.

Hansman, R.J., Jr.; and Kirby, M.S.: Measurement of Ice Accretion Using Ultrasonic Pulse-Echo Techniques. AIAA Paper 85-0471, Jan. 1985.

Haworth, L.A.; and Graham, M.S.: Flight Tests of the Helicopter Pneumatic Deicing System. Proceedings, American Helicopter Society, 41st Annual Forum, 1985, pp. 725-733.

Hovenac, E.A.; Hirleman, E.D.; and Ide, R.: Calibration and Sample Volume Characterization of PMS Optical Array Probes. Presented at the International Conference on Liquid Atomization and Spray Systems (ICLASS), London, England, July 1985.

Kim, J.J.: Computational Particle Trajectory Analysis on a Three-Dimensional Engine Inlet. AIAA Paper 85-0411, Jan. 1985.

Korkan, K.D.; Dadone, L.; and Shaw, R.J.: Performance Degradation of Helicopters Due to Icing - A Review. Proceedings, 41st Annual Forum, American Helicopter Society, 1985.

Lee, J.D.; and Shaw, R.J.: The Aerodynamics of Rotor Blades with Ice Shapes Accreted in Hover and in Level Flight. Proceedings, 41st Annual Forum, American Helicopter Society, 1985, pp. 735-742.

Masiulaniec, K.K., et al.: Full Two-Dimensional Transient Solutions of Electrothermal Aircraft Blade Deicing. AIAA Paper 85-0413, Jan. 1985.

Mikkelsen, K.L., et al.: Icing Flight Research: Aerodynamic Effects of Ice, and Ice Shape Documentation with Stereo Photography. AIAA Paper 85-0468, Jan. 1985.

Miller, T.L.; Korkan, K.D.; and Shaw, R.J.: Analytical Determination of Propeller Performance Degradation Due to Ice Accretion. AIAA Paper 85-0339, Jan. 1985.

Norment, H.G.: Calculation of Water Drop Trajectories To and About Arbitrary Three-Dimensional Lifting and Nonlifting Bodies in Potential Airflow. NASA CR-3935, 1985.

Norment, H.G.: Three-Dimensional Airflow and Hydrometeor Trajectory Calculation with Applications. AIAA Paper 85-0412, Jan. 1985.

Potapczuk, M.G.; and Gerhart, P.M.: Progress in Development of a Navier-Stokes Solver for Evaluation of Iced Airfoil Performance. AIAA Paper 85-0410, Jan. 1985.

Shaw, R.J.; and Richter, G.P.: The UH-1H Helicopter Icing Flight Test Program: An Overview. AIAA Paper 85-0338, Jan. 1985.

Zumwalt, G.W.: Icing Tunnel Tests of Electro-Impulse De-Icing of an Engine Inlet and High Speed Wings. AIAA Paper 85-0466, Jan. 1985.

1986

Bernhart, W.D.; Gien, P.H.; and Wilson, B.K.: A Structural Dynamics Investigation Related to EIDI Application. AIAA Paper 86-0550, Jan. 1986.

Bragg, M.B.; and Coirier, W.J.: Aerodynamic Measurements of an Airfoil With Simulated Glaze Ice. AIAA Paper 86-0484, Jan. 1986.

- Hansman, R.J., Jr.; and Kirby, M.S.: Real-Time Measurement of Ice Growth During Simulated and Natural Icing Conditions Using Ultrasonic Pulse-Echo Techniques. AIAA Paper 86-0410, Jan. 1986.
- Hovenac, E.A.: Calibration of Droplet Sizing and Liquid Water Content Instruments: Survey and Analysis. (FAA-CT-86-19, Sverdrup Technology Inc., NASA Contract NAS3 24105) NASA CR 175099, 1986.
- Hovenac, E.A.: Use of Rotating Reticles for Calibration of Single Particle Counters. LIA, vol. 58, 1987, pp. 129-134.
- Ingebo, R.D.: Formation and Characterization of Simulated Small-Droplet Icing Clouds. AIAA Paper 86-0409, Jan. 1986. (NASA TM-87180.)
- Jordan, J.L.; Platz, S.J.; and Schinstock, W.C.: Flight Test Report of the NASA Icing Research Airplane: Performance, Stability, and Control After Flight Through Natural Icing Conditions. (KSR-86-01, Kohlman Systems Research; NASA Contract NAS3-24547) NASA CR-179515, 1986.
- Kim, J.J.: Particle Trajectory Computation on a 3-Dimensional Engine Inlet. (DOT-FAA-CT-86-1, Wichita State Univ.; NASA Grant NAG3-566) NASA CR-175023, 1986.
- Kim, J.J.; and Elangovan, R.: An Efficient Numerical Computation Scheme for Stiff Equations of Droplet Trajectories. AIAA Paper 86-0407, Jan. 1986.
- McKnight, R.C.; Palko, R.L.; and Humes, R.L.: In-Flight Photogrammetric Measurement of Wing Ice Accretions. AIAA Paper 86-0483, Jan. 1986. (NASA TM-87191.)
- Mikkelsen, K., et al.: In-Flight Measurements of Wing Ice Shapes and Wing Section Drag Increases Caused by Natural Icing Conditions. NASA TM-87301, 1986.
- Nelepovitz, D.O.; and Rosenthal, H.A.: Electro-Impulse De-Icing of Aircraft Engine Inlets. AIAA Paper 86-0546, Jan. 1986.
- Olsen, W.: Experimental Evaluation of Icing Scaling Laws: A Progress Report. AIAA Paper 86-0482, Jan. 1986.
- Olsen, W.; and Walker, E.: Experimental Evidence for Modifying the Current Physical Model for Ice Accretion on Aircraft Surfaces. NASA TM-87184, 1986.
- Papadakis, M., et al.: An Experimental Method for Measuring Droplet Impingement Efficiency on Two- and Three-Dimensional Bodies. AIAA Paper 86-0406, Jan. 1986.
- Ranaudo, R.J., et al.: The Measurement of Aircraft Performance and Stability and Control After Flight Through Natural Icing Conditions. AIAA Paper 86-9758, Apr. 1986. (NASA TM 87265.)
- Ross, R.: Application of Electro-Impulse De-Icing to the NASA Lewis Altitude Wind Tunnel (AWT) Turning Vanes. AIAA Paper 86-0548, Jan. 1986.

Ruff, G.A.: Verification and Application of the Icing Scaling Equations. AIAA Paper 86-0481, Jan. 1986.

Shaw, R.J.: NASA's Aircraft Icing Analysis Program. NASA TM-88791, 1986.

Shaw, R.J., et al.: The Use of a Three Dimensional Water Droplet Trajectory Analysis to Aid in Interpreting Icing Cloud Data, AIAA Paper 86-0405, Jan. 1986.

Zumwalt, G.W.; and Friedberg, R.A.: Designing an Electro-Impulse De-Icing System. AIAA Paper 86-0545, Jan. 1986.

1987

Alexander, D.R.: Comparison of UNL Laser Imaging and Sizing System and a Phase/Doppler System for Analyzing Sprays from a NASA Nozzle. NASA CR-182437, 1987.

Bragg, M.B.: An Experimental Study of the Aerodynamics of a NACA 0012 Airfoil with a Simulated Glaze Ice Accretion. NASA CR-179897, 1987.

Cebeci, T.: Effects of Environmentally Imposed Roughness on Airfoil Performance. NASA CR-179639, 1987.

Henderson, R.A.; and Schrag, R.L.: Theoretical Analysis of the Electrical Aspects of the Basic Electro-Impulse Problem in Aircraft De-Icing Applications. NASA CR-180845, 1987.

Hovenac, E.A.: Fresnel Diffraction by Spherical Obstacles. Am. J. Phys., vol. 57, no. 1, Jan. 1989, pp. 79-84.

Hovenac, E.A.: Performance and Operating Envelope of Imaging and Scattering Particle Sizing Instruments. NASA CR-180859, 1987.

Miller, T.L.; Shaw, R.J.; and Korkan, K.D.: Evaluation of Icing Drag Coefficient Correlations Applied to Iced Propeller Performance Prediction. SAE Paper 871033, Apr. 1987.

Miller, T.L.; Korkan, K.D.; and Shaw, R.J.: Analytical Determination of Propeller Performance Degradation Due to Ice Accretion. J. Aircraft, vol. 24, no. 11, Nov. 1987, pp. 768-775.

Newton, J.E.: Icing of Flow Conditioners in a Closed-Loop Wind Tunnel. NASA TM-89824, 1987.

Oldenburg, J.R.: Analysis of Counting Errors in the Phase/Doppler Particle Analyzer. NASA TM-100231, 1987.

Olsen, W.; Van Fossen, J.; and Nussle, R.: Measured Performance of the Heat Exchanger in the NASA Icing Research Tunnel Under Severe Icing and Dry Air Conditions. NASA TM-100116, 1987.

Potapczuk, M.G.: Numerical Analysis of a NACA 0012 Airfoil with Leading-Edge Ice Accretions. AIAA Paper 87-0101, Jan. 1987. (J. Aircraft, vol. 25, no. 3, Mar. 1988, pp. 193-194).

Reehorst, A.L.; and Richter, G.P.: New Methods and Materials for Molding and Casting Ice Formations. NASA TM-100126, 1987.

Scavuzzo, R.J.; and Chu, M.L.: Structural Properties of Impact Ices Accreted on Aircraft Structures. NASA CR-179580, 1987.

Shaw, R.J.; and Reinmann, J.J.: NASA's Rotorcraft Icing Research Program. NASA/Army Rotorcraft Technology, Vol. 2, NASA CP-2495-VOL-2, 1987, pp. 802-832.

1988

Khatkhate, A.A.; Scavuzzo, R.J.; and Chu, M.L.: A Finite Element Study of the EIDI System. AIAA Paper 88-0022, Jan. 1988.

VanFossen, J.G., et al.: Measurement of Local Convective Heat Transfer Coefficients from a Smooth and Roughened NACA-0012 Airfoil: Flight Test Data. AIAA Paper 88-0287, Jan. 1988. (NASA TM-100284).

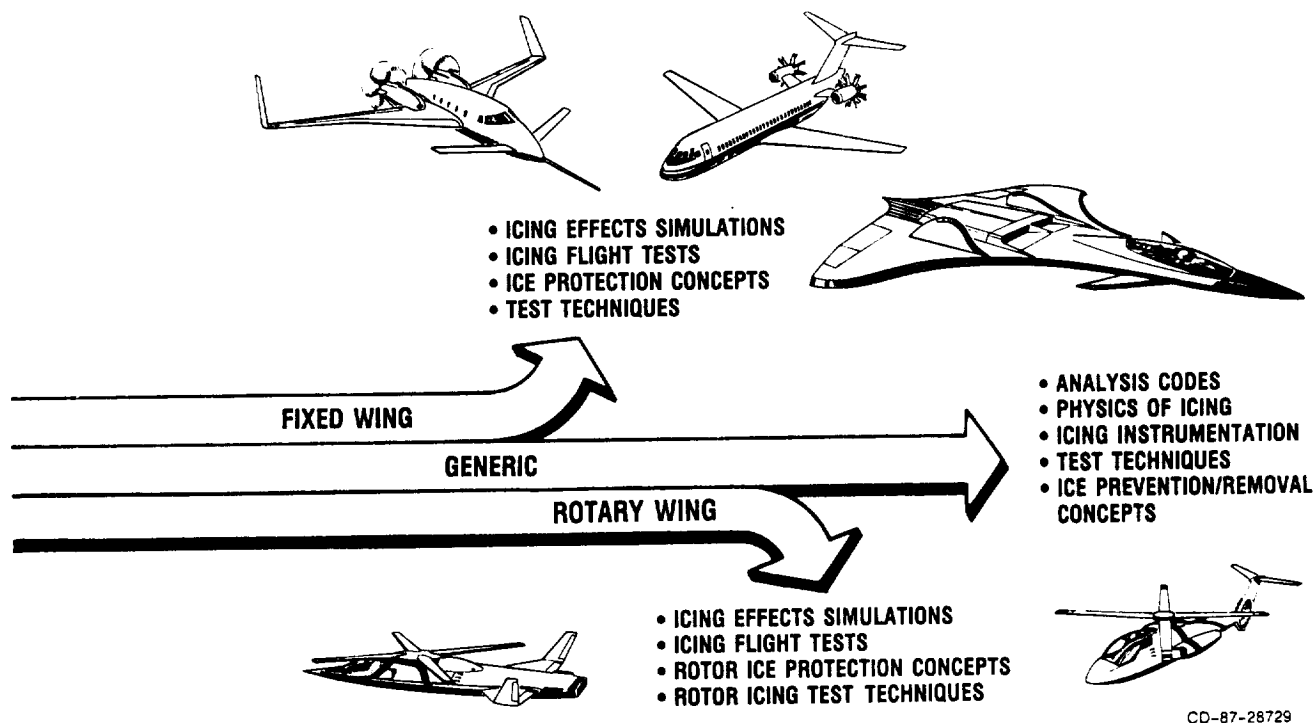


Figure 1. - Aircraft icing technology program.

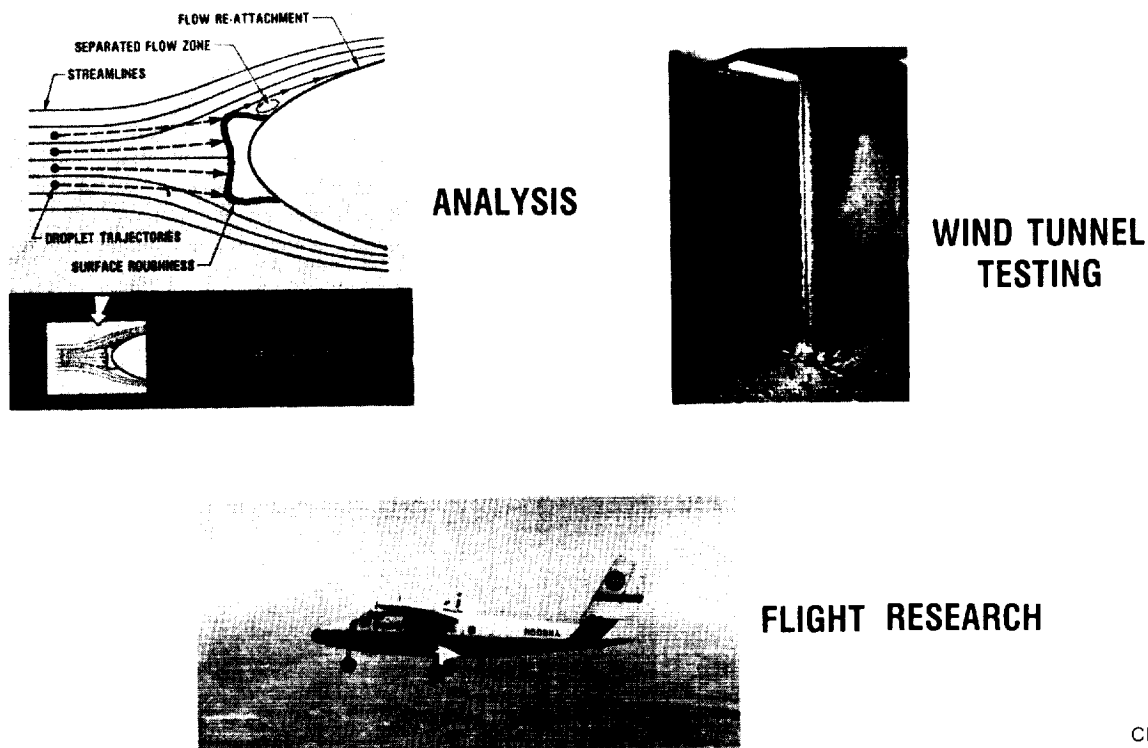


Figure 2. - Icing research.

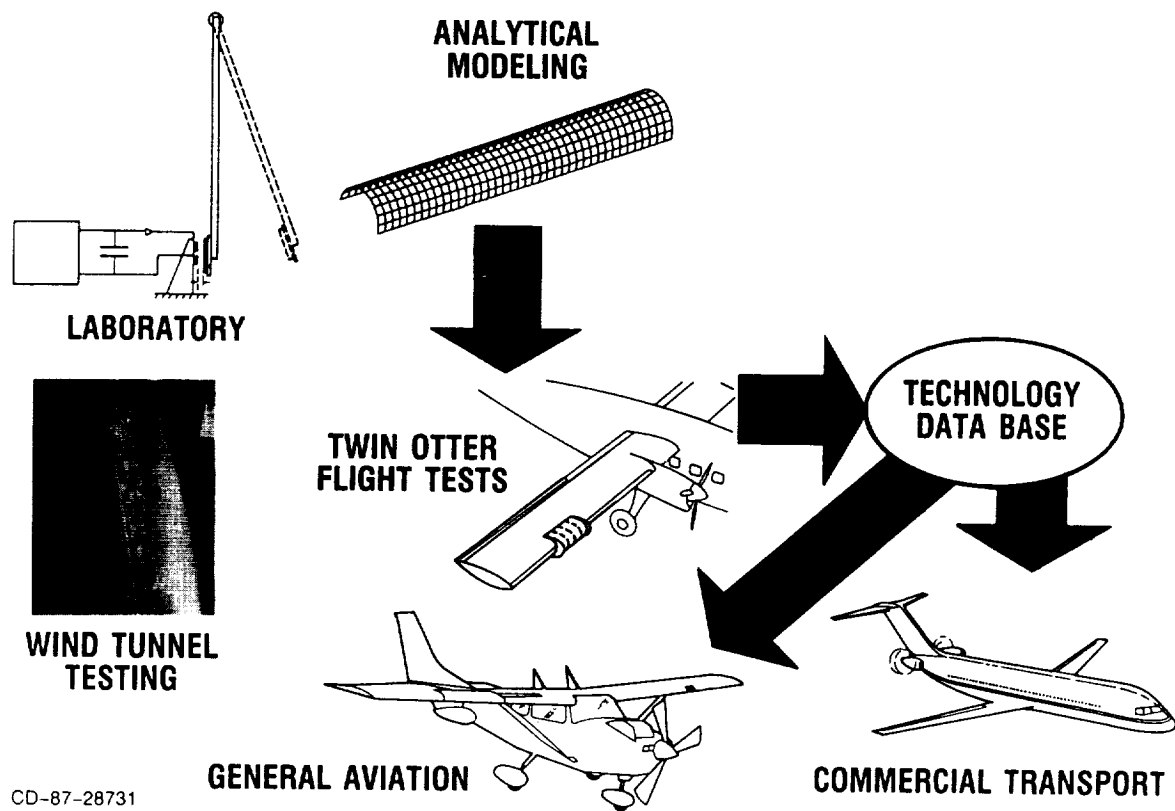


Figure 3. - NASA electromagnetic impulse deicer program.

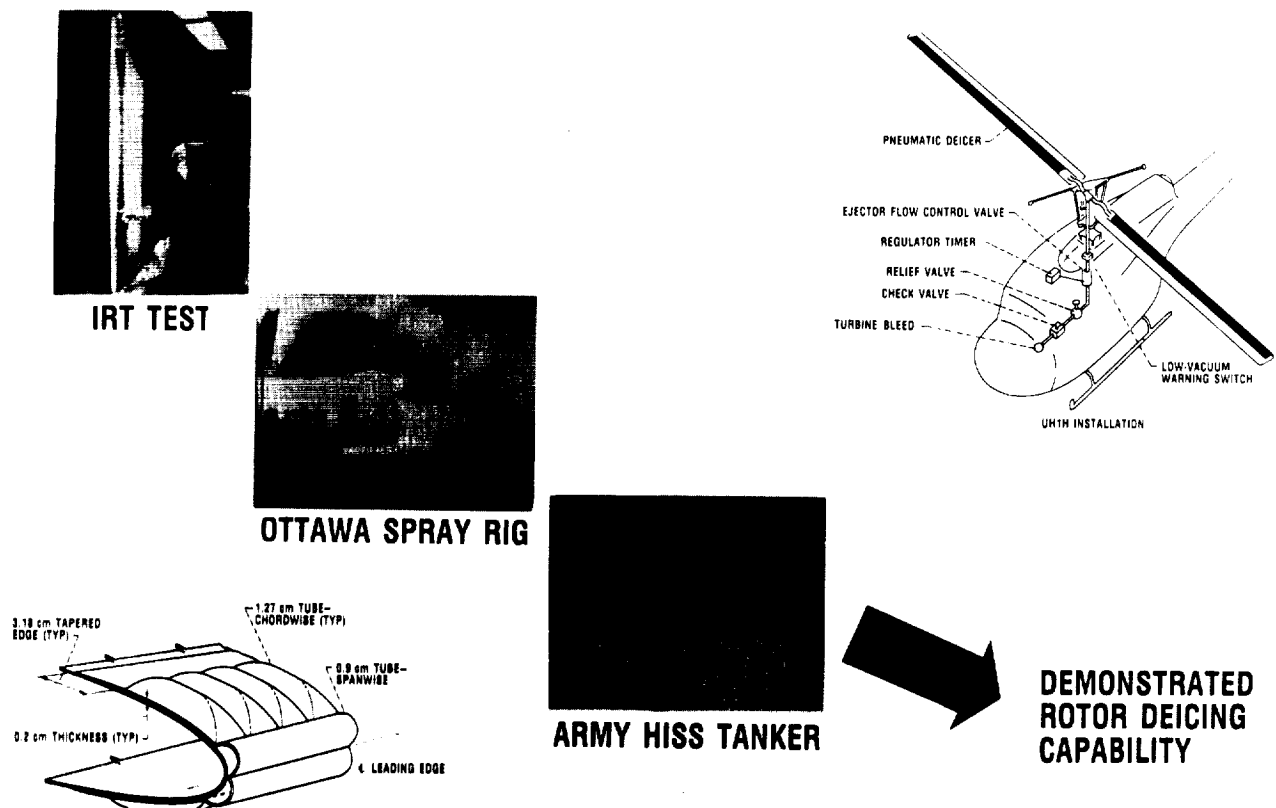


Figure 4. - NASA/Army/industry rotor pneumatic boot program.

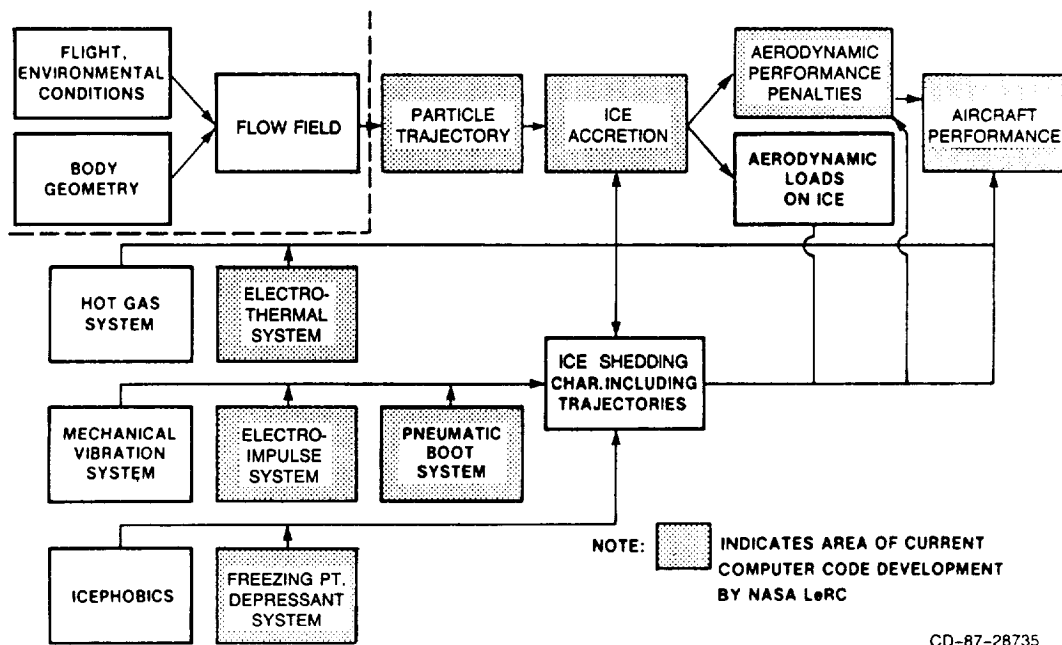


Figure 5. - Aircraft icing analysis methodology.

OBJECTIVE - ACQUIRE A DATA BASE TO VALIDATE TRAJECTORY CODES

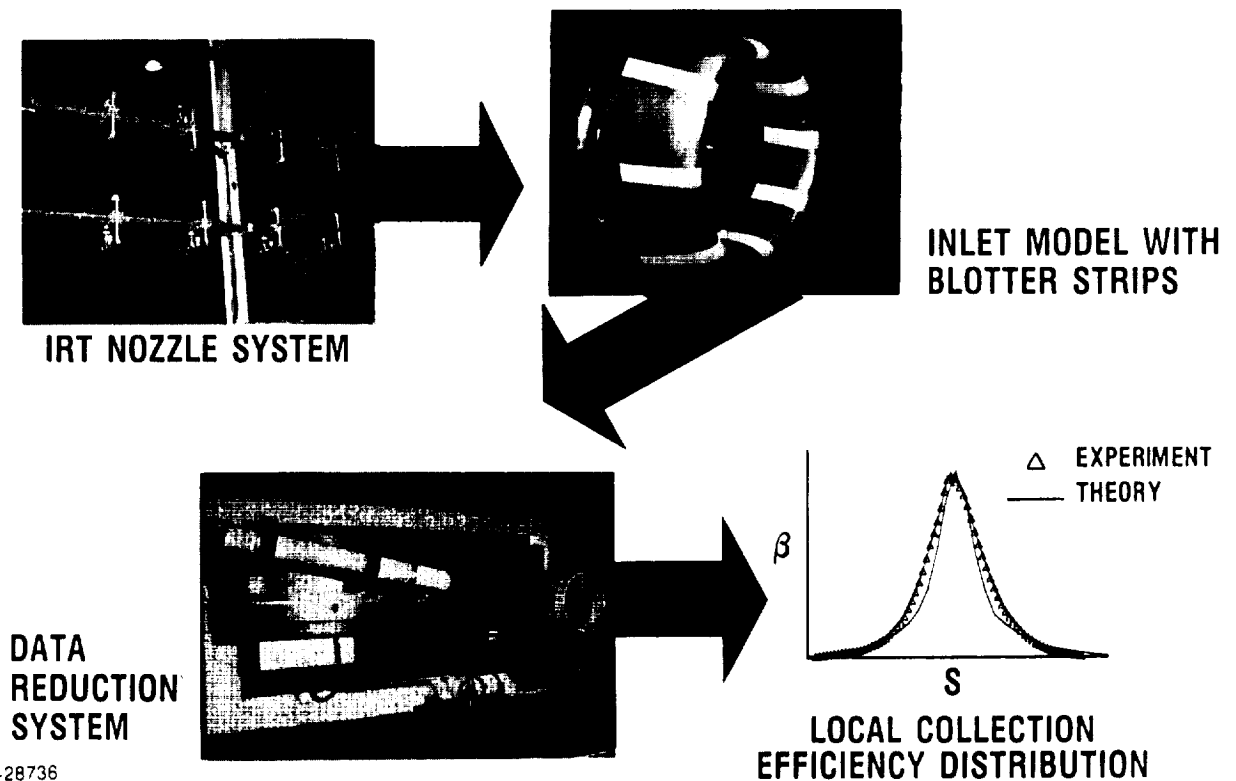
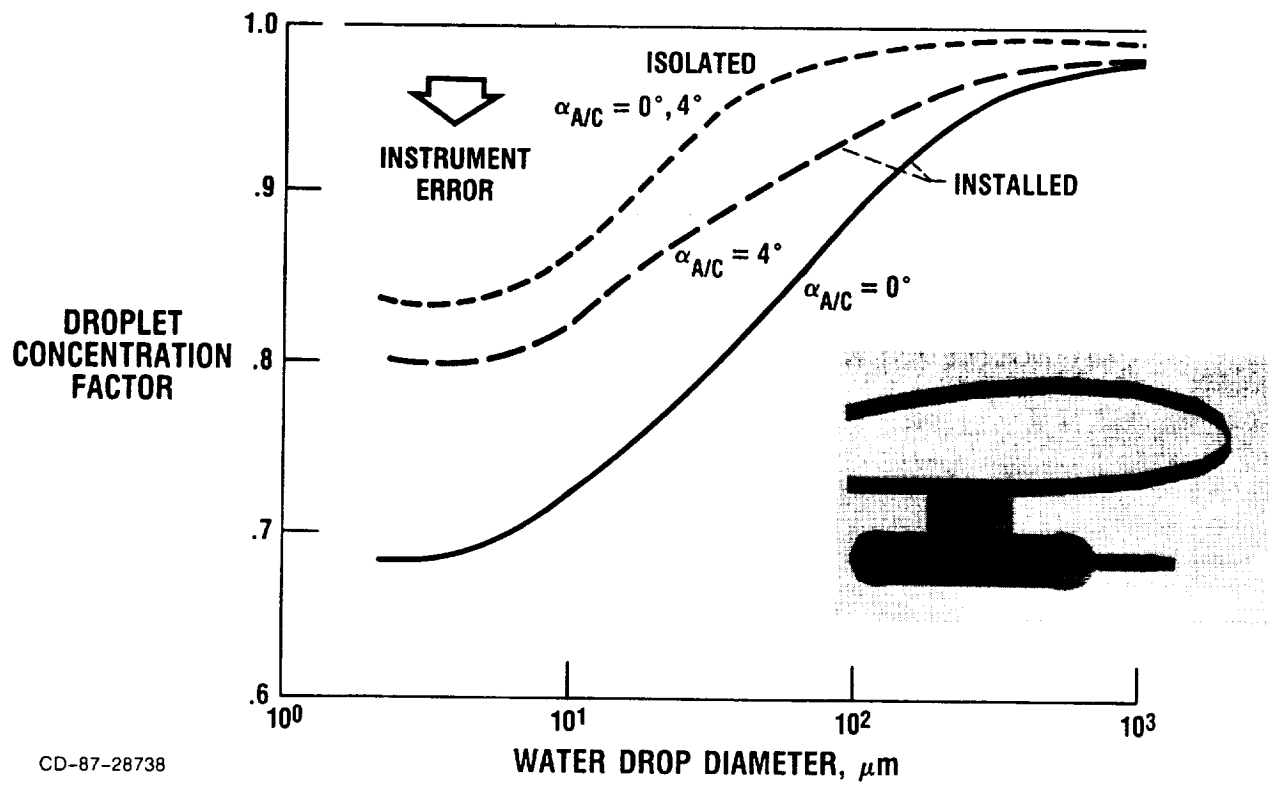


Figure 6. - NASA/FAA water droplet impingement research program.



Figure 7. - Twin Otter trajectory analysis.

CD-87-28737



CD-87-28738

Figure 8. - Trajectory analysis for laser spectrometer.

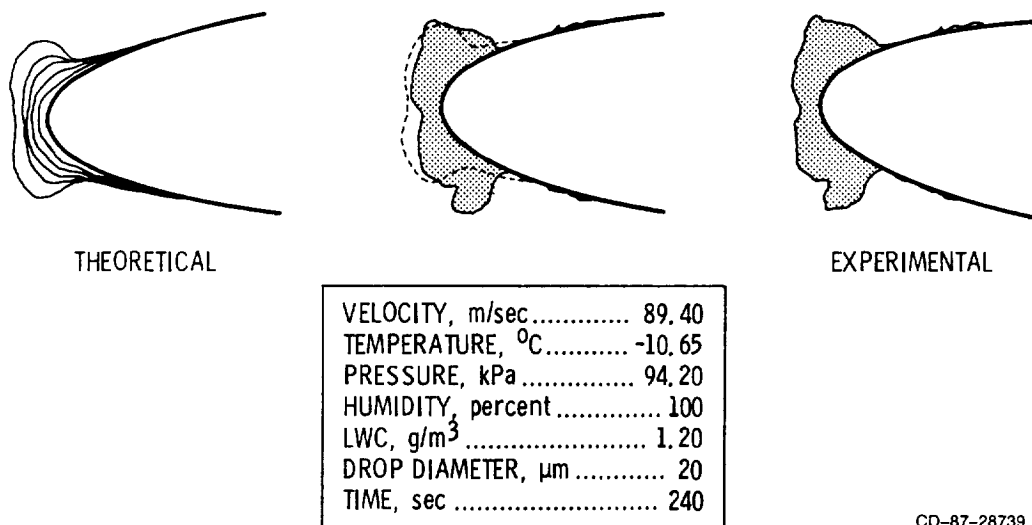
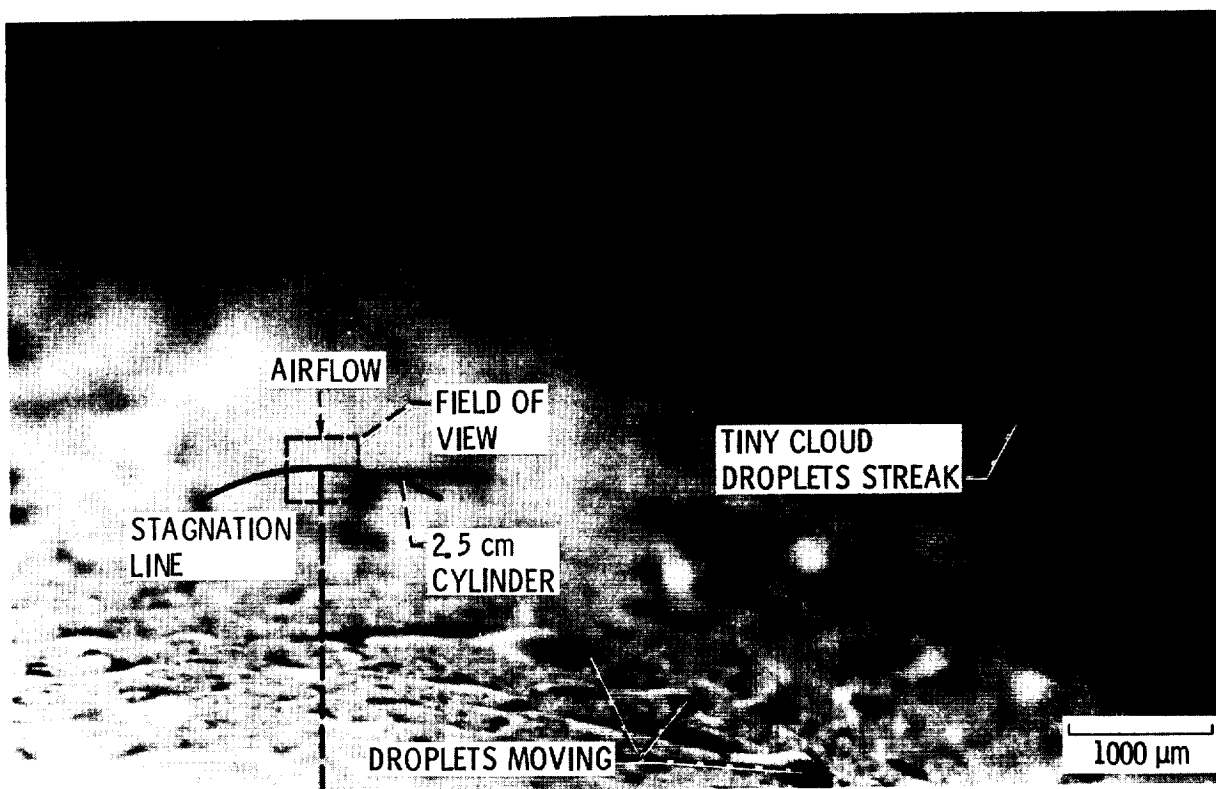
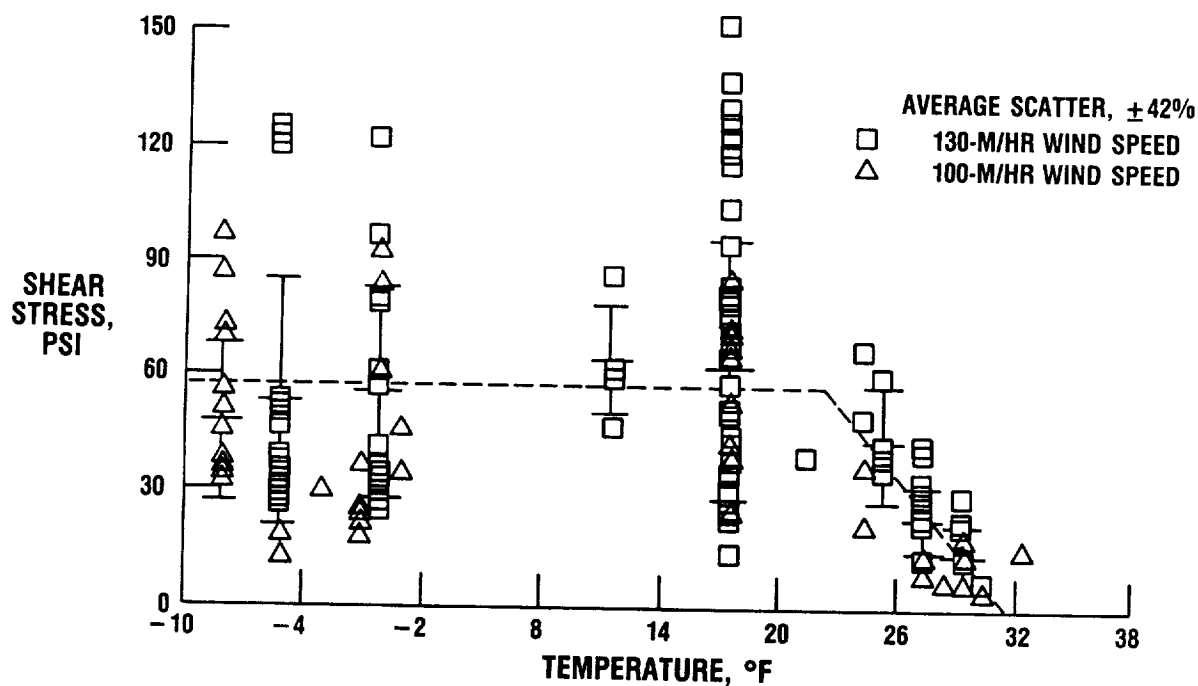


Figure 9. - NASA airfoil ice accretion code (LEWICE) comparison of glaze ice shapes (NACA 0012 airfoil, 21-in. chord).



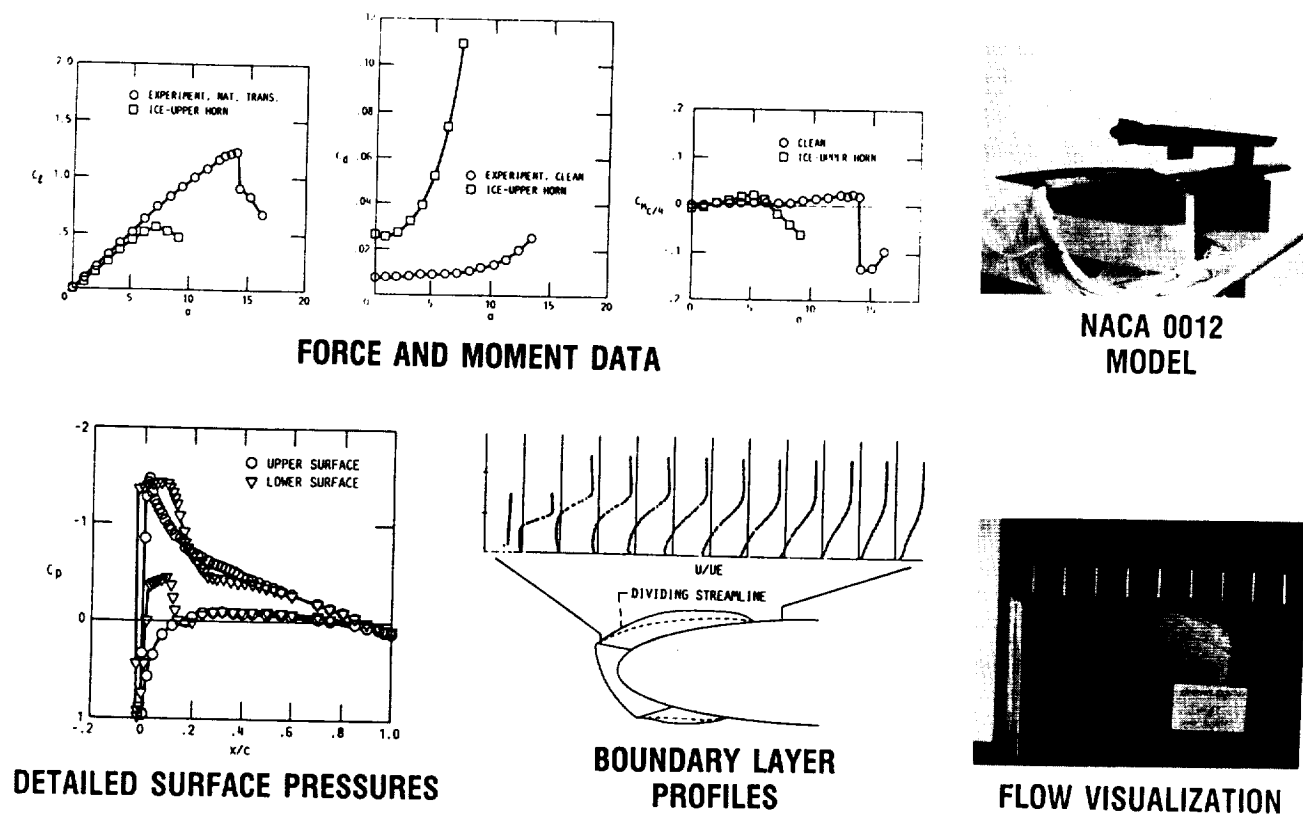
CD-87-28740

Figure 10. - Closeup flash picture of droplet impingement.



CD-87-28741

Figure 11. - Adhesive shear stress versus interface temperature.



CD-87-28742

Figure 12. - Code validation studies - iced airfoil analysis.

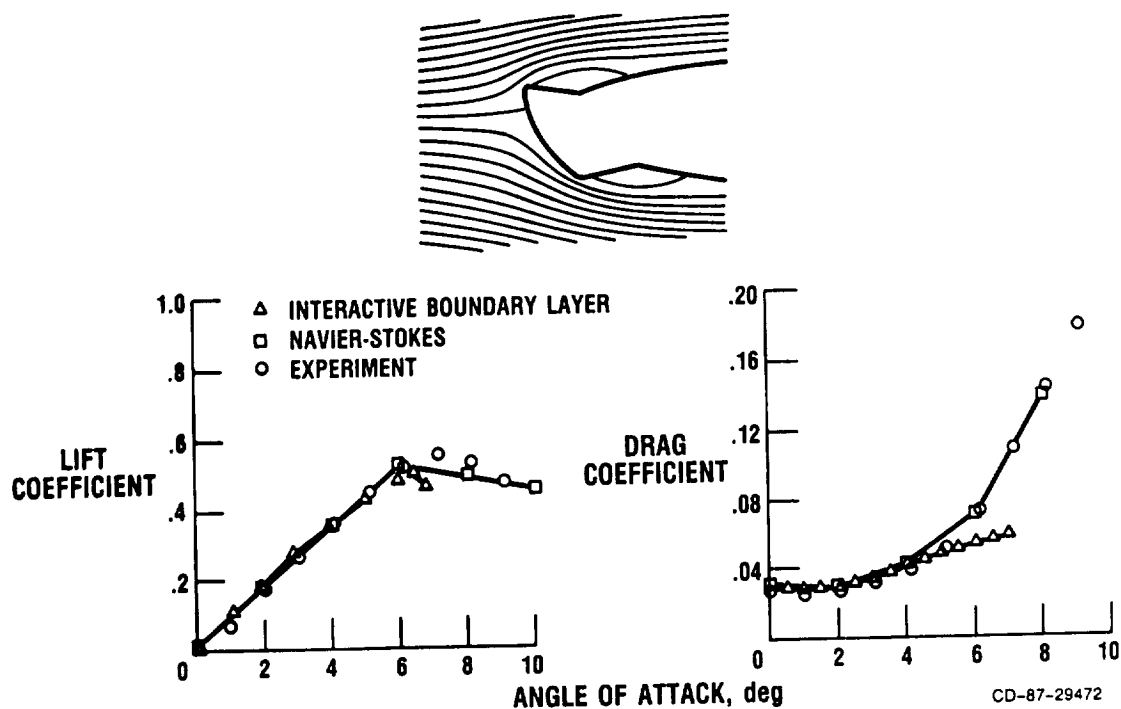


Figure 13. - Iced airfoil analysis.

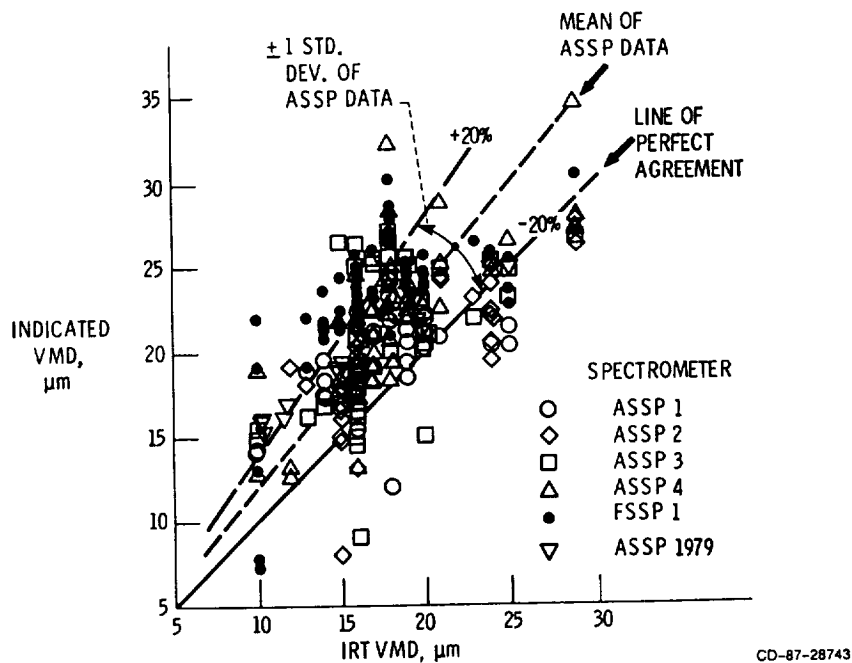


Figure 14. - Comparison of laser spectrometer drop size indications to old IRT calibration (range of conditions: VMD, 10 to 30 mm; LWC, 0.3 to 3 g/m³; velocity, 80 to 460 km/hr; ASSP and ISSP denote axial scattering and forward scattering spectrometer probes, respectively).

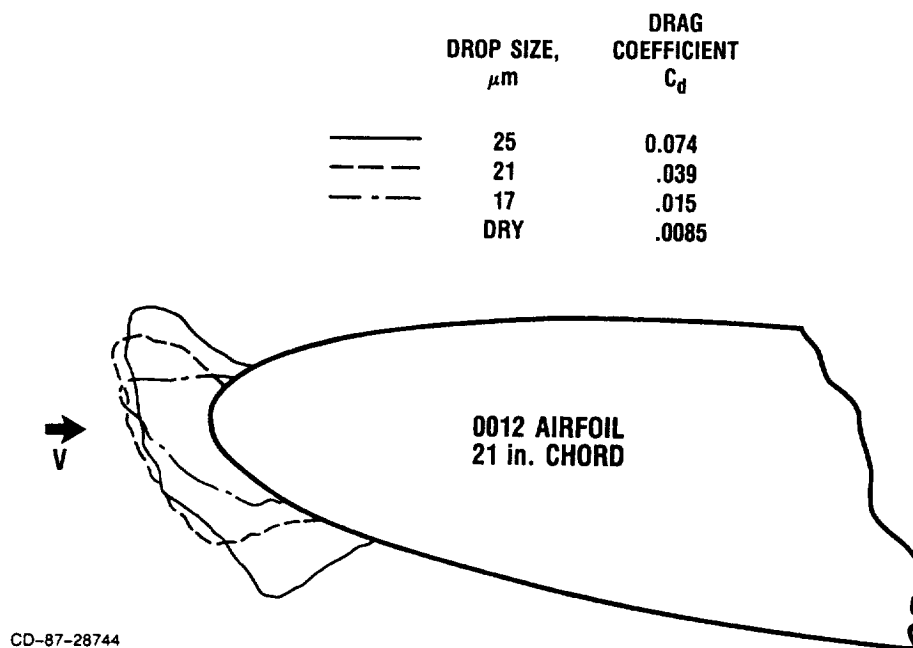
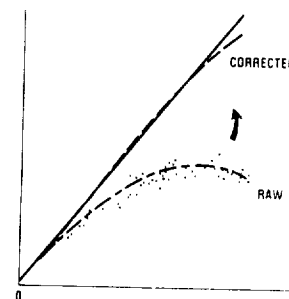


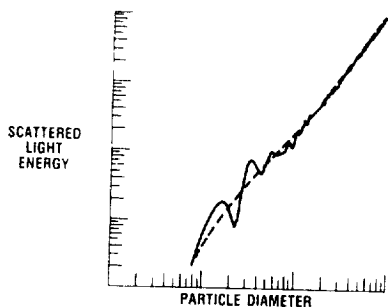
Figure 15. - Effects of drop size measurement errors.



CALIBRATION DEVICES

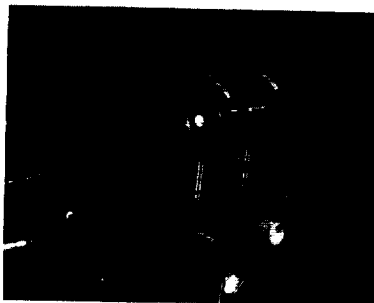


DATA CORRECTION
ALGORITHMS



THEORETICAL MODELING

CD-87-28745

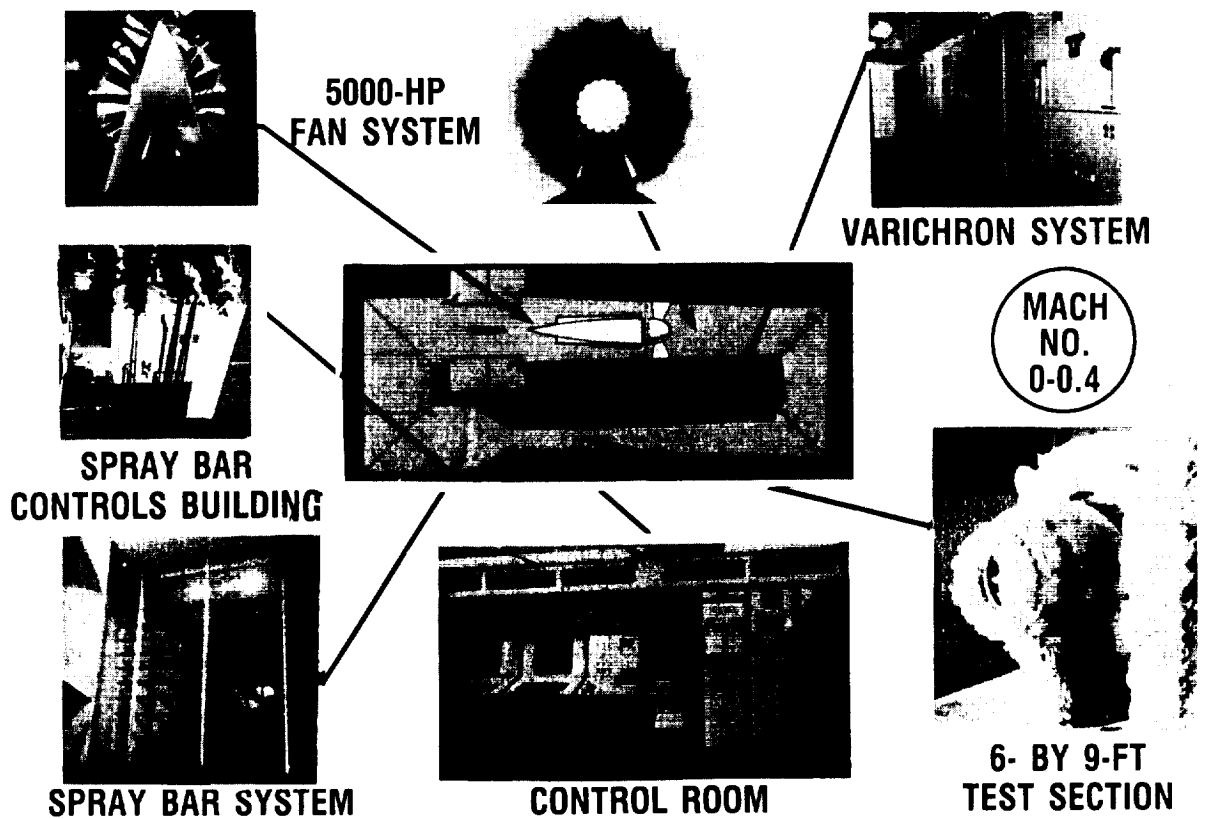


FUNDAMENTAL
RESEARCH



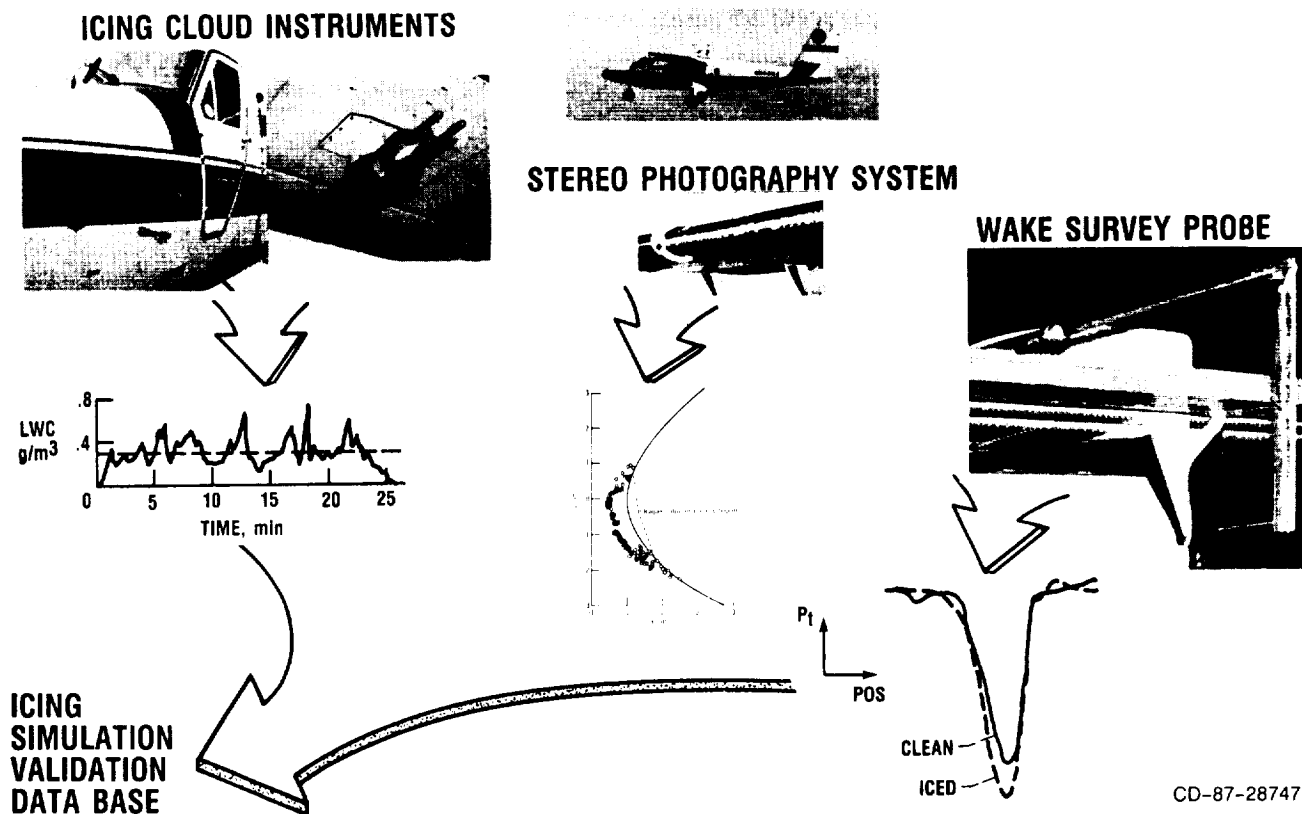
INSTRUMENT
COMPARISONS

Figure 16. - Particle sizing instrumentation research.



CD-87-28746

Figure 17. - Icing Research Tunnel.



CD-87-28747

Figure 18. - Twin Otter wing icing/aeroperformance.

EXPERIMENTAL DATA BASE IS BEING
ACQUIRED, RELATING AIRCRAFT PERFORMANCE
DEGRADATION TO A MATRIX OF MEASURED
NATURAL ICING CONDITIONS



GLAZE ICING ENCOUNTER

VMD - $13 \mu\text{m}$ ICING TIME - 26 min
LWC - 0.31g/m^3 STATIC TEMP. - -4°C

NASA DHC-6 TWIN OTTER
ICING RESEARCH AIRCRAFT

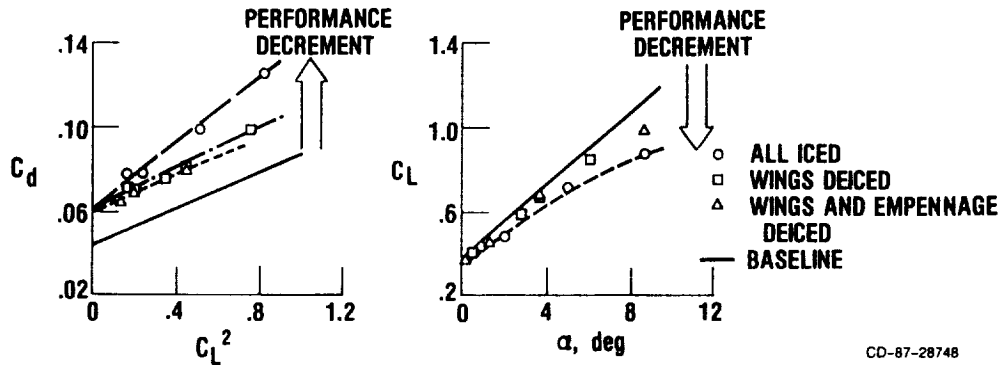
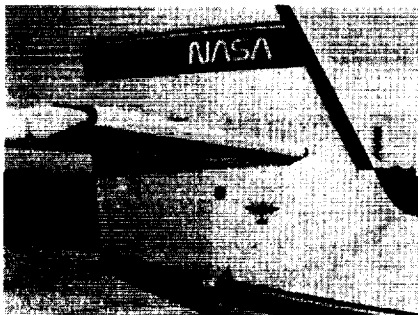


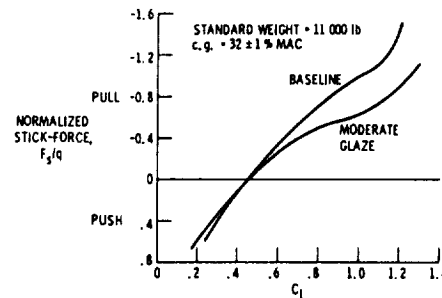
Figure 19. - Aircraft performance in natural icing.

OBJECTIVE: EMPLOY STATIC LONGITUDINAL FLIGHT TEST METHODS TO A DHC-6
AIRCRAFT WITH AN ARTIFICIAL ICE SHAPE ATTACHED TO THE
HORIZONTAL TAIL PLANE TO MEASURE THE CHANGE IN STATIC MARGIN

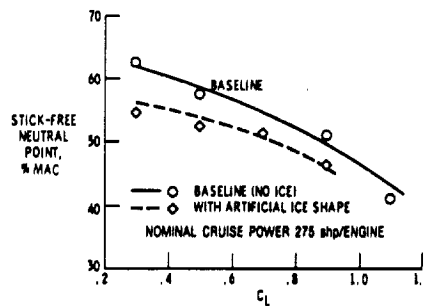
RESULTS: A REDUCTION IN STATIC MARGIN WAS MEASURED THROUGHOUT
THE NORMAL FLAPS-UP CRUISE ENVELOPE



ARTIFICIAL MODERATE GLAZE ICE SHAPE
ATTACHED TO HORIZONTAL TAIL



VARIATION IN NORMALIZED CONTROL FORCE
FOR THE "ICED" VERSUS BASELINE TAIL



REDUCTION IN STICK-FREE STATIC
MARGIN DUE TO TAIL ICE

CD-87-28749

Figure 20. - Reduction of aircraft static longitudinal stability due to icing.

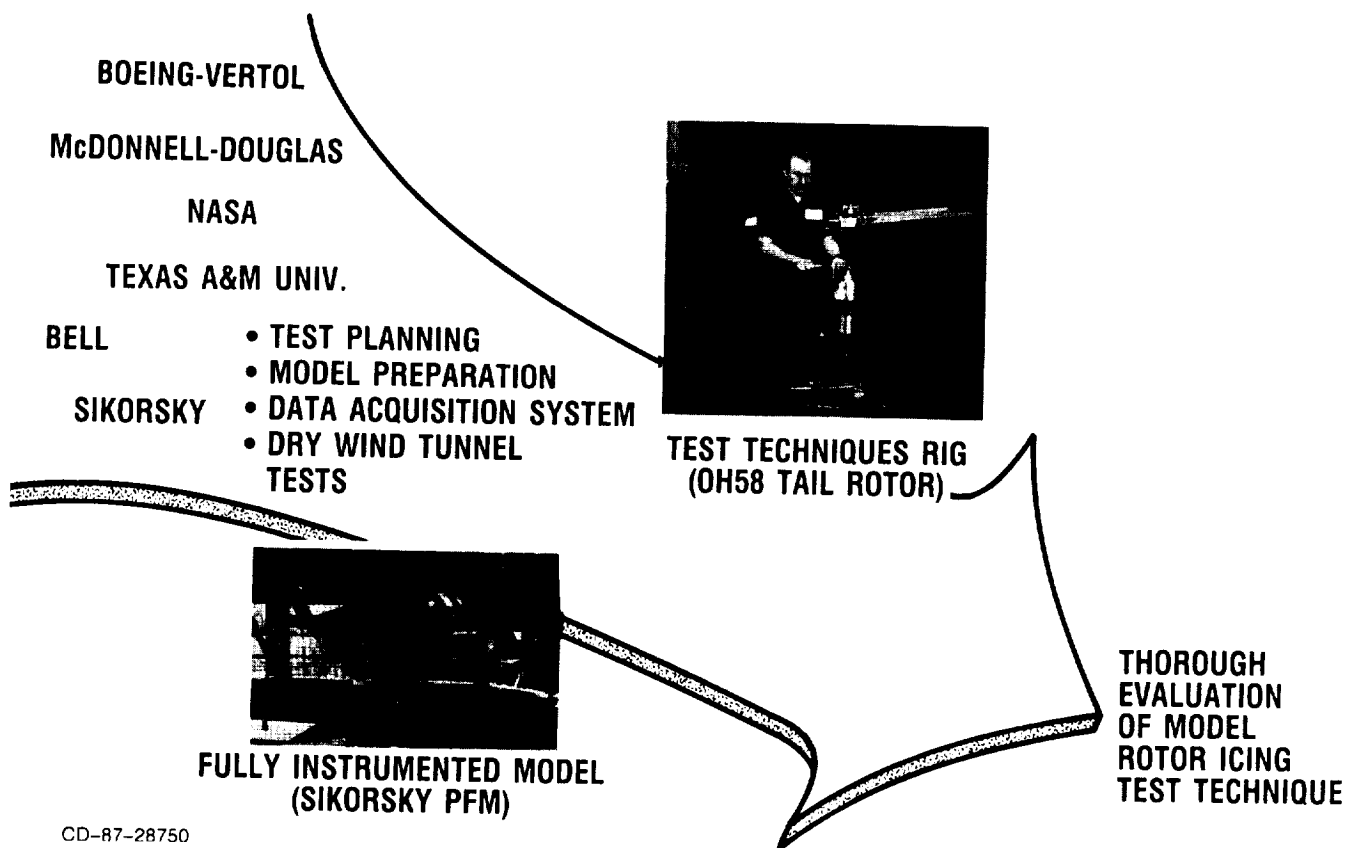
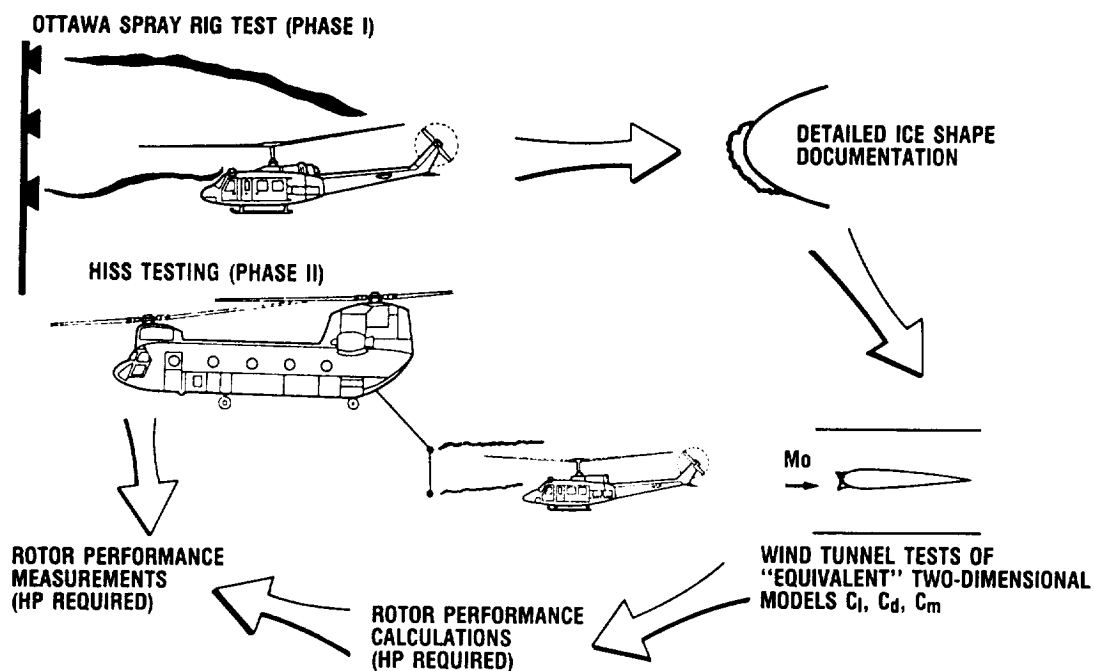


Figure 21. - Model rotor icing program.



CD-87-28751

Figure 22. - Helicopter icing flight test program.

**AIRCRAFT ENGINE HOT SECTION TECHNOLOGY -
AN OVERVIEW OF THE HOST PROJECT**

Daniel E. Sokolowski
and
Marvin H. Hirschberg

SUMMARY

NASA sponsored the Turbine Engine Hot Section Technology (HOST) Project to address the need for improved durability in advanced aircraft engine combustors and turbines. Analytical and experimental activities aimed at more accurate prediction of the aerothermal environment, the thermomechanical loads, the material behavior and structural responses to loads, and life predictions for cyclic high-temperature operation were conducted from 1980 to 1987. The project involved representatives from six engineering disciplines who are spread across three work sectors - industry, academia, and NASA. The HOST Project not only initiated and sponsored 70 major activities, but also was the keystone in joining the multiple disciplines and work sectors to focus on critical research needs. A broad overview of the project is given along with initial indications of the project's impact.

INTRODUCTION

Since introduction of the gas turbine engine to aircraft propulsion, the quest for greater performance has resulted in a continuing upward trend in overall pressure ratio for the engine core. Associated with this trend are increasing temperatures of gases flowing from the compressor and combustor and through the turbine. For commercial aircraft engines in the foreseeable future, compressor discharge temperature will exceed 922 K (1200 °F), while turbine inlet temperature will be approximately 1755 K (2700 °F). Military aircraft engines will significantly exceed these values.

In 1973 increasing fuel prices created the demand for energy conservation and more fuel-efficient aircraft engines. In response to this demand, engine manufacturers continually increased the performance of current-generation gas turbine engines. Soon afterward, the airline industry began to experience a notable decrease in the durability or useful life of critical parts in the engine hot section - the combustor and turbine. This was due primarily to cracking in the combustor liners, turbine vanes, and turbine blades. In addition, spalling of thermal barrier coatings that protect combustor liners also occurred.

For the airlines, reduced durability for in-service engines was measured by a dramatic increase in maintenance costs, primarily for high-bypass-ratio engines. Higher maintenance costs were especially evident in the hot section. As shown by Dennis and Cruse (ref. 1), hot section maintenance costs account

for almost 60 percent of the engine total. Widespread concern about such soaring maintenance costs led to a new demand - to improve hot section durability.

Durability can be improved in hot section components by using any combination of the following four approaches. They are the use of (1) materials having higher use temperatures, (2) more effective cooling techniques to reduce material temperatures, (3) advanced structural design concepts to reduce stress, and (4) more accurate analytical models and computer codes in the design analysis process to identify hot spots, high stresses, and so on.

High-temperature metallic materials currently include nickel- and cobalt-based superalloys. Certain elements of these alloys, such as cobalt, are in short supply and are expensive. Ways for reducing these alloying elements were presented by Stephens (ref. 2). Advanced high-temperature superalloy components also include directionally solidified, single-crystal, and oxide-dispersion-strengthened materials. Development time for new materials is lengthy, fabrication is sometimes difficult, and again, costs are high. Thus, successful use of these materials requires a balance among design requirements, fabrication possibilities, and total costs.

Current cooling techniques tend to be sophisticated, while fabrication is moderately difficult. In higher performance engines cooling capability may be improved by increasing the amount of coolant. But the penalty for doing this is a reduction of thermodynamic cycle performance of the engine system. In addition, the coolant temperature of such advanced engines is higher than that for current in-service engines. Consequently, more effective cooling techniques are being investigated. Generally, they are more complex in design, demand new fabrication methods, and may require a multitude of small cooling holes, each of which introduces potential life-limiting high stress concentrations. Acceptable use of the advanced cooling techniques will require accurate models for design analysis.

The introduction of advanced structural design concepts usually begins with a preliminary concept that then must be proven, must be developed, and - most critically - must be far superior to entrenched standard designs. Acceptance certainly is time consuming, and benefits must be significant. For improved durability in high-performance combustors, an excellent example of an advanced structural design concept is the segmented liner as discussed by Tanrikut et al. (ref. 3). The life-limiting problems associated with high hoop stresses were eliminated by dividing the standard full-hoop liners into segments. At the same time, designers realized increased flexibility in the choice of advanced cooling techniques and materials, including ceramic composites.

Finally, the design analysis of hot section component parts, such as the combustor liners or turbine vanes and blades, involves the use of analytical or empirical models. Such models often involve computer codes for predicting and analyzing the aerothermal environment, the thermomechanical loads, heat transfer, and material and structural responses to such loading. When the parts are exposed to high-temperature cyclic operation as in an aircraft turbine engine, the repetitive straining of the materials invariably leads to crack initiation and propagation until failure or breakaway occurs. The useful life of a part is usually defined as the number of mission cycles that can be accumulated before initiation and propagation of significant cracks. Thus, designers need

to predict useful life accurately so they can design a part to meet requirements.

Efforts to predict the life of a part generally follow the flow of analytical models shown in figure 1. Thus, designing a part such as a turbine blade to meet a specified life goal may require several iterations through the life prediction system of figure 1, varying the blade geometry, material, or cooling effectiveness in each pass, until a satisfactory life goal is predicted.

Fortunately, at the time of demands for improved hot section durability, dramatic increases were occurring in mathematical solution techniques, electronic computer memory, and computer computational speed. The time was ripe for significant improvements in analytical predictive capability.

Analysis models and codes have frequently predicted physical behavior qualitatively but have exhibited unacceptable quantitative accuracy. To improve predictive capability, researchers generally need (1) to understand and model more accurately the basic physics of the phenomena related to durability, (2) to emphasize local as well as global conditions and responses, (3) to accommodate nonlinear and inelastic behavior, and (4) to expand some models from two to three dimensions.

REVIEW OF THE HOST PROJECT

To meet the needs for improved analytical design and life prediction tools, especially those used for high-temperature cyclic operation in advanced combustors and turbines, NASA Lewis Research Center sponsored the Turbine Engine Hot Section Technology (HOST) Project. The project was initiated in October 1980 and completed in late 1987.

Objective

The HOST Project developed improved analytical models for the aerothermal environment, the thermomechanical loads, material behavior, structural response, and life prediction, along with more sophisticated computer codes, which can be used in design analyses of critical parts in advanced aircraft engine combustors and turbines. Use of these more accurate analytical tools during the design process will ensure improved durability of future hot section engines components.

Approach

The complex durability problem in high-temperature, cyclically operated turbine engine components requires the involvement of numerous research disciplines. This involvement must include not only focused research, but also interdisciplinary and integrated efforts. The disciplines included in HOST were instrumentation, combustion, turbine heat transfer, structural analysis, fatigue and fracture, and surface protection.

Most disciplines in the HOST Project followed a common approach. First, phenomena related to durability were investigated, often using benchmark

quality experiments. With known boundary conditions and proper instrumentation, these experiments resulted in a better characterization and understanding of such phenomena as the aerothermal environment, the material and structural behavior during thermomechanical loading, and crack initiation and propagation. Second, state-of-the-art analytical models were identified, evaluated, and then improved upon through use of more inclusive physical considerations and/or more advanced computer code development. When no state-of-the-art models existed, researchers developed new models. Finally, predictions using the improved analytical tools were validated by comparison with experimental results, especially the benchmark data.

Programs

In fulfillment of its objective, the HOST Project initiated and sponsored 70 major research and technology programs. HOST management issued contracts for 40 separate activities with private industry, most of which were multiyear and multiphased. In several activities, more than one contractor was involved because of the nature of the research and each contractor's unique qualifications. Thirteen more separate activities were conducted through grants with universities. Finally, at the NASA Lewis Research Center, 17 major efforts were supported by the project.

TECHNOLOGY TRANSFER

This report summarizes research needs and results for the HOST Project. The HOST Project research activities were usually organized, conducted, and reported along the discipline lines noted above. This report does the same.

Numerous publications provide further details about research results from the HOST Project. Six annual workshops were conducted, with conference proceedings being provided for each one (refs. 4 to 9). Each of the proceedings generally covers research results for the preceding year. The last two proceedings (refs. 8 and 9) also include a bibliography of definitive research reports. A comprehensive bibliography of the HOST Project is given in reference 10, and a comprehensive final review of the HOST Project's research accomplishments and their impact is provided in reference 11.

INSTRUMENTATION

The instrumentation work entailed five programs, covering a combustor viewing system, a dynamic gas temperature system, laser anemometry, heat flux sensors, and high-temperature strain measurement.

Combustor Viewing System

To allow visual diagnoses of abnormal operation of combustors, fuel injectors, liners, and nozzle guide vanes, HOST researchers developed a combustor viewing system that provides qualitative images during component operation. The viewing system consists of a water-cooled optical probe, a probe actuator, an optical interface unit that couples the probe to cameras and to an illumination source, and system controls. This system has been used in both combustor

component and full-scale engine tests, for combustor liner durability studies, and for flowpath diagnostics. It has been used to examine light-off and blow-out characteristics and appears to have considerable potential for other time-dependent phenomena and for flame radiometry.

Dynamic Gas Temperature System

Prior to HOST, researchers had no techniques to accurately measure fluctuating hot gas temperatures at frequencies above 10 Hz. Through HOST we developed a dynamic gas temperature measurement system and tested it in an F-100 engine facility and a high-pressure component test facility. Accurate gas temperature measurements are now possible up to 1-KHz and 3000 °F peaks. This helps with modeling combustor flows and better defines the environment imposed on turbine airfoils.

Laser Anemometry

The laser anemometer (LA) has become a valuable tool for nonintrusive gas velocity measurements in turbine engine work. Under HOST, we developed technology needed to apply LA to high-temperature turbines. Specific work areas included seeding, data acquisition, system optimization, and optical design.

Seeding. - Seed materials and high-volume seed generators were evaluated in a small combustor facility. We examined various refractory materials dispersed with a fluidized bed and titanium dioxide seed produced by the chemical reaction of titanium tetrachloride and water vapor.

Data acquisition. - Efficient data acquisition requires minimum operator intervention during test runs. To accomplish this, we developed a computer-controlled signal preprocessor for counterprocessors. This preprocessor controls filter settings, photomultiplier tube (PMT) voltage, and radiofrequency (RF) gain, as well as monitoring the PMT current.

System optimization. - A computer model was developed to determine optimal designs for fringe-type LA's. Prediction analysis methods were used to determine optical designs that provide minimum measurement uncertainties for given particle size, proximity to surfaces, and signal processor parameters. Experiments were conducted to measure surface reflectance properties - data needed for system optimization. A study of filter-induced errors was conducted to determine the best filter designs for use with counterprocessors.

Optical design. - The conventional fringe-type LA is not necessarily optimal for measurements within turbomachines. It has the required large acceptance angle, but its relatively large probe volume precludes accurate measurements close to flow passage walls. Under HOST, a unique four-spot time-of-flight LA was developed and tested. The four-spot LA has both a large acceptance angle and the capability to measure close to walls. In testing, we obtained successful measurements as close as 75 μm from a surface normal to the viewing direction. Another optical design project conducted under HOST was the development of an optical corrector for use with the cylindrical windows used in turbine facilities. This corrector eliminates the aberrations caused by the window.

Heat Flux Sensors

Heat flux sensors were developed and tested in both combustor liner and turbine airfoil applications. Tests in combustor liners provided useful heat flux data. However, the sensors proved to be too sensitive to transverse temperature heat flux gradients for most applications to turbine airfoils. This was particularly true for the Gardon gage sensor because of its lack of symmetry. Sensor configurations with lower transverse sensitivity have been considered but not tested.

High-Temperature Strain Measurements

The program's goal was to improve the capability for static strain measurement from the pre-HOST temperature limits of roughly 700 to 1800 °F. This was the most ambitious research effort of HOST's instrumentation subproject. We used three approaches in this work: (1) to develop improved resistance strain gage alloys, (2) to learn how to use available strain gages more effectively, and (3) to evaluate alternative optical strain measuring systems.

Improved strain gage alloys. - Improved strain gage alloys in the FeCrAl and PdCr systems were developed, but neither has been demonstrated as a successful high-temperature strain gage. Work continues on developing wire and thin film strain gages of PdCr.

More effective use of available strain gages. - Evaluation tests of strain gages mainly from the FeCrAl system (including wire gages from China) have provided a better understanding of FeCrAl gage characteristics. As a result, an experiment to measure combustor liner strain in which strain gage cooling rates were carefully controlled to match those used in pre- and post-test calibrations provided useful strain data at temperatures up to 1250 °F.

Alternative strain measuring systems. - Optical systems appear to have potential for high-temperature noncontact strain measurements. One such system, a laser speckle photogrammetric system, was tested and shown to be capable of measuring thermal expansion of a Hastelloy-X plate at temperatures up to 1600 °F. However, problems related to index refraction gradients in the gas within the viewing path must be solved (or at least controlled) to permit this technology to be applied widely.

Thin-Film Sensors

In addition to the work described above, we have been working on technology to put thin-film sensors on turbine engine hot section components. Thin-film thermocouple technology has been developed and such sensors are in use in engine testing. Current work in this area is focused on three goals: basic improvements in sensor processing technology, extension to other sensors such as strain gages and heat flux sensors, and accommodating changes in substrate materials. This work was partially supported by the HOST Project.

COMBUSTION

The HOST Project combustion work emphasized aerothermal modeling. The original plan called for three work phases. During phase 1, researchers assessed existing gas turbine combustion models. They then made suggestions for improving existing models, particularly for numerical accuracy. In phase 2 they improved models for interacting and nonreacting fluid flows. Phase 3 was to improve models for interacting and reacting fluid flows. Phase 3 work was not performed (because HOST Project funding was curtailed), but it is still important work that substantially affects our understanding and the predictive accuracy of combustion fluid flow models.

A separate work element involved dilution jet mixing. This work started before the HOST Project, but was subsequently funded by HOST. While the dilution jet mixing work had an independent existence, it became an integral part of the HOST research environment. This work was less ambitious in scope than the three-phase aerothermal modeling task, but it contributed significantly to the aerothermal phase 1 modeling assessment.

Assess Combustor Aerothermal Modeling - Phase 1

Gas turbine combustor models include submodels of turbulence, chemical kinetics, turbulence/chemistry interaction, spray dynamics, evaporation/combustion radiation, and soot formation/oxidation. During phase 1 model assessment work, three HOST contractors made extensive assessments of numerics, physical submodels, and the suitability of available data. They tested several models: K-E turbulence, algebraic stress and its modifications, scalar transport, and turbulence/chemistry interaction. Their major conclusion was that available computational fluid dynamics codes provided a useful combustor design tool, but the codes were only qualitatively accurate. Further study was needed to improve the numerical scheme and specified experimental data before various emerging physical submodels (for turbulence, chemistry, sprays, turbulence/chemistry interactions, soot formation/oxidation, radiation, and heat transfer) could be properly assessed.

The assessment identified a serious deficiency in numerical accuracy for data on flows, particularly where the false diffusion is of the same order of magnitude as the turbulent diffusion. This masked differences between turbulence models such that very different models gave essentially the same result and sometimes caused undeservedly good agreement between data and predictions.

Improved Spatial Property Variations and Quantitative Accuracy - Phase 2

During the second phase of the aerothermal modeling work, HOST researchers undertook three tasks: improved numerical methods, a flow interaction experiment, and fuel injector/air swirl characterization. We improved the resolution of spatial property variations and quantitative accuracy of aerothermal codes through three-dimensional numerical schemes, improved turbulence and chemistry models, and relevant benchmark data. We concentrated on nonreacting single- and two-phase swirling and nonswirling flows.

Improved numerical methods. - Here we found CONDIF and fluxspline useful. For improved computational efficiency, modifications such as SIMPLER and PISO have proven beneficial.

Flow interaction experiments. - Here researchers (1) studied the interactions between the combustor and diffuser systems and (2) obtained comprehensive mean and turbulence measurements for velocity and species concentration in a three-dimensional flow model of the primary zone of combustion chambers. These experiments were conducted with both air and water multiple-swirler rigs, as well as single swirler and swirling jet rigs. A key feature of this program provided a comparison of model calculations against data obtained, to ensure that data are complete and consistent and that they satisfy the boundary condition input requirements of current three-dimensional codes.

Fuel injector/air swirl characterization. - Here we sought to obtain fully specified mean and turbulence measurements of both gas and droplet phases downstream from a fuel injector and air swirler typical of those used in gas turbine combustion chambers. The flowfield of interest is an axisymmetric particle-laden jet flow with and without confinement and coannular swirling air flow. The comprehensive experimental data generated in these programs will be used to validate advanced models for turbulence, flow, stress, and spray.

Interacting-Reacting Flows - Phase 3

Although just as important as phase 2 aerothermal modeling programs that have led to significant improvements in our technical ability to predict non-reacting gas turbine combustor flow fields, work planned for phase 3 was not performed during the HOST Project. This phase 3 work would have collected fully specified reacting flow data, similar to that being gathered for non-reacting flows. Work should continue on the models for reacting sprays and multidimensional heat transfer.

Dilution Jet Mixing

This recently completed NASA work involved our ability to predict combustor exit temperature profiles (limited previously to jet trajectory analyses). The program provided a broad database and developed an empirical model for mixing diluting air jets with combustion gases. It also let us predict combustor exit temperatures accurately within the database's range.

The dilution jet mixing effort identified key flow parameters, collected data on the effect of varying these characteristics, and developed an empirical flow field model.

Conducted jointly by NASA Lewis and Garrett, this work concentrated on mixing of single-sided and opposed rows of jets in a confined duct flow to include effects of noncircular orifices and double rows of jets. The database was extended to include realistic effects of combustion chamber flow area convergence, nonisothermal mainstream flow, opposed (two-sided) in-line and staggered injection, and orifice geometry. Analysis of the mean temperature data obtained in this investigation showed that the effects of orifice shape and double rows are most significant in the region close to the injection plane.

This dilution jet mixing database is also being used to guide development of three-dimensional numerical codes so they provide broader and more accurate predictive capability. The dilution jet mixing work folded in with aerothermal modeling programs because (1) data was used in aerothermal modeling assessment and (2) the empirical model provides an alternative to numerical modeling for flows within the range of the dilution jet mixing experiments.

TURBINE HEAT TRANSFER

The major goal for the heat transfer program was to improve our basic understanding of the physics of aerothermodynamic phenomena in turbine components. Toward this end researchers gathered data for broad databases and, thus, prepared for future research. The development work was of two types: experimental databases and analytical tools. The experimental databases covered both stationary and rotational work. The experimental work is discussed first.

Local Gas-to-Airfoil Heat Transfer Rates

HOST researchers obtained broad databases and modified the STAN5 code to accurately predict heat transfer coefficients, especially at the transition point, for film- and non-film-cooled airfoils.

Allison researchers did initial work on the stator airfoil heat transfer. They checked the effects of several factors such as Reynolds number, turbulence level, and Mach number on heat transfer coefficients for various airfoil geometries at simulated engine conditions. This research was conducted for non-film-cooled airfoils, showerhead film-cooled designs, and showerhead/gill-region film cooling concepts. They obtained an extensive dataset that systematically shows the important effects of film cooling schemes on modern airfoils. The dataset went beyond the traditional effectiveness correlations to provide actual heat transfer data. It should provide a valuable baseline for emerging analysis codes.

Stanford University conducted a systematic study of the physical phenomena affecting heat transfer in turbine airfoil passages. Experimental research dealt with high free-stream turbulence intensity and large turbulence scale that might be representative of combustor exit phenomena. Their results show that heat transfer augmentation can be as high as 5X at a high value of free-stream turbulence intensity, but only 3X if the length scale is changed. These results suggest that the designer must know a great deal more about the aerodynamic behavior of the flow field in order to predict successfully the thermal performance of the turbine components.

The rotation work divided into concentrations on the gas-side airfoil and the coolant effect within passages.

Airfoil Rotation Effects on Heat Transfer

Scientists at United Technologies Research Center worked on determining the effects of airfoil rotation on heat transfer for the blade. This effort produced single-stage turbine data for both high and low inlet turbulence, one

and one-half stage turbine data (focusing on the second vane row), and aerodynamic quantities such as interrow time-averaged and rms value of velocity, flow angle, inlet turbulence, and surface pressure distributions. The results varied depending on location and surface. Work in this area indicates that pressure surface heat transfer still requires more study to explain high heat transfer.

Work in the blade's tip region was done at Arizona State University. The group at ASU experimentally modeled a blade tip cavity region and determined heat transfer rates by a mass transfer analogy with naphthalene. The dataset produced an important new addition to a traditionally neglected area and shows that with carefully designed datasets and analyses researchers can obtain an optimal design for tip cavities.

Coolant Rotation in Smooth-Wall Passages

Pratt & Whitney performed heat transfer experiments in a square passage with two 180° flow turns, with and without turbulators, and with and without rotation. Results for the smooth surface configuration show a strong rotational effect. Pratt also modified the three-dimensional Navier-Stokes TEACH code to predict flow and heat transfer in internal passages and rotation. It is adequate for simple geometric cases; however, it requires revision before application to more complex cases. Results for the turbulated passages also show strong rotational effects and significant differences in augmentation between leading and trailing surfaces.

The other half of the heat transfer subproject concentrated on developing analytical tools for boundary layer analysis and viscous flow analysis.

Three-Dimensional Boundary Layer

In this area HOST work concentrated on improving prediction accuracy for three-dimensional effects on heat transfer. This involved assessing three-dimensional boundary layer codes that were not designed for heat transfer work to determine what revisions were needed to make the code useful in heat transfer efforts.

Contracts were let for two efforts. United Technologies Research Center assessed the applicability of its three-dimensional boundary layer code to calculate heat transfer, total pressure loss, and streamline flow patterns in turbine passages. The results indicate a strong three-dimensional effect on a turbine blade, and they agree qualitatively with experimental data. The same code was modified for use as a two-dimensional unsteady code to analyze the rotor-stator interaction phenomena.

The other boundary layer study at the University of Minnesota addressed numerical turbulence modeling, particularly for turbine airfoils. This work extended modeling to apply to transitional flows for both free stream turbulence and pressure gradients. There was a reasonable improvement in predictive ability. This effort is a good start in establishing a methodology for moving away from heavy dependence on empirical constants.

Analytic Flow and Heat Transfer Modeling

Scientific Research Associates (SRA) worked on a fully elliptic, three-dimensional Navier-Stokes code. This group modified the code to handle turbine applications. Comparisons of predictions with analytical experimental data are good when researchers can specify location for the boundary layer transition. Ideally, the code would allow researchers to handle various locations. In this respect, work still remains on improving turbulence and transition modeling.

STRUCTURAL ANALYSIS

Under this heading, there are six major thrusts, involving an interface code between heat transfer and structural analysis, three-dimensional inelastic codes, constitutive models, component-specific modeling, liner cyclic life testing, and substantiated design analysis methods and codes.

Heat Transfer/Structural Analysis Interface Code

With HOST support, General Electric researchers developed an interface code, called TRANSITS, that transfers up to three-dimensional thermal information automatically from heat transfer codes (that generally use coarse finite element grids) to structural analysis codes (that use finer grids). Key features include independent heat transfer and stress model meshes, accurate transfer of thermal data, computationally efficient transfer, steady-state and transient data, user friendly program, flexible system, internal coordinate transformations, automated exterior surfacing techniques, and geometrical and temporal windowing.

Three-Dimensional Inelastic Codes

HOST provided development of three-dimensional inelastic structural analysis codes, involving two contractors, for nonlinear behavior at high thermomechanical loads. At Pratt & Whitney, three developed codes covered different approaches and degrees of complexity: MOMM, MHOST, and BEST3D. These codes provide a tenfold increase in computational efficiency - with improved accuracy. They embody a progression of mathematical models for increasingly comprehensive representation of the geometrical features, loading conditions, and forms of nonlinear material response. MOMM, a mechanics of materials model, is a stiffness method finite element code that uses one-, two-, and three-dimensional arrays of beam elements to simulate hot section component behavior. MHOST employs both shell and solid (brick) elements in a mixed method framework to provide comprehensive capabilities for investigating local (stress/strain) and global (vibration, buckling) behavior of hot section components. BEST3D is a general purpose, three-dimensional, structural analysis program using the boundary element method.

General Electric, the second contractor on the inelastic work, also developed a code that performs three-dimensional, inelastic structural analysis. The objective of this program was to develop analytical methods for evaluating the cyclic time-dependent inelasticity that arises in hot section engine components. Because of the large excursions in temperature associated with hot section engine components, the techniques developed must be able to accommodate

large variations in material behavior including plasticity and creep. To meet this objective, General Electric developed a matrix consisting of three constitutive models and three element formulations. A separate program for each combination of constitutive model/element model was written, making a total of nine programs. Each program can stand alone in performing cyclic nonlinear analysis.

The three constitutive models assume distinct forms: a simplified theory (simple model), a classical theory, and a unified theory. The 3-element formulations used an 8-node isoparametric shell element, a 9-node shell element, and a 20-node isoparametric solid element.

For linear structural analysis, the nine codes use a blocked-column skyline, out-of-core equation solver. To analyze structures with nonlinear material behavior, the codes use an initial stress interactive scheme. This code contains a major advance in our ability to handle a dynamic time incrementing strategy.

Constitutive Models

Before HOST, there was no capability to perform combined elastic-plastic creep structural analyses. There were limited high-temperature databases for constitutive model formulations and verifications. Through the HOST Project, researchers developed viscoplastic constitutive models for both isotropic and anisotropic materials, broadened the database capability, and verified models for a range of test conditions. These efforts led to a 30-percent improvement in high-temperature stress-strain prediction. These factors combined to make Lewis an internationally recognized leader in constitutive model development.

Isotropic material modeling. - In efforts aimed at isotropic material modeling, theorists from three organizations provided new models. The first organization, Southwest Research Institute, developed two existing models (Walker and Bodner-Partom) of the unified type for application to isotropic, cast, nickel-base alloys used for air-cooled turbine blades and vanes. Both models demonstrated good correlation with experimental results for two PWA alloys, B1900+Hf and MAR-M247. The program also demonstrated rather conclusively that the unified constitutive model concept is a powerful tool for predicting material response in hot section components under complex, time-varying thermomechanical loadings. At General Electric, researchers evaluated several viscoplastic constitutive theories against a large uniaxial and multi-axial database on René 80 material, which is a cast nickel-base alloy used in turbine blade and vane applications. No available approach for modeling the high-temperature, time-dependent behavior of René 80 was satisfactory, so GE developed a new theory that predicts with good accuracy the 90° out-of-phase tension-torsion experimental results at elevated temperatures. Finally, at a third organization, the University of Akron, researchers developed a time-dependent description potential function based on constitutive theory with stress dependence on J2 and J3 integrals that reduces to a J2 theory as a special case.

Anisotropic material modeling. - Modeling of anisotropic material also had three groups involved, all universities. Turbine manufacturers have been

developing nickel-base monocrystal superalloys for years. University of Connecticut theorists successfully modeled the deformation behavior of these materials by using both a macroscopic constitutive model and a micromechanical formulation based on crystallographic slip theory. The University of Cincinnati developed a model for nickel-base single-crystal alloy René N4 using a crystallographic approach. The current equations modified a previous model proposed by Dame and Stouffer, where a Bodner-Partom equation with only the drag stress was used to account for the local inelastic response in each slip system. The University of Akron developed a continuum theory for representing the high-temperature, time-dependent, hereditary deformation behavior of metal composites that can be idealized as pseudohomogeneous continua with locally definable directional characterizations.

Component-Specific Modeling

HOST allowed us to develop a modular code for nonlinear structural analyses that predicts temperatures, deformation, and stress and strain histories. It also gave us an automatic solution strategy for liners, with similar strategies underway for blades and vanes. The package contains five modular elements that are linked by an executive module. The thermodynamic engine model (TDEM) translates a list of mission flight points and time differences into time profiles of major engine performance parameters. The thermodynamic loads model (TDLM) works with the output of the TDEM to produce the mission cycle loading on the individual hot section components. The component specific structural modeling module provides a generic geometry pattern for each component. General Electric also created a software recipe that contains default values for point coordinates, lengths, thicknesses, angles, and radii. Users may modify specific values, but the software has saved them the effort of identifying basic geometry and parameters. Once a researcher defines specific values, the software develops a finite element model of this geometry consisting of 20-noded isoparametric elements. The fourth subsystem performs incremental nonlinear finite element analysis on complex three-dimensional structures under cyclic thermomechanical loading with temperature-dependent material properties and material response behavior. A major advance in the ability to perform time-dependent analyses is a dynamic time incrementing strategy incorporated in this software. The fifth element, COSMO, is an executive module that controls the whole system.

Liner Cyclic Life Testing

Through a cooperative effort, Pratt & Whitney and NASA Lewis Research Center developed a unique vehicle to obtain cyclic thermal and mechanical test data under realistic but controlled test conditions by using annular combustor hardware. Pratt & Whitney provided the test rig, while Lewis supplied the test facility, integrated the rig into the facility, conducted tests, and analyzed the data. The program initially tested a conventional liner of sheet metal, seam welded louver construction from Hastelloy-X material. Later, the program tested an advanced segmented liner made from materials developed by Pratt & Whitney. The tests radiantly heated segments (cylindrical sections) of turbine engine combustor liners. Quartz lamps provided cyclical heating of the test liners. This caused axial and circumferential temperature variations as well as through-the-wall temperature gradients in the test liner. The thermally induced stresses and strains were similar to those of in-service liners. A

typical engine mission cycle (i.e., takeoff, cruise, landing, and taxi) of 3 to 4 hr was simulated in 2 to 3 min. On the basis of nonlinear structural analyses of the two liners, researchers determined that the critical stress-strain location in the conventional liner was at the seam weld. For the advanced liner, it was at the retention loop. For the same heat flux, the advanced liner will have a much longer life than the conventional liner, because it has a lower operational temperature (440 °F) and has no structural or hoop constraint in the circumferential direction. The predicted life is greater than one million cycles. There is good agreement between predicted life and measured life.

Substantiated Design Analysis Methods and Codes

An important goal in the structural analysis discipline was concerned with developing user confidence in the models and codes discussed earlier in this section. Confidence comes with experimental validation. HOST allowed scientists to validate many technologies: time-varying thermomechanical load models, component-specific automated geometric modeling and solution strategy capabilities, advanced inelastic analysis methods, inelastic constitutive models, high-temperature experimental techniques and experiments, and nonlinear structural analysis codes. Under HOST, test facilities were upgraded, and codes in two major areas were developed. We also conducted experiments to calibrate and validate the codes. Unique high-temperature cyclic thermomechanical tests on tubular and solid bar specimens were conducted in upgraded structures test laboratories at the Lewis Research Center. Categories for validation activities included (1) new types of multiaxial viscoplastic constitutive models for high-temperature isotropic and anisotropic superalloys and metal matrix composites (2) nonlinear structural analysis methods and codes and (3) uniaxial and multiaxial thermomechanical databases for René N4, René 80, Hastelloy-X, MAR-M247, B1900+Hf, PWA 1480, and Haynes 188.

FATIGUE AND FRACTURE

Prior to HOST work in fatigue and fracture, we had no confidence in life predictions involving complex loading conditions, multiaxial stress states, or thermomechanical loading conditions until components had service experience. Now we have far more confidence in constitutive equations and life models for advanced configurations and materials under complex, multiaxial, and thermomechanical loading circumstances. Five major accomplishments are summarized in the following paragraphs.

Crack-Initiation Life-Prediction Methods

This is the first major fatigue-fracture work element. Two new crack-initiation, life-prediction methods have been developed for application to complex creep-fatigue loading of nominally isotropic superalloys at high temperatures (at Pratt & Whitney and at Lewis). The Pratt work led to a new method, called cyclic damage accumulation (CDA), for predicting high-temperature fatigue life. Under the Lewis program, the strainrange partitioning (SRP) method was advanced to allow researchers to express the approach in terms of total strain range versus cyclic life.

Cyclic Constitutive Models - Protective Coatings and Single-Crystal Alloys

HOST efforts in this second fatigue-fracture concern developed and verified cyclic constitutive models for oxidation protective coatings and for highly anisotropic single-crystal turbine blade alloys. Pratt & Whitney formulated a viscoplastic constitutive model for two fundamentally different coating types: a plasma-sprayed NiCoCrAlY overlay coating and a pack-cementation-applied NiAl diffusion coating. Pratt & Whitney also developed a unified constitutive model for PWA 1480 single-crystal material; it is in the final development stages.

Preliminary Cyclic Crack-Initiation Life-Prediction Model

Pratt & Whitney is also the contractor proposing a model for a preliminary cyclic crack-initiation life-prediction model. It is being evaluated. The model utilizes tensile hysteretic energy and frequency as primary variables.

Two High-Temperature, Cyclic Crack-Growth Life-Prediction Models

Two models have been proposed for the fourth fatigue and fracture work element. Micromechanistic and phenomenological engineering approaches have been taken. The micromechanistic approach, being developed by University of Syracuse scientists, is based on oxidation interactions with mechanical deformation at the crack tip. The engineering approach, at General Electric, has its origins in the path-independent integrals approach, which describes the necessary fracture mechanics parameters.

High-Temperature Fatigue and Structures Laboratory

Lewis Research Center created an advanced high-temperature fatigue and structures research laboratory. Test facilities have been significantly upgraded to allow uniaxial, high cycle/low cycle, and axial torsional fatigue research. Additionally, the laboratory contains a powerful computer facility that is among the best in the world for this kind of effort.

The uniaxial test facility now includes 12 load frame systems. The original eight frames are rated for $\pm 20\,000$ lb. Lewis added two more frames rated at $\pm 20\,000$ lb and two at $\pm 50\,000$ lb. Commercially available servocontrollers control each test system. The test facility provides both diametral and axial extensometers. Computer enhancements have had a major impact on the lab's uniaxial capabilities because each uniaxial system has its own minicomputer for experimental control and data acquisition. To further aid in simulating operating conditions, two machines allow tests to be conducted under two closely controlled environmental conditions, high temperature and vacuum.

To improve our understanding of cumulative cyclic loadings, Lewis bolstered its facility in this area as well. A new system produces arbitrary load or deformation histories corresponding to fatigue lives up to 10 million in less than 10 hr, using state-of-the-art servohydraulic materials test systems.

The third type of test enhancement relates to multiaxial stress. The load frames for each test system are rated for loads of $\pm 50\,000$ lb axial and

$\pm 25\ 000$ in.-lb torsional. These systems allow tests involving rapid thermal transients. A number of experimental projects are currently underway. Thus far the testing has been biaxial; eventually it will be triaxial.

The high-temperature fatigue and structures lab computer offers a versatile system, with a Data General Eclipse MV/4000 connected with 14 satellite computers in a multiprocessor class of computing configuration. This configuration also introduced the first validated ADA language compiler within NASA.

SURFACE PROTECTION

The surface protection subproject involved two programs: thermal barrier coating (TBC) life prediction and an airfoil deposition process/deposition model.

TBC Life Prediction

HOST provided pioneering research on thermal barrier coatings (TBC) involving three approaches to TBC life-prediction modeling. Lewis Research Center, Pratt & Whitney, Garrett, and General Electric worked on this modeling effort. The state-of-the-art coating system consists of about 0.25 mm of zirconia-yttria ceramic over 0.13 mm of an MCrAlY alloy bond coat. Both layers are applied by plasma spraying onto a structural base material. Benefits arise from thermal insulation of the structure that is provided by the ceramic layer.

Following an in-house model development program, Lewis awarded contracts (1) to determine thermomechanical properties, (2) to analyze coating stresses and strains, and (3) to develop life models for thermal barrier coatings.

Thermomechanical properties. - The effort to determine thermomechanical properties achieved general agreement that (1) these coatings fail primarily because of stresses induced by the thermal expansion mismatch between ceramic and metallic base layers and that (2) these stresses are greatly influenced by time-at-temperature processes - oxidation and possibly sintering.

Coating stresses and strains. - Next, researchers developed a laboratory model. This model represented a first step, but it was not in a form useful to engine designers.

Life models. - The model developed by Pratt & Whitney and its subcontractor, Southwest Research, is a fatigue-based coating life model. The model is accurate to plus or minus a factor of three, which is acceptable. The Garrett model considers bond coat oxidation, zirconia toughness reduction, and damage due to molten salt deposits. This model analyzes thermal data for specific elements in terms of mission. The General Electric model employs time-dependent, nonlinear, finite element modeling of stresses and strains present in the thermal barrier coating system, followed by correlation of these stresses and strains with test lives. This model was the only one to check failure induced by edges and, hence, the only one to consider shear strain.

Airfoil Deposition Process/Model

This activity raised fundamental questions about hot corrosion of blades and about deposition of corrosive salts. Scientists needed to identify what corrosive species and deposits were accumulating, how deposits reached the blade, and then what effect they had on the surface protection. Through HOST, researchers identified the corrosive as sodium sulfate, but they also learned from process studies that prior to reaching the blade it was not yet sodium sulfate (it was sodium carriers, sulfate carriers, etc.). People had been performing static studies, but research results in this area indicated that dynamic studies were needed. The reason was that in real-life situations the sodium sulfate supply continually accumulates and then, because of heat, becomes molten, creating a film that flows on the blade surface. The result is that salt deposition and flow rates are variable, prompting the need for a deposition model.

The deposition model that Lewis researchers developed assumes that the sodium-sulfate dissolution rate correlates with corrosion rate. This was the first attempt to correlate the process - initial corrosive species diffusing, moving, depositing, forming, filming, dissolving metal, and starting the corrosive effect. Researchers completed the model; however, funding limitations prevented validation experiments. This model is a significant step toward reality - modeling a real-life, dynamic environment.

CONCLUSIONS

The HOST Project activities encompassed researchers from industry, academia, and government. For a variety of reasons, it drew high-caliber people, including outstanding experts in each discipline. This was perhaps due to the project's difficult technical challenges, its size, and its visibility.

We could have addressed durability issues via several approaches: higher temperature materials, more effective cooling techniques, advanced structural design concepts, and improved design analysis tools. The last option attracted us because of the potential gains given the current breakthroughs in computer hardware technology and software development techniques.

To better understand the physics involved in the development of these design analysis tools for combustors and turbines, researchers developed high-quality experiments. Early project plans called for significant testing in the new High Pressure Facility at NASA Lewis Research Center. Unfortunately, technical problems limited testing to less than full test facility capability. Soon afterwards, Lewis moved away from component testing, with the facility being "mothballed" early in 1986. This change significantly affected HOST, because it greatly reduced model/code verification testing and the use of HOST-developed instrumentation in hot section research.

Most HOST research results were generic. They were applied to both large and small turbine engines. In addition, certain codes were used outside the HOST Project for durability improvements in the space shuttle main engine and for design analysis in an advanced communications technology satellite. There are, however, unique durability challenges in small turbine engines that the

HOST Project could not address because of funding constraints. These challenges include higher turbine blade attachment stresses, faster thermal transients, and different materials. Such challenges in today's small engines are believed to be the challenges in tomorrow's large engines.

Experience has shown that, in general, acceptance of new design analysis tools comes slowly. In some cases this has been true with HOST. Generally, users accept the new tools more quickly during a crisis involving, for example, in-service engine problems.

While a return on the investment in HOST has already been realized, additional returns will become visible as analysts use HOST codes more and as they incorporate these codes within new design analysis systems that are applicable to high-temperature composite and structural ceramic materials, which the HOST Project did not address.

REFERENCES

1. Dennis, A.J.; and Cruse, T.A.: Cost Benefits from Improved Hot Section Life Prediction Technology for Aircraft Engine Combustor and Turbine Parts. AIAA Paper 79-1154, June 1979.
2. Stephens, J.R.: COSAM Program Overview. COSAM (Conservation of Strategic Aerospace Materials) Program Overview, NASA TM-83006, 1982, pp. 1-11.
3. Tanrikut, S.; Marshall, R.L.; and Sokolowski, D.E.: Improved Combustor Durability--Segmented Approach with Advanced Cooling Techniques. AIAA Paper 81-1354, July 1981.
4. Turbine Engine Hot Section Technology (HOST). NASA TM-83022, 1982.
5. Turbine Engine Hot Section Technology (HOST). NASA CP-2289, 1983.
6. Turbine Engine Hot Section Technology (HOST). NASA CP-2339, 1984.
7. Turbine Engine Hot Section Technology (HOST). NASA CP-2405, 1985.
8. Turbine Engine Hot Section Technology (HOST). NASA CP-2444, 1986.
9. Turbine Engine Hot Section Technology (HOST). NASA CP-2493, 1987.
10. Sokolowski, D.E.: Comprehensive Bibliography of the Turbine Engine Hot Section Technology (HOST) Project. NASA TM-100275, to be published, 1989.
11. Sokolowski, D.E.: Toward Improved Durability in Advanced Aircraft Engine Hot Sections. NASA TM-4087, 1989.

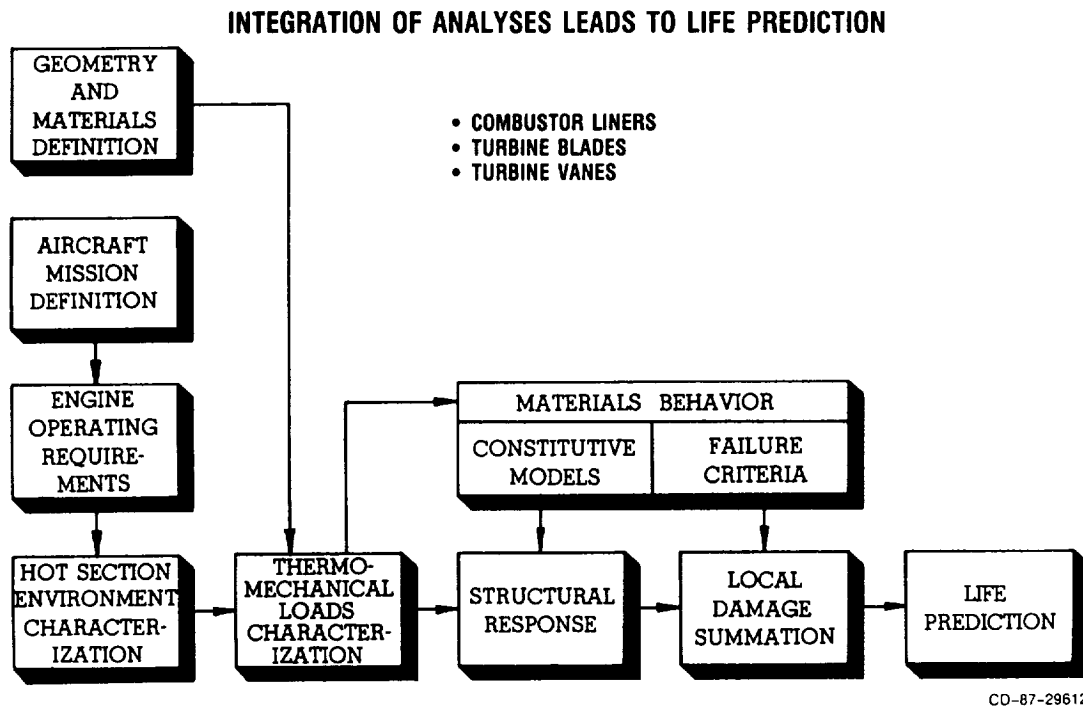


Figure 1. - Framework for HOST Project.

OVERVIEW OF NASA PTA PROPFAN FLIGHT TEST PROGRAM

Edwin J. Graber

SUMMARY

During the last several years, high-speed propellers have made the transition from a wind tunnel curiosity to a very likely near-term, fuel-efficient propulsion system that could revolutionize the subsonic commercial air transport industry. A key ingredient in this remarkable progress is the advanced turboprop program. Working together, NASA and industry have developed and flight-tested two propeller propulsion systems to provide answers to key technical questions and concerns. An industry team is currently developing a third propeller propulsion system for flight testing early in 1988. This report covers, in particular, the progress of the NASA-sponsored Propfan Test Assessment (PTA) flight test program. Lockheed-Georgia is the prime contractor for PTA with Allison, Hamilton Standard, Rohr, Gulfstream, and Lockheed-California serving as major subcontractors. In PTA, a 9-ft-diameter propfan has been installed on the left wing of a Gulfstream GII executive jet and is undergoing extensive flight testing at Dobbins Air Force Base to evaluate propfan structural integrity, near- and far-field noise, and cabin interior noise characteristics. This research testing includes variations in propeller tip speed and power loading, nacelle tilt angle, and aircraft Mach number and altitude. As a result, extensive parametric data will be obtained to verify and improve computer codes for predicting propfan aeroelastic, aerodynamic, and acoustic characteristics. Over 600 measurements are being recorded for each of approximately 600 flight test conditions.

INTRODUCTION

The major elements of the NASA-sponsored Advanced Turboprop (ATP) program, as shown in figure 1, are the Large-Scale Advanced Propeller (LAP) contract with Hamilton Standard, the Propfan Test Assessment (PTA) contract with Lockheed-Georgia, the Unducted Fan (UDF) contract with General Electric, and the Advanced Gearbox Technology contracts with both Allison and Pratt & Whitney.

In the LAP contract, Hamilton Standard designed, built, and ground-tested an eight-bladed, 9-ft-diameter, advanced single-rotation SR-7 propeller. Before delivery of the two SR-7 assemblies to PTA, Hamilton Standard conducted thorough bench tests at their research facilities, static tests with facility power at Wright Patterson Air Force Base, and wind tunnel tests at the Onera 26-ft tunnel in Modane, France. In the Modane tests, depicted in the photo on the left in figure 2, the propfan blades were instrumented to measure both steady and unsteady blade pressure distributions. Up to six of the eight blades were removed in the Modane tunnel testing in order to properly simulate

the correct power loading per blade with the limited facility power available. These unique data are currently being used to validate and improve propfan aerodynamic and acoustic performance prediction codes. One of the completed SR-7 assemblies for delivery to the PTA program is shown in the right-hand photo of figure 2.

The Unducted Fan program was a cooperative NASA-GE program to design, build, and static-test an 11-ft-diameter gearless counterrotating propeller propulsion system. The GE ground static test at Peebles, Ohio, is shown in the top photo of figure 3. In this 25 000-lb-thrust demonstrator engine, the propeller blades are mounted directly to the frames of a counterrotating turbine, eliminating the need for a high-horsepower gearbox. The UDF was static tested in August 1985 and later flight tested on the Boeing 727 and Douglas MD-80 aircraft. These two UDF flight-test configurations are shown in the two lower photos of figure 3. Flight-test results with both an 8 by 8 and 10 by 8 blade configuration indicate that a product UDF can meet the stringent FAR-36 noise standards, provide a quiet cabin environment, and burn from 40 to 50 percent less fuel than the low-bypass turbofans in use today in narrow-body aircraft such as the 727 and DC-9.

Both Allison and Pratt & Whitney were involved in the early phases of the NASA Advanced Gearbox Technology program. However, because of funding problems, only Allison (with their own funds) completed gearbox testing. Allison's 13 000-hp gearbox design used an in-line differential planetary gear system. In nose-to-nose rig tests at Allison's new gearbox test facility, shown in figure 4, an efficiency of over 99 percent was verified. Test results also indicated that the durability goal of 30 000-hr mean time between removals is achievable. Allison is using these results to build the lightweight gearbox for the 578-DX counterrotating propeller drive system being developed jointly by Pratt & Whitney and Allison. Hamilton Standard has designed and built a counterrotation propeller assembly for the 578-DX which draws upon SR-7 (LAP) technology and the results of counterrotation model testing of similar configurations. Testing of the 578-DX on the Douglas MD-80 will begin in 1989.

In just a few years, the propfan has made the transition from small-scale wind tunnel models to the flight test of several large-scale systems, as illustrated in the series of photographs in figure 5. The balance of this paper will focus on the NASA-sponsored PTA flight test program.

OBJECTIVES AND PROGRAMMING ASPECTS OF PTA PROGRAM

The PTA program focused on two fundamental concerns: propfan structural integrity and noise, as detailed in figure 6. NASA had to be sure that the thin, highly swept propfan blades would behave aeroelastically as predicted and that propfan-generated noise was not a problem. Source noise, cabin noise, community noise, and en route noise were investigated.

Figure 7 shows how the PTA program has progressed from its inception in August 1984. The Allison model 570 industrial gas turbine engine and T56 gearbox were modified and checked out by early 1986 for the static testing at Rohr's Brown Field test site in June 1986. Following the Rohr test, the propfan was installed on the left wing of the Gulfstream GII executive jet, and flight testing began in March 1987. In support of the flight test, several

scale-model wind tunnel tests were conducted to verify predicted aircraft flutter, performance, stability and control, and handling characteristics. The flight research testing was completed with the test of an advanced, lightweight, acoustically-treated interior in March 1988.

Figure 8 shows the team responsible for implementing the PTA program. Lockheed-Georgia, prime contractor to NASA for PTA, led a team consisting of five major subcontractors: Allison for the turboshaft engine and gearbox to power the propfan, Hamilton Standard for the SR-7 propfan, Rohr for the QEC or forward nacelle, Gulfstream for all aircraft modifications, and Lockheed-California for their expertise in the acoustic arena. All contractors did a remarkable job of pulling together as a team to make the total program a success.

AIRCRAFT MODIFICATION AND SUPPORT ACTIVITIES

Although installing the propfan on the wing of an aircraft may sound simple, it was actually very complex. Almost all of the aircraft systems (fuel, hydraulic, air conditioning, electrical, control, and so forth) had to be modified. The modifications made to the G-II airplane to convert it to the PTA testbed are summarized in figure 9. Of particular note is the over-2000-lb static balance boom added to the right wing to offset the 6500-lb propulsion system on the left wing. A dynamic boom was installed on the left wing to assure adequate wing flutter margin. Wing structural beef-up involved adding doublers to the front and rear beams, adding a rib near the nacelle attach point, and adding doublers to the ribs and skin. It should also be noted that, in addition to these modifications, a 700-lb armor plate of 3/8-in. stainless steel was installed on the fuselage during the early part of the flight testing to protect the crew in the event of a blade failure.

Because of the research objectives of the PTA flight test effort, it was necessary to highly instrument the airplane, as indicated in figure 10, thus adding to the complexity of the modification effort. Over 600 research and operational parameters were added for this test, including microphones, accelerometers, pressures, temperatures, fuel flow rates, propfan strains, and aircraft and propfan operation conditions. All parameters were continuously recorded by on-board recorders. In addition, propfan stresses were monitored in real time by an on-board Hamilton Standard engineer whenever the propfan was powered. A telemetry system also sent selected key parameters to a ground recording system.

To verify propfan integrity, the propfan had to be tested over a range of conditions including forward speed, altitude, and inflow angle of attack. Speed and altitude were easy to control, but the propfan inflow angle was more difficult. The variation in aircraft weight due to fuel burnoff during testing did not provide a sufficient angle-of-attack change. Lockheed came up with a unique way of solving this problem - a tiltable forward nacelle. With this system, which is illustrated in figure 11, tilt was adjustable from 2° up, to 3° down, simply by changing the forward-to-aft nacelle mounts. With tilt adjustment, the desired range of inflow conditions was attainable over a range of flight operating conditions. Figure 12 shows how nacelle tilt, combined with aircraft weight change (i.e., weight changing as fuel is burned off during flight), gives the desired range of a propfan flow parameter called excitation

factor. Excitation factor is a measure of flow nonuniformity and in its simplest form is the product of propfan inflow angle and the flow dynamic head. Shown in figure 12 are three representative flight conditions: Mach 0.3 at sea level, Mach 0.6 at 20 000-ft altitude, and Mach 0.8 at 30 000-ft altitude. In each case, an excitation factor range of about 2 to 4 is possible.

In support of the PTA design modification and analysis effort, several ground and wind tunnel tests were conducted. The models are shown installed in the test facilities in figure 13. These tests provided the data necessary to confirm predictions, verify analytical models, reduce program risk, and allow the proper interpretation of flight test data. Testing included a 1/3-scale inlet diffuser test to evaluate inlet recovery and distortion characteristics, a 1/9-scale full-span aeroelastic model test in NASA Langley's 16-ft transonic dynamics tunnel to verify aircraft flutter margins, a 1/9-scale full-span model test in two tunnels (NASA Langley's 16-ft transonic tunnel and 4- by 7-m low-speed tunnel to evaluate aircraft stability, control, and performance), and a 1/9-scale semi-span model in the NASA Lewis 8- by 6-ft wind tunnel to obtain data on the flow field coming into the propfan. This flow field information is needed for interpreting the propfan stress data obtained in flight.

The drive system for the SR-7 propfan consisted of an extensively modified Allison T-56 gearbox and a somewhat modified Allison model 570 industrial gas turbine engine. The model 570 is a ground-based version of the XT701 experimental engine developed by Allison for the Army heavy lift helicopter. Because this is one-of-a-kind hardware, the gearbox and engine were thoroughly ground tested before being combined with the Hamilton Standard SR-7 propfan and static tested at Rohr's static test stand in Chula Vista, California. The gearbox and engine testing at the Allison plant in Indianapolis are shown in the photos on the left in figure 14, while the Rohr test configuration is shown on the right. The 50-hr propulsion system checkout test over simulated flight conditions at Rohr was a real surprise, as it went almost exactly according to plan with only minor adjustments required before proceeding with the flight test program.

In figure 15 are shown a few photos of the Gulfstream GII airplane during various stages of modification. In the upper left-hand photo is the serial number 118 GII as purchased by Lockheed in May 1986. Wing beef-up, the attachment of the wing to the fuselage, and the nacelle installation on the wing are also shown in this series. The lower right-hand photo clearly shows the split line between the forward and aft nacelle assemblies. It is in this region that the attachment mounts are changed to adjust nacelle tilt angle.

FLIGHT TESTING

Figure 16 shows the completed PTA airplane as it was first tested in April 1987 with the propfan installed. Previous aircraft checkout testing without the propfan installed started in March. Note the static balance boom on the right wing, the microphone boom and flutter boom on the left wing, the Rose-mount aerohead boom on the nose, the fuselage protective shield in the plane of the propfan, and of course the SR-7 propfan and nacelle on the left wing. The top photograph shows that the propfan was not operated and that the blades were in the feather position during takeoff because of structural restrictions on allowable flap hinge moments. The Allison propfan engine is air started after takeoff with bleed air from the Spey engines at an altitude of about 5000 ft.

The flight test program was sequenced as shown in figure 17 to keep risk to a minimum. All systems were carefully checked out on the ground before going to flight testing. In flight, the complete flight research envelope (and beyond, to provide a safety margin) was systematically cleared before proceeding with the flight research testing. The initial airworthiness flight test phase was conducted with the protective armor plate installed on the fuselage until confidence was gained in the structural integrity of the propfan over the extremes of the operating conditions to be encountered in the test effort. The airworthiness tests consisted of evaluations of aircraft/propfan propulsion systems, flight flutter, and handling characteristics. The objective of the flight research phase was to verify propfan structural integrity, to determine propfan source noise, to obtain community and en route noise characteristics, to define cabin noise environment, and to determine lateral noise attenuation characteristics. Approximately 80 percent of the total flight time was devoted to flight research testing.

Over 500 high-altitude test conditions were recorded over the flight envelope shown in figure 18. The large number of test points is a result of the parametric approach to obtaining data. Nacelle tilt, propfan tip speed, and propfan power were all varied independently for the altitudes and speeds shown. In addition, baseline acoustic data were obtained with the propfan removed at most of these flight conditions so that propfan noise at various conditions could be compared with similar baseline conditions without the prop. The program emphasis was on getting good research data for verifying computer prediction codes. These codes can then be used by industry in the design of future propfan propulsion systems.

Figure 19 is a closeup photo of the installed SR-7 propfan with the spinner removed. Note the strain gages on each of the blades. Forty six strain gages were installed on the blades and blade root area. As mentioned earlier, key gages were continuously monitored during flight, and 32 were recorded.

Figure 20, which is representative of in-flight measured propfan blade inboard bending stress data, shows that these stresses were consistently below the infinite life limit criterion set by Hamilton Standard. These data show that although nacelle tilt angle variations affect blade stressing in a predictable manner, the trends vary as a function of airspeed. The results also show that blade stress increases with decreasing rotational speed (closed versus open symbols) because of increased 2-per-rev response as a critical speed is approached at the lower rotational speed.

The fuselage surface has been instrumented with a total of 44 microphones which are concentrated near the plane of propfan rotation, as shown in figure 21. This microphone placement allows mapping of the propfan noise contours in the area where they are likely to maximize. Internal cabin noise microphones at analogous locations will allow an assessment of the acoustic attenuation due to the cabin wall. The acoustic boom located near the wing tip contains five microphones at axial stations identical to five of the fuselage microphone planes. The boom is located at the same distance from the propfan as the closest points on the fuselage. The boom microphones will show the acoustic impact of rotation directionality, when the results are compared with

the output from the analogous fuselage microphones. This is because the propfan blades on the inboard side are rotating upward with the flow due to circulation over the wing, whereas on the outboard side the blades are moving downward against the circulatory flow.

Figure 22 compares fuselage-surface blade passing tone for measured flight test noise data, prediction, and Lewis 8- by 6-ft wind tunnel data acquired with a subscale propfan model. As can be seen, there is good correlation of the measured flight data with both the prediction and the corrected model test data. The peak surface noise occurs slightly downstream of the propfan plane and in magnitude is slightly below that obtained with the prediction and the wind tunnel data.

Community noise testing at the NASA Wallops Flight Facility was completed in October 1987. Twelve flights of about 2 hr each were flown over the microphone array shown to obtain a matrix of data at several altitudes (from 850 to 1600 ft), propfan tip speeds, power settings, and nacelle tilt angles. Acoustic baseline data with the propfan blades removed were also obtained. As shown in figure 23, sideline microphones beyond the normal 1476-ft distance required by FAR-36 were located at intervals out to a distance of 8100 ft from the flight path in order to assess lateral noise attenuation characteristics of the propfan in addition to the usual community noise measurements. A quick-look analysis of the acoustic data from each of the seven microphone sites was performed after each flight, and the data quality appears to be excellent. Detailed analysis of this data is now in progress.

After completion of the Wallops low-altitude noise tests, the PTA airplane returned to Dobbins Air Force Base in Marietta, Georgia, for maintenance and preparation for high-altitude en route noise testing, which was completed in November 1987. The en route noise testing was a joint effort with the FAA, which was primarily interested in verifying an analytical code for the prediction of atmospheric acoustic attenuation. In addition, NASA was interested in determining the acoustic characteristics for the propfan propulsion system from the standpoint of an observer on the ground when the airplane is in high-altitude flight. To assess the atmospheric acoustic attenuation characteristics, it was necessary to measure the propfan noise near the source as well as on the ground. The Lewis Learjet, equipped with wing-tip and fuselage microphones and special video and still camera equipment for distance measuring, was used for the acquisition of source noise data. The FAA installed a line of microphones on level ground at five stations beneath and perpendicular to the flight path, as shown in figure 24. To quantify atmospheric conditions during these flights, the Air Force launched weather balloons four times each day. Because it was necessary for the Learjet to fly beneath and close to the PTA at locations where pilot visibility of the other aircraft was restricted, the NASA T-38 chase plane was also flown on these formation flights to assure adequate separation between the two aircraft. Analysis of the data acquired in this testing is now in progress. Data quality appears to be excellent.

An advanced cabin acoustic treatment enclosure was fabricated under a NASA-Langley contract by Lockheed-California for flight test in the PTA testbed aircraft in March 1988. The enclosure, located as shown in figure 25, consists of tuned Helmholtz resonator panels attached to a framework, which was mounted to the cabin floor through vibration isolators. A comparison will be made between the interior noise levels with the advanced treatment and that obtained

in the earlier flight tests of the same airplane with bare, untreated cabin walls. These flight tests complete the currently planned PTA flight test program.

CONCLUDING REMARKS

The PTA flight testing was completed with the cabin acoustic enclosure testing in March 1988. The results obtained thus far are preliminary because analysis of the massive quantities of data acquired in this program will not be completed until late 1988. The PTA flight test effort is summarized as follows:

1. Over 600 measurements recorded
2. Over 500 high-altitude flight test conditions, including propfan tip speed from 600 to 840 ft/sec, propfan power from minimum to 100 percent, three nacelle tilts (to vary excitation factor), speed to Mach 0.89, and altitudes from 2000 to 40 000 ft
3. Community noise data obtained at NASA Wallops Flight Facility
4. En route noise data obtained

Resulting conclusions and status of the program are highlighted as follows:

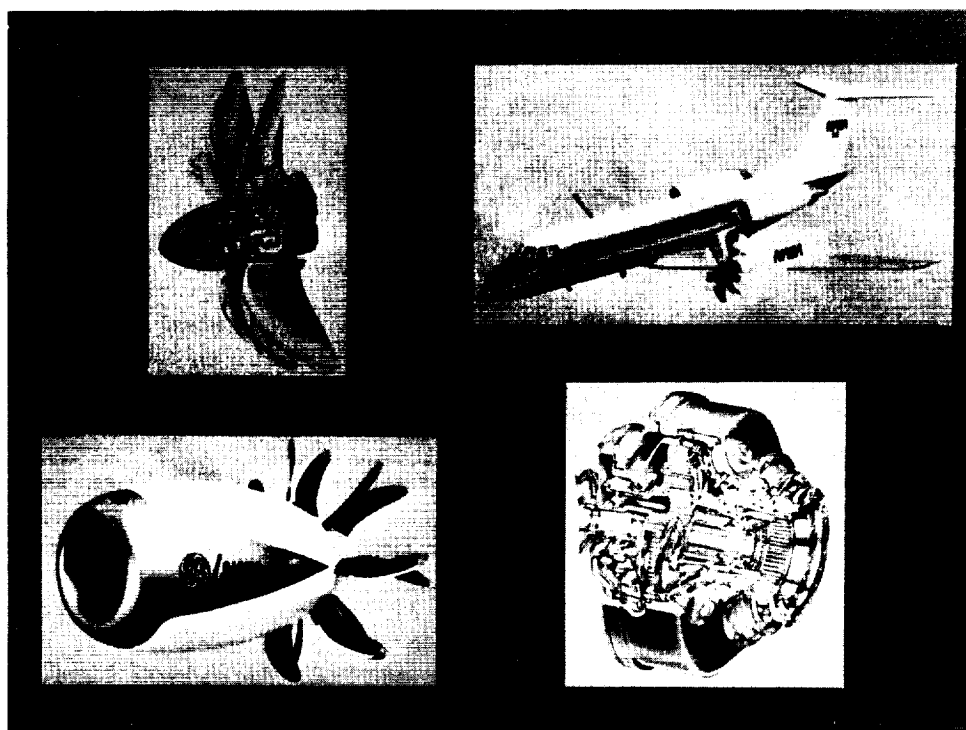
1. Propfan structural and aeroelastic response in good agreement with predictions
2. Measured near-field noise trends were consistent with predictions and data acquired in wind tunnel tests on subscale models
3. Community noise test data being analyzed by NASA and Lockheed
4. FAA and NASA using en route noise data to validate atmospheric attenuation codes
5. Interior noise tests completed in March 1988

In the high-altitude research tests, over 600 data parameters were recorded at more than 500 flight conditions. The effects of propfan tip speed and power level on blade stress and acoustics were recorded over a spectrum of flight conditions. A spectrum of inflow conditions was obtained over the flight Mach number/altitude matrix by varying nacelle tilt. A further perturbation to inflow conditions was obtained by a limited variation in yaw angle. Research data were acquired for a flight envelope extending from near the low-speed stall region to a flight speed of Mach 0.85 at altitudes up to 40 000 ft. Airworthiness testing verified that the aircraft was free of flutter up to Mach 0.89. For the wide range of inflow and flight conditions investigated for the propfan in this flight test program, blade stresses were always well within the limits specified by Hamilton Standard for unlimited fatigue life. The source noise measured on the fuselage in the high-altitude research testing was close to analytical prediction and wind tunnel model data. The peak noise at the fuselage surface occurred slightly downstream of the propfan plane.

Additional data were acquired in a series of low-altitude community noise evaluation flights at NASA Wallops in September and October, 1987. In addition to normal community noise measurements, lateral noise attenuation characteristics were also evaluated. Community noise data from Wallops is of good quality and is now being analyzed. Subsequently, high-altitude en route noise testing was performed over northern Alabama in conjunction with the FAA to verify an

atmospheric attenuation model and to determine the general characteristics of propfan noise measured on the ground. A preliminary look at the data indicated that it is of good quality, with the stable weather conditions necessary for code verification.

The final flight testing in PTA was a test of the advanced cabin acoustic treatment enclosure in March 1988. These tests allowed a direct comparison to be made between noise levels in flight with the treatment and with a bare-wall cabin. Because of the extensive source noise data acquisition throughout this research program, the propfan source noise will be well understood and will be beneficial in understanding any further treatment improvements which may be desired after analysis of the test results.



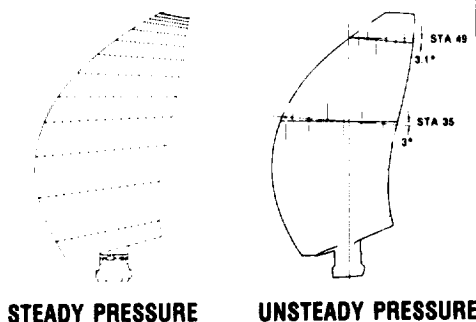
CD-87-28790

Figure 1. - Major contractual elements of ATP.



**TWO-BLADE
SR-7 IN MODANE,
FRANCE, WIND
TUNNEL**

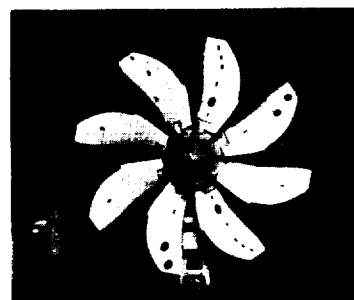
TRANSDUCER LOCATIONS



STEADY PRESSURE

UNSTEADY PRESSURE

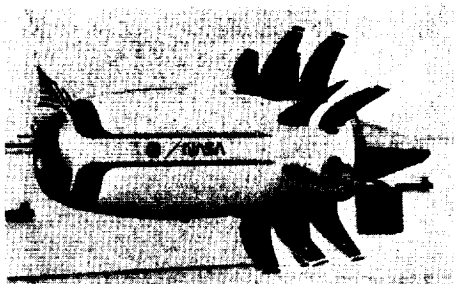
INSTRUMENTATION FOR MODANE TESTING



**TWO SR-7
ASSEMBLIES
DELIVERED
TO PTA**

CD-87-28791

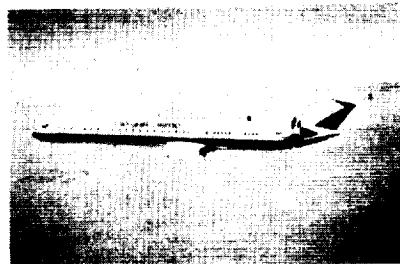
Figure 2. - LAP project.



GE STATIC TEST AT PEBBLES, OHIO



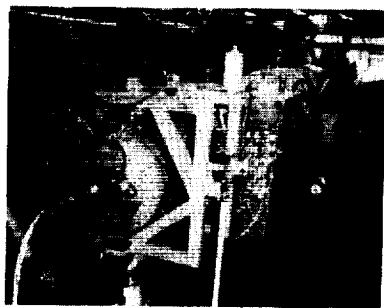
**BOEING 727 FLIGHT
TEST**



**DOUGLAS MD-80
FLIGHT TEST**

CD-87-28792

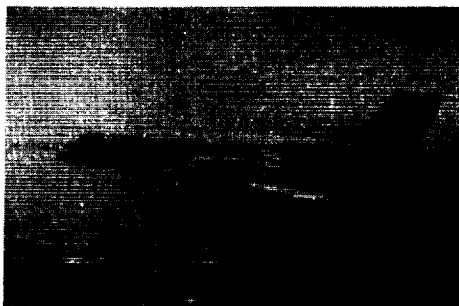
Figure 3. - NASA/GE unducted fan (UDF).



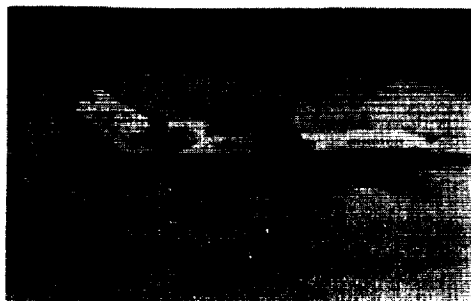
- ALLISON CONTRACT
- COUNTERROTATING IN-LINE DIFFERENTIAL PLANETARY GEAR SYSTEM
- 13 000-shp CLASS
- 99 PERCENT EFFICIENCY
- DURABILITY GOAL OF 30 000-hr MTBR

CD-87-28793

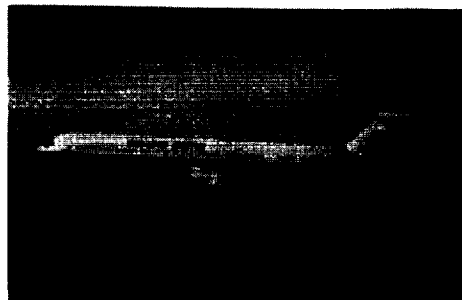
Figure 4. - Advanced counterrotation gearbox systems.



PTA/GULFSTREAM GII



UDF/BOEING 727



UDF/MD-80 AND
578DX/MD-80

CD-87-28794

Figure 5. - Flight testing of advanced turboprops.

**EVALUATE THROUGH THE DEVELOPMENT OF A FLIGHTWORTHY DRIVE SYSTEM AND
SUBSEQUENT GROUND AND FLIGHT TESTING OF A LARGE-SCALE PROPFAN**

- PROPFAN STRUCTURAL INTEGRITY
- PROPFAN SOURCE NOISE
- ASSOCIATED PROPFAN-RELATED CABIN NOISE
AND VIBRATION
- FAR-36 COMMUNITY NOISE
- ENROUTE CRUISE NOISE (GROUND)

CD-87-28795

Figure 6. - Propfan Test Assessment (PTA) objectives.

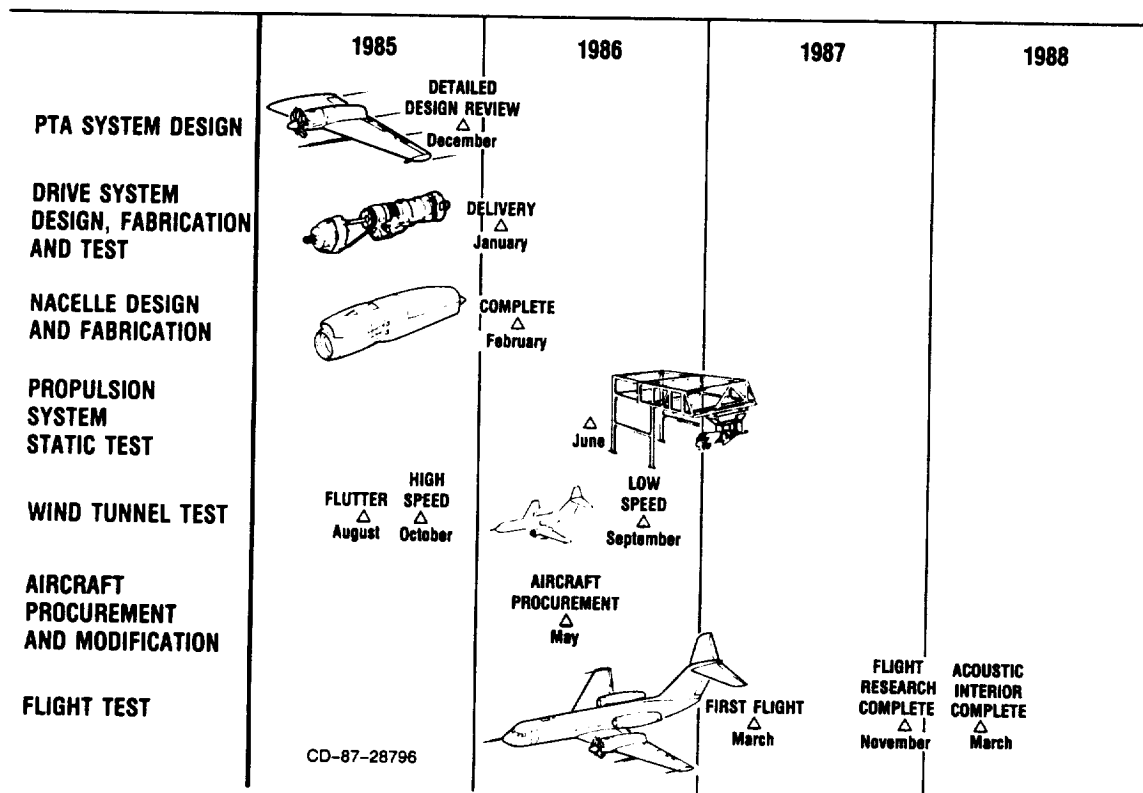
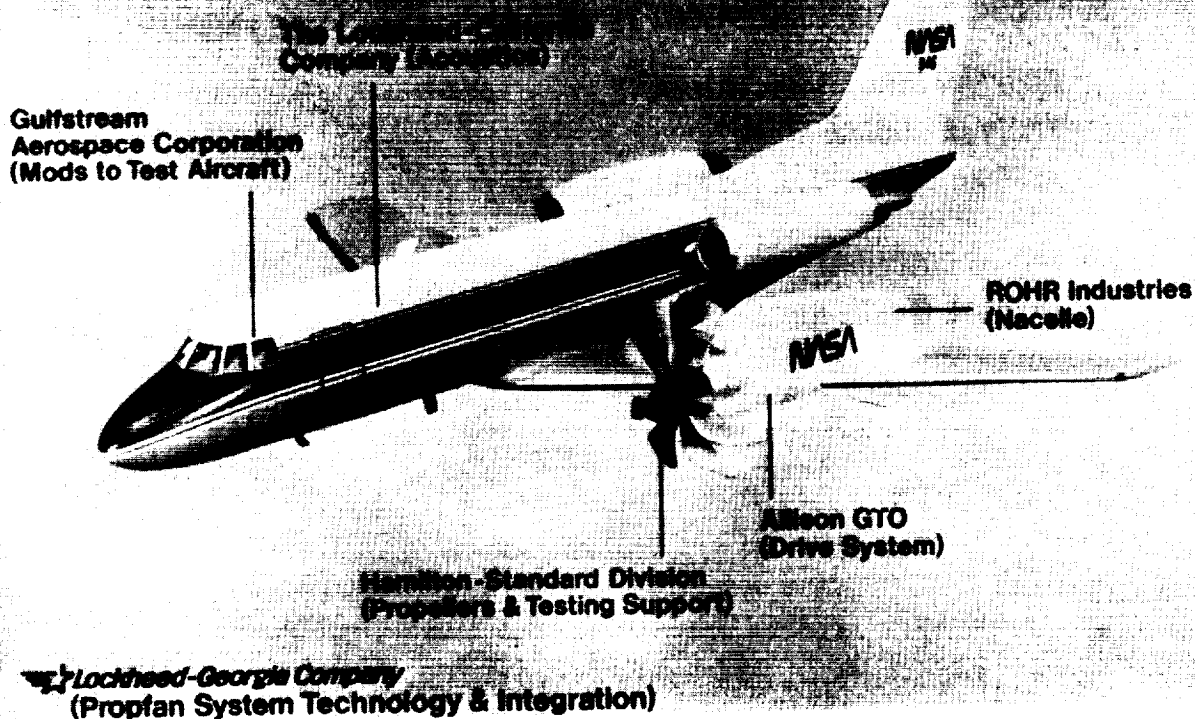


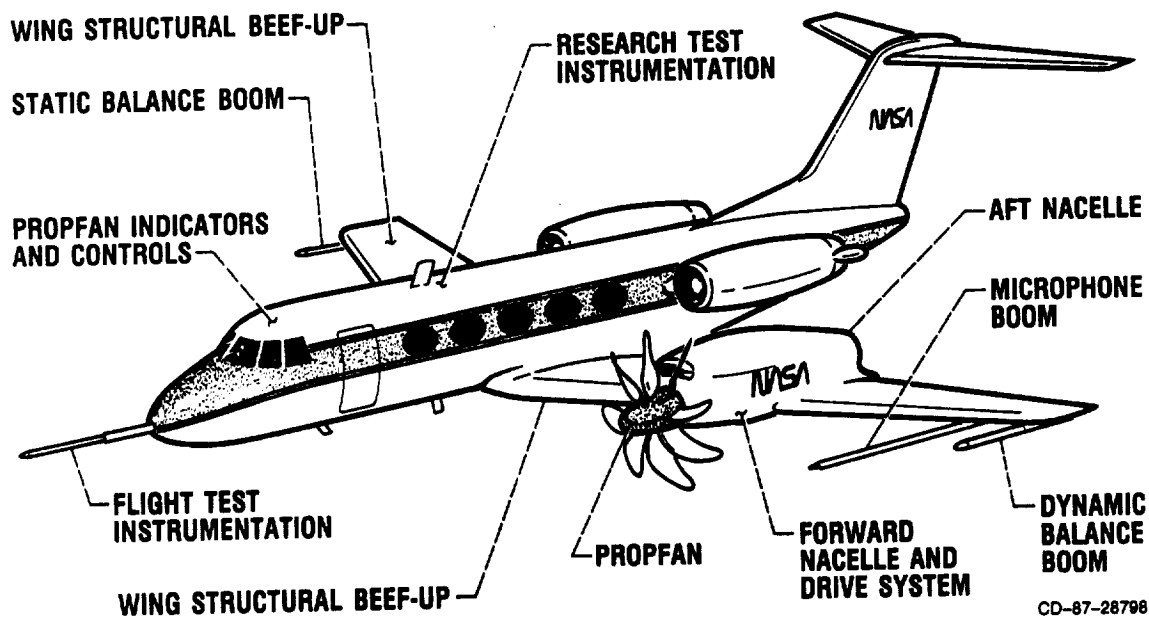
Figure 7. - PTA schedule.

PTA Team Members



CD-87-28797

Figure 8. - PTA team members.



CD-87-28798

Figure 9. - Aircraft modifications.

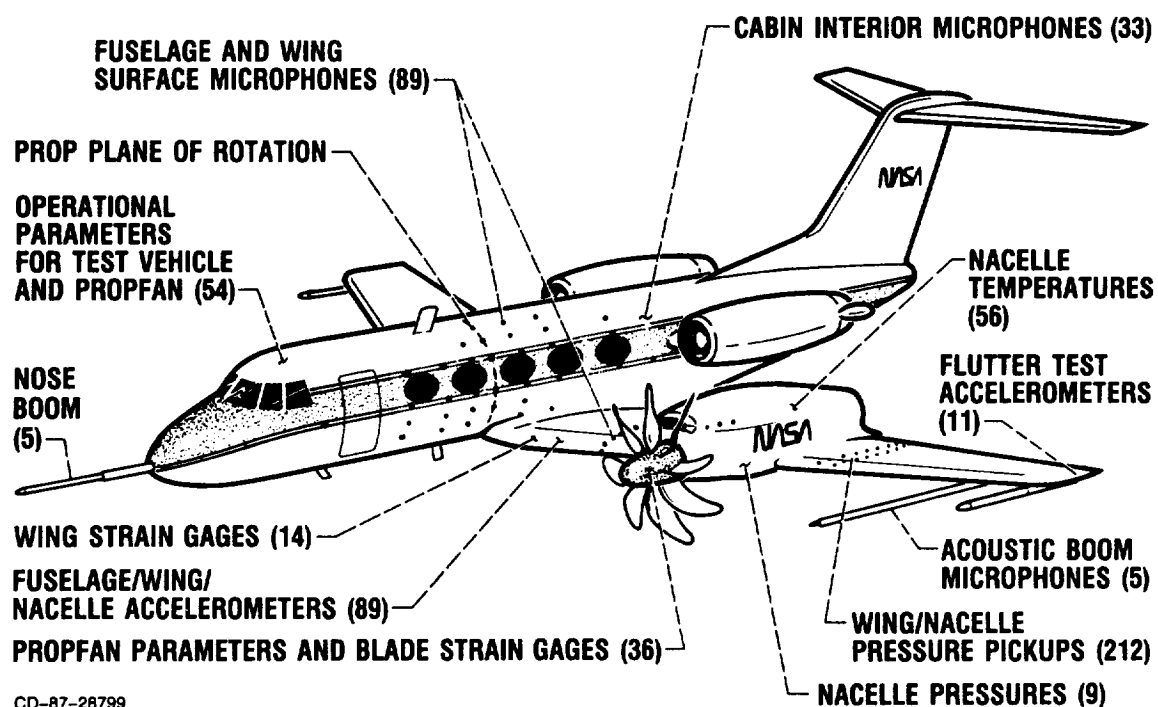
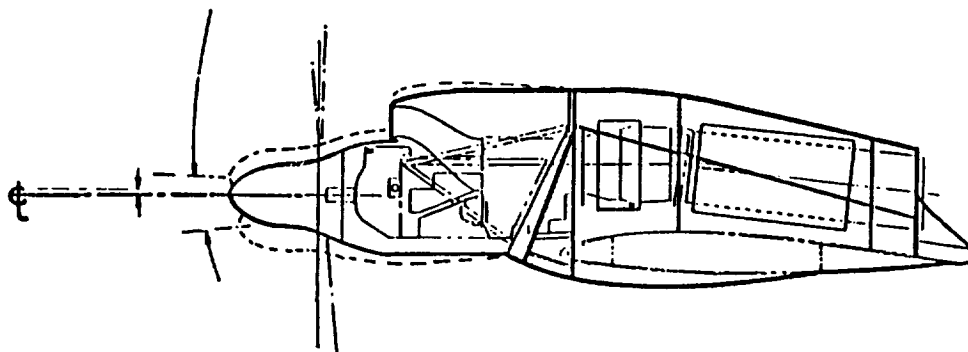


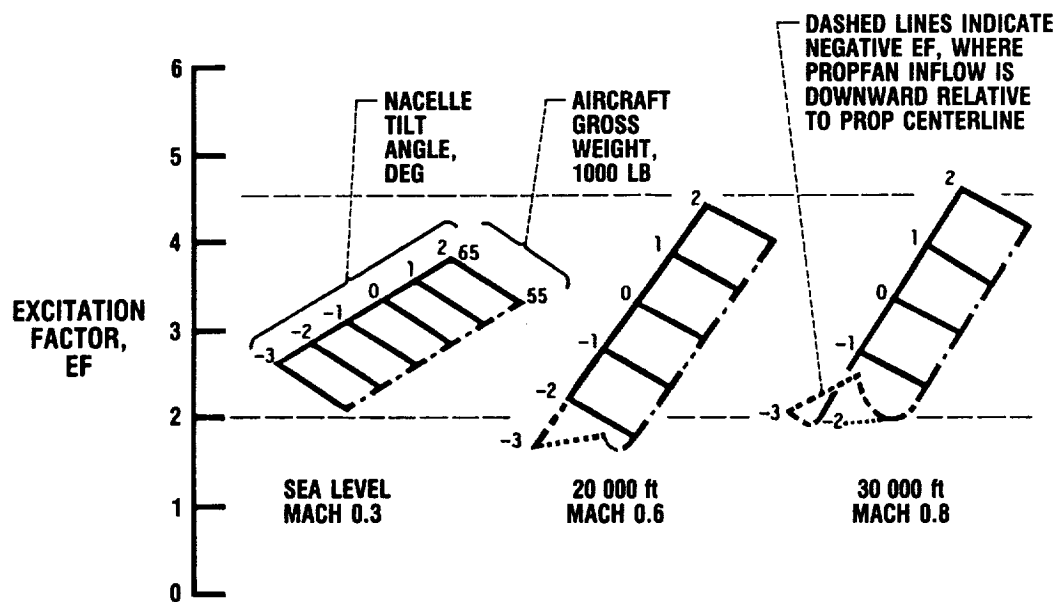
Figure 10. - Research instrumentation (613 parameters).

2° UP
1° DOWN—NOMINAL
3° DOWN



CD-87-28800

Figure 11. - Nacelle tilt range.

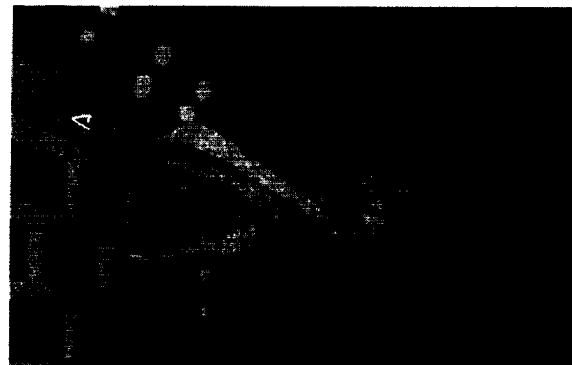


CD-87-28801

Figure 12. - Predicted propfan excitation factors.



1/3-SCALE INLET



1/9-SCALE FLUTTER



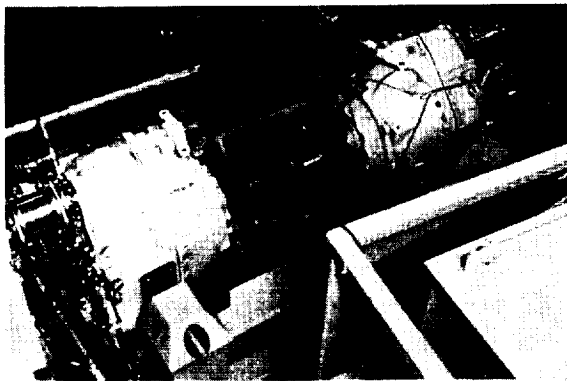
1/9-SCALE STABILITY, CONTROL, AND PERFORMANCE



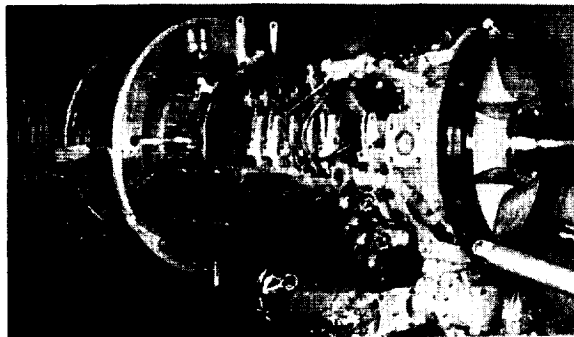
1/9-SCALE PROP FLOWFIELD

CD-87-28802

Figure 13. - Scale-model testing.



GEARBOX ENDURANCE



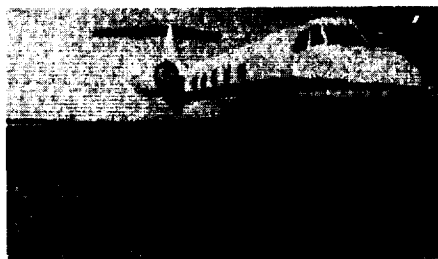
ENGINE DURABILITY



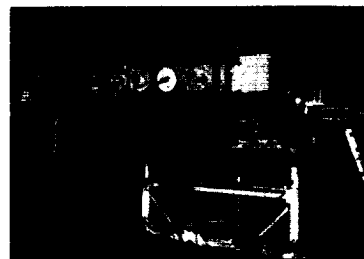
PROPULSION SYSTEM STATIC TEST

CD-87-28803

Figure 14. - Ground testing.



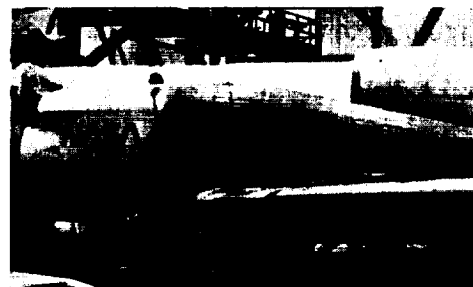
SERIAL NO. 118 GII



WING BEEF-UP



WING-TO-FUSELAGE ATTACHMENT



NACELLE ON WING

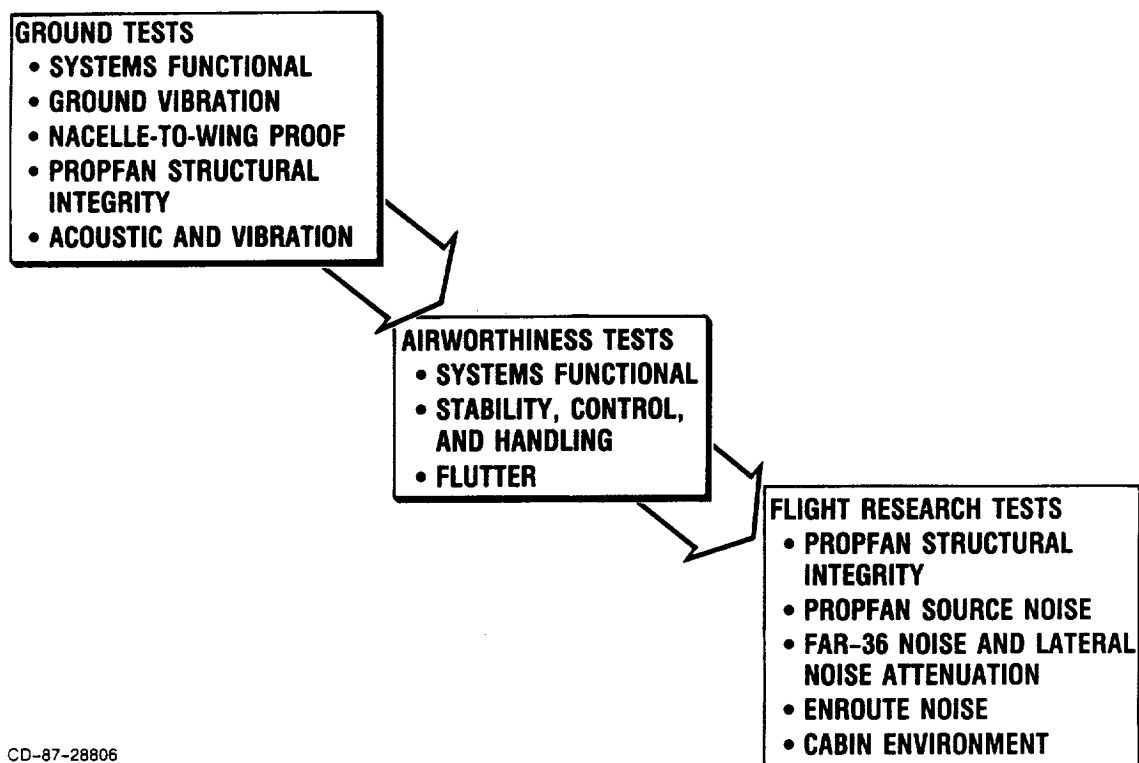
CD-87-28804

Figure 15. - Aircraft and stages of modification.



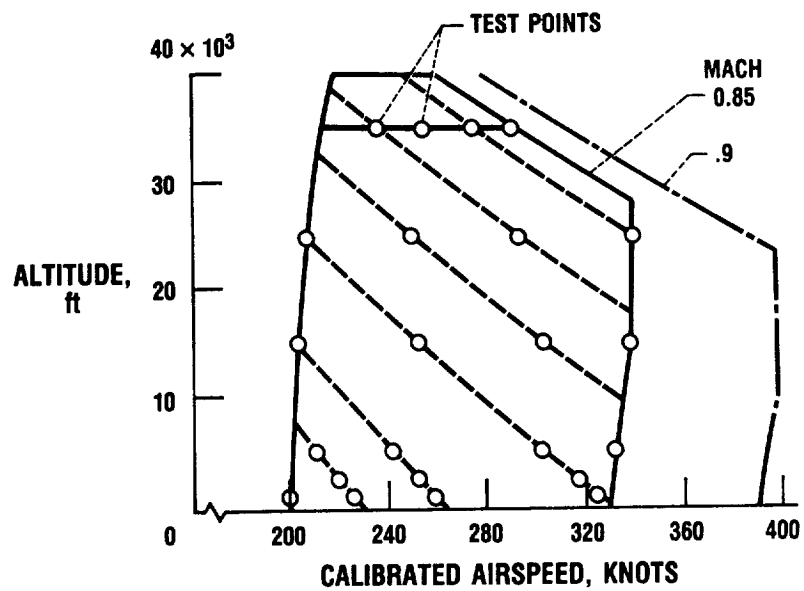
CD-87-28805

Figure 16. - PTA flight testing begun in March 1987.



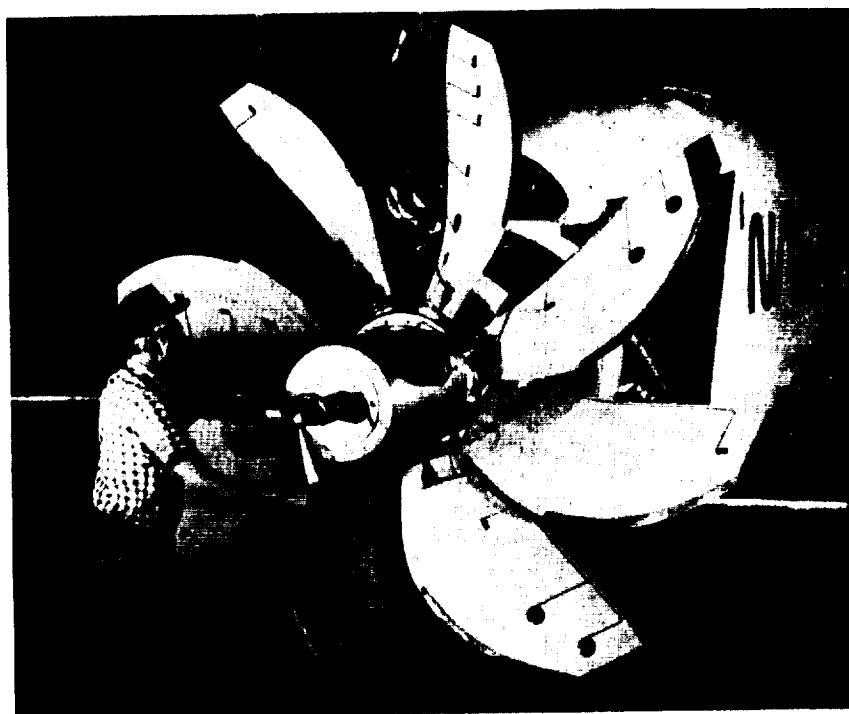
CD-87-28806

Figure 17. - PTA flight test program.



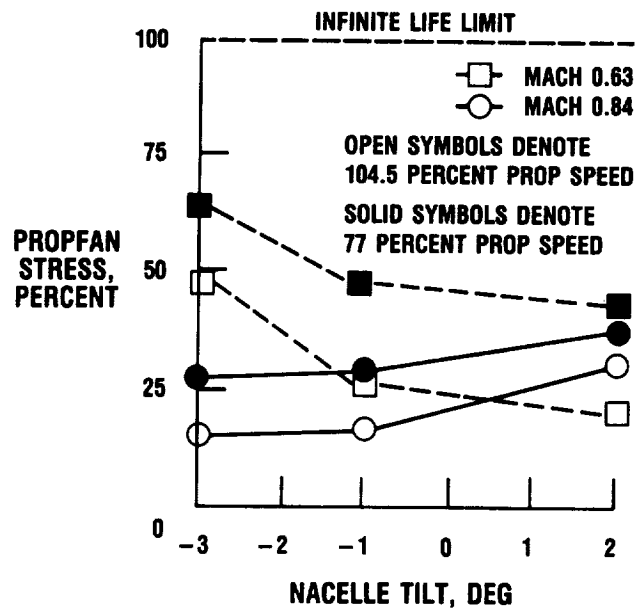
CD-87-28807

Figure 18. - Flight test envelope.



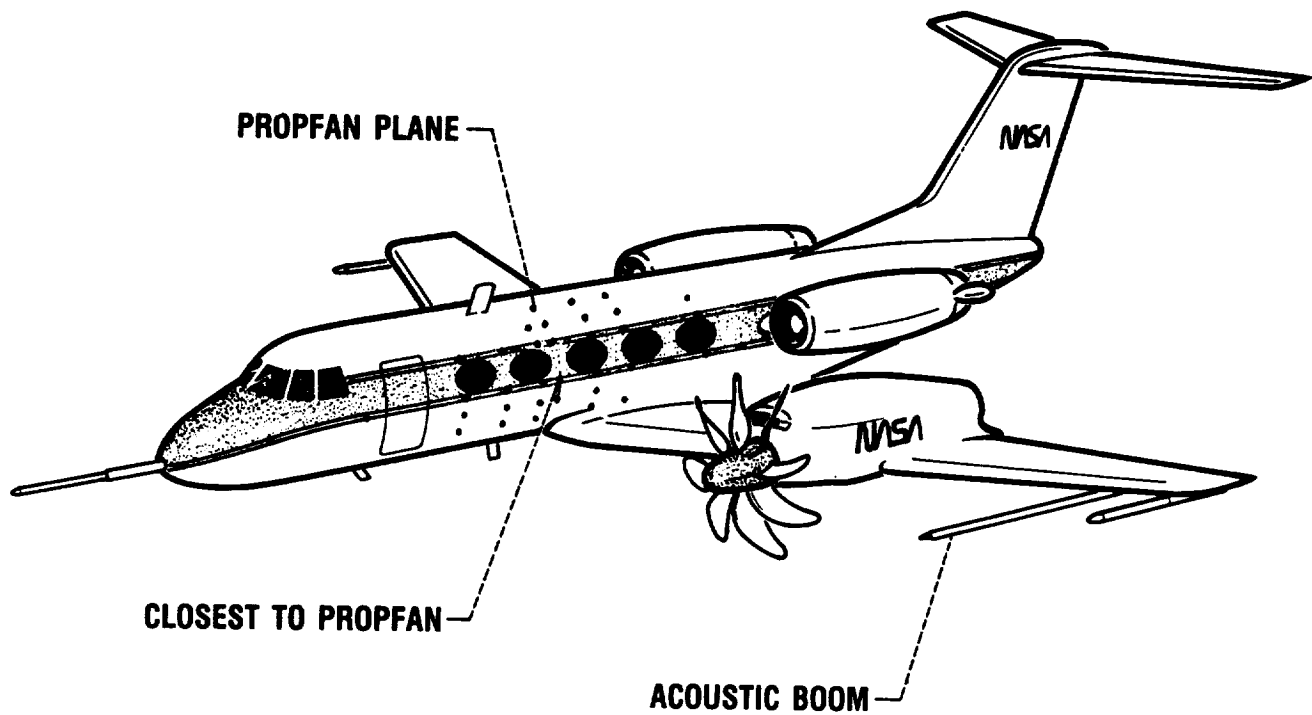
CD-87-28808

Figure 19. - Installed SR-7 propfan.



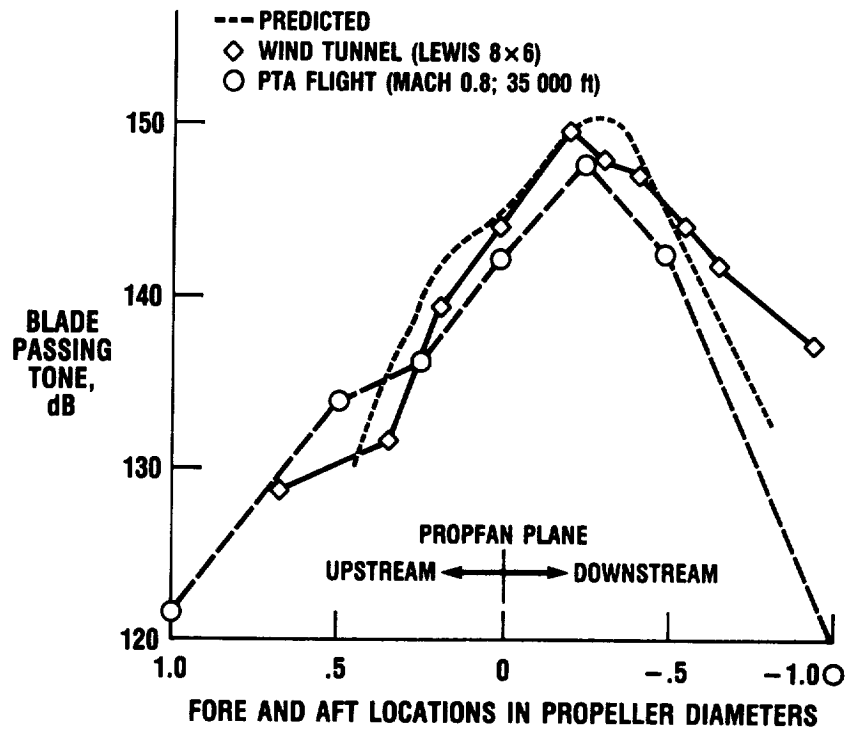
CD-89-40051

Figure 20. - Propfan in-flight stress (altitude, 27 000 ft).



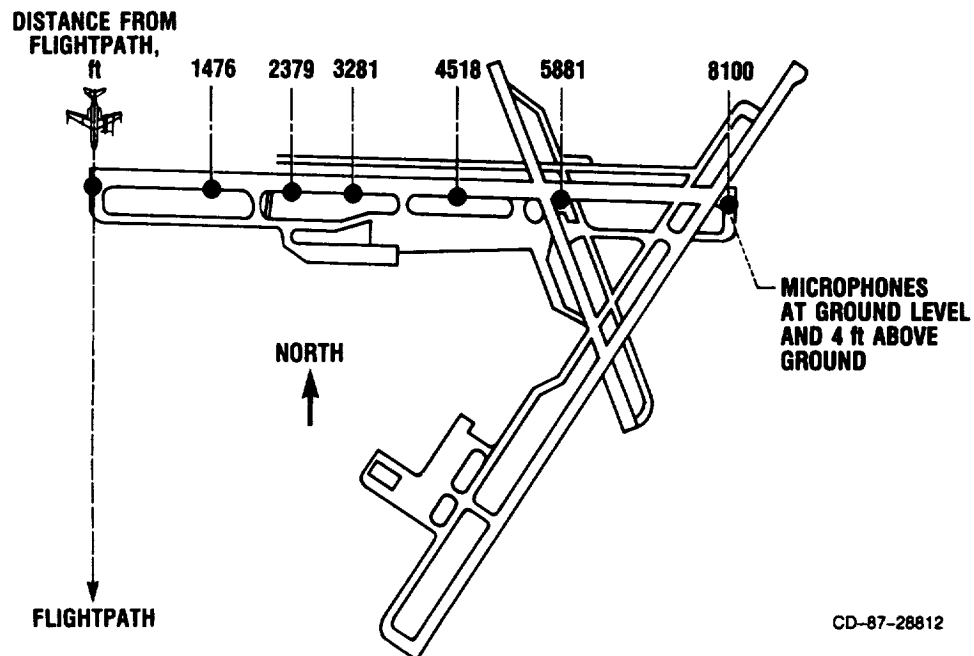
CD-87-28810

Figure 21. - Fuselage surface microphones.



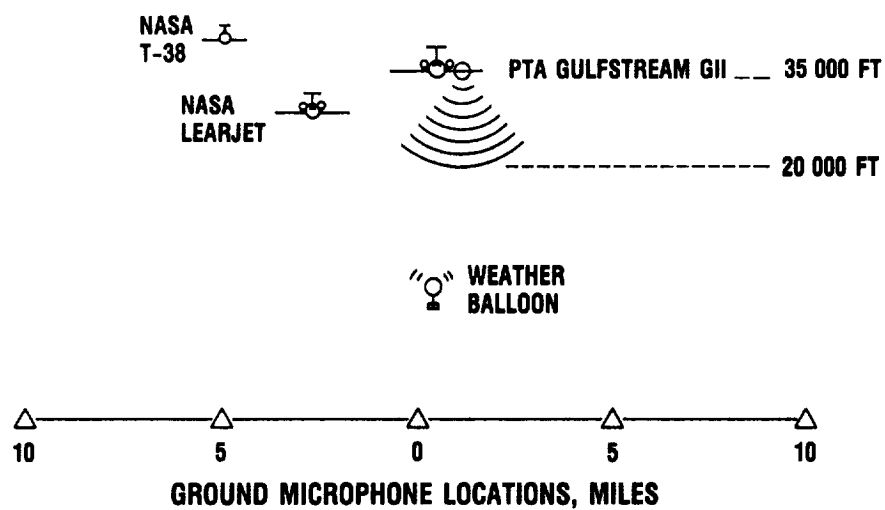
CD-87-28811

Figure 22. - Fuselage exterior noise.



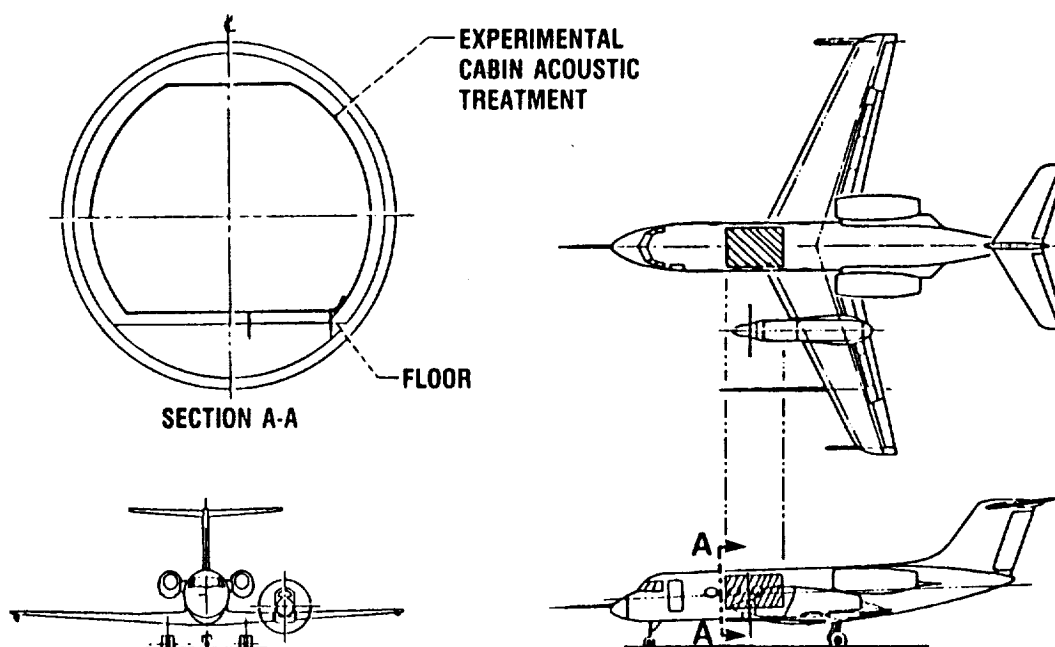
CD-87-28812

Figure 23. - Community noise testing, NASA Wallops Flight Facility.



CD-87-29512

Figure 24. - En route noise testing (cooperative NASA/FAA program).



CD-87-28813

Figure 25. - Cabin noise testing.

ADVANCED PROPELLER RESEARCH

John F. Groeneweg
and
Lawrence J. Bober

SUMMARY

Recent results of aerodynamic and acoustic research on both single-rotation and counterrotation propellers are reviewed. Data and analytical results are presented for three propellers: SR-7A, the single-rotation design used in the NASA Propfan Test Assessment (PTA) flight program; CRP-X1, the initial 5+5 Hamilton Standard counterrotating design; and F7-A7, the 8+8 counterrotating General Electric design used in the proof-of-concept Unducted Fan (UDF) engine. In addition to propeller efficiencies, cruise and takeoff noise, and blade pressure data, off-design phenomena involving formation of leading-edge vortexes are described. Aerodynamic and acoustic computational results derived from three-dimensional Euler and acoustic radiation codes are presented. Research on unsteady flows which are particularly important for understanding counterrotation interaction noise, unsteady loading effects on acoustics, and flutter or forced response is described. The first results of three-dimensional unsteady Euler solutions are illustrated for a single-rotation propeller at angle of attack and for a counterrotation propeller. Basic experimental and theoretical results from studies of the unsteady aerodynamics of oscillating cascades are outlined. Finally, advanced concepts involving swirl recovery vanes and ultra-high-bypass ducted propellers are discussed.

INTRODUCTION

This review addresses three aspects of propeller research: analysis, verification of the analysis with experiment, and studies of advanced concepts. Single-rotation and counterrotation sections address cruise performance, noise at both cruise and takeoff, and specific topics such as blade pressure measurements, leading-edge vortexes associated with off-design operation, and results from steady Euler analysis. In the area of unsteady aerodynamics, recent unsteady three-dimensional Euler results are shown together with theoretical and experimental results from work on transonic cascades. A concluding section discusses advanced concepts and the future work emphases required to address them.

Recent wind tunnel tests (refs. 1 to 3) have provided data on the three advanced high-speed propeller models described in table I. The SR-7A model is the most recent in a series of single-rotation designs (ref. 4) and is an aerodynamically scaled model of the 9-ft-diameter Large-Scale Advanced Propeller (LAP) being used in the Propfan Test Assessment (PTA) Flight Program (refs. 5

and 6). The F7-A7 is a scale model of the counterrotation pusher propeller being used on the Unducted Fan (UDF) demonstrator engine (ref. 7). The CRP-X1 model simulates a counterrotation tractor propeller. All three propeller models have a nominal diameter of 2 ft. Note that the F7-A7 has the highest hub-to-tip ratio and cruise loading.

SINGLE-ROTATION TECHNOLOGY

Figure 1 shows the SR-7A installed in the NASA Lewis 8- by 6-Foot Wind Tunnel, where its aerodynamic, acoustic, and aeroelastic performances were measured at cruise conditions. The laser beams are part of a system used to measure mean blade deflections during propeller operation (i.e., the so-called "hot" blade shape).

Net efficiency of the SR-7A propeller model is shown in figure 2, together with results from five earlier models. Detailed design parameters for each of the propellers are listed in table II. Measured net efficiencies are shown in figure 2 as a function of free-stream Mach number, with each propeller's design loading parameter C_p/J^3 kept constant with Mach number. At Mach 0.80, the design point for SR-7A, its efficiency lies on the upper bound of measured efficiencies. The SR-2 propeller has the lowest performance because it is the only one of these models which has no blade sweep.

The peak fundamental tone levels for SR-7A are plotted in figure 3 as a function of helical tip Mach number (ref. 8). Advance ratio is constant at 3.06, and the near-field measurements were made on a sideline parallel with the propeller axis at 0.3 propeller diameter from the propeller tip. Data for three loading levels are shown as indicated by the blade setting angles bracketing the design value. The striking feature of the tone variation with helical tip Mach number is the behavior in the supersonic range beyond 1.1. The peak fundamental tone levels no longer increase and may peak, level off, or decrease depending on loading. This result indicates that higher cruise and propeller speeds do not necessarily mean increased cabin noise problems.

The SR-7A propeller model was also tested in the NASA Lewis 9- by 15-Foot Anechoic Wind Tunnel to measure far field noise and performance at typical takeoff and approach conditions (Mach 0.2). Figure 4 shows the model installed on a swept wing used to determine installation effects. The entire propeller-wing assembly may be rotated to angle of attack in the horizontal plane. The continuously traversing microphones (at right) measure far field noise corresponding to levels measured below an aircraft during flyover. Fixed microphones on the walls measure noise in the other three directions and are staggered with respect to the tunnel flow to avoid wake interference on downstream microphones. The walls are acoustically treated to provide anechoic conditions down to a frequency of 250 Hz, well below the fundamental frequency for the propeller model.

The effect of angle of attack on the flyover noise of SR-7A without the wing is shown in figure 5 (ref. 9). Fundamental tone directivities are shown for four angles of attack ranging from 0° to 15°. The peak levels, approximately in the plane of rotation, increased by about 10 dB. A typical maximum takeoff angle of the propeller centerline with respect to the aircraft flight

path is about 8° ; thus takeoff noise would be increased on the order of 5 dB because of unsteady loading at that angle of attack.

A detailed knowledge of propeller blade surface pressures is important for aerodynamic code validation and as input to acoustic calculations. A two-blade version of the eight-blade Large-Scale Advanced Propeller (LAP) was tested in the ONERA S1 wind tunnel to obtain steady and unsteady blade pressures over a wide range of operating conditions (fig. 6). Only two blades were used because of the limited total power available to drive the propeller. In this way the propeller could be operated at a reasonable power per blade. The large size of this propeller (9-ft diam) allowed much more detailed measurements than could be obtained on the 2-ft-diameter models tested previously.

Sample results of the steady blade pressure distributions measured are shown in figure 7 at several spanwise locations on the LAP at a low-speed, high-power condition. The pressure distributions at the two locations nearest the tip lack the high suction peaks of the inboard locations because of the presence of leading-edge and tip vortexes at the outboard locations. Similar data were obtained at 12 additional operating conditions, providing valuable data for code verification.

A schematic of leading-edge and tip vortexes is shown in figure 8, together with curves showing the consequences of using analyses which neglect their presence. When the propeller is operating appreciably off the cruise design point, such as at takeoff, a leading-edge vortex which merges with the tip vortex is expected to form, as shown schematically. The phenomenon is similar to the vortex structure on a delta wing aircraft at high angle of attack. If the associated altered loading distribution is not accounted for in analytical models, errors in aerodynamic performance and the tone noise level predictions will result as illustrated.

In addition to the blade pressure data, flow visualization of propeller blade surface flows at off-design conditions has indicated the presence of leading-edge and tip vortexes (refs. 1 and 10). Fluorescent oil flow patterns on the pressure side of the SR-3 blade at the Mach 0.8, windmill condition are shown in figure 9. Streaks in the oil at the blade surface are influenced by two main factors. Centrifugal forces cause radial flow in the oil film. Shear flow forces at the surface act mainly along streamlines. Over much of the blade the streaks are at an angle determined by these two forces. However, near the leading edge on the outboard portion of the blade and at the tip, the lines are primarily radial. This indicates a different flow regime, interpreted as the existence of a leading-edge vortex merging with a tip vortex.

This flow phenomenon has recently been predicted computationally. An Euler code developed at NASA Lewis (ref. 11) was run at United Technologies Research Center (UTRC) with an order of magnitude increase in grid points to about 200 000. When particle paths were traced they revealed the leading-edge vortex which merges with the tip vortex flow, as shown in figure 10. The operating condition at Mach 0.2 and advance ratio of 1.0 is typical of a takeoff situation which involves high incidence angles. Apparently, numerical "viscosity" is sufficient to trigger vortex formation and produce at least a qualitative description of this flow phenomenon.

COUNTERROTATION TECHNOLOGY

The counterrotation tractor propeller model, designated CRP-X1, was designed and built by Hamilton Standard under contract to NASA Lewis and is shown installed in the UTRC high-speed wind tunnel in figure 11. The front and rear propellers are independently driven by two air-driven turbines. Propeller performance and flow field data, as well as blade stresses, were measured during these tests (ref. 2). Propeller acoustic data were obtained during separate tests in the UTRC Acoustic Research Tunnel (ref. 12).

Figure 12 shows the net efficiency of the CRP-X1 propeller model as a function of power loading at three free-stream Mach numbers. At the design power loading of 37.2 shp/D^2 , the data indicate a net efficiency of approximately 85 percent for Mach numbers in the range of 0.7 to 0.8. The efficiency also remains high over a wide range of power loadings. The predicted efficiency agrees very well with the data at Mach 0.8, but somewhat overpredicts the efficiency at the lower Mach numbers.

An example of acoustic data obtained on CRP-X1 (ref. 12) is shown in figure 13. Levels of the first five harmonics of single-rotation (SRP) and counterrotation (CRP) propeller noise are shown at three axial locations in the far field: forward, aft, and in the plane of rotation. The single-rotation fundamental tone levels are adjusted upward 3 dB to compare the equivalent noise of two independent propellers with the CRP-X1 counterrotation configuration. Single-rotation and counterrotation fundamental tones are then roughly equal, but the counterrotation harmonic levels are dramatically higher at all locations due to the unsteady aerodynamic interactions between blade rows. This characteristic of high forward and aft harmonic levels must be dealt with to achieve acceptable counterrotation community noise levels.

In figure 14 the NASA Lewis counterrotation pusher propeller test rig is shown installed in the 8- by 6-Foot Wind Tunnel. The propeller shown is the F7-A7 configuration described in table I. The tunnel has holes in the walls equivalent to about 6 percent porosity to minimize wall interactions at transonic speeds. The rig is strut mounted and is powered by two turbines using 450-psi drive air. Performance, flow field, and acoustic measurements are made.

Examples of the blade configurations tested are shown in figure 15 and include designs for Mach 0.72 cruise (top row) and Mach 0.8 cruise (bottom row). The designs differed in tip sweep, planform shape, airfoil camber, and a significantly shortened aft rotor (A3). The planform shapes for most forward and aft rotors were very similar. The A21 aft rotor planform is included since it differs so much from the F21 front rotor. The F1-A1 configuration is very similar to F7-A7 but with reduced camber, which is expected to improve cruise efficiency. F1-A3 was run to see the aerodynamic and acoustic effects of a short aft rotor. These blades were designed and built by the General Electric Company, several under contract to NASA Lewis.

Net efficiencies for F7-A7 are shown in figure 16 as a function of Mach number for three loadings: design, 80 percent, and 120 percent of design. Tip speed was held constant at the design value of 780 ft/sec. At the design Mach number of 0.72, efficiency depends quite strongly on loading: increased loading decreases efficiency. At Mach numbers significantly higher than design,

compressibility losses dominate, and efficiencies fall off nearly independent of loading.

Counterrotation fundamental tone levels at cruise conditions are shown in figure 17. Fundamental tone directivities for F7-A7, the proof-of-concept UDF configuration, are compared for model data from the NASA Lewis 8- by 6-Foot Wind Tunnel scaled to full-scale cruise conditions, full-scale flight data obtained by the formation flight of the instrumented NASA Lewis Learjet with the UDF engine on the 727, and predicted levels from a frequency domain model developed by General Electric. There is good agreement between the model wind tunnel measurements and full-scale flight data, particularly since the in-flight automation pitch control system did not allow the full-scale aft blade pitch angles to be matched with available model data. Predicted levels agree quite well with the data except for the forward angles.

Noise and performance measurements were also made on counterrotation models at takeoff/approach conditions. In figure 18 the model of the 8+8 configuration of the propeller used on the UDF proof-of-concept engine is shown in the 9- by 15-Foot Anechoic Wind Tunnel, where extensive community noise tests were conducted. Unequal blade numbers, differential diameter, rotor-to-rotor spacing, angle of attack, and effects of an upstream support pylon were investigated. A continuously traversing microphone (not shown) was also used to map the asymmetric sound field with the model at angle of attack or with a pylon installed. The tunnel walls are acoustically treated to make the test section anechoic down to 250 Hz, well below the fundamental tone frequency of the model.

Examples of counterrotation propeller noise at the takeoff conditions are shown in figure 19 (ref. 13). Measured and predicted directivities of the front rotor fundamental and the first interaction tone for F7-A7 at Mach 0.2 are compared. The predictions are from a frequency domain theory developed at General Electric. Note again the high levels of interaction tone noise at both forward and aft angles, in contrast to the forward rotor alone fundamental which peaks in the plane of rotation. Agreement between theory and data is very good for the front rotor fundamental. The predicted shape of the first interaction tone agrees well with the data, but the levels are underpredicted at the extremes in angle, indicating that more code development work is required for the interaction noise sources.

A counterrotation Euler code developed at NASA Lewis (ref. 12) has been used to obtain numerical predictions of the flow about one version of the UDF. The solution is obtained by iterating between the front and rear blade rows. The coupling between rows is done in a circumferentially averaged sense, so there are no blade-wake interactions included. The results in figure 20 show the pressure distribution on the nacelle and blade surfaces as well as on a plane perpendicular to the axis of rotation at the aft end of the nacelle. The flow field pressures were taken from the flow field of the rear row and show near-field acoustic pressure perturbations spiraling out into the flow. The calculations were done at Cray Research, and the flow field was displayed by using the code MOVIE-BYU.

UNSTEADY AERODYNAMICS

Fully unsteady, three-dimensional Euler code solutions have recently been obtained for advanced propeller geometries (ref. 14). Results from the unsteady Euler code solution for the SR-3 propeller with its axis at 4° to the mean 0.8 Mach number flow are shown in figure 21. As the propeller rotates, downward moving blades (on the right in the figure) experience the highest incidence, upward blades (on the left) the lowest, and top and bottom are near the mean. Pressure contours for regions where the absolute flow velocities are supersonic are plotted in alternate blade passages. Large regions of supersonic flow are shown for the high incidence, high loading positions with much smaller supersonic regions corresponding to lower incidences and loadings.

The unsteady Euler solution algorithms were also applied to the 8+8-configuration F7-A7 counterrotation propeller to obtain a full unsteady, three-dimensional solution for the flow field. A sample of the results in the form of pressure contours in a plane just downstream of both blade rows is shown in figure 22 (ref. 14). These contours, which are for a particular instant in time, show a low pressure island structure indicative of the tip vortexes shed by the blades. Current solution methods handle equal blade numbers in each row and are being extended to treat the general case of unequal blade numbers.

An experimental and analytical research program is being conducted to understand the flutter and forced response characteristics of advanced high-speed propellers. A comparison of measured and calculated flutter boundaries for a propfan model, called SR3C-X2, is shown in figure 23 (refs. 15 and 16). The theoretical results from the NASA Lewis-developed ASTROP3 analysis include the effects of centrifugal loads and steady-state, three-dimensional air loads. The analysis does reasonably well in predicting the flutter speeds and slopes of the boundaries. However, the difference between the calculated and measured flutter Mach numbers is greater for four blades than for eight blades. This implies that the theory is overcorrecting for the decrease in the aerodynamic cascade effect with four blades.

Wind tunnel tests of the SR-5 propeller demonstrated that cascade effects and sweep effects have a destabilizing influence on the flutter boundary at relative Mach numbers approximately equal to 1. Experimental research conducted in the NASA Lewis transonic oscillating cascade will investigate the subsonic and transonic steady and unsteady aerodynamics relevant to advanced turboprops. (See fig. 24.) An unswept cascade will provide baseline data. Following that, the aerodynamics of a cascade of airfoils with sweep will be quantified. Both subsonic and transonic flow fields will be investigated as the airfoils undergo torsional oscillations at realistic reduced frequency values.

A compressible, unsteady, full Navier-Stokes, finite-difference code has been developed for modeling transonic flow through two-dimensional, oscillating cascades (ref. 17). The procedure introduces a deforming grid technique to capture the motion of the airfoils, as shown on the left portion of figure 25, which is for an interblade phase angle of 90° . The use of the deforming grid is convenient for treatment of the outer boundary conditions since the outer boundary can be fixed in space, while the inner boundary moves with the blade motion. The code is an extension of the isolated airfoil code developed at the Georgia Institute of Technology (ref. 18). The motion of the shock wave

is evident in the chordwise pressure distributions shown at the right in figure 25.

ADVANCED CONCEPTS

The swirl recover vane experiment will investigate the fuel-saving and noise benefits available by adding swirl recovery vanes (SRV) behind a propfan, as shown in figure 26. Thus, the 1000-hp, single-rotation propeller test rig will be modified to accept a new balance and eight swirl recovery vanes. These tests will determine the fuel-saving benefits of the SRV concept over its Mach number operating range (0 to 0.85). Other parametric variations will include vane angle and vane axial spacing relative to the propfan. Design calculations indicate that as much as two-thirds of the efficiency increment available from counterrotation (8 to 10 percent) can be obtained with the swirl recovery vanes.

For long-range aircraft with wing-mounted engines, ducted propellers (ultra-high-bypass fans) have installation advantages in terms of limiting the diameter required for a given thrust. Technical issues associated with these configurations which require research are noted for high-speed cruise in the upper half of figure 27 and for low-speed takeoff or approach in the lower half. At cruise, the drag of the large-diameter thin cowl must be minimized while achieving acceptable near-field sound levels. A synthesis of propeller and fan aerodynamic design methods is required to arrive at an optimum combination of sweep and of axial and tip Mach numbers. At low speed, far-field community noise, cowl-lip separation at high angles of attack with the associated blade stresses, and reverse thrust operation must each be addressed.

CONCLUDING REMARKS

The status of current and future propeller research in each of the three disciplines (aerodynamics, acoustics, and aeroelastics) is summarized in figure 28. Presently, aerodynamic work emphasizes three-dimensional steady Euler solutions and performance measurements with some diagnostics, while future work is moving toward three-dimensional unsteady Euler and Navier-Stokes codes with more emphasis on detailed flow field diagnostics. Acoustically, three-dimensional codes are used with detailed steady aerodynamic input, and extensive cruise and takeoff signatures have been measured for both single rotation and counterrotation. Future efforts will emphasize unsteady aerodynamic inputs to the codes to describe interaction and installation effects, and experiments will concentrate on detailed noise maps for installed configurations. Current aeroelastics focus has been on prediction and measurement of flutter boundaries and constructing the first generation of structural design optimization codes. In the future, flutter boundary measurement and prediction will be extended to counterrotation, and the phenomena of stall flutter and forced response will receive more emphasis. Future emphasis in all three disciplines will involve addressing the technical issues associated with ultra-high-bypass ducted propellers.

REFERENCES

1. Stefko, G.L.; Rose, G.E.; and Podboy, G.G.: Wind Tunnel Performance Results of an Aeroelastically Scaled 2/9 Model of the PTA Flight Test Prop-Fan. AIAA Paper-87-1893, June 1987 (NASA TM-89917).
2. Wainauski, H.S.; and Vaczy, C.M.: Aerodynamic Performance of a Counter Rotating Prop-Fan. AIAA Paper 86-1550, June 1986.
3. Sullivan, T.J.: Aerodynamic Performance of a Scale-Model, Counter-Rotating Unducted Fan. Advanced Technology for Aero Gas Turbine Components, AGARD CP-421, AGARD, Neuilly-Sur-Seine, France, 1987, pp. 22-1 to 22-16. (Avail. NTIS, AD-A198664.)
4. Mikkelson, D.C.; Mitchell, G.A.; and Bober, L.J.: Summary of Recent NASA Propeller Research. AGARD Conference Paper, Oct. 1984 (NASA TM-83733).
5. Whitlow, J.B., Jr.; and Sievers, G.K.: Fuel Savings Potential of the NASA Advanced Turboprop Program. NASA TM-83736, 1984.
6. Graber, E.J.: Overview of NASA PTA Propfan Flight Test Program. Aero-propulsion '87, NASA CP-10003, 1987.
7. Stuart, A.R.: The Unducted Fan Engine. AIAA Paper 85-1190, July 1985.
8. Dittmar, J.H.; and Stang, D.B.: Cruise Noise of the 2/9 Scale Model of the Large-Scale Advanced Propfan (LAP) Propeller, SR-7A. AIAA Paper 87-2717, Oct. 1987 (NASA TM-100175).
9. Woodward, R.P.: Measured Noise of a Scale Model High Speed Propeller at Simulated Takeoff/Approach Conditions. AIAA Paper 87-0526, Jan. 1987.
10. Vaczy, C.M.; and McCormick, D.C.: A Study of the Leading Edge Vortex and Tip Vortex on Propfan Blades. J. Turbomachinery, vol. 109, no. 3, July 1987, pp. 325-331.
11. Celestina, M.L.; Mulac, R.A.; and Adamczyk, J.J.: A Numerical Simulation of the Inviscid Flow Through a Counter-Rotating Propeller. NASA TM-87200, 1986.
12. Magliozzi, B.: Noise Characteristics of a Model Counter-Rotating Propfans. AIAA Paper 87-2656, Oct. 1987.
13. Woodward, R.P.: Noise of a Model High Speed Counterrotation Propeller at Simulated Takeoff/Approach Conditions (F7/A7). AIAA Paper 87-2657, Oct. 1987 (NASA TM-100206).
14. Whitfield, D.L., et al.: Three-Dimensional Unsteady Euler Solution for Propfans and Counter-Rotating Propfans in Transonic Flow. AIAA Paper 87-1197, June 1987.
15. Kaza, K.R.V., et al.: Analytic Flutter Investigation of a Composite 14. Kaza, Propfan Model. NASA TM-88944, 1987.

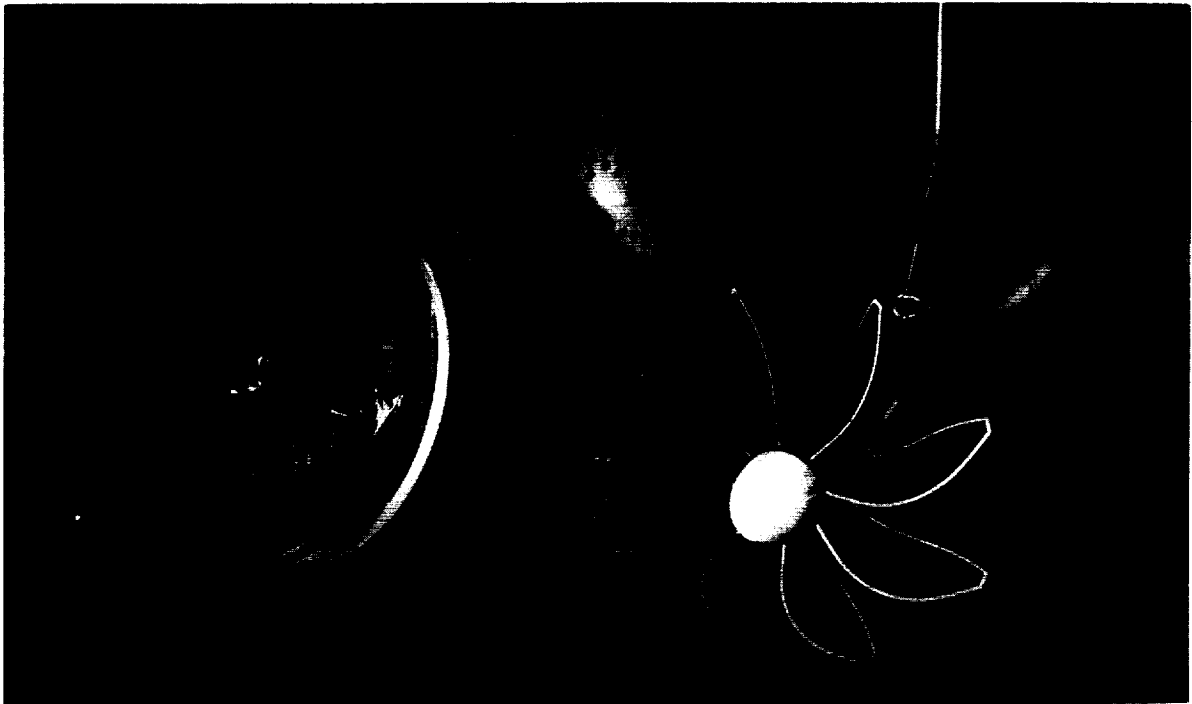
16. Ernst, M.A.; and Kiraly, L.J.: Determining Structural Performance. Aero-propulsion '87, NASA CP-10003, 1987.
17. Huff, D.L.: Numerical Simulations of Unsteady, Viscous, Transonic Flow Over Isolated and Cascade Airfoils Using a Deforming Grid. AIAA Paper 87-1316, June 1987 (NASA TM-89890).
18. Sankar, N.L.; and Tang, W.: Numerical Solution of Unsteady Viscous Flow Past Rotor Sections. AIAA Paper 85-0129, Jan. 1985.

TABLE I. - ADVANCED PROPELLER DESIGN PARAMETERS

Design	Number of blades	Radius ratio	Cruise Mach number	Cruise loading, shp/D ²	Tip speed, ft/sec
SR-7	8	0.24	0.80	32.0	800
F7-A7	8+8	.425	.72	55.5	780
CRP-X1	5+5	.240	.72	37.2	750
		.275	.72	37.2	750

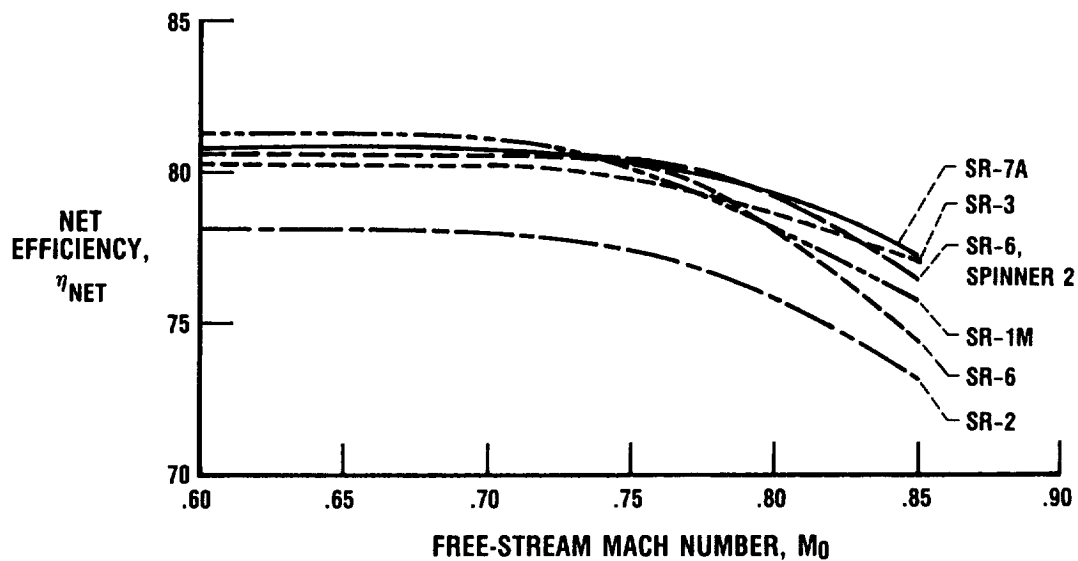
TABLE II. - SINGLE-ROTATION PROPELLER DESIGN PARAMETERS

Design	Number of blades	Sweep angle, deg	Power coefficient, C _p	Advance ratio, J	Loading parameter, C _p /J ³	Tip speed, ft/sec
SR-7A	8	41	1.45	3.06	0.0509	800
SR-6	10	40	2.03	3.50	.0474	700
SR-3	8	45	1.70	3.06	.0593	800
SR-1M	8	30	1.70	3.06	.0593	800
SR-2	8	0	1.70	3.06	.0593	800



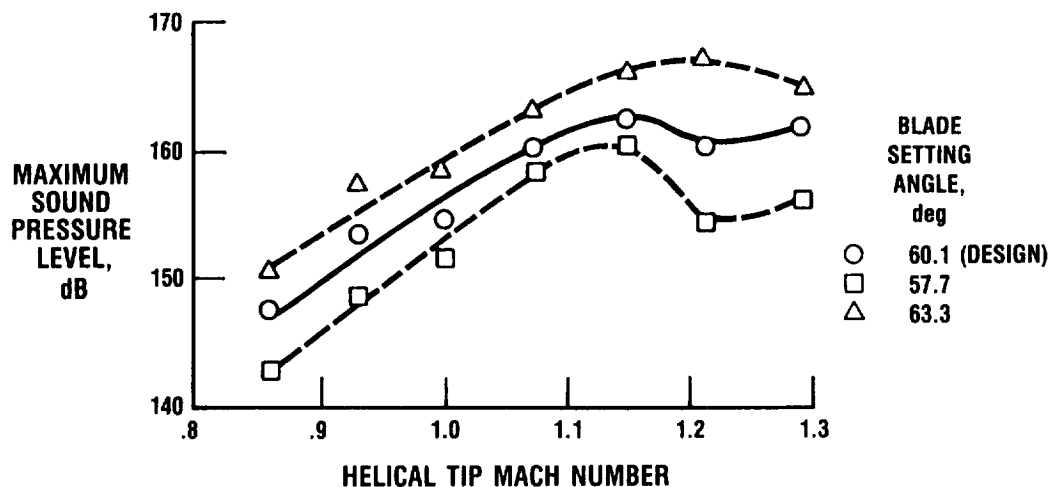
CD-87-29482

Figure 1. - SR-7A propeller in Lewis 8- by 6-Foot Wind Tunnel.



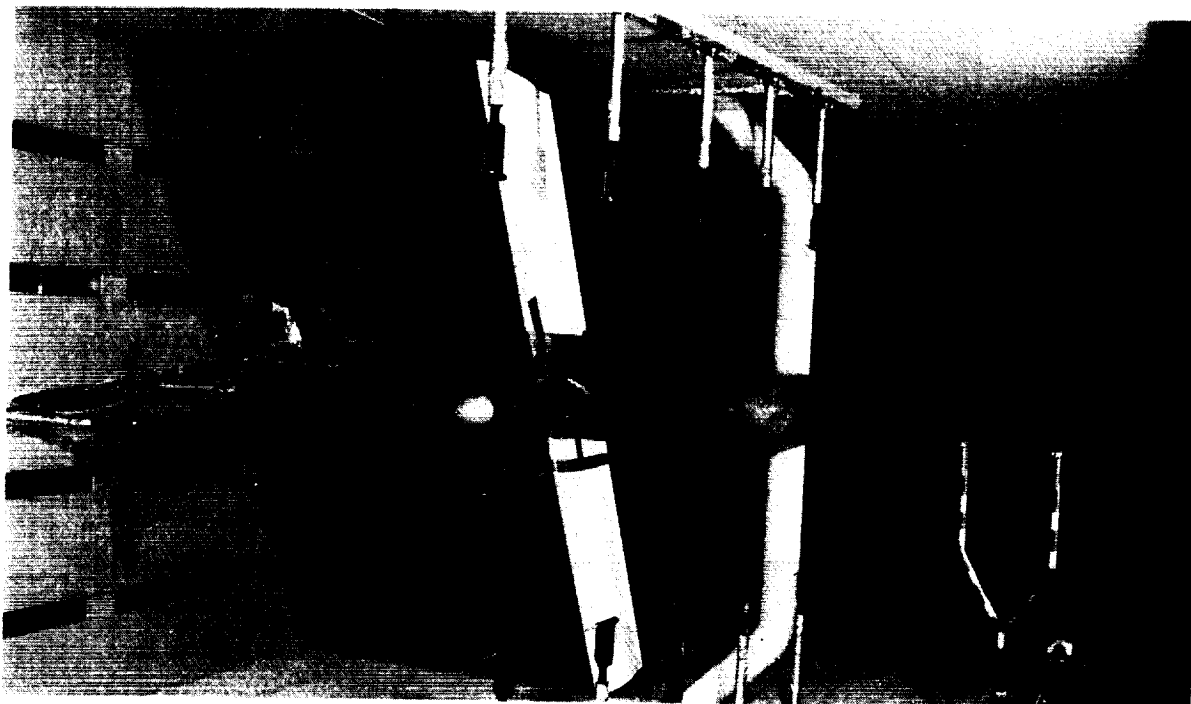
CD-87-29483

Figure 2. - Single-rotation propeller performance.



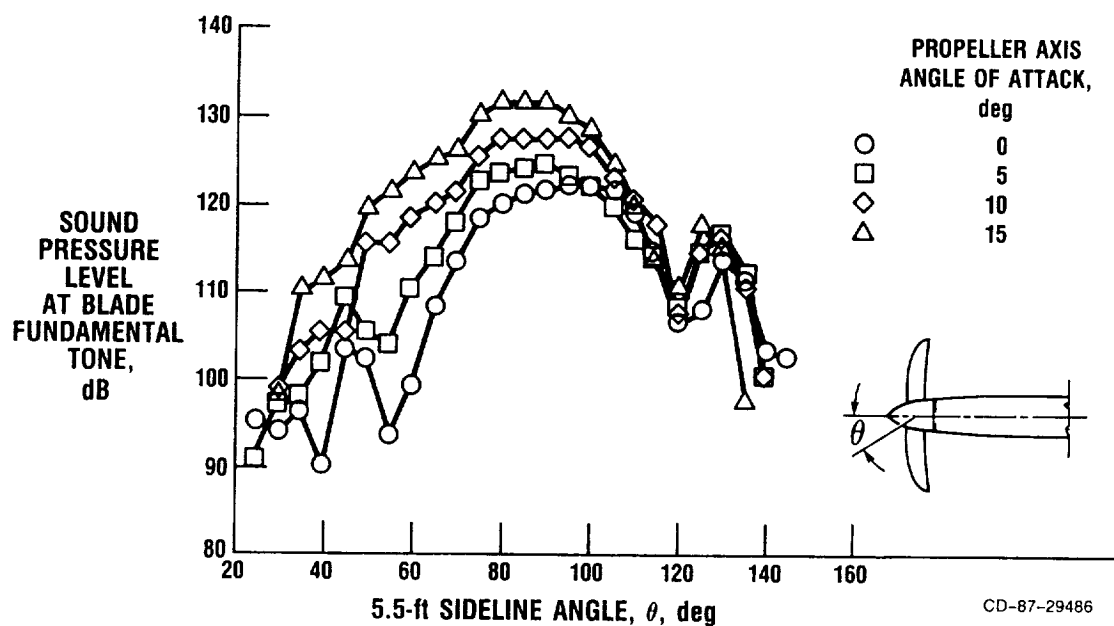
CD-87-29484

Figure 3. - SR-7 peak blade passing tone variation with helical tip Mach number (constant advance ratio, 3.06).



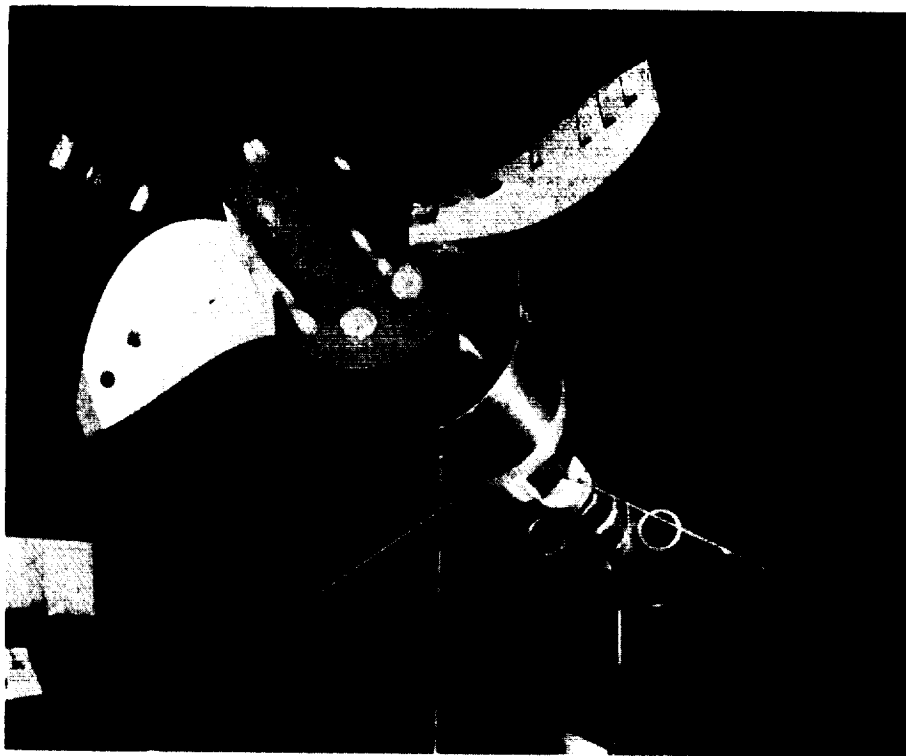
CD-87-29485

Figure 4. - SR-7A propeller model in 9- by 15-Foot Anechoic Wind Tunnel.



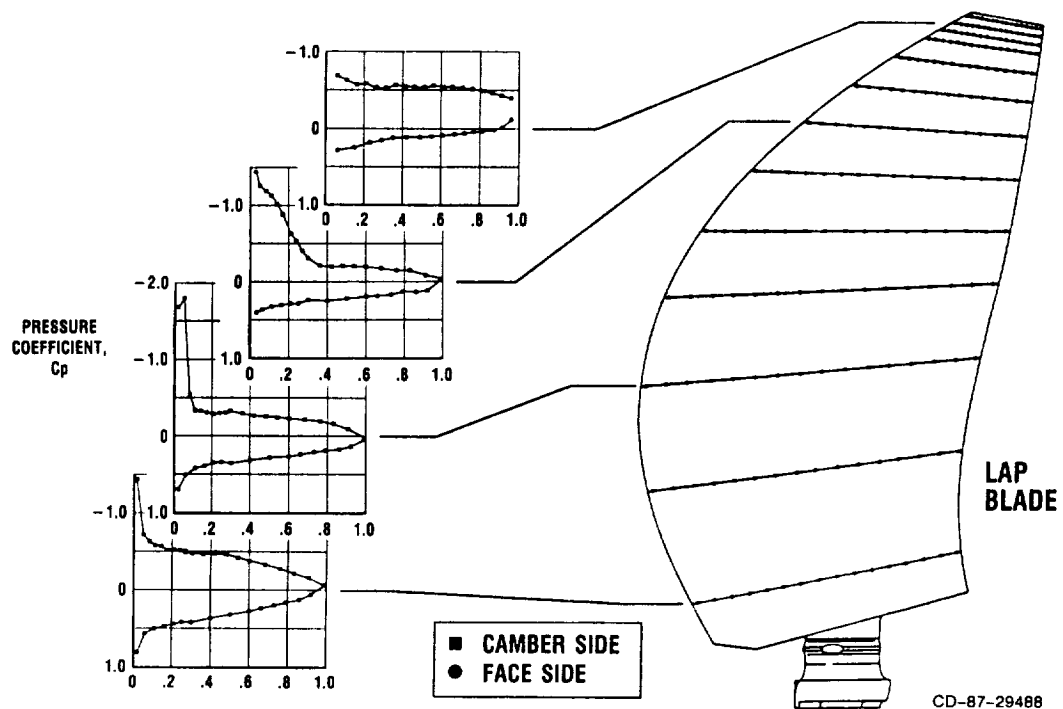
CD-87-29486

Figure 5. - Effect of angle of attack on flyover noise (single-rotation propeller SR-7A; 9- by 15-Foot Wind Tunnel; takeoff blade angle, 37.8°; tip speed, 800 ft/sec; tunnel Mach number, 0.2).



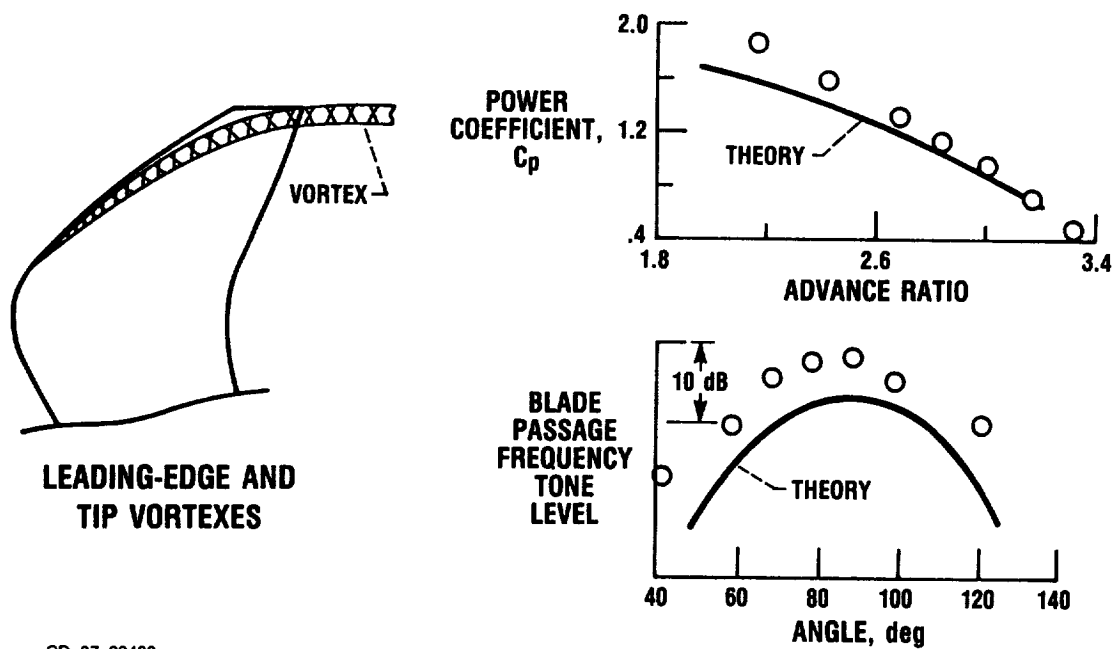
CD-87-29487

Figure 6. - Two-blade version of large-scale advanced propfan (LAP).



CD-87-29488

Figure 7. - Blade pressure measurements on full-scale propeller (low-speed conditions).



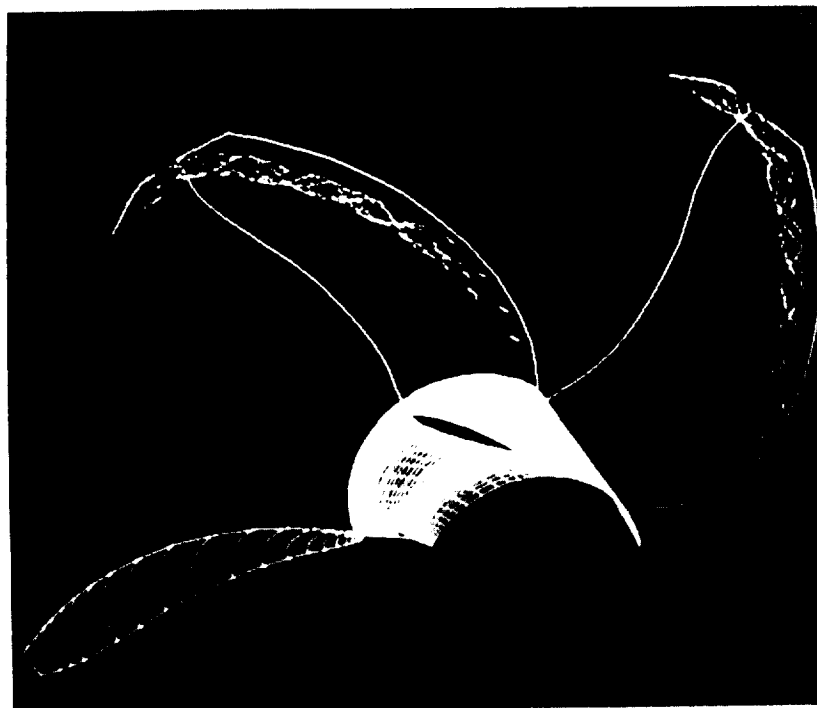
CD-87-29489

Figure 8. - Off-design operation.



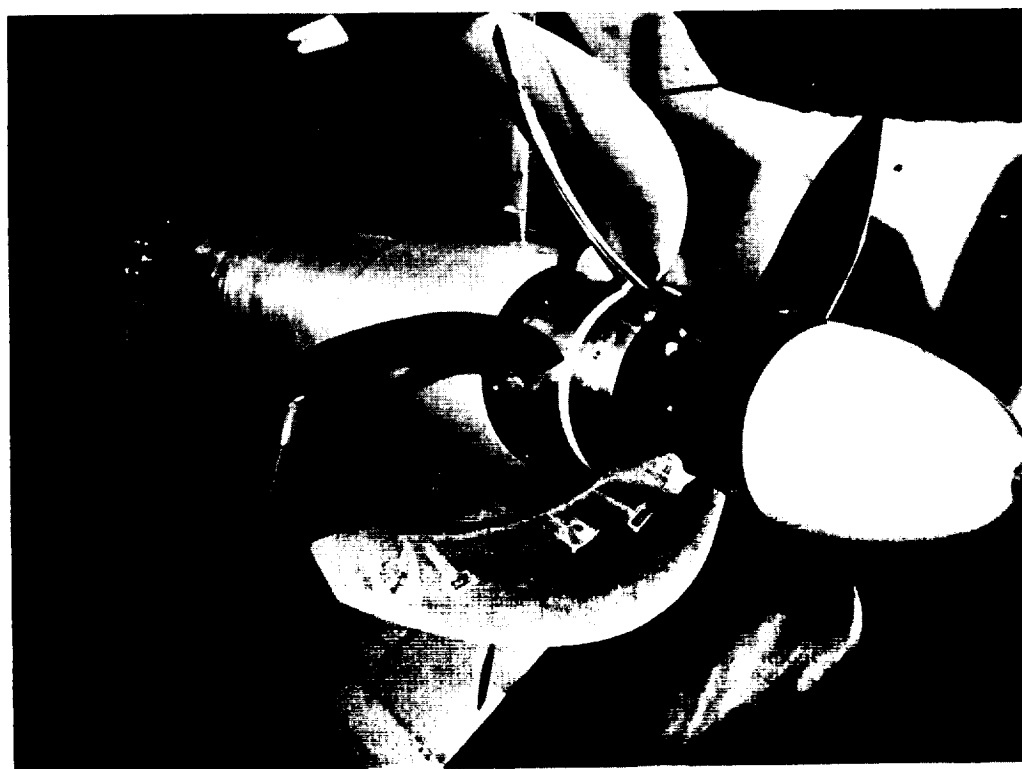
CD-87-29490

Figure 9. - Visualization of propeller blade surface flow (off-design conditions).



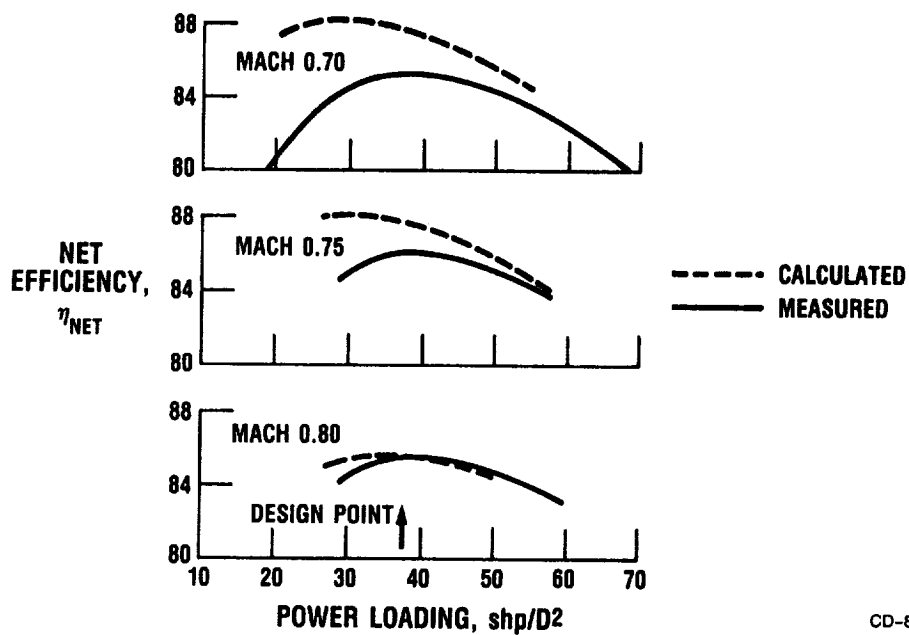
CD-87-29491

Figure 10. - Computed streamlines on CRP-X1 propeller (Mach 0.2; $J = 1.0$).



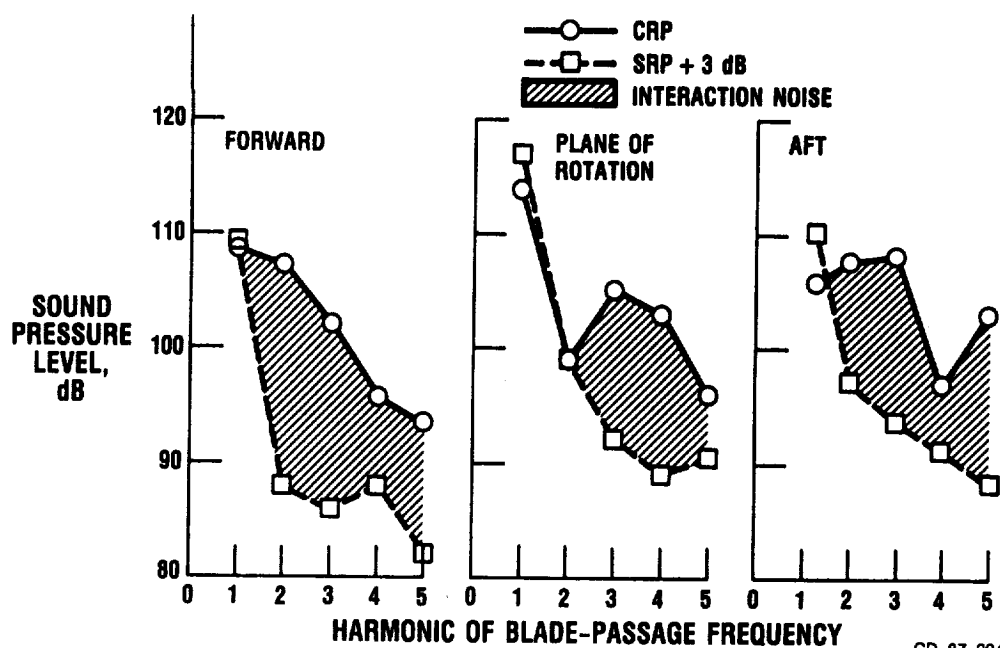
CD-87-29492

Figure 11. - Counterrotating propeller (CRP-X1) in UTRC wind tunnel.



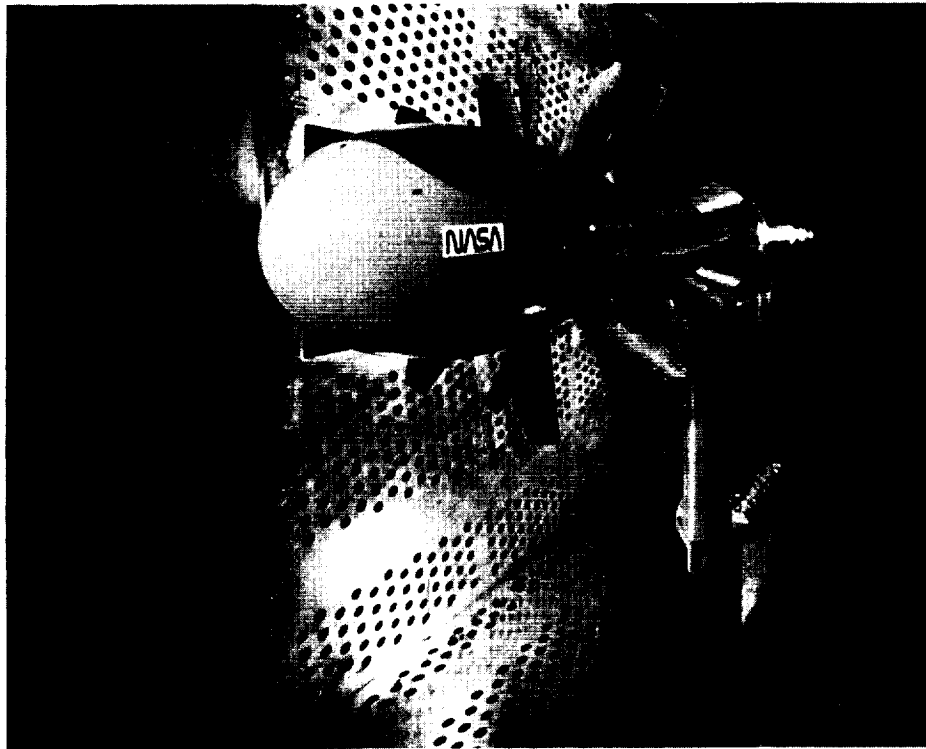
CD-87-29493

Figure 12. - CRP-X1 performance comparison ($\Delta\beta = 2.6$; tip speed, 750 ft/sec).



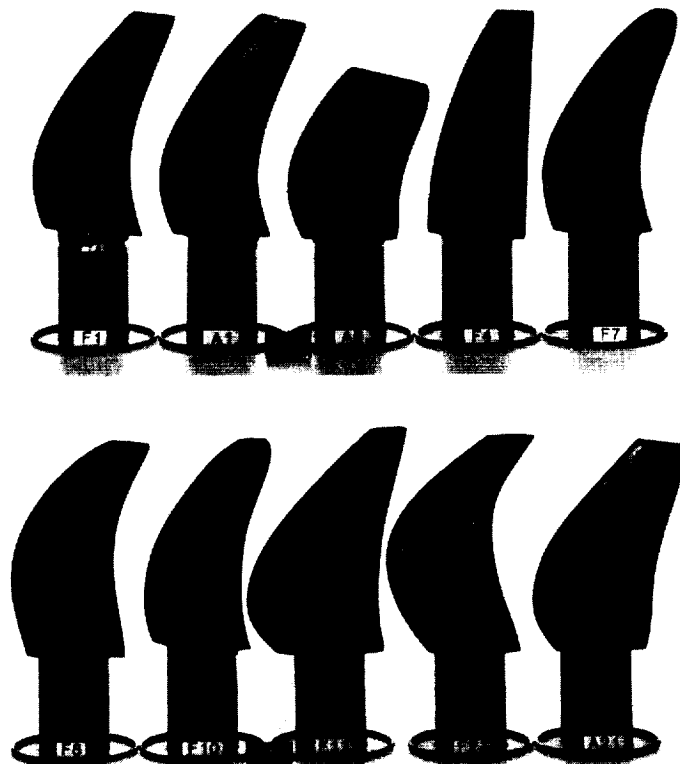
CD-87-29494

Figure 13. - Counterrotation propeller interaction noise (CRP-X1 at takeoff conditions: $V_T = 650$ ft/sec; 100 shp/rotor).



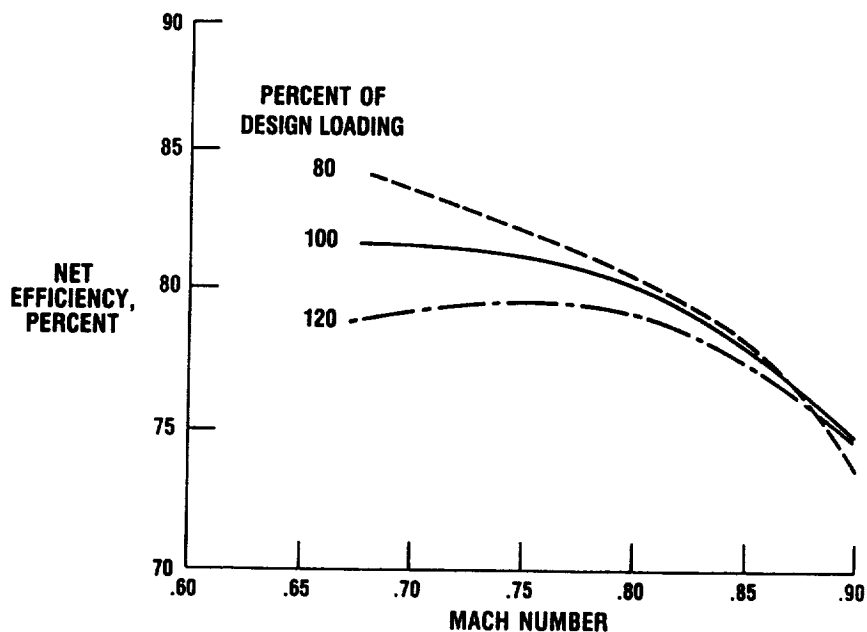
CD-87-29495

Figure 14. - Counterrotation propeller in Lewis 8- by 6-ft wind tunnel.



CD-87-29496

Figure 15. - Model counterrotation propeller blades.



CD-87-29497

Figure 16. - F7-A7 performance summary (8+8 blade configuration; nominal spacing; matched speed; tip speed, 780 ft/sec).

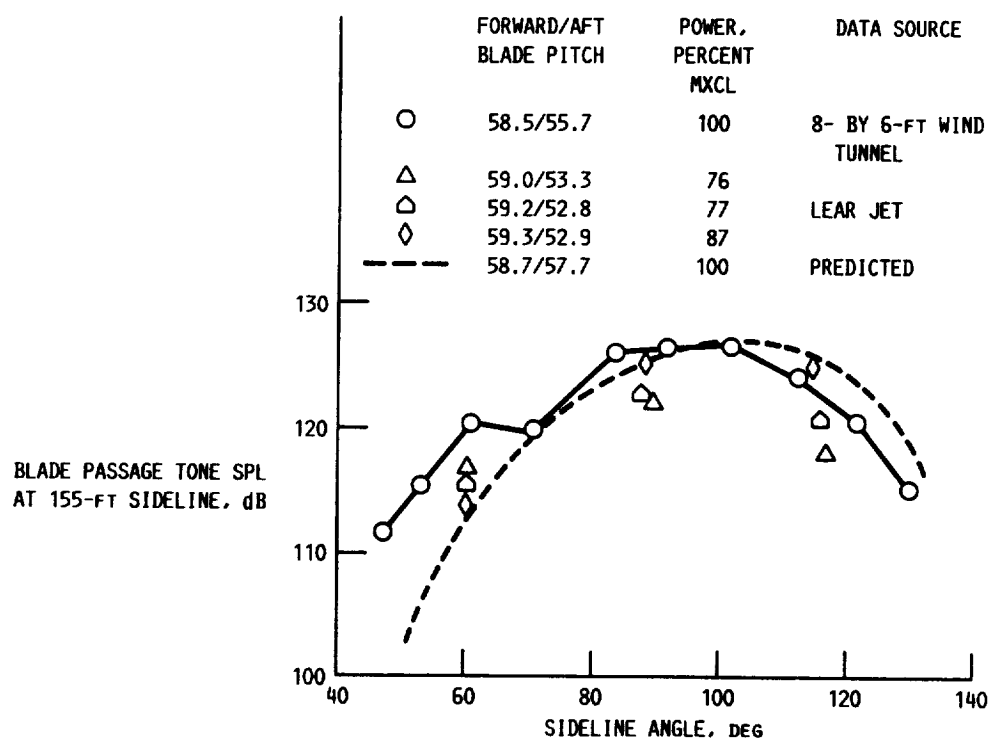
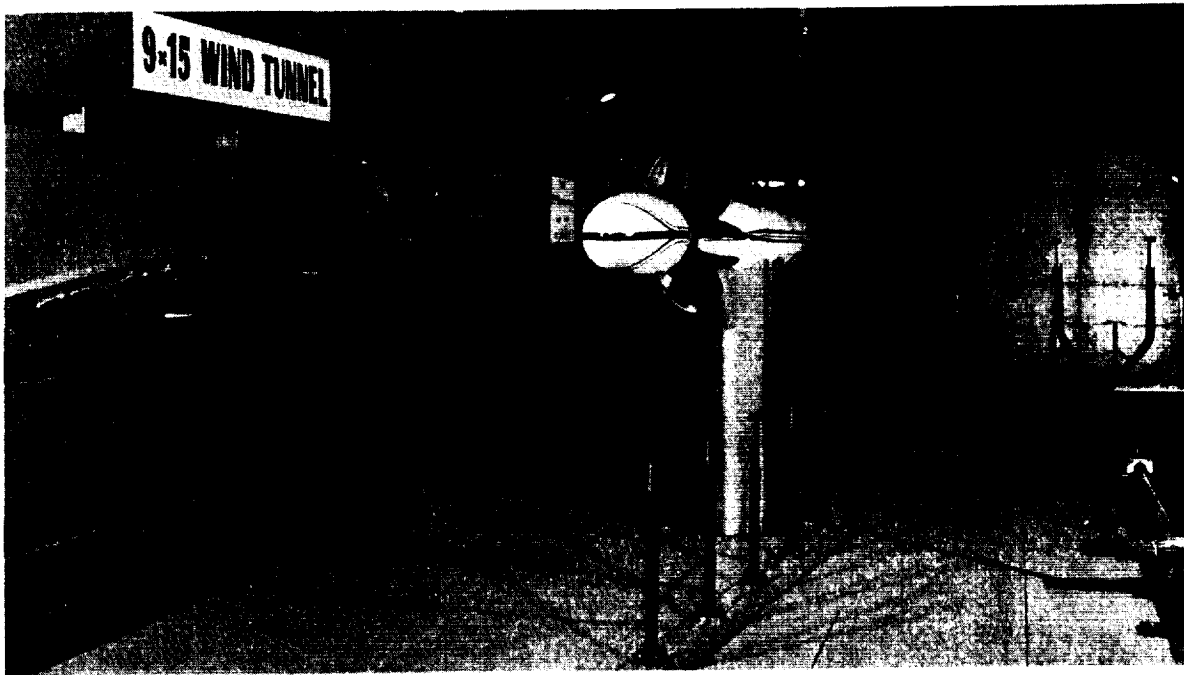
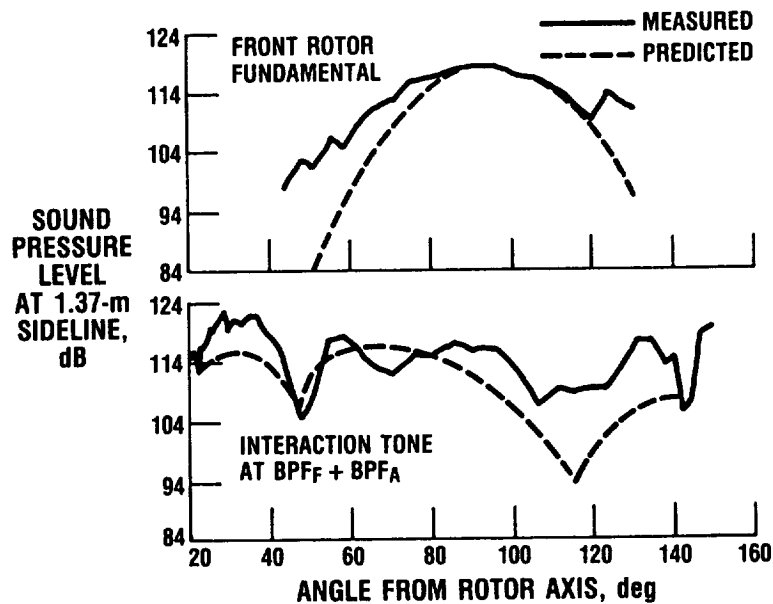


Figure 17. - Counterrotation tone levels at cruise (propeller F7-A7; Mach 0.72; altitude, 35 000 ft).



CD-87-29499

Figure 18. - Counterrotation model F7-A7 in Lewis 9- by 15-Foot Anechoic Wind Tunnel.



CD-87-29500

Figure 19. - Counterrotation propeller noise at takeoff (propeller F7-A7; Mach 0.2; 9- by 15-Foot Anechoic Wind Tunnel).

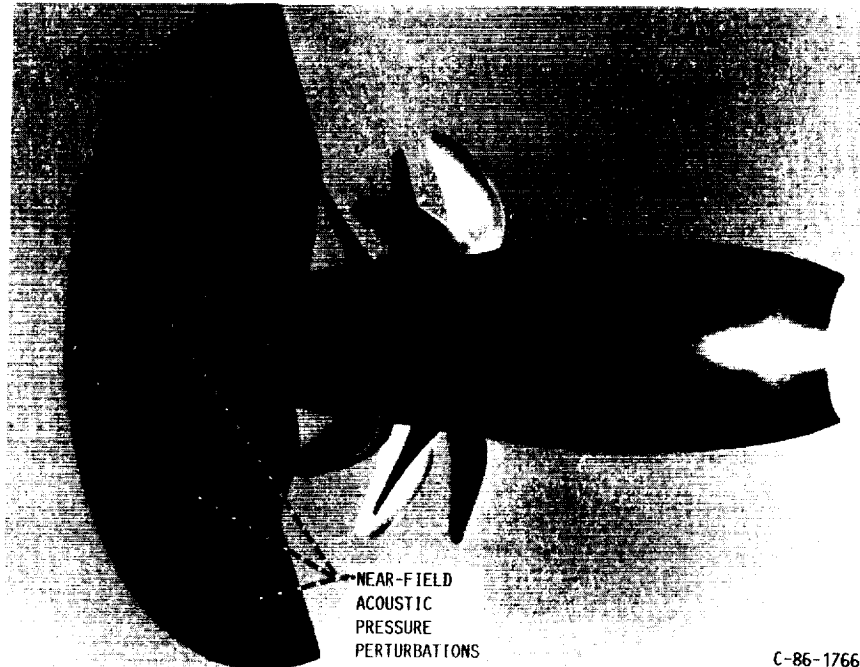


Figure 20. - Three-dimensional Euler analysis of counterrotation propeller flow field.

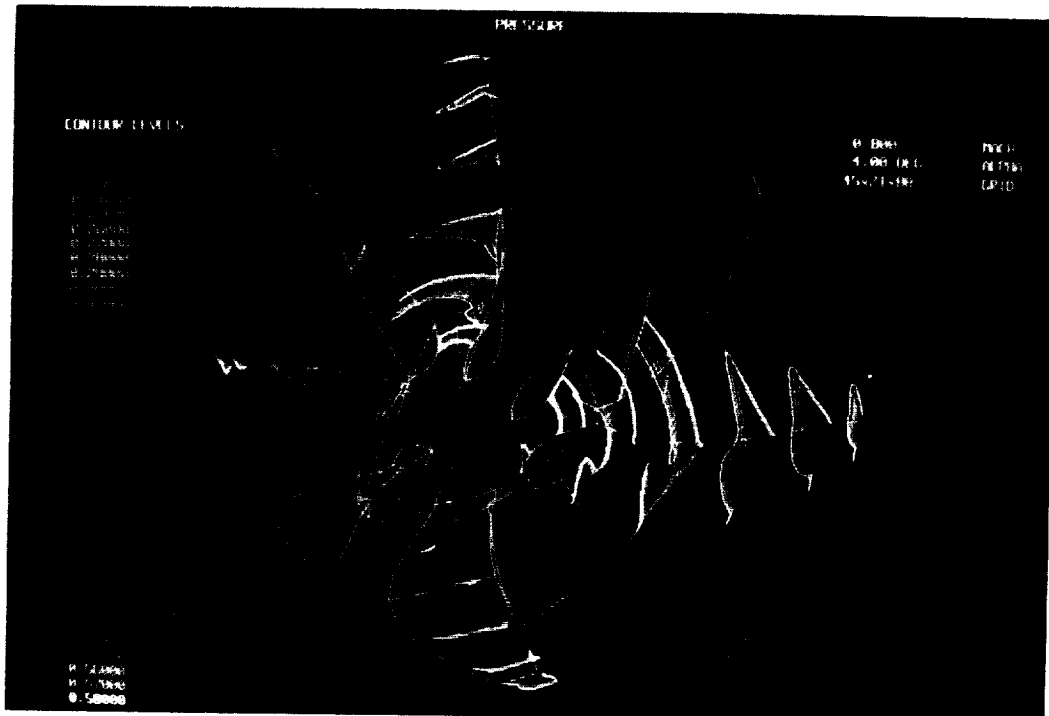
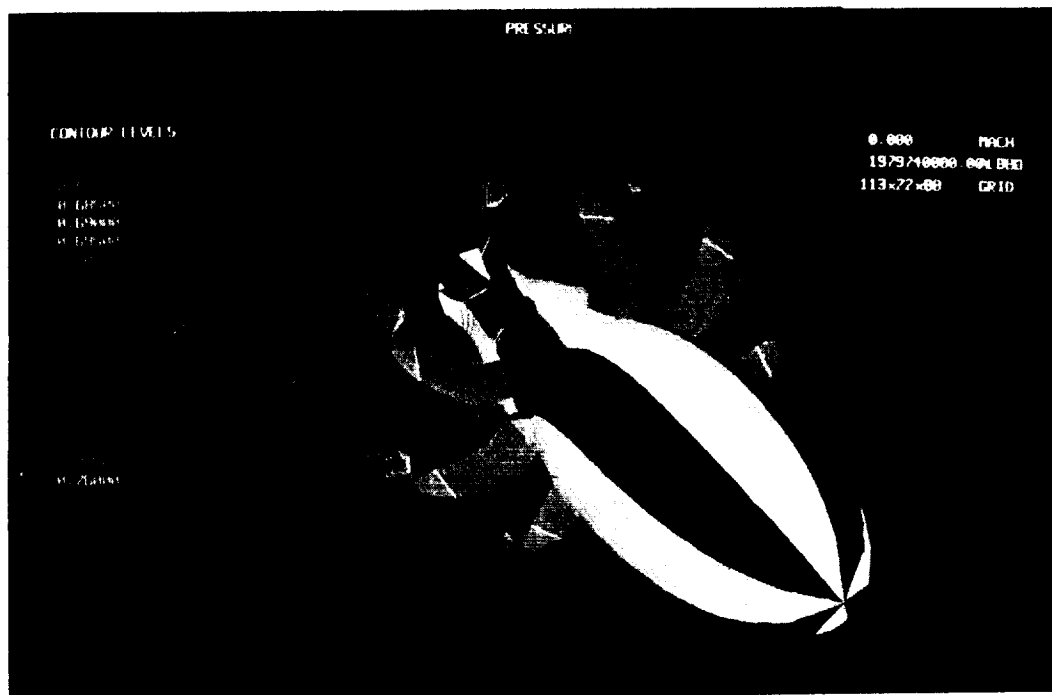
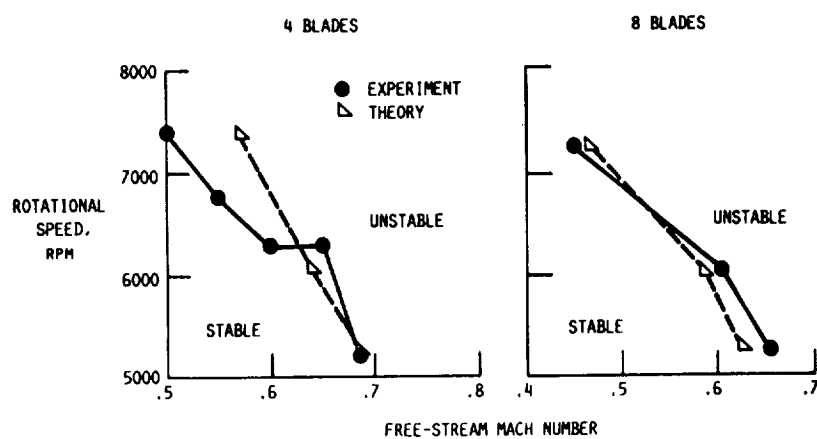


Figure 21. - Unsteady three-dimensional Euler code solution for propeller at angle of attack.



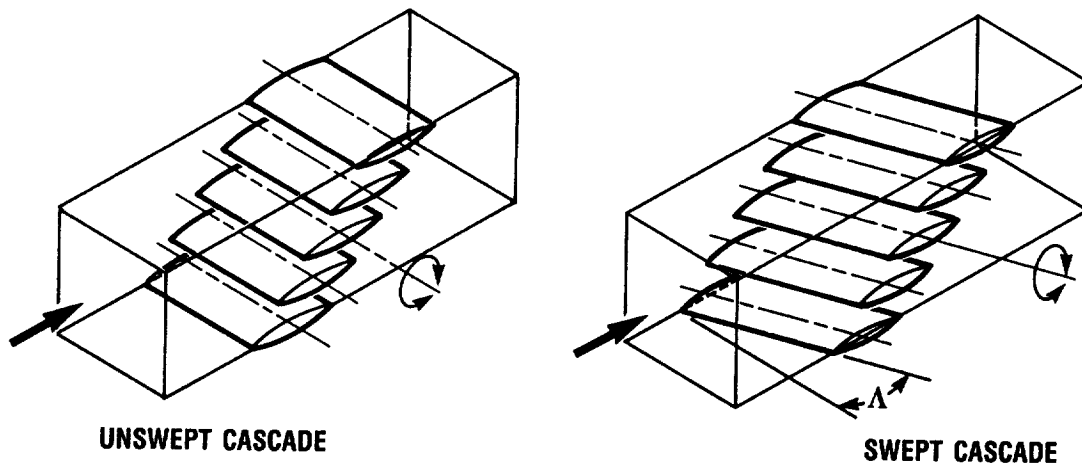
CD-87-29503

Figure 22. - Unsteady three-dimensional Euler solution for counterrotation propeller.



CD-87-29586

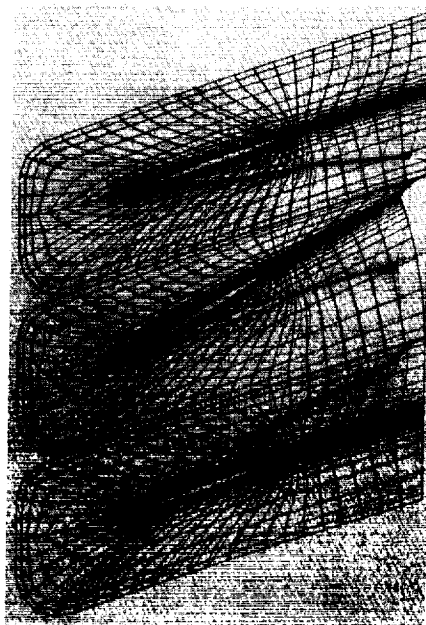
Figure 23. - Comparison of measured and calculated flutter boundaries (SR3C-X2 propfan model).



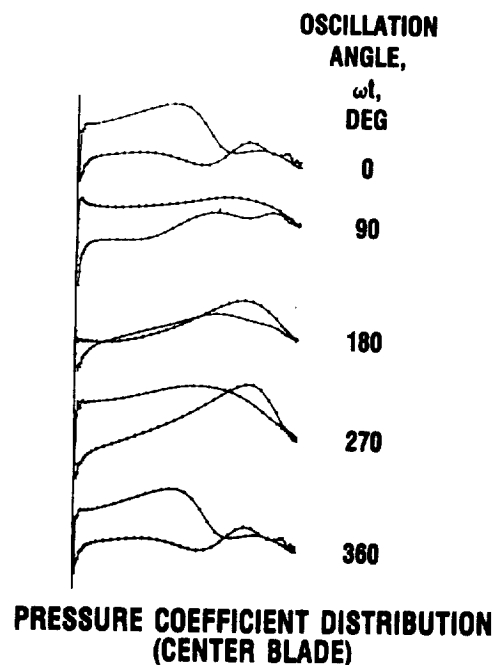
- EXPERIMENT TO DETERMINE EFFECT OF BLADE SWEEP, Δ , ON TRANSONIC CASCADE AERODYNAMICS
- STEADY AND UNSTEADY BLADE SURFACE PRESSURES
- TORSIONAL BLADE OSCILLATION
- DATA USED TO BENCHMARK STEADY AND UNSTEADY ANALYSES

CD-87-29505

Figure 24. - Swept cascade experiment.



DEFORMING GRID (EXAGGERATED MOTION)



CD-87-29506

Figure 25. - Two-dimensional unsteady, Navier-Stokes, oscillating cascade analysis (NACA 16-004 cascade; $M_1 = 0.75$; $g = 1.0$; $\alpha_m = 21^\circ$; $\alpha_1 = \pm 2.0^\circ$; $k = 0.20$; $Re = 5.0 \times 10^6$; $\theta = 20^\circ$; $\sigma = 90^\circ$).

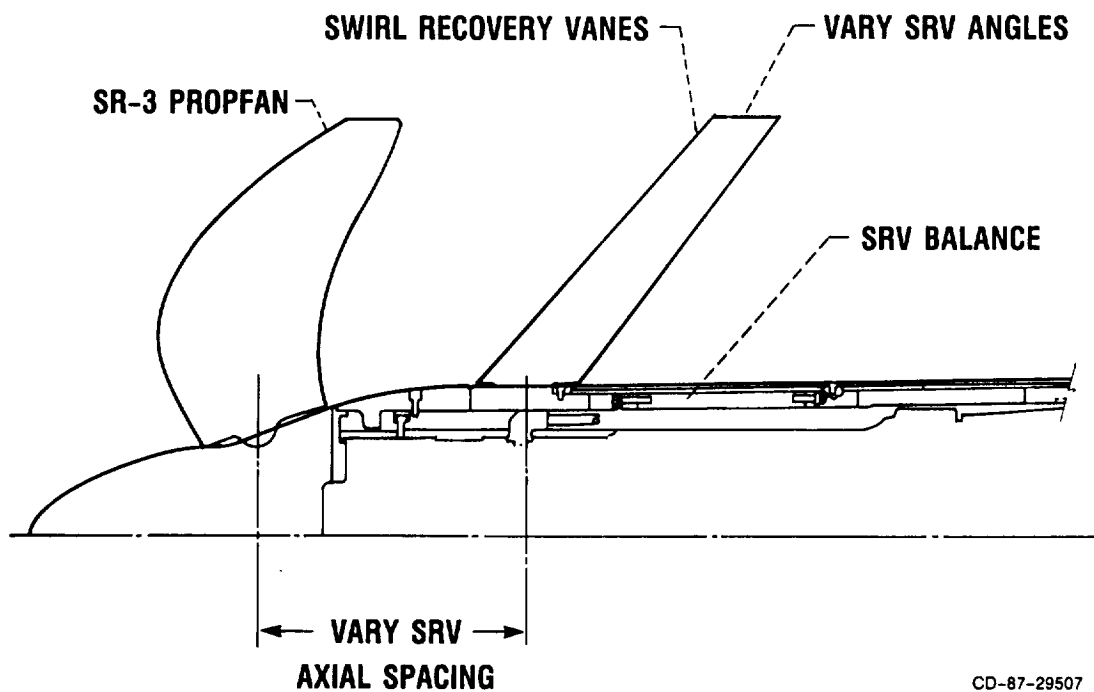


Figure 26. - Swirl recovery vane experiment.

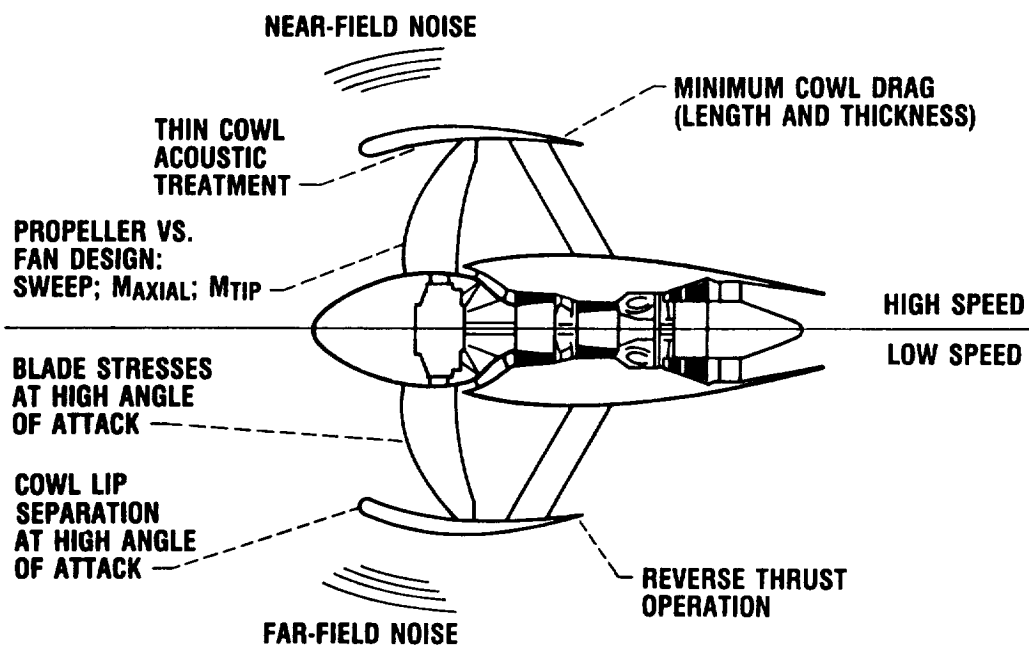


Figure 27. - High-speed ducted propeller issues.

	PRESENT	FUTURE
AERODYNAMICS	<ul style="list-style-type: none"> • 3D STEADY EULER CODES • PERFORMANCE MEASUREMENT, PROBE SURVEYS, & BLADE PRESSURES 	<ul style="list-style-type: none"> • 3D UNSTEADY EULER & NAVIER-STOKES CODES • DETAILED FLOW FIELD DIAGNOSTICS - LASER VELOCIMETER • ULTRA-HIGH BYPASS DUCTED PROPELLER PERFORMANCE
ACOUSTICS	<ul style="list-style-type: none"> • 3D CODES USING DETAILED STEADY AERO INPUT • CRUISE AND TAKEOFF SIGNATURES FOR SRP & CRP INSTALLATIONS 	<ul style="list-style-type: none"> • INTERACTION & INSTALLATION EFFECTS FROM DETAILED UNSTEADY AERO INPUT • DETAILED NOISE MAPS FOR INSTALLED CONFIGURATIONS • CODES & DATA FOR SHORT, THIN DUCTS
AEROELASTICS	<ul style="list-style-type: none"> • FLUTTER BOUNDARY MEASUREMENT & PREDICTION FOR SRP'S • FIRST GENERATION STRUCTURAL OPTIMIZATION CODES 	<ul style="list-style-type: none"> • FLUTTER BOUNDARY MEASUREMENT & PREDICTION FOR CRP'S • STALL FLUTTER & FORCED RESPONSE FOR SRP'S & CRP'S

CD-87-29509

Figure 28. - Propeller research areas of emphasis.

SESSION 6 - HIGH-SPEED PROPULSION TECHNOLOGY

NASA THRUSTS IN HIGH-SPEED AEROPROPULSION RESEARCH AND
DEVELOPMENT - AN OVERVIEW

Joseph A. Ziemianski

INTRODUCTION

NASA is conducting aeronautical research over a broad range of Mach numbers. In addition to the advanced conventional takeoff or landing (CTOL) propulsion research described in a separate session at this conference, the Lewis Research Center has intensified its efforts towards propulsion technology for selected high-speed flight applications. In a companion program, the Langley Research Center has also accomplished significant research in supersonic combustion ramjet (SCRAM) propulsion. What will be presented in this session is an unclassified review of some of the propulsion research results that are applicable for supersonic to hypersonic vehicles. This overview not only provides a preview of the more detailed presentations which follow, it also presents a viewpoint on future research directions by calling attention to the unique cycles, components, and facilities involved in this expanding area of work.

NASA THRUSTS IN AERONAUTICAL RESEARCH AND DEVELOPMENT

The Lewis Research Center is conducting high-speed propulsion research over a broad range of Mach numbers. In addition, the Langley Research Center has accomplished related research in supersonic combustion ramjet (SCRAM) propulsion. What will be presented here is an overview of some of the propulsion research results that are applicable to the classes of supersonic/hypersonic vehicles shown in figure 1. The research program associated with the National Aerospace Plane (NASP) will not be discussed because of classification, but the final paper of this session describes hypersonic propulsion research at Langley Research Center.

Session 5 of this conference described the advanced conventional takeoff or landing (CTOL) propulsion research results.

NASA THRUSTS IN AEROPROPULSION

The propulsion concepts that NASA has identified with the vehicle classes shown in figure 1 are illustrated in figure 2. The papers presented in this session describe the following:

- (1) An evaluation of the merits of a high-speed transport and the associated propulsion technology barriers

- (2) A further exposition of a propulsion research concept that may have applicability to the high-speed transport - a supersonic throughflow fan
- (3) High-speed inlet studies in the Mach 5 range
- (4) Propulsion research results associated with a supersonic short takeoff and vertical landing (SSTOVL) vehicle
- (5) A summary of hypersonic propulsion research at the Langley Research Center

FUTURE DIRECTIONS IN HIGH-SPEED PROPULSION RESEARCH AND DEVELOPMENT

The future of NASA's propulsion research will shift towards the higher Mach propulsion concepts because of the renewed emphasis on such challenging programs as SSTOVL, high-speed civil transports, and NASP. What is required is the identification of propulsion unique cycles and associated components that could lead to new vehicle capabilities in the high Mach regimes. Because of the complexity and limited data base at high Mach numbers, considerable discipline research must first be accomplished before any component program can begin. Integration of the propulsion system is complex; because of the high Mach numbers, the propulsion and airframe become an integral system.

UNIQUE TECHNOLOGIES FOR HIGH-SPEED PROPULSION

Unique technologies required for high-speed propulsion are shown in figure 3. They range from high-speed inlets and the associated computational fluid dynamic codes needed to address the complex flows to high-temperature materials/structures needed in the hot section of the engines. For application such as the high-speed civil transport, unique nozzles and suppressors are required for performance and community noise considerations.

Supersonic compression is an identified technology that can lead to more fuel-efficient propulsion concepts, in the Mach 2 to 4 range. Supersonic combustion is needed around Mach 6 for a scram propulsion mode but may have promise at lower speeds in a complete supersonic throughflow machine. How all these technologies are brought together in a viable propulsion concept is the challenge of today's researchers.

PUTTING IT ALL TOGETHER

One configuration that shows considerable promise is the supersonic throughflow engine (fig. 4), but it will require major progress in a variety of discipline and component research areas and careful matching of those elements. If successful, our analyses indicate for a high-speed civil application that this concept will be 10 percent more efficient and that the weight will be 25 percent less than that of a variable cycle engine.

HIGH-SPEED AEROPROPULSION RESEARCH WIND TUNNEL FACILITIES

NASA Lewis Research Center has positioned itself in the high-speed regime by developing additional capabilities in our complex of wind tunnel testing facilities, which are listed in table I. The Propulsion Systems Laboratory (PSL) now has the capability to run turbomachinery to Mach 6 with gaseous

hydrogen and oxygen. In addition, heaters have been added in our 1- by 1-ft tunnel to eliminate condensation shocks to Mach 6. These additions, together with the current 10- by 10-ft supersonic (Mach 3.5) and 8- by 6-ft transonic tunnels, give NASA the capability to test over a broad Mach range.

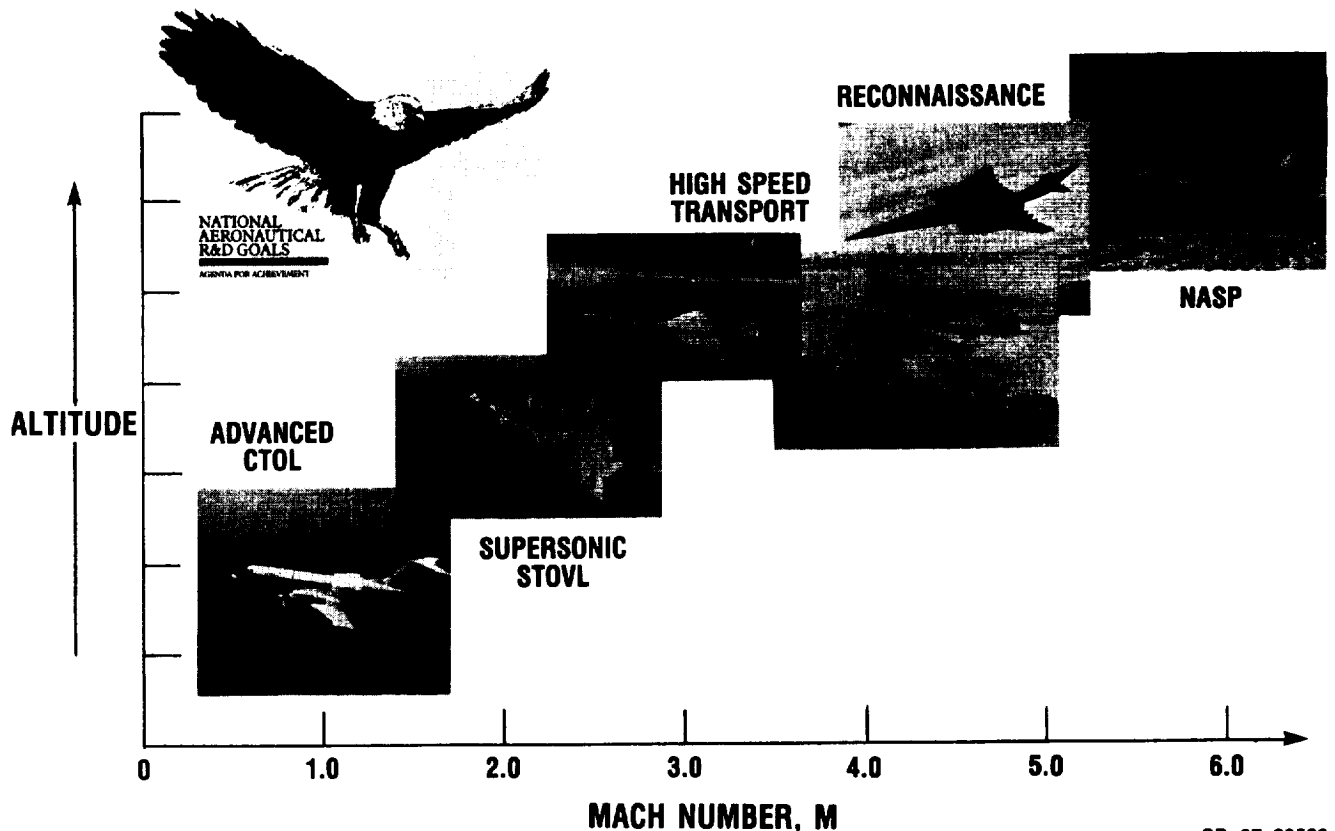
In addition, we are investigating reopening our Hypersonic Test Facility (HTF) at Plum Brook, which if successful will have capabilities to test at Mach numbers of 5, 6, and 7 in a nonvitiated mode. In addition, if heaters are added, the facility capabilities can be expanded substantially.

TABLE I. - HIGH-SPEED AEROPROPULSION RESEARCH
WIND TUNNEL FACILITIES

Facility	Speed capability, Mach number
10- by 10-Foot Supersonic Wind Tunnel	≤ 3.5
Propulsion Systems Laboratory 4	^a ≤ 6
1- by 1-Foot Supersonic Wind Tunnel	^a ≤ 6
8- by 6-Foot Supersonic Wind Tunnel	Transonic
Plum Brook Hypersonic Test Facility ^b	5, 6, and 7
Nonvitiated	
Vitiated	≤ 6

^aNew capability.

^bProposed for NASP testing.



CD-87-29522

Figure 1. - NASA thrusts in aeronautical research and development.

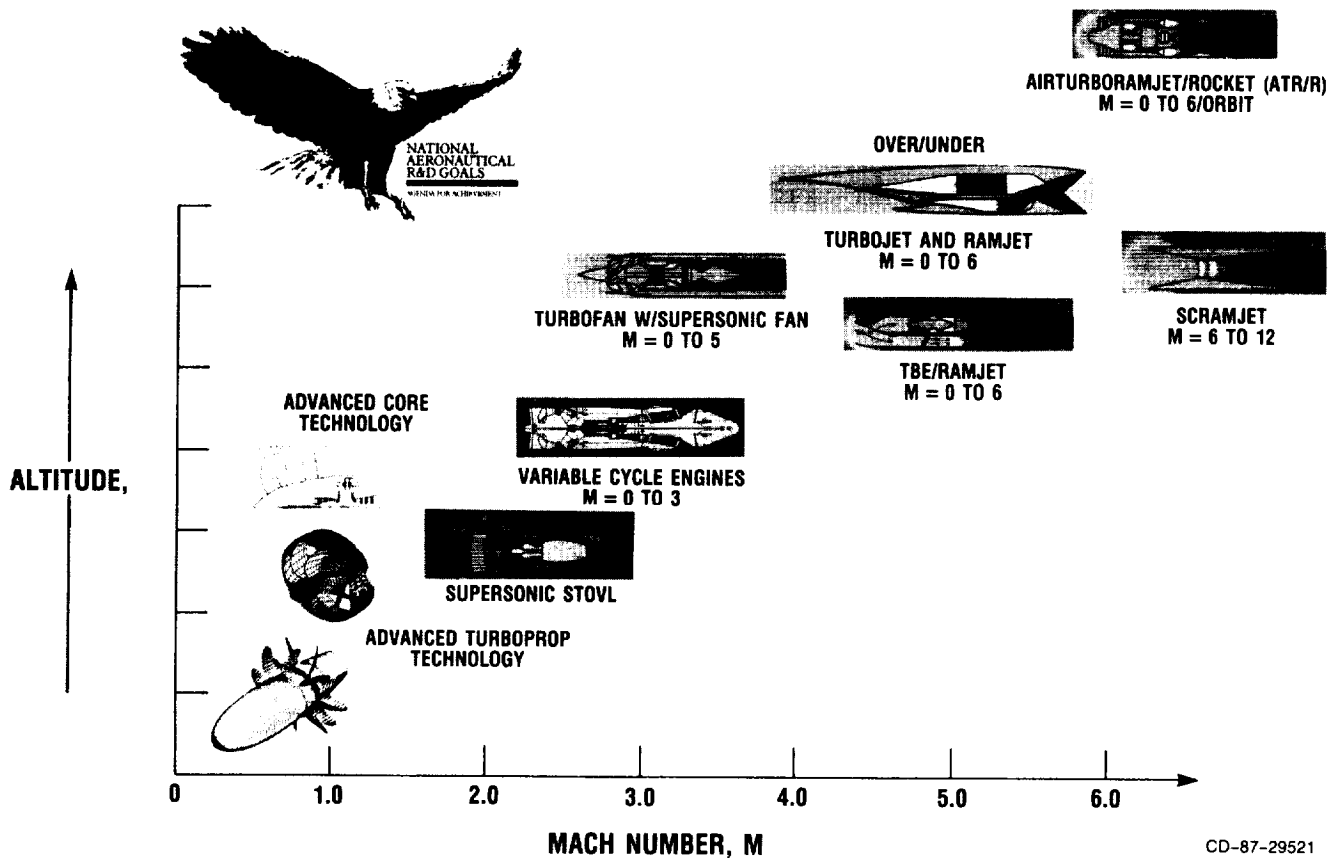
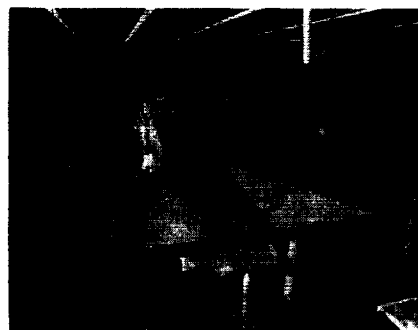
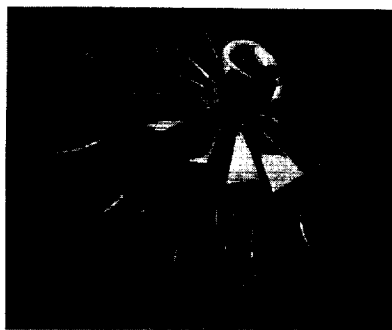


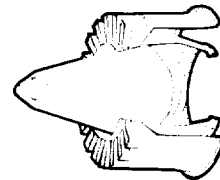
Figure 2. - NASA thrusts in aeropropulsion.



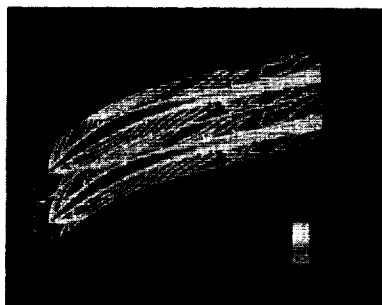
HIGH-SPEED INLETS



HIGH TEMPERATURE
MATERIALS/STRUCTURES



ADVANCED NOZZLES
AND SUPPRESSORS



SUPERSONIC COMPRESSION



SUPERSONIC COMBUSTION

CD-87-29520

Figure 3. - Unique technologies for high-speed propulsion.

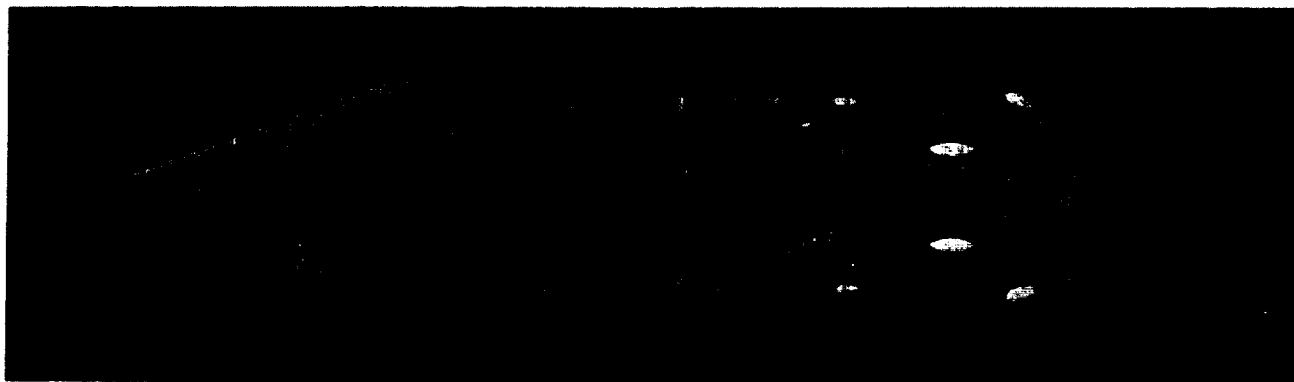


Figure 4. - Supersonic throughflow engine.

CD-87-29519

SUPERSONIC STOVL PROPULSION TECHNOLOGY PROGRAM - AN OVERVIEW

Bernard J. Blaha and Peter G. Batterton

SUMMARY

Planning activities are continuing between NASA, the Department of Defense (DOD), and two foreign governments to develop the technology and to demonstrate the design capability by the mid-1990's for advanced, supersonic, short-takeoff and vertical-landing (STOVL) aircraft. These planning activities have resulted in a Memorandum of Understanding (MOU) with the United Kingdom to jointly pursue the STOVL technology, and an MOU with Canada is expected to be signed shortly. Propulsion technology is key to achieving viable STOVL aircraft, and NASA Lewis Research Center will play a lead role in the development of these required propulsion technologies. The initial research programs are focused on technologies common to two or more of the possible STOVL propulsion system concepts. This paper will present an overview of the Lewis Research Center's role in the overall program plan and recent results of the research program. The future research program will be focused on one or possibly two of the propulsion concepts seen as most likely to be successful in the post-advanced-tactical-fighter (ATF) time frame.

INTRODUCTION

New interest has recently been generated in developing the capability for a supersonic short-takeoff and vertical-landing (STOVL) fighter/attack aircraft which could be developed in the post-ATF time frame. This interest has resulted in the initiation of several separate programs and separate Memorandums of Understanding (MOU's) between the U.S. and other governments. An MOU has recently been established with the United Kingdom (U.K.) to jointly pursue the required technologies, and an MOU with Canada is expected to be signed shortly. In these joint programs and others a minimum of five different propulsion concepts for a supersonic STOVL aircraft are being studied.

There have been few successful STOVL fighter/attack aircraft designs. The most notable success is the AV-8 Harrier. The reasons for the few successes are many, but the obvious ones are that the propulsion system becomes much more complex, and considerably more is asked of it. That is, it must provide levels of upward thrust capable of supporting the landing weight of the aircraft and controlling its attitude, yet be capable of switching to provide high levels of forward thrust for normal flight and possibly assisting the flight control. Required weight and volume of the resulting propulsion system has in the past been large and inefficient, forcing the weight of the total aircraft higher,

and ultimately resulting in an undesirable aircraft design. Therefore one concludes that for supersonic-capable STOVL aircraft to be successful, advanced propulsion technology is the key to allowing it to happen (refs. 1 and 2).

It has always been a goal of NASA aeronautics research to address and resolve high-risk, long-lead technologies. An attempt to design a current advanced, supersonic-cruise-capable STOVL fighter aircraft would lead to the conclusion that the required propulsion technologies are not yet available. Further, demonstration of these technologies will be required before the DOD and industry will attempt even a prototype. NASA Lewis Research Center will play a leading role in the development of the required propulsion technologies, which have been identified as being critical to achieve viable STOVL aircraft. Planning activities have already resulted in initial research programs focused on technologies common to two or more of the proposed propulsion system concepts. This paper will identify these concepts, and will present an overview of the program goals and the Lewis Research Center's role in the overall program plan, and recent results in the development of the required propulsion technologies.

PROPOSED CONCEPTS AND PROGRAM GOAL

Currently, as shown in silhouette in figure 1, five propulsion concepts are being considered for an advanced, supersonic STOVL aircraft which could be developed in the post-ATF time frame (late 1990's). These concepts are shown here in silhouette because they have been identified in the past and have been discussed in detail in many previous references (e.g., refs. 1 and 2), but studies have failed to prove one as being better than the other. In the order shown in the figure, these include

- (1) Remote augmenter lift system (RALS), a concept with burners and nozzles located remotely from the engine and forward of the center of gravity (CG) and which use air provided by the engine fan bypass
- (2) Vectored thrust (e.g., the AV-8 Harrier), which uses a separate flow bypass engine supplying nozzles forward and aft of the aircraft CG
- (3) Ejector augmenter, a concept with an airflow augmenting ejector located forward of the CG with primary air provided by the engine fan bypass
- (4) Tandem fan, a variable-cycle engine concept in which the fan stages can be separated so that the front stage provides air for nozzles forward of the CG for vertical mode. The front stage supercharges the aft fan stage for normal flight.
- (5) Lift plus lift/cruise (e.g., the YAK-36), a concept that uses a separate lift engine forward of the CG during vertical thrust of operation. This engine is used at this time only.

The current supersonic STOVL Program will study these systems in greater depth than before in the hope of generating data to identify which one or two may be better than the others. The joint U.S./U.K. program is studying the first four concepts shown. The U.S./Canada program is focused on the ejector concept

alone. General Dynamics and deHavilland have been working on this concept for some time and are convinced that it is a viable concept. NASA and the DOD have recently added the lift plus lift/cruise concept to their investigations. This concept has always proved favorable in past studies, so it has been added for completeness. There are many other propulsion concepts as well, but these can be considered as hybrids of the five just described.

The goal of the supersonic STOVL technology program is to have the required technologies in place by the early 1990's, so that a decision to start a research aircraft program can be made with relatively low risk. As stated before, the key technologies to be developed are primarily propulsion related. The design of fighter/attack aircraft which can dash and cruise supersonic (e.g., F-14, F-15, and F-16) is a standard practice. A subsonic aircraft for vertical takeoff and landing (e.g., the AV-8B Harrier) has been successfully designed. The challenge therefore is to combine these capabilities into a new, efficient, high-performance supersonic fighter/attack aircraft for the post-advanced-tactical-fighter (ATF) time frame. This will involve developing those unique engine system components with multifunction capabilities (e.g., vectoring and deflecting nozzles and, in particular, new control systems).

REQUIRED PROPULSION TECHNOLOGIES

The propulsion technologies, identified as key to the supersonic STOVL program, cover a broad spectrum and are listed in figure 2. Some of these are related to and will be developed in other ongoing NASA and U.S. Air Force (AF) base research and technology (R&T) programs combined with the STOVL program. As indicated in the figure, the supersonic STOVL program will benefit from related research programs going on during the same time frame. Examples are the Supermaneuver programs which currently exist in DOD and NASA. These include the AF F-15 STOL/Maneuver Technology Demonstrator (S/MTD) program; the joint Defense Advanced Research Projects Agency (DARPA)/U.S. Navy/West Germany Enhanced Fighter Maneuverability (EFM) program; a Navy F-14 program including a nozzle with deflecting paddles, at Pax River Naval Air Station; and the NASA F-18 High-Alpha Research Vehicle (HARV) program at the Dryden Flight Research Facility. In these programs high-angle-of-attack inlets, propulsive controls, and multiplane vectoring nozzle technology will be developed which will be directly applicable to STOVL. Most of these programs will be completed before the STOVL program achieves its goal. Likewise the new higher thrust-to-weight ratio (15 to 20) engine core technology required for supersonic STOVL will come from programs such as IHPTET and NASA's base technology efforts. The rest of the needed developments will be made in the supersonic STOVL program.

The first technology issue to be resolved in the supersonic STOVL program is the propulsive lift concept, which may be the best to pursue for a research aircraft. Each of the propulsive lift concepts being studied, including RALS, vectored thrust, ejector augments, tandem fan, and lift plus lift/cruise, has technical problems with performance, volume, weight, etc. The supersonic STOVL program is actively addressing some of the key issues which will be shown shortly. A downselect will have to be made early in the program to manage the scope of this effort to appropriate levels.

As mentioned earlier in this section, the new higher thrust-to-weight ratio (T/W) engines required will come from other existing programs such as

Integrated High Performance Turbine Engine Technology (IHPTET). However the impact of those things which will be unique to STOVL on these new higher energy and smaller core engines, for example, compressor bleed (for reaction control), will be evaluated in this program.

New short diffuser inlets with high alpha capability will be required for the supersonic application. The Harrier (AV-8) has a inlet which works well even at the extreme angles of attack associated with takeoff and transition. This inlet, however, has a thick lip and auxiliary inlets well suited to the local flow conditions. Similar capabilities will have to be developed for the thin lip supersonic inlet, which may also have the added complication of a shorter diffuser. The shorter diffuser will result from the STOVL requirement of locating the engine closer to the aircraft center of gravity (CG) for better balance and better location of the lift vectors.

New lightweight modulating, deflecting, and vectoring nozzles will have to be developed for the supersonic STOVL. The issue here is not a small scale one. Much work has been done at small scale over the last few years, demonstrating that high internal nozzle efficiency can be obtained with deflected thrusts exceeding 90° (refs. 3 and 4). What has to be researched is how to make these nozzles at large scale with real actuators, seals, materials, and cooling. These will be supersonic nozzles with normal CD area variations as well as the capability of 90° or more deflection for takeoff and landing. Some of these nozzles will also have to be able to perform with afterburning. All of these capabilities will have to be included at reasonable weights. A new type of nozzle may also have to be researched, namely, ventral nozzles located on the side of the engine nacelle with a variable blocker downstream.

Efficient low-loss ducts, valves, and fan air collectors will also have to be developed, particularly for the RALS and ejector systems. Past attempts at designing ejector systems were unsuccessful due in large part to high internal pressure losses (ref. 5).

Two of the more notable issues to be resolved for a supersonic STOVL include hot gas ingestion (HGI) and integrated flight/propulsion controls. The higher T/W engines will enhance the HGI problem already seen with the Harrier. Likewise the propulsion controls will become more critical at takeoff, transition, and landing, where the traditional aerodynamic controls are relatively ineffective. This last issue may be the most difficult to solve, and as a result was one of the first programs initiated. The work load seen with the Harrier is particularly high at takeoff and landing. With the higher performance aircraft a new control system will be required which does a more efficient job of allowing the pilot to manage the aircraft.

SUPERSONIC STOVL PROGRAM PLAN

As stated in the program goal there is interest in being able to develop and fly a research aircraft in the mid-1990's. The need for such an effort was clarified in the recent AF Forecast II study results, which identified requirements for an aircraft with VSTOL capabilities in the post-ATF time frame (beyond the year 2000). As previously stated, propulsion is key to achieving these capabilities. With that in mind an enabling plan was developed (fig. 3). To meet the technology demonstration schedule the required technologies have to be developed now, and a ground demonstration of the complete propulsion system

(for the research aircraft) will have to be completed early in the 1990's. As shown, several of the research programs have already been initiated. These include the NASA and DOD ongoing base technology programs, the joint U.S./U.K. program, the U.S./Canada ejector program, and a series of contracted efforts with the major engine companies to investigate advanced engine concepts and, in particular, integrated flight/propulsion controls. These efforts include studies, experimental test programs, and some design (conceptual and detailed) development activities.

As shown, the base NASA and DOD R&T efforts include many different programs. However each will develop new technology that will be useful to future STOVL vehicles. The U.S./U.K. STOVL aircraft conceptual design study efforts have been ongoing and are scheduled to be finished shortly. They will then be followed by an approximate 6-month downselect phase. In this phase the study data will be analyzed in an attempt to be able to identify one or two configurations on which to focus further research. During the configuration study phase, a parallel common technology program was initiated to research those technologies which are common to two or more of the proposed configurations (e.g., fan air collectors, ducts, and valves; hot gas ingestion; and integrated flight/propulsion controls). Once the downselect process is complete, a concept-specific phase of the program will be initiated to study in greater detail the chosen concept(s).

The U.S./Canada program is dedicated totally to the ejector concept. General Dynamics and deHavilland have been researching ejector aircraft for some time, and as a result the program has evolved to the point of developing and testing large-scale hardware. A large-scale model of the E-7 aircraft configuration is being fabricated for testing in the 40- by 80-ft wind tunnel at NASA Ames early next year. This model will incorporate a Spey engine initially. As indicated in figure 3, the Spey engine will eventually be replaced by an F110 engine. The F110 will be more representative of the weight flows and fan pressure ratios required for an advanced supersonic STOVL application. Lastly, as indicated in the figure, a series of contracts has been established to study the capabilities of current advanced engine cores (e.g., the PW5000) to meet the supersonic STOVL mission. Future engine requirements for the mid- to late-1990's are also being investigated in these studies. These contracts are also being used to support NASA's and the DOD's efforts in addressing integrated flight/propulsion controls. The contractors will develop hardware for testing advanced control systems and will develop control algorithms.

All of the technology efforts shown in figure 3 will culminate in a full ground propulsion technology validation program to take place in the late 1980's and early 1990's. This program plans to include a complete STOVL engine system. This system is currently planned to be a nearly full-scale ejector system with all components in place, including inlet, engine, fan air collector, ducting and valving, nozzle(s), and integrated flight/propulsion control system. The ejector system is currently being planned for this phase because, as a matter of convenience, it is already being tested at large size in the joint U.S./Canada program. None of the other proposed STOVL concepts are at this stage of testing and consequently would not be ready in the planned time frame. The intent of the ground validation program will be to validate a complete STOVL engine system, including real-time comparisons with the computer simulations. A pilot in-the-loop capability may also be employed. At the completion of this program enough of the required technologies will have been developed and validated such that a reasonable, low-risk decision can be made

to initiate a flight technology validation program in the time frame shown in the figure.

STOVL STUDY CONTRACTS

In figure 4 is presented a collage of the supersonic STOVL configuration study contracts currently in existence to generate the data necessary for detailed comparisons of the identified possible engine concepts. Three propulsion system contracts, with General Electric (GE), Pratt & Whitney (P&W), and Allison Gas Turbine (AGT) Division of General Motors are being managed at Lewis. Also, four airframe contracts, with McAir, General Dynamics (GD), Grumman, and Lockheed are being managed at Ames. As mentioned in the section Proposed Concepts and Program Goal, four of the engine concepts are being studied under the joint U.S./U.K. ASTOVL program, and the fifth concept was added for consideration by NASA and the DOD to generate an appropriate data base with this configuration for comparison with the others. Three of the propulsion concepts were assigned to multiple contractors in order to generate comparisons. Each airframer was teamed with an engine company for each concept so that consideration of the joint requirements of each could be factored into the studies of each. These contract efforts, which have been completed, will be followed by a phase whereby the data from these studies will be compared, and an attempt will be made to identify one or two of these configurations to pursue in the following technology programs.

BASE PROGRAM

The current Lewis base R&T program elements for the supersonic STOVL are shown in figure 5. Because the favored propulsion concept has not yet been identified, if it can ever be, the current technology research activities tend to be focused on common technology issues. These are issues which would be applicable to two or more of the propulsion system concepts currently being studied in the supersonic STOVL technology program. The individual thrusts are either in existence today or, as shown, are planned to begin shortly. The programs already in existence include fan air collectors, valves, and ducting (for ejector and RALS systems); hot gas ingestion (HGI); short diffuser supersonic inlets with high alpha capability; and integrated flight/propulsion controls. Each of these is important for all the proposed engine concepts. Information from each of the existing programs will be presented in the following figures. Plans are being developed to initiate in the near future corresponding programs in thrust augmentation by burning, and thrust deflecting and vectoring nozzles. In general, each of these program elements has both analytical and experimental phases. The program and results to date are now described for the four active program elements.

FAN AIR COLLECTORS, VALVES, DUCTING, AND EJECTORS

U.S./Canada Ejector Technology

The research activities associated with fan air collectors, valves, ducting, and ejectors are being accomplished in the joint U.S./Canada Ejector Program. NASA, the Canadian Government, deHavilland, and General Dynamics (GD) have for a number of years been highly interested in demonstrating the ejector

lift concept. More recently, DARPA has also provided support to the concept. NASA Lewis is not only addressing the ejector performance, but also the performance of the engine to the ejector air delivery system. Shown in figure 6 is a collage of the various elements of the joint U.S./Canada ejector technology program. In this program, a large-scale model of the General Dynamics E-7 supersonic STOVL aircraft configuration will be tested in the Ames 40- by 80-ft wind tunnel. This aircraft incorporates the ejector augmentor propulsion concept to provide the required lift at takeoff and landing. As shown in the upper left corner of the figure, the ejectors are located in the wing root on each side of the fuselage. The model will be tested with a complete engine system (first with a Spey engine, then eventually with an F110). A schematic of the engine system is shown in the upper right corner. In anticipation of the complete aircraft test, a series of large-scale component tests have recently been made. An example of a fan air collector design is shown in the figure. These large-component tests were conducted on the new Lewis Powered Lift Facility (PLF). This program provided the strong impetus to develop this new facility, which uses a research air supply system to evaluate full-scale STOVL components and systems in a static, ground environment. After the wind tunnel tests, the complete large-scale aircraft system will also be tested on the PLF at Lewis. Results from the initial large-scale ejector tests on the PLF will be presented in the following figures.

Powered Lift Facility

The new Lewis Powered Lift Facility (PLF), shown in figure 7, was initially designed and built to support testing for the U.S./Canada program. The system includes a large triangular (30-ft on a side) frame supported 15 ft above the ground. This frame is supported by load cells, which provide a six-component force measuring system. Vertical (20 000 lb), axial (30 000 lb), and lateral (5000 lb) forces as well as pitch, roll, and yaw moments can be measured in plus and minus directions. High-pressure (95 psig) and heated air (to 300 °F) with flows greater than 160 lb/sec can be supplied to the stand to simulate fan bypass air. The high-pressure air is brought onto the system through a series of bellows, oriented 90° to the force system, to minimize delivery system momentum tare forces. The facility was completed, and flow tests were initiated in September 1986. Initial force calibrations were made in April 1987, and performance tests began in June 1987.

As stated in the preceding paragraph, the PLF was initially designed to support ejector component and system testing. However, because of its unique capabilities, it is completely suitable for evaluation of components and systems for all of the supersonic STOVL propulsion concepts. It also could be used as a static test facility for multi-axis nozzle tests for supermaneuverable aircraft.

Ejector Performance

The first test on the new Lewis Powered Lift Facility (PLF) mentioned in the preceding section included the full-scale internal fan flow ducting and valving scheduled to be installed in the large-scale GD E-7 aircraft model. A schematic of the installation on the aircraft model is shown in figure 8. The fan flow will be collected and fed through a plenum to either a forward or aft duct. The forward duct will direct the flow to the ejector augmentor in the

aircraft wing. The aft duct will lead to a thrust nozzle in the back. Flow direction will be controlled by butterfly valves. This arrangement is unique to the E-7 configuration. A photograph of the duct and valve hardware installed on the PLF is also shown. The purpose of these tests was to evaluate the pressure loss performance of the system before the ejector was installed. Typical pressure loss data are shown and compared with previous predictions (lined curves). As seen in the figure the data for the rear duct show less loss (than predicted) and slightly higher loss for the ejector duct. These results were considered as being favorable and are expected to have minimal impact on the overall system performance.

After the internal duct and valve pressure loss tests were completed, the PLF force system was calibrated, and the first force test was initiated. As shown in figure 9, one-half (side) of the large-scale ejector was attached to the system ducting and tested on the PLF. These initial tests were completed in June 1987. This figure includes photographs of the model installed on the PLF and some of the more significant results. The upper photo is a view looking at the downstream end of the ejector. The lower photo is a closeup view looking at the inlet of the ejector secondary with the primary nozzles (12) clearly visible. For these tests the ejector was positioned on its side to avoid possible, and not currently understood, facility support interference effects. The test ejector measures approximately 10 by 2 ft and is supplied by 42-lb/sec primary airflow at the design point. The ejector achieved 3300 lb of thrust at that condition.

Preliminary thrust augmentation data are shown in the figure as a function of primary nozzle pressure ratio. The system design was for a thrust augmentation ratio of about 1.6 at a nozzle pressure ratio of 2.5 (corresponding to a Spey engine test condition). Previous deHavilland test results with another smaller scale model and lower flow facility are also shown for comparison. The Lewis data show excellent agreement with the previous data, and both exceeded the design by a considerable amount. The augmentation data shown are based on nozzle exit conditions. Correcting for the valve and duct pressure loss reduces this performance by only 3 percent. The resulting augmentation performance would still exceed the design requirement. It should be noted here that this test is somewhat analogous to a typical isolated nozzle test. Further, it can be expected that some of this performance may be lost upon installation in the aircraft model. This good agreement and sizable performance margin raises the confidence level for both the capabilities of the PLF and feasibility of an ejector system as one of the viable concepts for a future supersonic STOVL.

The next step in the U.S./Canada Ejector Program will be to install this same hardware in the complete E7 model and to test it in the Ames 40- by 80-ft wind tunnel. On the basis of the results discussed in the preceding paragraph, confidence in the success of this program is high. Follow-on work for the PLF will include a static evaluation of the E-7 model with the ejectors, evaluation of alternate ejectors, and an integrated flight/propulsion control system, which will be discussed later.

HOT GAS INGESTION

Hot gas ingestion (HGI) will be a problem for all of the currently proposed supersonic STOVL engine concepts. The problem, as demonstrated in

figure 10, is extremely complex and results from, in the case of a vectored thrust configuration, the jet flow impinging upon the ground and creating either of two conditions: (1) a fountain upwash is formed, which flows up to the fuselage and then forward to the inlet (near field) or (2) the ground flow, feeding forward, either interacts with the oncoming flow and gets recirculated or lifts off the ground because of buoyancy (far field). The fountain upwash essentially is the desired reflection of the jet exhaust off the ground upon the underside of the aircraft, which increases lift by offsetting jet-induced suckdown effects. However, this hot gas can run along the underside of the fuselage and enter the engine inlet system, producing a temperature distortion to the engine, loss of thrust, and at worst an engine compressor stall. The far-field phenomena can have the same result. These phenomena have already been a problem for the Harrier (ref. 6) and have been addressed in earlier V/STOL programs. With the higher T/W engines required for the supersonic STOVL it will be a worse problem. Therefore either control devices or operational procedures will have to be developed to reduce or eliminate the problem. The following figures will describe the Lewis program in place to work on the problem.

Analytical Results

An integral part of each Lewis supersonic STOVL program includes analytical development. An example of where significant progress has been made is illustrated in figure 11 for the case of hot gas ingestion (HGI). Shown in the figure are preliminary results from calculations made by using a three-dimensional Navier-Stokes code based on the TEACH code of Imperial College. This code assumes incompressible gas, but allows temperature differences between gases and their corresponding different densities, so results at this stage are purely qualitative (ref. 7). As shown calculations were made around a simplified forebody/inlet configuration, which included two subsonic jets close to a ground plane. A reflection plane down the middle of the fuselage thereby resulted in an equivalent four-jet (vectored thrust), two-inlet configuration. For the model, the inlet mass flow rate was matched to the exhaust nozzle flow rate.

The results shown are temperature profiles on planes at various heights from the ground to the aircraft inlets. As seen on the ground (plane 4) the jets show strong interactions, and the fountain upwash, typically seen with these configurations, is predicted together with the corresponding outflows and interactions with the free stream. The calculation for a location about midway between the ground and the fuselage (plane 3) indicates the strong development of the fountain between the nozzles and some spreading of the flow in the forward direction. Near the underside of the fuselage a stronger forward flow is observed (plane 2), and then hot flow is actually seen entering the inlet (plane 1). Qualitatively, these results are just about what one would expect to see. At present more analytical studies of these phenomena are being made with more complicated three-dimensional codes. Advanced studies will include compressible effects and more realistic forebody/inlet shapes and wing flows.

Scale-Model Results

A 1/10 scale model of a McDonnell Aircraft Company (McAir) 279-3 supersonic STOVL aircraft configuration, seen in figure 12, was tested in the Lewis 9- by 15-ft low-speed wind tunnel. The objective of these tests is to assess at scale-model sizes HGI and the distortion which must be accommodated by an engine, and to investigate possible approaches for either avoiding HGI and/or controlling it. Data from this model will also be valuable in validating the analytical codes used to assess the problem. This is a joint program between DARPA, NASA, and McAir. The model is a four-nozzle (post) vectored thrust configuration and includes high-pressure heated air (500 °F). Exhaust air provides inlet flow. A heater external to the tunnel was used to heat the nozzle flow, and flow to each nozzle could be individually controlled. Temperature and pressure rakes are included at the compressor face station to evaluate ingestion and to determine distortion profiles. As seen in the left photograph, the model was mounted from a fairly rigid support, which did provide some (but limited) model attitude and height variation. The tunnel installation included a ground plane which, as seen in the closeup view (right photo), included a trap door beneath the model. This allowed the hot gas to be ducted out of the tunnel while test conditions were being established. This door closed in about 0.5 sec, and then data were taken.

Preliminary results of the effect of model height on inlet temperature are shown in figure 13. In this figure the average temperature increase at the compressor face is presented as a function of free-stream velocity. Conditions were for a nozzle pressure ratio of 3.0 and exhaust gas temperature of 500 °F. The model height is expressed in feet for a full-scale aircraft rather than model scale to give a better understanding of the test results. As shown, hot gas began to be ingested with the landing gear, scaled up to full scale, about 4 ft above the ground for these simulated model and tunnel flow conditions. Hot gas ingestion is shown to increase as the model height was reduced. Basically, the data indicate that free-stream velocity had little effect. To use the model temperature on a full-scale basis it has to be scaled up, in this case, by a factor of about four since the nozzle supply was only at 500 °F. Investigation of temperature scaling was a part of these studies. Preliminary results indicate that the predicted scaling factors were validated for some conditions but not for others. Basically the trends observed in the data were as predicted. This test provided extremely valuable information to enhance the basic test technique for future tunnel entries and to develop possible solutions.

An example of this is shown in figure 14. In this figure the data shown indicate that model geometry seems to have a more significant impact on HGI than either tunnel or model flow conditions. As shown, hot gas ingestion can be significantly reduced if the proper flow diverter were added to the model. A series of supposed lift improvement devices (LID's) were also tested. These devices were extremely effective in reducing the HGI. A change in nozzle splay angle could result in further reductions in HGI. It became apparent in this testing that each aircraft concept will probably be subject to HGI in some degree. There are many possible solutions indicated, but the effectiveness of each will vary with the individual geometry.

As shown in figure 12, the 1/10 scale model was mounted in the test section from a relatively rigid support system. For future HGI tunnel entries a new model integrated support system (MISS), shown in figure 15, is currently

being fabricated. This support will allow testing at increased temperatures (1000 °F) and have remotely variable height, angle of attack, pitch, roll, and yaw. This support will again include exhaust for inlet flows and be capable of being used in other types of model testing. Thrust reverser, isolated inlet, and forebody inlet models could be tested over wide ranges of model and test conditions. The current model also will be modified to accept different nozzle configurations and locations. Both the model and MISS should be ready for a new series of tests in about a year.

SUPERSONIC INLET WITH SHORT DIFFUSER

Conventional supersonic dash or cruise inlets have long diffusers which maintain well behaved attached flows over wide ranges of aircraft angle of attack and attitude. The engine location in a typical supersonic STOVL may have to be moved forward for better weight and balance and to better locate the thrust vectors. This will then result in a problem for the diffuser design, particularly for operation at angle of attack. A two-dimensional supersonic inlet model, shown in the upper right corner of figure 16 with a conventional length diffuser, was built and tested in the Lewis 9- by 15-ft wind tunnel at angles of attack exceeding 100°. In these tests, variations in lip geometry and auxiliary inlets were investigated to improve alpha performance. Results of these tests show that good performance can be obtained even at the high alpha's. A modification to this model has been designed and fabricated which includes a short diffuser, as shown in the lower left corner, more appropriate to STOVL configurations. As indicated in the lower right corner of the figure, analysis has shown that this short diffuser will separate and have poor performance unless something is done to affect the boundary layer.

Short Diffuser Analysis

An analytical methodology was applied to the design of this diffuser, which incorporates techniques of boundary-layer control successfully studied and validated with subsonic V/STOL inlets at high angles of attack (ref. 8). In these previous studies both boundary-layer bleed and jet blowing were effective in maintaining attached diffuser flows in subsonic inlets at angles of attack approaching 100°. An example of these same methodologies applied to the design of the new short diffuser is shown in figure 17. As shown in the figure, the methodology was applied by McAir to the short diffuser including natural bleed. The short diffuser ($L/D = 1.25$) was designed without bleed (using typical techniques, including potential flow codes) and then with viscous corrections. Shown in the figure is the Mach number distribution along the top of the diffuser just outside the boundary layer. The analysis of this case indicated that the flow was separated at about halfway back even without any angle-of-attack considerations. This result is reflected also in the calculated skin friction, indicating that it approaches zero near this station. Varying distributions of boundary-layer bleed were then analytically applied until this separation was eliminated (also reflected in the skin friction calculation). As shown in the figure, this result was achieved with reasonable amounts of bleed required. Analyses including jet blowing were also made, again with favorable results.

Model Hardware

As a result of this work a new short diffuser section was then designed for the existing NASA Lewis/McAirm two-dimensional inlet model shown previously. This model will permit experimental incorporation of several different methods of boundary-layer control including suction, blowing (discrete and distributed), and other devices (e.g., vortex generators). The short diffuser model has been fabricated and is being readied for test in the Lewis 9- by 15-ft low-speed tunnel. A photograph of this model is shown in figure 18. The model can use any of the systems indicated either individually or in combination. Data from these tests will be used to validate these analyses. This hardware is currently being instrumented and is planned for evaluation at low speed and angle of attack in late 1988.

INTEGRATED FLIGHT/PROPULSION CONTROLS

One of the most difficult technology issues relative to supersonic STOVL will be integrated flight/propulsion controls. The supersonic STOVL aircraft goals require integration of supersonic flight, highly maneuverable flight, short takeoff, and vertical landing technologies. These modes of flight all are different and require different control strategies to implement. A pilot in combat cannot be expected to deal with all of these modes, some occurring simultaneously; hence the interest in developing integrated flight/propulsion control (IF/PC) systems has become paramount. In the joint U.S./U.K. program this was identified as being critical enough to be started immediately. As a result a joint effort was organized between NASA Ames and NASA Lewis to develop IF/PC technology. The collage shown in figure 19 represents that joint effort. Ames will work the flight aspects and Lewis the propulsion. Aircraft and engine simulations will be developed, and various control architectures will be pursued. A new real-time simulation computer has been installed at Lewis to model the propulsion and airframe dynamics. The future goal will be to eventually develop a pilot in the loop simulation capability, test these systems on the Ames Vertical Motion Simulator, and eventually verify the technology in a flight research program.

The initial effort in this joint program is an extension of the U.S./Canada Ejector Program because the characteristics of this system are currently the most clearly known. In this initial effort contracted support will provide the required hardware and develop initial control law algorithms. Participants in these efforts include GE, GD, Systems Control Technology, and deHavilland. The initial objectives will be to apply and evaluate the new Design Methodology for Integrated Control Systems (DMICS) technologies (refs. 9 and 10) as extended to STOVL. The goal of the program is the successful closed-loop demonstration of an operational engine with the ejector augmentor and simulated aircraft.

Figure 20 is a schematic of the currently proposed ground engine and integrated flight/propulsion controls demonstration test. Although the control logic is being evaluated here on an ejector-based system, the number of control loops, nonlinearities, etc., that must be dealt with are typical of the STOVL propulsion concepts. The configuration shown includes the GE F110 engine and ejector system that will be mounted on the Lewis Powered Lift Facility (PLF). The model will include a vectorable, two-dimensional convergent/divergent (CD) aft nozzle and a ventral nozzle for vertical thrust. Again

these items are typical of many of the STOVL propulsion concepts. This system will be tested with a real-time aircraft simulation running in parallel. The control computers will be fitted with the integrated control algorithms, first based on the contractors design methodology for integrated control systems (DMICS), and then with some new NASA-developed methodologies. Testing on the PLF will focus on vertical and transition operation at static conditions. This program is currently scheduled to take place in late 1989 and early 1990, and will be followed by a further evaluation of the ejector concept powered by an F110 in the NASA Ames 40- by 80-ft wind tunnel.

CONCLUDING REMARKS

A comprehensive program has been put in place that will develop the required propulsion technology to allow the initiation of a research aircraft in the early- to mid-1990's. A supersonic STOVL technology program is important, as indicated by the interest and involvement of three separate governments. The DOD is involved. Specifically, the Air Force is already an active participant, and there is indication that the Navy will soon be involved. Successful studies which will lead to more certainty on a concept specific effort are nearing completion. And, test programs are already in place and generating promising results. New facilities and research capabilities have also been developed which will be useful not only to this effort but also to others such as highly maneuverable fighter aircraft.

With adequate resources, considerable progress can be expected over the next several years, thus allowing supersonic STOVL to be a promising candidate for future fighter/attack aircraft.

REFERENCES

1. Kidwell, G.H., Jr.; and Lampkin, B.A.: An Evaluation of Supersonic STOVL Technology. AIAA Paper 83-2493, Oct. 1983.
2. Lewis, W.J.; and Palfreyman, D.: Supersonic V/STOL Ready for Technology Push. Aerospace America, vol. 22, no. 10, Oct. 1984, pp. 46-51.
3. Re, R.J.; and Leavitt, L.D.: Static Internal Performance of a Thrust Vectoring and Reversing Two-Dimensional Convergent-Divergent Nozzle with an Aft Flap. NASA TP-2549, 1986.
4. Mason, M.L.; and Burley, J.R., II: Static Investigation of Two STOL Nozzle Concepts with Pitch Thrust-Vectoring Capability. NASA TP-2559, 1986.
5. Bevilaqua, P.M.: Advances in Ejector Thrust Augmentation. AIAA Paper 84-2425, Oct. 1984.
6. Lewis, W.J.; and Hurd, R.: Augmented Vectored Thrust Engines and the Problem of Avoiding Hot Gas Recirculation. ASME Paper 79-GT-10, Mar. 1979.

7. Bruce, T.W.; Mongia, H.C.; and Reynolds, R.S.: Combustor Design Criteria Validation. Vol. 1: Element Tests and Model Evaluation. USARTL-TR-78-55A, Mar. 1979. (Avail. NTIS, AD-A067657.)
8. Hwang, D.P.: Analytical Study of Blowing Boundary-Layer Control for Subsonic V/STOL Inlets. Computation of Internal Flows; Methods and Applications, P.M. Sockol and K.N. Ghia, eds., ASME, New York, 1984, pp. 151-157 (NASA TM-83576).
9. Smith, K.L.; Kerr, W.B.; and Hartmann, G.L.: Design Methods for Integrated Control Systems. AFWAL-TR-84-2088, Dec. 1984. (Avail. NTIS, AD-B096089.)
10. Joshi, D.W., et al.: Design Methods for Integrated Control Systems. AFWAL-TR-84-2037, Feb. 1985. (Avail. NTIS, AD-B093646.)

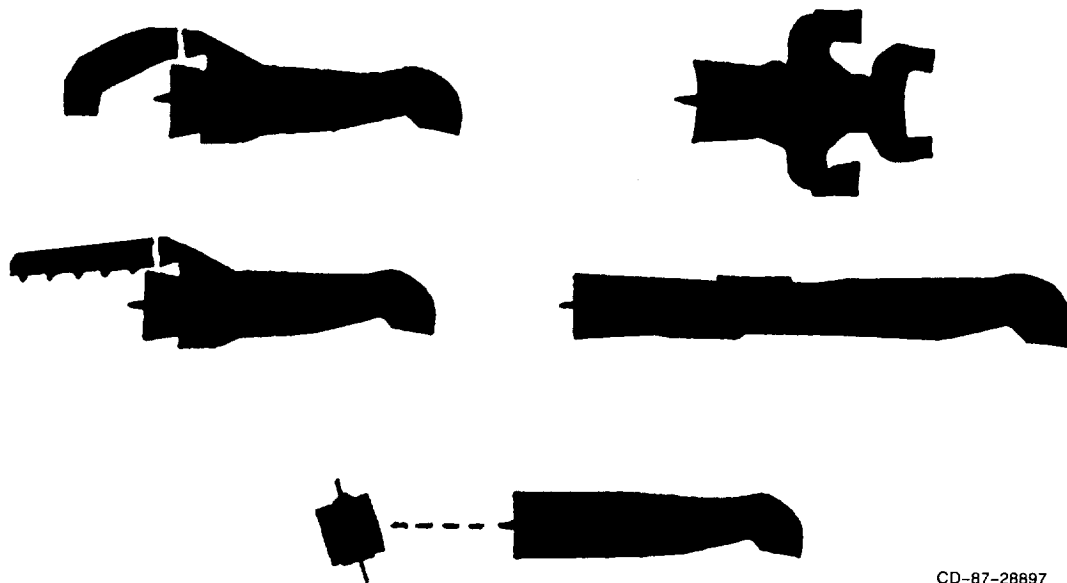
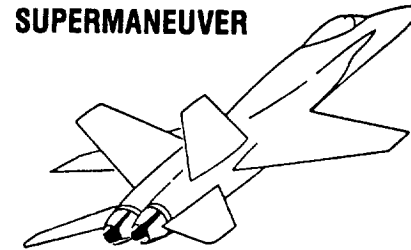
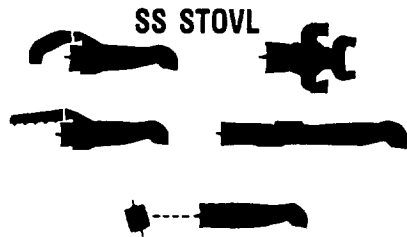


Figure 1. - Supersonic STOVL propulsion technology program.

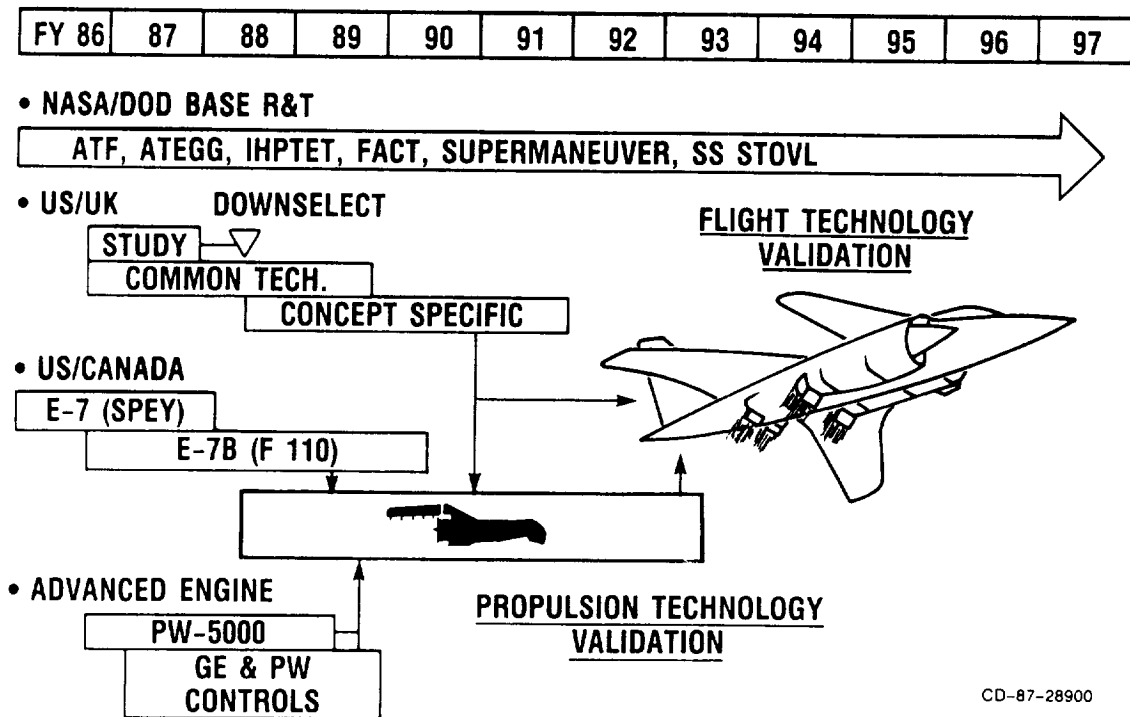


TECHNOLOGY ISSUES:

- PROPULSIVE LIFT CONCEPTS
- HIGH T/W ENGINES AND IMPACT OF ATTITUDE CONTROL SYSTEMS (BLEED)
- SUPERSONIC INLETS WITH HIGH ALPHA LOW SPEED CAPABILITY
- LIGHTWEIGHT MODULATING, DEFLECTING, AND VECTORING NOZZLES
- EFFICIENT LOW LOSS DUCTS, VALVES, AND COLLECTORS
- HOT GAS INGESTION AVOIDANCE/ACCOMMODATION
- INTEGRATED FLIGHT/PROPULSION CONTROLS

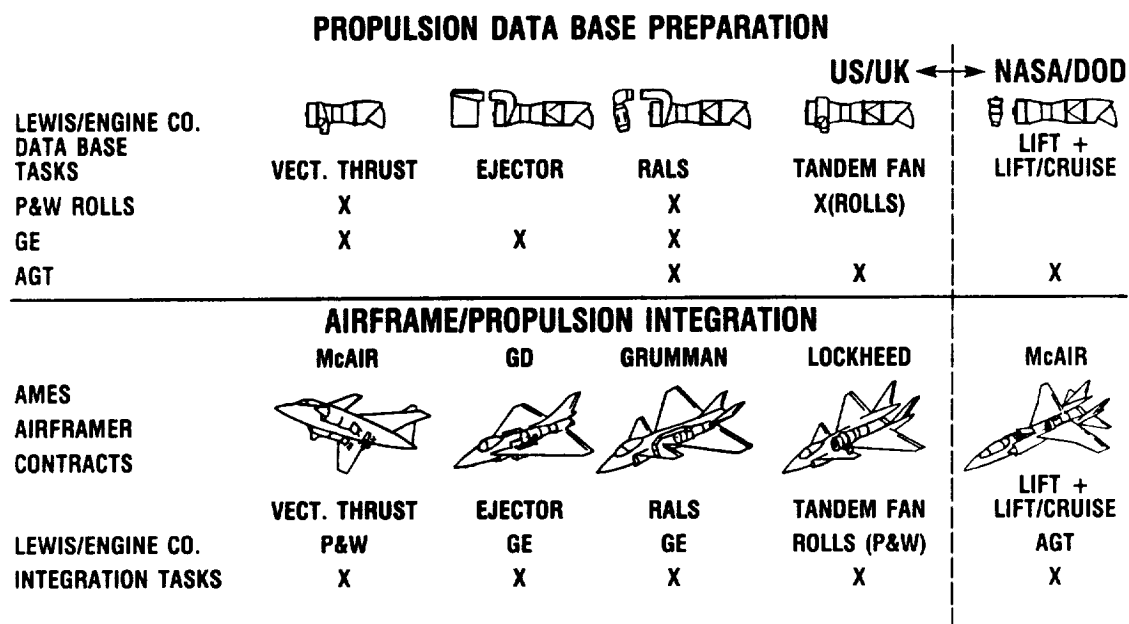
CD-87-28899

Figure 2. - STOVL supersonic and supermaneuver propulsion technology.





CD-87-28900

Figure 3. - Supersonic STOVL program plan.



CD-87-28901

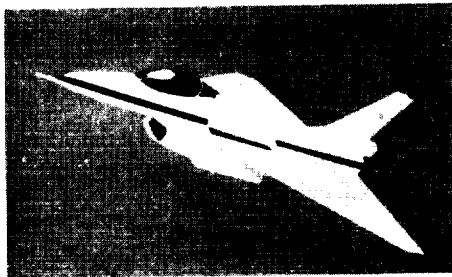
Figure 4. - STOVL study contracts -- FY87.

COMMON TECHNOLOGY ISSUES	FISCAL YEAR					STATUS
	87	88	89	90	91	
• FAN AIR COLLECTORS, VALVES, AND DUCTING (EJECTORS)						PROGRAMS IN PROGRESS
• HOT GAS INGESTION						
• SHORT DIFFUSER SUPERSONIC INLETS WITH HIGH-ALPHA CAPABILITY						
• INTEGRATED FLIGHT/PROPULSION CONTROLS						
• THRUST AUGMENTATION BY BURNING						PROGRAM PLANS BEING DEVELOPED
• THRUST DEFLECTING AND VECTORING NOZZLES						

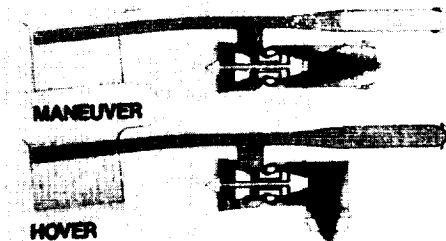
CD-87-28902

Figure 5. - Base program.

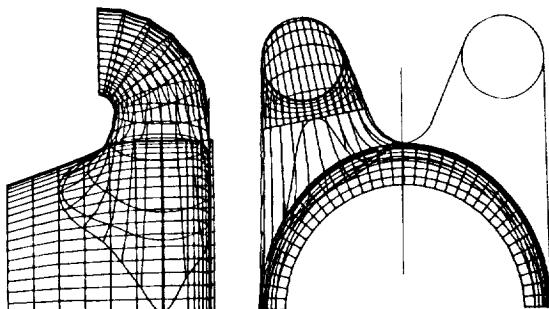
EJECTOR AIRCRAFT CONFIGURATION



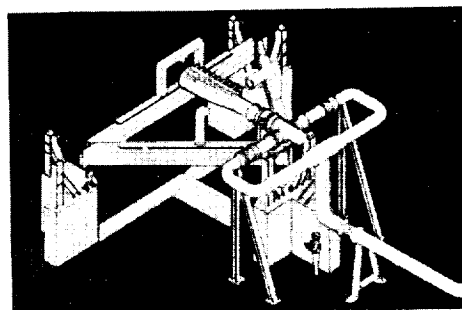
EJECTOR AUGMENTED LIFT SYSTEMS



FAN AIR COLLECTORS

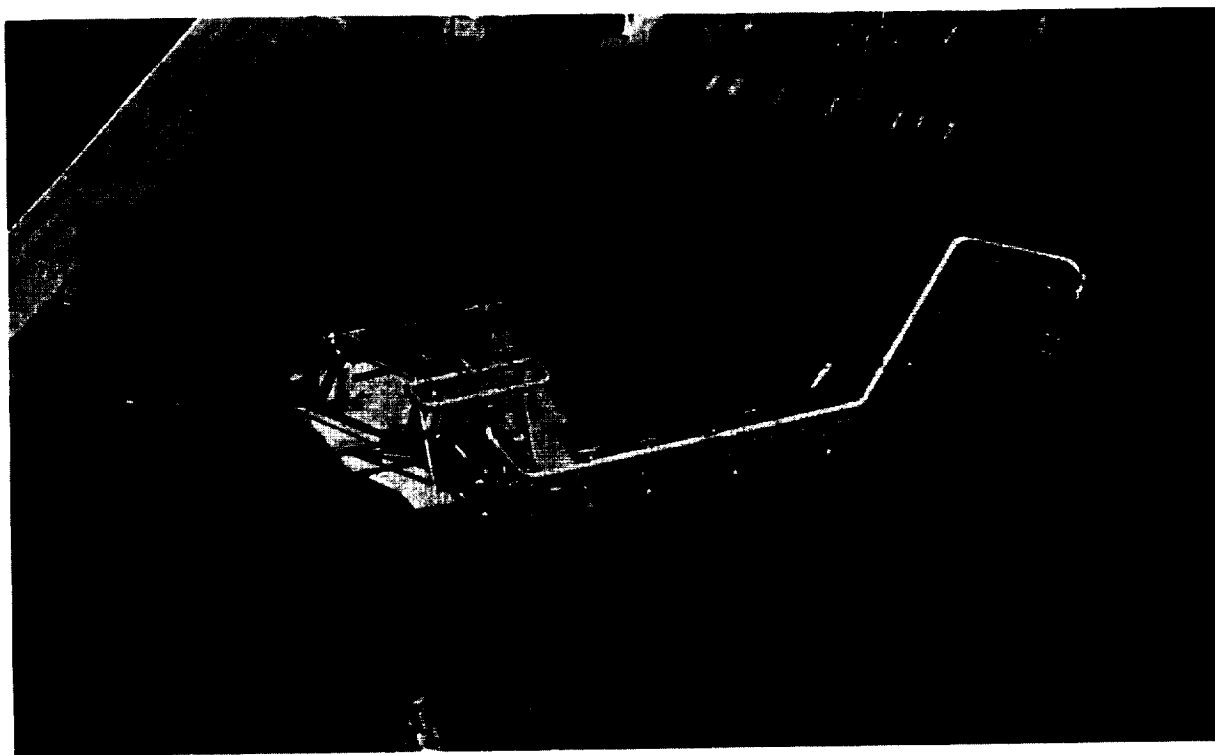


POWERED LIFT FACILITY (PLF)



CD-87-28903

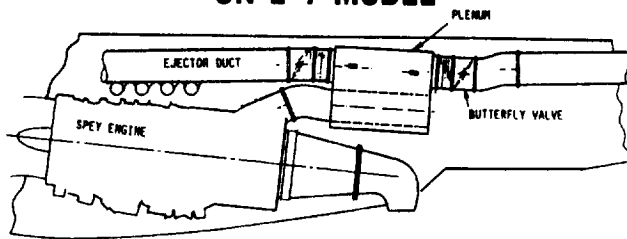
Figure 6. - U.S./Canada ejector technology.



CD-87-28904

Figure 7. - Powered Lift Facility.

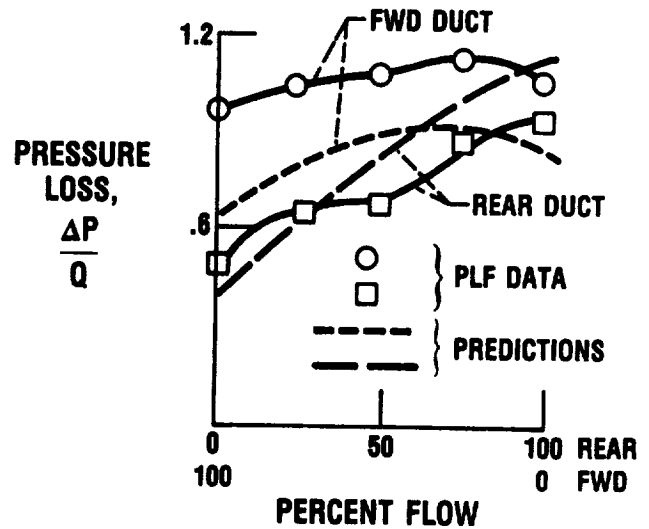
SCHEMATIC OF INSTALLATION ON E-7 MODEL



INSTALLED ON PLF



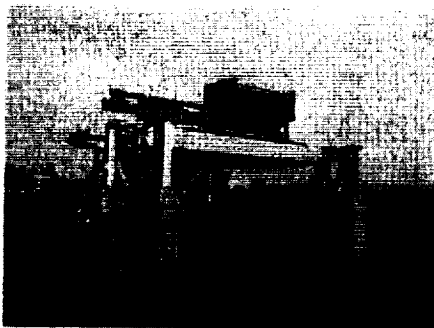
PRESSURE LOSS PERFORMANCE (SIM. FPR = 2.5)



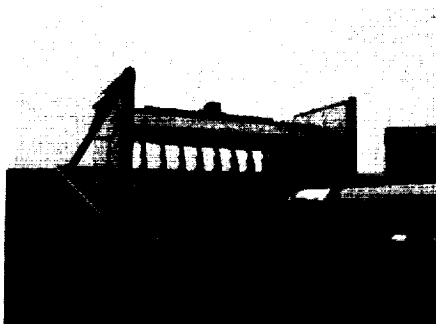
CD-87-28905

Figure 8. - DeHavilland full-scale duct and valve test on PLF.

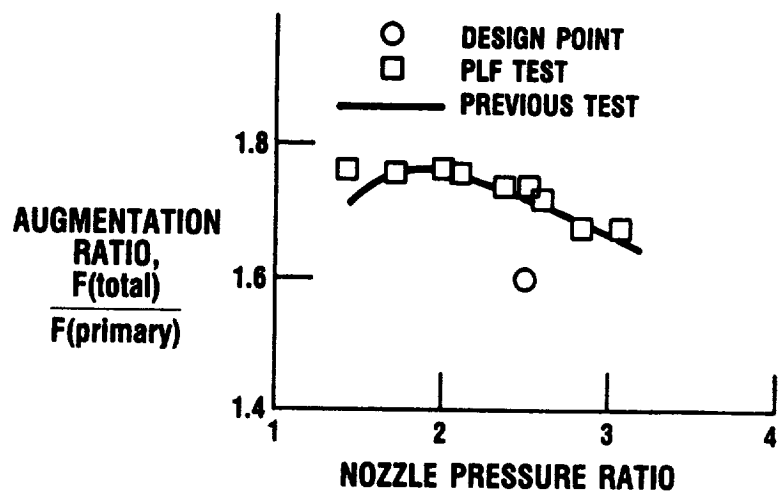
INSTALLED ON PLF



CLOSEUP VIEW



LIFT/THRUST PERFORMANCE



CD-87-28906

Figure 9. - DeHavilland full-scale ejector test on PLF.

STOVL DEFLECTED THRUST CONCEPT 279-3 AIRCRAFT

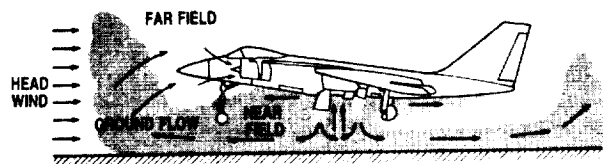


SOURCES

- NEAR FIELD
 - FOUNTAIN UPWASH
- FAR FIELD
 - SEPARATED GROUND FLOW

CD-87-28907

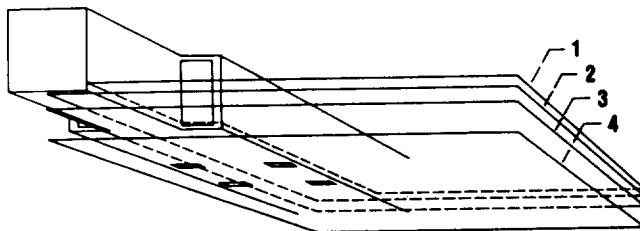
EXHAUST GAS INGESTION PHENOMENA



CONTROL

- LIFT IMPROVEMENT/FLOW DEFLECTOR
- INBOARD SPLAYING FRONT NOZZLES
- OPERATIONAL PROCEDURES
- ZONE BURNING FRONT NOZZLES
- INLET WATER INJECTION

Figure 10. - Hot gas ingestion (HGI).



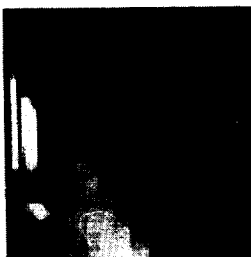
OBJECTIVE

ASSEMBLE AND VALIDATE 3-D
COMPUTER CODES TO ANALYZE
EFFECTS OF AIRCRAFT CONFIGURATION,
FLIGHT SPEED, AND GROUND PROXIMITY
ON HOT GAS ENVIRONMENT AROUND
STOVL AIRCRAFT.

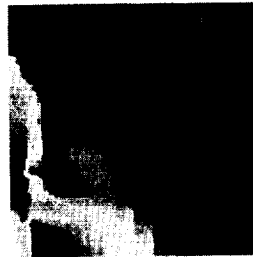
FORWARD VELOCITY = 28 m/s
EXHAUST VELOCITY = 300 m/s

TEMPERATURE CONTOURS

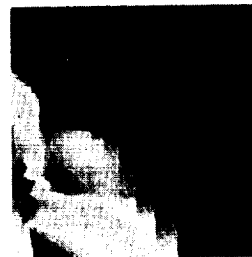
1000 F
70 F



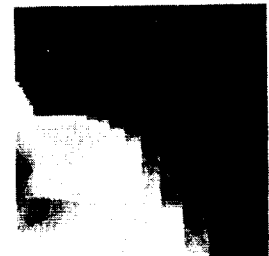
PLANE 1



PLANE 2



PLANE 3

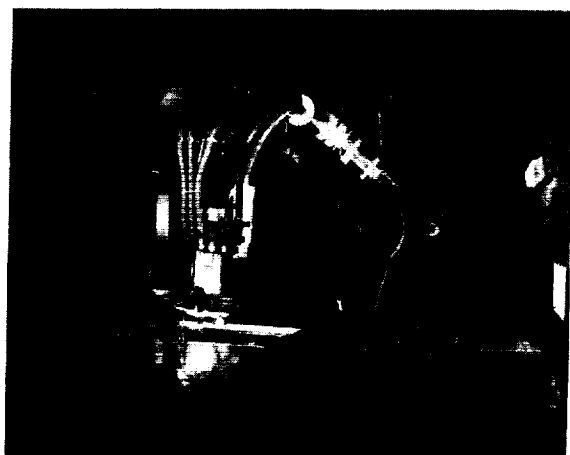


PLANE 4

CD-87-28908

Figure 11. - Hot gas ingestion analytical results.

MODEL INSTALLED IN TUNNEL



CLOSEUP VIEW



CD-87-28909

Figure 12. - One-tenth scale McAir 279-3 supersonic STOVL model hot gas ingestion (HGI) test in Lewis 9- by 15-ft wind tunnel.

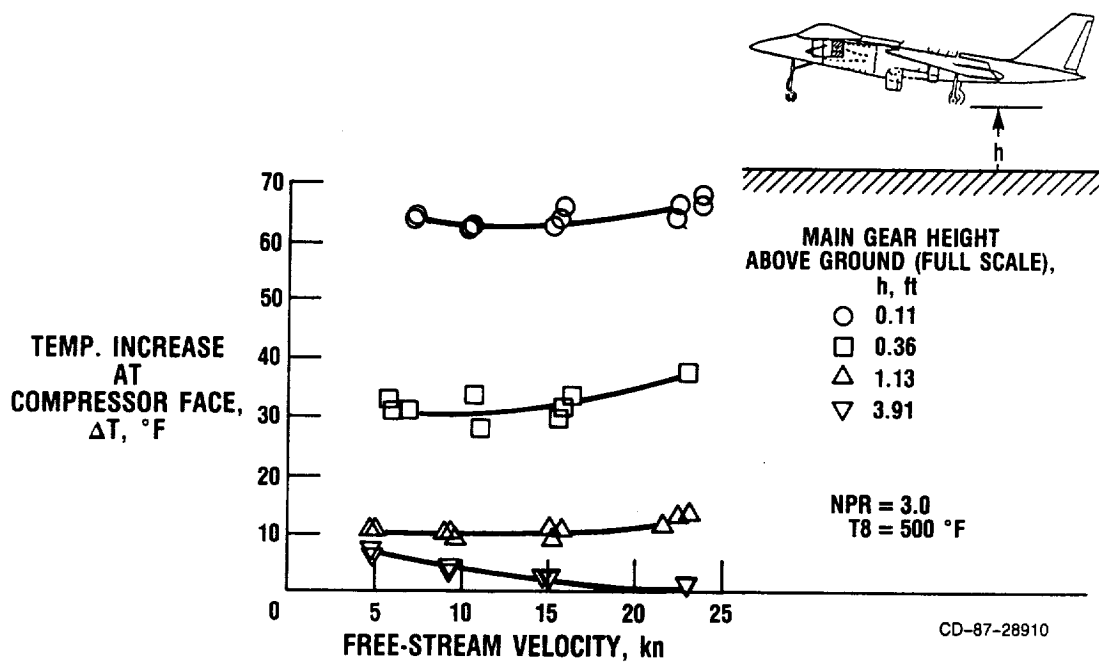
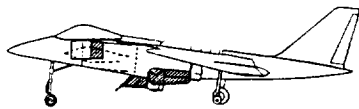
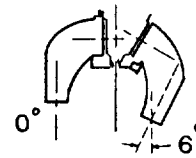


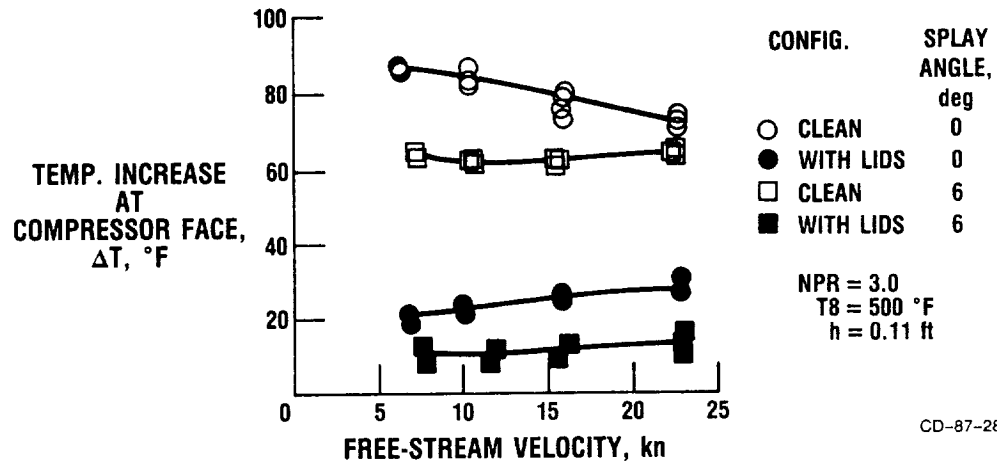
Figure 13. - Effect of ground proximity on hot gas ingestion (HGI) with basic 279-3 model.



LIFT IMPROVEMENT DEVICES (LIDS)



NOZZLE SPLAY ANGLE



CD-87-28911

Figure 14. - Effect of geometry on hot gas ingestion (HGI).

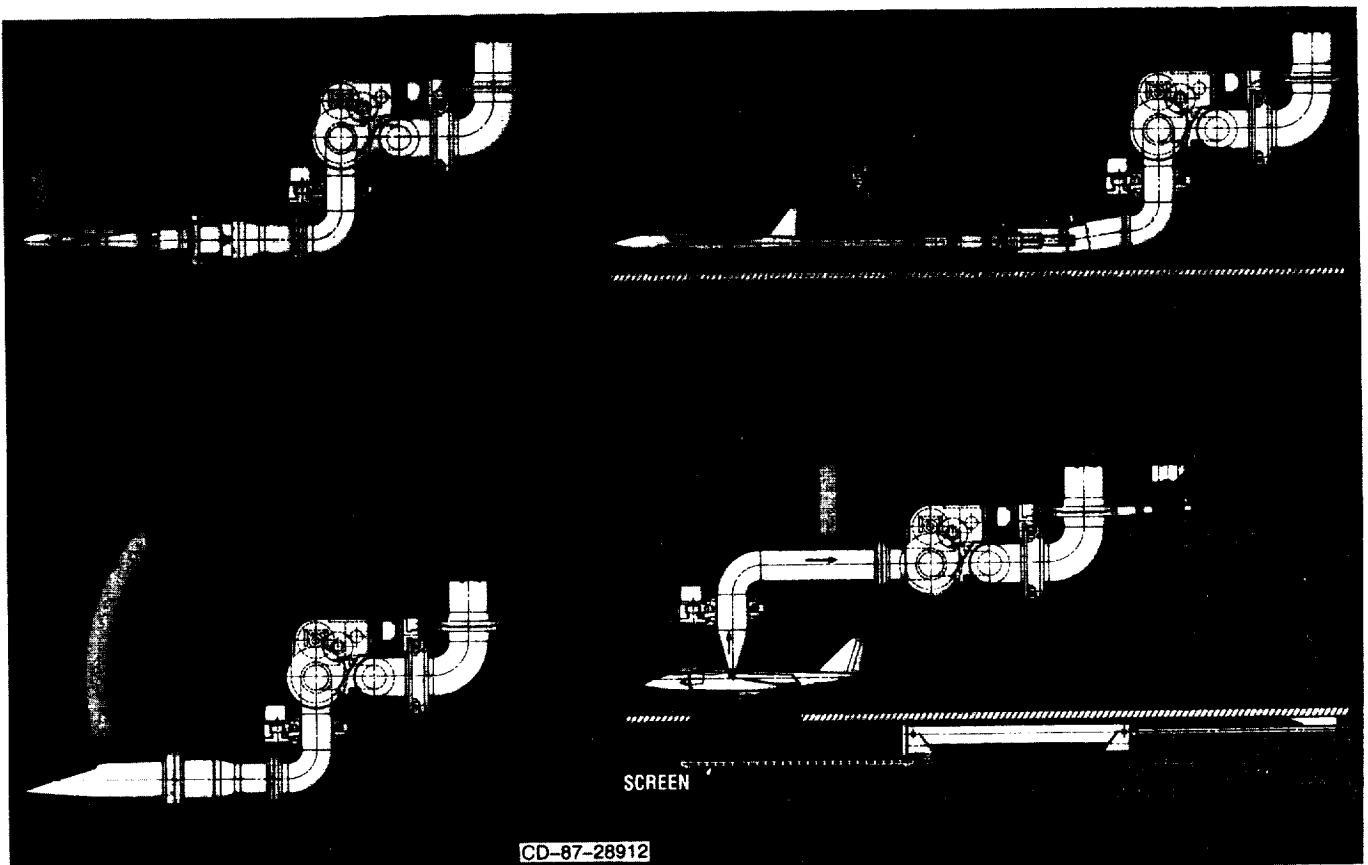
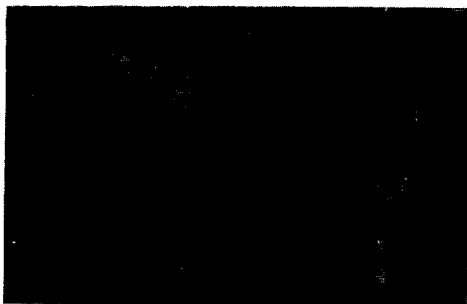
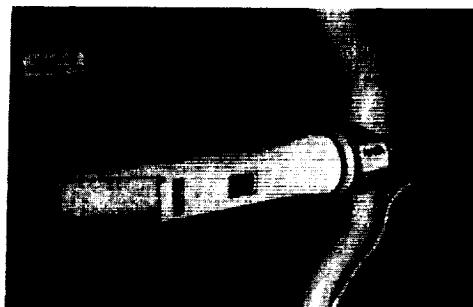


Figure 15. - Model integrated support system (MISS) for versatile and efficient research testing.

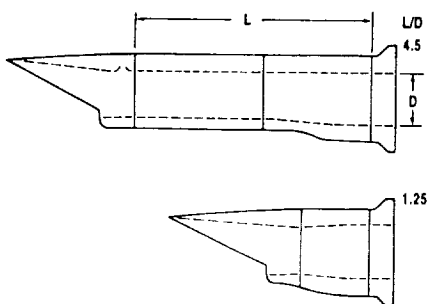
AIRCRAFT CONFIGURATION



2-D SUPERSONIC INLET



DIFFUSER VARIATIONS



CD-87-28913

DIFFUSER FLOW RANGE

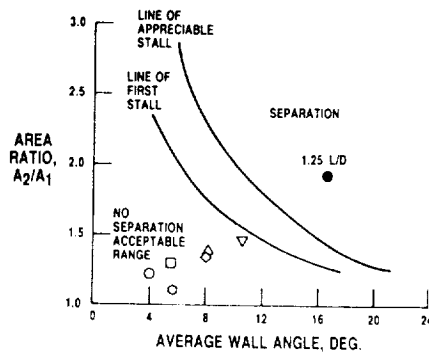
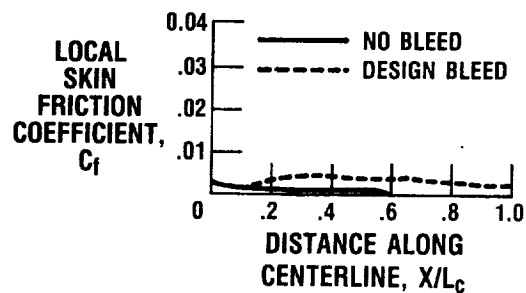
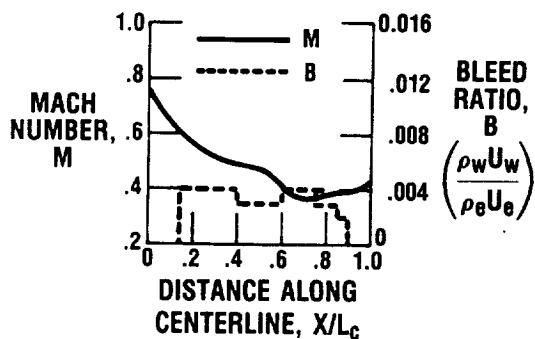
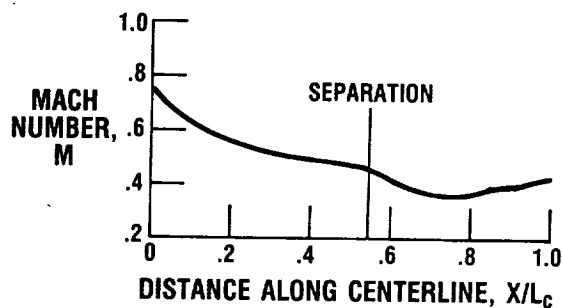
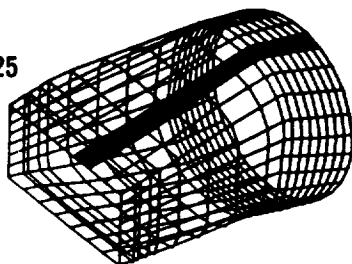


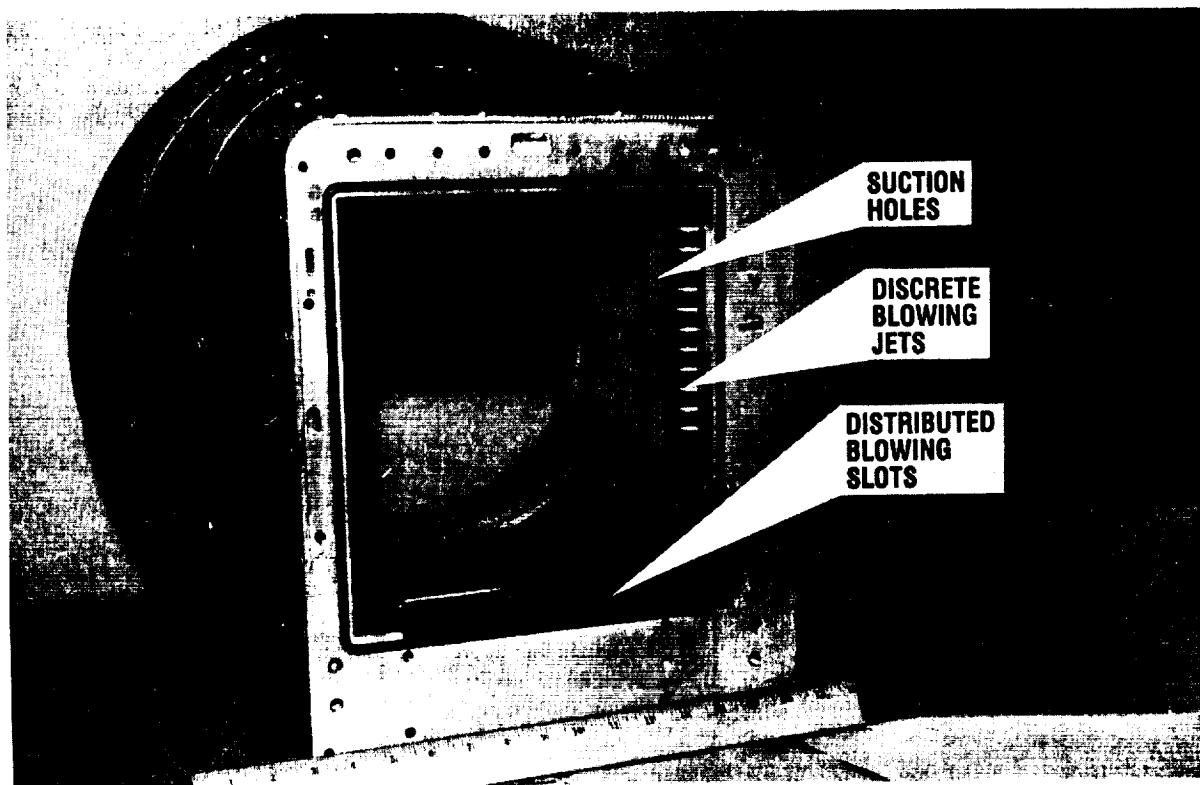
Figure 16. - Supersonic inlet with short diffuser.

$L/D = 1.25$



CD-87-28914

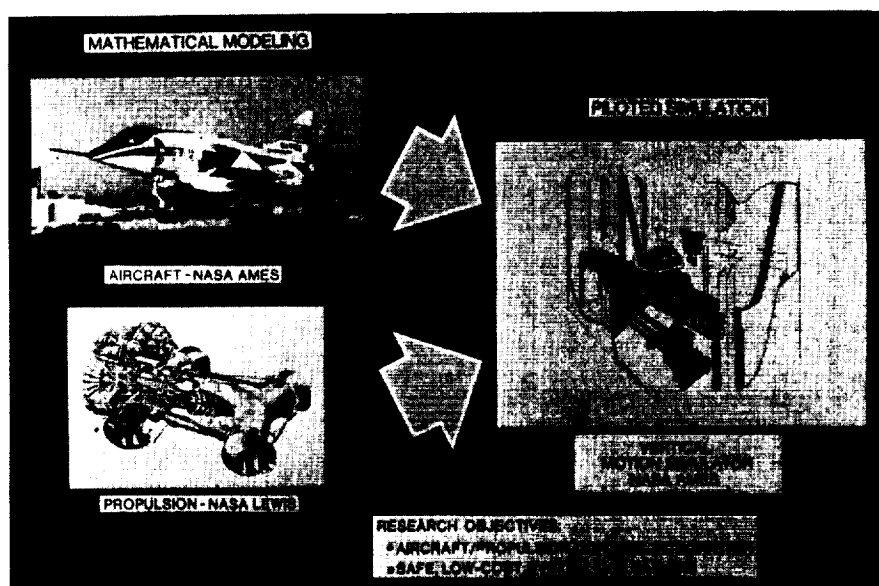
Figure 17. - Short diffuser analysis - effect of bleed.



CD-87-28915

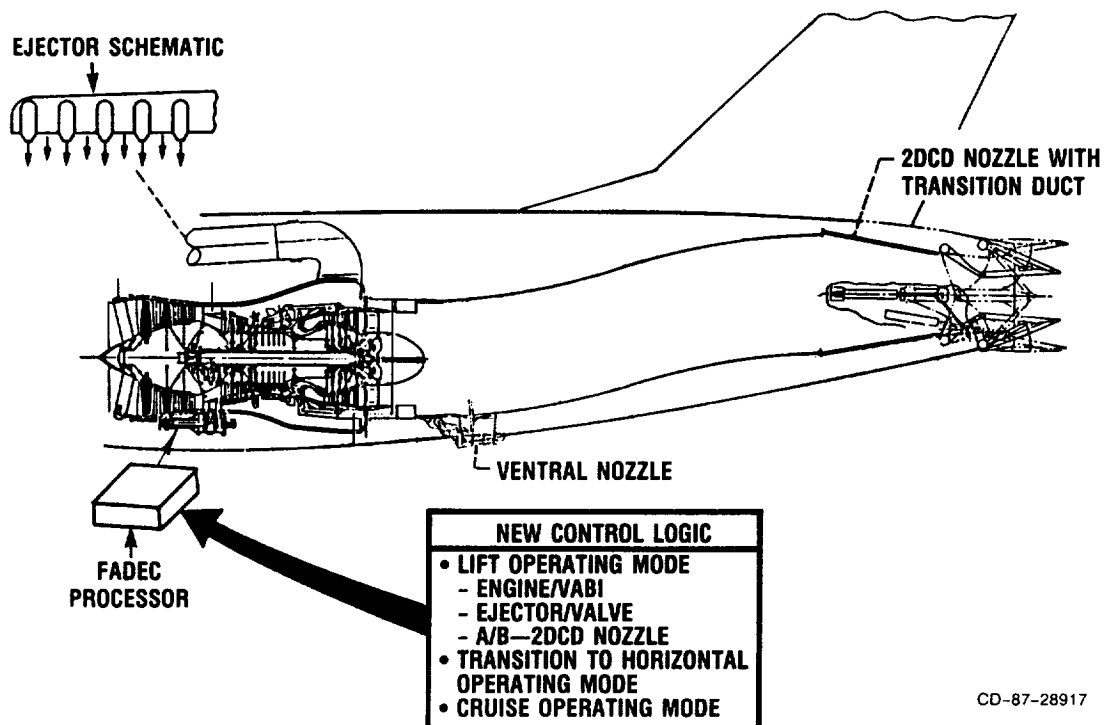
Figure 18. - Short supersonic diffuser model.

INTEGRATED FLIGHT/PROPULSION SIMULATION AND CONTROLS



CD-87-28916

Figure 19. - STOVL supersonic and supermaneuver propulsion technology.



CD-87-28917

Figure 20. - NASA/DARPA ejector/controls configuration.

PROPULSION CHALLENGES AND OPPORTUNITIES FOR HIGH-SPEED TRANSPORT AIRCRAFT

William C. Strack

SUMMARY

The major challenges confronting the propulsion community for supersonic transport (SST) applications are identified. Both past progress and future opportunities are discussed in relation to perceived technology shortfalls for an economically successful SST that satisfies environmental constraints.

A very large improvement in propulsion system efficiency is needed both at supersonic cruise and subsonic cruise conditions. Toward that end, several advanced engine concepts are being considered that, together with advanced discipline and component technologies, promise up to 25 percent better efficiency than the Concorde engine.

The quest for higher productivity through higher speed is also thwarted by the lack of a conventional, low-priced fuel that is thermally stable at the higher temperatures associated with faster flight. Extending Jet A-type fuel to higher temperatures and the adoption of liquid natural gas or methane are two possibilities requiring further investigation.

Airport noise remains a tough challenge because previously researched concepts fall short of achieving FAR 36 Stage III noise levels. Innovative solutions may be necessary to reach acceptably low noise.

While the technical challenges are indeed formidable, it is reasonable to assume that the current shortfalls in fuel economy and noise can be overcome through an aggressive propulsion research program.

OVERVIEW OF SST CHALLENGES

For several years there has been a growing interest in the subject of efficient, sustained supersonic cruise technology applied to a high-speed transport aircraft. Although the Concorde ushered in the supersonic transport era, it has not been a commercial success for a variety of reasons. Its poor fuel consumption (three times equivalent technology subsonic airplanes) is largely responsible for its uncompetitive economics - twice the total operation cost (TOC) as similar technology long-range subsonic transports (fig. 1). Very large airframe and propulsive efficiency improvements will be required to alter this situation. In our quest for greater productivity through increased speed, we are confronted with ever-increasing difficulties arising from high ram temperature levels. The challenge is to utilize advanced materials to cope

with the high temperatures without incurring excessive weight and cost penalties. In addition, the inability of readily available low-cost fuels to provide adequate thermal stability seriously impedes the pursuit of higher speeds. Expensive JP-type fuels reach thermal stability limits at approximately Mach 4, but low-cost Jet A is limited to slightly above Mach 2.

There are also several challenging environmental issues. While the sonic boom problem is airframe driven, the excessive airport noise levels are due to the very high takeoff exhaust velocities associated with supersonic engines. Engine exhaust gas emissions is another environmental issue requiring attention.

In the remainder of this report, each of these issues will be discussed in more detail, including a summary of previous progress, current status, and future research requirements.

FUEL ECONOMY

Figure 2 summarizes prior progress made in reducing SST engine thrust specific fuel consumption (TSFC). Results are normalized by the cruise TSFC of the 1971 U.S. engine that was first proposed for a U.S. SST. This afterburning turbojet (GE4) performed relatively well at supersonic cruise conditions. But its subsonic efficiency was very inferior to comparable high-bypass-ratio subsonic engines. To mitigate this mismatch between a fixed-cycle engine and varying mission requirements, the nation embarked on a 10-year NASA-sponsored variable-cycle engine (VCE) research program that achieved considerable progress during the 1970's. Compared to the 1971 GE4 afterburning turbojet, the hypothetical VCE engines defined in 1981 (which assumed technology levels beyond 1981) consumed 10 percent less fuel at supersonic and transonic conditions, and 25 percent less at subsonic speeds - reflecting the cycle changing feature of VCE's. A simultaneous 25 percent reduction in engine weight occurred as a result of improved materials. Nevertheless, these gains are insufficient by themselves to obtain good enough fuel economy to enable competition with subsonic aircraft. The subsonic efficiency of the 1981 VCE engines, for example, is still only one-half that of today's high-bypass-ratio turbofans.

The primary cause of the Concorde's high fuel consumption is the dramatic fall in airplane lift-to-drag ratio (L/D) at supersonic speeds - on the order of one-half that of subsonic transports. This is only partially offset by the trend towards increasing overall engine efficiency with flight speed, as shown in figure 3. Installed cruise efficiency shown here includes inlet and nozzle losses, but not nacelle drag, and represents design point values. The lowest curve represents currently operational powerplants. The middle curve indicates that significant improvement is possible with today's available technology for both subsonic and supersonic regimes. The top band projects future opportunities based principally on NASA cycle analyses. Several alternative cycle concepts are represented, including very advanced VCE and turbine bypass engines (lower boundary), and radically different concepts such as supersonic through-flow turbofans (upper boundary). These advanced technology concepts extend the peak propulsion efficiency levels from Mach 2+ to at least Mach 4. Gains of as much as 25 percent over Concorde's Olympus are possible.

Using a simple criterion such as design point efficiency is insufficient to properly convey the overall impact of advanced technology. For example, this plot shows a relatively modest 8 percent gain between 1987-technology VCE's and advanced VCE's (lower line of top band). Not shown, but vitally important, are even larger gains in climb efficiency and engine weight for advanced VCE's. For example, figure 4 displays an example of a "goal" VCE, representing what payoffs would accrue if revolutionary advances in materials and structures technology are achieved. This particular design was generated by General Electric in their recent NASA-sponsored Revolutionary Opportunities for Materials and Structures (ROMS) study (ref. 1). It assumes essentially uncooled stoichiometric engine materials coupled to advanced aerodynamics and structural design technologies. This implies extensive use of nonmetallics and intermetallic materials.

Two levels of technology are quoted here: (1) the uncooled stoichiometric goal level is denoted by the right-hand values (GE ROMS), and (2) a 600 °F cooler level is denoted by the left-hand values (NASA estimate). One-third of the 32-percent ultimate fuel reduction potential is due to a 45-percent engine weight reduction relative to a hypothetical 1984 technology-readiness baseline engine. While achieving uncooled stoichiometric technology is certainly a very long term goal, the magnitude of the payoff is so large that pursuit of high-temperature, minimally cooled cores and advanced VCE components is key to substantial improvement in supersonic flight efficiency.

To obtain even better powerplant performance than afforded by applying advanced technology to the traditional VCE, novel high risk concepts will be required. One potential SST breakthrough is the supersonic fan concept (fig. 5). Instead of using a long and heavy inlet system to efficiently decelerate the intake airflow to the subsonic speeds required by conventional turbomachinery, the supersonic fan efficiently processes air at supersonic throughflow velocities. The advantages include much lower inlet system weight, lighter fan (less stages required for a given pressure ratio), less boundary-layer bleed drag, better inlet pressure recovery, and better matching of bypass ratio variations to flight speed. Of course, there are many unknowns and challenges. What are such a fan's low-speed operating characteristics? How can the core inlet losses associated with unsteady, swirling, supersonic inflow be controlled - or is an aft fan configuration a better solution? Little effort has been expended on this concept to date, although NASA has initiated a concept feasibility research effort.

The potential payoff of supersonic throughflow fan (SSTF) technology for a typical SST application has been analyzed by NASA (ref. 2). One of the major contributors is the inlet size and weight reduction to about one-half that of a conventional supersonic inlet. This also reduces the inlet bleed drag penalty about 70 percent. The installed efficiency is improved nearly 10 percent relative to a comparable-technology conventional engine, the propulsion system weight is reduced about 25 percent, and together these improvements would yield approximately a 22-percent reduction in mission fuel (fig. 6).

Figure 7 displays the impact of potential future technology advances on airplane fuel consumption - recognizing that the key to viable SST economics is fuel cost levels approaching those for future subsonic airplanes. Achieving 100-percent fuel usage parity with the subsonic competition is not necessary because of the increased productivity associated with SST's. However, it is

important to at least be in the same neighborhood, which the Concorde and previous SST study airplanes cannot achieve despite their relatively short range capabilities. The impact of advanced propulsion technology is impressive, enabling fuel consumption rates not much different than current long-range subsonic airplanes. Coupling the most optimistic propulsion technology with potential airframe advances (18-percent better L/D and 15-percent lighter structure than SPF/DB titanium at Mach 3) produces encouraging results in the Mach 2 to 4 speed range. Of course these are preliminary first order results subject to refinement as the ongoing studies evolve. Another uncertainty is the possible introduction of a very advanced all-new subsonic airplane with an estimated 11-percent L/D improvement, a 15-percent structural weight (W_{str}) improvement, and a 33-percent propulsion efficiency improvement. The conclusion to be drawn from this analysis is that the SST fuel consumption impediment can be overcome, but it will require very large technology gains in all disciplines: propulsion, airplane aerodynamics, and airframe structures.

MIXED COMPRESSION SUPERSONIC INLETS

Commercial supersonic flight at moderate Mach 2 Concorde speeds can be viewed as relatively straightforward and within industry's technological grasp. Pushing the cruise speed substantially higher is certainly desirable, but introduces a series of ever-increasing technological challenges beyond the fuel economy of just the engine by itself. One of these new challenges is illustrated in figure 8. Conventional external compression inlets accomplish all of their diffusion outside of the intake duct through several oblique shocks and a terminal normal shock located at the cowl lip. This type of inlet delivers adequate performance and is well behaved (stable) under all transport flight conditions up to Mach 2. Beyond Mach 2, though, the performance of external compression inlets rapidly deteriorates because of the excessive cowl drag associated with the increasing cowl lip angle and the inability to increase the number of oblique shocks due to excessive inlet length and weight penalties. Flight beyond Mach 2, therefore, requires a mixed compression type inlet that performs some of the diffusion inside the intake duct through more oblique shocks and a normal shock near the throat. This introduces other problems, notably more boundary-layer bleed to avoid adverse shock - boundary-layer interactions (separation) and inlet shock system instability. The result is a much more complex inlet and control system. Neither transports nor fighters have been flown with such inlets, yet the need for utmost propulsion efficiency will require it for high-speed transports.

Mixed-compression inlets are quite susceptible to a phenomenon known as inlet instability, or "unstart," as illustrated in figure 9. Whenever a flow-retarding disturbance occurs, the internal shock system moves abruptly upstream and repositions itself completely outside the intake duct. This causes an abrupt and severe drop in thrust due to lower recovery and mass flow, and an increase in drag. The precipitating disturbance could be relatively small, such as encountering a strong gust or rapidly changing the angle-of-attack. If the initial disturbance is large (e.g., compressor stall), the transient response can be very severe - possibly unstating neighboring inlet-engine systems, which would likely throw the airplane into a violent yaw and roll maneuver. To prevent such unacceptable behavior, some form of stability control system is needed.

One inlet stability improvement concept consists of a set of self-actuating bleed valves located in the inlet nacelle (fig. 10). These rapid-response-rate pneumatic valves will open in response to the increase in duct pressure produced by a transient excursion of the inlet terminal shock forward from its steady-state position. As the shock moves forward it exposes the stability bypass plenum to increased pressure and automatically activates the bleed valves which spill inlet bleed air overboard. This increases the inlet mass flow and forces the shock rearward, and thereby reestablishes stability. The valves close when the transient disturbance subsides and the shock has retreated to its steady-state position (refs. 3 and 4).

An experimental wind tunnel test program at NASA Lewis verified the feasibility of this concept during the mid-1970's. A five-fold increase in stability margin was demonstrated by using a YF-12 system simulation. While encouraging, these initial tests represent just a beginning, not an established data base. Considerable research lies ahead to adequately address this important issue.

EXHAUST NOZZLE PERFORMANCE

The exhaust nozzle for an SST must perform well at three critical flight conditions: takeoff, subsonic cruise, and supersonic cruise. The experimental model test results shown in figure 11 (Lewis 8- by 6-ft wind tunnel) of an ejector nozzle show that, while good takeoff and cruise performance was achieved, the subsonic cruise performance was disappointingly low because of flow separation over the inlet doors of the ejector. This shortfall is important because it significantly increases the reserve fuel allowance required to reach an alternate airport. For long-range SST's, the amount of reserve fuel is quite large, equal in magnitude to the payload weight. In addition, it is critical to obtain high nozzle performance at the transonic thrust minus drag "pinch point" to minimize inlet-engine flow matching penalties.

TRANSONIC PROPULSION SYSTEM DRAG

Just as exhaust nozzle performance is critical during subsonic flight, so is the minimization of transonic installation losses associated with inlets and nozzles. The transonic inlet spillage drag, for example, can exceed the entire airframe drag for high design Mach numbers. This problem arises from a major mismatch in inlet flow swallowing capacity (too much) compared to the engine demand (fig. 12). Likewise, the nozzle boattail drag penalty rises rapidly with design cruise speed. Finding solutions to these installation problems is absolutely essential to achieve an acceptable airplane design.

THE HIGH-SPEED TRANSPORT FUEL ISSUE

Conventional jet fuels cannot withstand the high temperatures associated with flight speeds in excess of about Mach 2. If subjected to temperatures above approximately 250 °C (time dependent also), they thermally decompose and form coke deposits that clog fuel supply components and fuel injectors. Consequently, a challenge exists to extend the thermal stability of conventional jet fuel (Jet A) to higher temperatures without incurring a significant fuel

price increase, associated with either the manufacture of fuel or special fuel transportation and handling requirements, such as with JP-7 and cryogenics (fig. 13). While the practical use of hydrogen lies far into the future, liquid methane or liquid natural gas remains an intriguing possibility due to its current low price and high thermal stability. Endothermic fuels offer more heat sink capacity, but are fraught with offsetting practical and economic penalties. Uncertain future fuel prices and infrastructure costs cloud the issue of fuel selection and, consequently, airplane design speed as well.

SST TAKEOFF NOISE REDUCTION

The first generation of hypothetical SST's of the early 1970's used after-burning turbojets and would have provoked the irritation of many people living around major airports. Reducing their high jet exhaust velocities (over 4000 ft/s) by oversizing the engines and throttling back during takeoff reduces noise somewhat, but it also increases airplane size too rapidly to be an effective method for more than a few decibels. Each curve in figure 14 represents a series of various amounts of engine oversizing for a fixed mission. Considerable noise reduction progress evolved during the 1970's through a combination of variable cycle features and many noise suppression concepts experimentally tested. However, even this progress is insufficient to meet current FAR 36 stage III requirements. The noise shortfall increases considerably if we select cruise speeds and airplane ranges in excess of those assumed in figure 14. Much research lies ahead if we are to achieve a quiet SST without excessive noise reduction penalties.

Some of the noise reduction concepts illustrated in figure 15 have been explored in axisymmetric configurations suitable for flight speeds up to Mach 2.5. These concepts need data base extensions to higher speeds in both axisymmetric and two-dimensional nozzle configurations. Other concepts have practically no data base at all and are quite speculative. For example, the concept of enhancing exhaust jet mixing with pneumatic oscillators represents a very speculative and technically challenging strategy. The remote augmented thrust system concept guarantees low noise with its high-mass-flow, low-pressure-ratio fan. But it introduces different problems - notably, how to integrate the deployable remote takeoff fans into the airframe.

SST EMISSIONS REDUCTION

Previous airport pollution concerns precipitated a NASA emissions reduction research program that led to several emission control mechanisms, including the development of two-zone combustors. The conventional single-zone combustors have their high power efficiency compromised to obtain good low-power ignition and stability. The improved two-zone combustors utilized a pilot stage optimized for idle conditions and a main stage optimized for cruise power. This resulted in leaner, well mixed high-power combustion with approximately one-half as much NO_x emissions assuming the engine cycle remains unchanged (fig. 16). However, our continued quest for higher overall engine efficiency produces even higher cycle temperatures, which increases NO_x production. Hence, the final engine designs of the supersonic cruise research (SCR)/VCE program, if built, would have produced about as much NO_x as the actual engines introduced a decade earlier. Today, we face the same dilemma -

performance-driven designs will increase NO_x, while emissions-driven designs will reduce performance.

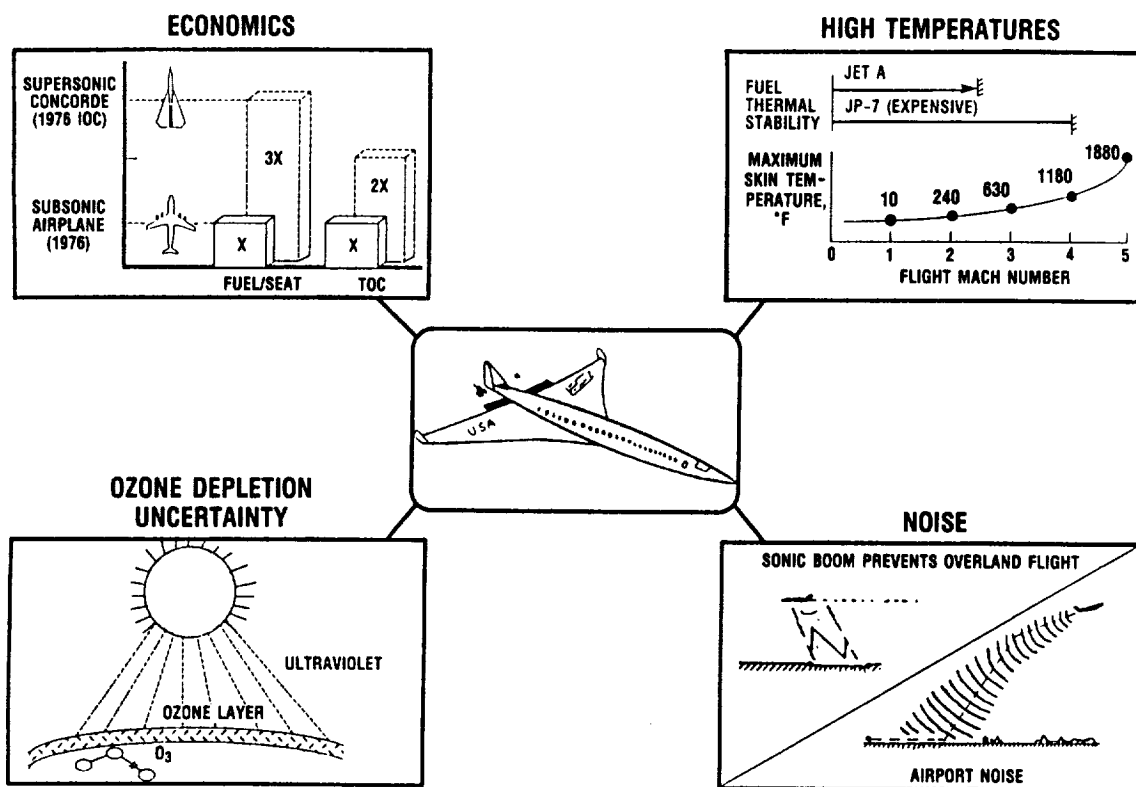
One approach to reduce NO_x emissions is to reduce the flame temperature. Another approach is to reduce the residence time of the combustion gas at high temperatures (fig. 17). In the latter approach, two concepts worth pursuing are (1) increasing the velocity through the combustor, and (2) avoiding large recirculation regions within the primary combustion zone. Increasing the combustion velocity involves finding means to avoid excessive pressure losses, as well as maintaining good combustion stability and ignition characteristics. Avoiding large pockets of recirculating hot gases in the primary zone also reduces stability characteristics, thereby requiring the implementation of other stability enhancing features.

CONCLUDING REMARKS

As the 21st century approaches, it is becoming increasingly clear that efficient supersonic cruise flight is within our technological reach. Many challenging propulsion problems need to be addressed, however, before a state of technology readiness is achieved. One possible program plan entails a two-pronged approach: a near-term effort aimed at variable-cycle engine concepts incorporating very aggressive discipline and component technologies, and a far-term effort focused on validating supersonic throughflow technology which offers even higher potential benefits (fig. 18). Continued propulsion system studies as well as a high-speed fuel and fuel systems effort are also needed. Achievement of the propulsion goals outlined herein would indeed revolutionize aircraft capability for the future.

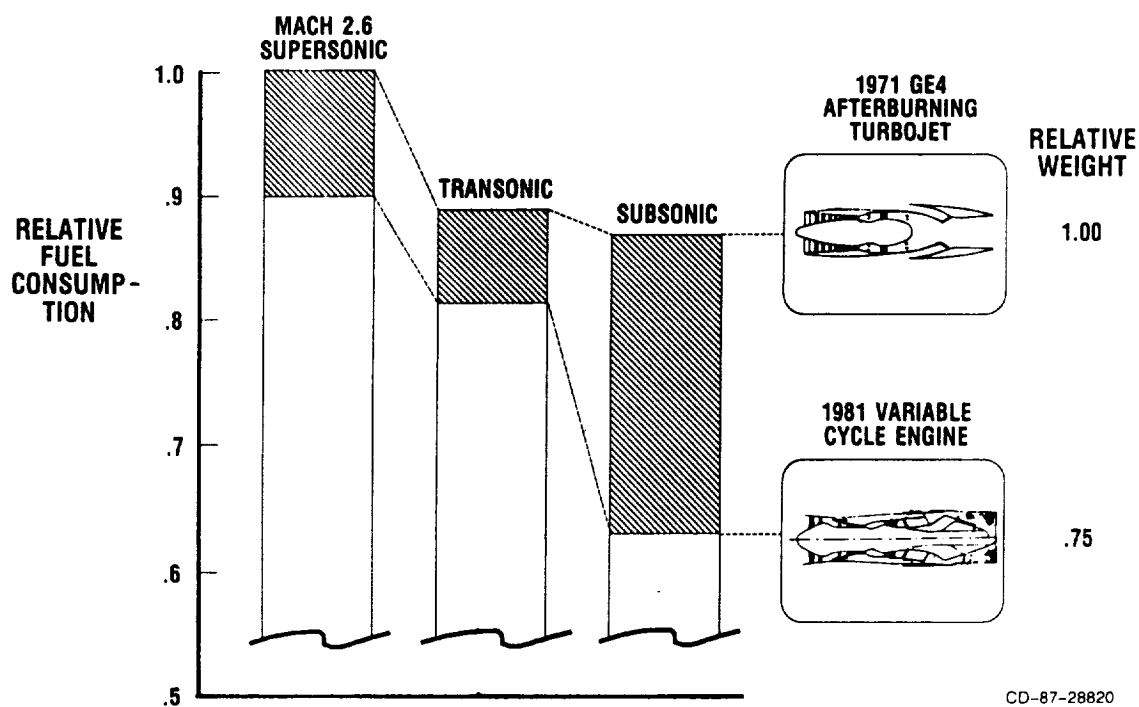
REFERENCES

1. Feig, P.D.: Revolutionary Opportunities for Materials and Structures Study. NASA CR-179642, 1987.
2. Franciscus, L.C.: The Supersonic Through-Flow Turbofan for High Mach Propulsion. AIAA Paper 87-2050, July 1987 (NASA TM-100114).
3. Sanders, B.W.; and Mitchell, G.A.: Increasing the Stable Operating Range of a Mach 2.5 Inlet. AIAA Paper 70-686, June 1970 (NASA TM X-52799).
4. Sanders, B.W.; and Mitchell, G.A.: Throat Bypass Bleed Systems for Increasing the Stable Air Flow Range of a Mach 2.50 Axisymmetric Inlet with 40-Percent Internal Contraction. NASA TM X-2779, 1973.



CD-87-28819

Figure 1. - Challenges to high-speed transports.



CD-87-28820

Figure 2. - SST propulsion progress.

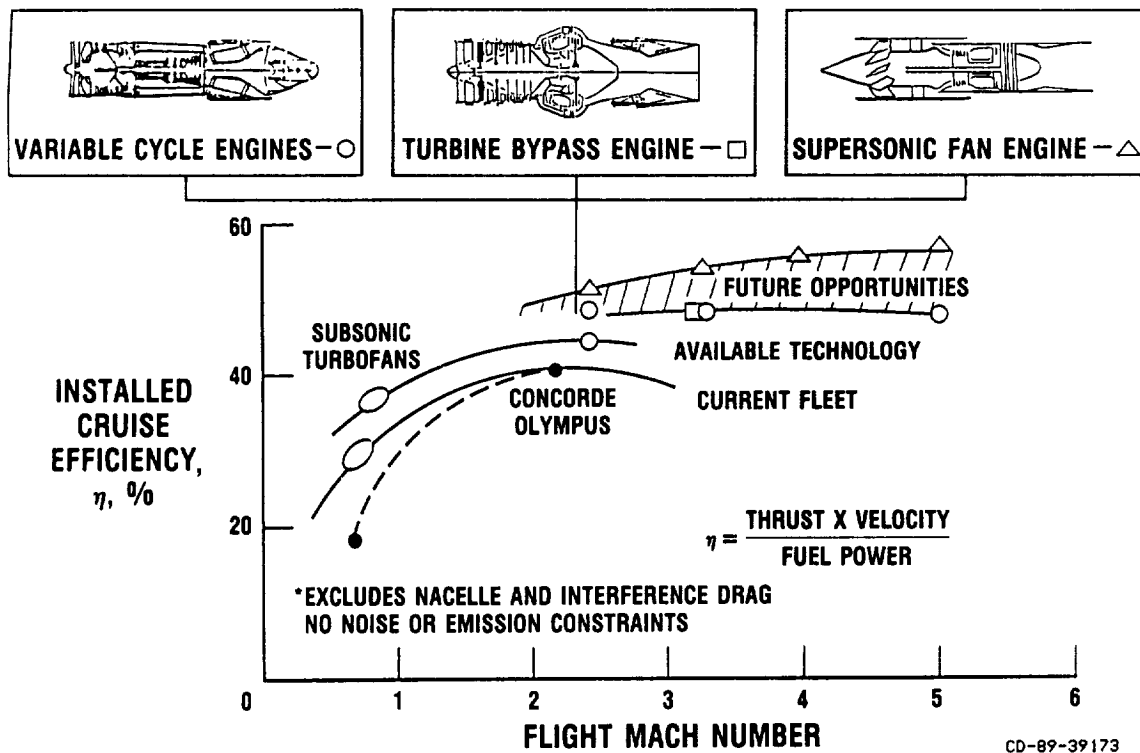
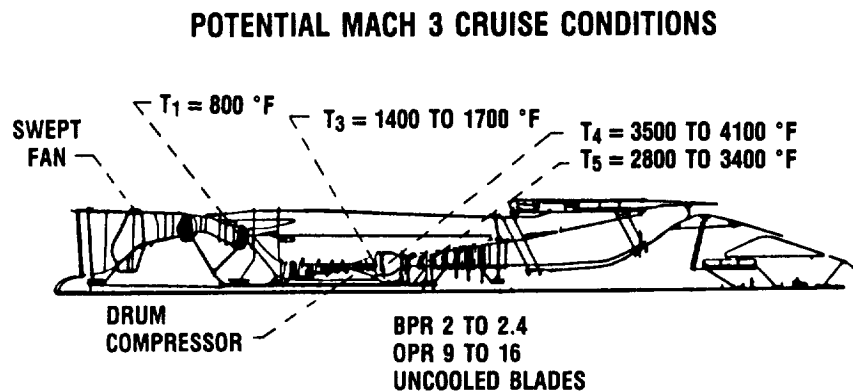


Figure 3. - Future high-speed propulsion performance potential.

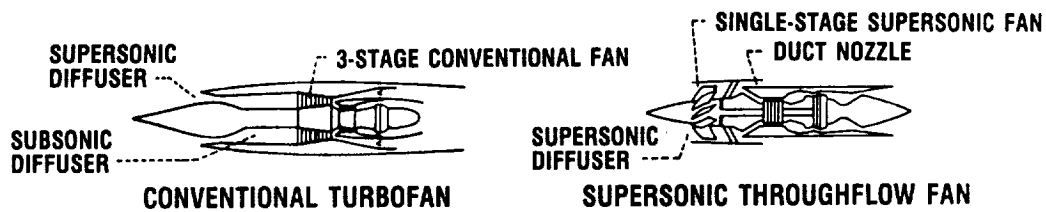


**BENEFITS (MATERIALS AND AERO): 290 PAX 5000 nmi TRANSPORT
RELATIVE TO CURRENT TECHNOLOGY AT 60¢/gal.**

FUEL	27 TO 32%
DOC	13 TO 15%

CD-87-28822

Figure 4. - Variable-cycle engine goal.



SUPERSONIC THROUGHFLOW FAN ENGINE FEATURES

- SHORT, ALL SUPERSONIC INLET
- SINGLE-STAGE SUPERSONIC FAN
- BPR DECREASES WITH M_0

IMPLICATIONS

- LOWER WEIGHT, LOWER INLET DRAG
- LOWER WEIGHT AND COST, RUGGED BLADING
- HIGHER CRUISE THRUST

CD-87-28823

Figure 5. - Supersonic throughflow fan engine.

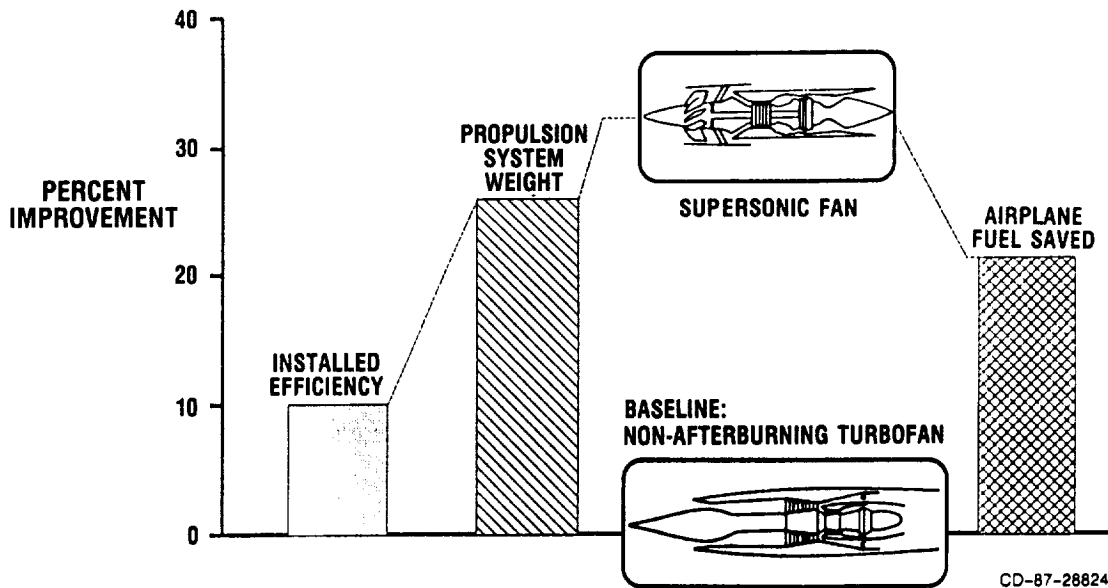


Figure 6. - Benefit of supersonic throughflow fan (Mach 3 commercial transport, 300 passengers, 5500 nmi range).

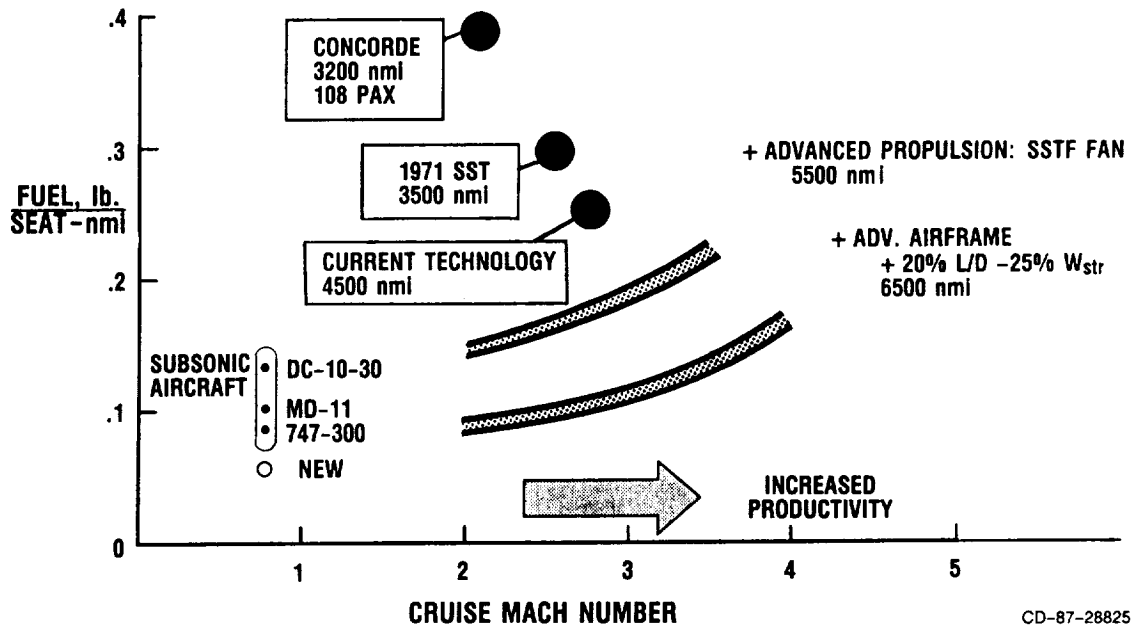


Figure 7. - Impact of technology on fuel economy (300 passengers).

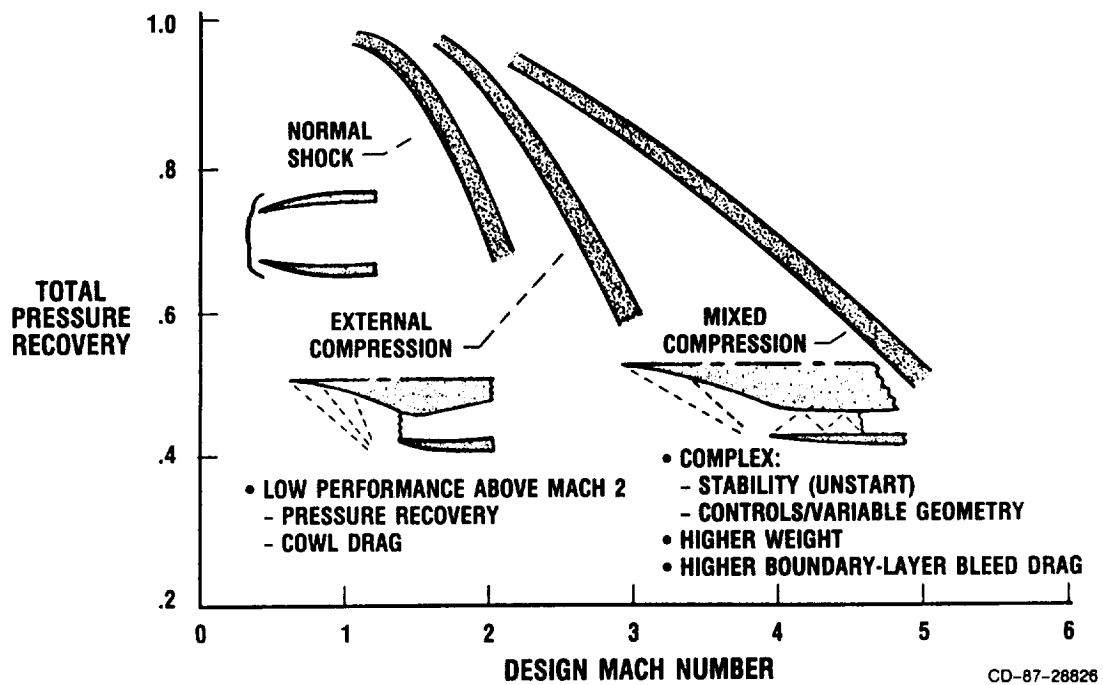


Figure 8. - Supersonic inlet performance.

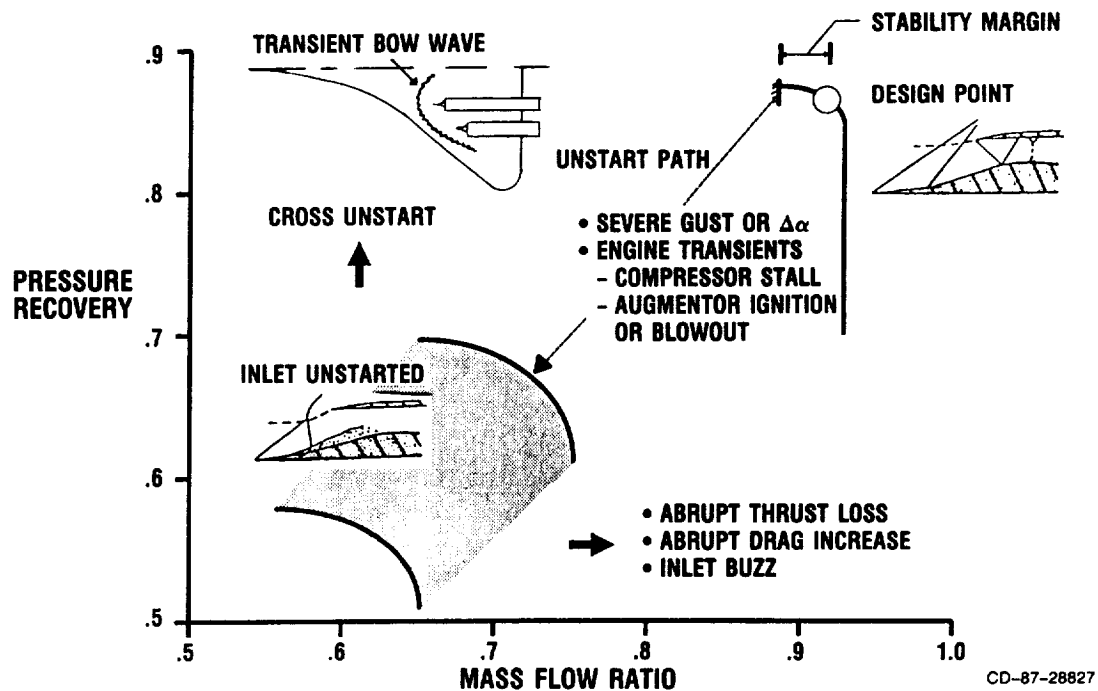


Figure 9. - Mixed-compression supersonic inlet instability.

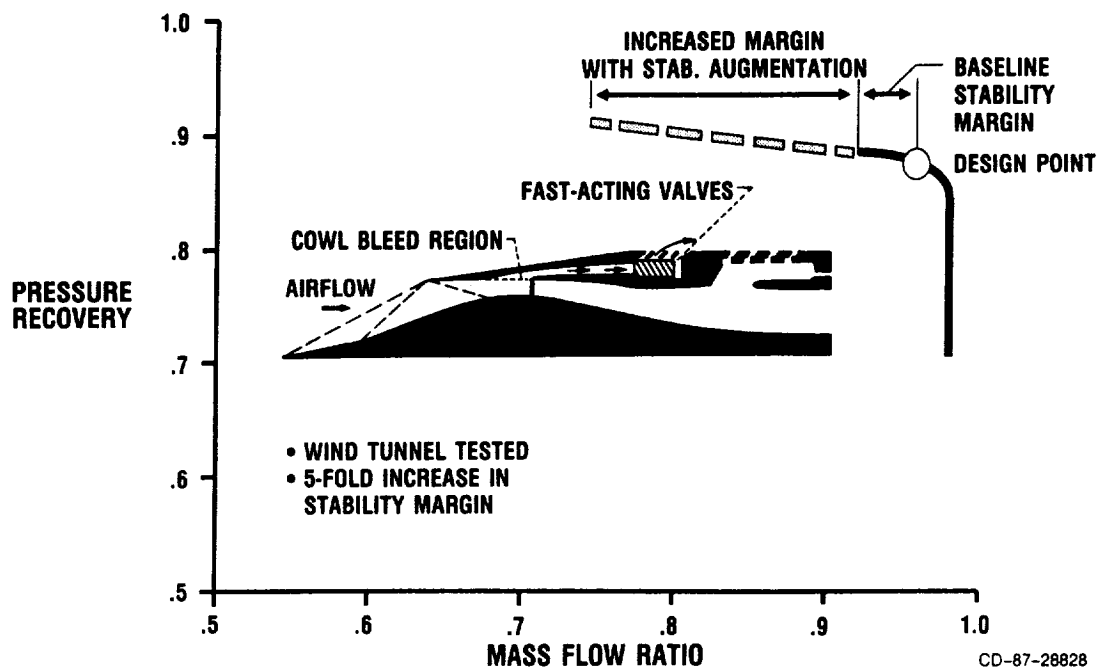


Figure 10. - Mixed-compression inlet stability improvements.

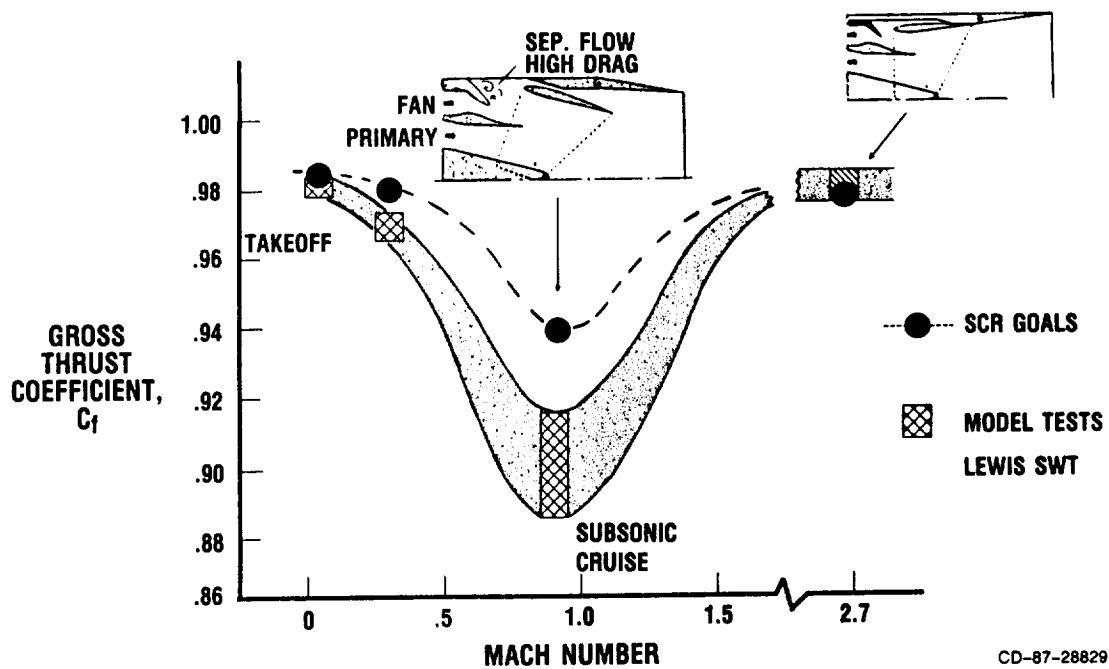


Figure 11. - Nozzle performance (VCE research ejector).

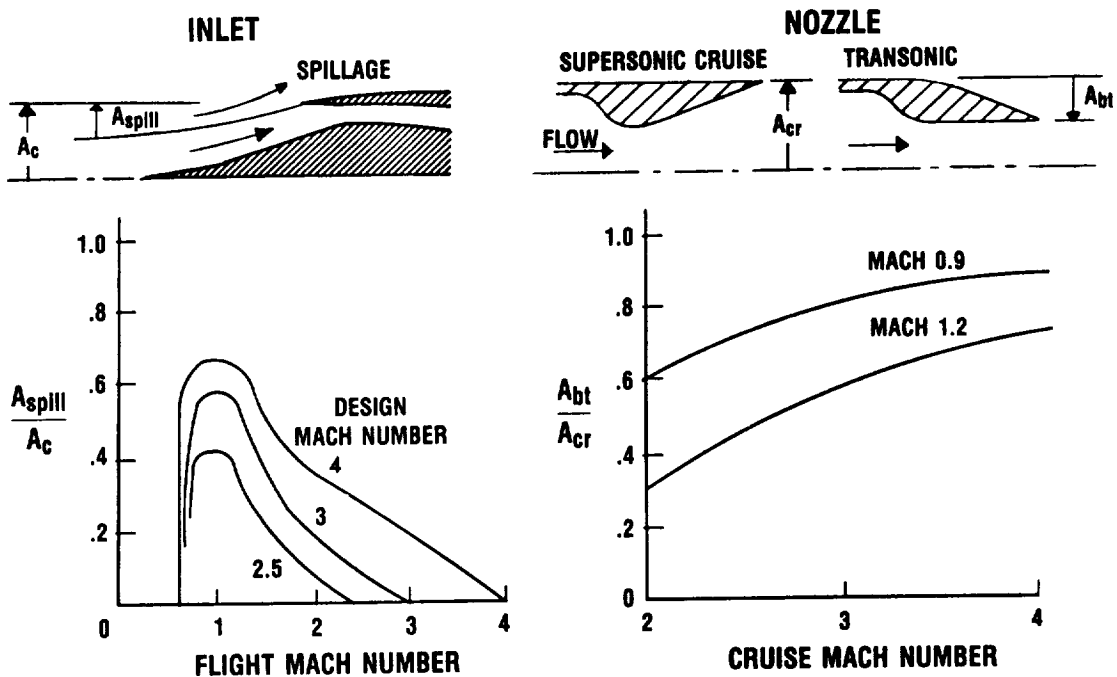
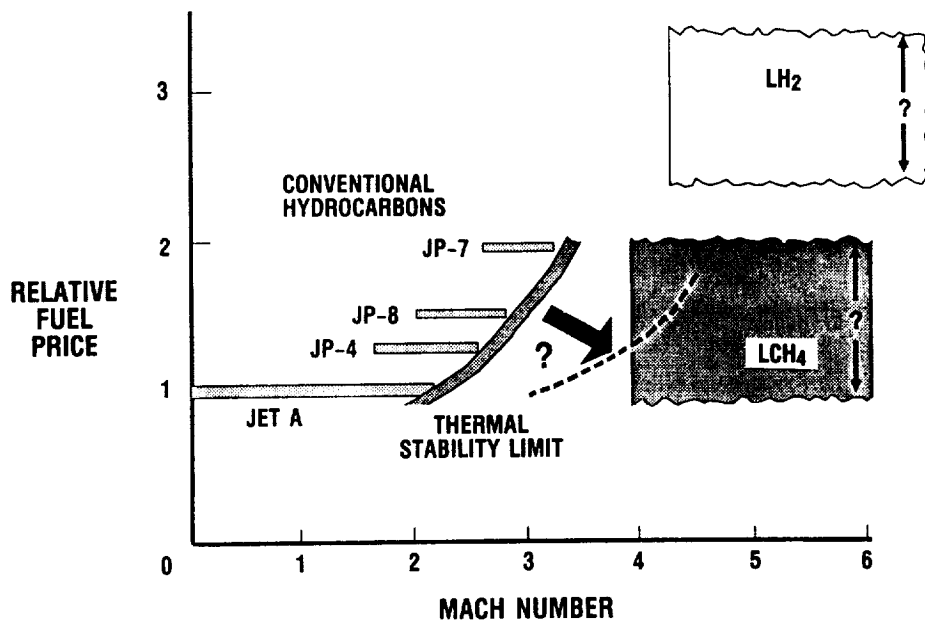
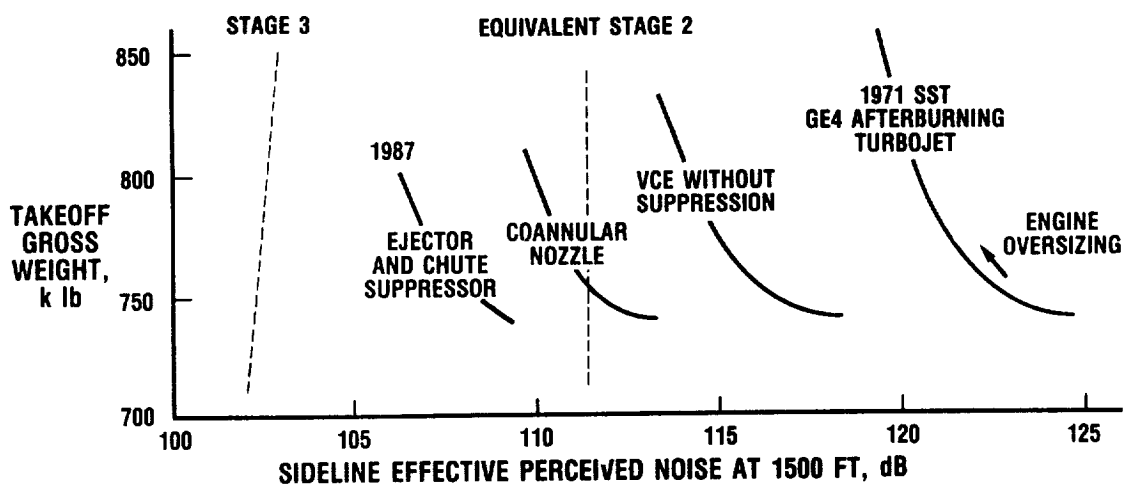


Figure 12. - Transonic propulsion system drag.



CD-87-28831

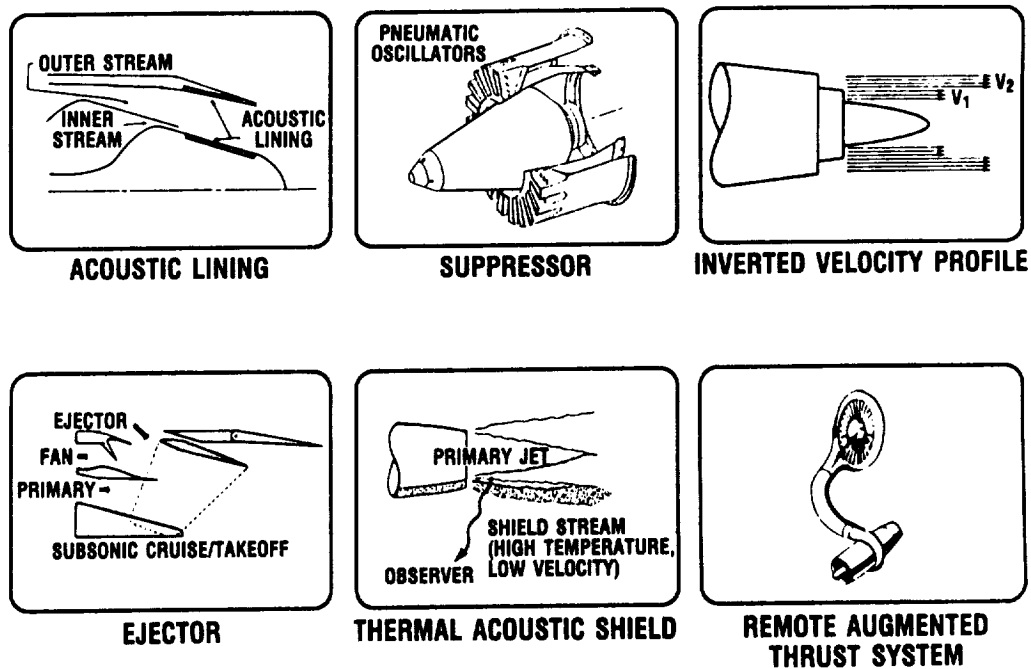
Figure 13. - The high-speed transport fuels issue.



CONCLUSION: CONSIDERABLE RESEARCH EFFORT WARRANTED

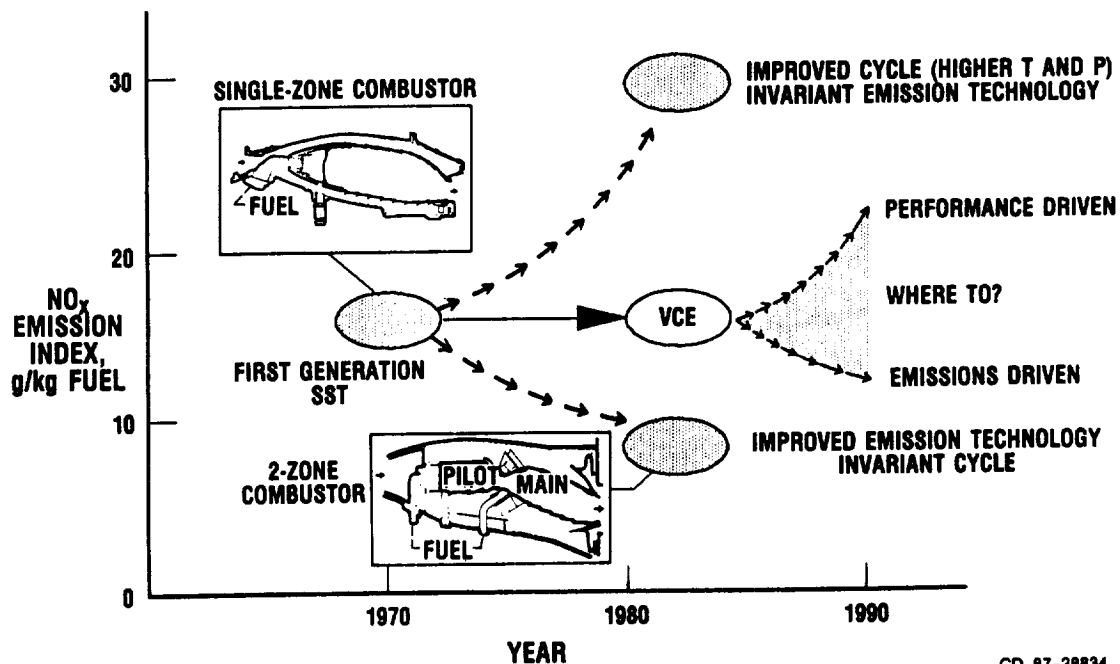
CD-87-28832

Figure 14. - Progress in SST takeoff noise reduction (Mach 2.4 to 3.2 experimental data base).



CD-87-28833

Figure 15. - Jet noise reduction concepts.



CD-87-28834

Figure 16. - Progress in SST cruise NO_x emission reduction.

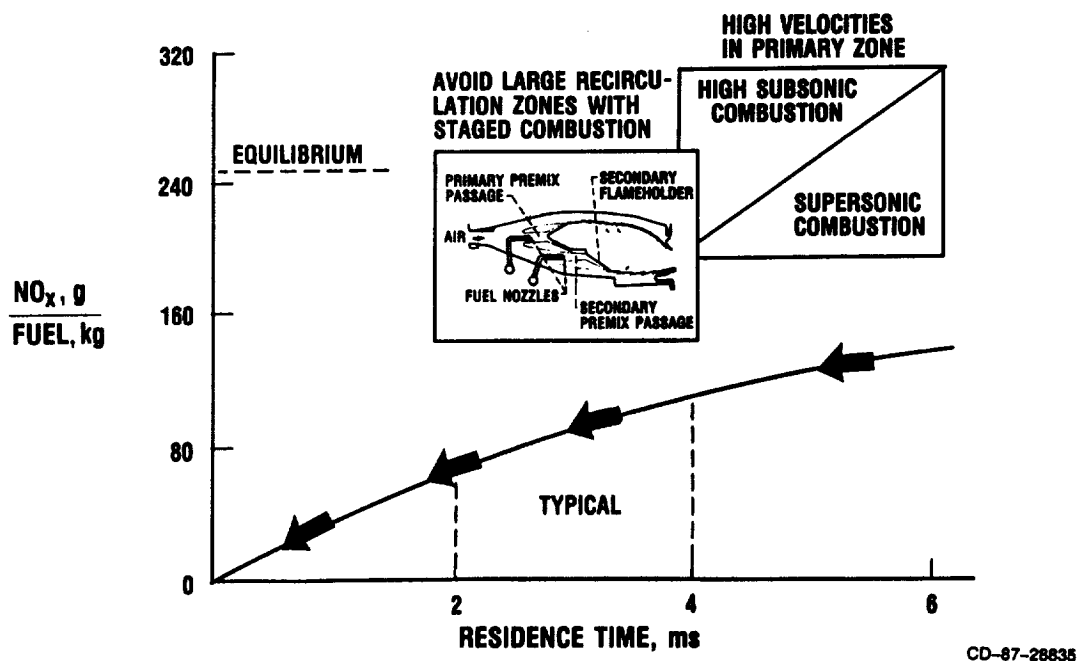


Figure 17. - NO_x emissions reduction concepts.

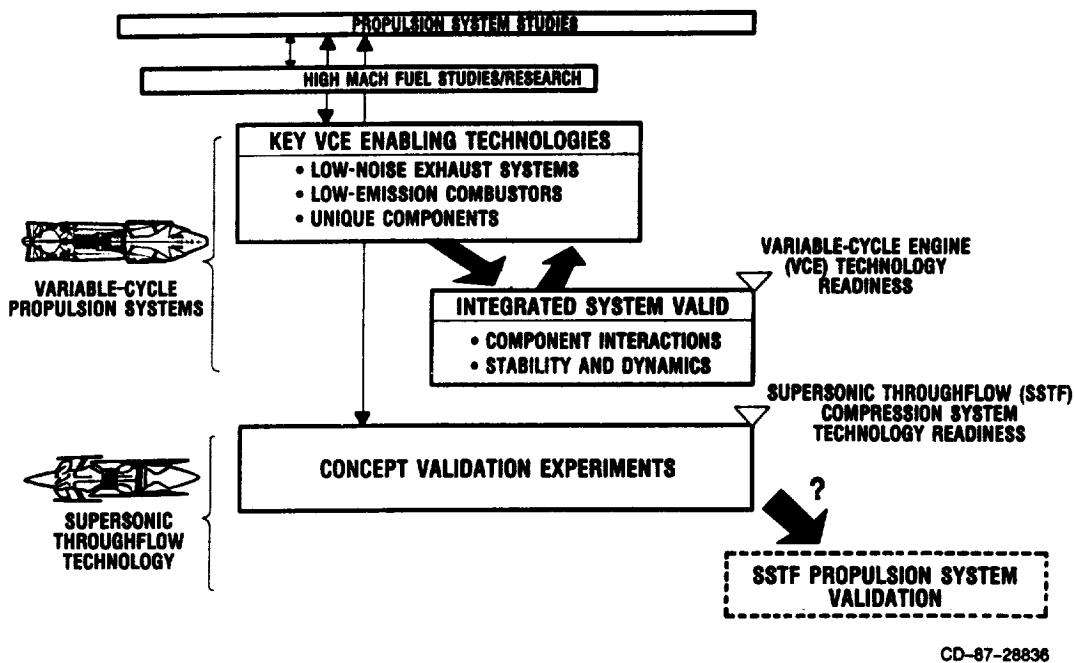


Figure 18. - Candidate high-speed propulsion program plan.

SUPERSONIC THROUGHFLOW FANS FOR HIGH-SPEED AIRCRAFT

Calvin L. Ball and Royce D. Moore

SUMMARY

This paper provides a brief overview of past supersonic throughflow fan activities; discusses technology needs; describes the design of a supersonic throughflow fan stage, a facility inlet, and a downstream diffuser; and presents the results from the analysis codes used in executing the design. Also presented is a unique engine concept intended to permit establishing supersonic throughflow within the fan on the runway and maintaining the supersonic throughflow condition within the fan throughout the flight envelope.

INTRODUCTION

Increased need for more efficient long-range supersonic flight has revived interest in the supersonic throughflow fan as a possible component for advanced high-speed propulsion systems. A fan that can operate with supersonic inlet axial Mach numbers would reduce the inlet losses incurred in diffusing the flow from supersonic Mach numbers to subsonic at the fan face. In addition, the size and weight of an all-supersonic inlet will be substantially lower than those of a conventional inlet. However, the data base for components of this type is practically nonexistent. Therefore, in order to furnish the required information for assessing the potential for this type of fan, the NASA Lewis Research Center has begun a program to design, analyze, build, and test a fan stage that is capable of operating with supersonic axial velocities from inlet to exit (refs. 1 and 2). The objectives are to demonstrate the feasibility and potential of supersonic throughflow fans, to gain a fundamental understanding of the flow physics associated with such systems, and to develop an experimental data base for design and analysis code validation.

BACKGROUND

Ferri, in 1956, was the first to point out the potential advantages of supersonic inflow compression systems for supersonic aircraft propulsion (ref. 3). In 1961, Savage, Boxer, and Erwin (ref. 4) studied the starting characteristics in transitioning to supersonic inflow by operating a transonic rotor at an overdesign tip speed. Under Air Force sponsorship in 1967, General Applied Science Laboratory (GASL), with Detroit Diesel Allison (DDA) as a subcontractor, and United Technologies Research Center (UTRC) conducted design studies and proposed turbojet engine concepts incorporating supersonic throughflow compressors (refs. 5 and 6). Also in 1967, Boxer proposed a high-bypass-ratio turbofan engine/ramjet combination with a variable-pitch supersonic inflow fan (ref. 7). In 1975, Breugelmans (ref. 8) conducted the most thorough

supersonic throughflow fan experiment to date. He tested a rotor designed for an inlet axial Mach number of 1.5. However, a mechanical failure precluded reaching the design speed, and only limited data were obtained. In 1978, Franciscus presented the results of his first analysis showing significant pay-offs of supersonic throughflow fan engines for supersonic cruise aircraft (ref. 9). Results from his later analysis, confirming potential payoffs, are presented in references 10 to 12.

TECHNOLOGY NEEDS

First, there is a need to extend and validate the computational codes for supersonic throughflows to include the associated endwall boundary-layer flows, blade row interactions, unsteady flows, and design and off-design performance predictions. In moving into the supersonic flow regime, where the data base is essentially nonexistent, applying computational methods in the design process should greatly enhance the quality of the experimental program.

There is also a need to conduct experiments to obtain data for flow physics modeling and code validation and to demonstrate subsonic performance, transition, and supersonic performance. Choke, stall, and unstart (which all occur near Mach 1 for supersonic throughflow) need to be investigated. Fan distortion tolerance and the flutter and forced response must also be experimentally evaluated in the supersonic flow regime.

CODE STATUS

The following design and analysis codes have been modified and applied to the supersonic throughflow fan, but they have not yet been validated for the supersonic flow regime with the exception of the three-dimensional parabolized Navier-Stokes code. This code was validated for duct flows.

- (1) Axisymmetric design code (ref. 13)
- (2) One-dimensional stage stacking code (ref. 14)
- (3) Axisymmetric off-design code (unpublished work by J.E. Crouse)
- (4) Quasi-three-dimensional thin shear layer Navier-Stokes code (ref. 15)
- (5) Three-dimensional passage average stage code (refs. 16 and 17)
- (6) Supersonic throughflow flutter code (ref. 18)
- (7) Three-dimensional Euler code with two-dimensional boundary layer model (ref. 19 and unpublished material by J.D. Denton, ASME Turbomachinery Institute Course on Fluid Dynamics of Turbomachinery, July 18-27, 1983)
- (8) Three-dimensional parabolized Navier-Stokes code (ref. 20)
- (9) Three-dimensional unsteady Euler code (ref. 21)

Modification of the axisymmetric design code for supersonic flow proved to be a key to the design of the supersonic throughflow fan. This code generates blade geometry which can then be analyzed by the other codes. Each of the codes will be validated as experimental results become available.

NASA SUPERSONIC THROUGHFLOW FAN

Fan Aerodynamic Design

In discussing the NASA supersonic throughflow fan design, particular attention will be given to the results obtained from the analysis codes and to how they were used to guide the design. The detailed flow physics gleaned from the codes will be highlighted.

Figure 1 depicts a supersonic throughflow fan, the facility inlet needed to accelerate the flow to supersonic velocities at the fan face, and the diffuser needed downstream to decelerate the supersonic flow leaving the fan to subsonic conditions downstream. The design fan-face Mach number is 2.0, and the exit Mach number is 2.9. The fan was designed with a constant annulus area. The design pressure ratio and tip speed were selected to be representative of those required of a turbofan engine fan operating at supersonic cruise conditions.

The following design criteria were established to guide the design of the baseline fan, the facility inlet, and the facility downstream diffuser:

- (1) Set the hub and tip radii constant throughout the fan stage to limit severe three-dimensional effects.
- (2) Apply computational two- and three-dimensional inviscid and viscous codes to the fan to (1) ensure started conditions, (2) maintain supersonic throughflow velocities throughout the compression system, (3) ensure that all shock structure is captured within the bladed passages, and (4) control suction and pressure surface gradients to minimize the strength of the internal compression and expansion wave system.
- (3) Apply computation codes to the facility inlet to (1) achieve uniform velocity distribution at the fan inlet and (2) minimize endwall boundary layers entering the fan.
- (4) Apply computation codes to the facility diffuser to (1) minimize diffusion losses through a series of controlled weak compression waves and (2) ensure started conditions.

In the design of the fan an axisymmetric design code was used to obtain initial blade shapes (fig. 2). The quasi-three-dimensional thin shear layer Navier-Stokes code was then used to analyze the design. The design was adjusted by using the axisymmetric design code, and the process was repeated until the desired loading distributions and wave patterns were achieved. In the lower half of the figure are the calculated Mach number contours from the quasi-three-dimensional thin shear layer Navier-Stokes code. The Mach number contours for the rotor and stator show that the waves off the leading edge are contained within the bladed passage. Also, the expansion waves off the suction surface tend to cancel the compression waves off the pressure-surface leading edge, thus reducing the pressure gradient along the suction surface. At the trailing edge the strength of the expansion and compression waves was minimized by controlling the loading near the trailing edge.

Figure 3 shows results obtained from a three-dimensional unsteady Euler code used to study the rotor/stator flowfield interactions with supersonic throughflow. Computer graphics were used to obtain the interactive wave patterns for a given index of the rotor relative to the stator. The picture can be thought of as a schlieren photograph with the light patterns being expansion waves and the dark patterns, compression waves. The effect of the time-dependent flowfields behind the rotor on the stator flowfield can best be seen from the next figure.

Figure 4 shows the stagnation enthalpy, and thus temperature, for two different indexes of the rotor blades relative to the stators. The interactive wave patterns within and exiting the rotor result in a time-dependent flowfield entering the stator. This unsteady flowfield relative to the stator appears to result in cyclic movement fore and aft of the stator leading-edge compression wave, which emanates from the pressure surface. Wave motion is nonlinear, with more energy being added when the shock moves forward than is subtracted when the shock moves rearward. Further analysis is needed to fully understand this phenomenon. The cyclic nature of the local temperature is apparent from the difference in the magnitudes of the local white (highest temperature) regions.

The predicted performance map for the supersonic throughflow fan (fig. 5) was derived by using a combination of codes including the off-design axisymmetric code and the quasi-three-dimensional viscous code. Presenting the performance as a function of inlet axial Mach number results in a performance map similar to subsonic/transonic fan maps. Also shown in the figure is the maximum flow condition calculated for subsonic flow and the unstart condition for the supersonic flow regime. Lines of constant incidence angles of 3° , 0° , and -3° are plotted on the map. The incidence angle range at design speed is greater than that normally predicted for subsonic/transonic fans.

The performance map presented in figure 6 is for the normal pressure ratio versus weight flow. This figure reflects the reduction in flow capacity on the supersonic throughflow side of the map as the inlet axial Mach number is increased.

Facility Variable-Inlet Nozzle Design

In order to test the fan over a range of Mach numbers and to provide transition from subsonic to supersonic flows, a variable-inlet nozzle is needed for the facility. The results obtained from a three-dimensional Euler code with an interactive boundary layer routine and from a three-dimensional parabolized Navier-Stokes code in analyzing the flowfield of the variable-inlet nozzle are presented in figure 7. The nozzle was positioned to achieve the design axial Mach number of 2.0. Good agreement existed between the codes. The codes indicated that at the design condition the flow was radially uniform at the fan face and the wall boundary layers were relatively thin.

Facility Variable Diffuser Design

A variable diffuser was designed to diffuse the flow from a fan exit Mach number of approximately 2.9 to Mach 1.8 prior to dumping the flow into the Lewis central exhaust system. The diffusion is taken primarily through two weak compression waves. The variable diffuser will be used to ease starting

conditions. A similar analysis was conducted for the diffuser as for the inlet. Again, good agreement was obtained between the Euler and the viscous codes (fig. 8).

Fan Aeroelastic Analysis

A new supersonic flutter code was developed to analyze the fan blades. This code indicated that a blade redesign was required. The results from an analysis of the flutter potential of the supersonic throughflow fan are presented in figure 9. Note the large reduction in stable operating range indicated by the supersonic throughflow flutter analysis at supersonic relative velocities. Even though the initially designed rotor blade was relatively low in aspect ratio, the analysis indicated a potential for supersonic torsional flutter. The design aspect ratio was further reduced in the final design to bring the rotor into the stable operating range.

Test Package

The layout of the supersonic throughflow fan test package is presented in figure 10. The variable-inlet nozzle and the variable downstream diffuser will be used to provide control over the fan-face Mach number and the diffusion of the supersonic fan exit velocities to subsonic conditions entering the exhaust system. Boundary layer bleed capability is provided at the inlet to the fan and the diffuser. Bleed air for the rotor inlet hub will exhaust down the centerbody and out of the inlet struts. The exit hub bleed air will exhaust out the back of the test package. Photographs of some of the test package hardware are shown in figure 11 in various phases of completion.

UNIQUE HIGH-SPEED ENGINE CONCEPT

Some of the problems raised in connection with supersonic throughflow fans for supersonic aircraft are how to "fly" such an engine system, how the fan can be made to transition to the supersonic side of the performance map and at what flight speed this would occur, how to select the design point, and unstart. The following figures present a unique engine concept that solves these problems. The transition to supersonic throughflow within the fan component is made while the airplane is on the runway. This concept's many advantages will be discussed.

A conceptual design for a supersonic throughflow turbofan high-speed engine is shown in figure 12 for a Mach 3 design condition. However, the basic concept also applies to turbojet and airturboramjet cycles. The concept incorporates a short annular inlet with a variable capture and throat area to ease transitioning to supersonic throughflow within the fan on the runway and to maintain supersonic flow at the fan face throughout the flight envelope. Located downstream of the fan are annular supersonic/subsonic diffusers, one in the bypass duct and the other in the core inlet duct. The core inlet also features a variable capture area to help in flow matching and in optimizing performance. The flow entering the core compressor is diffused to subsonic conditions throughout the flight envelope. However, the duct flow is diffused subsonically for only subsonic flight Mach numbers and remains supersonic for

supersonic flight. The variable-geometry features in the diffuser and nozzle are intended to achieve these goals. Duct burning may or may not be required. Some of the advantages of this concept are no forward transmission of fan noise on takeoff, ease of meeting pressure ratio requirements for takeoff and aircraft acceleration through Mach 1, potentially good subsonic cruise performance for overland operation, and, it is hoped, no variable geometry in the fan rotor.

The flowpath shown for the turbofan is consistent with the Mach 3 design. The design flight Mach number has a significant effect on the fan geometry. The effect of flight Mach number on the fan geometry is illustrated in figure 13. For the Mach 3 condition, as shown in figure 12, the fan hub/tip ratio is about 0.7. As the flight Mach number is increased, the passage height decreases and the hub/tip ratio increases. At Mach 5 the fan hub/tip ratio is above 0.8. The reduction in the fan tip diameter in relation to the inlet diameter is adequate to achieve the desired change in throat area with acceptable axial translation of the nozzle. By limiting the reduction in fan diameter, the gooseneck is minimized and the strength of the expansion and compression waves is reduced during supersonic operation. To achieve the low hub/tip ratio typical of transonic fans while achieving satisfactory supersonic operation would require a prohibitive gooseneck.

In order to examine how the inlet would be configured over the flight envelope, a climb flight path was established. The assumed flight path is shown in figure 14. Mach 0.3 was assumed for takeoff, transition to supersonic flight Mach numbers at 35 000 ft, and Mach 3.0 cruise at 70 000 ft.

The fan performance map (fig. 15) shows the startup, transition, and flight operating lines. The design point was assumed to be Mach 3.0 cruise with a fan-face Mach number of 2.0 and a pressure ratio of approximately 2.5, consistent with that derived from mission analysis studies conducted by Franciscus for a Mach 3.0 transport aircraft. These same studies indicated fan pressure ratio requirements of approximately 3.3 and 3.0 for takeoff and aircraft transition to supersonic flight Mach numbers, respectively. The inlet is set to the lower design fan-face Mach number during takeoff and transition to maximize the flow and to minimize inlet bleed requirements. Predicted maximum subsonic flow before startup is shown along with the predicted unstart boundary on the supersonic side of the performance map. Note the large supersonic flow range. The startup method is to increase speed to approximately 80 percent and then close the inlet nozzle slightly. In so doing, it is predicted that the normal shock will transition through the fan. The concept requires a low load line to keep the fan out of stall during subsonic operation, even though the fan incidence will be high just prior to transitioning. As the normal shock passes through the fan, the operating point will jump to the supersonic side along the 80 percent speed line. The inlet will be adjusted to achieve the desired fan-face Mach number, and the speed will then be increased to takeoff conditions. The reverse procedure would be employed during landing.

Figure 16 shows the inlet geometry configurations for Mach 0 to 0.3, 1.0, 2.0, and 3.0 (the assumed design point). From Mach 0 to 0.3 the inlet cowl is extended forward so that the flowpath will converge to accelerate the air to Mach 1.0 at the throat. The throat area is set relative to the fan inlet area to achieve the desired fan-face Mach number, in this case 1.5. As the flight Mach number is increased to supersonic conditions, a bow wave is formed off the

inlet spike. As the Mach number becomes supersonic behind the shock, the inlet cowl is set to control the position of the internal reflected wave. At the design point of Mach 3.0 the cowl is positioned such that the leading-edge bow wave is attached to the cowl lip. The throat is opened up at Mach 2.0 and 3.0 flight to achieve the desired fan-face Mach number.

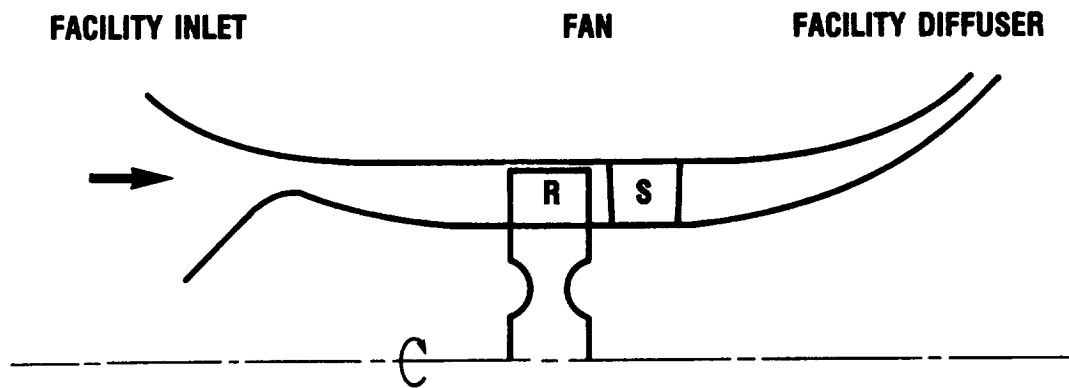
CONCLUDING REMARKS

In summary, mission studies conducted by Franciscus have shown significant benefits from supersonic throughflow fans. The design and analysis conducted on the NASA supersonic throughflow fan shows promise for such a stage. However, an experiment is strongly needed to demonstrate transition and to validate the computational codes. Off-design analysis is continuing with emphasis on the use of Chima's quasi-three-dimensional viscous code. Rotor/stator interactions will be investigated at off-design conditions by using Whitfield's code. The fan is now in fabrication, and testing is scheduled for the end of 1989.

REFERENCES

1. Wood, J.R., et al.: Application of Advanced Computational Codes in the Design of an Experiment for a Supersonic Throughflow Fan Rotor. ASME Paper 87-GT-160, May 1987 (NASA TM-88915).
2. Schmidt, J.F., et al.: Supersonic Through-Flow Fan Design. AIAA Paper 87-1746, June 1987 (NASA TM-88908).
3. Ferri, A.: Problems Related to Matching Turbojet Engine Requirements to Inlet Performances as Function of Flight Mach Number and Angle of Attack. Air Intake Problems in Supersonic Propulsion, J. Fabri, ed., Agardograph No. 27, AGARD, France, 1956, pp. 48-62.
4. Savage, M.; Boxer, E.; and Erwin, J.R.: Resume of Compressor Research at the NACA Langley Laboratory. J. Eng. Power, vol. 83, no. 3, July 1961, pp. 269-285.
5. Lipfert, F.W.: Supersonic Axial Velocity Compressor Study, Vol. 1, AFAPL-TR-67-68, 1967. (Avail. NTIS, AD-383675.)
6. Gadbois, S.E.; and Dunn, B.M.: Investigation of the Supersonic Through-Flow Compressor Concept, Vol. II, AFAPL-TR-67-60-VOL-2, 1967. (Avail. NTIS, AD-815963.)
7. Boxer, E.: The Variable-Pitch Supersonic Inflow Compressor and Its Application in a Hypersonic Engine. Conference on Hypersonic Aircraft Technology, NASA SP-148, 1967, pp. 401-416.
8. Breugelmans, F.A.E.: The Supersonic Axial Inlet Component in a Compressor. ASME Paper 75-GT-26, Mar. 1975.
9. Franciscus, L.C.: Supersonic Through-Flow Fan Engines for Supersonic Cruise Aircraft. NASA TM-78889, 1978.

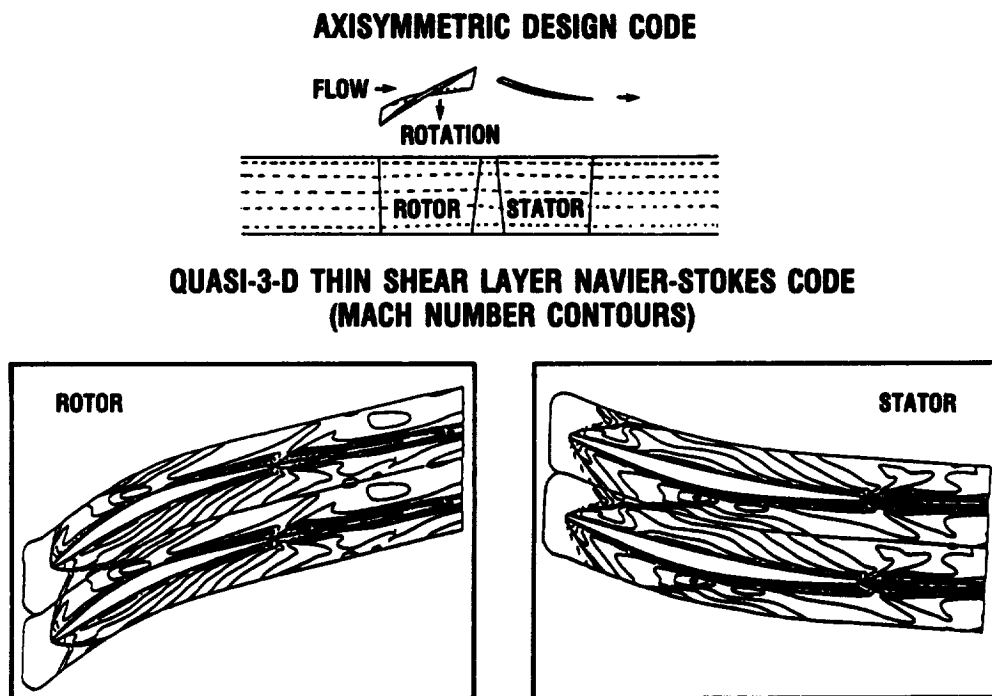
10. Franciscus, L.C.: The Supersonic Fan Engine - An Advanced Concept in Supersonic Cruise Propulsion. AIAA Paper 81-1599, July 1981 (NASA TM-82657).
11. Franciscus, L.C.: Supersonic Fan Engines for Military Aircraft. AIAA Paper 83-2541, Oct. 1983 (NASA TM-83499).
12. Franciscus, L.C.: The Supersonic Through-Flow Turbofan for High Mach Propulsion. AIAA Paper 87-2050, June 1987 (NASA TM-100114).
13. Crouse, J.E.; and Gorrell, W.T.: Computer Program for Aerodynamic and Blading Design of Multistage Axial-Flow Compressors. NASA TP-1946, 1981.
14. Steinke, R.J.: STGSTK - A Computer Code for Predicting Multistage Axial Flow Compressor Performance by a Meanline Stage Stacking Method. NASA TP-2020, 1982.
15. Chima, R.V.: Explicit Multigrid Algorithm for Quasi-Three-Dimensional Viscous Flows in Turbomachinery. J. Propulsion Power, vol. 3, no. 5, Sept.-Oct. 1987, pp. 397-405.
16. Adamczyk, J.J.; Mulac, R.A.; and Celestina, M.L.: A Model for Closing the Inviscid Form of the Average-Passage Equation System. J. Turbomachinery, vol. 108, no. 2, Oct. 1986, pp. 180-186.
17. Celestina, M.L.; Mulac, R.A.; and Adamczyk, J.J.: A Numerical Simulation of the Inviscid Flow Through a Counterrotation Propeller. J. Turbomachinery, vol. 108, no. 2, Oct. 1986, pp. 187-193.
18. Ramsey, J.K.; and Kielb, R.E.: A Computer Program for Calculating Unsteady Aerodynamic Coefficients for Cascades in Supersonic Axial Flow. NASA TM-100204, 1987.
19. Denton, J.D.: An Improved Time-Marching Method for Turbomachinery Flow Calculations. J. Eng. Power, vol. 105, no. 3, July 1983, pp. 514-524.
20. Buggeln, R.C., et al.: Development of a Three-Dimensional Supersonic Inlet Flow Analysis. NASA CR-3218, 1980.
21. Whitfield, D.L., et al.: Three-Dimensional Unsteady Euler Solutions for Propfans and Counter-Rotating Propfans in Transonic Flow. AIAA Paper 87-1197, June 1987.



PRESSURE RATIO 2.45
 AXIAL MACH NUMBER
 INLET 2.0
 EXIT 2.9
 ROTOR TIP SPEED 1500 ft/sec

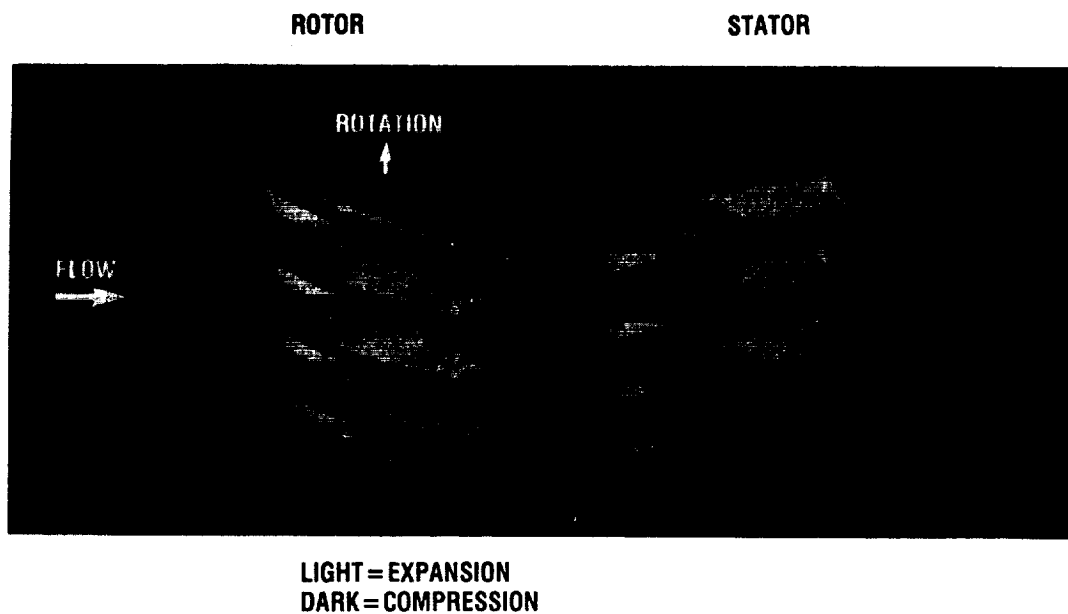
CD-87-29431

Figure 1. - Supersonic throughflow fan.



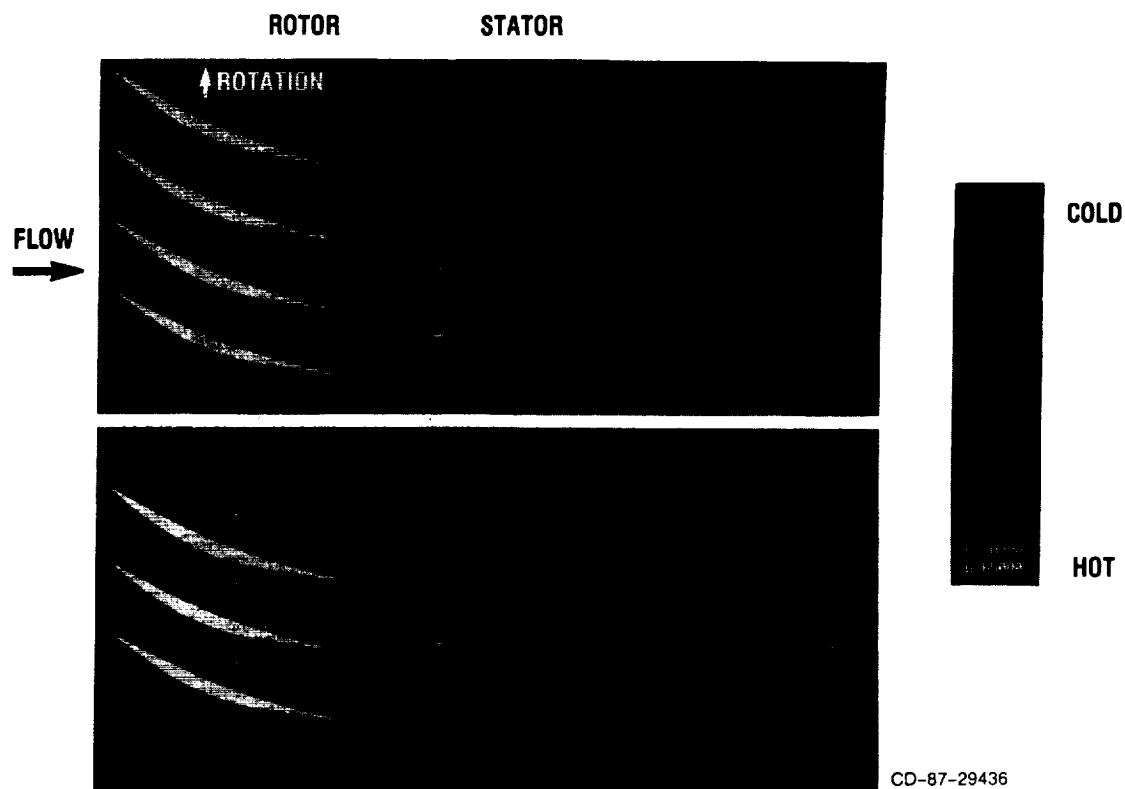
CD-87-29434

Figure 2. - Design procedure.



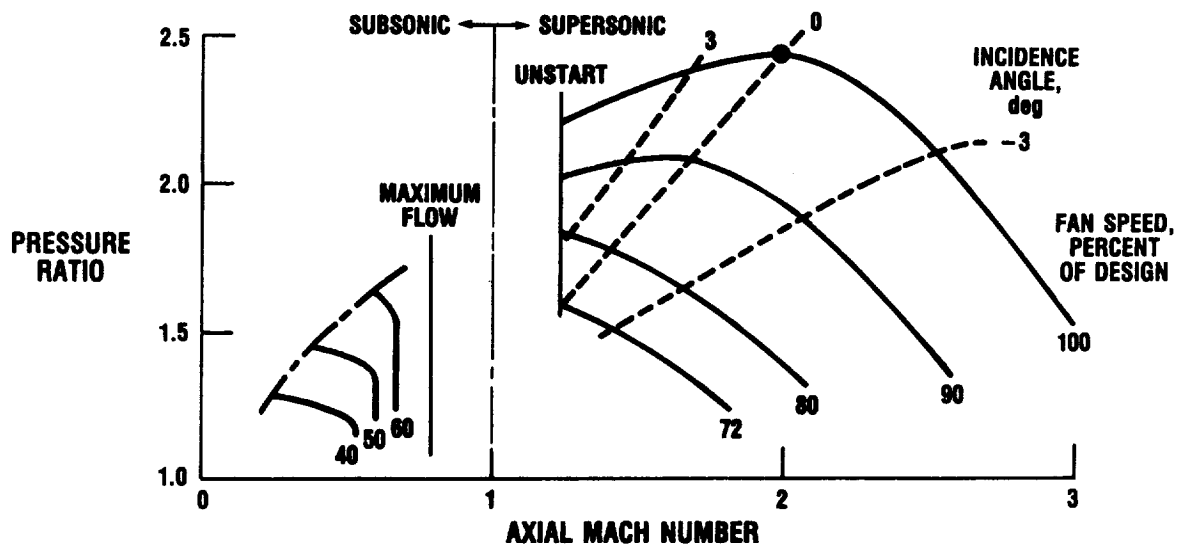
CD-87-29435

Figure 3. - Three-dimensional unsteady Euler code (interactive wave patterns).



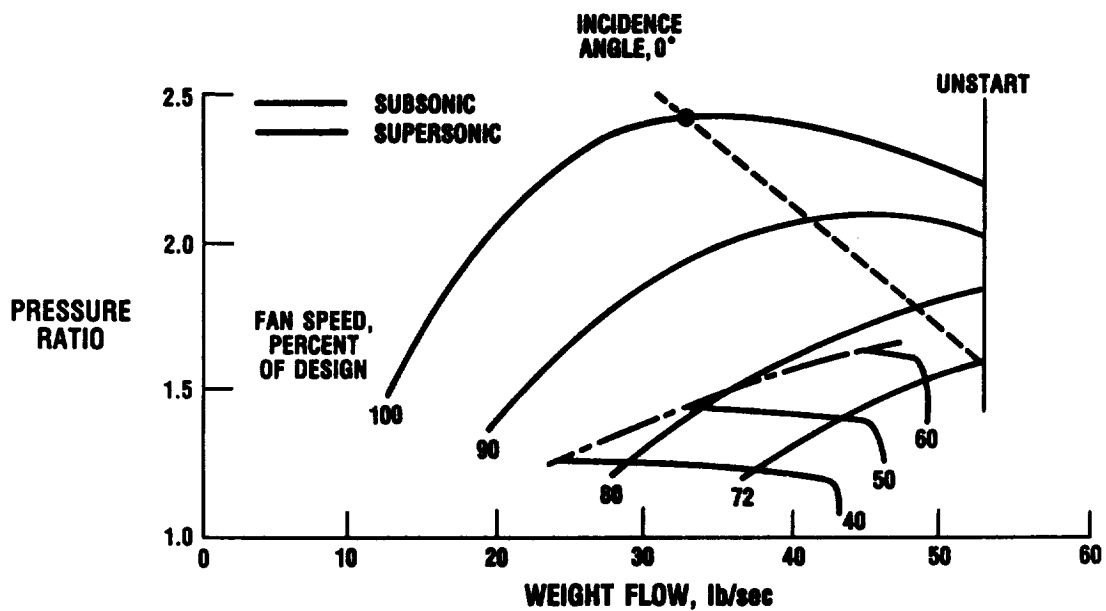
CD-87-29436

Figure 4. - Three-dimensional Euler code (stagnation enthalpy).



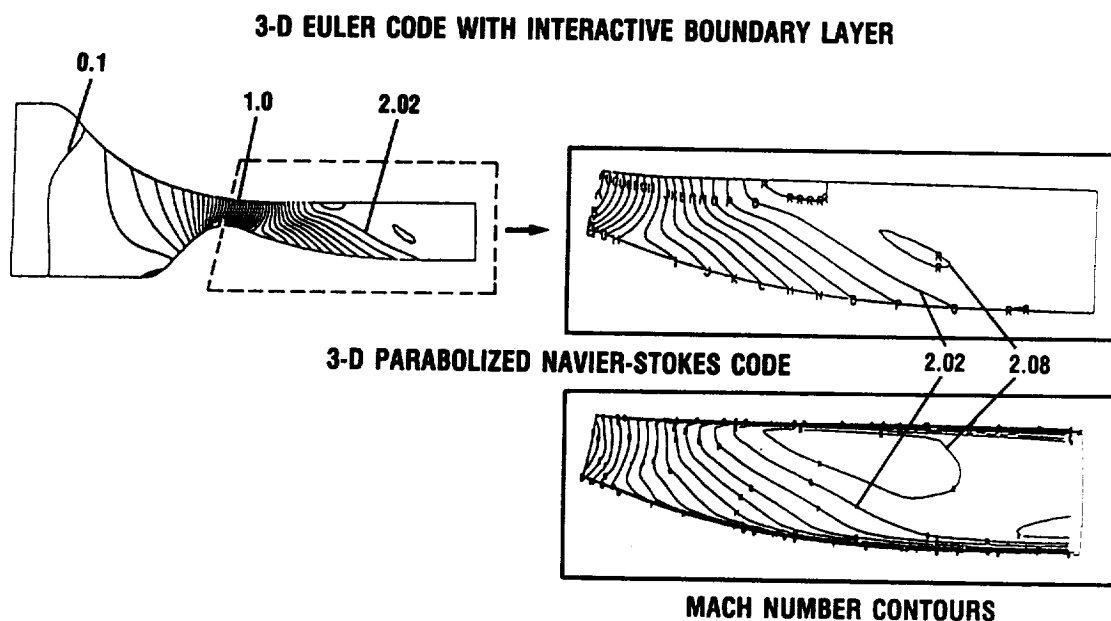
CD-87-29437

Figure 5. - Predicted fan performance map (pressure ratio versus axial Mach number).



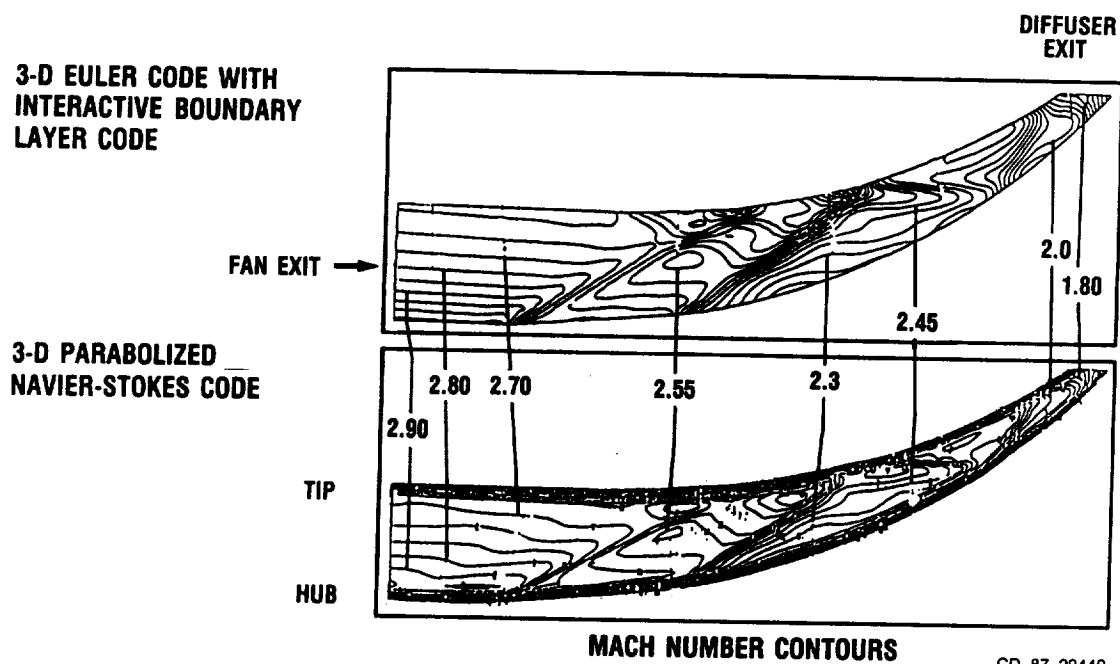
CD-87-29438

Figure 6. - Predicted fan performance map (pressure ratio versus weight flow).



CD-87-29439

Figure 7. - Facility variable-inlet nozzle.



CD-87-29440

Figure 8. - Facility variable diffuser.

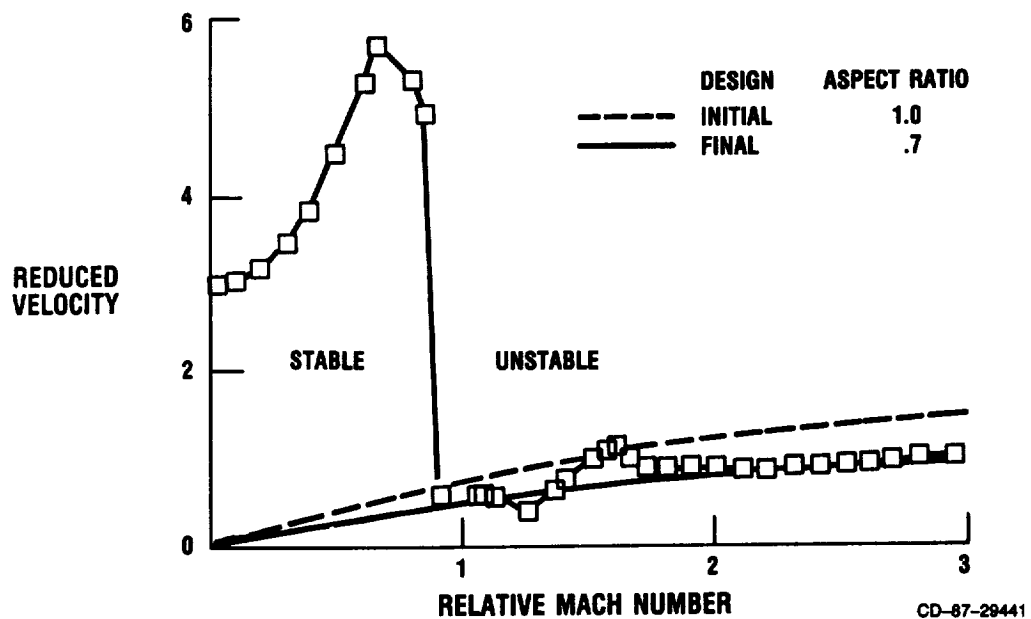
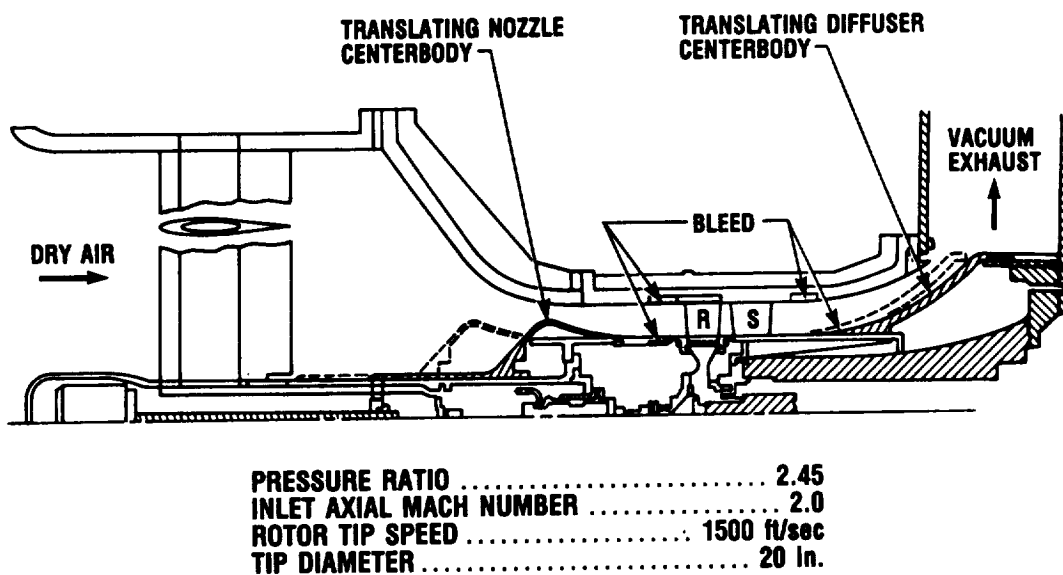


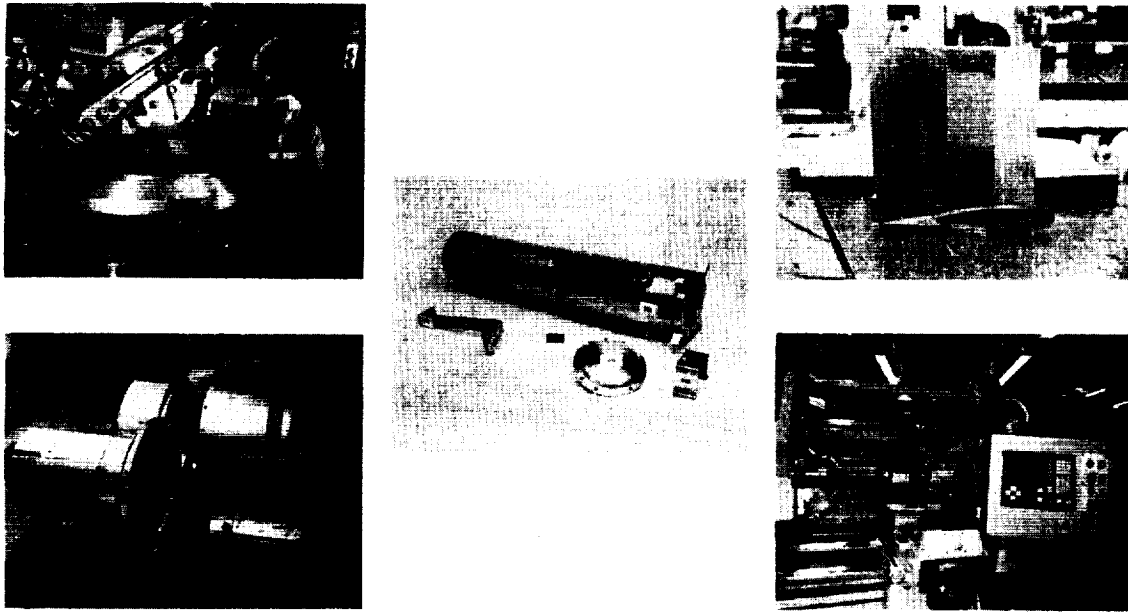
Figure 9. - Aeroelastic analysis of supersonic throughflow fan torsional flutter.



CD-87-29442

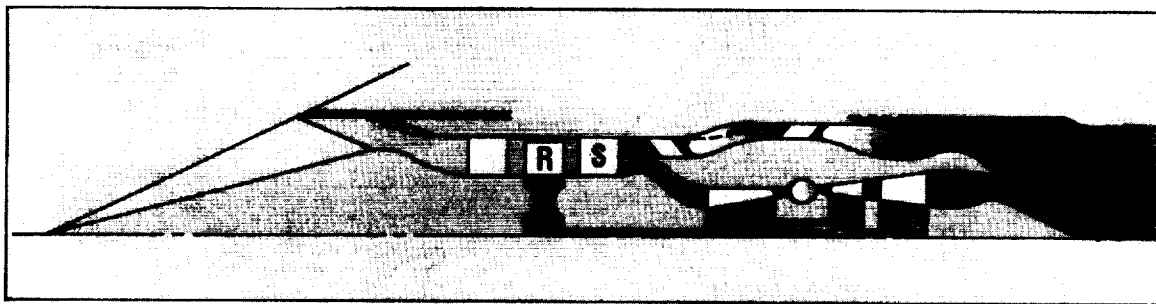
Figure 10. - Test package.

ORIGINAL PAGE
BLACK AND WHITE PHOTOGRAPH



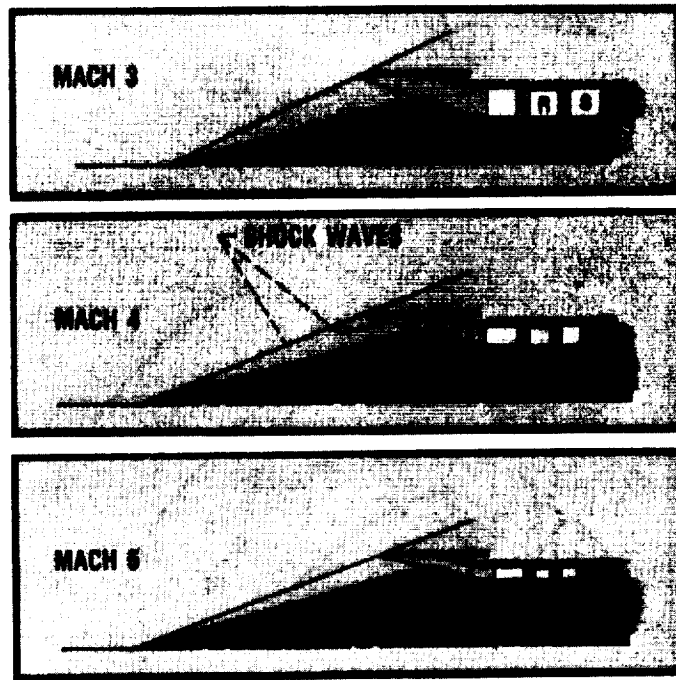
CD-87-29443

Figure 11. - Hardware fabrication.



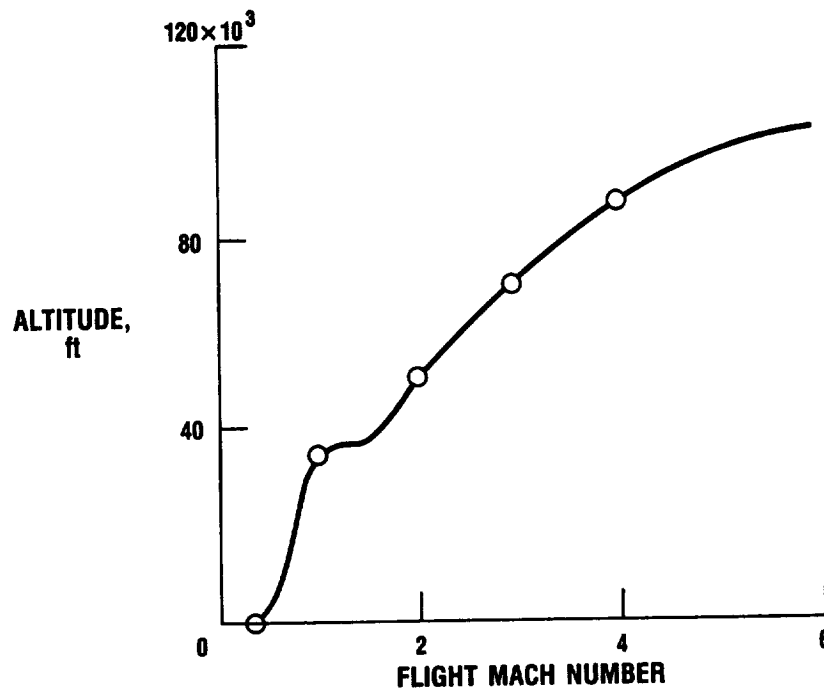
CD-87-29445

Figure 12. - Supersonic throughflow turbofan high-speed engine concept (Mach 3 design).



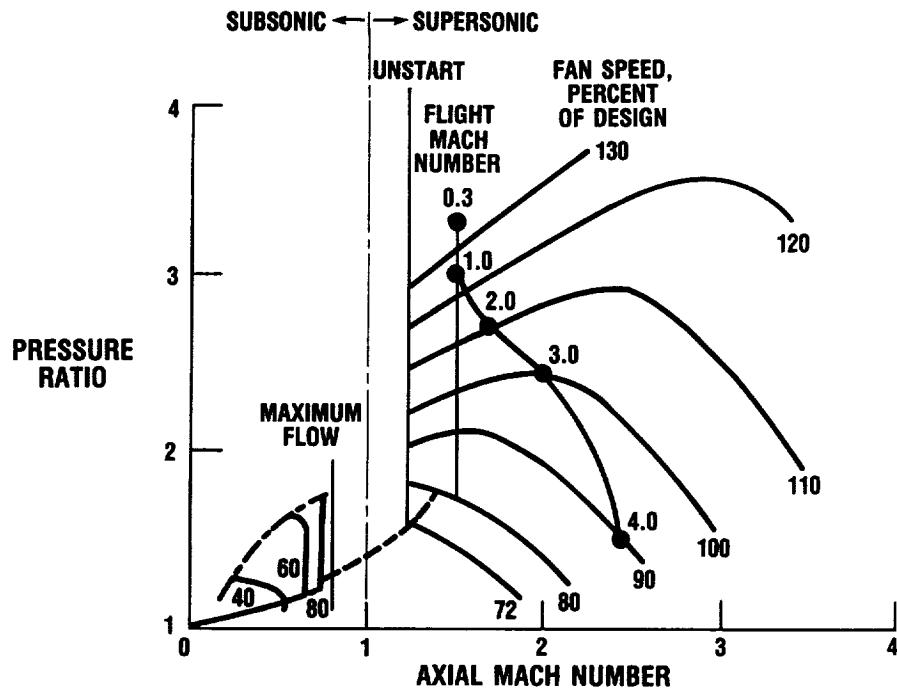
CD-87-29446

Figure 13. - Various flight Mach number designs for supersonic throughflow turbofan.



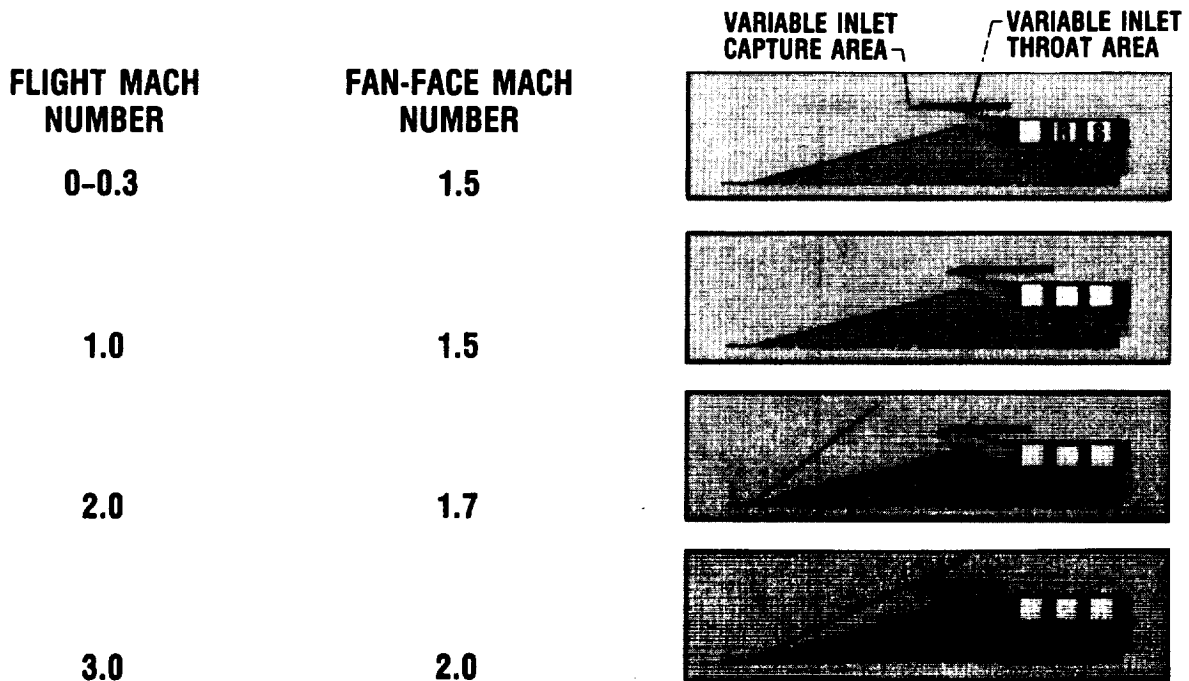
CD-87-29448

Figure 14. - Assumed high-speed aircraft climb flight path.



CD-87-29449

Figure 15. - Supersonic throughflow turbofan fan operating line.



CD-87-29447

Figure 16. - Inlet geometry configurations for supersonic throughflow turbofan.

HIGH-SPEED INLET RESEARCH PROGRAM AND SUPPORTING ANALYSIS

Robert E. Coltrin

SUMMARY

The technology challenges faced by the high-speed-inlet designer are discussed by describing the considerations that went into the design of the Mach 5 research inlet. It is shown that the emerging three-dimensional viscous computational fluid dynamics (CFD) flow codes, together with small-scale experiments, can be used to guide larger scale full inlet systems research. Then, in turn, the results of the large-scale research, if properly instrumented, can be used to validate or at least to calibrate the CFD codes.

INTRODUCTION

The design of a relatively simple-looking high-speed inlet is a complex task which presents many technology challenges. The inlet design process is much more difficult than the single development of an on-design configuration. The actual design is an iterative process in which inlet designers use their expertise to develop an overall system that will meet mission goals. The final design not only must represent a configuration that provides high performance at the design condition, but also must (1) function at off-design, (2) maintain acceptable shock stability for safety, (3) have minimum bleed requirement, (4) employ a reasonable variable geometry system, (5) allow boundary layer control systems and ducting, (6) provide required engine/combustor airflow, (7) be lightweight, (8) minimize drag, (9) provide for unstart and restart, (10) minimize sealing requirements, (11) incorporate additional systems for takeoff and landing and for control functions, and (12) be compatible with other engines and modules and with propulsion/airframe integration. Many designs that can provide very high internal performance for the design condition become unacceptable when the overall requirement is considered. Thus, in the past, most inlets have been designed by a few inlet experts using empirical methods to lay out the initial inlet lines, and then relying on their expertise based on years of experience (and a little "magic" where required) to accomplish the majority of the inlet design effort.

The state of the art of inlet design technology still relies on these same experts using their empirical methods. Method of characteristics codes are used to lay out the inviscid inlet lines at design conditions. Boundary-layer codes are then exercised, and the inviscid inlet lines are corrected for the boundary layer displacement thickness. However, there are new tools becoming available that the experts can use to help guide the inlet research once the lines are defined. These tools are the emerging three-dimensional viscous flow codes. This paper will use the Mach 5 inlet research program to show how these three-dimensional codes, together with small-scale research, can be used to guide the larger scale inlet systems research. The results of this large-scale

research, if properly instrumented, can then be used to validate or at least to calibrate the emerging CFD codes.

SYMBOLS

H_{c1}	height of cowl lip, m
M	Mach number
P_T/P_{REF}	local total pressure, ratioed to free-stream total pressure
X	horizontal length, m
Y	vertical length, m
α	angle of attack relative to first inlet ramp, deg

Subscripts:

I	local
∞	free stream

DISCUSSION

In the third paper of this session, Propulsion Challenges and Opportunities for High-Speed Transport Aircraft, Strack has described the importance of the inlet to high-speed aircraft (see also refs. 1 to 3), and has also described some of the important inlet characteristics as a function of cruise Mach number. Figure 1 shows some additional inlet features as a function of cruise speed. This is a simple generic plot of altitude versus Mach number with photographs of four typical research inlets. These photographs are placed on the plot in the altitude/Mach number arena in which they would be applicable.

In the low supersonic speed range up to Mach 2, inlets tend to be simple fixed-geometry configurations which employ entirely external compression. Normal shock inlets, like the HiMAT (Highly Maneuverable Aircraft Technology) research inlet (ref. 4) shown on the left, are often used. As discussed by Strack in this session, aircraft operating above Mach 2 must employ mixed compression in order to maintain high efficiency. Inlets in the Mach 2 to 4 range are usually pod mounted; therefore axisymmetric configurations are usually favored, but two-dimensional configurations can be considered. The second photograph from the left is of a variable-diameter centerbody (VDC) inlet that was studied as part of the Supersonic Cruise Aircraft Research Program in the 1970's (ref. 3). In the Mach 4 to 6 range, inlets tend to be more integrated into the airframe. Because of this integration, two-dimensional configurations are favored, but axisymmetric or half-axisymmetric configurations can be considered. A two-dimensional Mach 5 research inlet model is shown in the third photograph from the left. Inlets for Mach 6+ aircraft must be fully integrated into the airframe, and are therefore normally two-dimensional configurations.

A Langley Research Center inlet model which employs both ramp and sidewall compression is shown in the photograph at the right. This type of inlet was tested as part of the Langley scramjet program, which is described in the sixth paper of this session, Hypersonic Propulsion Research.

The remainder of this paper will describe the technique that was used for the design of the Mach 5 research inlet (third photograph from the left). This technique is generically representative of that used for any typical high-speed inlet design.

The Mach 5 inlet resulted from a program that was initiated in 1980 by NASA Langley, with NASA Lewis as a partner. The research study was a contractual program with Lockheed-California as prime contractor and Pratt & Whitney as subcontractor. The purpose of this study was to define an aircraft capable of sustained high-speed cruise in the Mach 5 arena, and specifically, to lay out the aircraft in enough detail so that the propulsion system and its integration with the aircraft could be defined. The final aircraft resulting from this study is shown in figure 2 and discussed in reference 5. The aircraft would employ four propulsion modules (two under each wing), with the inlets integrated into the wings but with the leading edge in the free stream. The propulsion system chosen for this aircraft is an over-under turbojet plus ramjet system with two-dimensional dual flow inlets and nozzles.

The various modes of operation for the over-under turbojet plus ramjet propulsion system are illustrated in figure 3. There are two flow paths through the propulsion system with a turbojet engine in the upper flow path and a ramjet engine in the lower flow path. The inlet and the nozzle each have a flow control diverter, which must be properly positioned at each point in the flight envelope to provide the required flow to each engine. At subsonic flight speeds, the turbojet engine only powers the aircraft, with cold flow through the ramjet duct. Near Mach 1 the ramjet is ignited, initially to help fill the large nozzle base area. Both systems are operating until the aircraft approaches Mach 3, where the ramjet engine then provides the total power. Between Mach 2.5 and 3 the turbojet spools down, and at Mach 3 the upper duct of the system is totally closed off. The turbojet engine is then in a sealed environment that can be cooled. From Mach 3 to cruise speed, the aircraft is powered by the ramjet engine only. Thus, this system takes maximum advantage of the turbojet engine in the low-speed range where it is most effective, and the ramjet engine in the high-speed range where it is most effective.

Once this propulsion system was defined, it was realized that there were many technology challenges associated with its design. One of the most challenging was the cruise performance and operating characteristics of the inlet. Could an inlet be designed that would provide sufficient performance, and how much boundary-layer bleed would be required to obtain this performance and maintain normal shock stability? This bleed question was crucial since excessive bleed drag could make the whole concept unacceptable. Therefore, the Mach 5 inlet program was initiated. The objective of the program was to design, analyze, build, and test a large-scale inlet for the cruise (ramjet) configuration and to define its performance and operating characteristics. Even though it was realized that the off-design operation and the transition from turbojet to ramjet operation posed many more challenges, it was decided that the make-or-break challenge was at cruise. If the cruise challenges could be met, the off-design challenges would be addressed in a later model.

The nozzle presents a similar set of design and off-design problems that would need to be addressed.

The aerodynamic design (cross section) of the Mach 5 inlet is shown in figure 4. The X- and Y-dimensions are nondimensionalized to the cowl lip height. Mach numbers in the various flow regions are shown for the cruise (Mach 5) condition. At cruise conditions, free-stream airflow is at an angle of 9° relative to the first ramp surface. The resulting first compression wedge of 9° and Mach 5 free-stream conditions gives a local Mach number of 4.1 on the first inlet wedge. The Mach conditions are successively reduced by additional wedges to obtain Mach 3.1 on the final external ramp surface. A cowl shock, additional distributed compression, and a terminal shock are employed for internal supersonic compression. The inlet was designed by using a conventional method-of-characteristics (MOC) approach to lay out the initial inlet inviscid lines. A boundary-layer code was then exercised, and the inviscid inlet lines were corrected for the boundary-layer displacement thickness. One of the main driving factors in the design was length minimization to reduce the weight as much as possible. In order to minimize length, the design calls for the cowl shock to be cancelled at the inlet shoulder, followed by a strong cowl generated compression fan. The design throat Mach number is 1.6 inviscidly, which is reduced to approximately 1.2 when boundary layer corrections are made. The design compression split is about 85 percent external (with four ramps) and 15 percent internal.

Once the inlet lines were established, the next step was to design the location and size of the boundary-layer bleed systems. This is where the inlet expert normally enters the picture. It is well known that on a two-dimensional basis, bleed will be required to control the oblique shock/boundary-layer and normal shock/boundary-layer interactions. But how much and where? And on a three-dimensional basis, how can the glancing sidewall shock/boundary-layer interactions and three-dimensional corner flow be controlled?

Figure 5 graphically demonstrates the glancing shock/boundary-layer interaction phenomena. The figure shows a simple 10° compression wedge installed across the entire width of the NASA Lewis 1- by 1-Foot Supersonic Wind Tunnel, which is operating at Mach 3. This wedge could represent the ramp of an inlet, and the tunnel wall the inlet sidewall. The oblique shock from this wedge interacts with the wall boundary layer, which has a thickness of approximately 1 in. The surface oil film shows flow patterns in the boundary layer. The oil flows indicate that the boundary layer on the wall is turned ahead of the oblique shock and follows the 27° shock angle rather than the 10° wedge angle that the free-stream flow follows. This boundary-layer flow is turned because of the pressure rise through the oblique shock wave, which is fed forward through the subsonic portion of the boundary layer. A large portion of the boundary-layer flow aft of the shock is also turned in a direction along the oblique shock angle. The low-energy boundary layer that has been turned ahead of the oblique shock migrates along the oblique shock wave and then interacts with the floor boundary layer, which could simulate an inlet cowl. This interaction produces a large three-dimensional glancing sidewall/corner shock wave interaction, which in an inlet would most likely cause an unstart.

Figure 6 shows a three-dimensional parabolized Navier-Stokes (PNS) solution for the configuration shown in figure 5. The code used for this analysis is PEPSIS, which is the supersonic code in the PEPSI series (described by

Abbott, Anderson, and Rice in session 3, and discussed in ref. 6). The graphics have been mechanized to show the surface velocity vectors, which should then be directly comparable to the experimental oil flow results of figure 5. By comparing the flow features of figure 5 with those of figure 6 (see also ref. 6), it can be seen that the PEPSIS results are qualitatively similar to the experimental results. These near-wall results gave us confidence to look at the PEPSIS results in midstream.

The lower portion of figure 7 shows the PEPSIS results for a very similar test case as was shown in figure 5. The results shown here are the analytical simulations (ref. 6) of an experiment conducted by Bogdonoff (refs. 7 to 9). Again, a simple 10° wedge spanned a wind tunnel operating at Mach 2.94. The wind tunnel wall was in the front plane of the paper and has been removed so that the flow patterns can be seen. In each plane cut across the flow path, the secondary velocity vectors in that plane are shown. The results are shown from the front wall to the centerline of the tunnel. Near the tunnel centerline, the wedge-generated oblique shock wave can be seen (horizontal line in the flow vectors) at each flow station. But as the shock wave glances along the sidewall boundary layer, a large interaction region can be seen. The velocity vectors indicate that the flow in this interaction region is along the ramp surface toward the sidewall, then up the sidewall forming a vortex. It can also be seen that, as in the case near the sidewall, the interaction region away from the sidewall extends well ahead of the oblique shock. The upper portion of figure 7 demonstrates what this glancing shock/sidewall interaction phenomenon means to an inlet. The boundary layer proceeding downstream on the sidewall is turned ahead of the oblique shock wave, and this low-energy flow migrates along the shock wave, eventually arriving at the inlet cowl lip. If the inlet employs multiple oblique shock waves, as does the Mach 5 inlet, this flow migration has a cumulative effect, with large regions of low-energy flow sweeping up the sidewall ready to be captured by the cowl.

The excellent comparison of the PEPSIS analysis with the Bogdonoff data (ref. 10), gave us confidence to next apply PEPSIS to the Mach 5 inlet. The result is shown in figure 8. The figure shows total pressure distributions on cross planes at several stations in the inlet aft of the cowl lip. Only half planes are shown, since flow is symmetrical. The cowl lip shock can be seen as a horizontal line in each cross plane near the inlet centerline. Near the sidewall it can be seen that the low energy flow that has swept up the sidewalls ahead of the cowl lip is captured by the cowl and continues to grow. At a station about halfway between the cowl lip and the ramp shoulder, the code predicts a very large flow separation.

Figure 9 shows a more detailed view of the last cross plane of figure 8. The figure shows the total pressure distribution for the entire cross section, and the secondary velocity vectors have been superimposed. The cowl oblique shock can be seen in midstream. The flow in the corner flows up the sidewall and across the cowl in vortex fashion. A separated zone is indicated. As can be seen, the flow within a relatively simple-looking two-dimensional inlet is highly three-dimensional. In fact, the only location in the cross plane where the flow may be nearly two-dimensional is along the vertical centerline. But even here potential flow problems are developing.

The midstream ramp boundary layer, which started at zero thickness at the leading edge of the ramp, is very thick at this station. If this boundary layer would be allowed to proceed down the inlet to where the cowl shock (or

later the normal shock) would interact with it, a separation would most likely occur. In order to analyze this phenomenon, which potentially could involve subsonic flow and separated zones, full Navier-Stokes (NS) codes must be employed.

A two-dimensional Navier-Stokes analysis of the Mach 5 inlet is shown in figure 10. This analysis was carried out by W. Rose and E. Perkins of Rose Engineering and Research, consultants to Lockheed on the Mach 5 project. The analytical code was developed by Kumar of the NASA Langley Research Center. The Mach number distribution for the no-bleed case shown on the left represents the area encompassed by the large (single cross-hatched) box in the inlet sketch at the top. The Y (vertical) axis has been expanded by 3 1/2 times that of the X (horizontal) axis. It can be seen that there is a massive separation on the ramp surface, most likely caused by the interaction of the cowl lip generated shock. This plot is for one instant in the time marching solution. Because of the separation, the inlet cannot swallow the required airflow, and the inlet is on its way to unstart. No started stable solution was obtained. The Mach contours on the right, with 17 percent bleed (4 percent near the ramp shoulder and 13 percent in the normal shock region) distributed through the inlet, represent the area in the inlet throat (double cross-hatched) region in the sketch. The bleed prevents the larger separation seen at the left. The cowl lip shock is not quite cancelled at the ramp shoulder, and normal shock has been stabilized in the inlet. This is a steady solution. These analyses indicate that the experimentalist will have a difficult task in providing a high-performance inlet while maintaining low inlet bleed.

These results from the PNS and NS codes have been used to locate and size bleed systems for the Mach 5 inlet and to locate instrumentation. An isometric sketch of the model to be tested in the NASA Lewis 10- by 10-Foot Supersonic Wind Tunnel is shown in figure 11. A good test model can often be more complex than the actual flight configuration, since in the research and development process many additional parameters are investigated to arrive at an optimum configuration. This is especially true if both steady state and the very important transient phenomena are to be investigated. The Mach 5 inlet is such a model, as it incorporates remotely variable ramp geometry, main duct mass-flow control, and 15 bleed exit plugs. The model is extensively instrumented with static pressure taps, total pressure rakes, translating flow angularity probes, and dynamic pressure transducers. It is a very large model, with an overall model length of about 20 ft. The cowl lip height is 16 in., with a capture width of 16 in. The acceleration plate is 100 in. wide.

The requirement for the acceleration plate is shown in figure 12. The Lewis 10- by 10-Foot Supersonic Wind Tunnel has a maximum Mach number capability of 3.5, and the inlet has a design of Mach 5. In order to overcome this tunnel Mach number deficiency, the inlet is mounted beneath the large accelerator plate or expansion plate. The plate is then operated at negative angle of attack, and by taking advantage of the resulting expansion fan, the correct Mach number of 4.1 is generated on the first ramp (fig. 4). This "accelerator plate" test technique duplicates the actual inlet internal flow conditions with the exception that the initial oblique shock (Mach 5 and 9° wedge) is not present. This oblique shock would lay just above the sideplate leading edges and just above the cowl lip so that no shock/boundary-layer interactions are lost. What is lost is the pressure reduction through this initial oblique shock. The data will be corrected for this total pressure loss.

Figure 13 shows two photographs of the Mach 5 inlet model. The model is made of stainless steel, except for the accelerator plate, which is aluminum. On the right, a side view of the inlet is shown with the sidewall removed to show the variable ramp mechanisms. A single, large pair of actuators raises and lowers all movable sections of the ramp simultaneously. The inlet duct is entirely two-dimensional, from leading edge to mass-flow control plug. All bleed regions are compartmented to prevent recirculation. Collapsible bellows are used to duct the compartmentalized ramp bleed through the ramp plenum.

Figure 14 demonstrates the impact of the PEPsIS analysis on the model instrumentation and bleed systems. As a result of the PEPsIS analysis indicating boundary-layer migration from sidewall shock/boundary-layer interactions, modifications were made to the original model design. The dark band on the sidewall indicates the location of bleed holes added to the sidewall. The plenum behind this bleed region is compartmented to avoid reverse bleed. This bleed will allow the low energy boundary layer to be bled off before it is captured by the cowl. The dark area on the cowl corners indicate the location of cowl bleed. This will permit the removal of the low energy flow once it has been captured by the cowl. Not shown is the extensive two-dimensional bleed regions that were added to the ramp and cowl surfaces as a result of the Kumar code results.

The large size of this inlet makes it adaptable to the installation of more instrumentation than is possible on small-scale models. Figure 14 indicates the additional instrumentation that was added on the forward ramp and sidewall to map the flow migration phenomena and to provide code validation data.

At present, the testing of this inlet is scheduled for the summer of 1988. However, a small-scale model of the inlet was tested in the NASA Lewis 1- by 1-Foot Supersonic Wind Tunnel, and some typical results are shown in figure 15. This model had capture dimensions of 1.6 by 1.6 in. and duplicated the large-scale inlet geometry back to the cowl lip and ramp shoulder. Aft of these stations, the inlet was opened up to allow inlet starting. The schlieren photo on the lower left is for design flow conditions, with the inlet accelerator plate at the negative angle of attack relative to free-stream conditions. The ramp tip is off the picture to the left, but the Mach line generated by the expansion plate can be seen in the upper left portion of the photograph. The dark horizontal line is the leading edge of the sideplates. (For this photograph the metal sideplates have been changed to plexiglass sideplates.) The oblique shock waves from the second, third, and fourth ramps, as well as the cowl shock, can be seen. The cowl shock hits ahead of the ramp shoulder, and the resulting reflection can be seen. The surface oil film photograph at the right is for an off-design Mach number (Mach 3 on the first ramp). For the condition shown in the photograph, the inlet was unstarted, as indicated by the ramp flow near the cowl lip station. Upstream of this location the sidewall boundary-layer flow migration that results from the boundary-layer/glancing shock interaction can be seen, as well as the almost vertical migration ahead of the terminal shock location. This kind of small-scale research gives us confidence that the acceleration plate test technique is valid, and that the flow migration patterns are about what the codes predicted.

The aerodynamic design approach used to reduce the weight of the Mach 5 inlet is to decrease the length over which the distributed cowl compression intersects the ramp surface. This is accomplished by increased curvature of

the cowl and results in a large pressure rise over a short distance on the ramp. These large pressure gradients with large approach boundary layers can result in separation. A simple experimental program was conducted to study ramp bleed configurations to control the interaction of the pressure gradient and boundary layer in this region. Figure 16 shows that for this test, the cowl was simulated by a contoured compression plate, and the ramp by the tunnel wall (photograph on the upper right in the figure). The tunnel wall incorporated a bleed plate in which various bleed patterns could be studied. A translating probe was used to survey the flow field. When no bleed was employed, the boundary layer separated as expected. The left figure shows that when a distributed porous bleed configuration was attempted, separation was still present. This was the result of recirculation of the high-pressure airflow in the aft part of the bleed plenum, reversing the flow in the forward part of the plenum. When the bleed plenum was compartmentalized, as shown on the right, the boundary layer was successfully controlled, and a healthy boundary layer exited this compression fan zone. Thus, a bleed pattern is in hand for use in the initial large-scale testing. Thus, maybe for the first time, three-dimensional PNS analysis, two-dimensional NS analysis, and small-scale research experiments have all been used to guide the design and test planning of a large-scale inlet system at high speed.

Figure 17 shows the benefits to be obtained from the Mach 5 inlet test program. The main goals of this test plan are (1) to determine overall inlet performance and bleed requirements, and (2) to provide data for code validation and for the development of inlet design codes. The validation goals, as shown in the left column, are to validate or at least to calibrate the codes that have been used to pre-analyze the inlet. The operational goals shown on the right are equally important but have not been covered in this paper. This test program will validate the overall use of the design approach described in this paper, as well as the acceleration plate test technique. The amount and location of required inlet bleed will be determined, together with the tradeoff between bleed and performance. The unstart/restart characteristics, as well as the control signals required to control the overall inlet, will also be determined.

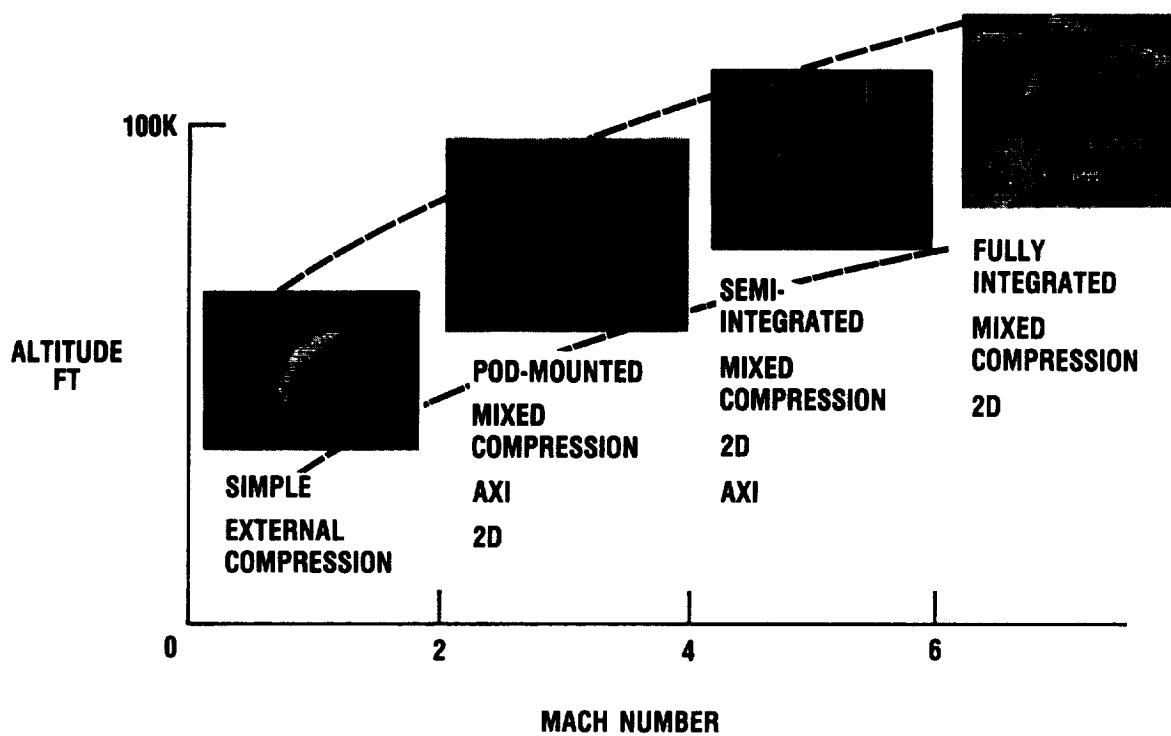
CONCLUDING REMARKS

The purpose of this paper was to describe the state-of-the-art inlet design and analysis techniques. These design techniques still rely on the traditional method-of-characteristics codes, with boundary-layer corrections. Thus, inlet experts are still the heart of the design process. However, the emerging three-dimensional viscous flow codes can now be used to guide the research in such areas as understanding local three-dimensional flow fields, placing and sizing bleed zones, and placing instrumentation. As the three-dimensional analytical codes become more validated and user friendly, they will become more and more a part of the design process. But the availability of a set of true three-dimensional viscous design codes that will generate the inlet surfaces on the basis of desired inlet flow properties is still a long way over the horizon. Even for the analytical codes, the inlet designer is continuously conceiving configurations that the existing codes cannot quite handle, and therefore they must be modified and revalidated. Thus, the few inlet experts will be required in the design loop for many years. The trick is to take maximum advantage of what each offers. The Mach 5 program may be the first large-scale high-speed inlet program to take maximum advantage of the inlet expert,

the tried and the true method-of-characteristics design code, the best available three-dimensional viscous flow codes, and small-scale experiments to guide the design and test planning of the inlet. We anxiously await the Mach 5 experimental results to determine the payoff of this design approach.

REFERENCES

1. Aircraft Propulsion. NASA SP-259, 1970.
2. Aeronautical Propulsion. NASA SP-381, 1975.
3. Aeropropulsion 1979. NASA CP-2092, 1979.
4. Neumann, H.E.; Povinelli, L.A.; and Coltrin, R.E.: An Analytical and Experimental Study of a Short S-Shaped Subsonic Diffuser of a Supersonic Inlet. AIAA Paper 80-0386, Jan. 1980 (NASA TM-81406).
5. Watts, J.D., et al.: Mach 5 Cruise Aircraft Research. Langley Symposium on Aerodynamics, NASA CP-2398, Vol. II, S.H. Stack, ed., 1985, pp. 285-304.
6. Anderson, B.H.: Three-Dimensional Viscous Design Methodology For Advanced Technology Aircraft Supersonic Inlet Systems. AIAA Paper 84-0194, Jan. 1984. (NASA TM-83558.)
7. Oskam, B.; Vas, I. E.; and Bogdonoff, S. M.: Mach 3 Oblique Shock Wave/Turbulent Boundary Layer Interactions in Three-Dimensions. AIAA Paper 76-336, July 1976.
8. Oskam, B.; Vas, I. E.; and Bogdonoff, S. M.: Oblique Shock Wave/Turbulent Boundary Layer Interactions in Three-Dimensions at Mach 3.0. AFFDL-TR-76-48-PT-I, June 1976.
9. Oskam, B.; Vas, I. E.; and Bogdonoff, S. M.: Oblique Shock Wave/Turbulent Boundary Layer Interactions in Three-Dimensions at Mach 3.0. AFFDL-TR-76-PT-II, Mar. 1978.
10. Anderson, B. H.; and Benson, T. J.: Numerical Solution to the Glancing Sidewall Oblique Shock Wave/Turbulent Boundary Layer Interaction in Three-Dimensions. AIAA Paper 83-0136, January 1983. (NASA TM-83056.)



CD-87-29935

Figure 1. - High-speed cruise inlets.



CD-87-28920

Figure 2. - Mach 5 cruise aircraft study.

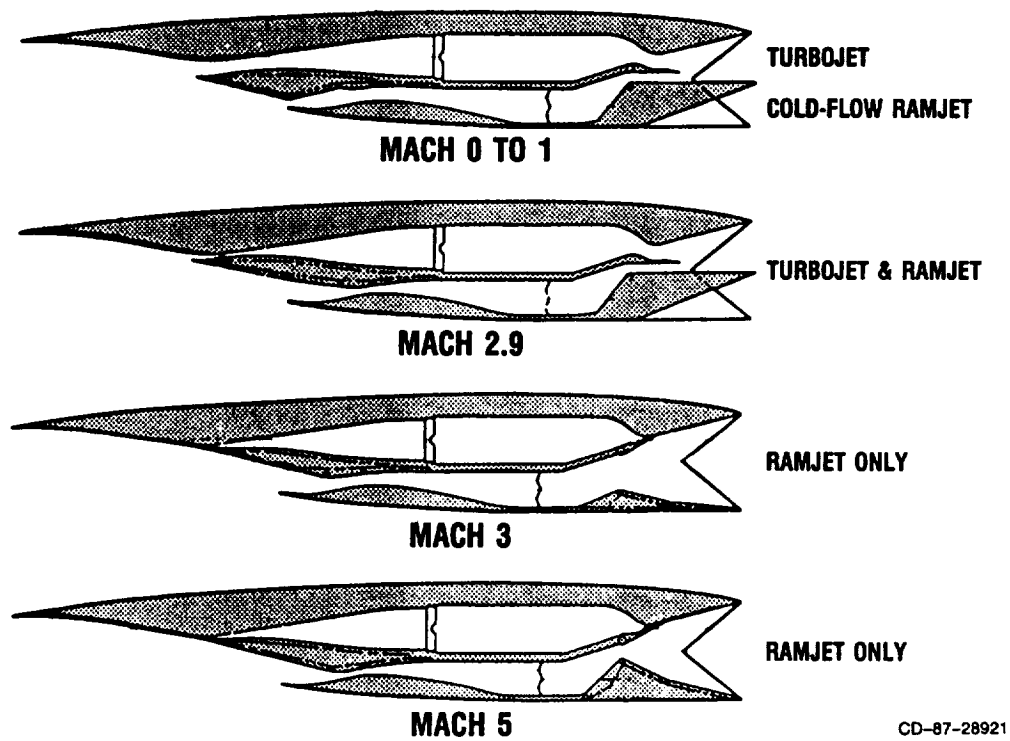
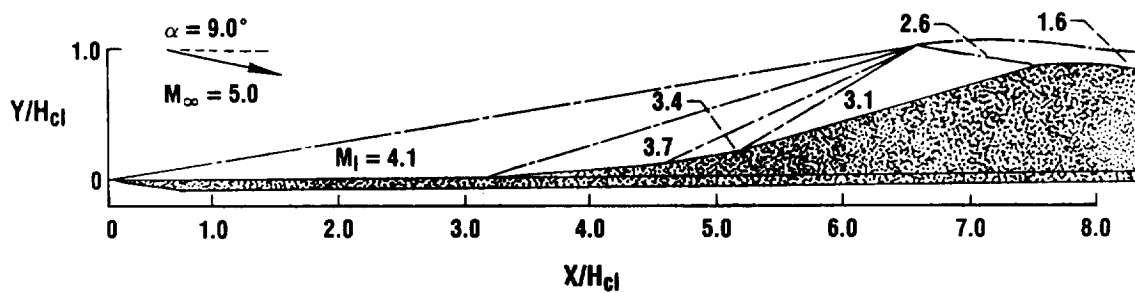
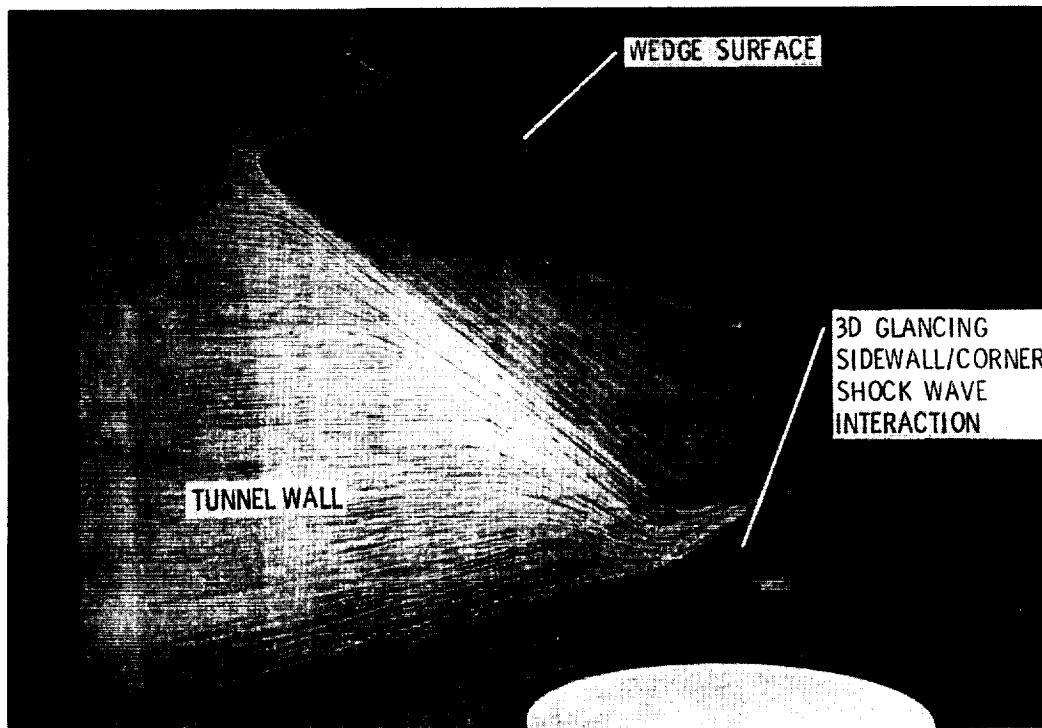


Figure 3. - Over-under turbojet/ramjet.



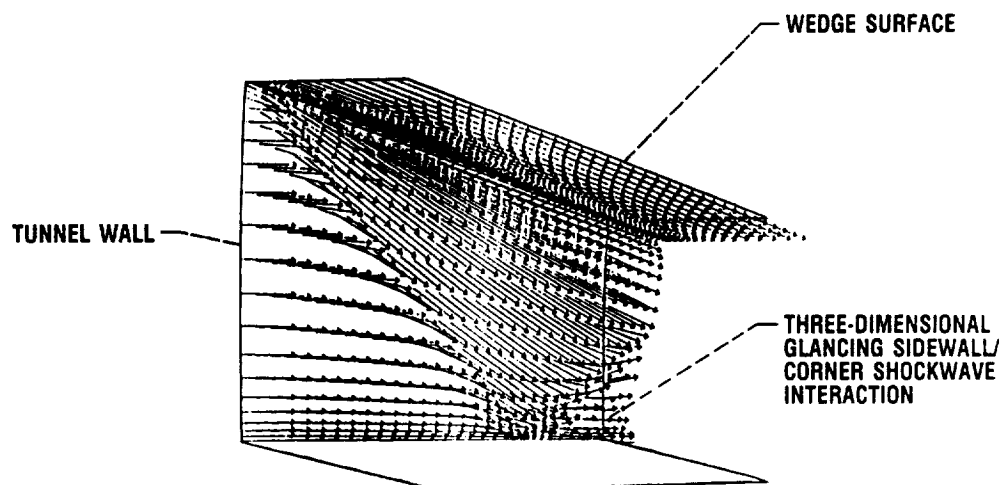
CD-87-28923

Figure 4. - Mach 5 inlet aerodynamic design configuration.



CD-87-28926

Figure 5. - Three-dimensional sidewall shock interaction (experimental surface oil film patterns).



CD-87-28927

Figure 6. - Three-dimensional sidewall shock interaction (PEPSIS analytical surface oil film patterns).

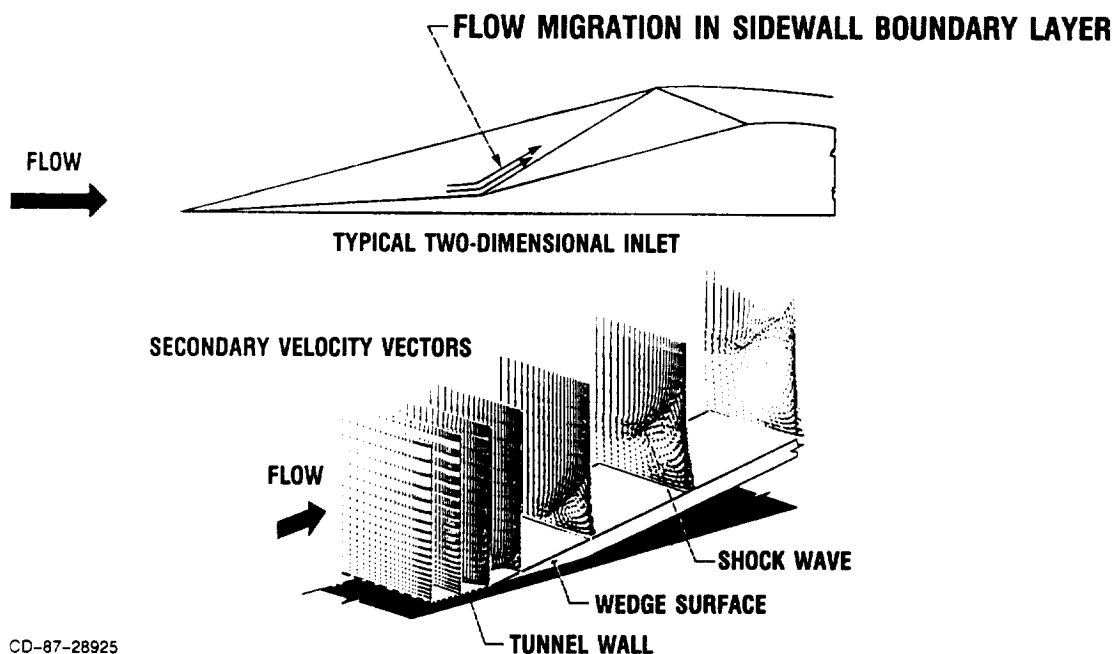


Figure 7. - Sidewall boundary-layer/glancing shock wave interaction - PEPSIS analysis.

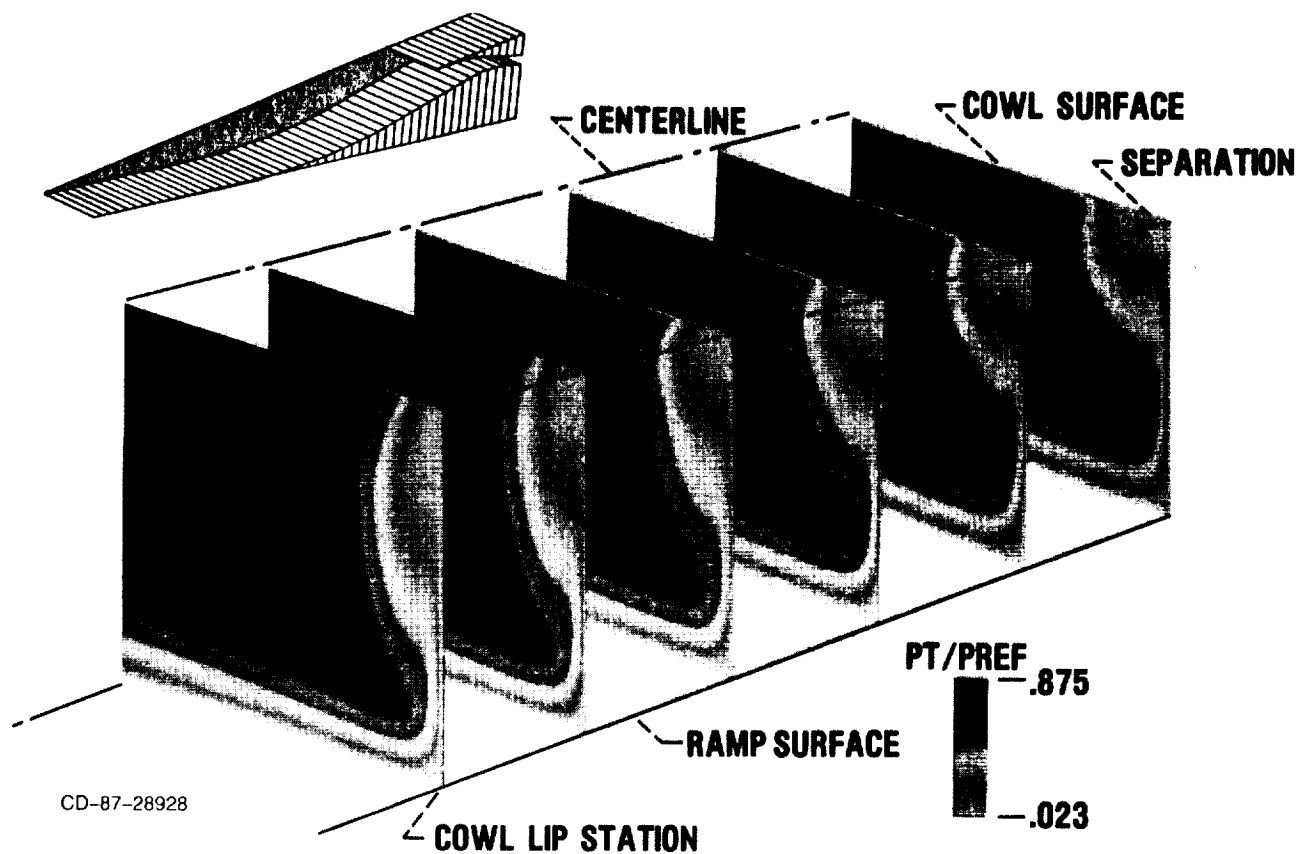


Figure 8. - PEPSIS analysis of Mach 5 inlet (total pressure distribution).

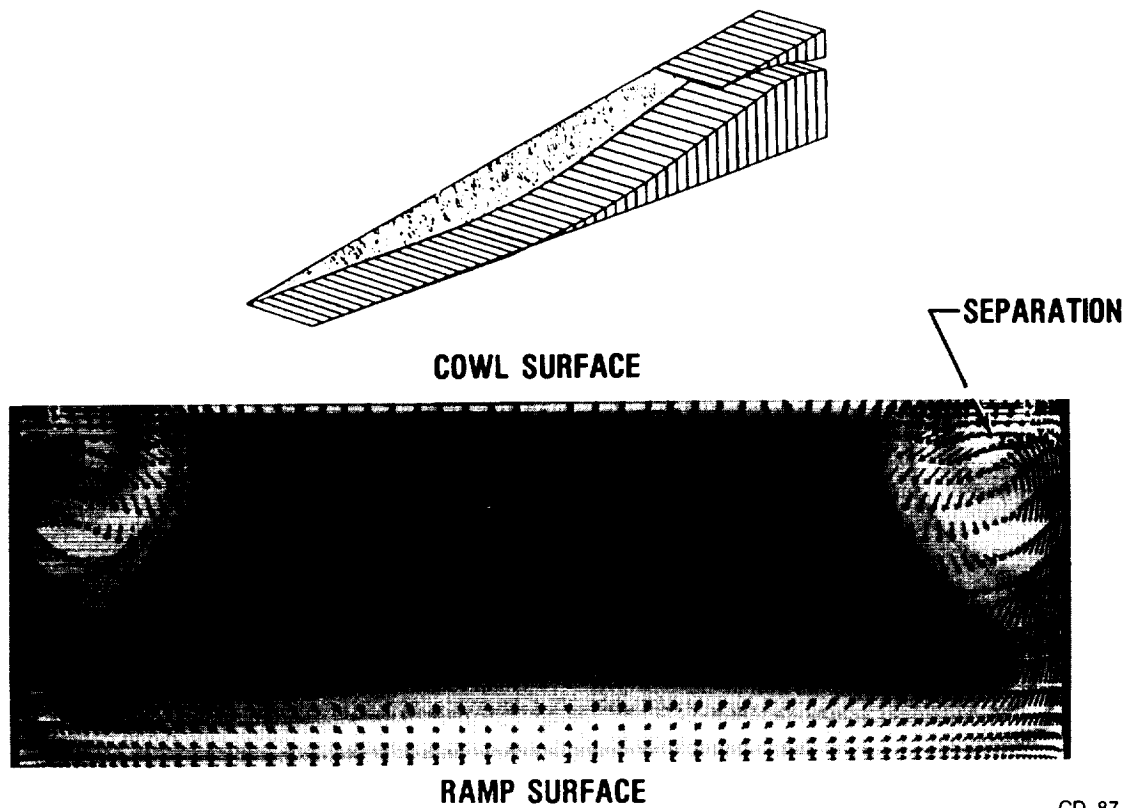


Figure 9. - Detailed PEPSIS analysis (total pressure).

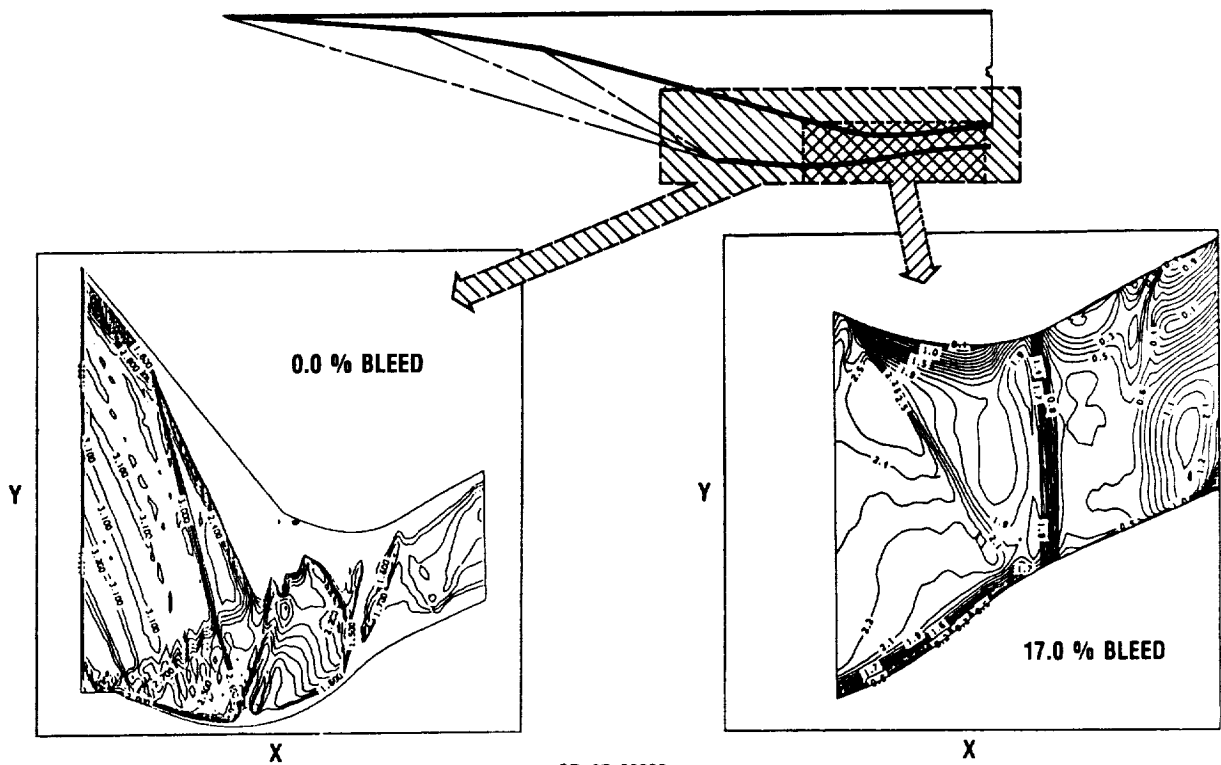
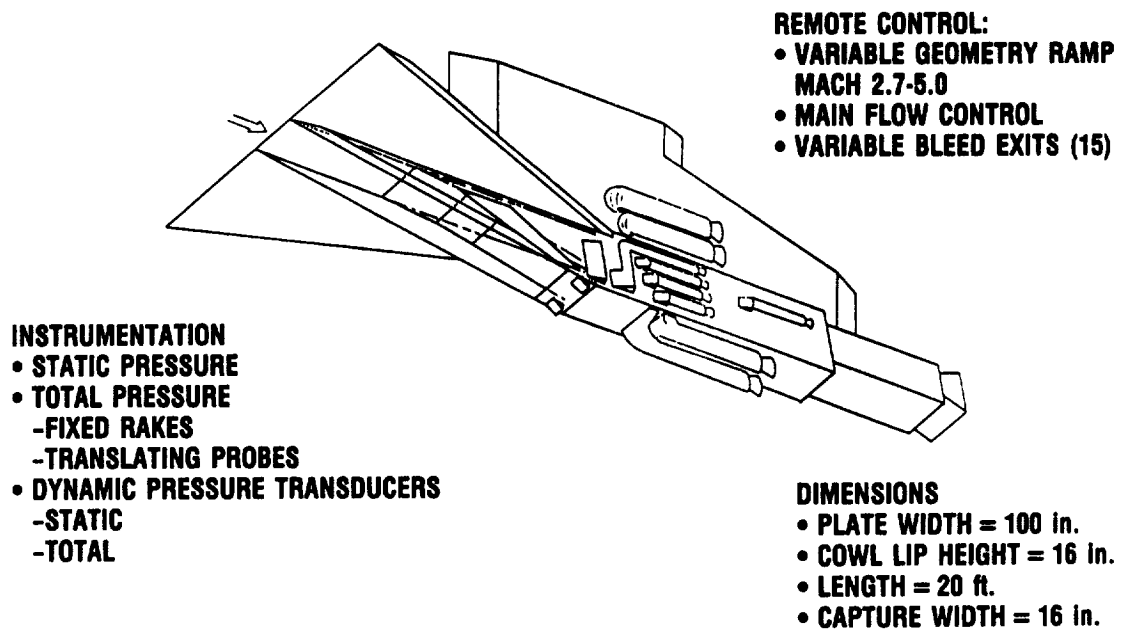
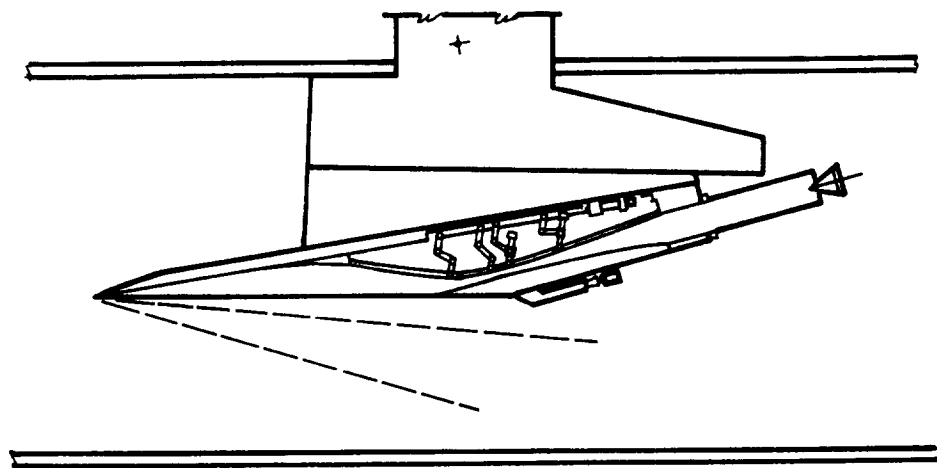


Figure 10. - Two-dimensional Kumar code analysis: Mach number contours.



CD-87-28933

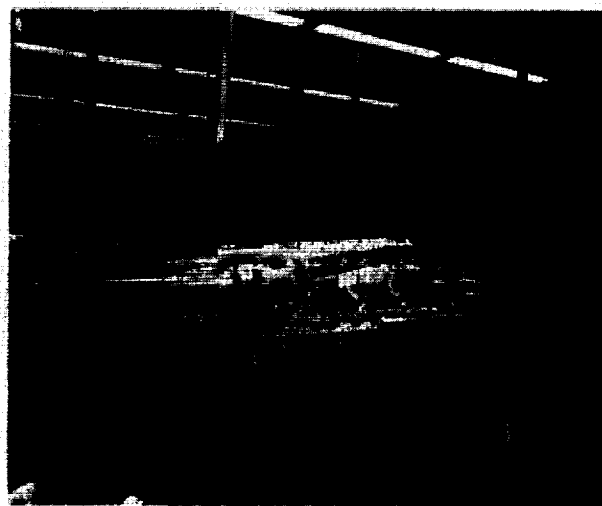
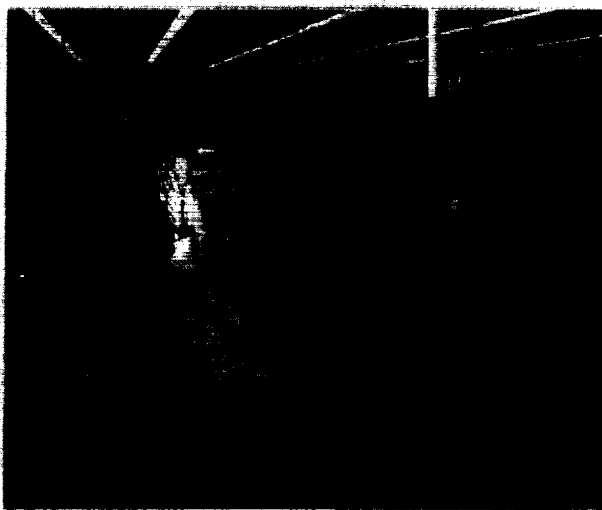
Figure 11. - Isometric sketch of Mach 5 inlet model.



TWO-DIMENSIONAL INLET INSTALLED IN 10 × 10 SWT

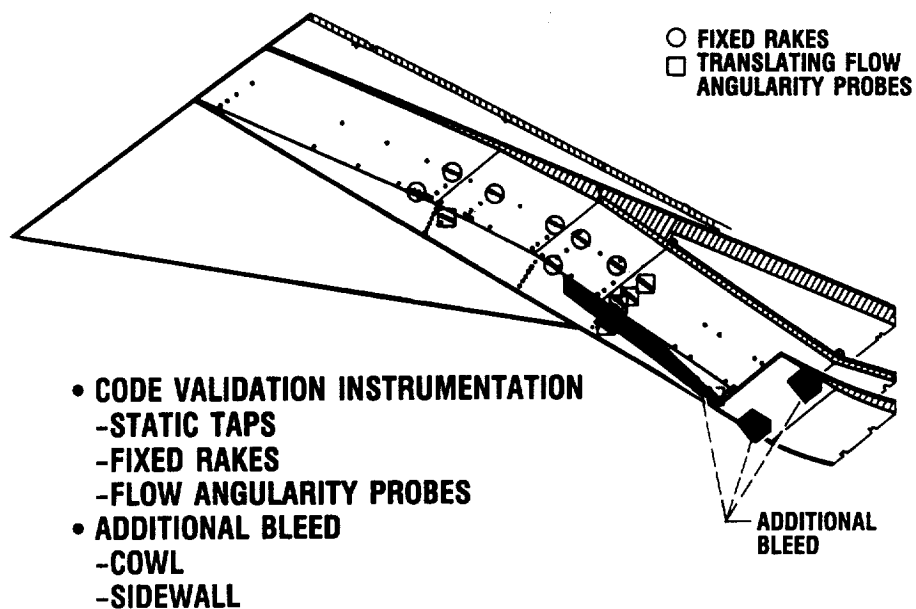
CD-87-28932

Figure 12. - Acceleration plate test technique.



CD-87-28934

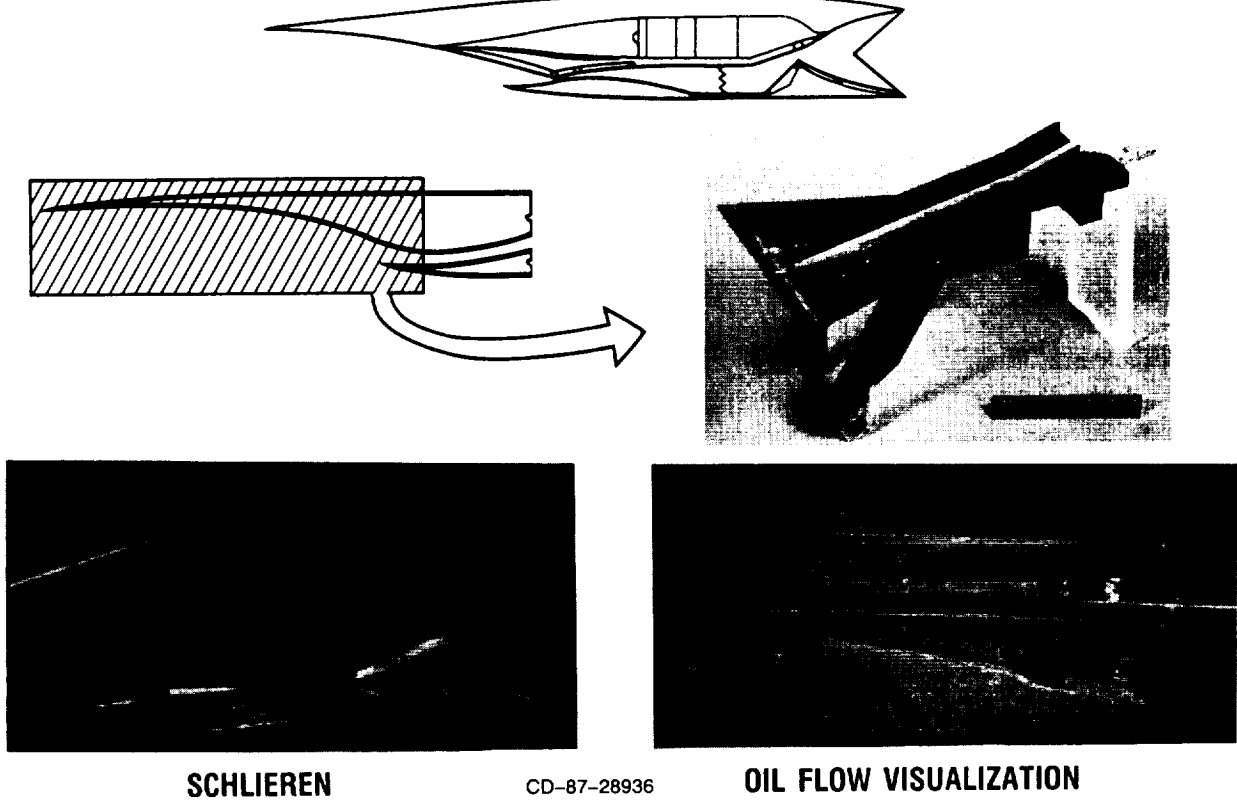
Figure 13. - Mach 5 inlet test model.



CD-87-28935

Figure 14. - Effect of PEPSIS analysis on placement of model instrumentation and bleed systems.

TURBOJET AND RAMJET

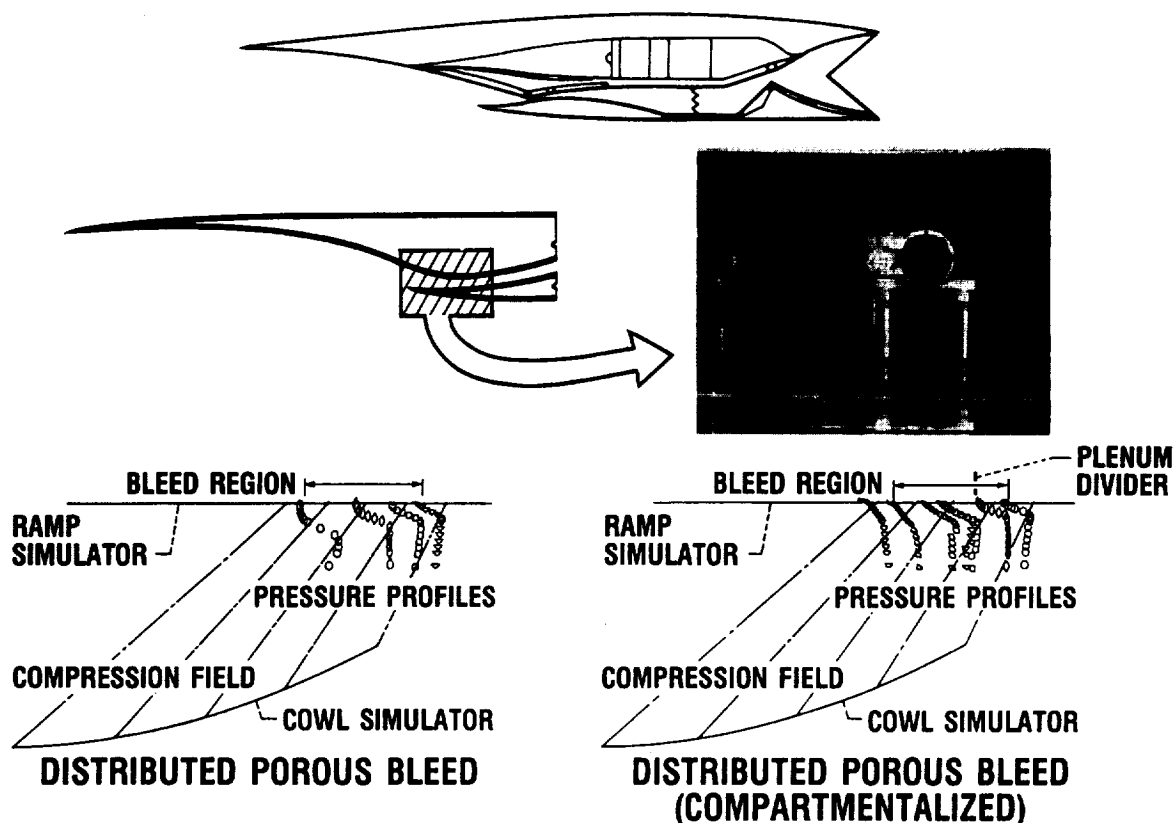


SCHLIEREN

CD-87-28936

OIL FLOW VISUALIZATION

Figure 15. - Small-scale plate/ramp model (1- by 1-Foot Supersonic Wind Tunnel).



CD-87-28937

Figure 16. - Bleed control studies (1- by 1-Foot Supersonic Wind Tunnel).

**PROVIDE FUNDAMENTAL AND DESIGN
DATA FOR CODE VALIDATION**

- GLANCING SIDEWALL SHOCK/
BOUNDARY LAYER INTERACTION
- THICK BOUNDARY LAYER/MULTIPLE
AND OBLIQUE SHOCK INTERACTION
- THICK BOUNDARY LAYER/NORMAL
SHOCK INTERACTION
- CORNER FLOW
- INLET DESIGN CODE DEVELOPMENT
DATA

**DETERMINE OVERALL INLET
PERFORMANCE**

- DESIGN AND OFF-DESIGN
AERODYNAMIC CHARACTERISTICS
- BLEED REQUIREMENTS
- UNSTART/RESTART CHARACTERISTICS
- CONTROL DATA SIGNALS
- VERIFICATION OF INLET DESIGN
TECHNIQUE
- VERIFICATION OF ACCELERATOR
PLATE TEST TECHNIQUE

CD-87-28931

Figure 17. - Benefits to be obtained from inlet test program.

HYPERSONIC PROPULSION RESEARCH

G. Burton Northam
Langley Research Center

INTRODUCTION

The NASA Langley Research Center has been conducting hypersonic propulsion research since the 1960's. In 1965, the Hypersonic Research Engine (HRE) project was undertaken to demonstrate internal performance of a scramjet with the X-15 as a test platform. The X-15 program was terminated in 1968 before the scramjet was ready for flight testing. However, two regeneratively cooled models were constructed and the internal performance of the engine was demonstrated in ground tests at the Lewis Research Center's Plum Brook test facility. Following the HRE program, the Hypersonic Propulsion Branch developed a modular airframe-integrated scramjet concept. This engine concept yields higher installed performance by reducing drag associated with mounting the engine. The airframe-integrated scramjet uses the vehicle forebody as a part of the compression surface, attaches engine modules directly to the underside of the vehicle, and uses the aft end of the airframe as a nozzle expansion surface. The development of technology for the modular airframe-integrated scramjet has been the focus of this research for the past several years.

As part of this research, a variety of inlet concepts have been explored and characterized. The emphasis of the inlet program has been the development of the short (light weight), fixed geometry, side-wall-compression inlets that operate efficiently over a wide Mach number range. As hypersonic combustion tunnels were developed, programs to study the parameters controlling fuel mixing and combustion with single and multiple strut models were conducted using direct connect test techniques. These various tests supported the design of subscale engine test hardware that integrated inlet and combustor technology and allowed the study of the effect of heat release on thrust and combustor/inlet interaction. A number of subscale (8-in.-high by 6-in.-wide) engine tests have demonstrated predicted performance levels at Mach 4 and Mach 7 simulated flight conditions.

This paper summarizes a few of the highlights from this research program.

ARTIST CONCEPT OF A SINGLE-STAGE-TO-ORBIT VEHICLE

An artist's concept of the current focus of much of the nation's hypersonic research is shown in figure 1. Since February 1985 when President Reagan announced that the country would build a National Aero-Space Plane (NASP) there has been an accelerated program at government and industrial laboratories to access and define the technology advances required to make single stage to orbit possible. NASA has teamed with the Defense Department, industry, and the universities to develop the technologies necessary to design and construct an experimental aircraft needed to demonstrate hypersonic flight by using airbreathing propulsion. The proposed research airplane, designated the X-30, is not an operational vehicle but a test bed to demonstrate the various technologies required for the design of three classes of vehicles - hypersonic transports that would cruise at Mach 5 or higher, space transports, and trans-atmospheric military vehicles.

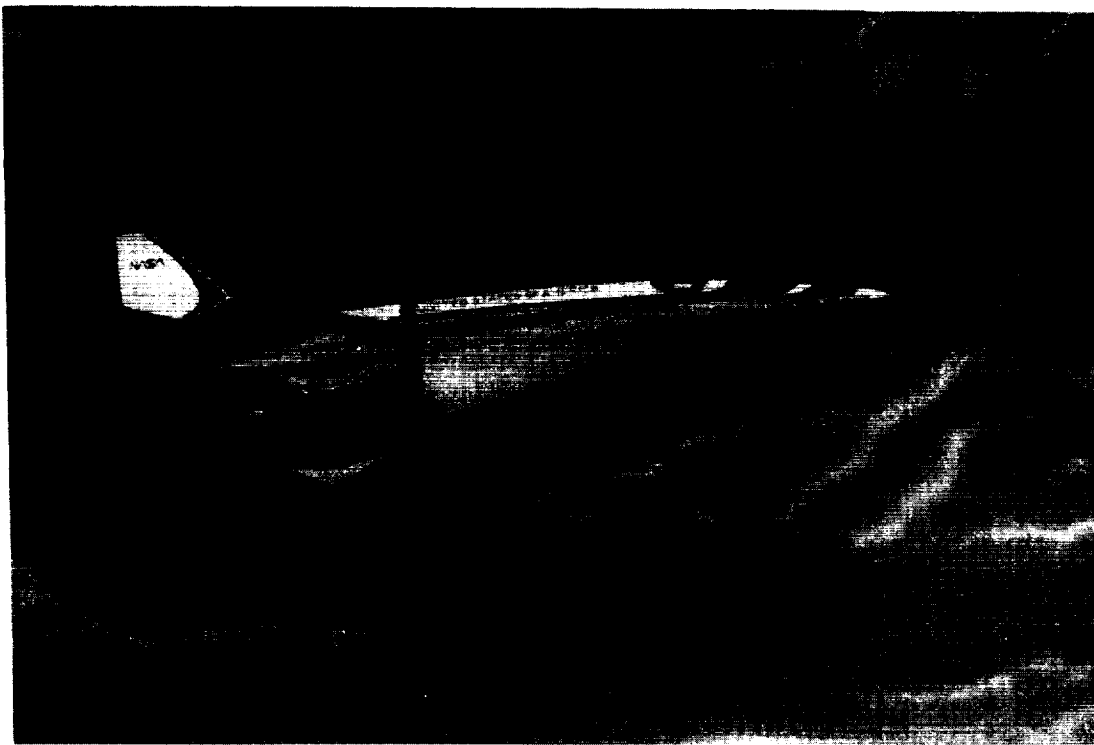


Figure 1. - Artist concept of a single-stage-to-orbit vehicle.

AIRFRAME-INTEGRATED SUPERSONIC COMBUSTION RAMJET

Figure 2 shows the Langley concept for an airframe-integrated supersonic combustion ramjet (scramjet). The engine modules are mounted on the underside of the vehicle and use the vehicle forebody as part of the nozzle compression. The compression is completed by the inlet sidewalls and the fuel injection struts. The use of fuel injection struts to complete the compression shortens the inlet and provides locations for distributing the fuel in the incoming compressed air. The relative amount of parallel and transverse injected fuel is used to control the mixing and thus the heat release distribution required for the desired performance as a function of flight Mach number. The modular design allows testing of a single engine in a smaller facility than that required if the total propulsion system had to be tested.

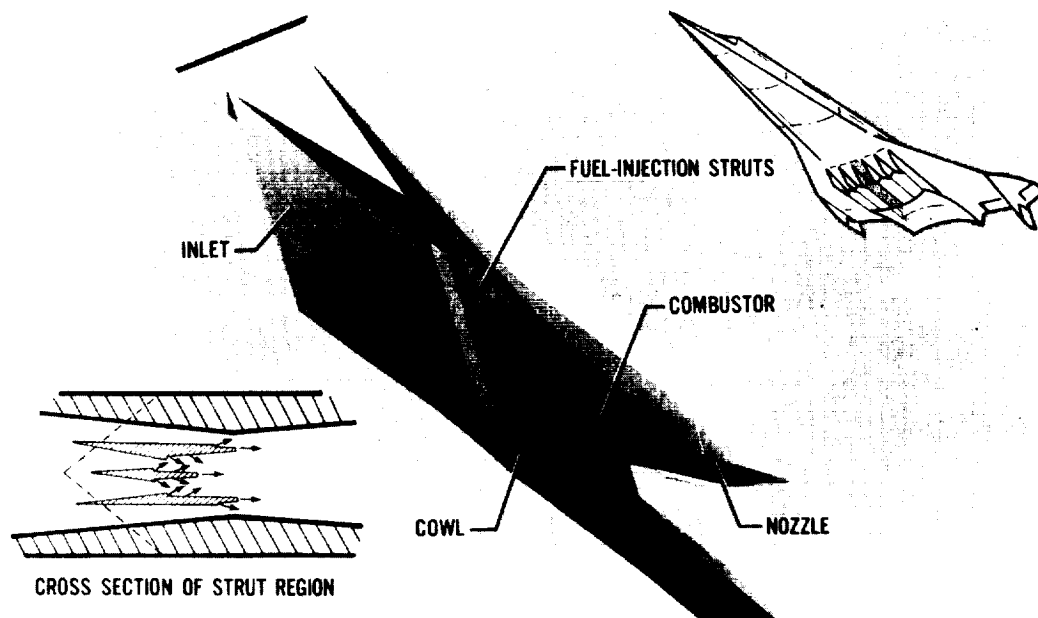


Figure 2. - Airframe-integrated supersonic combustion ramjet.

HYPersonic INLET DESIGN

Several inlet designs (fig. 3) have been constructed and evaluated at Mach 3 to 6. Currently the testing range is being extended to Mach 18 to support the NASP program. The three strut inlet with a swept combustor was the first inlet of this class completely characterized - mass capture, pressure recovery, contraction ratio, and throat Mach number as a function of free stream Mach number. Computational fluid dynamics is becoming more mature and is being used to design and evaluate alternate inlet designs like the rectangular to circular inlet and the two strut inlets shown. The three-module inlet model is being used to determine the effect of an inlet unstart on the performance of the remaining started inlets.

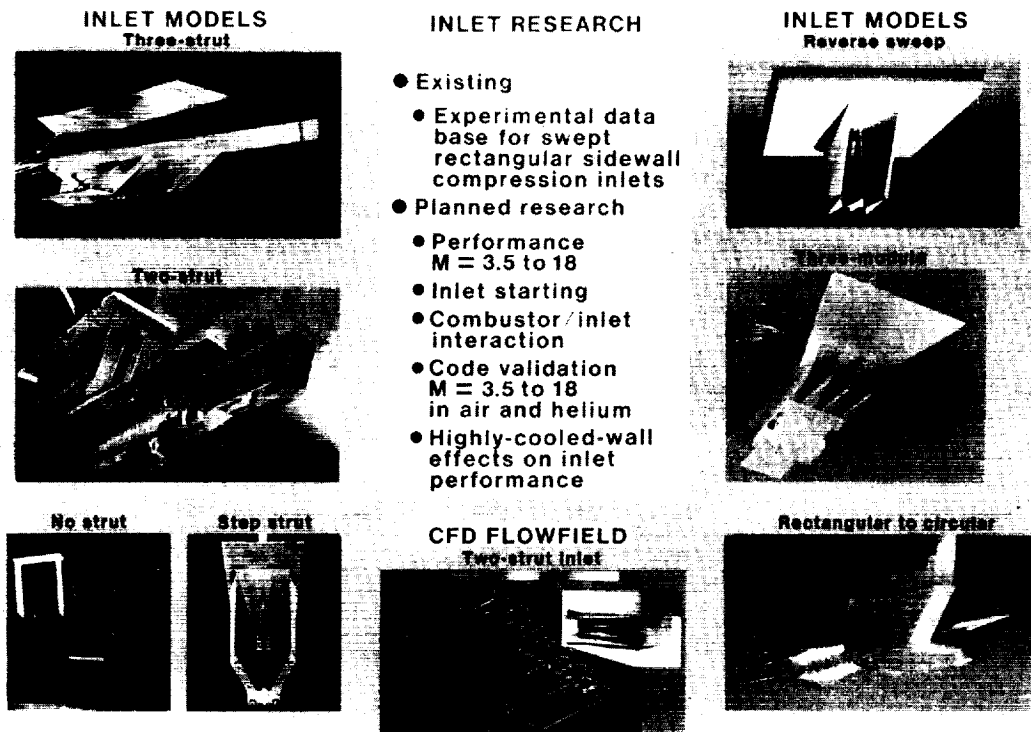


Figure 3. - Hypersonic inlet design.

SCHEMATIC OF DIRECT CONNECT TEST APPARATUS

In order to reduce the size of the facility required to test a scramjet engine, direct connect tests of the combustor are conducted by simulating the inlet flow into the combustor region. Typical direct connect test hardware are shown in figure 4. This hardware is being used to determine combustor geometry effects on scramjet performance. The figure shows some of the geometry variables being investigated.

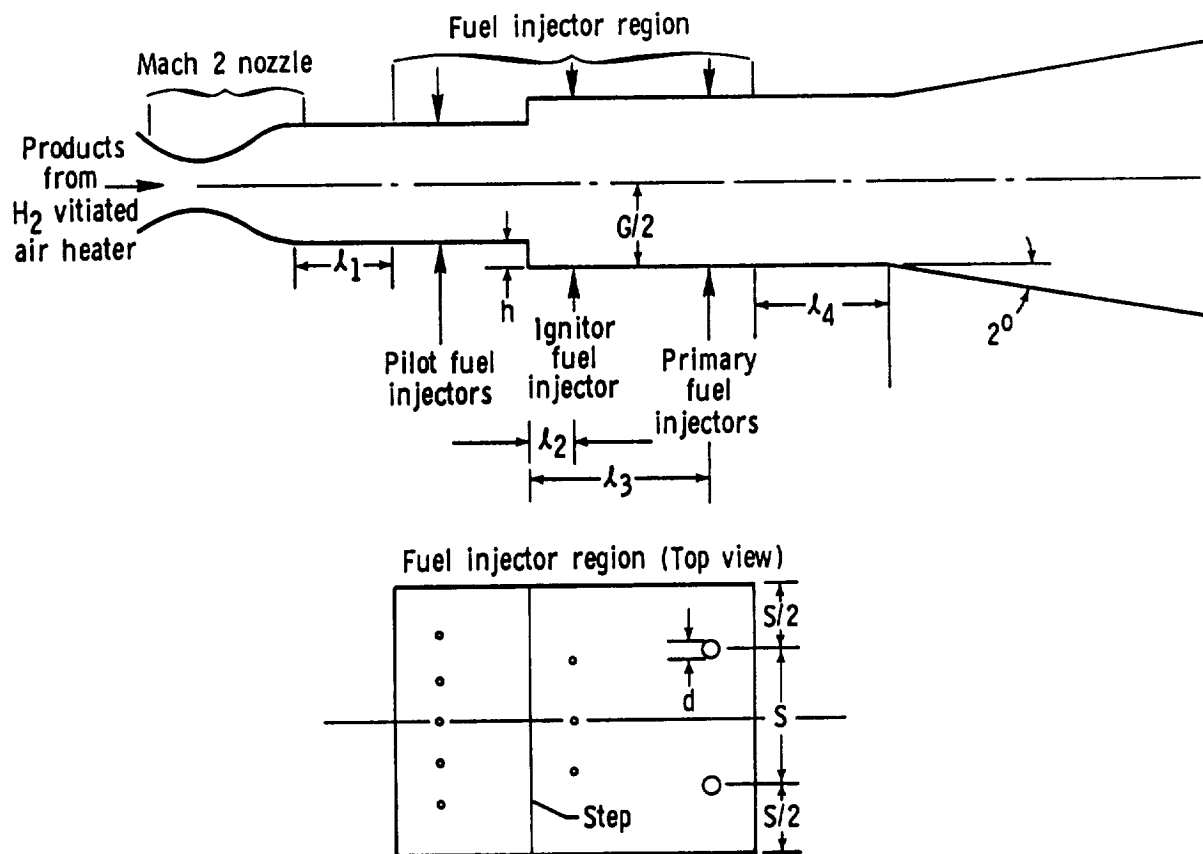


Figure 4. - Schematic of direct connect test apparatus.

DUAL-MODE COMBUSTOR OPERATION

Using direct connect test hardware, the two different pressure distributions shown in figure 5 were obtained by varying the total temperature and the fuel injection location with the Mach number at the combustor entrance held constant at 1.7. The Mach 4 distribution with a major portion of the duct operating subsonic had most of the fuel injected parallel to the flow. For the Mach 7 total temperature data, most of the fuel was injected perpendicular to the air flow and much of the combustion occurred at supersonic conditions.

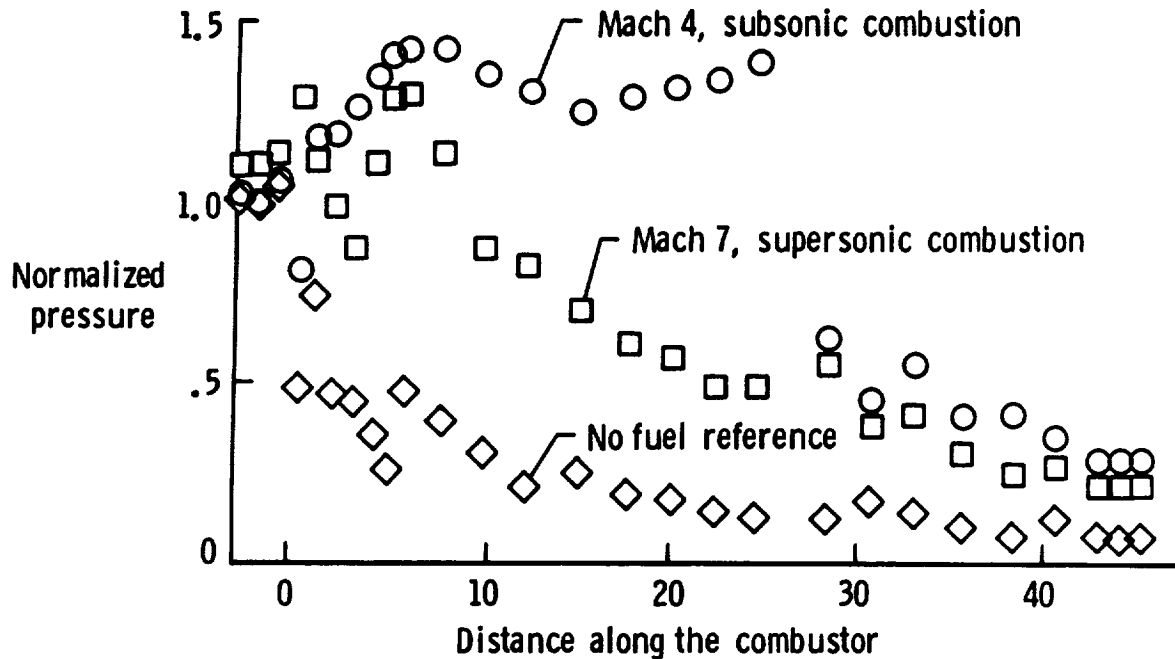


Figure 5. - Dual-mode combustor operation.

UPSTREAM INTERACTION LIMIT

Figure 6 shows the maximum equivalence ratio that can be injected in the direct connect hardware as a function of total temperature. The Mach number entering the combustor from the facility nozzle was 2.0. Adding a constant area section 2.2 duct heights downstream of the fuel injector region reduced the amount of fuel that could be added without causing a pressure rise at the combustor entrance station. The duct divergence downstream of the fuel injectors of the constant area section was 2° on the top and bottom walls.

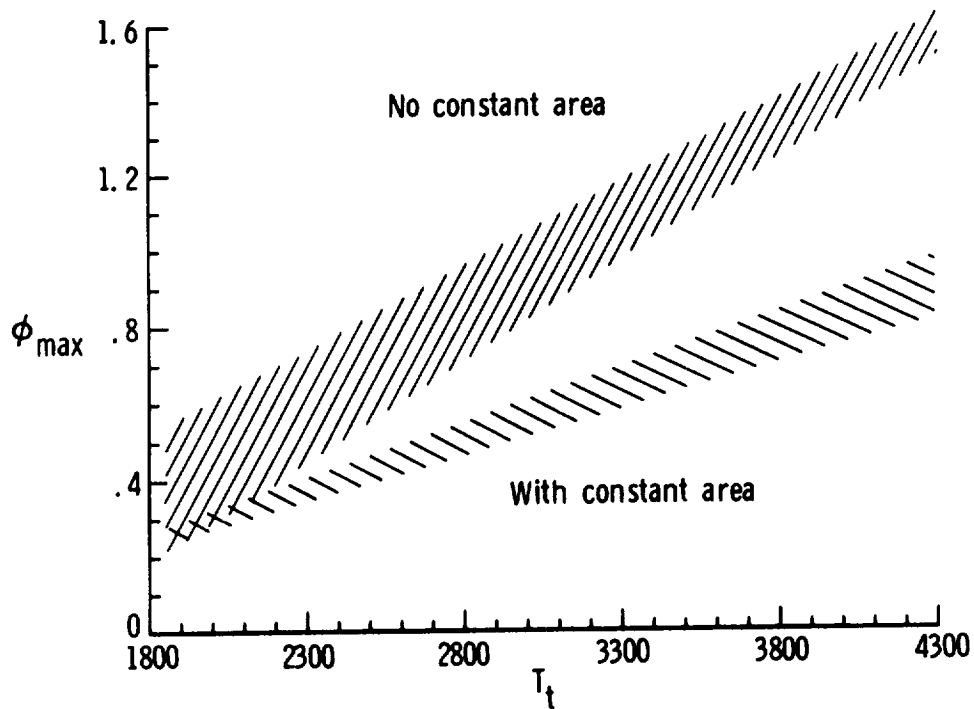


Figure 6. - Upstream interaction limit (effect of constant area combustion).

PRESSURE DISTRIBUTIONS FOR PILOTED TESTS

A number of tests have been conducted to explore ignition and flame-holding techniques for hypersonic combustion. At low flight speeds, the total temperature is not high enough for autoignition; at high speeds the reduced residence time may make flameholding difficult. One ignition technique explored was the use of an electrically driven plasma jet operating on a hydrogen/argon mixture. Figure 7 shows the pressure distributions for a Mach 2 combustor operating below the autoignition temperature (total temperature 1400 °R). When 50 percent hydrogen/argon mixture was used in the plasma jet operating at less than 1 kW, the pressure distribution indicated considerable pressure rise. However, when the torch was operated on all argon the pressure distribution was similar to the no fuel distribution. These results indicate that the hydrogen atoms generated in the plasma, not the thermal heating of the gases were the ignition source.

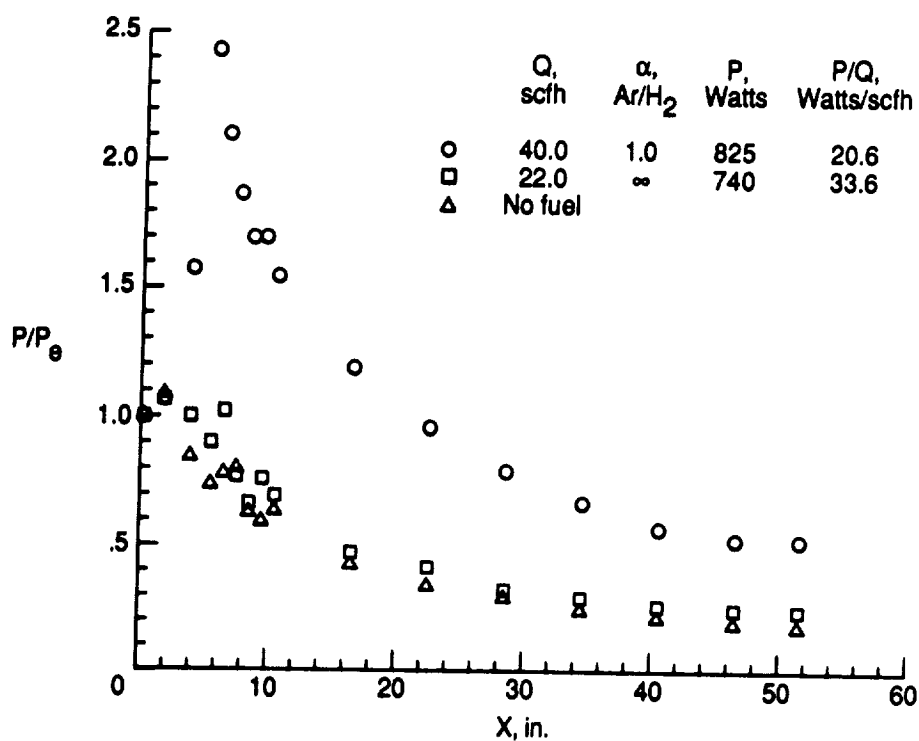
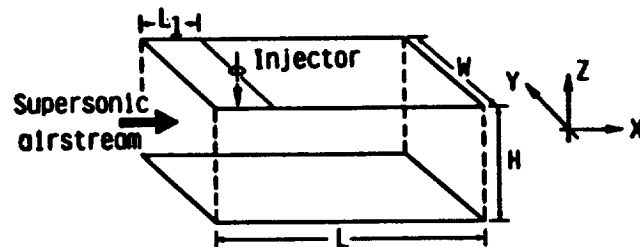


Figure 7. - Pressure distributions for piloted tests (AR/H₂ and argon plasmas, $T_t = 1400$ R, $\phi = 0.28$).

COMPARISON OF CFD AND EXPERIMENTAL MIXING RESULTS

The use of large computers for the calculations of complex flows is a new tool available to the scramjet designer. In order for these codes to be used with confidence, validation tests with well defined boundary conditions must be conducted and compared with the corresponding computed results. Figure 8 shows that the result of one such experiment where a sonic transverse jet was injected into supersonic Mach 2.06 flow. The lines are the calculated mass contours and the dots are the edge of the jet as defined by laser induced fluorescence of iodine. This favorable comparison indicates that the CFD code could be extended to other similar geometries with confidence. In fact, the code has been modified to include chemical reactions and similar reacting flow experiments are planned.



	Injected air	Main airstream
Mach number	1.0	2.06
Static temperature (K)	240.0	170.0
Static pressure (KPa)	152	36.0

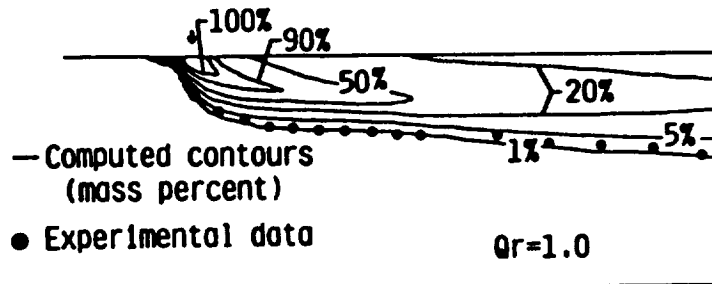
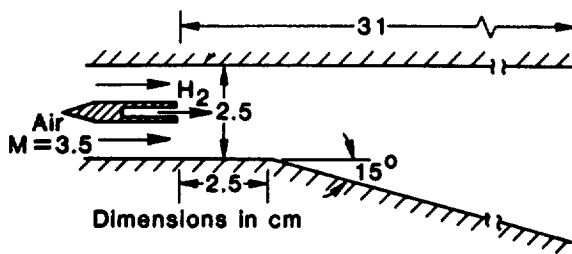


Figure 8. - Comparison of CFD and experimental mixing results.

SHOCK TUNNEL SUPERSONIC COMBUSTION

At high hypersonic speeds, there are no steady state facilities capable of simulating the total enthalpy and pressure encountered in flight. The best experimental simulation of hypersonic combustion is conducted in pulse facilities that operate on the order of 1/1000 of a second. Results from such tests are shown in figure 9 for Mach 9 and 16 simulated flight conditions. Again CFD calculations were used to predict the flow. The Mach 16 results were not predicted as well as the lower speed test results. At these higher speeds where ground tests facilities are not available, CFD will have to be used to predict performance for NASP.



- Reasonable match between data and theory in Mach 8 to 12 speed range
- Indication of combustion effects at Mach 16
 - Unexplained difference between data and theory
 - Short residence time, low pressure, oxygen dissociation
- Additional analysis and tests at higher pressure planned

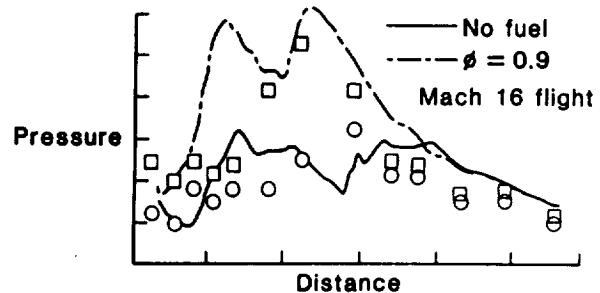
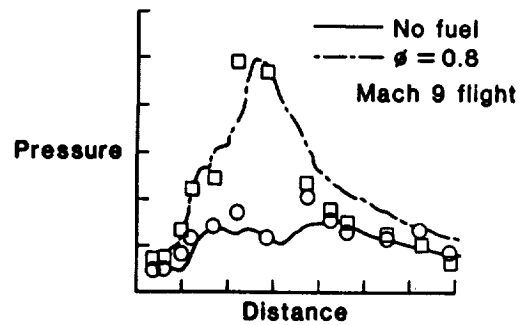


Figure 9. - Shock tunnel supersonic combustion (University of Queensland).

MULTISPECIES CARS SCHEMATIC

In order to validate CFD codes, instream measurements of temperature and species profiles are required. In reacting supersonic streams it is difficult to use sampling probes for the measurements due to shock effects. Nonintrusive optical techniques are being developed to replace probe measurements. One technique being used is Coherent AntiStokes Raman Scattering, CARS. A schematic of the CARS system is shown in figure 10. This system can measure temperature, oxygen, and nitrogen during a 10-nanosecond laser pulse at 10-Hz rate. The short pulse time allows measurements to be made in high speed turbulent flow.

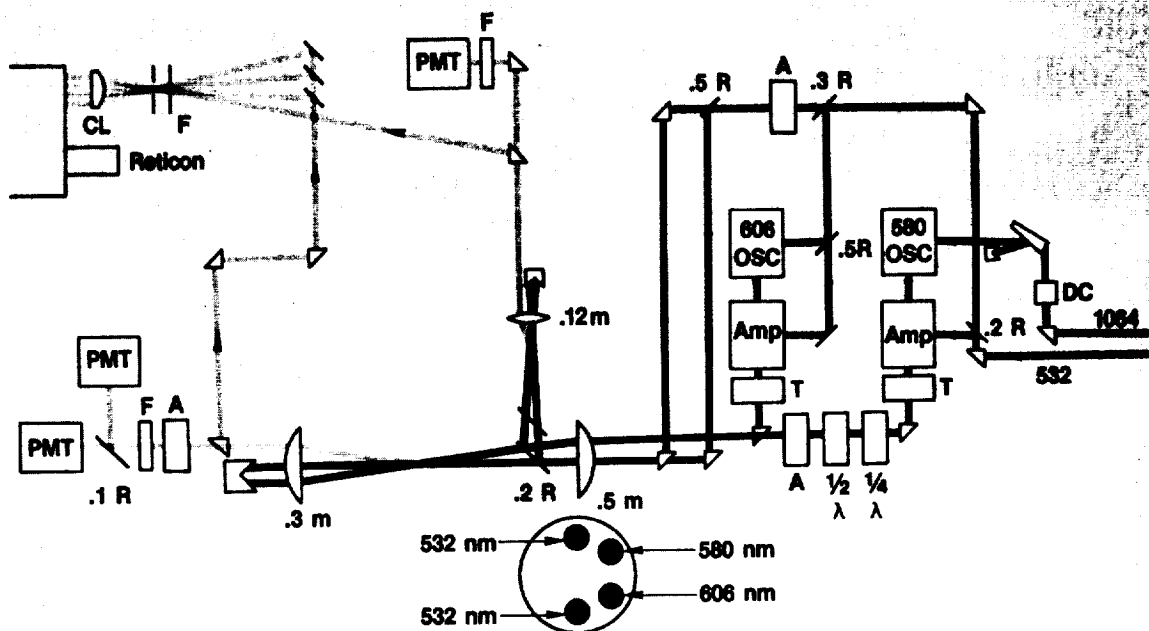


Figure 10. - Multispecies cars schematic.

SUPERSONIC COMBUSTION EXPERIMENTS

A simple coaxial-jet, supersonic combustion experiment has been developed for CFD validation. The sonic jet is injected into a Mach 2 high enthalpy simulated air stream generated by the combustion and expansion of hydrogen and air with oxygen make up. A cross section of the apparatus is shown in figure 11 along with data taken in the exit plane. On the data plots the dashed lines are the calculated means and the solid lines are the CARS measurements. Tests are underway to make similar measurements to map the radial and axial profiles with and without fuel injection. This experiment is also being simulated by using a reacting flow CFD code.

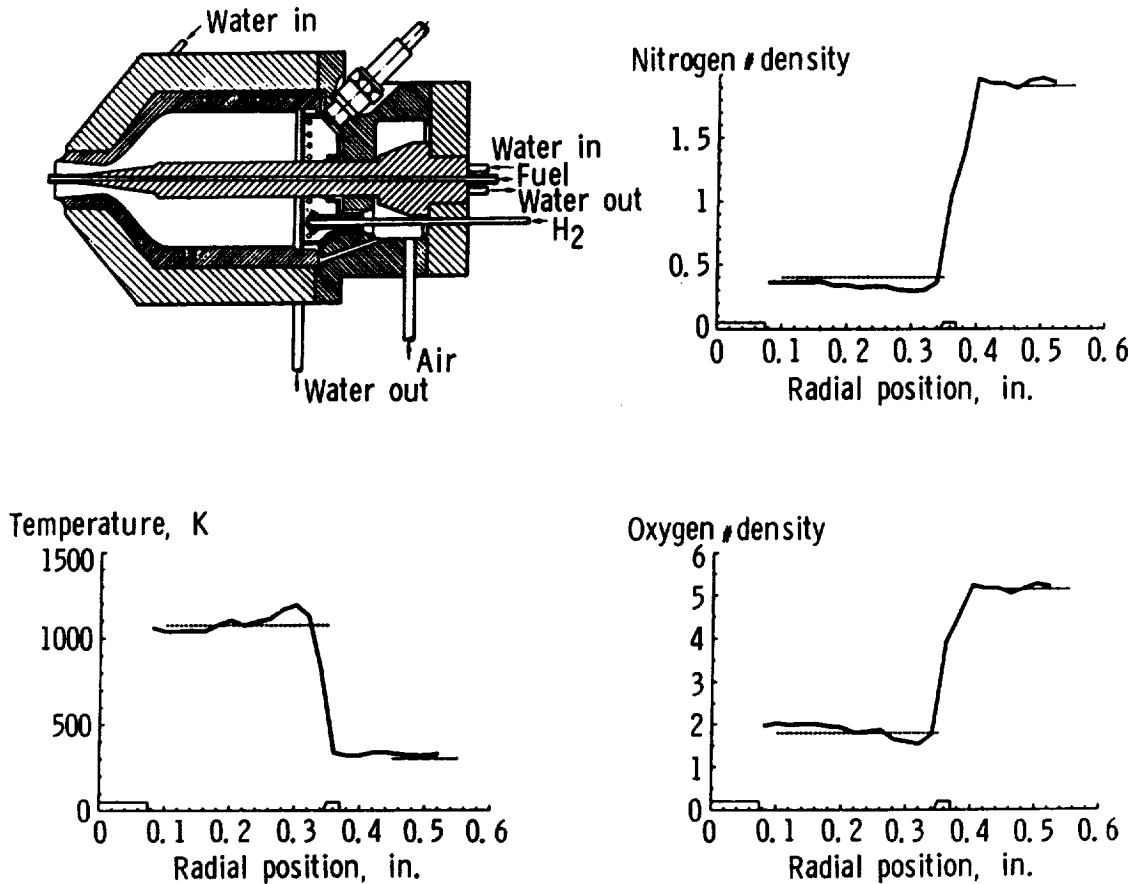


Figure 11. - Supersonic combustion experiments.

SIMULATION REQUIREMENTS FOR HYPERSONIC SCRAMJET COMBUSTOR

In order to demonstrate scramjet performance in ground test, large high enthalpy facilities are required. Figure 12 shows the total enthalpy required as a function of flight Mach number up to Mach 25 or near orbital speed. Also shown on the figure are the static temperatures, stagnation temperatures and the stagnation pressures required for proper simulation. The right most curve shows the flight path energy and the band shows the combustor flow conditions after the air is processed by the inlet. Even the combustor conditions rise rapidly with flight Mach number. In fact, hydrogen or air heaters can only be used to simulate flight speeds up to about Mach 8. Beyond this speed pulse facilities are required.

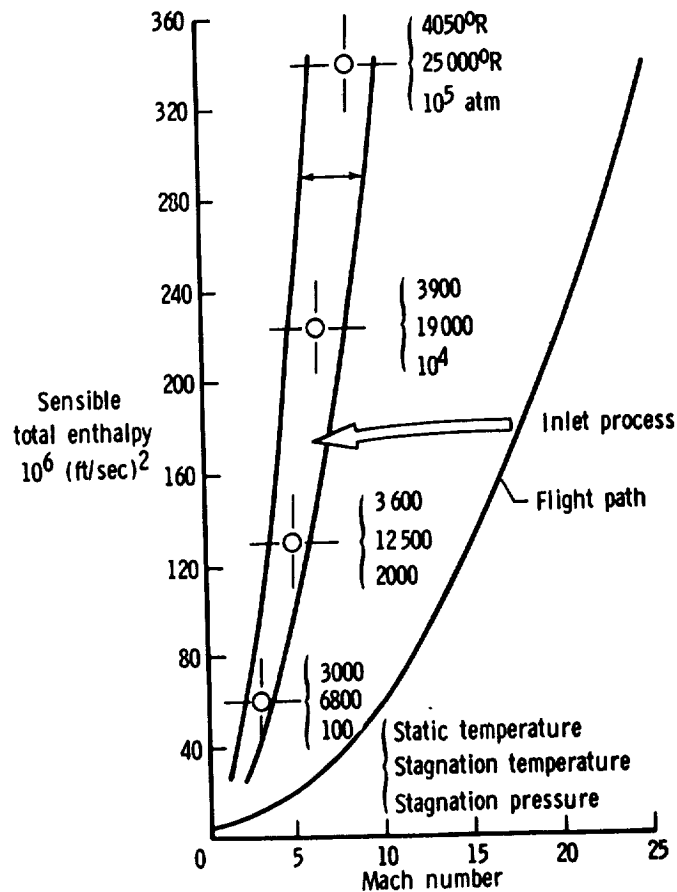


Figure 12. - Simulation requirements for hypersonic scramjet combustor tests.

SIMULATION CAPABILITIES OF OPERATIONAL AND NEAR-TERM FACILITIES

Figure 13 shows, on similar coordinates, the operational range of several combustion tunnels. Note that the T3 tunnel at the University of Queensland in Australia is the only facility that covers the higher Mach numbers. This facility has been used to produce flow simulating Mach 12.

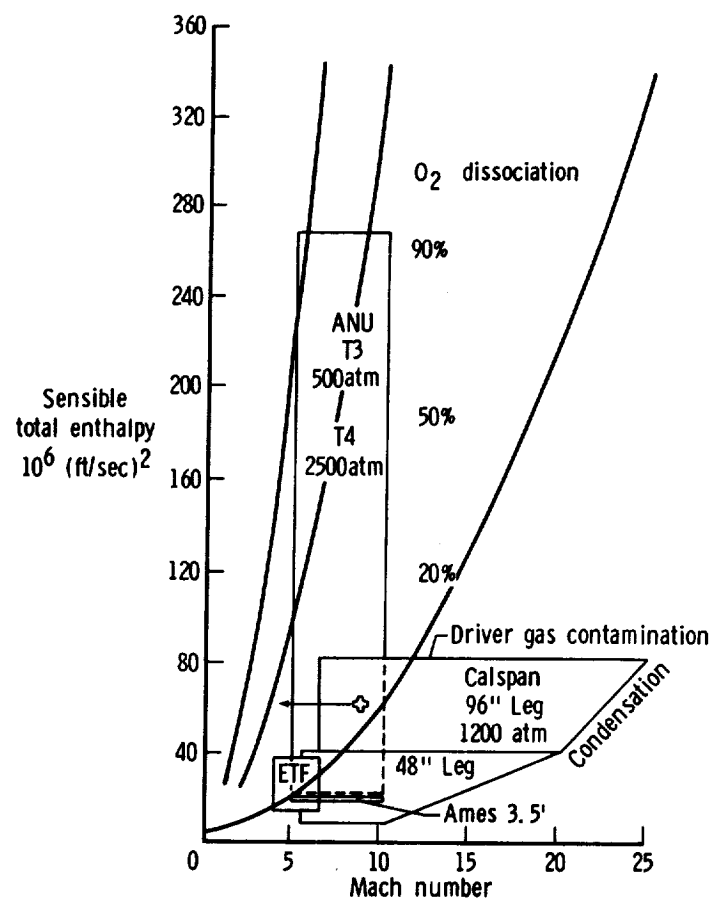


Figure 13. - Simulation capabilities of operational and near-term facilities.

EFFECTS OF VITIATION ON IGNITION TIME FOR STOICHIOMETRIC H_2 IN EQUILIBRIUM AIR

One of the problems associated with testing in high enthalpy ground test facilities is the fact that the energy is usually added to the flow by some mechanical, electrical, or combustion process that contaminates or dissociates the air. Engine test facilities that use combustion of hydrogen or hydrocarbons can produce simulated Mach numbers of about 7 with oxygen content maintained at atmospheric levels. When these facilities are used, the tests are said to be conducted in vitiated air. Figure 14 shows the effects of vitiation on the ignition delay of hydrogen as a function of static pressure and temperature. At low temperatures and pressures the effects become significant.

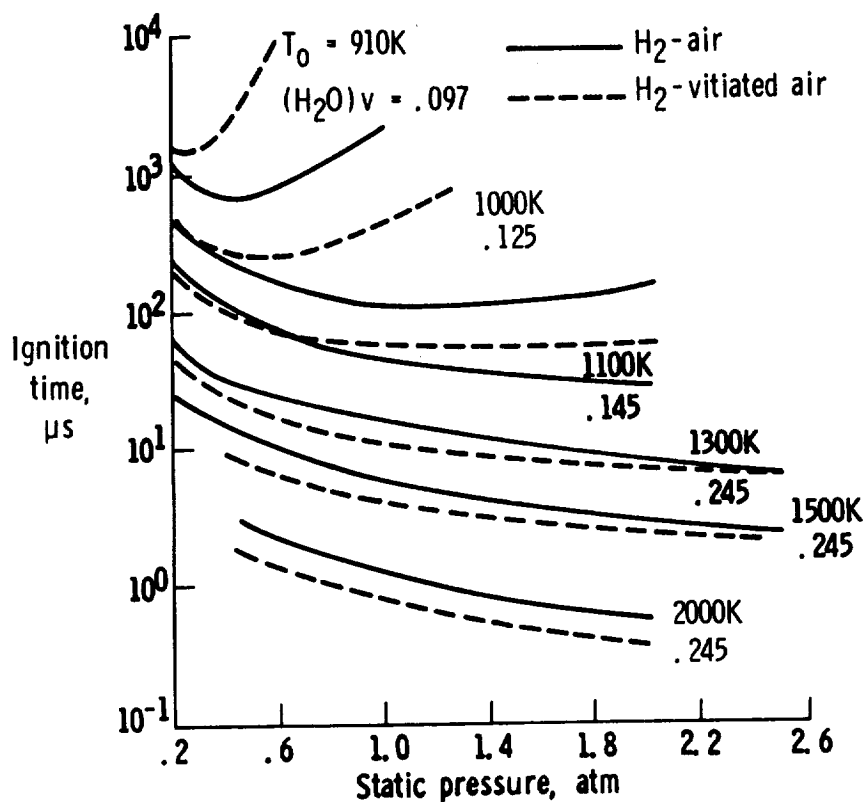


Figure 14. - Effects of vitiation on ignition time for stoichiometric H_2 in equilibrium air.

STRUTLESS PARAMETRIC ENGINE MODEL

In order to integrate the inlet and combustor technology, subscale engine tests are conducted in arc or vitiated scramjet test facilities at Langley from Mach 3.4 to 7 flight conditions. Figure 15 shows the strutless parametric engine that is being used to study the sensitivity of performance to engine geometric variables, fuel injection location, fuel level, contraction ratio and inlet sweep.

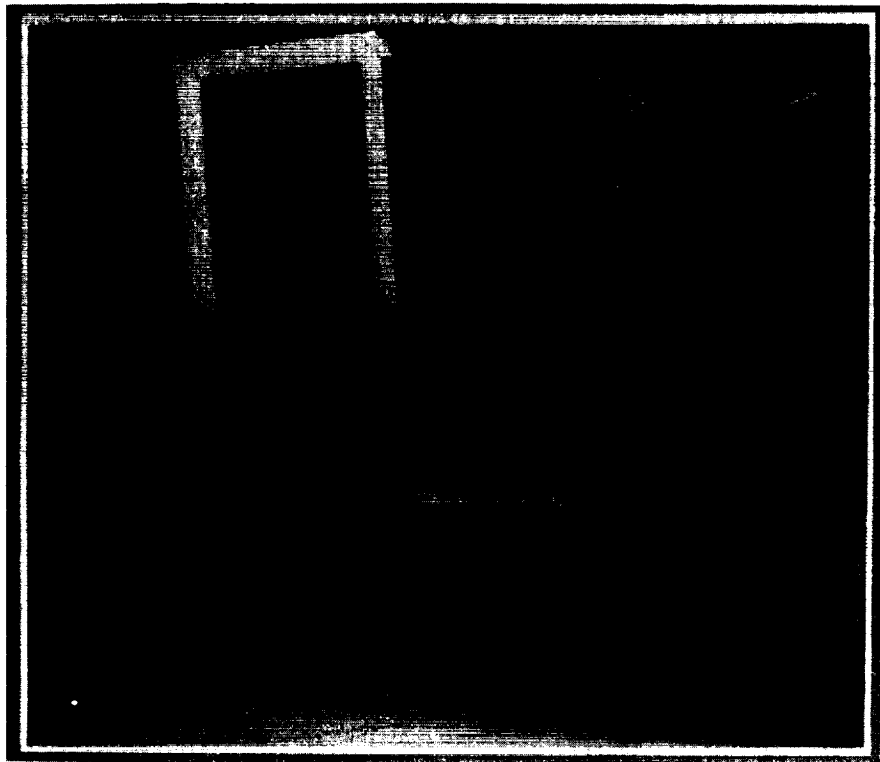


Figure 15. - Strutless parametric engine model.

ORIGINAL PAGE
BLACK AND WHITE PHOTOGRAPH

STRUTLESS PARAMETRIC ENGINE MODEL DETAILS

The sketch in figure 16 shows the details of the strutless model. The sidewalls are adjustable and the segmented side wall locations can be independently moved to tailor the internal geometry. Fuel can be injected from a number of side wall locations. The engine is mounted on a thrust balance in the tunnel and has numerous pressure ports to measure wall pressures.

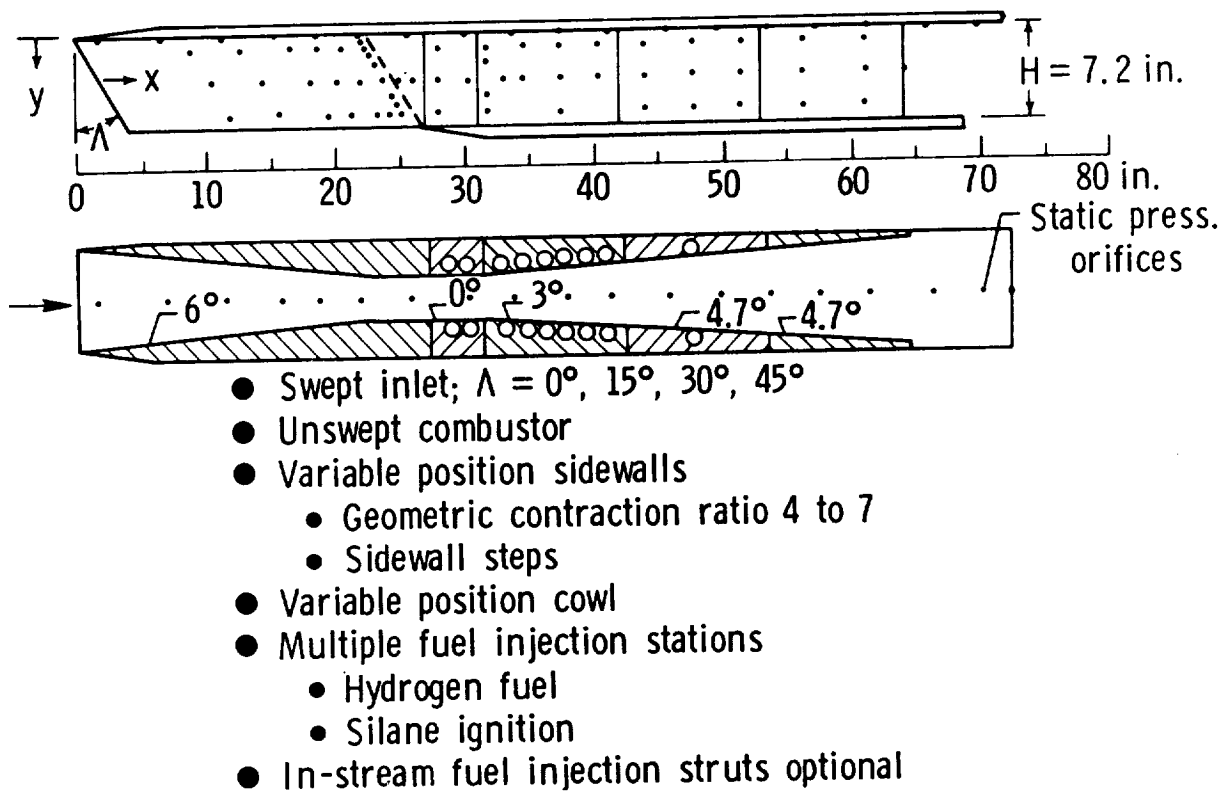


Figure 16. - Strutless parametric engine model details.

MACH 4 ENGINE PERFORMANCE

Figure 17 shows typical pressure and force data obtained in Mach 4 tests of the strutless scramjet shown in the schematic. The peak pressure in the combustor increases as more fuel is injected into the engine and the pressure rise moves upstream closer to the inlet exit. However, no combustor-inlet interaction occurred since the combustion-induced pressure rise did not move onto the forward-facing sidewalls of the inlet.

The thrust curve shows a comparison of data from the strutless engine with that from an earlier version of a scramjet and with theory assuming mixing-controlled combustion. Solid symbols indicate that combustion of the primary hydrogen fuel was assisted by a pilot gas (silane/hydrogen) while the open symbols indicate that the fuel was all hydrogen. Agreement of the two sets of data (piloted and unpiloted) indicate that the wedges shown in the schematic were good flameholders. Agreement of the data with theory indicates that the combustion was mixing-controlled. And, finally, comparison of the data with that from the other scramjet shows the improvement in performance obtained by redesign.

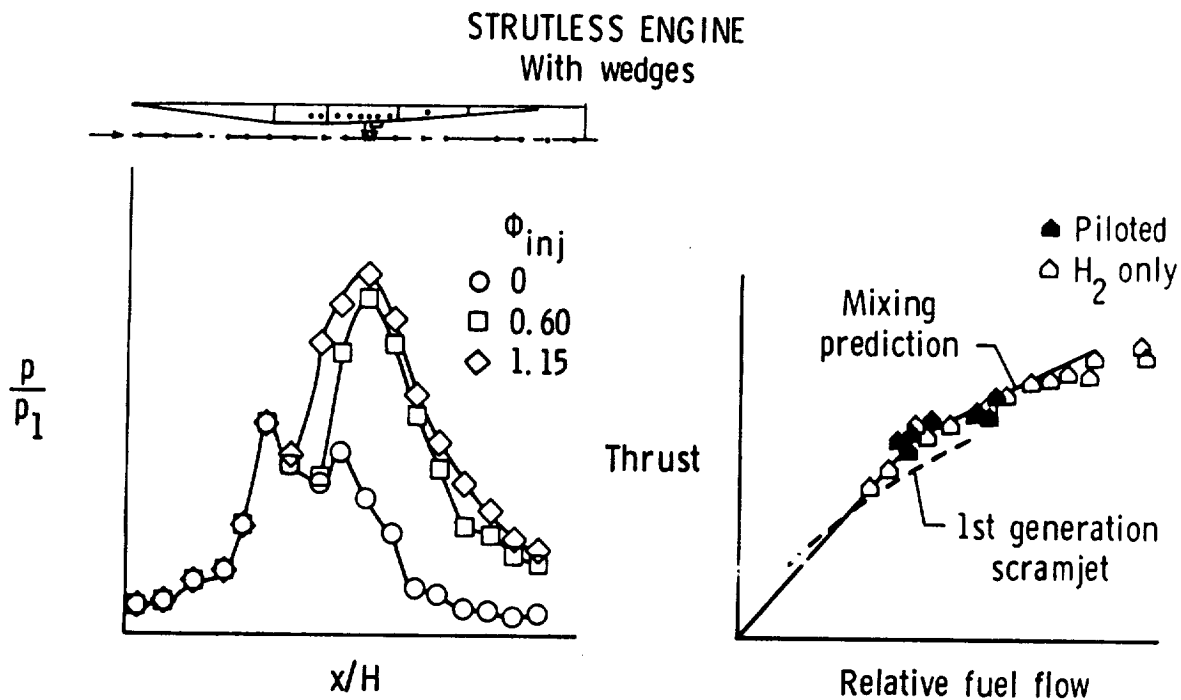
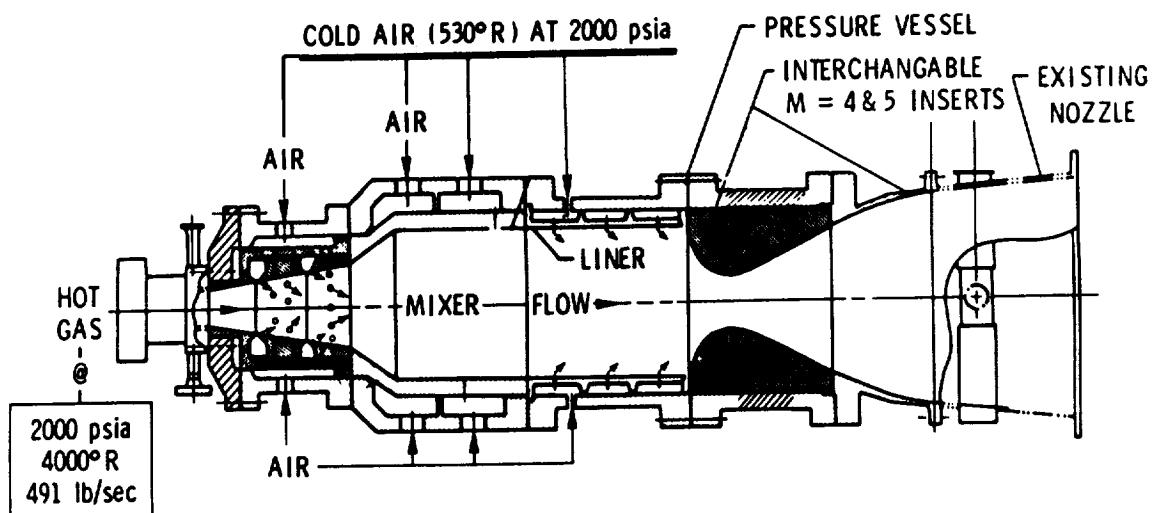


Figure 17. - Mach 4 engine performance.

MIXER/ALTERNATE MACH NUMBER NOZZLES FOR 8-FOOT HTT

The Langley 8-foot test diameter high temperature tunnel is being modified for propulsion testing. When completed this facility will allow testing of larger scale models and complete missile size scramjets. Figure 18 indicates the operating points at maximum total pressure of the 8-foot HTT with the Mach 4, 5, and 7 nozzles. A schematic is also shown of the mixer/throat section which is used with the Mach 4 and Mach 5 nozzles. When the Mach 7 nozzle is in service, the entire mixer/throat section (shown in section view) is replaced by the first portion of the Mach 7 nozzle. The hardware upstream and downstream of the cross-hatched section is used with all three nozzles.

During Mach 7 tests, no unheated air is added to the 4000 °R vitiated air exiting combustion heater. However, to obtain the lower Mach 4 and Mach 5 total enthalpies, unheated bypass air is added as shown in the schematic in a fashion similar to that employed in the Langley Arc-Heated Scramjet Test Facility.



MACH NUMBER	THROAT DIAMETER, in.	MIXER TOTAL PRESSURE, psia	MIXER TOTAL TEMPERATURE, °R	COLD AIR FLOW RATE, lb/sec	TOTAL FLOW RATE, lb/sec
4.0	28.5	234	1640	1436	1927
5.0	17.1	444	2350	597	1088
7.0	5.6	2000	4000	0	491

Figure 18. - Mixer/alternate Mach number nozzles for 8-foot HTT.

SCRAMJET DEVELOPMENT

As high speed propulsion matures and new larger facilities become available, testing will move from single module subscale testing to testing of larger scale and multi-engine modules in the 8 ft tunnel and then to flight testing (fig. 19). The larger or near full scale tests will build confidence in the mixing and flameholding models and will allow realistic engine cooling evaluations in flight type hardware. The multi mode test will be used to study the influence of one module on the inlet flow of an adjacent module and allow the study of an inlet unstart on the total engine performance.

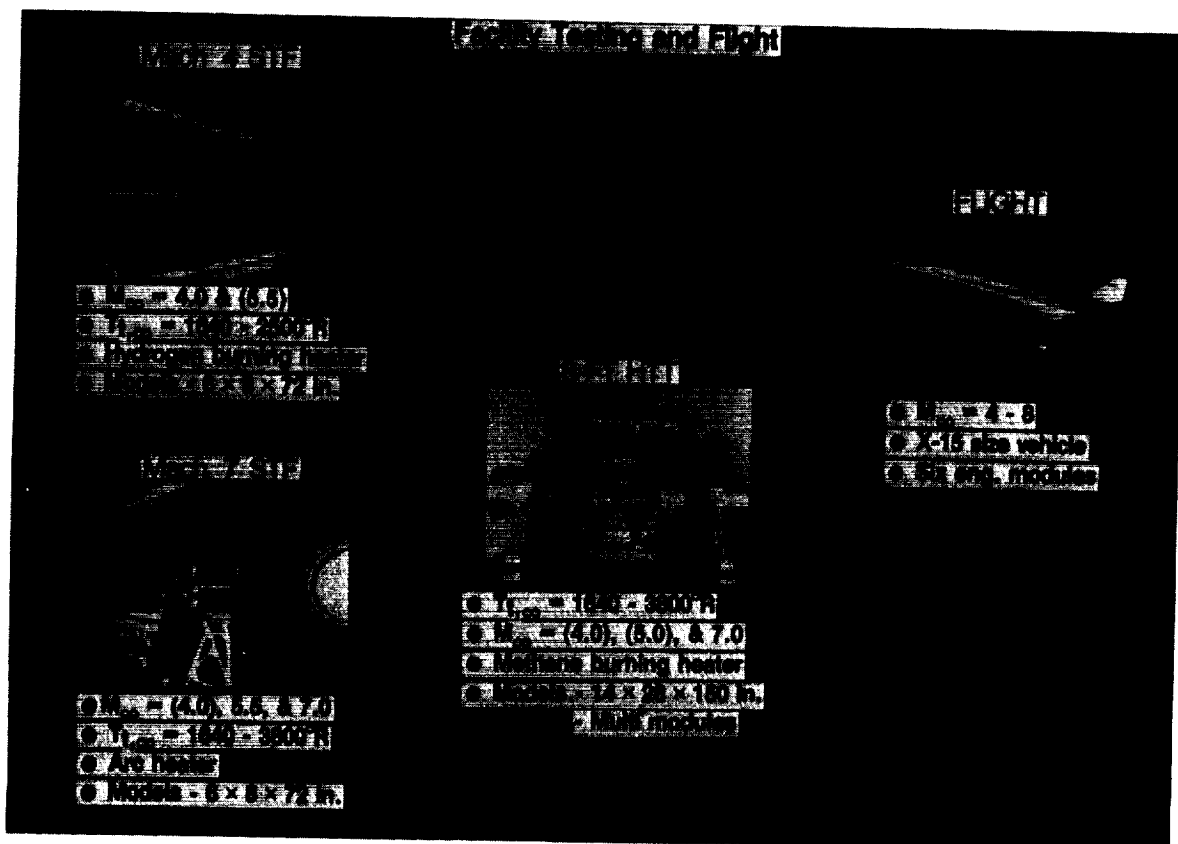


Figure 19. - Scramjet development.

ORIGINAL PAGE
BLACK AND WHITE PHOTOGRAPH



National Aeronautics and
Space Administration

Report Documentation Page

1. Report No. NASA CP-3049		2. Government Accession No.		3. Recipient's Catalog No.	
4. Title and Subtitle Aeropropulsion '87				5. Report Date February 1990	
				6. Performing Organization Code	
7. Author(s)				8. Performing Organization Report No. E-3798	
				10. Work Unit No. 505-62-3B	
9. Performing Organization Name and Address National Aeronautics and Space Administration Lewis Research Center Cleveland, Ohio 44135-3191				11. Contract or Grant No.	
				13. Type of Report and Period Covered Conference Publication	
12. Sponsoring Agency Name and Address National Aeronautics and Space Administration Washington, D.C. 20546-0001				14. Sponsoring Agency Code	
15. Supplementary Notes This publication supercedes the Aeropropulsion '87 session preprints (NASA CP-10003).					
16. Abstract This publication records the Proceedings of the Aeropropulsion '87 Conference, held at the NASA Lewis Research Center, Cleveland, Ohio, on November 17 to 19, 1987. Unclassified presentations by Lewis and NASA Headquarters senior management and many Lewis technical authors covered the philosophy and major directions of the Lewis aeropropulsion program, and presented a broad spectrum of recent research results on materials, structures, internal fluid mechanics, instrumentation and controls, and both subsonic and high-speed propulsion technology. Primary emphasis is on research accomplished in fiscal years 1985 through 1987.					
17. Key Words (Suggested by Author(s)) Aeronautical propulsion research; Materials; Structures; Internal fluid mechanics; Instrumentation; Controls; Subsonic propulsion; Supersonic propulsion; Hypersonic propulsion			18. Distribution Statement Unclassified - Unlimited Subject Category 07		
19. Security Classif. (of this report) Unclassified		20. Security Classif. (of this page) Unclassified		21. No of pages 516	22. Price* A22

1

**National Aeronautics and
Space Administration
Code NTT-4**

**Washington, D.C.
20546-0001**

**Official Business
Penalty for Private Use, \$300**

NASA
